National Park Service
U.S. Department of the Interior

Northeast Region
Natural Resource Stewardship and Science

Assessment of Air Quality and Related Values in Shenandoah National Park

Technical Report NPS/NERCHAL/NRTR-03/090

Assessment of Air Quality and Related Values in Shenandoah National Park

Technical Report NPS/NERCHAL/NRTR-03/090

Timothy J. Sullivan[1], Bernard J. Cosby[2], John A. Laurence[3], Robin L. Dennis[4], Kristi Savig[5], James R. Webb[2], Arthur J. Bulger[2], Mark Scruggs[6], Christi Gordon[7], John Ray[6], E. Henry Lee[8], William E. Hogsett[8], Heather Wayne[5], Debbie Miller[6], and Jeffrey S. Kern[9]

U.S. Department of the Interior
National Park Service
Northeast Region
Natural Resource Stewardship and Science
Philadelphia, Pennsylvania

[1] E&S Environmental Chemistry, Inc., Corvallis, OR
[2] Department of Environmental Sciences, University of Virginia, Charlottesville, VA
[3] Formerly with U.S. Environmental Protection Agency, National Health and Environmental Effects Laboratory, Western Ecology Division, Corvallis, OR; now with USDA Forest Service, Pacific Northwest Research Station, Corvallis, OR
[4] National Oceanic and Atmospheric Administration, Air Resources Laboratory, Atmospheric Sciences Modeling Division, Research Triangle Park, NC
[5] Air Resource Specialists, Inc., Fort Collins, CO
[6] National Park Service, Air Resources Division, Denver, CO
[7] Shenandoah National Park, Luray, VA
[8] U.S. Environmental Protection Agency, National Health and Environmental Effects Laboratory, Western Ecology Division, Corvallis, OR
[9] Dynamac Corporation, Corvallis, OR

ON THE COVER
A view of Massanutten Mountain (right middle ground) and the Shenandoah Mountains from a Skyline Drive overlook in Shenandoah National Park

As the nation's primary conservation agency, the Department of the Interior has responsibility for most of our nationally owned public land and natural resources. This includes fostering sound use of our land and water resources; protecting our fish, wildlife, and biological diversity; preserving the environmental and cultural values of our national parks and historical places; and providing for the enjoyment of life through outdoor recreation. The department assesses our energy and mineral resources and works to ensure that their development is in the best interests of all our people by encouraging stewardship and citizen participation in their care. The department also has a major responsibility for American Indian reservation communities and for people who live in island territories under U.S. administration.

NPS D-271, May 2003

National Park Service
U.S. Department of the Interior

Northeast Region
Natural Resource Stewardship and Science
200 Chestnut Street
Philadelphia, PA 19106-2878

The Northeast Region of the National Park Service comprises national parks and related areas in 13 New England and Mid-Atlantic states. Biological, physical, and social science research results, natural resource inventory and monitoring data, scientific literature reviews, bibliographies, and proceedings of technical workshops and conferences related to 38 of these park units in Pennsylvania, New Jersey, Maryland, Virginia, and West Virginia are disseminated through the NPS/NERCHAL Technical Report and Natural Resources Report series. The reports are a continuation of series with previous acronyms of NPS/PHSO and NPS/MAR, although they retain a consecutive numbering system. Individual parks may also disseminate information through their own report series.

The National Park Service (NPS) is responsible for preserving and protecting air quality and "air quality related values" in the National Park System by ensuring compliance with the requirements of the Clean Air Act, the National Park Service Organic Act, and other pertinent laws, regulations, and policies. This report focuses on the estimated historical, current, and projected future conditions of air quality, acidic deposition, and known air quality related values in Shenandoah National Park—visibility, streams, fish, aquatic insects, soils, and vegetation—and the human-made air pollutants that most affect them.

This technical document was peer-reviewed by internal and external scientists.

Mention of trade names or commercial products does not constitute endorsement or recommendation for use by the National Park Service or Shenandoah National Park.

A limited number of hard copies and compact disks are available from the Superintendent, Shenandoah National Park, 3655 U.S. Highway 211 East, Luray VA 22835.

Hard copies may also be obtained (a copy charge may be involved) from the NPS Technical Information Center (TIC), Denver Service Center, PO Box 25287, Denver CO 80225-0287. To order from TIC, refer to document D-271.

NPS D-271, May 2003

TABLE OF CONTENTS

LIST OF FIGURES vii

LIST OF TABLES xiii

ACRONYMS xvii

ACKNOWLEDGMENTS xxi

EXECUTIVE SUMMARY xxiii

I. INTRODUCTION I-1
- A. PURPOSE I-1
- B. BACKGROUND I-2
- C. LEGAL RESPONSIBILITIES AND MANAGEMENT POLICIES I-6
  - 1. National Park Service Organic Act I-7
  - 2. Enabling Legislation for Shenandoah National Park I-7
  - 3. Government Performance and Results Act I-8
  - 4. Clean Air Act I-10
  - 5. Clean Air Act Implementation Developments I-14
  - 6. Federal Water Pollution Control (Clean Water) Act I-17
  - 7. Wilderness Act I-19
  - 8. Other Pertinent Laws I-19
  - 9. National Park Service Management Policies I-21
- D. SCOPE I-22

II. ENVIRONMENTAL SETTING II-1
- A. BACKGROUND II-1
- B. CLIMATE II-8
- C. SCENERY II-9
- D. SURFACE WATERS II-11
- E. AQUATIC BIOTA II-12
  - 1. Fish II-12
  - 2. Invertebrates II-15
- F. GEOLOGY AND SOILS II-16
- G. VEGETATION II-28
- H. WILDLIFE II-33
- I. DISTURBANCE II-34

III. SCIENTIFIC BACKGROUND III-1
- A. PURPOSE III-1
- B. GASEOUS POLLUTANTS III-1
  - 1. Ground-level Ozone III-1
  - 2. Sulfur Dioxide III-3
  - 3. Volatile Organic Compounds and Nitrogen Oxides III-3
- C. ATMOSPHERIC DEPOSITION III-4

D. AQUATIC RESOURCES AND SENSITIVE INDICATORS . . . III-6
1. Water Chemistry . . . III-6
2. Aquatic Fauna . . . III-12
E. TERRESTRIAL INDICATORS . . . III-19
1. Plant Symptomatology . . . III-20
2. Physiological Effects . . . III-23
3. Nitrogen Saturation and Forest Decline . . . III-24
4. Soil Acidification . . . III-27
F. VISIBILITY . . . III-29
1. Visibility Degradation . . . III-29
a. Sources of Visibility Degradation . . . III-29
b. Types of Visibility Degradation . . . III-30
c. Visibility Scales/Metrics . . . III-33
2. Background on the Visibility Monitoring Program . . . III-34
a. Particle Monitoring . . . III-35
b. Optical Monitoring . . . III-36
c. View Monitoring . . . III-36

IV. EMISSIONS AND AIR POLLUTANT TRANSPORT . . . IV-1
A. PURPOSE . . . IV-1
B. RECENT AND PROJECTED FUTURE REGIONAL EMISSIONS . . . IV-1
C. PATTERNS OF AIR POLLUTANT TRANSPORT . . . IV-12
1. Source Areas . . . IV-12
2. Airsheds . . . IV-16
3. Top Five Air Pollutant Source Subregions for Shenandoah National Park . . . IV-23
4. Relative Contributions by State . . . IV-24
D. IN-PARK EMISSIONS . . . IV-28

V. AIR QUALITY AND DEPOSITION . . . V-1
A. BACKGROUND ON MONITORING EFFORTS . . . V-1
B. ESTIMATED NATURAL CONDITIONS . . . V-3
1. Ground-level Ozone . . . V-3
a. Average Observed Ground-level Ozone Concentrations at Remote Locations . . . V-4
b. Probability Distribution Methods . . . V-4
c. Correlation Methods with Ground-level Ozone Precursors . . . V-5
d. Computer Simulation Modeling . . . V-6
2. Visibility . . . V-6
3. Deposition . . . V-8
C. CURRENT CONDITIONS AND TRENDS . . . V-10
1. Air Quality . . . V-10
a. Ambient Conditions . . . V-10
b. Trends in Air Quality . . . V-17
c. Ground-level Ozone Formation . . . V-20
2. Visibility . . . V-29
a. National Conditions and Trends . . . V-29
b. Current Conditions and Trends in Shenandoah National Park . . . V-37

3. Deposition V-59
a. Ambient Deposition V-59
b. Trends in Deposition V-68
D. PROJECTED CHANGES IN FUTURE AIR QUALITY AND DEPOSITION . . V-73

VI. ENVIRONMENTAL RECEPTORS AND EFFECTS OF AIR QUALITY VI-1
A. PURPOSE VI-1
B. AQUATIC ECOSYSTEMS VI-1
1. Current Status of Streamwater Chemistry VI-1
a. Relationships between Geology and Streamwater Chemistry VI-11
b. Relationships between Soils and Streamwater Chemistry VI-18
c. Influence of Forest Defoliation on Streamwater Chemistry VI-22
d. Regional Context VI-24
2. Trends in Streamwater Chemistry VI-24
a. Methods and Data VI-25
b. Results VI-26
c. Summary of Trends in Streamwater Chemistry in Shenandoah National Park VI-38
3. Biological Effects VI-39
a. Acidification Effects on Aquatic Invertebrates in Shenandoah National Park VI-39
b. Acidification Effects on Fish in Shenandoah National Park VI-43
4. Episodic Acidification Effects VI-55
C. VEGETATION VI-64
1. Effects of Ground-level Ozone and Other Gaseous Pollutants VI-64
a. Visible Injury Caused by Ground-level Ozone VI-65
b. Effects of Sulfur and Nitrogen Oxides VI-67
2. Sensitivity of Plant Species in Shenandoah National Park VI-67
3. Acidification Effects VI-70

VII. FUTURE CONDITIONS AND PROGNOSIS FOR RECOVERY VII-1
A. PURPOSE VII-1
B. 1990 CLEAN AIR ACT AMENDMENTS AND ALTERNATIVE EMISSIONS CONTROL SCENARIOS VII-1
C. FUTURE PROJECTIONS VII-3
1. Aquatic Ecosystems VII-3
a. Background VII-3
b. Modeling Methods for Aquatic Effects VII-4
c. Aquatic Modeling Results VII-22
d. Implications for Aquatic Biota VII-43
e. Prognosis for Recovery of Aquatic Ecosystems VII-64
2. Vegetation VII-78
a. Background VII-78
b. Modeling Methods for Ground-level Ozone Effects VII-78
c. Vegetation Modeling Results VII-89
d. Prognosis for Recovery of Terrestrial Ecosystems VII-111
3. Visibility VII-113

VIII. SUMMARY OF SENSITIVE RECEPTOR IMPACTS AND CONCLUSIONS . . . VIII-1
A. AQUATIC ECOSYSTEMS VIII-1
B. TERRESTRIAL ECOSYSTEMS VIII-2
C. VISIBILITY VIII-4
D. CONCLUSIONS VIII-5

IX. REFERENCES IX-1

APPENDICES
Appendix A. Weighting Function for W126 Ground-level Ozone Exposure Index
Appendix B. Description of Metrics Used to Quantify Visibility Effects
Appendix C. Description of the Extended RADM Model
Appendix D. Characteristics of Streams Surveyed within Shenandoah National Park
Appendix E. Water Chemistry Trends Data
Appendix F. Description of the MAGIC Model and Application Methods Employed
Appendix G. Details of TREGRO Parameterization
Appendix H. Details of Regional Ground-level Ozone Interpolation
Appendix I. Equations Describing the Simulated Effect of Ground-level Ozone on Vegetative Mass
Appendix J. Projected Changes in Tree Mass in Response to Ambient Ground-level Ozone Exposure During the Period 1997 to 1999, for Species That Showed Only Minor Response

LIST OF FIGURES

I-1 Locational map for Shenandoah National Park I-3
II-1 Shenandoah National Park and division into three management districts II-2
II-2 Location of roads, trails, streams, and scenic historical overlooks within park boundaries II-3
II.3 Examples of outstanding scenery within Shenandoah National Park II-10
II-4 Lithologic and geological sensitivity maps of Shenandoah National Park II-24
II-5 Soils types in Shenandoah National Park II-29
II-6 Major forest types within Shenandoah National Park, by district II-30
III-1 Export of base cations from watershed soils III-27
III-2 Uniform haze, coherent plume, and layered haze: three ways that air pollution can visually degrade a scenic vista III-31
IV-1 New source permit reviews during the period January 1987 to June 2002 . . . . . IV-2
IV-2 Bar chart of SO_2 emissions showing surface and point emissions for the top 10 states in 1990, 1996, and each of the scenarios IV-8
IV-3 Bar chart of NO_X emissions for surface and point source emissions for the top 10 states in 1990, 1996, and each of the scenarios IV-9
IV-4 Pie chart of SO_2 emissions broken down by five source categories comparing 1990, Scenario 3, and Scenario 4 . . . . . IV-11
IV-5 Pie chart of NO_X emissions by five-source categories comparing 1990 and Scenario 4 . . . . . IV-13
IV-6 Range of influence of sulfur deposition, oxidized nitrogen deposition, reduced nitrogen deposition, and sulfate air concentrations expressed as the percent contribution from Subregion 20, a 160x160 km square centered at the joining of the state boundaries of WV, KY, and OH in the Ohio River Valley . . . IV-15
IV-7 Major airsheds for Shenandoah National Park for oxidized nitrogen deposition, sulfur deposition, sulfate air concentrations IV-18
IV-8 Geographic subdivision of the Shenandoah major airsheds IV-21
IV-9 Top 5 source regions contributing air pollution in Shenandoah National Park . . . IV-25
IV-10 First-ranked state percent contribution contour for oxidized nitrogen deposition (VA), sulfur deposition (WV), and sulfate air concentrations (OH) IV-27
IV-11 In-park Shenandoah National Park emissions relative to emissions from surrounding counties IV-30
V-1 Estimated natural background particle contributions to visibility reduction in the eastern and western United States V-9
V-2 Ozone monitoring locations in and near Shenandoah National Park V-11
V-3 Box and whisker plot showing the monthly maximum 1-hour ozone averages at Big Meadows for the period 1995 to 1997 . . . . . V-13
V-4 Three-year average of the 4th highest 8-hour ozone average concentrations V-14
V-5 Diurnal ozone patterns at Big Meadows during each of the four seasons V-15
V-6 May-September diurnal ozone patterns at Washington D.C. for the period 1995 to 1999 . . . . . V-16
V-7 Adjusted SUM06 values for Fauquier County, Frederick County, and Big Meadows monitoring sites for the period 1990 through 2000 . . . . . V-18
V-8 Adjusted W126 values for Fauquier County, Frederick County, and Big Meadows monitoring sites for the period 1990 through 2000 . . . . . V-18

V-9 Mean daily ozone production rates during the modeling period in 1995 . . . . . V-24
V-10 Domain plot of the simulated average VOC loss (L_{VOC}) due to photochemistry . . V-25
V-11 Simulated values of VPOP, the O_3 production efficiency of VOC photochemistry V-26
V-12 Sensitivity to added VOC V-28
V-13 IMPROVE Monitoring Sites V-30
V-14 Average 3-year visibility (March 1996 - February 1999) reconstructed from IMPROVE aerosol data and represented as extinction coefficient (Mm^{-1}), haziness (deciview), and standard visual range (km) V-31
V-15 Current visibility impairment expressed in deciviews for the clearest, middle, and haziest 20 percent days based on 1997-1999 IMPROVE data V-32
V-16 Trends in 75th percentile visual range over the United States from 1950 through 1994 . . . . . V-34
V-17 Summary plot of calculated light extinction and the fractional contribution of each species for the 20 monitoring regions in the IMPROVE network V-36
V-18 Class I area significant trends in haziness for the clearest 20%, middle 20%, and haziest 20% days V-37
V-19 Class I area significant trends in light extinction due to sulfate for the clearest 20%, middle 20%, and haziest 20% days V-38
V-20 Fine mass budgets for the mean of the cleanest, middle, and haziest 20% of days for Shenandoah National Park (March 1988 - February 2000) V-40
V-21 Calculated extinction coefficient budgets for Shenandoah National Park, March 1988-February 2000 . . . . . V-42
V-22 Monthly contributions of total light extinction contributed by sulfate, nitrate, organics, light absorbing carbon, and soil for Shenandoah National Park (1996 – 1998) V-43
V-23 Seasonal and annual average calculated extinction for Shenandoah National Park, March 1988 – February 2000 . . . . . V-44
V-24 Calculated aerosol light extinction in Shenandoah National Park for the cleanest 20%, middle 20%, and haziest 20% of the days in the distribution, February 1988 - March 2000 . . . . . V-46
V-25 Trends in annual averages for aerosol extinction, standard visual range, and deciview, February 1988 - March 2000 . . . . . V-47
V-26 Seasonal and annual arithmetic means for transmissometer data (filtered) at Shenandoah National Park during the period 1988 to 2000 . . . . . V-53
V-27 Seasonal and annual arithmetic means, Shenandoah National Park, nephelometer data, 1996 to 1999 . . . . . V-55
V-28 Photographs illustrating visibility conditions at Skyland in Shenandoah National Park. V-57
V-29 Photographs illustrating visibility conditions at Shenandoah National Park, Dickie Ridge vista V-58
V-30 Annual wet deposition of sulfate throughout the eastern United States during the most recent year of record V-60
V-31 Annual wet deposition of nitrate throughout the eastern United States during the most recent year of record V-61
V-32 Annual wet deposition of inorganic nitrogen throughout the eastern United States during the most recent year of record V-62
V-33 Wet sulfur deposition for the period of record at three monitoring sites in Shenandoah National Park V-69

V-34 Wet inorganic nitrogen deposition for the period of record at three monitoring sites in Shenandoah National Park V-70
V-35 Wet ammonium deposition for the period of record at three monitoring sites in Shenandoah National Park V-71
V-36 Wet nitrate deposition for the period of record at three monitoring sites in Shenandoah National Park V-72
V-37 Representation of the 80-km grid domain of the RADM model, with the nested 20-km grid that was created for this assessment V-74
VI-1 Primary study watersheds in Shenandoah National Park shown in relation to the distribution of major bedrock types VI-2
VI-2 Distribution of streamwater ANC determined in the 1992 spring survey of water chemistry within 11 watersheds in Shenandoah National Park VI-12
VI-3 Comparison of estimated natural background and current median sulfate concentrations among streams located on major bedrock types in Shenandoah National Park VI-18
VI-4 Median percent base saturation for soils associated with Shenandoah National Park's three bedrock types VI-20
VI-5 Median spring ANC of streams in SWAS watersheds during the period 1988 to 1999 versus median base saturation of watershed soils VI-21
VI-6 Effect of watershed defoliation by the gypsy moth caterpillar on nitrate flux in streamwater VI-23
VI-7 Trends in solute concentrations for the 14 SWAS streams in Shenandoah National Park VI-27
VI-8 Median values of annual and seasonal trends in streamwater ANC concentrations among VTSSS and SWAS watersheds: 1988-2001 . . . . . VI-32
VI-9 Median values of annual and seasonal trends in streamwater SO_4^{2-} concentrations among VTSSS and SWAS watersheds: 1988-2001 . . . . . VI-33
VI-10 Median values of annual and seasonal trends in streamwater SBC concentrations among VTSSS and SWAS watersheds: 1988-2001 . . . . . VI-34
VI-11 Life stages of brook trout VI-36
VI-12 Trends in streamwater SO_4^{2-} concentrations in relation to median SO_4^{2-} concentrations for VTSSS and SWAS streams VI-37
VI-13 Average number of families of aquatic insects in a sample for each of 14 streams in Shenandoah National Park versus the mean or minimum ANC of each stream VI-44
VI-14 Average total number of individuals of aquatic insects in a sample for each of 14 streams in Shenandoah National Park versus the mean or minimum ANC of each stream VI-45
VI-15 Average EPT index in a sample for each of 14 streams in Shenandoah National Park versus the mean or minimum ANC of each stream VI-46
VI-16 Number of fish species among 13 streams in Shenandoah National Park VI-50
VI-17 Length-adjusted condition factor, a measure of body size in blacknose dace (*Rhinichthys atratulus*) among 11 populations in Shenandoah National Park VI-53
VI-18 Minimum streamwater ANC sampled at each site during each year versus median spring ANC for all samples collected at that site during that spring season VI-56

VI-19 Relationship between ANC and runoff for streamwater samples collected at intensively-studied sites in Shenandoah National Park VI-60
VI-20 Decrease in ANC and pH and increase in dissolved aluminum in response to a sharp increase in stream flow in three watersheds within Shenandoah National Park during a hydrological episode in 1995 . . . . . VI-62
VI-21 Visible injury caused by ozone on milkweed and yellow poplar at Shenandoah National Park VI-66
VII-1 Calibration results for the MAGIC model, expressed as predicted versus observed values in the calibration year for sulfate, nitrate, sum of base cations, sum of mineral acid anions, calculated ANC, and pH VII-17
VII-2 Simulated versus observed soils characteristics for modeled watersheds in Shenandoah National Park, expressed as exchangeable Ca, Mg, Na, and K; base saturation; and soil pH VII-18
VII-3 Simulated versus observed ANC over a ten year period for modeling sites VII-19
VII-4 MAGIC hindcast projections for modeled sites VII-23
VII-5 MAGIC model projections of streamwater sulfate under the scenario of constant deposition at 1990 levels and the four emissions control scenarios for modeled sites VII-27
VII-6 MAGIC model projections of streamwater nitrate under the scenario of constant deposition at 1990 levels and the four emissions control scenarios for modeled sites VII-30
VII-7 MAGIC model projections of streamwater sum of base cations under the scenario of constant deposition at 1990 levels and the four emissions control scenarios for modeled sites VII-33
VII-8 MAGIC model projections of streamwater ANC under the scenario of constant deposition at 1990 levels and the four emissions control scenarios for modeled sites VII-36
VII-9 Predicted and observed number of fish species in 13 Shenandoah National Park streams for the year 2000 . . . . . VII-45
VII-10 Projected number of fish species in 14 Shenandoah National Park streams for past and present conditions VII-45
VII-11 Projected number of fish species in 14 Shenandoah National Park streams for the year 2040 in response to simulated constant deposition at 1990 levels and the four emissions control scenarios VII-48
VII-12 Predicted and observed brook trout categories in 14 Shenandoah National Park streams for 1988-1992 . . . . . VII-49
VII-13 Projected brook trout categories in 14 Shenandoah National Park streams for past and present conditions VII-50
VII-14 Projected brook trout categories in 14 Shenandoah National Park streams for the year 2040 in response to simulated constant deposition at 1990 levels and the four emissions control scenarios VII-51
VII-15 Projected condition factor for blacknose dace and observed presence/absence of blacknose dace in 13 Shenandoah National Park streams for the year 2000 . . VII-54
VII-16 Projected condition factor for blacknose dace in 14 Shenandoah National Park streams for past and present conditions VII-55

VII-17 Projected condition factor for blacknose dace in 14 Shenandoah National Park streams for the year 2040 in response to simulated constant deposition at 1990 levels and the four emissions control scenarios VII-58
VII-18 Projected suitability of streamwater pH for, and observed presence/absence of, nine fish species in 13 Shenandoah National Park streams for the year 2000 . . . . . VII-60
VII-19 Projected suitability of streamwater pH for nine fish species in 14 Shenandoah National Park streams for past and present conditions VII-61
VII-20 Projected suitability of streamwater pH for nine fish species in 14 Shenandoah National Park streams for the year 2040 in response to simulated constant deposition at 1990 levels and the four emissions control scenarios VII-62
VII-21 Relationship between the simulated sulfur deposition load and the percent of modeled streams in Shenandoah National Park that have ANC less than or equal to a critical value (0, 20, or 50 µeq/L) in three different future years (2020, 2040, 2100) VII-72
VII-22 Relationship between the simulated sulfur deposition load and the percent of modeled streams in Shenandoah National Park that have ANC less than or equal to a critical value (0, 20, or 50 µeq/L), depending on the future year examined (2020, 2040, or 2100) VII-73
VII-23 Sulfur critical load simulated by the MAGIC model to protect streams in Shenandoah National Park against acidification to ANC below 0, 20 µeq/L, and 50 µeq/L by the year 2040, as a function of 1990 ANC and geologic sensitivity class VII-75
VII-24 Ozone exposures (total for 1997-1999) used in TREGRO simulations VII-82
VII-25 Ozone exposures (5 month SUM06) for each of the three simulation years VII-82
VII-26 Percent change, compared to the lowest ozone exposure, in the mass of the total tree, shoot, stem, and root of basswood, black cherry, chestnut oak, red maple, red oak, sugar maple, white ash, and yellow poplar simulated by TREGRO. VII-90
VII-27 Simulated effects of ozone on the density of trees, total woody biomass, and basal area of the stand, and the growth of major species in the Chestnut Oak forest type as affected by ozone VII-93
VII-28 Simulated effects of ozone on the density of trees, total woody biomass, and basal area of the stand, and the growth of major species in the Cove Hardwood forest type as affected by ozone VII-96
VII-29 Simulated effects of ozone on the density of trees, total woody biomass, and basal area of the stand, and the growth of major species in the Yellow Poplar forest type as affected by ozone VII-98
VII-30 Comparison of the effects of ozone on the basal area of species simulated as individuals over three years versus as a member of a stand over 100 years . VII-100
VII-31 Interpolated ozone exposure for Shenandoah National Park in 1997 . . . . . VII-102
VII-32 Interpolated ozone exposure for Shenandoah National Park in 1998 . . . . . VII-103
VII-33 Interpolated ozone exposure for Shenandoah National Park in 1999 . . . . . VII-104
VII-34 Interpolated total ozone exposure for Shenandoah National Park, 1997-1999 . VII-105
VII-35 Projected change in stem and total mass of white ash in response to ozone exposures in 1997-1999 . . . . . VII-106

VII-36 Projected change in basal area and woody biomass in Cove Hardwood forests in response to ozone over 100 years VII-107
VII-37 Projected change in basal area and woody biomass in Chestnut Oak forests in response to ozone over 100 years VII-108
VII-38 Projected change in basal area and woody biomass in Yellow Poplar forests in response to ozone over 100 years VII-109

LIST OF TABLES

I-1 National Ambient Air Quality Standards published by the U.S. Environmental Protection Agency I-11
I-2 Prevention of significant deterioration increments I-13
II-1 Fish species recorded in Shenandoah National Park streams (as of 2002) II-13
II-2 Total number of invertebrate families of each order present in Shenandoah National Park streams II-17
II-3 Invertebrate presence in Shenandoah National Park streams II-18
II-4 Interquartile distribution of pH, cation exchange capacity, and percent base saturation for soil samples collected in Shenandoah National Park study watersheds during the 2000 soil survey II-27
III-1 Common symptoms of ozone-induced foliar injury III-21
IV-1 State-level annual emissions totals of SO_2 for the 1990 Base Case, the 1996 case, and the four scenarios IV-3
IV-2 State-level annual emissions totals of NO_X for the 1990 Base Case, the 1996 case, and the four scenarios IV-4
IV-3 Summary of annual SO_2 and NO_X emissions subdivided into Surface and Point Sources for the 1990 Base, 1996 and the four scenarios IV-8
IV-4 Summary of the percent changes in annual SO_2 and NO_X emissions from the 1990 Base Case to 1996 and the four future scenarios for the Surface and Point Source categories IV-9
IV-5 Characteristics of major airsheds that contribute air pollution to Shenandoah National Park IV-17
IV-6 1990 emissions for the states nominally covered by the Shenandoah airsheds . . . IV-20
IV-7 Contributions from geographic subdivisions of Shenandoah National Park major airsheds and efficiency for causing pollution in the park IV-22
IV-8 Percent of the pollution in Shenandoah National Park explained by accumulating geographic subdivisions of the major airsheds IV-23
IV-9 Percent of the pollution in Shenandoah National Park explained by state emissions, expressed as the individual state contributions to deposition and atmospheric concentrations IV-26
IV-10 Shenandoah National Park 1999 emissions summary IV-28
IV-11 Annual emissions totals from within Shenandoah National Park and comparison with surrounding counties IV-29
V-1 Visibility, air quality and atmospheric deposition monitoring at Shenandoah National Park V-1
V-2 Values for the 10th and 30th percentile O_3 measurements at remote inland locations compared with generally comparable data from Shenandoah National Park V-5
V-3 Estimated natural background particulate concentrations and light extinction V-7
V-4 Estimates of historical deposition in Shenandoah National Park of sulfur and oxidized nitrogen at five year intervals V-10
V-5 Three-year averages of annual 4th highest daily maximum 8-hr ozone concentrations and annual exceedances V-14
V-6 May Through September SUM06 and W126 ozone exposure values, for the period 8AM-8PM, adjusted by percent of data completeness V-17

V-7 Trends in May through September (8 AM-8 PM) ozone exposure in and around Shenandoah National Park during the period 1990-2000 . . . . . V-19
V-8 Trends in May through September daily maximum 1-hour average ozone concentration V-20
V-9 Summary of Class I area extinction trend analysis V-36
V-10 Measured fine and coarse aerosol mass concentrations for Shenandoah National Park V-39
V-11 Seasonal and annual average standard visual range and calculated extinction at Shenandoah National Park, March 1988 - February 2000 . . . . . V-43
V-12 Seasonal and annual arithmetic means, Shenandoah National Park, transmissometer data December 1988 through February 2000 . . . . . V-50
V-13 Seasonal and annual 20% cleanest visibility metric statistics, Shenandoah National Park, transmissometer data, December 1988 through February 2000 . . . V-51
V-14 Seasonal and annual 20% haziest visibility metric statistics, Shenandoah National Park, transmissometer data, December 1988 through February 2000 . . . V-52
V-15 Seasonal and annual arithmetic means, Shenandoah National Park, nephelometer data, 1996 through February 2000 . . . . . V-54
V-16 Precipitation volume and measured concentrations of major ions in precipitation at monitoring sites within Shenandoah National Park V-63
V-17 Measured wet deposition fluxes at monitoring sites within Shenandoah National Park V-65
V-18 Estimated dry deposition fluxes at Big Meadows, based on data and calculations from CASTNet V-67
V-19 Percent changes in pollutants and pollutant metrics relative to the 1990 Base Case as predicted by the Extended RADM model V-76
VI-1 Interquartile distributions of ANC, sulfate and sum of base cations for Shenandoah National Park study streams during the period 1988 to 2001 . . . . . VI-5
VI-2 Bedrock distribution in Shenandoah National Park and SWAS watersheds VI-10
VI-3 Range and distribution of streamwater concentrations within Shenandoah National Park associated with major bedrock VI-16
VI-4 Interquartile distribution of pH, cation exchange capacity, and percent base saturation for soil samples collected in Shenandoah National Park study watersheds during the 2000 soil survey VI-19
VI-5 Interquartile distributions for each bedrock class of pH, cation exchange capacity, and percent base saturation for all soil pits excavated within the 2000 soil survey VI-22
VI-6 Median trends in solute concentrations within geographically or lithologically defined classes for the 14-year period 1988-2001 (water years) VI-28
VI-7 Minimum, average and maximum ANC values in the 14 Shenandoah National Park study streams during the period 1988 to 2001 for all quarterly samples VI-42
VI-8 Critical pH thresholds for fish species of Shenandoah National Park. VI-47
VI-9 Streamwater acid neutralizing capacity categories for brook trout response VI-49
VI-10 Median streamwater ANC and watershed area of intensively-studied streams in Shenandoah National Park. VI-51
VI-11. List of plant species in Shenandoah National Park known to be sensitive to visible injury on foliage from ozone exposure levels found within the park VI-68

VI-12 Calcium and aluminum data collected for soil water samples from three watersheds in Shenandoah National Park during the period 1999-2000 . . . . . VI-75
VII-1 Annual deposition of sulfur and nitrogen projected by the Enhanced Regional Acid Deposition Model for the four scenarios VII-3
VII-2 Five-year average estimates of wet, dry, and total deposition of sulfur and nitrogen, which were used to calibrate the MAGIC model to watersheds modeled in Shenandoah National Park for streamwater chemistry VII-6
VII-3 Wet and dry deposition input data for Shenandoah National Park sites VII-9
VII-4 Assignment of historical deposition sequences at Shenandoah National Park, based on ASTRAP modeled deposition VII-10
VII-5 Percent changes in sulfur and nitrogen deposition relative to 1990 base, calculated for emissions control scenarios VII-11
VII-6 Streamwater input data for Shenandoah National Park modeling sites VII-13
VII-7 Soils input data for Shenandoah National Park modeling sites VII-14
VII-8 ANC in streams within Shenandoah National Park derived from MAGIC simulations for the past, the present, and for selected years in the future VII-39
VII-9. pH in streams within Shenandoah National Park derived from MAGIC simulations for the past, the present, and for selected years in the future VII-41
VII-10 Projected number of fish species in streams within Shenandoah National Park estimated from simulations for the past and for the future in response to simulated constant deposition at 1990 levels and the four emissions control scenarios VII-46
VII-11 Projected brook trout categories in streams within Shenandoah National Park estimated from simulations for the past and for the future in response to simulated constant deposition at 1990 levels and the four emissions control scenarios VII-52
VII-12 Projected condition factor for blacknose dace in streams within Shenandoah National Park estimated from simulations for the past in response to historical deposition and for the future in response to simulated constant deposition at 1990 levels and the four emissions control scenarios VII-56
VII-13 Estimated critical load of sulfur to achieve a variety of ANC endpoints in a variety of future years for modeled streams in Shenandoah National Park VII-69
VII-14 Median and range of estimated critical load values for sulfur deposition, by principal geologic sensitivity class within the watershed VII-70
VII-15 Estimated percent change in 1990 sulfur deposition required to produce a variety of ANC endpoints in a variety of future years for streams in Shenandoah National Park VII-71
VII-16 Regression equations for estimating critical load of sulfur deposition to protect against having ANC below a given threshold in a given endpoint year, based on 14 modeled streams in Shenandoah National Park VII-76
VII-17 Total three-year daylight (0800-2000) ozone exposure metrics calculated from hourly concentrations used for TREGRO simulations VII-80
VII-18 Twelve-month ozone exposure metrics, by year, calculated from hourly concentrations used for TREGRO simulations VII-81
VII-19 Modifiers of ZELIG processes calculated from TREGRO simulations VII-85
VII-20 Species included in three forest types simulated with ZELIG VII-86
VII-21 Degree of visibility improvement associated with emission reductions scenarios VII-114

LIST OF ACRONYMS

AERP	Aquatic Effects Research Program
Al	Aluminum
ANC	Acid neutralizing capacity
AQRV	Air quality related value
ARD	Air Resources Division
ASTRAP	Advanced Statistical Trajectory Regional Air Pollution model
BART	Best Available Retrofit Technology
BEA	Bureau of Economic Analysis
C	Carbon
Ca	Calcium
CAA	Clean Air Act
CAAA	Clean Air Act Amendments
CARB	California Air Resources Board
CASTNet	Clean Air Status and Trends Network
CEC	Cation exchange capacity
Cl	Chloride
CIRA	Cooperative Institute for Research in the Atmosphere
CO	Carbon monoxide
CPOM	Coarse particulate organic matter
DDF	Dry deposition factor
DOC	Dissolved organic carbon
DOI	U.S. Department of the Interior
DOM	Dissolved organic matter
dv	Deciview
EGU	Electric generating unit
EPA	U.S. Environmental Protection Agency
EPT	Ephemeroptera-Plecoptera-Trichoptera
FIA	Forest Inventory Analysis
FISH	Fish in Sensitive Habitats Project
FLM	Federal Land Manager
FMP	Fisheries Management Plan
FPOM	Fine particulate organic matter
GIS	Geographic Information System
GPRA	Government Performance and Results Act
GRSM	Great Smoky Mountains National Park
HAP	Hazardous Air Pollutant
HBEF	Hubbard Brook Experimental Forest
HDDV	Heavy Duty Diesel Vehicle
IFS	Integrated Forest Study
IMPROVE	Interagency Monitoring of Protected Visual Environments Program
IPM	Integrated Planning Model
LAC	Light absorbing carbon
LTEMS	Long-Term Ecological Monitoring System
L_{VOC}	Average simulated VOC loss due to photochemistry
MACA	Mammoth Cave National Park

MAGIC	Model of Acidification of Groundwater in Catchments
MAQSIP	Multiscale Air Quality Simulation Platform model
MOU	Memorandum of Understanding
MVCP	Maximum VOC capacity point, the point at which further addition of VOCs reduced ozone concentration
N	Nitrogen
NAAQS	National ambient air quality standards
NADP	National Atmospheric Deposition Program
NADP/NTN	National Atmospheric Deposition Program/National Trends Network
NAPAP	National Acid Precipitation Assessment Program
NAS	National Academy of Sciences
NEI	National Emissions Inventory
NH_3	Ammonia
NH_4	Ammonium
NO_2	Nitrogen dioxide
NO_3	Nitrate
NO_x	Nitrogen oxides
NO_y	Reactive oxides of nitrogen
NPS	National Park Service
NWS	National Weather Service
O_3	Ozone
OTC	Ozone Transport Commission
PAN	Peroxyacetylnitrate
P_{O3}	Mean daily total ozone production through photochemical reactions
PO_4	Phosphate
POM	Particulate organic matter
ppb	Parts per billion
ppbv	Parts per billion by volume
ppm	Parts per million
PSD	Prevention of significant deterioration
RADM	Regional Acid Deposition Model
RHR	Regional Haze Rule
S	Sulfur
SAMAB	Southern Appalachian Man and the Biosphere program
SAMI	Southern Appalachian Mountains Initiative
SBC	Sum of base cations
SHEN	Shenandoah National Park
SIP	State Implementation Plan
SKT	Seasonal Kendal Test
SO_2	Sulfur dioxide
SO_4	Sulfate
SO_x	Sulfur oxide
SUM06	Sum of all hourly ozone concentrations that are greater than or equal to 0.06 parts per million
SVR	Standard visual range
SWAS	Shenandoah Watershed Study
TMDL	Total maximum daily load

USDA	U.S. Department of Agriculture
USFWS	U.S. Fish and Wildlife Service
USGS	U.S. Geological Survey
VDGIF	Virginia Department of Game and Inland Fisheries
VMT	Vehicle miles traveled
VOCs	Volatile organic compounds
VPOP	Ozone production per unit of VOC consumed
VR	Visual range
VTSSS	Virginia Trout Stream Sensitivity Study
W126	Sum of all hourly ozone concentrations, where each is weighted by a function that gives greater emphasis to the higher concentrations

Acknowledgments

We wish to thank the National Park Service (NPS) staff who assisted in many aspects of this effort. John Karish and Dee Morse assisted with agreement and contract management. Dan Hurlbert coordinated GIS data for Shenandoah National Park and assisted in the mapping activities. Shane Spitzer prepared the tabular summary of the park's past and present ambient air quality, visibility, and deposition monitoring, and assisted with Shenandoah-relevant publications distribution and tracking. Tonnie Maniero and Bruce Nash provided information regarding the sensitivity of plants in the park to ozone foliar effects. Bill Malm calculated future visibility conditions. Gary Rosenlieb provided the Clean Water Act summary. Wendy Cass provided information on wildfires; rare plant communities (notably red spruce and boreal species); and white ash species composition in chestnut oak, cove hardwood, and yellow poplar forests. Alan Williams assisted with natural resource data base queries and data summaries. Jim Atkinson updated the wildlife and fish sections. In-park emissions data were compiled by Aaron Worstell.

Bryan Bloomer assisted with development of emissions control scenarios for model projections of future change. Kai Snyder, Erin Gilbert, Deian Moore, and Jayne Charles assisted with data analyses, graphics, and map construction. Word processing and document production were provided by Jayne Charles and Deian Moore.

Constructive comments and criticisms were provided on an earlier draft of this report by a group of external and NPS peer and administrative reviewers, including: James Akerson, Jim Atkinson, Steve Bair, Michael Barna, Tamara Blett, John Bunyak, Robbins Church, Reed Engle, Keith Eshleman, Alan Herlihy, Dan Hurlbert, Roy Irwin, Tonnie Maniero, Gordon Olson, Marc Pitchford, Gary Rosenlieb, Holly Salazer, William Sharpe, Shane Spitzer, George Taylor, Kathy Tonnessen, Helga Van Miegroet, John Vimont, and David Weinstein.

EXECUTIVE SUMMARY

Introduction

Shenandoah National Park overlies the crest of the northern Blue Ridge Mountains of Virginia. The park has one of the most comprehensive air quality monitoring and research programs of all national parks and wilderness areas that are afforded special protection under the Clean Air Act. Under the Clean Air Act (as amended), the Assistant Secretary for Fish, Wildlife and Parks (acting through the park Superintendent) has an "affirmative responsibility" to protect air quality related values from the adverse effects of human-made air pollution.

The park's air-related science program has emphasized particulate matter, gaseous pollutants, acidic deposition, visibility, and the acid-base status of streams. Over 20 years of monitoring and research show that, despite some recent improvements, the park's sensitive scenic and aquatic resources remain degraded by human-made air pollution. Furthermore, the park's air quality does not currently meet the 8-hour ground-level ozone standard set by the U.S. Environmental Protection Agency to protect public health and welfare.

In the late 1990s, park managers determined the need for a comprehensive, state-of-the-science assessment of the park's air quality and related values in support of air-related regional, state, and park planning, policy-making, permit review, and scientific and outreach activities. This report provides that assessment as well as key resource information. The National Park Service assembled a team of scientists to evaluate the estimated historic, current, and projected future status of air quality and air pollution effects on sensitive resources in the park. This assessment addresses the park's known air quality related values, including visibility, vegetation, soils, streamwater chemistry, fish, and aquatic insects, as well as the human-made air pollutants that most affect them. This report also summarizes pertinent national and park-specific laws and policies, and describes the park's current and estimated historic air quality and resource conditions. It synthesizes knowledge on the visibility and ecological effects of atmospheric pollutants, and documents park-specific critical load ranges for the effects of sulfur deposition on surface waters and ground-level ozone on tree growth, forest growth, and species composition. It also projects future air quality, acidic deposition, and resource conditions and recovery, assuming implementation of four emissions control scenarios.

The atmospheric and deposition modeling described herein was conducted using the Extended Regional Acid Deposition Model to: (1) determine principal emissions source

subregions, known as airsheds, responsible for the majority of acidic deposition and sulfate haze affecting the park; (2) apportion the relative contribution of the airshed emissions, as a function of distance from the park, to the acidic deposition and sulfate air concentrations in the park; (3) define the top-ranked source subregions within the airsheds responsible for the largest fraction of acidic deposition and sulfate air concentrations affecting the park; (4) illustrate the relative contributions of 13 eastern states to acidic deposition and sulfate haze in the park; and (5) project future air quality and acidic deposition in response to the emissions control scenarios considered. Park and regional monitoring data were used to characterize recent and current conditions and to evaluate model performance. Four emissions control scenarios were considered. Scenarios 1 and 2 were based on emissions regulations required by the 1990 Clean Air Act Amendments and projected to 2010 and 2020, respectively. Scenario 3 was based on more stringent controls on sulfur dioxide and nitrogen oxides emissions from electric utilities sources than were mandated by the 1990 Clean Air Act Amendments. Scenario 4 was based on the same emissions controls on electric utilities sources as required by Scenario 3, plus more stringent controls on emissions from industrial point sources and mobile sources than required by the 1990 Clean Air Act Amendments.

Dose-response calculations and simulation modeling were used to estimate potential future changes in the extent of damage to visibility, aquatic, and forest resources in Shenandoah National Park in response to Scenarios 1 through 4. The Model of Acidification of Groundwater in Catchments was used to simulate aquatic ecosystem effects and determine ranges of critical sulfur deposition loadings. The TREGRO model was used to simulate the isolated effects of ground-level ozone on tree growth. The ZELIG gap succession model was used to simulate the isolated effects of ozone on forest stand composition and growth. Future visibility conditions were projected for each of the emissions control scenarios on the basis of expected reductions in fine sulfate particle concentrations in the atmosphere and the known contribution of each particle type to light extinction. These analyses augmented a broader literature review pertinent to the effects of human-made air pollutants on visibility and aquatic and terrestrial ecosystems.

Overall, this assessment found that implementation of emissions controls, especially Scenarios 3 and 4, would be expected to make progress toward, but not fully restore, the park's estimated natural visibility conditions and acid-base chemistry of the most sensitive aquatic ecosystems. Full implementation of the 1990 Clean Air Act Amendments (Scenario 2) should also make substantial progress toward protecting park forests from the isolated effects of ground-

level ozone. In addition, thirteen eastern states and several source subregions were identified that can contribute the most toward restoring and protecting air quality and related values in Shenandoah National Park. The following is a summary of key assessment findings by major topic.

Detailed Summary of Assessment Findings

Emissions and Air Pollutant Transport

- Major emissions source subregions impacting the park are found in the Ohio River Valley, northeastern West Virginia, southwestern Pennsylvania, and central and eastern Virginia.

- In descending order of importance, Ohio, Virginia, West Virginia, Pennsylvania, and Kentucky comprise the top five of thirteen key states causing sulfate air concentration and haze impacts at the park. West Virginia, Ohio, Virginia, Pennsylvania, and Kentucky comprise the top five states causing sulfur deposition impacts at the park. Virginia, West Virginia, Ohio, Pennsylvania, and North Carolina comprise the top five states causing oxidized nitrogen deposition impacts at the park.

- Emission sources within about 200 kilometers (125 miles) cause greater visibility and acidic deposition impacts at the park**,** *on a per ton basis*, than more distant sources.

- Because of the non-linear production of sulfur pollutants during transport, changes in sulfur dioxide emissions do not translate into proportionate changes in sulfate air concentrations or sulfur deposition. These non-linearity effects are more pronounced for haze than deposition, especially at higher sulfate air concentrations.

- For five air pollutants (sulfur dioxide, nitrogen oxides, volatile organic compounds, carbon monoxide, coarse particulate matter), in-park emissions comprise less than 1% of total human-made emissions from the eight counties encompassing the park.

Ambient Air Quality and Acidic Deposition

The park has among the highest monitored concentrations of airborne sulfate particles, acidic deposition, and ground-level ozone of all national parks.

Ground-level Ozone

- Many experts consider 25 parts per million-hour (ppm-hr SUM06) to be an important ozone exposure threshold above which vegetation begins to show effects. The mean and maximum ozone exposures at Big Meadows were 47 ppm-hr and 87 ppm-hr, respectively, during the period 1990-2000.

- The park's air quality from 1997 through 2001 did not meet the 8-hour ground-level ozone standard set in 1997 by the U.S. Environmental Protection Agency to protect public health and welfare.

Acidic Deposition

- Estimated total (wet + dry) annual deposition values at Big Meadows are currently about 13 kg/ha/yr for sulfur and 8 kg/ha/yr for nitrogen.

- The park does not routinely monitor cloud and fog deposition, but limited in-park research suggests its contribution toward the total deposition budget is relatively small compared to higher elevation sites such as Whitetop Mountain, Virginia.

- Concentrations of sulfur in wet deposition have shown a decreasing trend over the past 15 to 20 years at Big Meadows, North Fork Dry Run and White Oak Run.

- Concentrations of nitrogen in wet deposition have shown evidence of some decline over the past 15 to 20 years at North Fork Dry Run and White Oak Run, but not at Big Meadows.

Visibility Status and Trends

Visibility has been degraded in the park, potentially detracting from visitor enjoyment of numerous vistas accessible from Skyline Drive (a Virginia State Scenic Highway), the Appalachian National Scenic Trail, and other trails and points in the park.

- Current annual average visual range is about 20% of the park's estimated natural visual range of approximately 185 kilometers (115 miles).

- Current annual average haziness is about three times greater than the park's estimated natural haziness of about 7.5 deciviews.

- Seasonal variability in visibility is driven primarily by changes in the atmospheric concentration of ammonium sulfate, and poorest visibility occurs in summer.

- Even the park's clearest 20% of days, which occur mainly in winter, are degraded by human-made particulate matter. The fine mass budget on these clearest days includes about 51% sulfates and 12% nitrates.

- Although the clearest 20% of days showed no consistent trend for March 1988 through February 2000, the haziest 20% showed a moderately improving trend.

Terrestrial Ecosystem Status and Trends

Ground-level Ozone

Ground-level ozone is considered to be a long-term, potentially debilitating stress to the park's ozone-sensitive vegetation that can interact with other, potentially exacerbating stresses such as drought, insects, and diseases. This assessment focuses on the isolated effects of ozone on trees and forests. Ground-level ozone also causes visible foliar damage to several plant species in the park, including but not limited to milkweed, black cherry, yellow poplar, and white ash. However, little is known about the relationship between visible foliar injury and the growth or vitality of sensitive plant species.

- Responses of eight tree species to the isolated effects of ground-level ozone exposures were simulated, and ranked in order from most to least sensitive to growth and species composition impacts:

  White ash>Basswood=Chestnut oak>Red maple>Yellow poplar>Black cherry=Red oak>Sugar maple.

- Simulations suggested that white ash is more sensitive to growth and species composition impacts than other species, both as an individual and as a component of a forest stand. Ambient ground-level ozone exposure caused an estimated 1% decrease in total growth of white ash, a long-lived species, over the three year simulation period.

Acidic Deposition

Sulfur retention in watershed soils reduces the potential for the acidification of surface waters because it decreases the mobility of sulfate. However, as the finite adsorption capacity of soils is exhausted, sulfate concentration can increase in soil waters and surface waters, potentially contributing to greater acidification. Based on published out-of-park research, it is unlikely that deciduous forest vegetation in the park has experienced sufficiently high deposition of sulfur or nitrogen to cause adverse acidification impacts, although high elevation and isolated coniferous forest areas may be more sensitive.

- The park's recently observed total (wet + dry) nitrogen deposition rates of close to 8 kilograms/hectare/year (kg/ha/yr) are approaching the 10 kg/ha/yr levels observed elsewhere to often be associated with nitrate leaching (an indicator of nitrogen saturation).

- Data from the 2000 soil survey of 14 park watersheds indicated that median base saturation (a reflection of soil acid-base status) was less than 10% for mineral soils associated with siliciclastic bedrock and less than about 14% for mineral soils associated with granitic bedrock in the park. This measure of watershed soil acid-base status is related to the stream's acid neutralizing capacity (ANC). All park watersheds that were characterized by soil base saturation less than about 14% had average streamwater ANC less than 100 microequivalents per liter (μeq/L). Watersheds that had higher soil base

saturation were dominated by the basaltic bedrock type and had average streamwater ANC greater than 100 μeq/L.

Aquatic Ecosystem Status and Trends

The acid-base status of the park's streamwater chemistry is closely related to the characteristics of bedrock geology and soils. The park has three major geologic types underlain by siliciclastic (quartzite and sandstone), granitic, and basaltic bedrock. Each of these bedrock types underlies about one-third of the park area. Siliciclastic sites have the greatest sensitivity to acidification, while granitic sites have moderate sensitivity and basaltic sites have low sensitivity. Sulfur is the primary determinant of precipitation acidity and sulfate is the dominant acid anion associated with acidic streams, both in the central Appalachian Mountains region and within the park. Sulfur deposition has acidified park streams and affected in-stream biota, particularly in watersheds dominated by siliciclastic bedrock types that give rise to soils with low base saturation and relatively low sulfur adsorption, and to streams with low ANC. In the absence of severe disturbance such as forest defoliation by the gypsy moth, nitrogen is generally tightly cycled within park watersheds and does not contribute significantly toward streamwater acidification.

- Of the 14 park streams modeled for this assessment, none had simulated pre-industrial streamwater ANC less than 50 μeq/L, suggesting that these streams may have supported a greater variety of aquatic fauna.

- Almost half of the siliciclastic streams in a 1992 in-park survey of small subwatersheds were chronically acidic (ANC < 0 μeq/L) in which lethal effects on brook trout are probable. The balance of siliciclastic streams had ANC in the episodically acidic range (having chronic ANC between 0 and 20 μeq/L) in which sub-lethal or lethal effects are possible. Many of the streams associated with granitic bedrock in this survey were in the indeterminate ANC range (20-50 μeq/L) for brook trout. In contrast, the streams associated with basaltic bedrock had relatively high ANC values that were well within the suitable range for brook trout. These thresholds were developed for brook trout, which is considered the most acid tolerant fish species in the park. Species which are more acid-sensitive, such as blacknose dace and some mayfly species, likely have higher suitable ANC ranges than brook trout. Generally, ANC values greater than 20 to 50 μeq/L should support greater diversity and larger populations of aquatic fauna.

- Episodic acidification of park streams can be attributed to acidic deposition and natural processes, and it is superimposed on baseflow chemistry that is more acidic than pre-industrial conditions. Episodic ANC values are generally about 20% lower than baseflow values.

- Acidic episodes in low ANC park streams killed young brook trout and adult blacknose dace in field bioassays.

- Modeling results suggested that park streams that occur on siliciclastic bedrock have generally lost one or two species, and some streams may have lost up to four species, of fish in response to acidic deposition.

- Low ANC park streams generally have lower fish species richness, lower population density, poorer blacknose dace condition, fewer age classes, smaller sizes, and lower field bioassay survival than higher ANC streams.

- Higher ANC streams generally have greater numbers of families and numbers of individuals in each of three important benthic insect orders: mayflies (Ephemeroptera), stoneflies (Plecoptera), and caddisflies (Trichoptera) than low-ANC streams.

- Park streamwater chemistry is showing signs of ANC recovery in response to decreased sulfur deposition, whereas streamwater chemistry within the larger western Virginia region is not. Recent changes in both streamwater sulfate concentrations and ANC are generally smaller than in the northeastern United States, are confounded by seasonal differences, and in many cases are not statistically significant.

- Most park streams do not show evidence of ANC recovery in the winter season when the brook trout is present in its early, more acid-sensitive life stages.

Future Conditions and Prognosis for Recovery

Visibility

- Future improvements in annual average visibility projected to result from the emissions control scenarios ranged from 13% to 38% for Scenarios 2 through 4.

- For the summer season, the degree of needed visibility improvement to restore estimated natural background conditions at the park is nearly 85%. Implementation of the most stringent emissions control scenario (4) was forecasted to achieve a 52.4% improvement in average summer-time visibility at the park.

Terrestrial Ecosystems

- 1997 through 1999 ambient ground-level ozone exposures were projected to cause a 50% decrease in white ash species composition in chestnut oak forests projected over the 100-year simulation period.

- Ground-level ozone exposures greater than ambient levels were projected to cause less than 10% decrease in white ash and yellow poplar species composition in cove hardwood forests over 100 years.

- Ground-level ozone exposure scenarios were projected to cause 0 to 3% decrease in growth or species in yellow poplar forests composition over 100 years.

- Model results suggested that the isolated effects of ground-level ozone on growth and composition of park forests should diminish under Scenarios 2 through 4.

- Foliar injury on sensitive vegetation that occurs at lower ground-level ozone exposures (i.e., 10-15 ppm-hr SUM06) should diminish as a forest stress factor under Scenarios 2 through 4. Foliar injury is projected to be rare under Scenario 4, which assumes more than 50% reduction in ozone exposure.

- Modeling results suggested that ground-level ozone exposures about 15% less than 1997 through 1999 ambient levels should protect against isolated changes in white ash growth and species composition in the park's forests.

Aquatic Ecosystems

Model projections of future streamwater ANC in streams on siliciclastic bedrock ranged from simulated changes less than 10 to greater than 40 µeq/L for scenarios 1 through 4.

- In response to substantial reductions in sulfur deposition (Scenario 4), model projections for the year 2100 suggested that park streams on siliciclastic bedrock would likely experience increases of one to two species of fish, improved suitability for brook trout, and improved condition of blacknose dace. However, none of these streams are projected to fully recover the estimated number of fish species lost in the past in response to acidic deposition.

- Levels of continuous future sulfur deposition that were simulated to cause streamwater ANC to change to three specified critical levels (0, 20 and 50 µeq/l) ranged from less than zero (not attainable) to several hundred kg/ha/yr, depending on the site, ANC endpoint, and evaluation year. The specified critical levels correspond to general aquatic fauna response categories.

- Modeled streams on siliciclastic bedrock showed critical sulfur deposition loads ranging from 9 to 15 kg/ha/yr in order to protect against chronic acidity (ANC less than 0) in the year 2100. Lethal effects on brook trout are probable at ANC less than 0.

- Modeled streams on siliciclastic bedrock showed critical sulfur deposition loads ranging from 6 to 11 kg/ha/yr in order to protect against acidification to ANC of 20 µeq/L in the year 2100. Sub-lethal or lethal episodic effects on brook trout are possible at ANC 0 to 20 µeq/L.

- Modeled streams on siliciclastic bedrock showed critical sulfur deposition loads ranging from less than 0 (not attainable in one modeled stream) to 6 kg/ha/yr to protect against acidification to ANC of 50 in the year 2100. Streams having ANC above 50 µeq/L generally support greater diversity and populations of aquatic fauna than do lower ANC streams.

Conclusions

This assessment reveals that the park's visibility and most sensitive aquatic ecosystems have been degraded by human-made air pollution, although there is some evidence of recent improvement, presumably as a result of Clean Air Act implementation**.** Full recovery of the park's estimated natural visibility conditions and acid-base chemistry of the most sensitive streams would not occur under any of the four emissions control scenarios, although varying degrees of progress would be made. Implementation of the 1990 Clean Air Act Amendments (Scenario 2) should make substantial progress toward or possibly achieve protecting park forests from the isolated effects of ground-level ozone on tree growth, forest growth, and changes in forest species composition. However, model simulations of isolated effects may underestimate ground-level ozone forest effects, since ozone does not act alone. The park's air quality and related values are primarily influenced by emission sources in Great Lakes States, Mid-Atlantic States, Southeastern States, and several key source subregions that transcend state boundaries. These states and subregions can contribute the most through collaborative, intra- and inter-regional efforts toward restoring and protecting clean air, clear views, and healthy aquatic and terrestrial ecosystems in Shenandoah National Park.

VIII. SUMMARY OF SENSITIVE RECEPTOR IMPACTS AND CONCLUSIONS

As discussed in previous sections, it is clear that impacts to aquatic, terrestrial, and visual resources have occurred at Shenandoah National Park (SHEN) in response to human-made air pollution. We have varying confidence, however, in our understanding of the extent and magnitude of such effects within the park. Where selected resource components have been damaged (e.g., acidification of streamwaters, loss of sensitive aquatic biota, decreased calcium (Ca) to aluminum (Al) ratio in soil solution, ground level (tropospheric) ozone (O_3) damage to foliage, ozone-mediated reduced tree growth, or occurrence of tree species), the range of response for a given type of receptor has been attributable to spatial and temporal variation in the sensitivity of the resources to adverse impacts more than to spatial variation in the severity of air pollution across the park. For example, it is primarily the streams that occur on siliciclastic bedrock that have been acidified and that have experienced loss of fish populations. Similarly, some plant species are more sensitive than others to damage at O_3 concentrations that currently occur in the park. In contrast, adverse impacts on visibility occur parkwide. However, the severity of the impact on visibility varies with season, as does the extent to which visibility degradation is associated with pollutants of anthropogenic origin.

A. AQUATIC ECOSYSTEMS

Although baseline, pre-industrial resource conditions are not well known, we have a general understanding of the likely range of conditions that would occur in the absence of air pollution impacts. For example, it is clear that none of the streams within SHEN were acidic in pre-industrial times and the number of streams having ANC $\leq$ 20 μeq/L was much lower than it is currently. MAGIC model estimates suggested that streams that currently exhibit streamwater ANC $\leq$ 20 μeq/L experienced, on average, a decrease in ANC of 73 μeq/L since pre-industrial times. Of the 14 streams modeled for this assessment, none had simulated pre-industrial streamwater ANC $\leq$ 50 μeq/L, compared with 5 that currently have ANC $\leq$ 26 μeq/L. Most streams that occur on siliciclastic bedrock now exhibit episodic decreases in streamwater ANC to values near or below zero during hydrological events. Model estimates suggest that the chronic ANC of streams was not sufficiently low for this to have been the case in pre-industrial times. In the most acid-sensitive streams, such episodic ANC depressions are accompanied by

pulses of increased acidity (decreased pH) and inorganic Al, which are toxic to many species of aquatic biota. Although episodic acidification is partly a natural process, it is also partly driven by sulfur (S) of atmospheric origin at SHEN, and it is superimposed on baseflow chemistry that is substantially more acidic than it was previously. This chronic and episodic loss of ANC has been accompanied by a loss of some fish species and other species of aquatic biota. Many streams have likely lost the more acid-sensitive species of fish and invertebrates. Species richness has declined, as has the condition of the acid-sensitive blacknose dace (*Rhinichthys atratulus*). In some streams, these impacts have been sufficiently large as to eliminate or reduce the population of brook trout (*Salvelinus fontinalis*), a rather acid-tolerant species.

B. TERRESTRIAL ECOSYSTEMS

Tropospheric ozone has caused foliar damage to sensitive plant species within SHEN, including but not limited to milkweed (*Asclepias* spp.), black cherry (*Prunus serotina* Ehrh.), and yellow poplar (*Liriodendron tulipifera* L.). Little is known, however, about the relationship between visible foliar injury and the growth or vitality of the plants. Thus, it is not possible to judge fully what the implications of such visible damages might be. It is also suspected, but has not been demonstrated in the park, that O_3 may result in premature foliar color change and casting. The chronology of foliar color change is important at SHEN because many visitors come to the park in order to enjoy the autumn change of season.

Model simulations were conducted using the TREGRO and ZELIG models to project vegetation (individual tree and stand, respectively) growth in response to a range of future O_3 exposures in SHEN. The O_3 forest effects modeling analysis is an attempt to isolate the effects of O_3 from those of other stresses. Other stresses do occur, potentially exacerbating the relatively small, with the exception of white ash, direct growth effects of O_3 at current concentrations. Results suggested that reductions greater than about 1% in the growth of forest trees are not occurring under ambient O_3 exposure conditions. Among the tree species simulated, white ash (*Fraxinus americana*) was most sensitive, both as an individual tree, and as a component of a forest stand. TREGRO estimated about a 1% decrease in total growth of white ash over the three year 1997 to 1999 simulation period, due to ambient O_3 exposure throughout the park. Long-term (100-year) simulations with ZELIG suggested impacts less than about 1% on simulated basal area per hectare for all tree species simulated, except white ash. For other

species, simulated changes in basal area over time were influenced by other aspects of stand dynamics to a far greater extent than by O_3 exposure. For white ash, however, the basal area per ha within the chestnut oak forest type was projected to decline after 100 years from 1.2 m^2/ha during the calibration period to about 1.1 m^2/ha under the lowest simulated O_3 exposure and 0.6 m^2/ha under continued ambient exposure. This is nearly a factor of two reduction in projected white ash basal area attributable to continued O_3 exposure at ambient levels.

Among the forest types simulated with ZELIG, however, there was little difference after 100 years in simulated results for overall stand basal area, density, or biomass in response to continued O_3 exposure at ambient levels as opposed to reduced O_3 exposures (to 20% of ambient five-month SUM06 exposure). Although white ash was simulated to experience reduced growth, its impact did not affect the simulated growth and development of any of the overall stands. This was because other species were projected to compensate for the projected adverse impacts on white ash. Nevertheless, protecting sensitive species, such as white ash, is an important NPS concern.

Forest soils within SHEN have probably acidified to some degree in response to acidic deposition. MAGIC model calibrations for 14 watersheds in SHEN suggested that the median decline in base saturation since pre-industrial times was 1.3%. For watersheds containing streams having ANC $\leq$ 20 μeq/L, the median simulated historical loss of base saturation was 1.2%. Compared with the median simulated pre-industrial value for base saturation (19%) for the watersheds that currently have ANC $\leq$ 20 μeq/L, this is not a large simulated change. Additional empirical data regarding soil acidification are needed, at least for the siliciclastic watersheds sampled as part of this effort, in order to more accurately evaluate the extent of soil acidification in the park.

It is not clear whether these estimates of past and/or future soil acidification have been, or will be, associated with adverse impacts on forest growth or health in SHEN. The park has no research to indicate that soil acidification has caused nutrient deficiencies in the forest to date or that the concentrations of inorganic Al in soil solution have increased to high enough levels to elicit toxicity responses. Soil solution empirical data in the park are limited, but do not suggest Ca:Al molar ratios near 1 (Table VI-12), the generally accepted threshold for protection of forest growth and health (c.f., Cronan and Griegal 1995). However, Nutrient Cycling Model (NuCM) simulations for White Oak Run suggested that the Ca:Al molar ratio in soil solution might

decrease in the future (by 2040) to levels below 1, even under substantially reduced S deposition (Sullivan et al. 2002b). Adverse forest health responses cannot be ruled out now or in the future, especially if acidic deposition levels remain high.

C. VISIBILITY

The current visibility conditions at SHEN are severely degraded as compared with estimates for natural conditions in the park of about 184 km (115 mi). The annual average calculated light extinction at SHEN (107.0 Mm^{-1}) is approximately five times greater than the estimated annual average for natural conditions in the East (22.2 Mm^{-1}). As shown in Section V, the average visual range on the clearest days (Figure V-20) is presently only about 90 km, or about 30% of what it could be in the absence of anthropogenic air pollution (270 km). Similarly, current average conditions of the middle 20% of days and the average haziest conditions are, respectively, 25% and 14% of what they could be in the absence of air pollution. Visibility degradation is greatest in the summer months when park visitation is high, with visual ranges averaging 20 km (Table V-11). Whereas winter visibility conditions are generally best, winter visual range seldom exceeds 70 km. Average visual range in the autumn, another high visitation period, seldom exceeds 45 km.

Seasonal average calculated light extinction ranges from 61.0 Mm^{-1} during winter to 193.5 Mm^{-1} during summer. Seasonal variability in visibility is driven primarily by ammonium sulfate ($[NH_4]_2SO_4$) extinction. Organics, fine soil, and coarse mass extinction contribute to seasonal variability to a lesser degree, but extinction due to light absorbing carbon and nitrate is similar among seasons at the park.

Calculated extinction for the clearest 20% of the days for March 1988 through February 2000 showed no consistent trend, with values ranging between about 38 Mm^{-1} and 50 Mm^{-1}. The clearest 20% days are substantially degraded by $[NH_4]_2SO_4$ (51% of fine mass budget) and ammonium nitrate (NH_4NO_3; 12% of fine mass budget; Figure V-20). The haziest 20% of the days for the same period showed a moderate improving (downward) trend, with values ranging between 163 Mm^{-1} and 251 Mm^{-1}. The fine mass budget on these haziest days is comprised largely of $[NH_4]_2SO_4$ (72%), with only 2% being NH_4NO_3 (Figure V-20).

D. CONCLUSIONS

To date, and as this assessment illustrates, it appears that the following adverse effects have occurred to the following sensitive receptors:

- aquatic chemistry - chronic and episodic acidification of streamwaters, most importantly those occurring in watersheds underlain by siliciclastic, and to a lesser degree, granitic bedrock
- aquatic biota - loss of sensitive species, changes in condition of sensitive species, reduction in species richness of fish and benthic insects
- forest health - O_3 damage to foliage, reduced growth and occurrence of white ash
- visibility - significant degradation of visual range and scenic quality relative to estimated natural conditions

In addition, it is possible, but has not been demonstrated, that soils have acidified in response to acidic deposition.

Additional and innovative measures will have to be implemented over time if continued progress is to be made toward the National Visibility Goal to reach natural conditions in Class I areas by 2064. Eastern states are required to submit State Implementation Plans to the U.S. EPA in 2008 that calculate the rate of progress needed to achieve the goal for each Class I area (using 2000-2004 ambient conditions as the baseline) and present the measures that will be adopted to make "reasonable progress" toward that goal through 2018. States must periodically assess (every 5 years) their rate of progress and, every 10 years, revise their plans in order to maintain reasonable progress toward the National Visibility Goal (see the discussion of the Regional Haze Regulation in Section I.B).

Similarly, it will be necessary for S deposition to be reduced substantially below current levels in order to prevent further acidification and associated biological impacts in acid-sensitive streams within SHEN. Emissions reductions required by the Clean Air Act Amendments will be sufficient to prevent further deterioration of some, but not all, acid-sensitive streams in the park (Table VII-8). Model analyses for this assessment suggested that recovery of all streams in the park to ANC levels above 20 µeq/L would occur within about 100 years if S deposition was reduced below about 5 kg S/ha/yr, which is less than 40% of the current deposition amount. It was projected that recovery of siliciclastic streams to ANC levels above 50 µeq/L by 2100 would require S deposition ranging from 1 kg/ha/yr (Meadow Run) to 6 kg/ha/yr (Paine Run) for all

siliciclastic sites except White Oak Run. For White Oak Run, it was projected that ANC = 50 μeq/L would not be attained by 2100 even if S deposition was reduced to 0.

VII. FUTURE CONDITIONS AND PROGNOSIS FOR RECOVERY

A. PURPOSE

The purpose of this section is to evaluate potential future air pollution impacts on sensitive receptors in Shenandoah National Park (SHEN) in response to various scenarios of emissions reductions. Simulation modeling was used to evaluate possible future changes in the extent of damage to aquatic, forest, and visibility resources in SHEN in response to changing levels of acidic deposition, ground-level (tropospheric) ozone (O_3) exposure, and ambient air quality, respectively. Alternative emissions scenarios were specified for aquatics and visibility projections on the basis of existing and substantially more stringent regulations, available emissions control technologies, and using the Regional Acid Deposition Model (RADM) to estimate future sulfate (SO_4^{2-}) air concentrations and deposition values at SHEN, as described in Section IV. Ozone exposure scenarios were based on measured 5-month SUM06 exposures for the period 1997 to 1999, and a suite of future exposure scenarios, ranging from about an 80% decrease to about a three-fold increase in the ambient 5-month SUM06 O_3 exposure. The effects modeling was conducted using the Model of Acidification of Groundwater in Catchments (MAGIC) for aquatic effects, the TREGRO model for growth of individual tree species, and the ZELIG gap succession model for forest stand composition and growth. Future visibility conditions were calculated for each of the emission scenarios based on expected reductions in fine SO_4^{2-} particle concentrations in the atmosphere, generated from RADM, and the known contribution of each particle type to light extinction.

The prognosis for future recovery of damaged resources in SHEN was also evaluated. In particular, this effort included a critical loads analysis of the effects of sulfur (S) deposition on aquatic resources, based on several chemical endpoint criteria and evaluation years.

B. 1990 CLEAN AIR ACT AMENDMENTS AND ALTERNATIVE EMISSIONS CONTROL SCENARIOS

Scenarios of future emissions were developed for this report following U.S. Environmental Protection Agency (EPA) methods regarding preparation of emissions inventory input into air quality modeling for policy analysis and rule making purposes (see, for example, Appendix A of U.S. EPA 1999). A base emissions inventory was created representing the future with economic assumptions obtained from the Bureau of Economic Analysis and emissions controls representative of the laws, rules, and regulations already on the books and final as of the date of

preparation of the inventory. These various control constraints include Federal, state and local requirements for emissions control for a wide variety of environmental and human health goals.

This report relies upon EPA projected emissions developed for the Heavy-Duty Engine and Vehicle Standards and Highway Diesel Fuel Rulemaking for the 1996, 2010 and 2020 base emissions for all sources other than electricity generation. Electricity generation emissions were modeled using the Integrated Planning Model (IPM) to develop the base emissions estimates for electricity generation for 2020. Additional control constraints were applied to the generation system nationwide to reflect the various levels of additional control considered. In addition, a control scenario was developed by E.H. Pechan and Associates under EPA contract for stationary point sources, representing the limit of current commercially available control technology. Finally, a set of mobile source emissions estimates were developed by Dyntel Corp., under contract to the EPA, reflecting the limit of technology for highway automobiles and light duty trucks based upon a California Air Resources Board (CARB) analysis of this sector (CARB 2001).

The 1990 base case and future emissions estimates were thus developed for this assessment based on existing regulations and future economic assumptions. Four emissions scenarios, described in more detail in Section IV.B, were implemented:

Scenario 1. Base with NO_x State Implementation Plan (SIP) Call - Assumes reasonable economic growth and emissions limitations according to existing regulations as of summer, 2000. Projections are provided to 2010.

Scenario 2. Base Projected to 2020 - Same assumptions as Scenario 1, but projected to 2020 to allow for continued implementation of Tier II Vehicle Standards and full implementation of Title IV and Heavy Duty Diesel Vehicle standards.

Scenario 3. Additional Stringent Utility Controls - Adds to Scenario 2 additional Electric Generating Unit (EGU) controls.

Scenario 4. Additional Stringent Controls on Utility, Industry-Point, and Mobile Sources - Adds to Scenario 3 additional, non-EGU emissions reductions.

The annual deposition of S and nitrogen (N) projected at SHEN under each of the scenarios is provided in Table VII-1. The deposition of S and, to a lesser extent, N is projected to decline substantially from the 1990 base under all scenarios, as are the O_3 exposures and fine particle air concentrations (Table V-19).

Table VII-1. Annual deposition of sulfur and nitrogen projected by the Enhanced Regional Acid Deposition Model for the four scenarios.

Constituent	1990 Base	Scenario 1	Scenario 2	Scenario 3	Scenario 4
Total Sulfur[a] (kg-S/ha/yr)	12.96	8.66	8.20	4.06	3.25
Total Nitrogen[b] (kg-N/ha/yr)	7.63	5.70	4.88	4.40	3.98

[a] Total sulfur deposition includes wet deposition of SO_4^{2-} and dry deposition of gaseous SO_2 and particulate SO_4^{2-}.
[b] Total nitrogen deposition includes wet deposition of NO_3^- and NH_4^+ ; dry deposition of gaseous NO_2, HNO_3, and NH_3 ; and dry deposition of particulate NO_3^- and NH_4^+. Ammonium total deposition was assumed to remain constant at 2.16 kg-N/ha/yr.

C. FUTURE PROJECTIONS

1. Aquatic Ecosystems

a. Background

Computer models can be used to predict pollution effects on ecosystems and to perform simulations of future ecosystem response (Cosby et al. 1985a,b,c; Agren and Bosatta 1988). The MAGIC model, a lumped-parameter, mechanistic model, has been widely used throughout North America and Europe to project streamwater and lakewater response and has been extensively tested against the results of diatom reconstructions and ecosystem manipulation experiments (e.g., Wright et al. 1986; Sullivan et al. 1992, 1996; Sullivan and Cosby 1995; Cosby et al. 1995, 1996). It has been used extensively in the eastern and western United States and Europe to determine the deposition levels at which environmental damage would be expected to occur (c.f., Skeffington 1999, Bulger et al. 2000, Cosby and Sullivan 2001, Sullivan et al. 2002a).

To estimate the past and future status of Virginia's headwater brook trout streams under different acid deposition scenarios, Bulger et al. (2000) applied the MAGIC model to 60 streams, including 14 SHEN streams, chosen to be regionally representative with respect to acidification sensitivity. This analysis suggested that only about half of all trout streams in Virginia have suitable acid-base chemistry for supporting the relatively acid-tolerant brook trout (*Salvelinus fontinalis*) and that acidic deposition is responsible for significant ecological damage in about one-third of the brook trout streams in Virginia.

The model projections by Bulger et al. (2000) suggested that neither a 40% nor a 70% reduction in S deposition would increase the number of streams that are suitable for brook trout in the year 2041. In fact, the results suggested that a 70% reduction in S deposition would be needed in the long-term just to maintain the current number of streams that are suitable for brook trout. Bulger et al. (2000) concluded that recovery of brook trout streams that have been lost due to acidification is not likely unless S deposition reductions in excess of 70% are achieved. In addition, many other ecologically important species, including blacknose dace (*Rhinichthys atratulus*), minnows, darters and aquatic insects, will be eliminated under conditions that are tolerable for brook trout.

Based on such model projections and the results of other research (c.f., Kaufman et al. 1988, Feldman and Connor 1992, SAMAB 1996, Kauffman et al. 1999, Moeykens and Voshell 2002), it appears that aquatic biodiversity in western Virginia has been reduced by acidification. This is not surprising, given the large number of species regionally, some of which are acid-sensitive. Furthermore, rain water is generally too acidic (pH $\leq$ 4.8; Table V-16) to support any fish life without buffering, and dilute, low-acid neutralizing capacity (ANC) waters are common. The results of model simulations presented by Bulger et al. (2000) suggested that, under currently mandated reductions in acidifying pollutants, biodiversity loss in some of Virginia's headwater brook trout streams is likely to continue.

b. Modeling Methods for Aquatic Effects

Site Selection

Fourteen streams were selected for aquatic effects modeling, to represent the range of geologic sensitivity and streamwater ANC found in SHEN (Table VI-1). The 14 streams chosen are all of the streams in SHEN for which water quality data are available in sufficient quantity and of sufficient quality for use in calibrating MAGIC to a long-term database. These streams are routinely sampled as part of the Shenandoah Watershed Study (SWAS) and the Virginia Trout Stream Sensitivity Study (VTSSS). The frequency of sampling ranges from weekly (6 streams) to quarterly (8 streams) and all streams have at least 12 years of monitoring data available. Five streams are underlain by rocks from each of the siliciclastic and basaltic geologic sensitivity classes. Four streams represent the granitic sensitivity class. The siliciclastic watersheds included four streams having ANC between 0 and 16 μeq/L (Paine, Deep, Meadow,

and Twomile Runs), and one stream (White Oak Run) having ANC = 26 μeq/L. The streamwater ANC in the granitic watersheds ranged from 60 (North Fork Dry Run) to 102 (Hazel River) μeq/L, and for the basaltic watersheds ranged from 126 (White Oak Canyon Run) to 258 (North Fork of Thornton River) μeq/L.

Deposition and Meteorology Data

MAGIC requires as atmospheric inputs estimates of the annual precipitation volume (m/yr) and the total annual deposition (eq/ha/yr) of eight ions: Ca, Mg, Na, K, NH_4, SO_4, Cl, and NO_3. These total deposition data are required at each site for each year of the calibration period (the years for which observed streamwater data are used for calibrating the model to each site). Estimated total deposition data are also required for the 140 years preceding the calibration period as part of the calibration protocol for MAGIC, and for each year of any future scenario that will be run using MAGIC.

Total deposition of an ion at a particular site for any year can be represented as combined wet, dry, and in some cases cloud deposition. Inputs to the model are specified as wet deposition (the annual flux in meq/m^2/yr) and a dry and cloud deposition enhancement factor (DDF, unitless) used to multiply the wet deposition in order to get total deposition:

$$\text{TotDep} = \text{WetDep} * \text{DDF}$$

where:

$$\text{DDF} = 1 + \text{DryDep} / \text{WetDep}$$

Thus, given an annual wet deposition flux (WetDep) and the ratio of dry plus cloud deposition to wet deposition (DryDep/WetDep) for a given year at a site, the total deposition for that site and year is uniquely determined.

In order to calibrate MAGIC and run future scenarios, time-series of the total deposition at each site must be estimated for each year of: a) the calibration period; b) the historical reconstructions; and c) the future scenarios. The procedure used to provide these input data for this assessment was as follows.

Wet deposition input data were collected at Big Meadows by the National Atmospheric Deposition Program (NADP) and at White Oak Run and North Fork Dry Run by the University of Virginia. Wet deposition input data were averaged for the three sites over a five-year period centered on 1990. Averaging over a number of years reduces the likelihood that an "outlier" year (i.e., very wet or very dry) would have a large influence.[1] Dry deposition was estimated based on a DDF, which was calculated using NADP and Clean Air Status and Trends Network (CASTNet) data from Big Meadows, also as a five-year average, using those years for which a complete record was available (all except 1994 and 1996). These five-year average estimates of wet and dry deposition for S and N (Table VII-2), derived from sites within the park, were used to define the Reference Year deposition of S and N for the modeling study. These Reference Year deposition values of S and N were used for model calibration (including the historical reconstructions) and for simulation of future deposition scenarios as described below.

Table VII-2. Five-year average estimates of wet, dry, and total deposition of sulfur and nitrogen, which were used to calibrate the MAGIC model to watersheds modeled in SHEN for streamwater chemistry.

Monitoring Site	Precipitation (m/yr)	Wet Deposition (kg/ha/yr)[a]		
		NH_4^+-N	NO_3^-N	SO_4^{2-}-S
White Oak Run	0.99	1.05	2.47	7.24
N. Fork Dry Run	1.14	2.12	2.76	6.96
Big Meadows	1.39	2.02	2.66	7.03
Average	1.17	1.73	2.63	7.08
Monitoring Site		Dry Plus Cloud Deposition (kg/ha/yr)[b]		
		NH_4^+-N	NO_3^--N	SO_4^{2-}-S
Big Meadows		0.51	2.87	5.83
Estimate Applied to All Modeling Sites		Total Deposition (kg/ha/yr)		
		NH_4^+-N	NO_3^--N	SO_4^{2-}-S
	1.17	2.24	5.50	12.91

[a] Five-year average (1988-1992)
[b] Five-year average, based on years having complete data: 1991-1998, except 1994 and 1996

[1] Note that selection of the calibration period does not have an appreciable effect on model projections or estimates of critical loads. The model is run forward to the evaluation year, based on measured or projected deposition values.

Given the Reference Year deposition values, the deposition data for historical and calibration periods can be calculated using the Reference Year absolute values and scaled time series of wet deposition and DDF that give the values for a given year as a fraction of the Reference Year value. For instance, to calculate the total deposition of a particular ion in some historical year j:

$$\text{TotDep}(j) = [\text{WetDep}(0) * \text{WetDepScale}(j)] * [\text{DDF}(0) * \text{DDF Scale}(j)]$$

where WetDep(0) is the Reference Year wet deposition (meq/m^2/yr) of the ion, WetDepScale(j) is the scaled value of wet deposition in year j (expressed as a fraction of the wet deposition in the Reference Year), DDF(0) is the dry deposition factor for the ion for the Reference Year, and DDFScale(j) is the scaled value of the dry deposition factor in year j (expressed as a fraction of the DDF in the Reference Year). In constructing the historical deposition data, the scaled sequences of wet deposition and DDF were derived from simulations using the Advanced Statistical Trajectory Regional Air Pollution (ASTRAP) model (Shannon 1998).

Given the same Reference Year deposition values, the deposition data for the future deposition scenarios can be calculated using the Reference Year absolute values and a scaled time series of changes in total deposition to give the total deposition values for a given future year as a fraction of the Reference Year value. For instance, to calculate the total deposition of a particular ion in some future year j:

$$\text{TotDep}(j) = [\text{WetDep}(0) * \text{DDF}(0)] * \text{TotDep Scale}(j)$$

where WetDep(0) is the Reference Year wet deposition (meq/m^2/yr) of the ion, DDF(0) is the dry deposition factor for the ion for the Reference Year, and TotDepScale(j) is the scaled value of the total deposition factor in year j (expressed as a fraction of the total deposition in the Reference Year).

Deposition Inputs for MAGIC

Four deposition inputs are required for each of the eight deposition ions in MAGIC in order to set the total deposition for all years required in the calibrations and future simulations:

1) the absolute value of wet deposition at the site for the Reference Year (meq/m^2/yr);

2) the absolute value of DDF (calculated from the DryDep/WetDep ratios) for the site for the Reference Year, (unitless);

3) time series of scaled values of wet deposition and scaled values of DDF covering all historical years necessary to calibrate the model (scaled to the Reference Year);

4) time series of scaled values of future total deposition covering all future years of interest to the scenario runs (scaled to the Reference Year).

The *absolute value of wet deposition* is time and space-specific, varying geographically and from year to year. It is desirable to have the estimates of wet deposition take into account the geographic location of the site as well as the year for which calibration data are available. The Reference Year wet deposition (derived above) for the park provides a single value for the deposition of each ion for the whole park for the Reference Year. To provide an estimate of the spatial variation in wet deposition across the 14 modeling sites within the park, the Reference Year average deposition values were corrected for geographical location and elevation using scaled deposition data for each ion at each site derived from the spatially explicit deposition model of Lynch et al. (1996). The Lynch model is based on spatial and elevational interpolation of wet deposition values of each ion from the NADP monitoring network. The outputs of the Lynch model for each of the 14 modeling sites were averaged over the same five-year period (1988-1992) to provide spatial patterns of wet deposition within the park over the period used to define the Reference Year. The resulting spatially-dependent wet deposition data were used for each site when calibrating MAGIC (Table VII-3). This spatial extrapolation procedure insures that the average deposition values of each ion across the 14 sites (Table VII-3) are equal to the Reference Year deposition values for the whole park.

The *absolute value of the DDF* specifies the ratio between the absolute amounts of wet and total deposition. This ratio is less variable in time and space than is the estimate of total deposition. That is, if in a given year the wet deposition goes up, then the total deposition usually goes up also (and conversely). Estimates of the DDF used for MAGIC may, therefore, be derived from a procedure that uses park-wide data (i.e., lacks spatial resolution). As described previously, the DDF values for S and N were derived from observed data for the Reference Year at a single site within the park, Big Meadows. The same DDF was used for S and N for all 14 modeling sites (Table VII-3). DDF values for chloride (Cl^-) and the base cations were calculated by assuming that Cl^- inputs and outputs should be in balance across the park. A single DDF (dry

Table VII-3. Wet and dry deposition input data for SHEN sites.[a]

Site[b]	Discharge (cm/yr)	Precip. (m/yr)	Yield (%)	Concentration in Precipitation (1990 Reference Year)								Dry Deposition Factor (DDF)							
				Ca	Mg	Na	K	NH^4	SO_4	Cl	NO_3	Ca	Mg	Na	K	NH^4	SO_4	NO_3	Cl
VT36	0.705	1.071	0.66	5.3	2.1	3.6	2.0	10.8	36.8	5.4	15.4	1.76	1.76	1.76	1.76	1.25	1.83	2.08	2.8
DR01	0.779	1.271	0.61	5.9	2.2	3.8	2.5	10.6	41.1	5.3	17.9	1.67	1.67	1.67	1.67	1.25	1.83	2.08	2.8
VT35 (PAIN)	0.814	1.213	0.67	6.0	2.3	4.0	2.6	10.4	41.4	5.6	18.3	1.68	1.68	1.68	1.68	1.25	1.83	2.08	2.8
VT53	0.885	1.332	0.66	6.0	2.4	4.1	2.7	10.4	41.4	5.7	18.5	1.68	1.68	1.68	1.68	1.25	1.83	2.08	2.8
WOR1	0.891	1.280	0.70	6.0	2.3	3.9	2.6	10.7	41.6	5.5	18.2	1.67	1.67	1.67	1.67	1.25	1.83	2.08	2.8
NFDR	0.649	1.343	0.48	5.0	2.0	3.6	1.9	10.4	35.3	5.3	14.5	1.76	1.76	1.76	1.76	1.25	1.83	2.08	2.8
VT58	0.744	1.172	0.63	5.4	2.1	3.5	2.0	10.7	37.1	5.3	15.4	1.73	1.73	1.73	1.73	1.25	1.83	2.08	2.8
VT59 (STAN)	0.750	1.188	0.63	5.6	2.2	3.8	2.3	10.5	39.6	5.4	17.0	1.70	1.70	1.70	1.70	1.25	1.83	2.08	2.8
VT62	0.712	1.163	0.61	5.0	2.1	3.6	2.0	10.8	36.3	5.4	15.1	1.76	1.76	1.76	1.76	1.25	1.83	2.08	2.8
VT75	0.578	1.123	0.51	4.8	2.0	3.7	1.9	10.4	34.6	5.4	14.3	1.78	1.78	1.78	1.78	1.25	1.83	2.08	2.8
VT66	0.526	1.066	0.49	4.6	2.0	3.9	1.9	10.1	33.6	5.5	13.8	1.80	1.80	1.80	1.80	1.25	1.83	2.08	2.8
VT51	0.522	1.107	0.47	4.7	2.0	3.9	2.0	10.3	34.7	5.5	14.4	1.79	1.79	1.79	1.79	1.25	1.83	2.08	2.8
VT60 (PINE)	0.530	1.053	0.50	4.8	2.0	3.7	1.9	10.6	35.3	5.5	14.6	1.78	1.78	1.78	1.78	1.25	1.83	2.08	2.8
VT61	0.517	1.055	0.49	5.2	2.1	3.7	2.0	10.7	36.5	5.5	15.2	1.76	1.76	1.76	1.76	1.25	1.83	2.08	2.8

[a] Yield and reference year deposition data were adjusted as necessary to produce mass-balance for chloride.
[b] For stream names, see Table VI-2. Intensively studied sites include Paine Run (PAIN), Staunton River (STAN), and Piney River (PINE).

enhancement) of Cl^- inputs was calculated for the whole park such that the average mass balance (input-output) for Cl^- across all 14 sites was equal to zero. This same DDF was used for Cl^- for all 14 sites (Table VII-3). The added Cl^- was balanced by base cations. A DDF for each base cation at each site was calculated using the ratio of the four base cations in wet deposition at each site. The DDF's for base cations thus vary from site-to-site but result in an exact balance for the added Cl^- at each site (Table VII-3).

Similarly, the *time series of scaled sequences* used for MAGIC simulations do not require detailed spatial resolution. That is, if for any given year the deposition goes up at one site, it also goes up at neighboring sites within the park. Time series of wet deposition and DDF were derived from the ASTRAP model (Shannon 1998), which produced wet, dry, and cloud deposition estimates of S and oxidized nitrogen (NO_x) every five years starting in 1900 and ending in 1990 for the Big Meadows site as part of the Southern Appalachian Mountains Initiative (SAMI) project (Sullivan et al., 2002a). The ASTRAP model outputs are smoothed estimates of deposition roughly equivalent to a ten-year moving average centered on each of the output years. Modeling sites for this project were assigned the historical sequences of the ASTRAP Big Meadows output. The time-series of wet deposition and DDF from 1900 to 1990 were normalized to the 1990 values to provide scaled historical sequences for the MAGIC calibration and reconstruction simulations. The same scaled historical sequences of wet deposition and DDF for S and N were used at all 14 sites (Table VII-4). Historical sequences of base cation and Cl^- deposition were assumed to be constant.

Table VII-4. Assignment of historical deposition sequences at SHEN, based on ASTRAP modeled deposition. [a]

Scaled Sequence	Year													
	1850[b]	1900	1915	1920	1925	1935	1945	1950	1960	1965	1975	1980	1985	1990
Wet S	0.050	0.302	0.620		0.717	0.526	0.829	0.776	0.870	0.920	1.161		0.973	1.000
S DDF	1.112	1.112		1.138			1.154		1.106	1.048	0.977	0.970	0.972	1.000
Wet N	0.000	0.143	0.247		0.363	0.321	0.481	0.531	0.712	0.787	0.977		0.970	1.000
N DDF	0.989	0.989		1.054			0.988		1.000	0.976	0.960	0.960	0.995	1.000

[a] Sequence values were multiplied by wet deposition and DDF values that were measured or estimated for the reference year (1990) in order to estimate total deposition for past years.
[b] The 1850 values of these sequences are assumed for the historical reconstruction as follows: wet deposition sequences were assumed to decline to near zero and DDF sequences were assumed to remain constant at 1900 values.

Specification of Deposition for Future Projections

For a given scenario, the deposition in future years was specified as a fraction of the total deposition in the reference year. In that the future deposition changes were specified only as changes in total deposition, these were implemented in MAGIC by assuming that wet, dry and cloud deposition all change by the same relative amount. The percent changes in total S and N deposition calculated for the emissions control scenarios described in Section IV.B using the RADM model are given in Table VII-5. The modeled percent changes in S deposition are slightly smaller than percent changes in S emissions, whereas the model percent changes in NO_x deposition are slightly larger than percent changes in NO_x emissions (Table IV-4).

Table VII-5. Percent changes in sulfur and nitrogen deposition relative to 1990 base, calculated for emissions control scenarios.

Constituent	Scenario	All	1	2	3	4
	Year	1996	2010	2020	2020	2020
Sulfur		-20.2	-33.2	-36.7	-68.7	-74.9
Oxidized Nitrogen		+2.7	-35.2	-50.3	-59.0	-66.8
Reduced Nitrogen		+29.9	+26.1	+25.7	+29.6	+20.0

Protocol for MAGIC Calibration and Simulation at Individual Sites

The aggregated nature of the MAGIC model requires that it be calibrated to observed data from a system before it can be used to examine potential system response. Calibration is achieved by setting the values of certain parameters within the model that can be directly measured or observed in the system of interest (called fixed parameters). The model is then run (using observed and/or assumed atmospheric and hydrologic inputs) and the outputs (streamwater and soil chemical variables - called criterion variables) are compared to observed values of these variables. If the observed and simulated values differ, the values of another set of parameters in the model (called optimized parameters) are adjusted to improve the fit. After a number of iterations, the simulated-minus-observed values of the criterion variables usually converge to zero (within some specified tolerance). The model is then considered calibrated. If new assumptions (or values) for any of the fixed variables or inputs to the model are subsequently adopted, the model must be re-calibrated by re-adjusting the optimized parameters until the simulated-minus-observed values of the criterion variables again fall within the

specified tolerance. The model and its application methods for this assessment generally conform with the approach followed in the SAMI Assessment (Sullivan et al., 2002a) and are further described in Appendix F.

Calibration Data

The calibration procedure requires that streamwater quality, soil chemical and physical characteristics, and atmospheric deposition data be available for each stream. The water quality data needed for calibration are the concentrations of the individual base cations (Ca^{2+}, Mg^{2+}, Na^{+}, and K^{+}) and acid anions (Cl^{-}, SO_4^{2-}, NO_3^{-}) and the stream pH. The soil data used in the model include soil depth and bulk density, soil pH, soil cation-exchange capacity, and exchangeable bases on the soil (Ca^{2+}, Mg^{2+}, Na^{+}, and K^{+}). The atmospheric deposition inputs to the model must be estimates of total deposition, not just wet deposition.

Ideally, the MAGIC water quality calibration data would be the volume-weighted annual average values of each water quality variable. However, the eight VTSSS streams included in this study do not have discharge data available, and only have water quality data on a quarterly basis. It is thus not possible to derive a volume-weighted annual average value for the water quality variables at these sites. Discharge gauges and weekly water quality sampling at the other six sites allowed calculation of the volume-weighted annual average for those streams. Those averages were most similar to the spring quarter sample in each of the streams. Therefore, the spring quarterly data were selected for calibration at all sites (even in watersheds for which weekly water quality data were available) to ensure compatibility of calibration results across all streams. The averages of spring quarterly samples over the five year period from 1988-1992 were used for calibration at each site (Table VII-6).

Soils data for model calibration were derived as areally averaged values of soil parameters determined from four to eight soil pits excavated within each of the 14 watersheds in 2000. The soils data for the individual soil horizons at each sampling site were averaged based on horizon, depth, and bulk density to obtain single vertically aggregated values for each soil pit. The vertically aggregated data were then spatially averaged to provide a single value for each soil variable in each watershed. Details of the soils data used for calibration at each site are given in Table VII-7. The deposition values used for calibration are summarized in Tables VII-3 and VII-4.

Table VII-6. Streamwater input data for SHEN modeling sites.

Site	Bedrock Class[a]	Discharge (m/yr)	Streamwater Concentration (µeq/L or pH units)												
			Ca	Mg	Na	K	NH_4	SO_4	Cl	NO_3	ANC	pH	SBC[b]	SAA[b]	Calk[b]
VT36	S	0.705	24.7	41.6	21.9	27.0	0.0	90.9	23.1	1.2	-2.4	5.44	115.2	115.2	0.1
DR01	S	0.779	22.8	46.1	25.1	42.9	0.0	108.7	24.4	2.1	-0.8	5.46	136.9	135.2	1.6
VT35[c]	S	0.814	27.2	50.6	24.2	45.7	0.0	111.3	23.5	6.3	4.1	5.81	147.7	141.1	6.6
VT53	S	0.885	28.0	48.1	27.8	38.6	0.0	99.2	24.1	3.5	10.1	6.03	142.5	126.8	15.8
WOR1	S	0.891	30.0	51.8	22.8	38.7	0.0	79.9	22.0	14.9	19.8	6.03	143.2	116.8	26.4
NFDR[c]	G	0.649	84.8	49.2	73.7	10.1	0.0	100.5	30.5	26.5	49.7	6.47	217.7	157.6	60.2
VT59	G	0.750	59.6	25.1	61.3	9.4	0.0	41.4	23.9	2.0	69.7	6.67	155.4	67.3	88.1
VT58	G	0.744	53.7	33.5	59.4	9.5	0.0	40.6	23.2	4.6	71.4	6.73	156.0	68.5	87.6
VT62	G	0.712	56.5	40.7	62.1	10.1	0.0	38.9	24.7	3.9	80.8	6.66	169.4	67.6	101.8
VT75	B	0.578	101.5	79.6	49.8	4.8	0.0	52.2	29.2	28.1	110.7	6.75	235.8	109.6	126.2
VT66	B	0.526	108.9	84.6	58.0	5.1	0.0	52.1	31.3	26.4	127.8	6.80	256.6	109.9	146.8
VT51	B	0.522	132.5	130.0	66.5	18.0	0.0	131.2	32.8	17.2	155.6	7.11	347.1	181.2	165.9
VT60[c]	B	0.530	134.9	112.5	76.7	6.6	0.0	66.5	30.4	30.0	185.2	7.10	330.7	126.9	203.8
VT61	B	0.517	154.7	140.5	97.4	10.3	0.0	89.5	31.2	24.5	234.4	7.12	402.9	145.2	257.7

[a] Siliciclastic, S; Granitic, G; Basaltic, B

[b] SBC, sum of base cations; SAA, sum of mineral acid anions; Calk, calculated ANC.

[c] Intensively-studied sites include VT35 (Paine Run), VT59 (Staunton River), and VT60 (Piney River). For other stream names, see Table VI-2.

Table VII-7. Soils input data for SHEN modeling sites.

Site[b]	Bedrock Class[c]	Soil Chemistry[a]						
		Exchangeable Cations (%)				Base Saturation (%)	pH	CEC (meq/kg)
		Ca	Mg	Na	K			
VT35 (PAIN)	S	10.63	4.06	5.16	0.51	20.4	4.5	70.0
WOR1	S	2.84	1.77	2.86	0.46	7.9	4.4	76.6
DR01	S	5.49	5.34	2.61	0.42	13.9	4.5	85.4
VT36	S	8.40	2.28	2.93	0.45	14.0	4.4	64.0
VT53	S	18.25	5.55	3.71	0.14	27.6	4.4	82.5
VT59 (STAN)	G	19.56	4.66	3.11	0.24	27.6	4.9	101.9
NFDR	G	7.01	2.97	3.20	0.19	13.4	4.5	89.5
VT58	G	7.09	2.85	2.87	0.35	13.2	4.7	100.0
VT62	G	12.32	4.64	3.22	0.71	20.9	4.7	71.0
VT60 (PINE)	B	22.76	12.10	3.24	0.48	38.6	5.0	90.0
VT66	B	36.47	8.84	2.45	0.51	48.3	4.9	134.1
VT75	B	18.15	12.89	2.20	0.40	33.6	5.3	98.4
VT61	B	37.49	15.37	2.47	0.39	55.7	5.3	108.0
VT51	B	19.38	10.81	2.49	0.58	33.3	5.2	87.8

[a] The following parameter values were assumed for all sites: porosity, 50%; bulk density, 1400 g/m^3; depth, 90 cm.
[b] For stream names, see Table VI-2. Intensively studied sites include Paine Run (PAIN), Staunton River (STAN), and Piney River (PINE).
[c] Siliciclastic, S; Granitic, G; Basaltic, B

Calibration and Simulation Procedures

The procedures for calibrating and applying MAGIC to an individual site involve a number of steps, use a number of programs, and produce several discrete outputs. The input data required by the model (streamwater, watershed, soils, and deposition data) were assembled and maintained in data bases (electronic spreadsheets) for each landscape unit. When complete, these data bases were accessed by a program (MAGIC-IN) that generated the initial parameter files (xxx.PR) and optimization (xxx.OPT) files for each site. The initial parameter files contain observed (or estimated) soils, deposition, and watershed data for each site. The optimization files contain the observed soil and streamwater data that are the targets for the calibration at each site, and the ranges of uncertainty in each of the observed values.

The initial parameter and optimization files for each site were sequentially passed to the optimization program (MAGIC-OPT). This program produced three outputs as each site was calibrated. The first (xxx.OUT) is an ASCII file of results that was passed to statistical routines for analysis and summary of model goodness-of-fit for the site. The second (xxx.PR1 ... xxx.PR10) was the multiple calibrated parameter set used in the fuzzy calibration procedure to

assess model uncertainty (see below). The third (xxx.PAR) was the average parameter set for each site (average of the multiple calibration parameter sets) which represents the most likely responses of the site.

The multiple calibrated parameter set (xxx.PR1…xxx.pr10) for each site was used by the program MAGIC-RUN with estimates of historical or future deposition to produce two outputs: 1) reconstructions of historical change at the site; or 2) forecasts of most likely future responses for the applied future deposition scenario. Both of these outputs are in the form of electronic spreadsheets giving simulated values for all modeled variables for each year of each scenario at the site. The multiple calibrated parameter sets were also used with the same estimates of future deposition and the program MAGIC-RUN to produce an analysis of the uncertainty in model projections for that scenario. The results of the uncertainty analysis are in the form of an electronic spreadsheet giving simulated ranges (upper and lower values) for all modeled variables for each year of each scenario at the site.

The implementation of this protocol for calibration and simulation provides a structure for quality control and serves to document the calibration procedure, providing a degree of objectivity in the calibration process. The input data files and programs have been archived along with the MAGIC program. The assumptions involved in the calibration of MAGIC have thus become "fixed and documented". That is, anyone given the input files and programs will generate the same intermediate and final products. There are no subjective decisions made during the calibration of any site that may be forgotten, obscured or confused. The intent is to keep any subjective bias in calibration from affecting scenario simulations. A similar objective protocol was used for MAGIC applications in the National Acid Precipitation Assessment Program (NAPAP) and has been used in a number of regional studies in the United States and Europe.

Performance Analysis

The multiple calibration procedure for each site produced summary statistics (mean, standard deviation, maximum and minimum) for the observed values, the simulated values and the differences (simulated-observed values) of each of the 15 stream variables and each of the 7 soil variables simulated for each of the sites. In addition, plots of simulated versus observed values for stream variables were constructed (Figures VII-1 and VII-2). These analyses showed

that the model calibration results were not biased and did not contain unacceptably large residual errors.

Analysis of Uncertainty

The estimates of the fixed parameters, the deposition inputs (past, current, and future), and the target variable values to which the model is calibrated all contain uncertainties. The multiple optimization procedure that was implemented for calibrating the model allows estimation of the effects of these uncertainties on simulated values from the calibrated model.

The procedure consists of multiple calibrations of each site using random values of the fixed parameters drawn from the observed range of values, and random values of deposition from the range of atmospheric model estimates. Each of the multiple calibrations begin with 1) a random selection of values of fixed parameters and deposition, and 2) a random selection of the starting values of the adjustable parameters. The adjustable parameters are then optimized to achieve a minimum error fit to the target variables. This procedure is repeated ten times for each site. The final calibrated model is represented by the ensemble of parameter values of all of the successful calibrations. To provide an estimate of the uncertainty (or reliability) of a simulated response to a given scenario, all of the ensemble parameter sets are run using the scenario. For any year in the scenario, the largest and smallest values of a simulated variable define the upper and lower confidence bounds for that site's response for the scenario under consideration. Applied for all variables and all years of the scenario, this procedure results in a band of simulated values through time that encompasses the likely response of the site for any point in the scenario. The distributions of these uncertainty estimates for each landscape unit can be regionalized to provide overall estimates of uncertainty for a scenario.

The variations between predicted and observed chemistry (Figure VII-3) may reflect the uncertainty in model structure and performance more accurately than do the results of multiple calibrations. Natural systems respond to processes and rates that are only partially captured by the model formulation. In addition, there is uncertainty associated with the measured values. Thus, it is not surprising that there is some divergence between simulated and observed streamwater ANC over the period of overlap (Figure VII-3). Nevertheless, the simulations are clearly representative of the overall pattern of response.

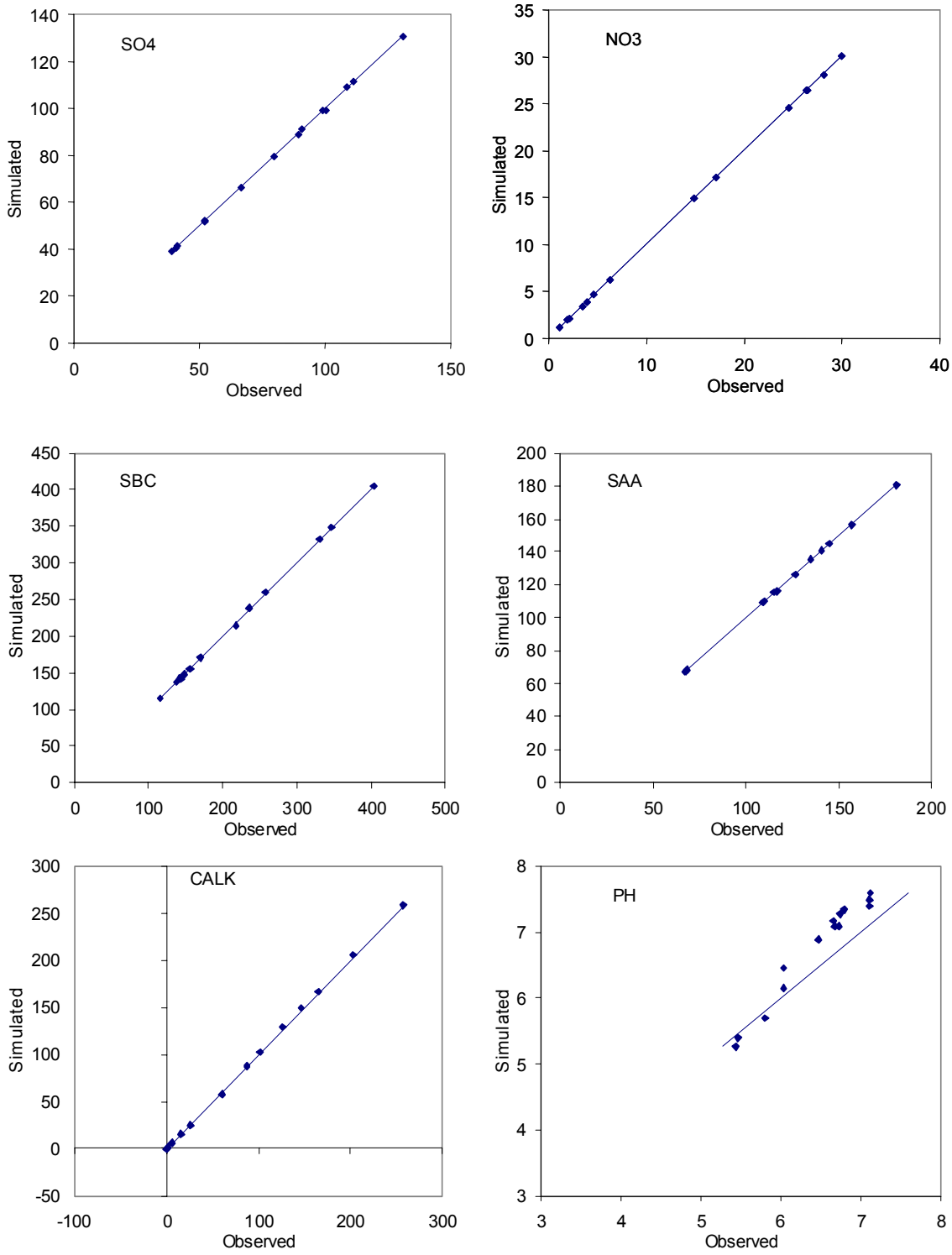

Figure VII-1. Calibration results for the MAGIC model, expressed as predicted versus observed values in the calibration year for sulfate, nitrate, sum of base cations (SBC), sum of mineral acid anions (SAA), calculated ANC (CALK), and pH. Equality lines (1:1) are added for reference.

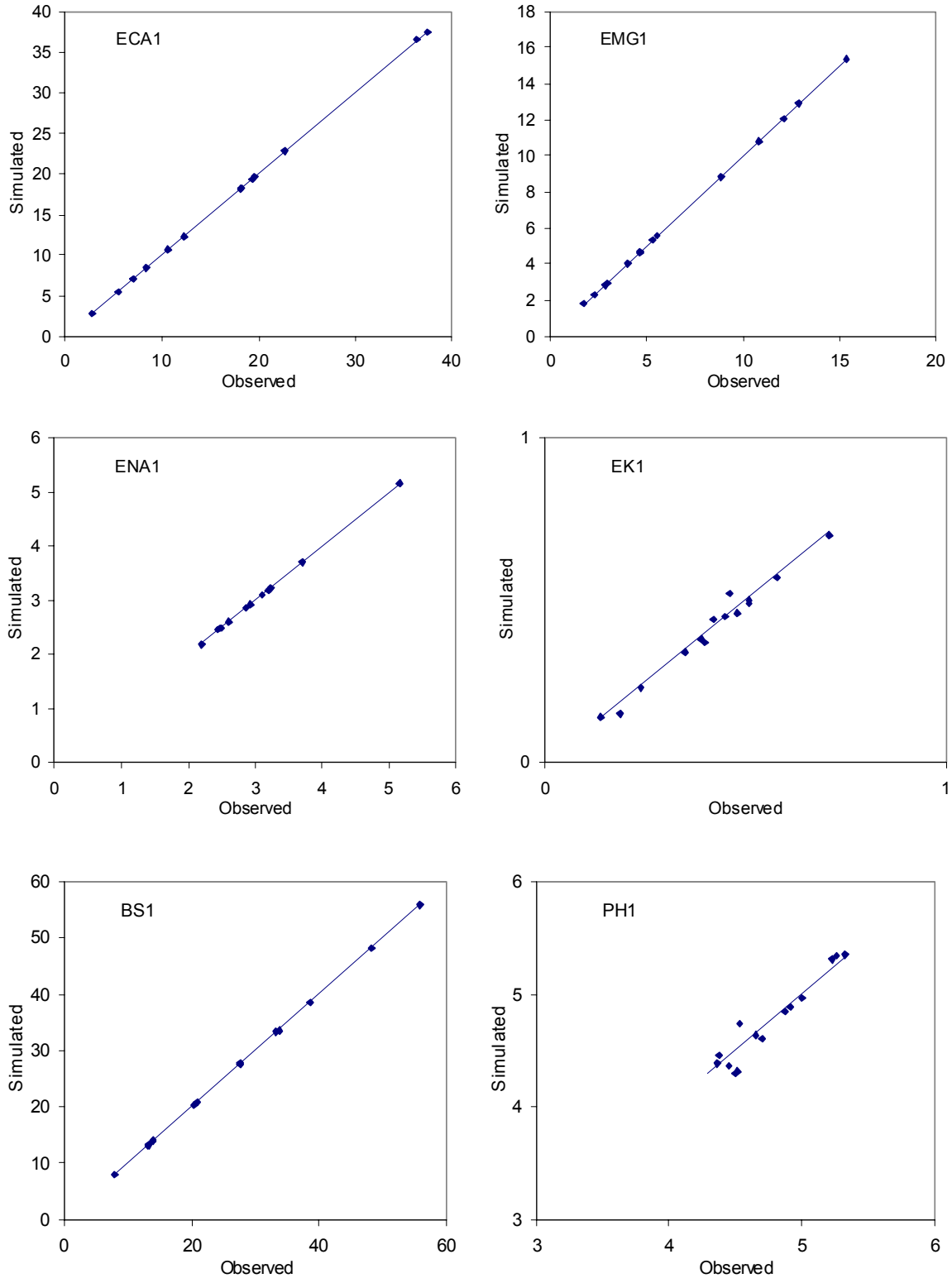

Figure VII-2. Simulated versus observed soils characteristics for modeled watersheds in SHEN, expressed as exchangeable Ca, Mg, Na, and K; base saturation; and soil pH. Equality lines (1:1) are added for reference.

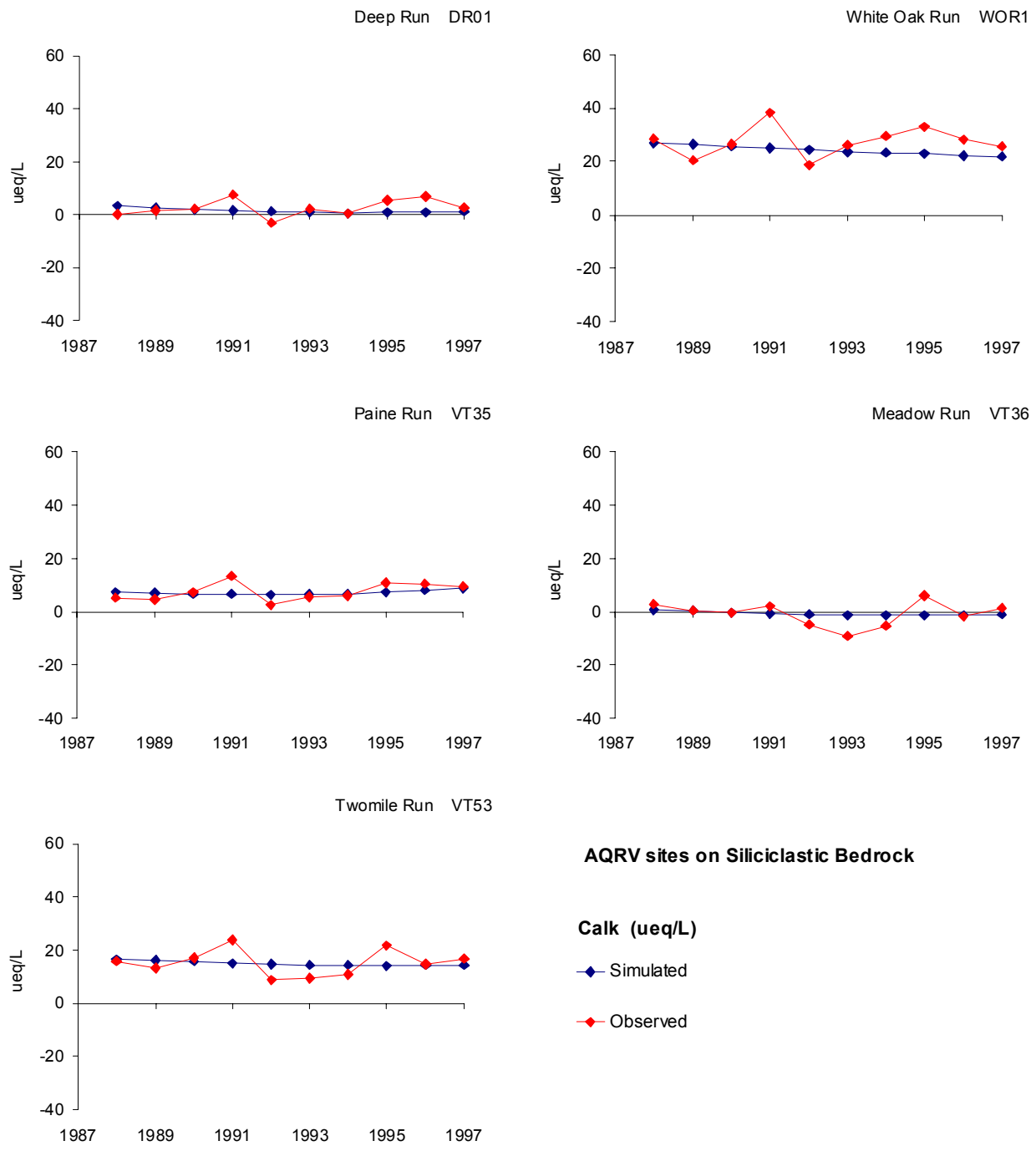

Figure VII-3a. Simulated versus observed ANC over a ten year period for modeling sites on siliciclastic bedrock. The calibration period for these sites was 1988-1992 (5 year average).

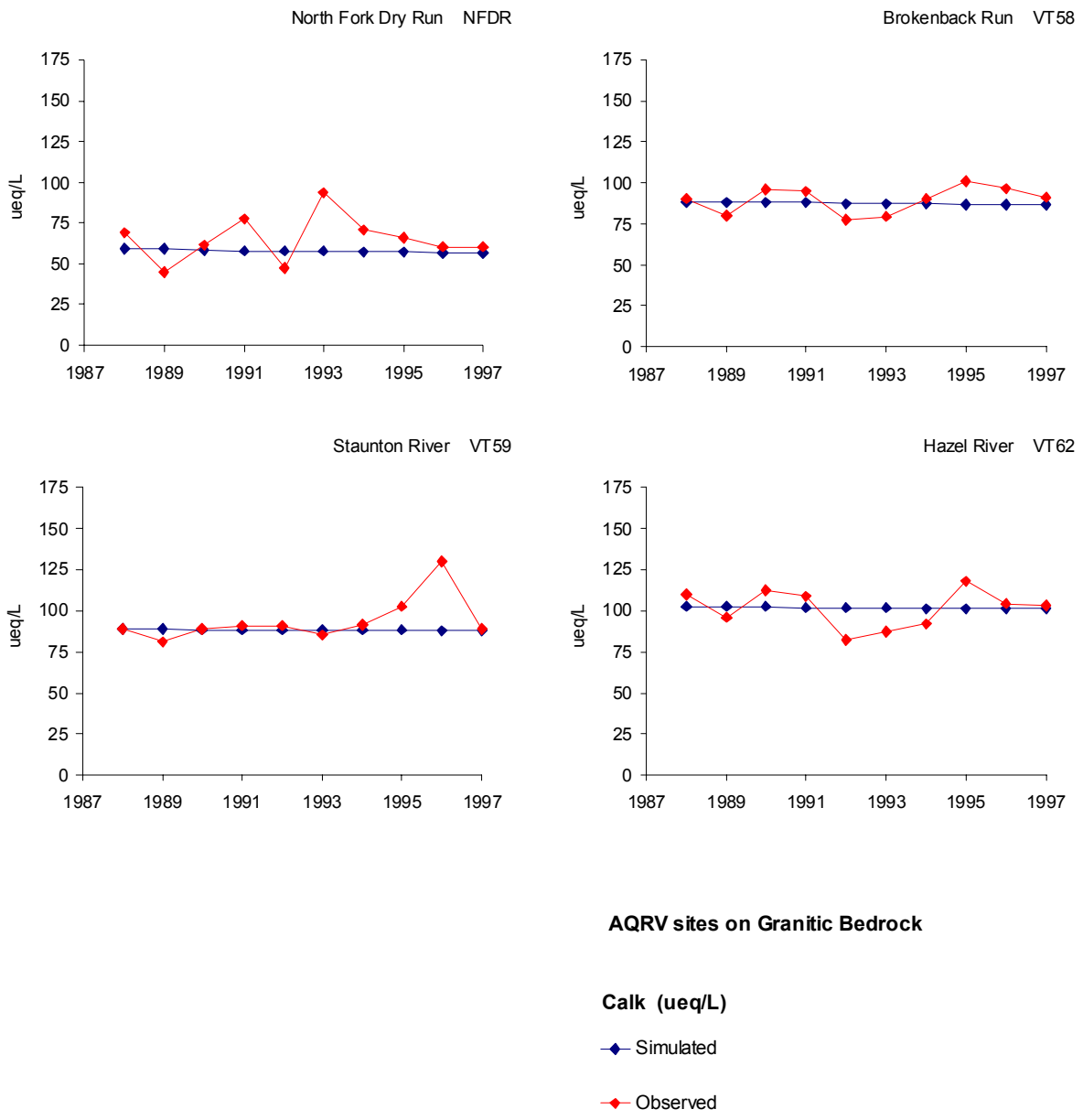

Figure VII-3b. Simulated versus observed ANC over a ten year period for modeling sites on granitic bedrock. The calibration period for these sites was 1988-1992 (5 year average).

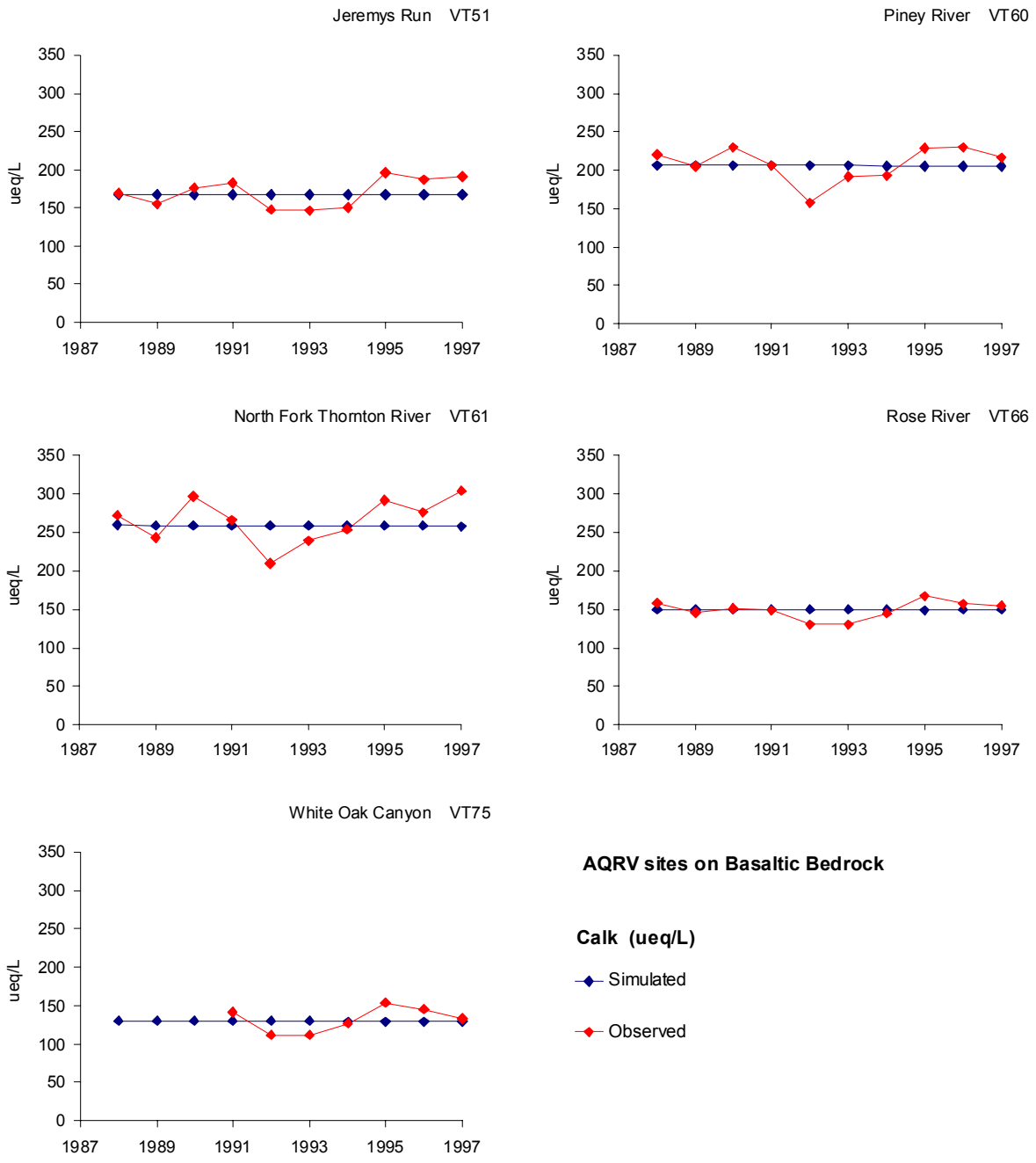

Figure VII-3c. Simulated versus observed ANC over a ten year period for modeling sites on basaltic bedrock. The calibration period for these sites was 1988-1992 (5 year average).

c. Aquatic Modeling Results

MAGIC was successfully calibrated to all modeled watersheds. Results of predicted versus observed chemistry in the calibration year are shown for all modeled sites in Figures VII-1 and VII-2. Agreement was very good for all variables, with the possible exception of pH. The MAGIC model calculates pH using a number of constituents, including the charge-balance ANC and the concentrations of dissolved organic carbon (DOC) and aluminum (Al). Values for DOC and/or Al were missing from some of the model site databases. This introduced additional uncertainty into the estimates of pH for the calibration year.

Demonstrated agreement between predicted and observed streamwater chemistry during the calibration period, as shown in Figures VII-1 and VII-2, does not necessarily demonstrate, however, that the model structure and fundamental assumptions are sufficiently accurate and representative of major watershed processes to yield correct simulations of future conditions. The MAGIC model has been confirmed in several studies that have examined model performance in comparison with independent estimates or measurements of chemical change (c.f., Cosby et al. 1995, 1996; Sullivan et al. 1996) and has been found to be reliable.

A further check on the success of the calibration procedure can be made by comparing yearly time series of simulated values with the observed values at each site for the period of observed data (1988-1997, Figure VII-3). While the model misses some of the observed year-to-year variability, the general agreement with the 10 years of observed data is good at each site. The model was calibrated to the average of the first five years of the observed data. The second five years of data at each site were not used in the calibration procedure.

Future streamwater chemistry was simulated for each site throughout the period 1990 to 2100, based on the scenario of continued constant deposition at 1990 levels and the four emissions control scenarios described in Section IV. Hindcast simulation results are shown in Figure VII-4, suggesting substantial acidification of the modeling sites that occur on siliciclastic bedrock (Figure VII-4a). Among the modeling sites on granitic bedrock, North Fork Dry Run showed evidence of moderate historic acidification, whereas other modeling sites on granitic bedrock and all of the sites on basaltic bedrock showed little historic acidification (Figure VII-4b,c). The inferred pre-industrial ANC of all of the siliciclastic sites and of North Fork Dry Run ranged between about 60 and 90 μeq/L, whereas other sites were inferred to have had pre-industrial ANC near or above 100 μeq/L.

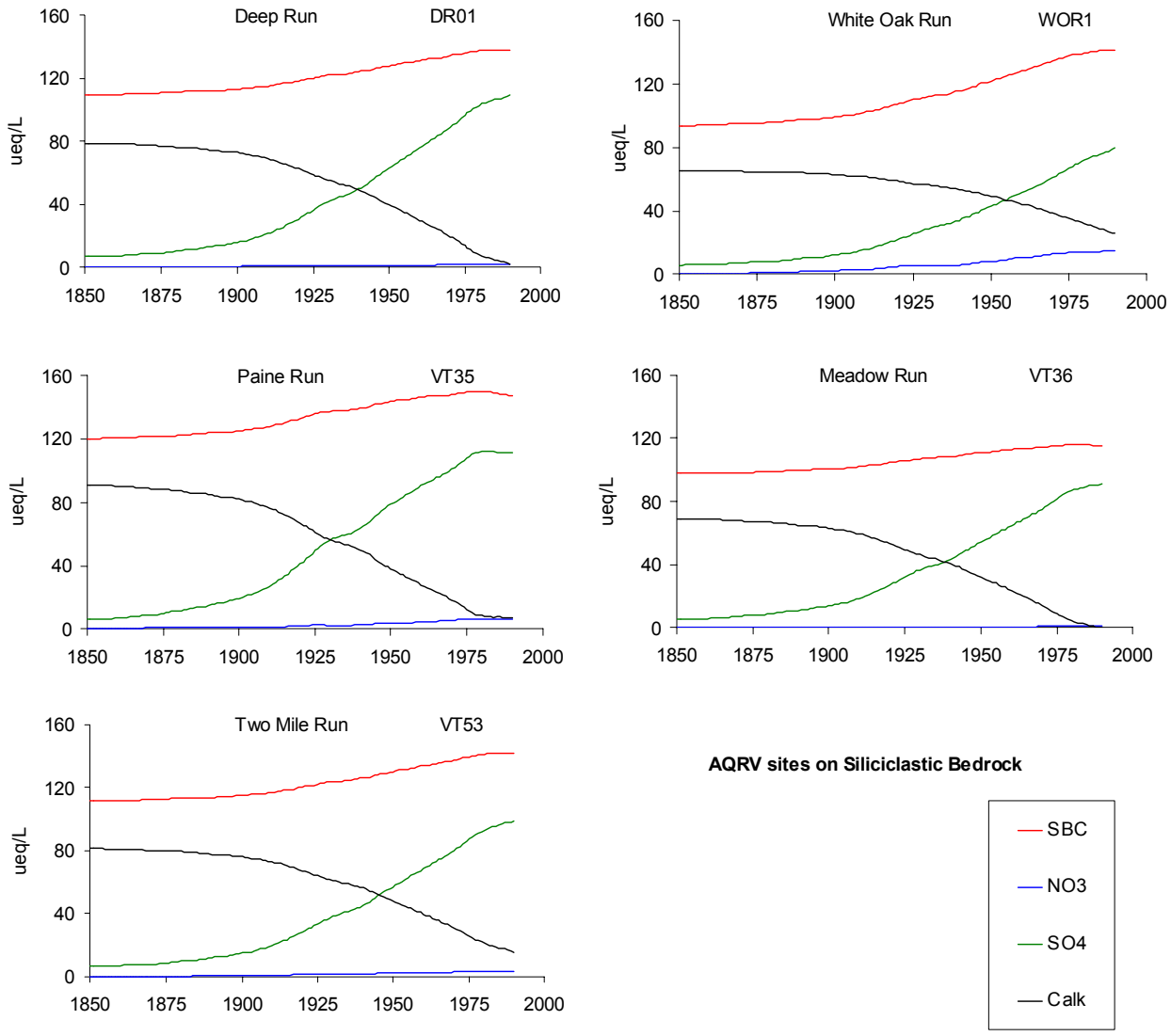

Figure VII-4a. MAGIC hindcast projections for modeled sites on siliciclastic bedrock.

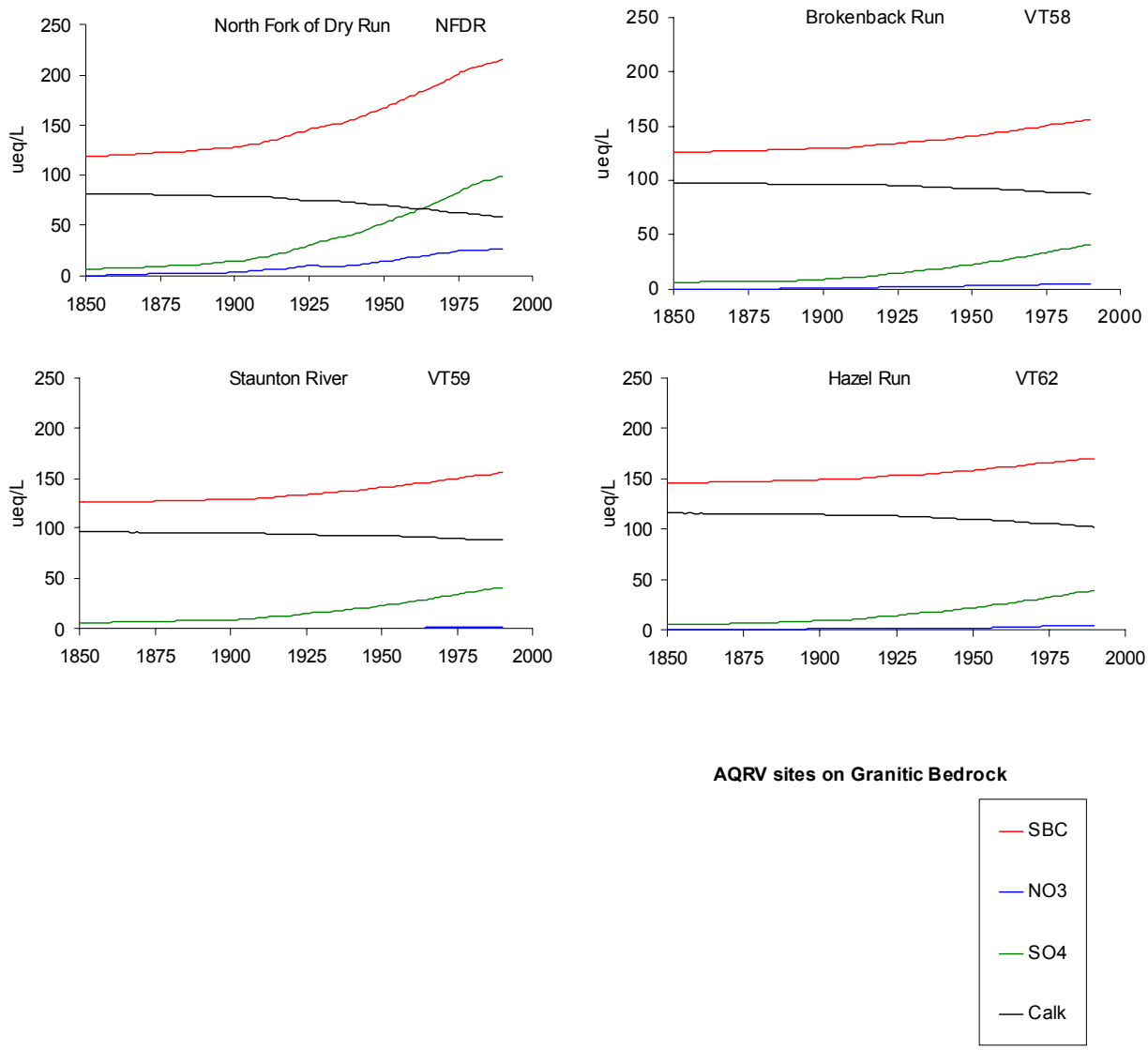

Figure VII-4b. MAGIC hindcast projections for modeled sites on granitic bedrock.

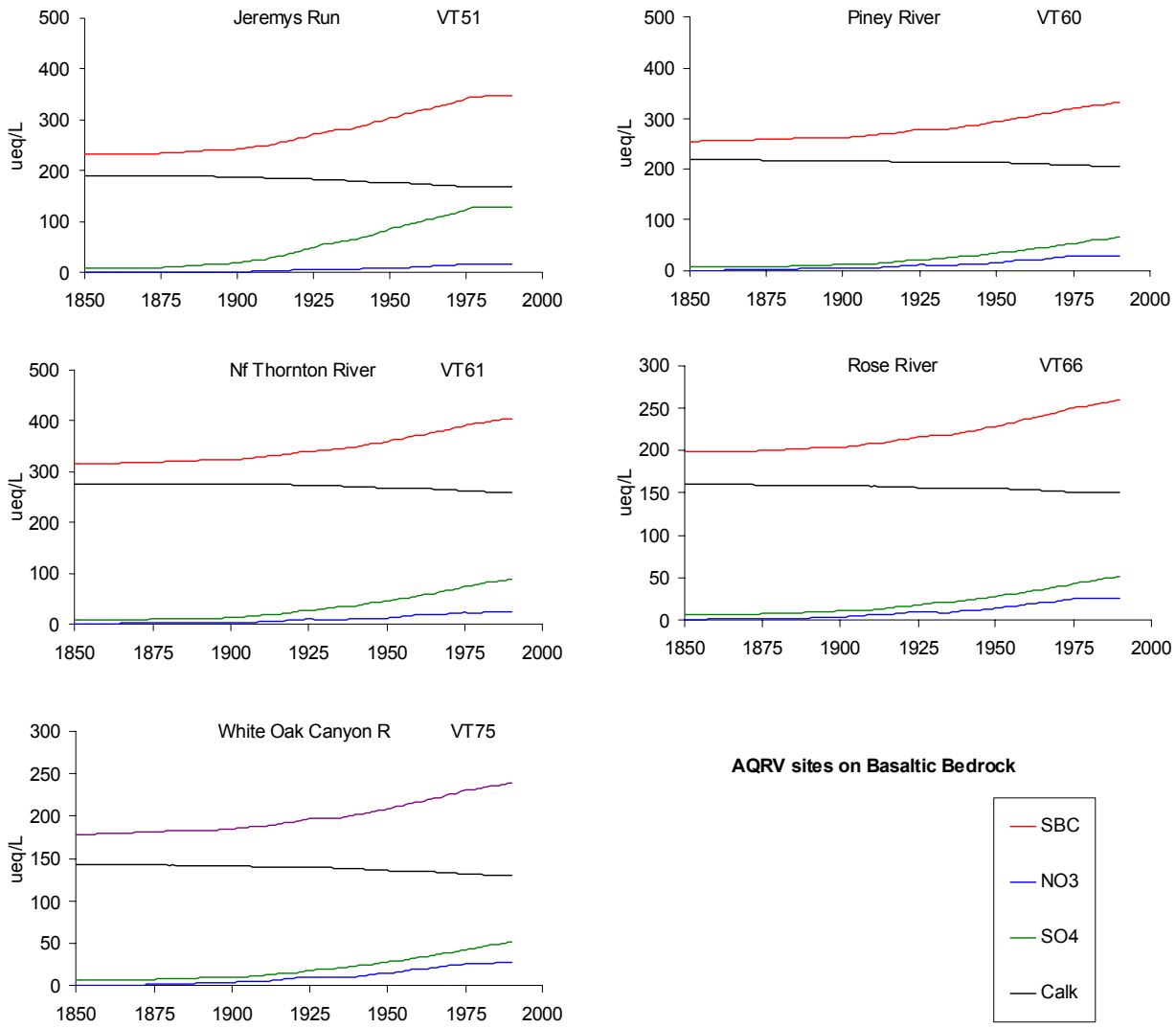

Figure VII-4c. MAGIC hindcast projections for modeled sites on basaltic bedrock.

Projected future concentrations of SO_4^{2-}, nitrate (NO_3^-), sum of base cations, and ANC are presented in Figures VII-5 through VII-8 and Table VII-8 for each of the modeled sites and scenarios. Projected pH values are summarized in Table VII-9 for each site and for each scenario. Sulfate concentrations in streamwater were projected to increase at all sites under the scenario of continued constant deposition. Under the four emissions control scenarios, streamwater SO_4^{2-} concentrations were projected to decrease at all of the sites on siliciclastic bedrock, but results were mixed for the various scenarios applied to sites on granitic and basaltic bedrock. The most stringent emissions control strategy (Scenario 4) resulted in substantial (> 25 μeq/L) projected decreases in streamwater SO_4^{2-} concentrations (Figure VII-5).

Changes in streamwater NO_3^- concentration in response to the scenarios were either negligible or were projected decreases in concentration that were less than about 12 μeq/L (Figure VII-6). Changes in streamwater base cation concentrations were projected to be smallest for the siliciclastic sites, which generally have the lowest base cation concentrations currently, and did not differ substantially among simulations. Base cation leaching was projected to be largest under continued constant deposition and progressively smaller with increasingly stringent emissions control scenarios (Figure VII-7). Projected changes in base cation concentrations were largest for the basaltic sites.

The combined effects of modeled changes in SO_4^{2-} and base cations resulted in projected future changes in streamwater ANC that ranged from less than 10 μeq/L for some siliciclastic sites under Scenarios 1 and 2 to projected ANC increases of more than 40 μeq/L at Deep Run and Paine Run for Scenarios 3 and 4 (Figure VII-8). All siliciclastic sites were projected to become acidic (ANC ≤ 0) by the year 2050 under continued deposition at 1990 levels. White Oak Run was projected to nearly become acidic under Scenarios 1 and 2 by 2100, but other sites on siliciclastic bedrock were projected to increase ANC in the future under all emissions control scenarios. In contrast, the majority of the sites on granitic and basaltic bedrock showed projected decreases in ANC under most of the scenarios, largely in response to changes in S adsorption on soils in response to continued S deposition.

We expect that episodic ANC depressions will be superimposed on these projected future chronic ANC values. We lack an approach to rigorously quantify the extent of episodic changes in ANC that would occur in the future, but we expect that such episodic ANC variability would be similar to current episodic behavior. In general, typical episodic ANC depressions of streams

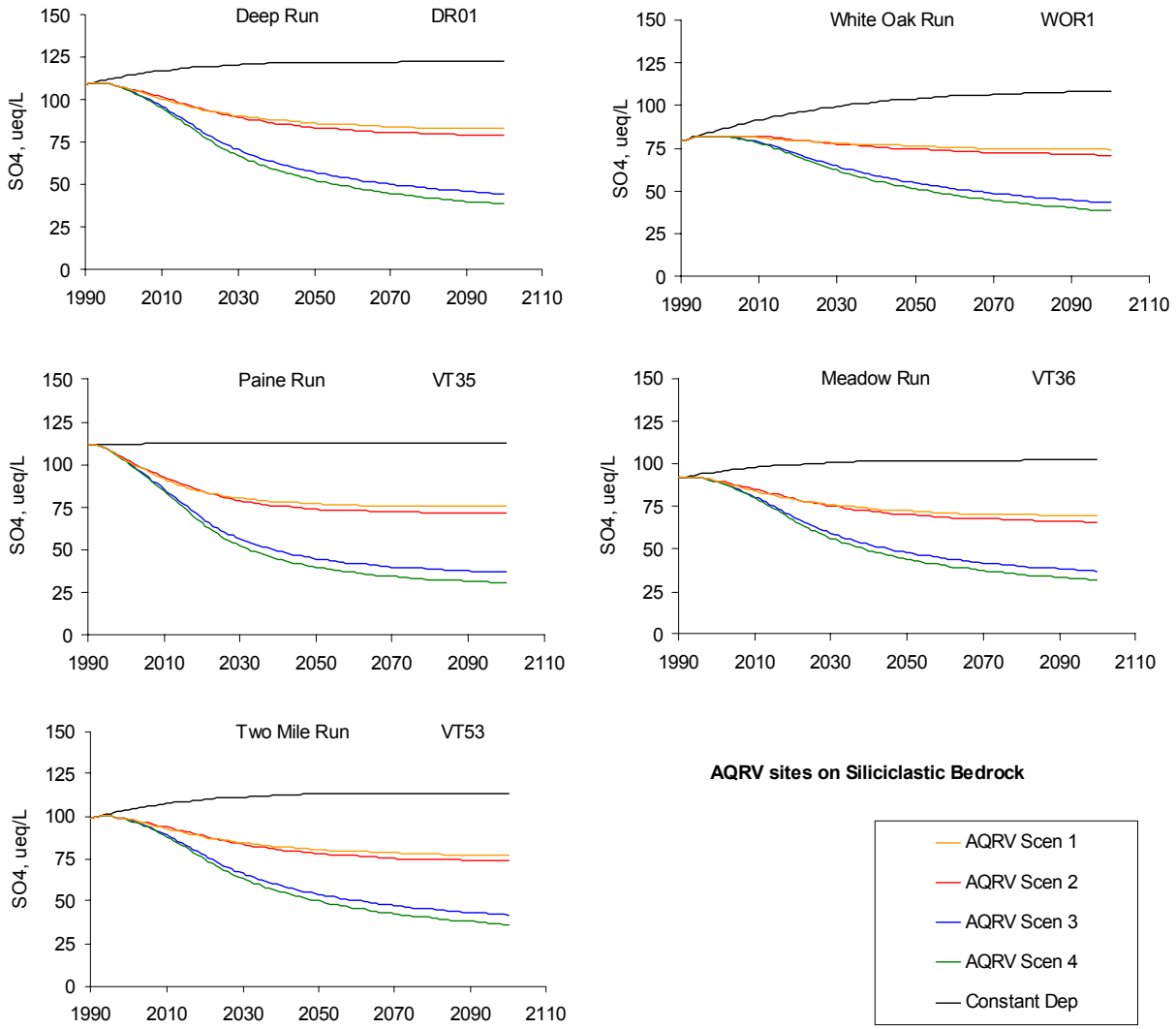

Figure VII-5a. MAGIC model projections of streamwater sulfate under the scenario of constant deposition at 1990 levels and the four emissions control scenarios described in Section IV for modeled sites on siliciclastic bedrock.

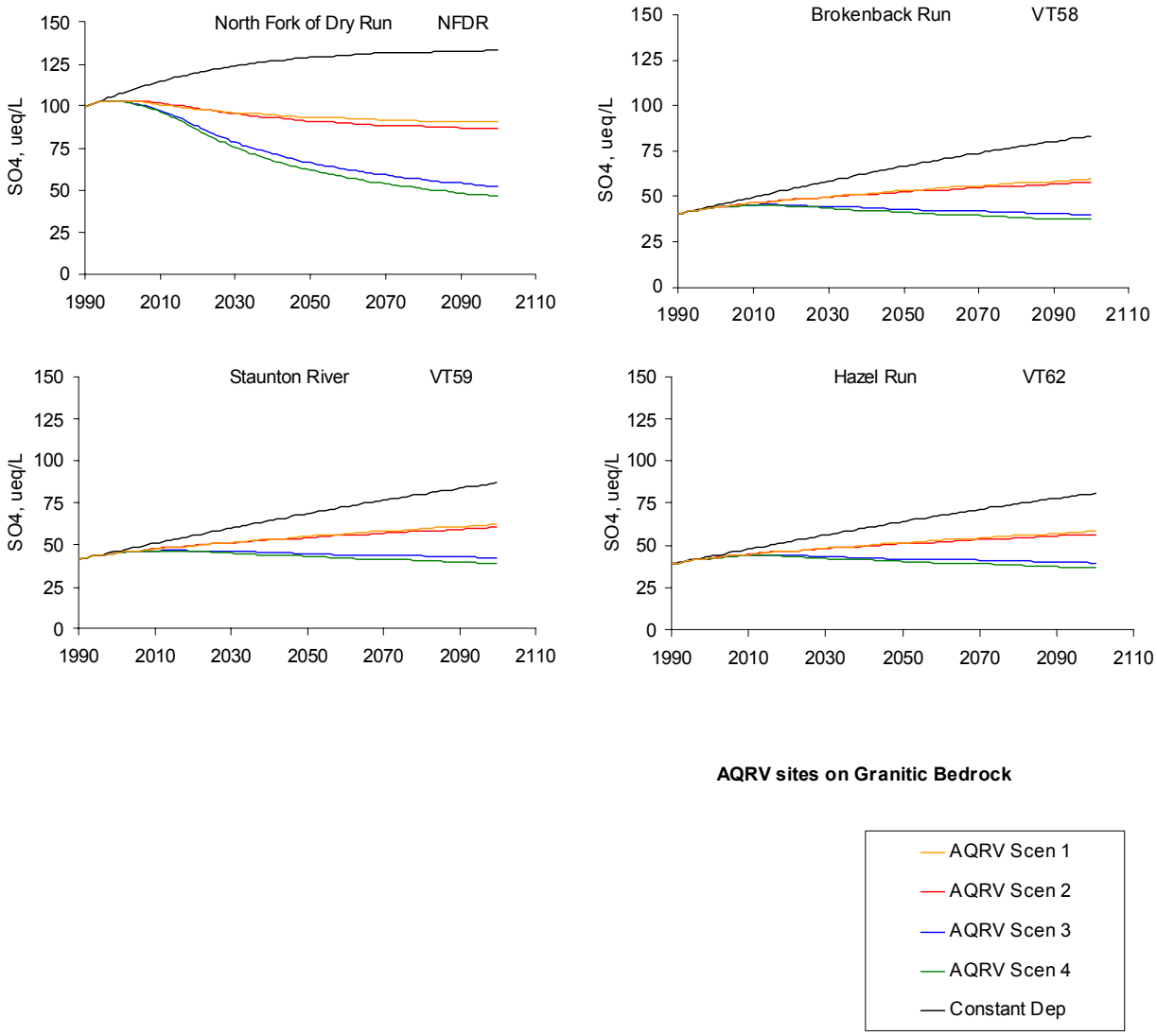

Figure VII-5b. MAGIC model projections of streamwater sulfate under the scenario of constant deposition at 1990 levels and the four emissions control scenarios described in Section IV for modeled sites on granitic bedrock.

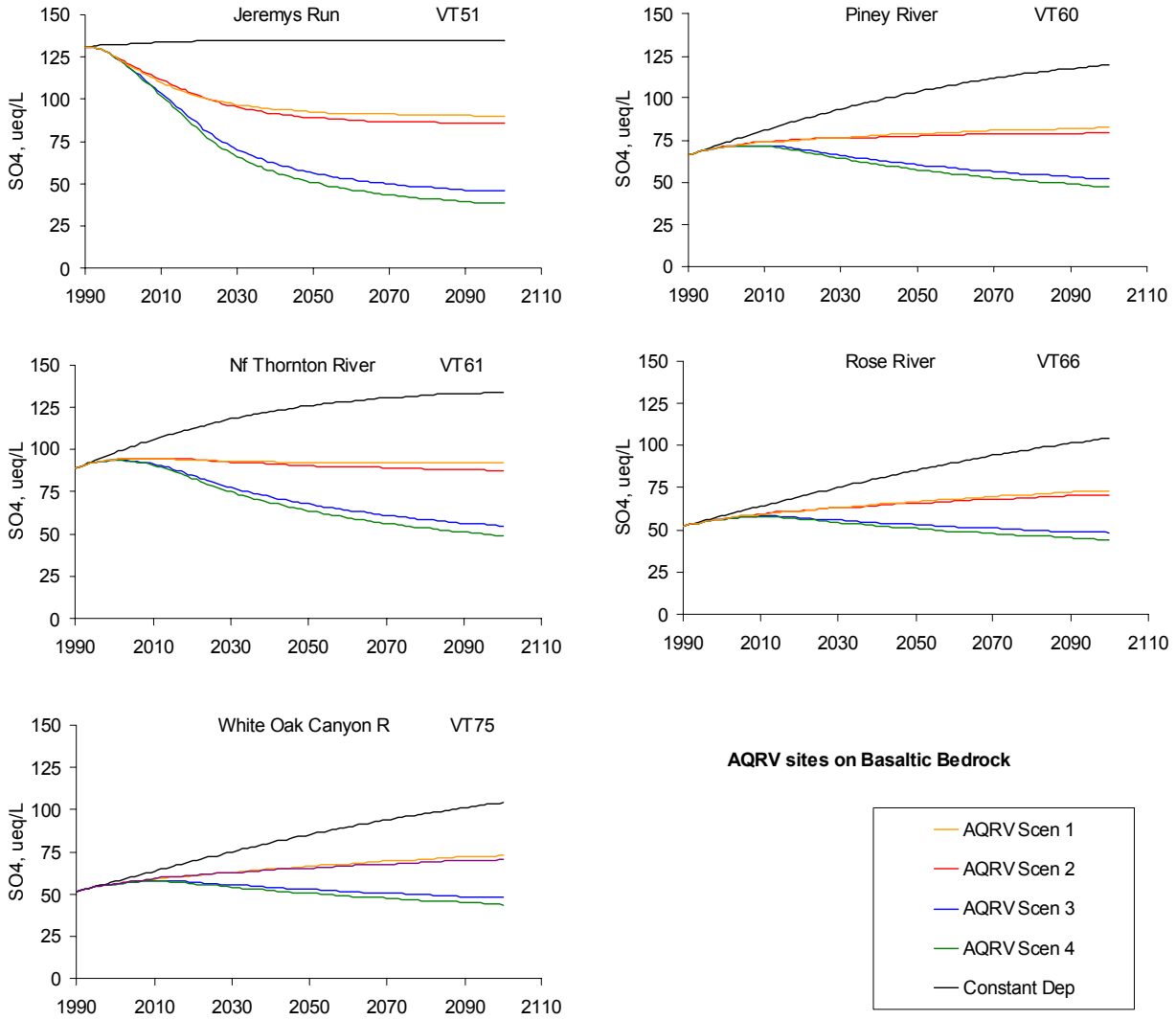

Figure VII-5c. MAGIC model projections of streamwater sulfate under the scenario of constant deposition at 1990 levels and the four emissions control scenarios described in Section IV for modeled sites on basaltic bedrock.

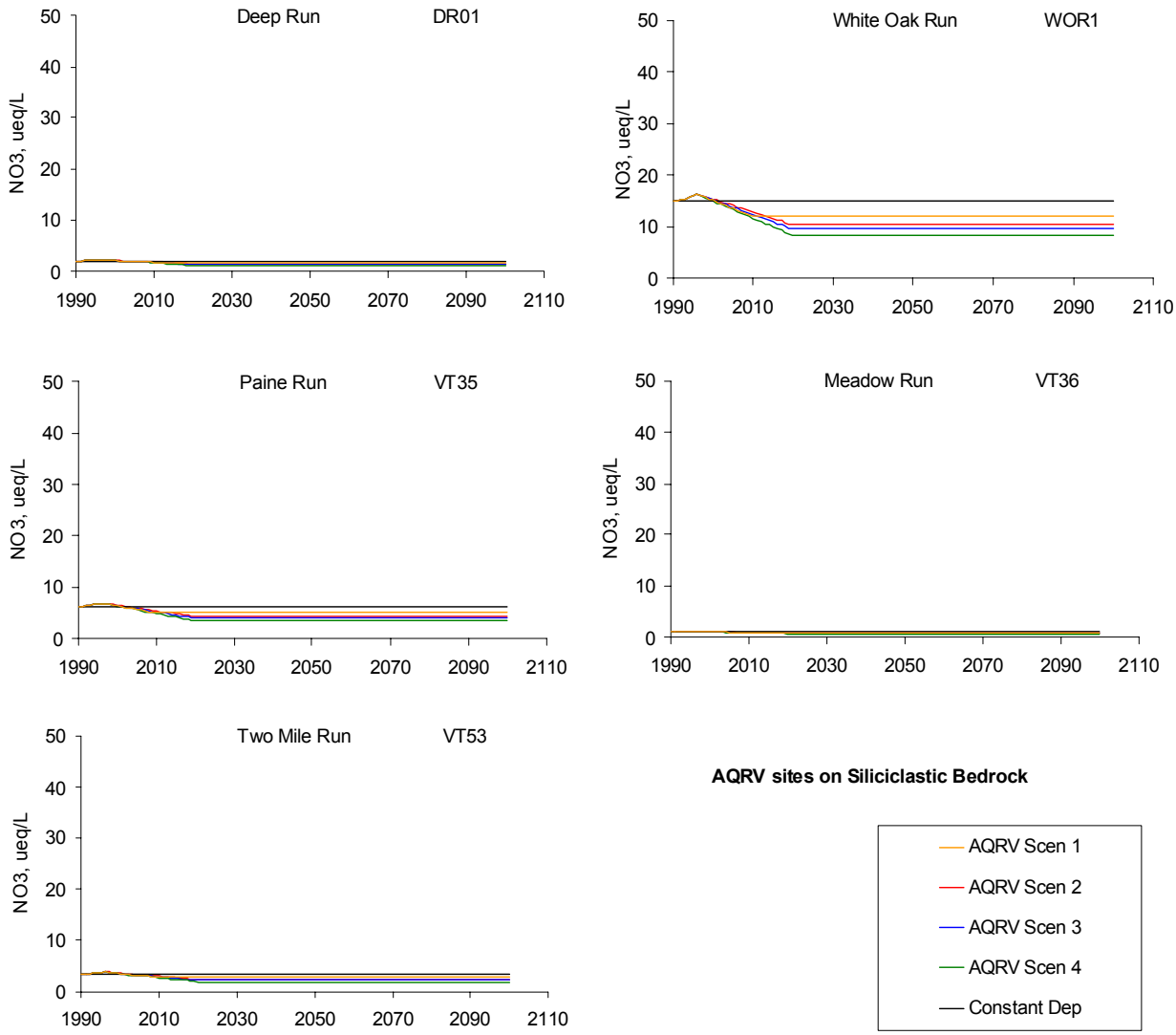

Figure VII-6a. MAGIC model projections of streamwater nitrate under the scenario of constant deposition at 1990 levels and the four emissions control scenarios described in Section IV for modeled sites on siliciclastic bedrock.

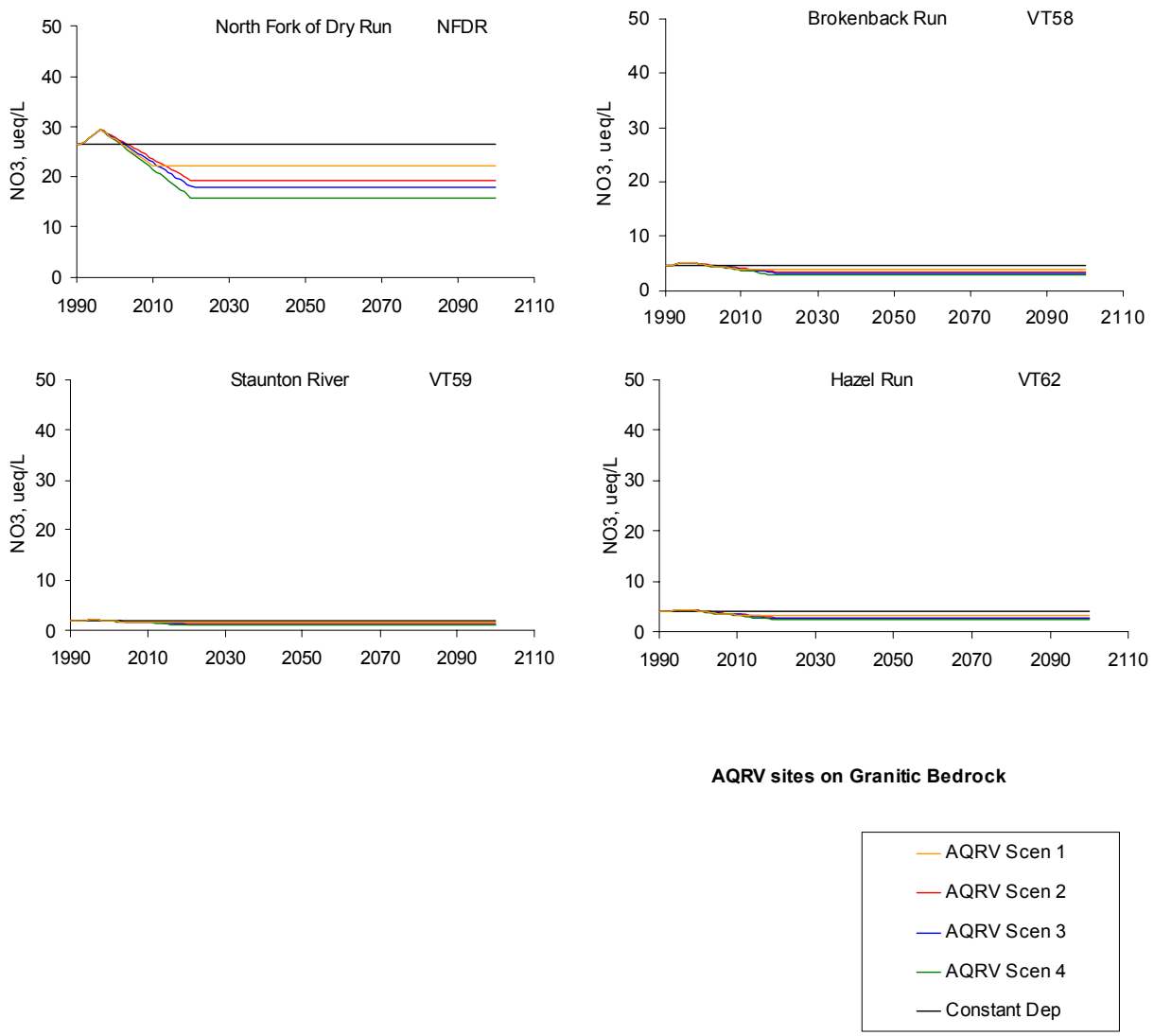

Figure VII-6b. MAGIC model projections of streamwater nitrate under the scenario of constant deposition at 1990 levels and the four emissions control scenarios described in Section IV for modeled sites on granitic bedrock.

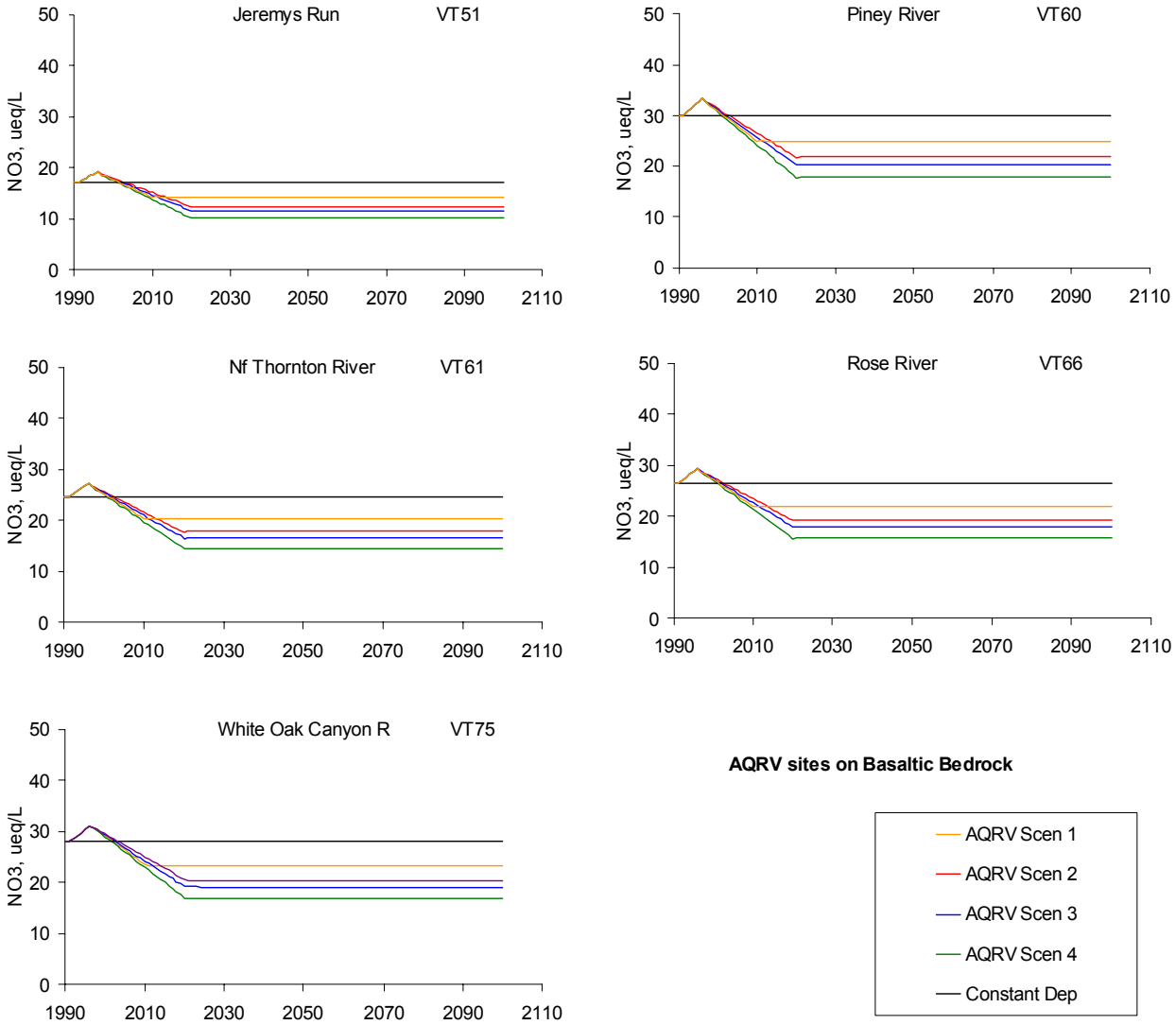

Figure VII-6c. MAGIC model projections of streamwater nitrate under the scenario of constant deposition at 1990 levels and the four emissions control scenarios described in Section IV for modeled sites on basaltic bedrock.

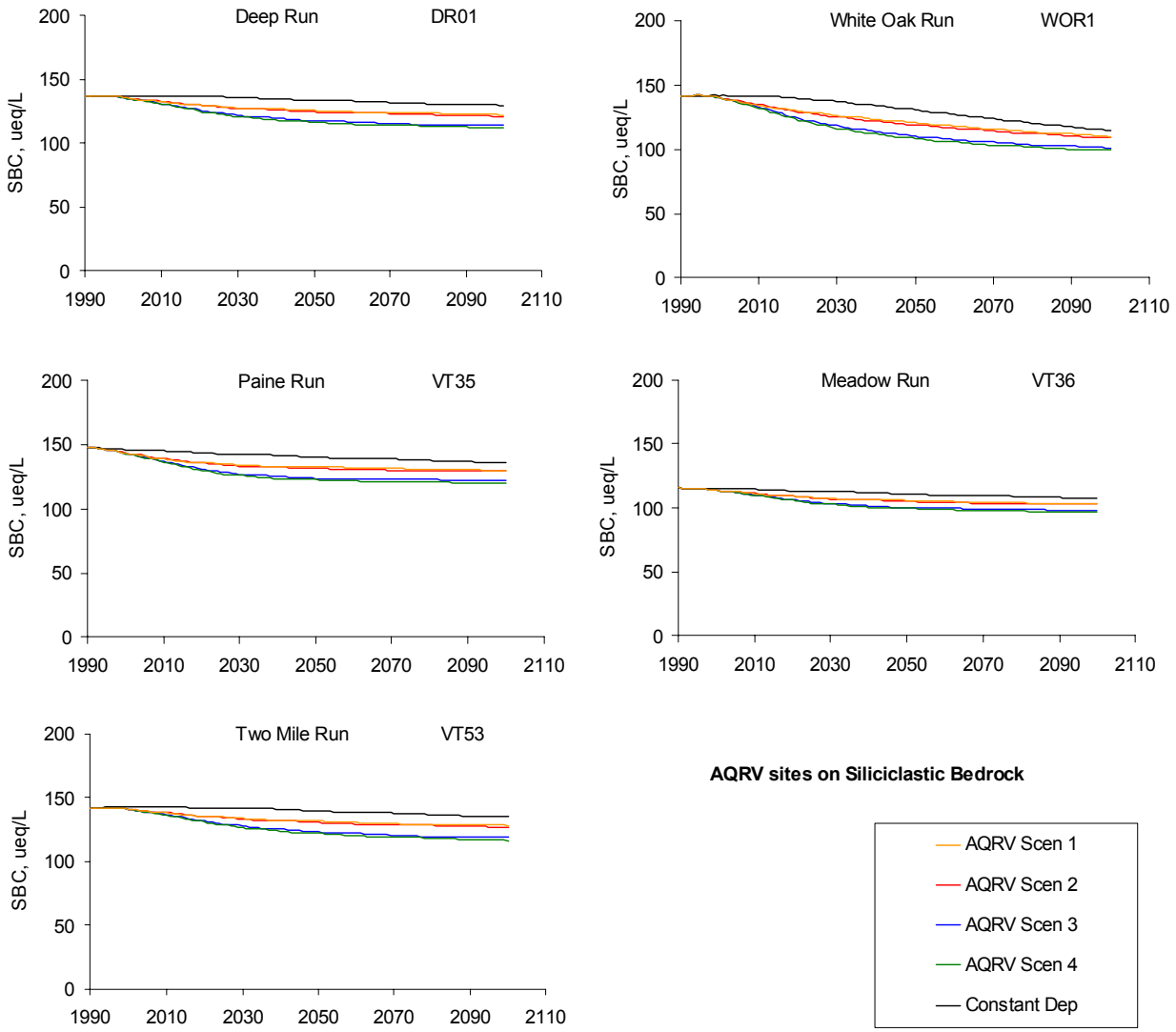

Figure VII-7a. MAGIC model projections of streamwater sum of base cations (SBC) under the scenario of constant deposition at 1990 levels and the four emissions control scenarios described in Section IV for modeled sites on siliciclastic bedrock.

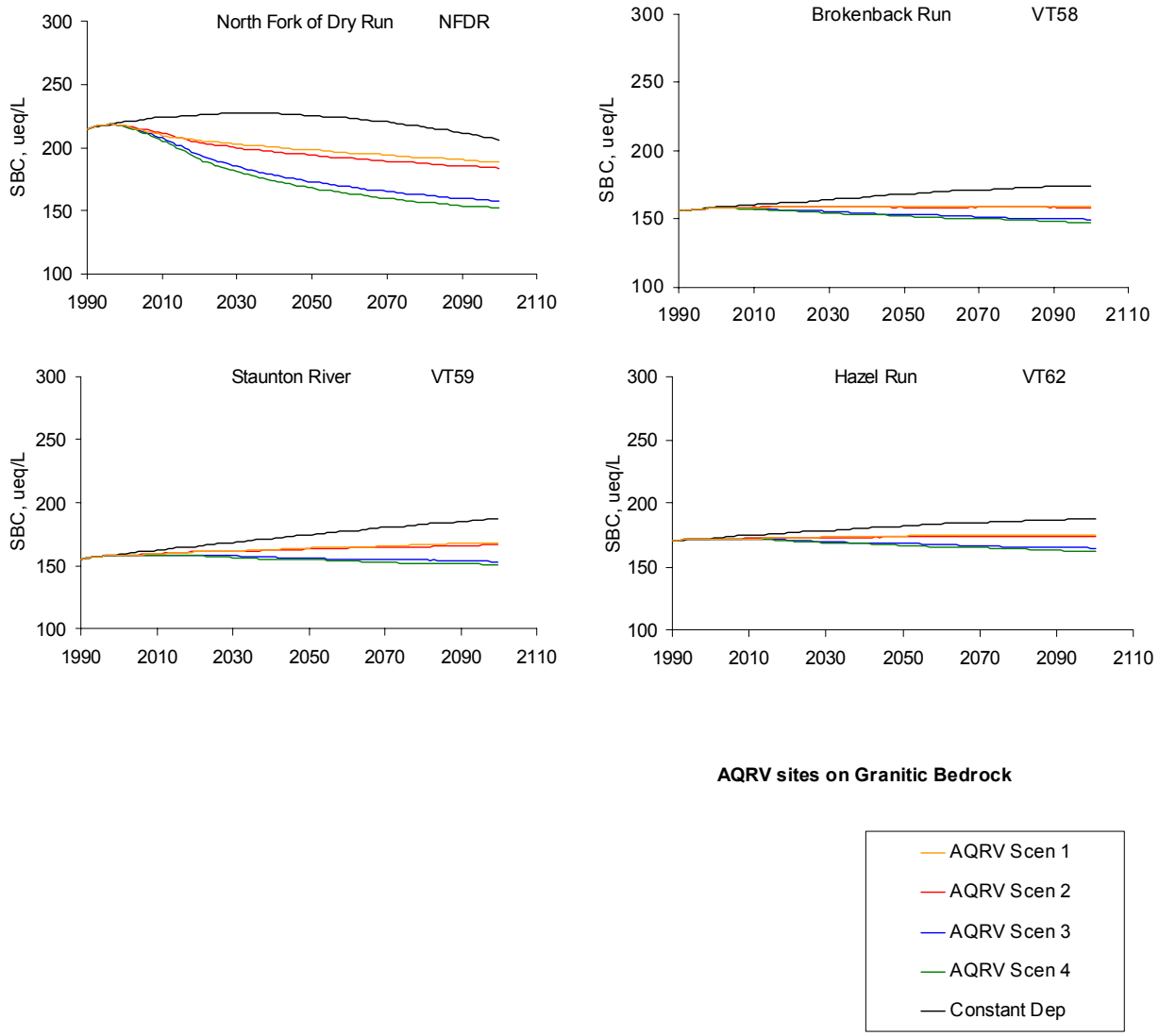

Figure VII-7b. MAGIC model projections of streamwater sum of base cations (SBC) under the scenario of constant deposition at 1990 levels and the four emissions control scenarios described in Section IV for modeled sites on granitic bedrock.

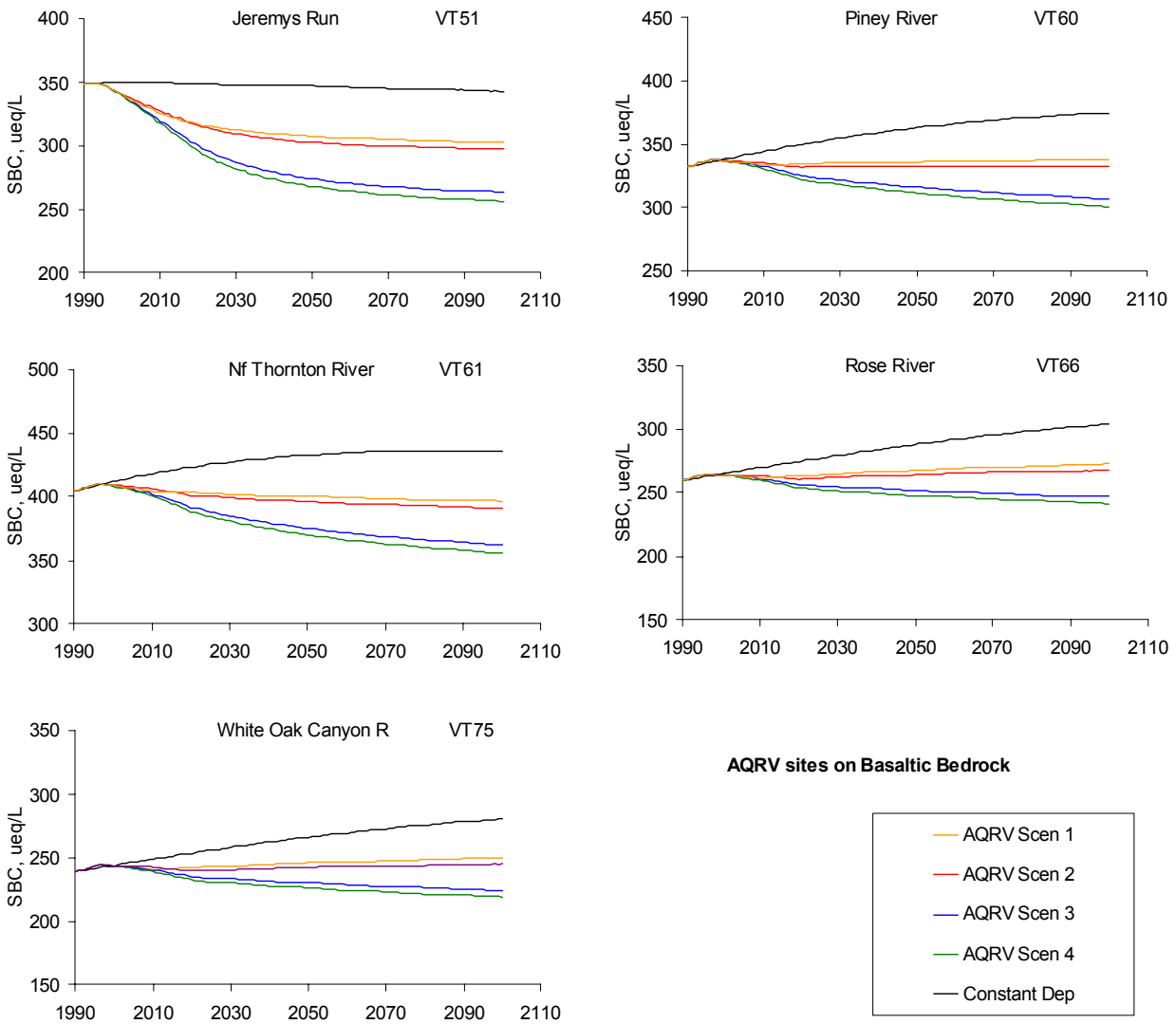

Figure VII-7c. MAGIC model projections of streamwater sum of base cations (SBC) under the scenario of constant deposition at 1990 levels and the four emissions control scenarios described in Section IV for modeled sites on basaltic bedrock.

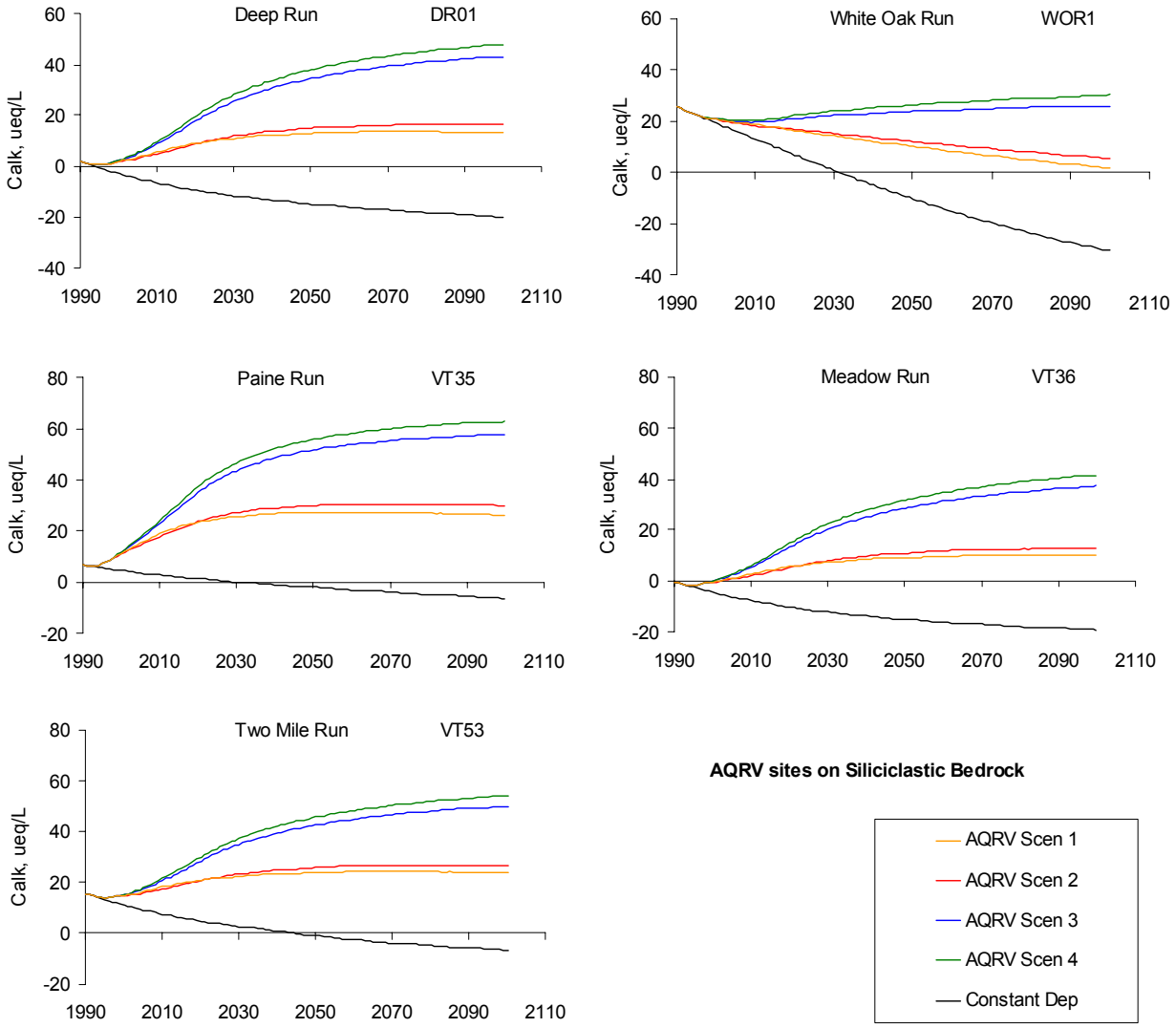

Figure VII-8a. MAGIC model projections of streamwater ANC under the scenario of constant deposition at 1990 levels and the four emissions control scenarios described in Section IV for modeled sites on siliciclastic bedrock. See model estimates of pre-industrial ANC in Table VII-8.

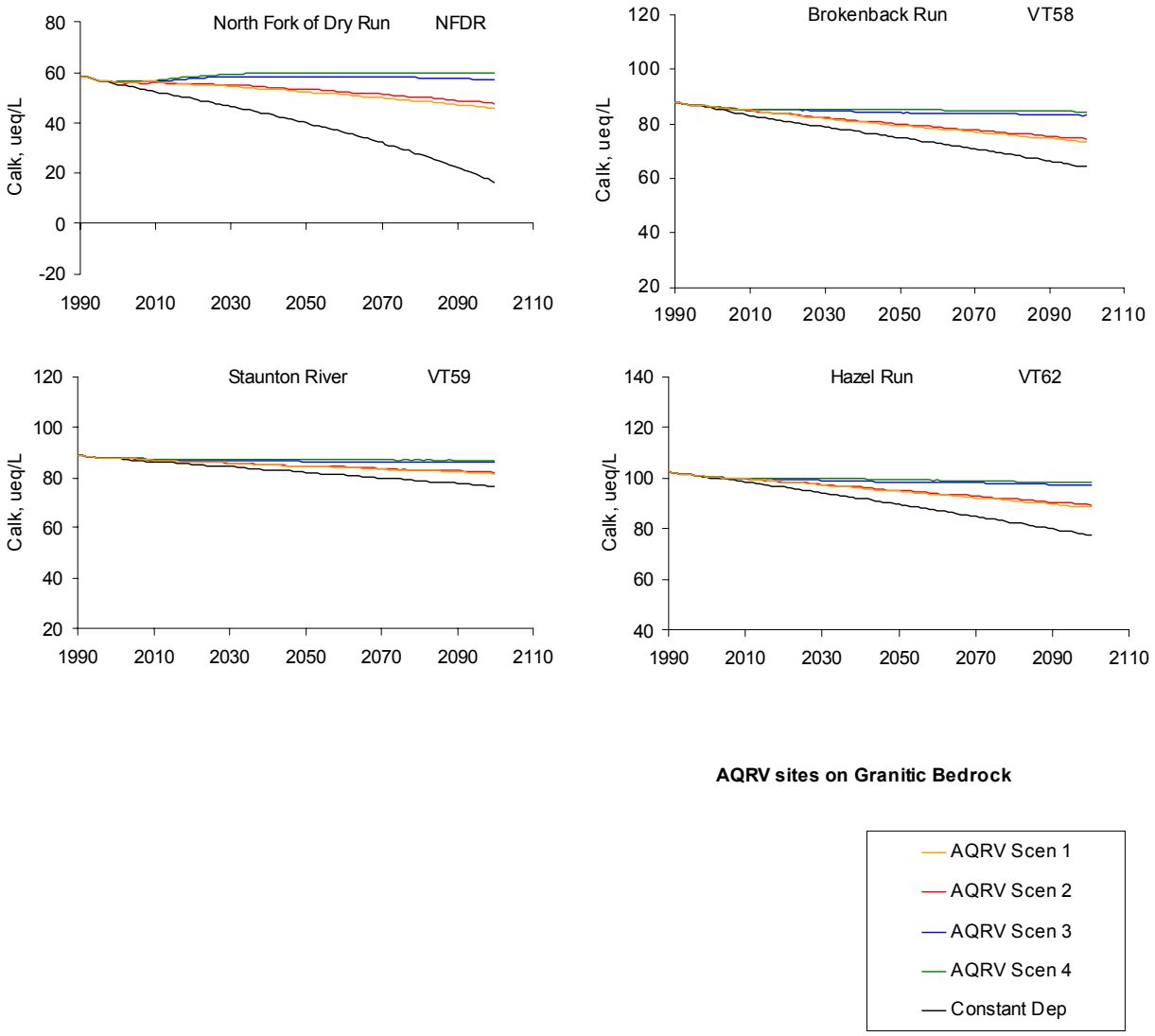

Figure VII-8b. MAGIC model projections of streamwater ANC under the scenario of constant deposition at 1990 levels and the four emissions control scenarios described in Section IV for modeled sites on granitic bedrock. See model estimates of pre-industrial ANC in Table VII-8.

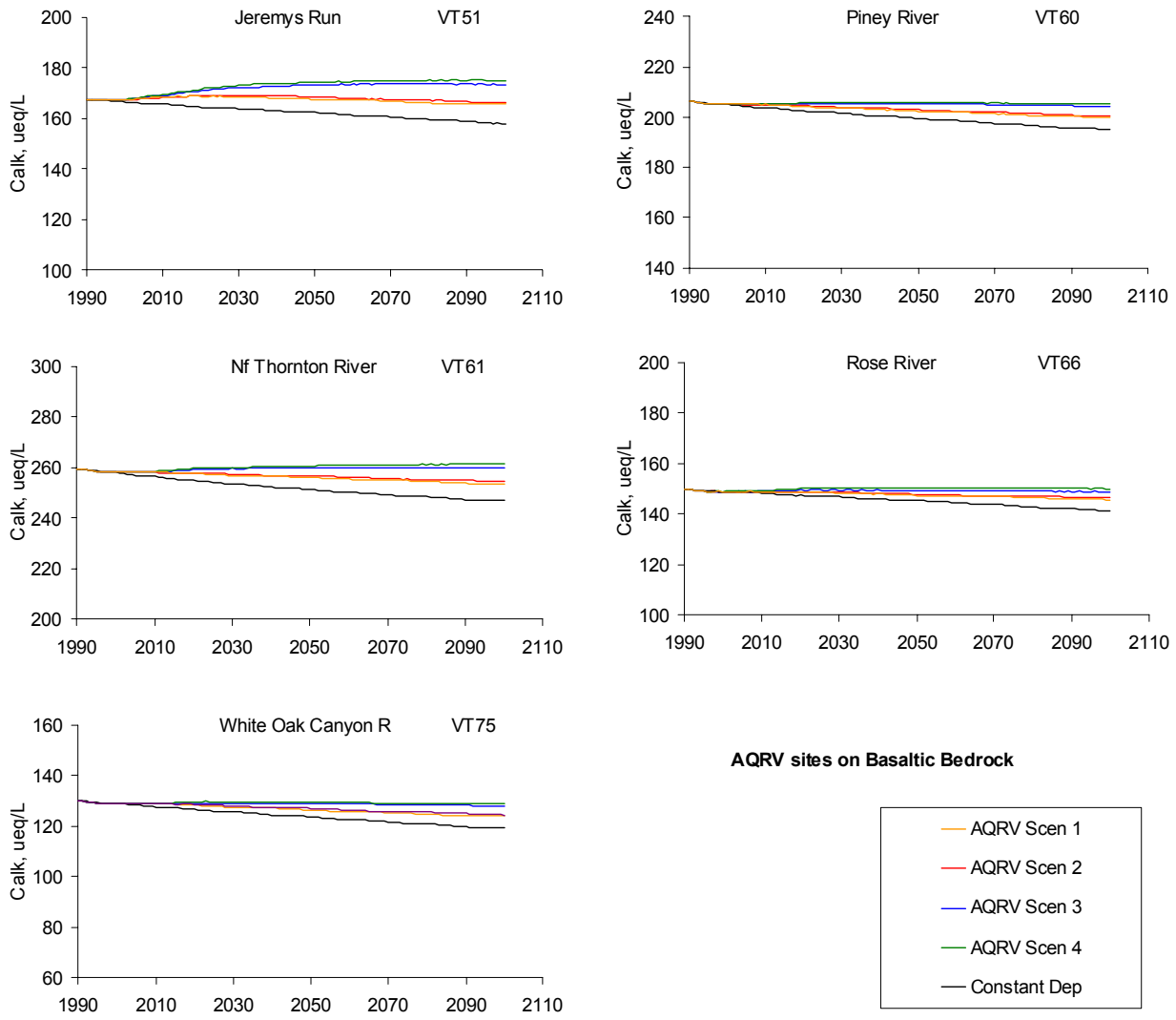

Figure VII-8c. MAGIC model projections of streamwater ANC under the scenario of constant deposition at 1990 levels and the four emissions control scenarios described in Section IV for modeled sites on basaltic bedrock. See model estimates of pre-industrial ANC in Table VII-8.

Table VII-8. ANC (ueq/L) in streams within SHEN derived from MAGIC simulations for the past (in response to historical deposition), the present, and for selected years in the future (in response to simulated constant deposition at 1990 levels and the four emissions control scenarios).

Site[a]	Scenario	Past	Year					
			1990	2000	2010	2020	2040	2100
Sites on Siliciclastic Bedrock								
DR01	Constant	78.5	2.1	-2.9	-6.6	-9.5	-13.3	-19.9
	1	78.5	2.1	2.0	5.8	9.1	12.4	13.2
	2	78.5	2.1	1.9	5.0	8.9	13.9	16.5
	3	78.5	2.1	2.3	8.9	18.0	30.9	43.2
	4	78.5	2.1	2.4	9.6	19.7	33.9	47.9
VT35 (PAIN)	Constant	90.7	6.8	4.5	2.8	1.4	-1.0	-6.3
	1	90.7	6.8	11.5	19.2	23.7	27.0	26.6
	2	90.7	6.8	11.3	18.1	24.0	29.4	30.3
	3	90.7	6.8	12.0	23.2	35.4	48.9	58.0
	4	90.7	6.8	12.1	24.3	37.6	52.4	63.2
VT36	Constant	69.0	-0.2	-4.5	-7.6	-10.1	-13.7	-19.0
	1	69.0	-0.2	-0.2	2.9	5.7	8.6	10.3
	2	69.0	-0.2	-0.3	2.2	5.4	9.9	13.1
	3	69.0	-0.2	0.0	5.6	13.5	25.1	37.4
	4	69.0	-0.2	0.1	6.2	15.0	27.8	41.6
VT53	Constant	81.1	15.7	11.1	7.5	4.8	0.8	-6.6
	1	81.1	15.7	14.9	18.3	20.9	23.5	24.0
	2	81.1	15.7	14.9	17.6	20.9	25.0	27.0
	3	81.1	15.7	15.2	20.8	28.6	39.6	50.0
	4	81.1	15.7	15.3	21.5	30.1	42.2	54.1
WOR1	Constant	65.5	25.6	19.4	13.2	7.0	-4.8	-30.5
	1	65.5	25.6	21.2	19.3	17.0	12.8	2.7
	2	65.5	25.6	21.1	18.8	17.6	14.4	6.6
	3	65.5	25.6	21.3	20.3	21.7	23.7	26.9
	4	65.5	25.6	21.3	20.7	22.7	25.7	30.7
Sites on Granitic Bedrock								
NFDR	Constant	81.6	58.5	55.3	52.3	49.5	43.3	16.5
	1	81.6	58.5	56.5	56.5	55.7	53.7	46.4
	2	81.6	58.5	56.5	56.1	56.0	54.6	48.5
	3	81.6	58.5	56.6	56.9	58.0	58.8	57.8
	4	81.6	58.5	56.7	57.2	58.6	59.8	60.0
VT58	Constant	97.6	87.7	85.8	83.0	80.8	76.9	64.1
	1	97.6	87.7	86.2	85.1	83.6	80.8	73.6
	2	97.6	87.7	86.3	84.9	83.8	81.1	74.6
	3	97.6	87.7	86.3	85.4	85.1	84.6	83.2
	4	97.6	87.7	86.3	85.5	85.5	85.2	84.5

Table VII-8. Continued.

Site[a]	Scenario	Past	Year					
			1990	2000	2010	2020	2040	2100
VT59 (STAN)	Constant	96.0	88.7	87.4	86.2	85.2	83.1	76.6
	1	96.0	88.7	87.7	86.9	86.2	85.1	81.7
	2	96.0	88.7	87.7	86.8	86.2	85.1	82.0
	3	96.0	88.7	87.8	87.1	86.9	86.6	86.0
	4	96.0	88.7	87.7	87.2	87.1	87.1	86.8
VT62	Constant	115.6	102.4	100.3	98.4	96.3	91.8	77.4
	1	115.6	102.4	100.7	99.7	98.6	96.0	88.6
	2	115.6	102.4	100.6	99.6	98.7	96.4	89.6
	3	115.6	102.4	100.7	99.9	99.5	98.9	97.3
	4	115.6	102.4	100.7	100.0	99.8	99.5	98.3
Sites on Basaltic Bedrock								
VT51	Constant	191.0	167.7	166.6	165.5	164.6	163.1	157.9
	1	191.0	167.7	167.7	168.6	168.9	168.3	165.5
	2	191.0	167.7	167.7	168.5	168.9	169.0	166.4
	3	191.0	167.7	167.8	169.3	171.3	173.2	173.6
	4	191.0	167.7	168.0	169.7	171.7	174.0	175.1
VT60 (PINE)	Constant	218.3	206.3	204.9	203.6	202.5	200.4	194.9
	1	218.3	206.3	205.3	205.1	204.4	203.2	200.0
	2	218.3	206.3	205.3	205.0	204.9	203.7	200.8
	3	218.3	206.3	205.4	205.3	205.7	205.6	204.8
	4	218.3	206.3	205.3	205.5	206.1	206.2	205.6
VT61	Constant	276.9	259.4	257.8	256.2	254.7	252.3	246.7
	1	276.9	259.4	258.4	258.3	257.7	256.7	253.6
	2	276.9	259.4	258.3	258.0	258.0	257.2	254.7
	3	276.9	259.4	258.5	258.6	259.3	259.8	260.1
	4	276.9	259.4	258.5	258.8	259.7	260.5	261.3
VT66	Constant	159.4	149.8	148.9	148.1	147.4	145.9	141.1
	1	159.4	149.8	149.2	149.2	148.7	148.0	145.9
	2	159.4	149.8	149.2	149.0	149.1	148.4	146.6
	3	159.4	149.8	149.2	149.3	149.7	149.7	149.3
	4	159.4	149.8	149.2	149.3	150.2	150.3	150.0
VT75	Constant	143.0	130.1	128.9	127.8	126.7	124.6	119.1
	1	143.0	130.1	129.2	129.2	128.6	127.4	124.2
	2	143.0	130.1	129.2	129.0	129.0	127.9	125.0
	3	143.0	130.1	129.2	129.3	129.6	129.3	128.5
	4	143.0	130.1	129.3	129.4	130.0	129.8	129.3

[a] For stream names, see Table VI-2.

Table VII-9. pH in streams within SHEN derived from MAGIC simulations for the past (in response to historical emissions), the present, and for selected years in the future (in response to simulated constant deposition at 1990 levels and the four emissions control scenarios).

Site	Scenario	Past	Year					
			1990	2000	2010	2020	2040	2100
Sites on Siliciclastic Bedrock								
DR01	Constant	7.1	5.4	5.1	5.0	4.9	4.9	4.8
	1	7.1	5.4	5.4	5.6	5.8	6.0	6.1
	2	7.1	5.4	5.4	5.6	5.8	6.1	6.2
	3	7.1	5.4	5.4	5.8	6.2	6.6	6.8
	4	7.1	5.4	5.4	5.9	6.3	6.6	6.8
VT35 (PAIN)	Constant	7.1	5.7	5.6	5.4	5.4	5.2	5.0
	1	7.1	5.7	6.0	6.3	6.4	6.5	6.5
	2	7.1	5.7	6.0	6.2	6.4	6.5	6.6
	3	7.1	5.7	6.0	6.4	6.6	6.8	6.9
	4	7.1	5.7	6.0	6.4	6.7	6.8	6.9
VT36	Constant	7.0	5.3	5.1	5.0	4.9	4.9	4.8
	1	7.0	5.3	5.3	5.5	5.6	5.8	5.9
	2	7.0	5.3	5.3	5.4	5.6	5.9	6.0
	3	7.0	5.3	5.3	5.6	6.1	6.4	6.7
	4	7.0	5.3	5.3	5.7	6.1	6.5	6.7
VT53	Constant	7.1	6.2	5.9	5.7	5.6	5.3	5.0
	1	7.1	6.2	6.1	6.3	6.3	6.4	6.4
	2	7.1	6.2	6.1	6.2	6.3	6.4	6.5
	3	7.1	6.2	6.1	6.3	6.5	6.7	6.8
	4	7.1	6.2	6.1	6.4	6.6	6.7	6.9
WOR1	Constant	7.0	6.5	6.3	6.1	5.7	5.1	4.7
	1	7.0	6.5	6.3	6.3	6.2	6.0	5.4
	2	7.0	6.5	6.3	6.3	6.2	6.1	5.7
	3	7.0	6.5	6.3	6.3	6.4	6.4	6.5
	4	7.0	6.5	6.3	6.3	6.4	6.5	6.6
Sites on Granitic Bedrock								
NFDR	Constant	7.1	6.9	6.9	6.8	6.8	6.7	6.2
	1	7.1	6.9	6.9	6.9	6.9	6.9	6.8
	2	7.1	6.9	6.9	6.9	6.9	6.9	6.8
	3	7.1	6.9	6.9	6.9	6.9	6.9	6.9
	4	7.1	6.9	6.9	6.9	6.9	6.9	6.9
VT58	Constant	7.2	7.1	7.1	7.1	7.1	7.0	6.9
	1	7.2	7.1	7.1	7.1	7.1	7.1	7.0
	2	7.2	7.1	7.1	7.1	7.1	7.1	7.0
	3	7.2	7.1	7.1	7.1	7.1	7.1	7.1
	4	7.2	7.1	7.1	7.1	7.1	7.1	7.1

Table VII-9. Continued.

Site	Scenario	Past	Year 1990	2000	2010	2020	2040	2100
VT59 (STAN)	Constant	7.1	7.1	7.1	7.1	7.1	7.1	7.0
	1	7.1	7.1	7.1	7.1	7.1	7.1	7.1
	2	7.1	7.1	7.1	7.1	7.1	7.1	7.1
	3	7.1	7.1	7.1	7.1	7.1	7.1	7.1
	4	7.1	7.1	7.1	7.1	7.1	7.1	7.1
VT62	Constant	7.2	7.2	7.2	7.2	7.1	7.1	7.0
	1	7.2	7.2	7.2	7.2	7.2	7.1	7.1
	2	7.2	7.2	7.2	7.2	7.2	7.1	7.1
	3	7.2	7.2	7.2	7.2	7.2	7.2	7.2
	4	7.2	7.2	7.2	7.2	7.2	7.2	7.2
Sites on Basaltic Bedrock								
VT51	Constant	7.5	7.4	7.4	7.4	7.4	7.4	7.4
	1	7.5	7.4	7.4	7.4	7.4	7.4	7.4
	2	7.5	7.4	7.4	7.4	7.4	7.4	7.4
	3	7.5	7.4	7.4	7.4	7.4	7.4	7.4
	4	7.5	7.4	7.4	7.4	7.4	7.4	7.4
VT60 (PINE)	Constant	7.5	7.5	7.5	7.5	7.5	7.5	7.5
	1	7.5	7.5	7.5	7.5	7.5	7.5	7.5
	2	7.5	7.5	7.5	7.5	7.5	7.5	7.5
	3	7.5	7.5	7.5	7.5	7.5	7.5	7.5
	4	7.5	7.5	7.5	7.5	7.5	7.5	7.5
VT61	Constant	7.6	7.6	7.6	7.6	7.6	7.6	7.6
	1	7.6	7.6	7.6	7.6	7.6	7.6	7.6
	2	7.6	7.6	7.6	7.6	7.6	7.6	7.6
	3	7.6	7.6	7.6	7.6	7.6	7.6	7.6
	4	7.6	7.6	7.6	7.6	7.6	7.6	7.6
VT66	Constant	7.4	7.4	7.3	7.3	7.3	7.3	7.3
	1	7.4	7.4	7.3	7.3	7.3	7.3	7.3
	2	7.4	7.4	7.3	7.3	7.3	7.3	7.3
	3	7.4	7.4	7.3	7.3	7.4	7.4	7.3
	4	7.4	7.4	7.3	7.3	7.4	7.4	7.4
VT75	Constant	7.3	7.3	7.3	7.3	7.3	7.3	7.2
	1	7.3	7.3	7.3	7.3	7.3	7.3	7.3
	2	7.3	7.3	7.3	7.3	7.3	7.3	7.3
	3	7.3	7.3	7.3	7.3	7.3	7.3	7.3
	4	7.3	7.3	7.3	7.3	7.3	7.3	7.3

[a] For stream names, see Table VI-2.

of the siliciclastic type within SHEN would be expected to be in the range of about 5 to 10 μeq/L, such as have been observed for Paine Run, White Oak Run, and Deep Run (Figure VI-18). In contrast, streams on granitic and basaltic bedrock are expected to continue to exhibit

somewhat larger episodic ANC depressions, such as the 20 to 30 μeq/L depressions found for Staunton River and North Fork Dry Run, and the greater than 40 μeq/L depressions found for Piney River (Figure VI-18). Such episodes are most likely to be accompanied by adverse biological effects in streams in which episodic ANC falls near or below zero.

d. Implications for Aquatic Biota

The projected changes in streamwater ANC and pH in response to future (or past) deposition that were summarized in the last section can be used to project expected changes in fish communities in SHEN streams. There are four measures of biological response that can be estimated and that provide information about the community, population and individual responses of fish in SHEN streams. The projected changes in stream ANC (Table VII-8) can be used to estimate: 1) the number of species expected in each stream (using the relationship between ANC and species richness described in Figure VI-16); and 2) the status of the brook trout fishery in each stream (using the relationship between ANC categories and brook trout responses described in Table VI-9). In addition, the projected changes in streamwater pH (Table VII-9) can be used to estimate: 3) the expected condition factor of the more acid-sensitive blacknose dace in each stream (using the relationship between pH and condition factor described in Figure VI-17); and 4) the expected presence or absence of nine different species of fish in each stream (using the data in Table VI-8 which describe upper and lower pH thresholds for loss of each species).

Each of these four measures of biological response was separately estimated for each of the 14 SHEN streams modeled by MAGIC (Table VI-4). In addition, each of the biological responses in each of the streams was estimated for each of the four future emissions controls scenarios discussed in Sections IV and V, as well as for the baseline case of no future change in deposition from the 1990 levels. Future biological responses are presented in tabular form for a number of years for each scenario, and are presented graphically and discussed for the year 2040.

As a means of assessing the relative importance and robustness of the projected future biological changes, each measure of biological response was also calculated for present and past conditions in each stream. The observed present conditions were compared to estimated present conditions as a measure of the precision and accuracy of the biological projections. This was

done by coupling the output of the geochemical model to the various empirical biological response models. The estimated past conditions provide a benchmark for assessing the efficacy of the future emissions control scenarios. We evaluated the extent to which fish communities, populations, or individuals in the streams might be expected to improve or to return to pre-acidification conditions in response to a given future deposition scenario.

Species Richness

A direct outcome of fish population loss as a result of acidification is a decline in species richness (the total number of species in a stream). This appears to be a highly predictable outcome of regional acidification, although the pattern and rate of species loss varies from region to region (see discussion in Section VI). A statistically robust relationship between the ANC of streamwater and fish species richness was found in SHEN as part of the Fish in Sensitive Habitats (FISH) project (Bulger et al. 1999). The numbers of fish species were compared among 13 SHEN streams spanning a range of ANC conditions. There was a highly significant ($p<0.0001$) relationship between stream ANC (during the seven-year period of record) and fish species richness among the 13 streams, such that the streams having the lowest ANC hosted the fewest species (Figure VI-16).

The linear relationship derived from the data in Figure VI-16 was used with the predicted streamwater ANC values (Table VII-8) to provide estimates of the expected number of fish species in each of the modeled streams for the past, present and future chemical conditions simulated for each stream with MAGIC. The coupled geochemical and biological model predictions were evaluated by comparing the predicted species richness in each of the 13 streams with the observed number of species that occur in each stream (Table II-1). The agreement between predicted and observed species numbers was good (Figure VII-9), with a root mean squared error (RMSE) in predicted number of species across the 13 streams of 1.2 species. The average error was 0.3 species, indicating that the coupled models are unbiased in their predictions. Model reconstructions of past species richness in the streams (Figure VII-10) suggested that historical loss of species has been greatest in the siliciclastic streams. The average number of species lost on the three bedrock types were estimated as: 1.6 species on siliciclastic bedrock; 0.4 species on granitic bedrock; and 0.4 species on basaltic bedrock. In the case of the siliciclastic streams, the projected past changes were much larger than the average error and RMSE of the coupled models, suggesting that the projections are reasonably robust.

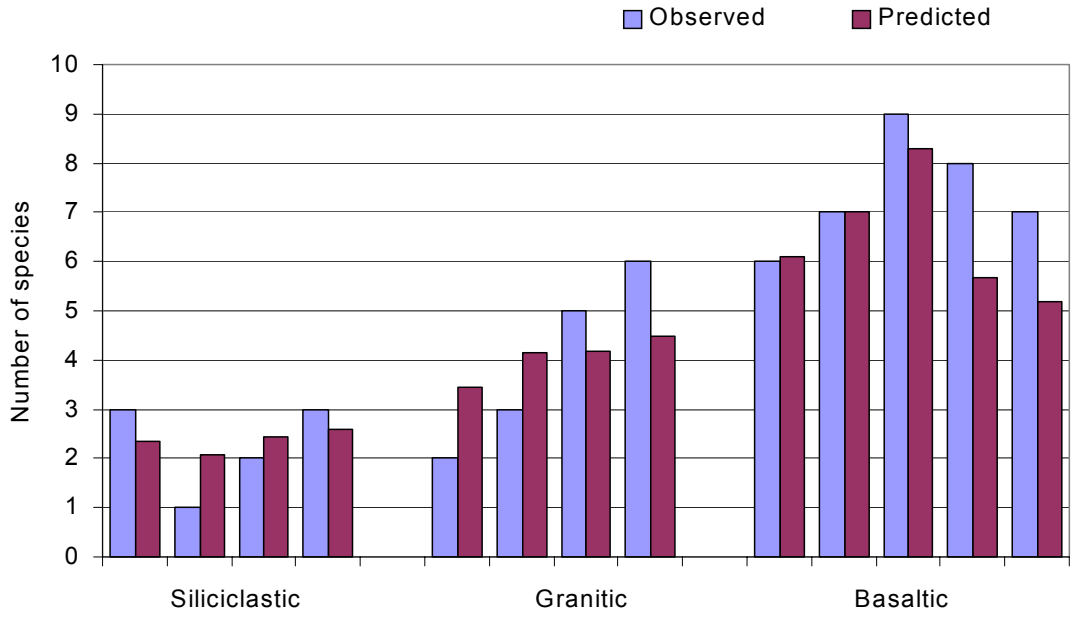

Figure VII-9. Predicted and observed number of fish species in 13 SHEN streams for the year 2000.

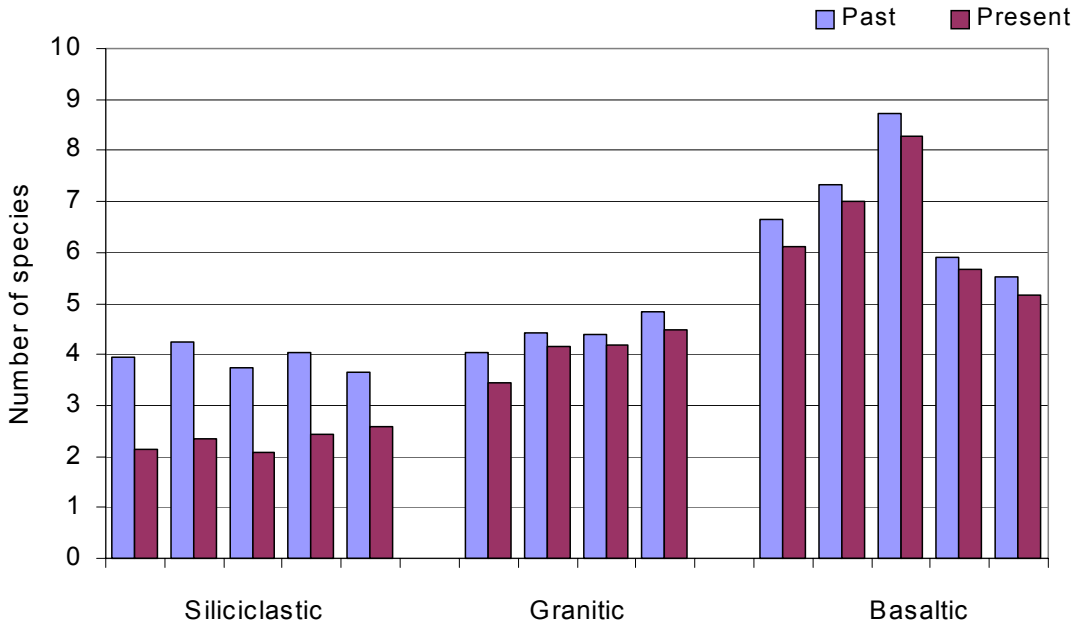

Figure VII-10. Projected number of fish species in 14 SHEN streams for past and present conditions.

The coupled geochemical and biological models were also used to predict expected changes in future numbers of species in each of the streams for selected years in each of the future deposition scenarios (Table VII-10). For all except the constant future deposition scenario, the models suggested that species richness will increase in the future, and that increases in species richness will be greatest in siliciclastic streams (Figure VII-11). The projected recovery of species richness, however, would not return these streams to their estimated past conditions (Figure VII-10) under any of the scenarios considered.

Table VII-10. Projected number of fish species in streams within SHEN estimated from simulations for the past in response to historical deposition and for the future in response to simulated constant deposition at 1990 levels and the four emissions control scenarios.

		Year						
Site[a]	**Scenario**	**Past**	**1990**	**2000**	**2010**	**2020**	**2040**	**2100**
Sites on Siliciclastic Bedrock								
DR01	Constant	4.0	2.1	2.0	1.9	1.8	1.8	1.6
	1	4.0	2.1	2.1	2.2	2.3	2.4	2.4
	2	4.0	2.1	2.1	2.2	2.3	2.4	2.5
	3	4.0	2.1	2.1	2.3	2.5	2.8	3.1
	4	4.0	2.1	2.1	2.3	2.5	2.9	3.2
VT35 (PAIN)	Constant	4.3	2.2	2.2	2.1	2.1	2.1	1.9
	1	4.3	2.2	2.4	2.5	2.6	2.7	2.7
	2	4.3	2.2	2.3	2.5	2.7	2.8	2.8
	3	4.3	2.2	2.4	2.6	2.9	3.2	3.5
	4	4.3	2.2	2.4	2.7	3.0	3.3	3.6
VT36	Constant	3.7	2.1	2.0	1.9	1.8	1.7	1.6
	1	3.7	2.1	2.1	2.1	2.2	2.3	2.3
	2	3.7	2.1	2.1	2.1	2.2	2.3	2.4
	3	3.7	2.1	2.1	2.2	2.4	2.7	3.0
	4	3.7	2.1	2.1	2.2	2.4	2.7	3.1
VT53	Constant	4.0	2.5	2.3	2.3	2.2	2.1	1.9
	1	4.0	2.5	2.4	2.5	2.6	2.6	2.7
	2	4.0	2.5	2.4	2.5	2.6	2.7	2.7
	3	4.0	2.5	2.4	2.6	2.8	3.0	3.3
	4	4.0	2.5	2.4	2.6	2.8	3.1	3.4
WOR1	Constant	3.6	2.7	2.5	2.4	2.2	2.0	1.3
	1	3.6	2.7	2.6	2.5	2.5	2.4	2.1
	2	3.6	2.7	2.6	2.5	2.5	2.4	2.2
	3	3.6	2.7	2.6	2.6	2.6	2.6	2.7
	4	3.6	2.7	2.6	2.6	2.6	2.7	2.8
Sites on Granitic Bedrock								
NFDR	Constant	4.0	3.5	3.4	3.3	3.3	3.1	2.5
	1	4.0	3.5	3.4	3.4	3.4	3.4	3.2
	2	4.0	3.5	3.4	3.4	3.4	3.4	3.2
	3	4.0	3.5	3.4	3.4	3.5	3.5	3.5
	4	4.0	3.5	3.4	3.4	3.5	3.5	3.5

Table VII-10. Continued.

Site	Scenario	Year						
		Past	**1990**	**2000**	**2010**	**2020**	**2040**	**2100**
VT58	Constant	4.4	4.2	4.1	4.1	4.0	3.9	3.6
	1	4.4	4.2	4.1	4.1	4.1	4.0	3.8
	2	4.4	4.2	4.1	4.1	4.1	4.0	3.9
	3	4.4	4.2	4.1	4.1	4.1	4.1	4.1
	4	4.4	4.2	4.1	4.1	4.1	4.1	4.1
VT59 (STAN)	Constant	4.4	4.2	4.2	4.1	4.1	4.1	3.9
	1	4.4	4.2	4.2	4.2	4.1	4.1	4.0
	2	4.4	4.2	4.2	4.2	4.1	4.1	4.0
	3	4.4	4.2	4.2	4.2	4.2	4.2	4.1
	4	4.4	4.2	4.2	4.2	4.2	4.2	4.2
VT62	Constant	4.8	4.5	4.5	4.4	4.4	4.3	3.9
	1	4.8	4.5	4.5	4.5	4.4	4.4	4.2
	2	4.8	4.5	4.5	4.5	4.4	4.4	4.2
	3	4.8	4.5	4.5	4.5	4.5	4.4	4.4
	4	4.8	4.5	4.5	4.5	4.5	4.5	4.4
Sites on Basaltic Bedrock								
VT51	Constant	6.7	6.1	6.1	6.0	6.0	6.0	5.9
	1	6.7	6.1	6.1	6.1	6.1	6.1	6.0
	2	6.7	6.1	6.1	6.1	6.1	6.1	6.1
	3	6.7	6.1	6.1	6.1	6.2	6.2	6.2
	4	6.7	6.1	6.1	6.1	6.2	6.3	6.3
VT60 (PINE)	Constant	7.3	7.0	7.0	7.0	6.9	6.9	6.8
	1	7.3	7.0	7.0	7.0	7.0	7.0	6.9
	2	7.3	7.0	7.0	7.0	7.0	7.0	6.9
	3	7.3	7.0	7.0	7.0	7.0	7.0	7.0
	4	7.3	7.0	7.0	7.0	7.0	7.0	7.0
VT61	Constant	8.7	8.3	8.3	8.2	8.2	8.1	8.0
	1	8.7	8.3	8.3	8.3	8.3	8.2	8.2
	2	8.7	8.3	8.3	8.3	8.3	8.2	8.2
	3	8.7	8.3	8.3	8.3	8.3	8.3	8.3
	4	8.7	8.3	8.3	8.3	8.3	8.3	8.3
VT66	Constant	5.9	5.7	5.7	5.6	5.6	5.6	5.5
	1	5.9	5.7	5.7	5.7	5.6	5.6	5.6
	2	5.9	5.7	5.7	5.7	5.7	5.6	5.6
	3	5.9	5.7	5.7	5.7	5.7	5.7	5.7
	4	5.9	5.7	5.7	5.7	5.7	5.7	5.7
VT75	Constant	5.5	5.2	5.2	5.1	5.1	5.1	4.9
	1	5.5	5.2	5.2	5.2	5.2	5.1	5.1
	2	5.5	5.2	5.2	5.2	5.2	5.1	5.1
	3	5.5	5.2	5.2	5.2	5.2	5.2	5.2
	4	5.5	5.2	5.2	5.2	5.2	5.2	5.2

[a] For stream names, see Table VI-2.

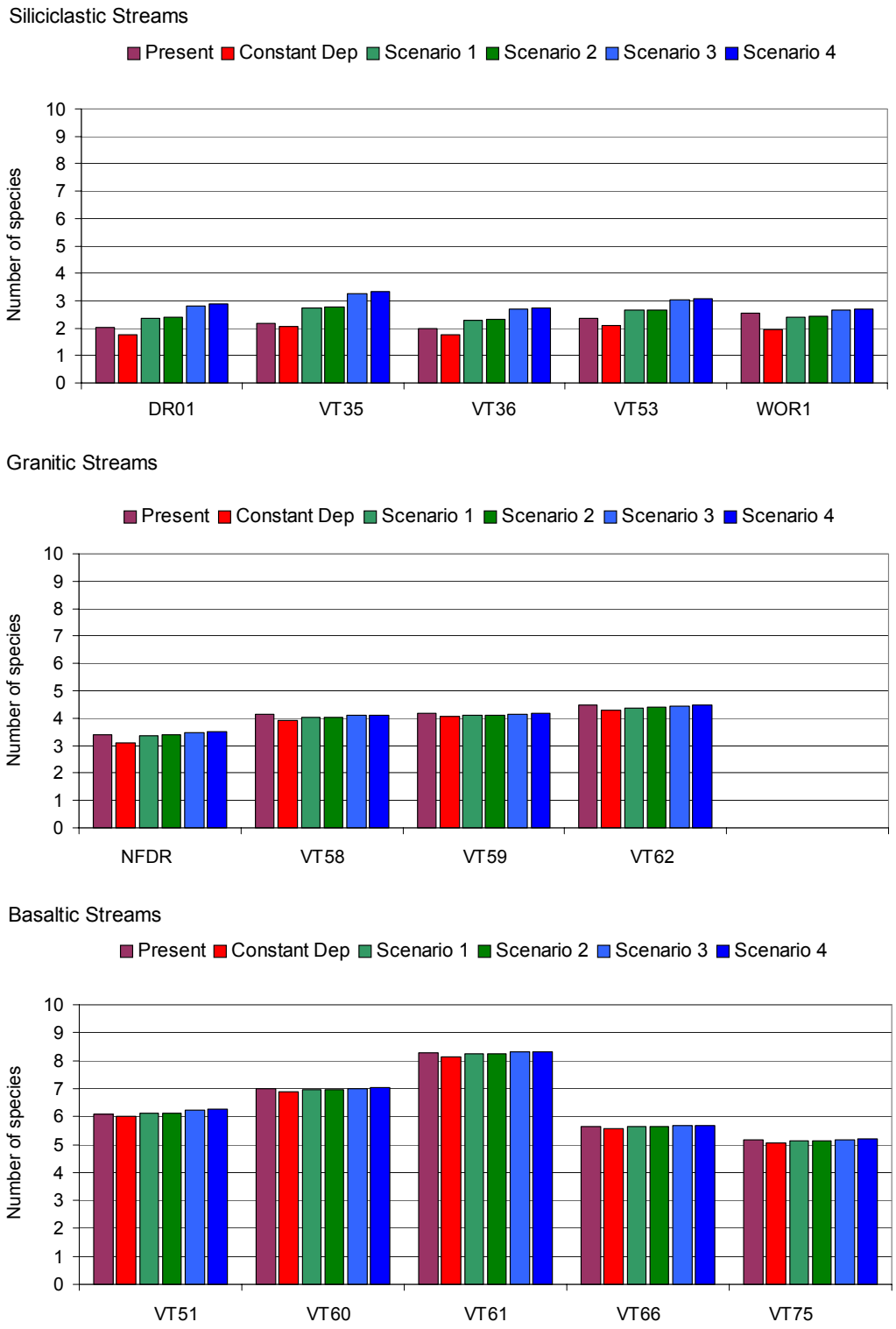

Figure VII-11. Projected number of fish species in 14 SHEN streams for the year 2040 in response to simulated constant deposition at 1990 levels and the four emissions control scenarios.

Brook Trout Status

ANC categories for brook trout response to acidification have been established for forested headwater catchments in western Virginia (Bulger et al., 2000; see Table VI-9). The ANC classes and brook trout status categories defined in Table VI-9 were used with the projected streamwater ANC values from Table VII-8 to provide estimates of the expected brook trout status in each of the modeled streams for the simulated past, present and future chemical conditions. The coupled geochemical and biological model projections were evaluated by comparing the observed brook trout status with the predicted brook trout status in each of the 13 streams, calculated from observed ANC values (Table VII-6). The agreement among categories was exact (Figure VII-12). As a further check, Table II-1 indicates that all modeled streams actually have brook trout present. The coupled models (and the observed ANC data) predicted that only one of the streams is currently unsuitable for brook trout, but the simulated ANC for that stream was only -1 ueq/L (observed = -2 ueq/L), just below the threshold for the unsuitable category.

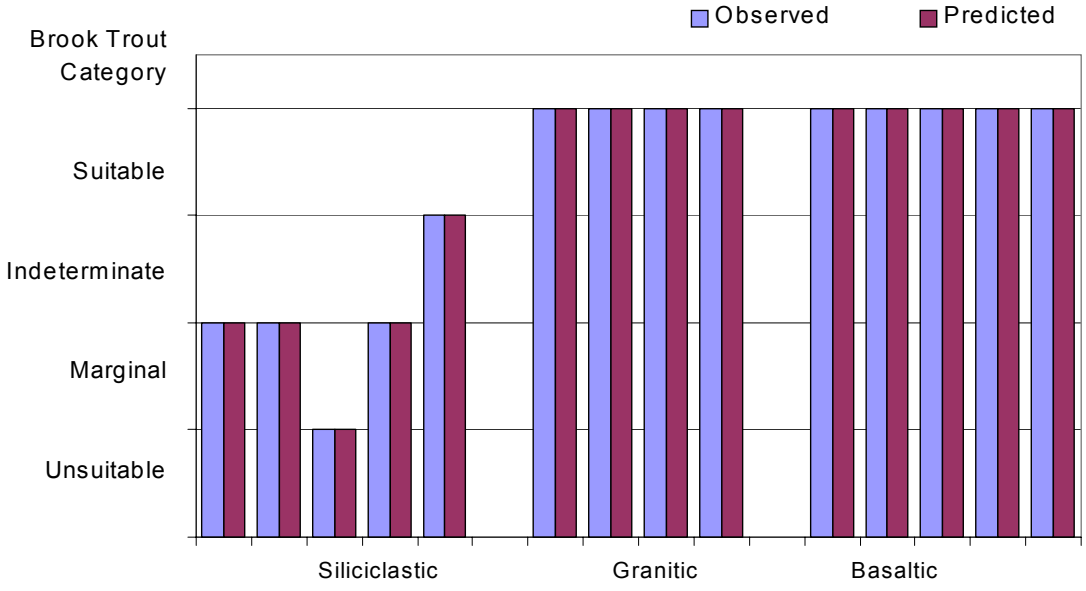

Figure VII-12. Predicted and observed brook trout categories in 14 SHEN streams for 1988-1992.

Model reconstructions of past brook trout status in the streams (Figure VII-13) suggested that all of the streams were suitable for brook trout in the past. The brook trout status has declined most in the siliciclastic streams. The brook trout status of streams draining granitic and basaltic catchments has not changed historically, even though the model suggests that these streams have lost ANC (Table VII-8).

The coupled geochemical and biological models were also used to predict the expected changes in brook trout status in each of the streams for selected years in each of the future deposition scenarios (Table VII-11). For all except the constant future deposition scenario, the models suggested that brook trout status will improve in all siliciclastic streams (Figure VII-14). The basaltic and granitic streams all showed increased ANC (Table VII-8) but no change in brook trout status because they are all already in the highest category (Figure VII-14).

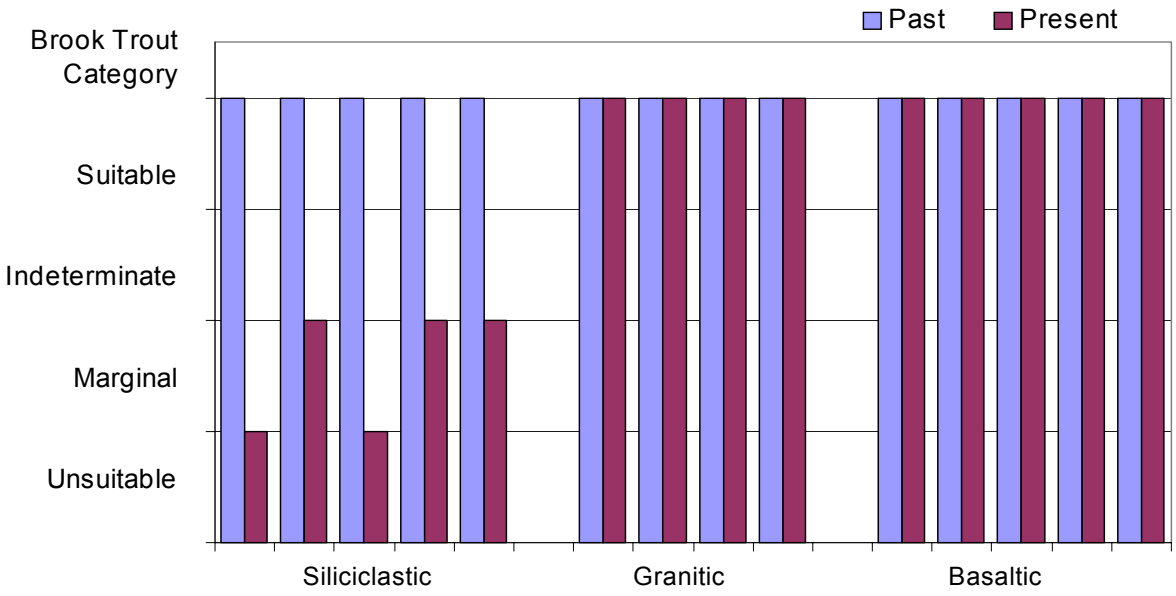

Figure VII-13. Projected brook trout categories in 14 SHEN streams for past and present (2000) conditions.

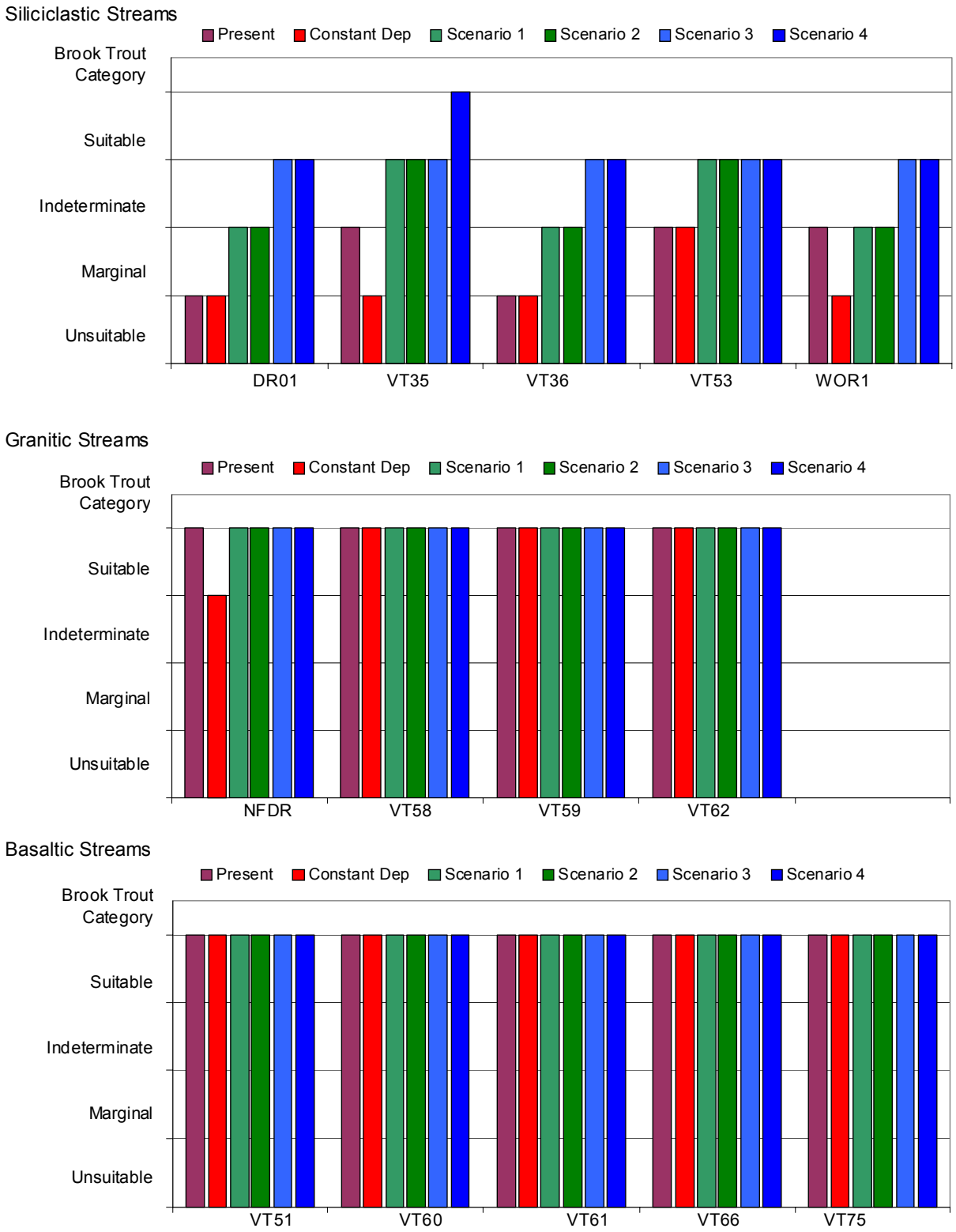

Figure VII-14. Projected brook trout categories in 14 SHEN streams for the year 2040 in response to simulated constant deposition at 1990 levels and the four emissions control scenarios.

Table VII-11. Projected brook trout categories in streams within SHEN estimated from simulations for the past in response to historical deposition and for the future in response to simulated constant deposition at 1990 levels and the four emissions control scenarios.

		Year						
Site[a]	**Scenario**	**Past**	**1990**	**2000**	**2010**	**2020**	**2040**	**2100**
Sites on Siliciclastic Bedrock								
DR01	Constant	Suitable	Marginal	Unsuitable	Unsuitable	Unsuitable	Unsuitable	Unsuitable
	1	Suitable	Marginal	Marginal	Marginal	Marginal	Marginal	Marginal
	2	Suitable	Marginal	Marginal	Marginal	Marginal	Marginal	Marginal
	3	Suitable	Marginal	Marginal	Marginal	Marginal	Indeterm	Indeterm
	4	Suitable	Marginal	Marginal	Marginal	Marginal	Indeterm	Indeterm
VT35 (PAIN)	Constant	Suitable	Marginal	Marginal	Marginal	Marginal	Unsuitable	Unsuitable
	1	Suitable	Marginal	Marginal	Marginal	Indeterm	Indeterm	Indeterm
	2	Suitable	Marginal	Marginal	Marginal	Indeterm	Indeterm	Indeterm
	3	Suitable	Marginal	Marginal	Indeterm	Indeterm	Indeterm	Suitable
	4	Suitable	Marginal	Marginal	Indeterm	Indeterm	Suitable	Suitable
VT36	Constant	Suitable	Unsuitable	Unsuitable	Unsuitable	Unsuitable	Unsuitable	Unsuitable
	1	Suitable	Unsuitable	Unsuitable	Marginal	Marginal	Marginal	Marginal
	2	Suitable	Unsuitable	Unsuitable	Marginal	Marginal	Marginal	Marginal
	3	Suitable	Unsuitable	Marginal	Marginal	Marginal	Indeterm	Indeterm
	4	Suitable	Unsuitable	Marginal	Marginal	Marginal	Indeterm	Indeterm
VT53	Constant	Suitable	Marginal	Marginal	Marginal	Marginal	Marginal	Unsuitable
	1	Suitable	Marginal	Marginal	Marginal	Indeterm	Indeterm	Indeterm
	2	Suitable	Marginal	Marginal	Marginal	Indeterm	Indeterm	Indeterm
	3	Suitable	Marginal	Marginal	Indeterm	Indeterm	Indeterm	Suitable
	4	Suitable	Marginal	Marginal	Indeterm	Indeterm	Indeterm	Suitable
WOR1	Constant	Suitable	Indeterm	Marginal	Marginal	Marginal	Unsuitable	Unsuitable
	1	Suitable	Indeterm	Indeterm	Marginal	Marginal	Marginal	Marginal
	2	Suitable	Indeterm	Indeterm	Marginal	Marginal	Marginal	Marginal
	3	Suitable	Indeterm	Indeterm	Indeterm	Indeterm	Indeterm	Indeterm
	4	Suitable	Indeterm	Indeterm	Indeterm	Indeterm	Indeterm	Indeterm
Sites on Granitic Bedrock								
NFDR	Constant	Suitable	Suitable	Suitable	Suitable	Indeterm	Indeterm	Marginal
	1	Suitable	Suitable	Suitable	Suitable	Suitable	Suitable	Indeterm
	2	Suitable	Suitable	Suitable	Suitable	Suitable	Suitable	Indeterm
	3	Suitable	Suitable	Suitable	Suitable	Suitable	Suitable	Suitable
	4	Suitable	Suitable	Suitable	Suitable	Suitable	Suitable	Suitable
VT58	Constant	Suitable	Suitable	Suitable	Suitable	Suitable	Suitable	Suitable
	1	Suitable	Suitable	Suitable	Suitable	Suitable	Suitable	Suitable
	2	Suitable	Suitable	Suitable	Suitable	Suitable	Suitable	Suitable
	3	Suitable	Suitable	Suitable	Suitable	Suitable	Suitable	Suitable
	4	Suitable	Suitable	Suitable	Suitable	Suitable	Suitable	Suitable
VT59 (STAN)	Constant	Suitable	Suitable	Suitable	Suitable	Suitable	Suitable	Suitable
	1	Suitable	Suitable	Suitable	Suitable	Suitable	Suitable	Suitable
	2	Suitable	Suitable	Suitable	Suitable	Suitable	Suitable	Suitable
	3	Suitable	Suitable	Suitable	Suitable	Suitable	Suitable	Suitable
	4	Suitable	Suitable	Suitable	Suitable	Suitable	Suitable	Suitable
VT62	Constant	Suitable	Suitable	Suitable	Suitable	Suitable	Suitable	Suitable
	1	Suitable	Suitable	Suitable	Suitable	Suitable	Suitable	Suitable
	2	Suitable	Suitable	Suitable	Suitable	Suitable	Suitable	Suitable
	3	Suitable	Suitable	Suitable	Suitable	Suitable	Suitable	Suitable
	4	Suitable	Suitable	Suitable	Suitable	Suitable	Suitable	Suitable

Table VII-11. Continued.

Site	Scenario	Year						
		Past	**1990**	**2000**	**2010**	**2020**	**2040**	**2100**
Sites on Basaltic Bedrock								
VT51	Constant	Suitable	Suitable	Suitable	Suitable	Suitable	Suitable	Suitable
	1	Suitable	Suitable	Suitable	Suitable	Suitable	Suitable	Suitable
	2	Suitable	Suitable	Suitable	Suitable	Suitable	Suitable	Suitable
	3	Suitable	Suitable	Suitable	Suitable	Suitable	Suitable	Suitable
	4	Suitable	Suitable	Suitable	Suitable	Suitable	Suitable	Suitable
VT60 (PINE)	Constant	Suitable	Suitable	Suitable	Suitable	Suitable	Suitable	Suitable
	1	Suitable	Suitable	Suitable	Suitable	Suitable	Suitable	Suitable
	2	Suitable	Suitable	Suitable	Suitable	Suitable	Suitable	Suitable
	3	Suitable	Suitable	Suitable	Suitable	Suitable	Suitable	Suitable
	4	Suitable	Suitable	Suitable	Suitable	Suitable	Suitable	Suitable
VT61	Constant	Suitable	Suitable	Suitable	Suitable	Suitable	Suitable	Suitable
	1	Suitable	Suitable	Suitable	Suitable	Suitable	Suitable	Suitable
	2	Suitable	Suitable	Suitable	Suitable	Suitable	Suitable	Suitable
	3	Suitable	Suitable	Suitable	Suitable	Suitable	Suitable	Suitable
	4	Suitable	Suitable	Suitable	Suitable	Suitable	Suitable	Suitable
VT66	Constant	Suitable	Suitable	Suitable	Suitable	Suitable	Suitable	Suitable
	1	Suitable	Suitable	Suitable	Suitable	Suitable	Suitable	Suitable
	2	Suitable	Suitable	Suitable	Suitable	Suitable	Suitable	Suitable
	3	Suitable	Suitable	Suitable	Suitable	Suitable	Suitable	Suitable
	4	Suitable	Suitable	Suitable	Suitable	Suitable	Suitable	Suitable
VT75	Constant	Suitable	Suitable	Suitable	Suitable	Suitable	Suitable	Suitable
	1	Suitable	Suitable	Suitable	Suitable	Suitable	Suitable	Suitable
	2	Suitable	Suitable	Suitable	Suitable	Suitable	Suitable	Suitable
	3	Suitable	Suitable	Suitable	Suitable	Suitable	Suitable	Suitable
	4	Suitable	Suitable	Suitable	Suitable	Suitable	Suitable	Suitable

[a] For stream names, see Table VI-2.

Blacknose Dace Condition Factor

As a measure of the non-lethal effects of acidification, Bulger et al. (1999) compared condition factor (a measure of robustness of individual fish) in populations of blacknose dace in 11 streams within SHEN spanning a range of pH/ANC conditions. They found (see Figure VI-17) a highly significant relationship between mean stream pH and condition factor in blacknose dace. The results of the condition factor comparisons among the 11 streams indicated that the mean length-adjusted condition factor of fish from the stream with the lowest ANC (and pH) was about 20% lower than that of the fish in best condition. Bulger et al. (1999) concluded that this lower condition factor was attributable to acid stress in the blacknose dace population of that stream, and more generally, that the range of condition factor for blacknose dace among the SHEN streams was a result of the range of observed streamwater pH.

The linear relationship derived from the data in Figure VI-17 was used with the predicted streamwater pH values (Table VII-9) to provide estimates of the expected condition factor of blacknose dace in each of the modeled streams for the past, present and future conditions simulated for the streams. The coupled geochemical and biological model projections were evaluated by comparing the predicted condition factor in each of the 13 streams with the presence or absence of blacknose dace in each stream (Table II-1) for the year 2000. There were no direct measurements of condition factor in the streams in 2000, so no direct evaluation could be made. The indirect comparison (Figure VII-15), however, showed that the stream with the lowest predicted condition factor for the year 2000 (condition factor < 8.0) did not support a population of blacknose dace. This suggests that the predicted condition factor may be a useful index of acid stress effects on blacknose dace populations in SHEN.

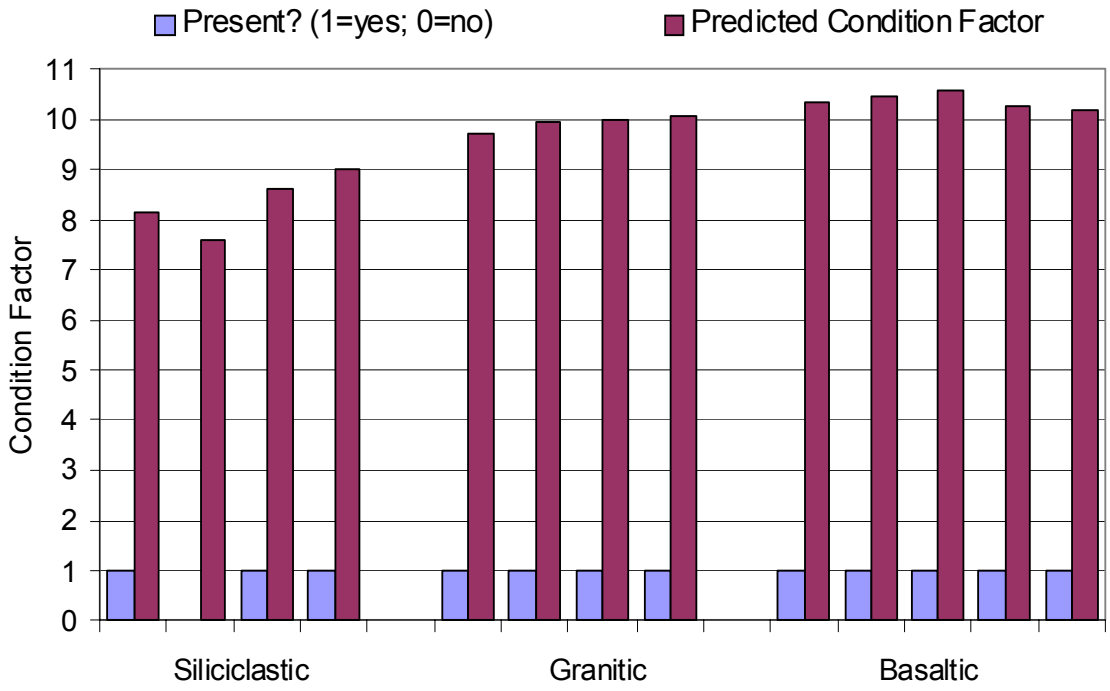

Figure VII-15. Projected condition factor for blacknose dace and observed presence/absence of blacknose dace in 13 SHEN streams for the year 2000.

Model reconstructions of past condition factor for blacknose dace in the streams (Figure VII-16) suggested that loss of condition factor (added acid stress) in blacknose dace populations has been greatest in the siliciclastic streams. Predictions of the expected changes in condition factor for blacknose dace in each of the streams for selected years in each of the future deposition scenarios (Table VII-12) showed that recovery of condition factor (reduction of acid stress) is expected in the siliciclastic streams for all future scenarios except constant deposition. The degree of recovery is greatest for Scenarios 3 and 4 (Figure VII-17).

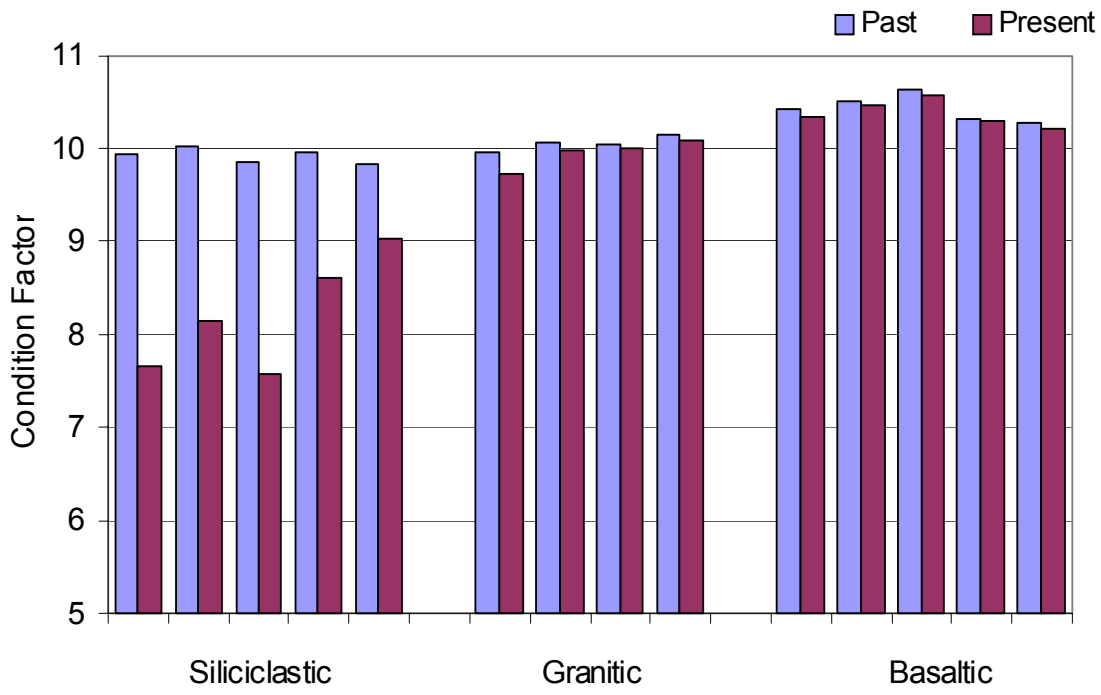

Figure VII-16. Projected condition factor for blacknose dace in 14 SHEN streams for past and present conditions.

Table VII-12. Projected condition factor for blacknose dace in streams within SHEN estimated from simulations for the past in response to historical deposition and for the future in response to simulated constant deposition at 1990 levels and the four emissions control scenarios.

		Year						
Site[a]	**Scenario**	**Past**	**1990**	**2000**	**2010**	**2020**	**2040**	**2100**
Sites on Siliciclastic Bedrock								
DR01	Constant	9.9	8.0	7.7	7.5	7.4	7.3	7.2
	1	9.9	8.0	8.0	8.3	8.5	8.7	8.7
	2	9.9	8.0	8.0	8.2	8.5	8.8	8.9
	3	9.9	8.0	8.0	8.5	9.0	9.4	9.6
	4	9.9	8.0	8.0	8.5	9.0	9.4	9.6
VT35 (PAIN)	Constant	10.0	8.3	8.1	8.0	7.9	7.8	7.5
	1	10.0	8.3	8.6	9.0	9.2	9.3	9.2
	2	10.0	8.3	8.6	9.0	9.2	9.3	9.3
	3	10.0	8.3	8.7	9.1	9.4	9.7	9.8
	4	10.0	8.3	8.7	9.2	9.5	9.7	9.8
VT36	Constant	9.9	7.8	7.6	7.5	7.4	7.3	7.2
	1	9.9	7.8	7.8	8.0	8.2	8.5	8.6
	2	9.9	7.8	7.8	8.0	8.2	8.5	8.7
	3	9.9	7.8	7.8	8.2	8.8	9.2	9.5
	4	9.9	7.8	7.8	8.3	8.8	9.3	9.6
VT53	Constant	9.9	8.9	8.6	8.4	8.2	7.9	7.5
	1	9.9	8.9	8.8	9.0	9.1	9.2	9.2
	2	9.9	8.9	8.8	8.9	9.1	9.2	9.3
	3	9.9	8.9	8.8	9.1	9.3	9.5	9.7
	4	9.9	8.9	8.9	9.1	9.3	9.6	9.7
WOR1	Constant	9.8	9.2	9.0	8.7	8.3	7.6	7.1
	1	9.8	9.2	9.1	9.0	8.9	8.7	8.0
	2	9.8	9.2	9.1	9.0	8.9	8.8	8.3
	3	9.8	9.2	9.1	9.1	9.1	9.2	9.3
	4	9.8	9.2	9.1	9.1	9.1	9.2	9.4
Sites on Granitic Bedrock								
NFDR	Constant	10.0	9.8	9.7	9.7	9.7	9.6	8.9
	1	10.0	9.8	9.7	9.7	9.7	9.7	9.6
	2	10.0	9.8	9.7	9.7	9.7	9.7	9.6
	3	10.0	9.8	9.7	9.7	9.7	9.8	9.7
	4	10.0	9.8	9.7	9.7	9.8	9.8	9.8
VT58	Constant	10.1	10.0	10.0	10.0	9.9	9.9	9.8
	1	10.1	10.0	10.0	10.0	10.0	9.9	9.9
	2	10.1	10.0	10.0	10.0	10.0	9.9	9.9
	3	10.1	10.0	10.0	10.0	10.0	10.0	10.0

Table VII-12. Continued.

Site	Scenario	Year						
		Past	**1990**	**2000**	**2010**	**2020**	**2040**	**2100**
	4	10.1	10.0	10.0	10.0	10.0	10.0	10.0
VT59 (STAN)	Constant	10.0	10.0	10.0	10.0	10.0	10.0	9.9
	1	10.0	10.0	10.0	10.0	10.0	10.0	9.9
	2	10.0	10.0	10.0	10.0	10.0	10.0	10.0
	3	10.0	10.0	10.0	10.0	10.0	10.0	10.0
	4	10.0	10.0	10.0	10.0	10.0	10.0	10.0
VT62	Constant	10.2	10.1	10.1	10.1	10.0	10.0	9.9
	1	10.2	10.1	10.1	10.1	10.1	10.0	10.0
	2	10.2	10.1	10.1	10.1	10.1	10.0	10.0
	3	10.2	10.1	10.1	10.1	10.1	10.1	10.1
	4	10.2	10.1	10.1	10.1	10.1	10.1	10.1
Sites on Basaltic Bedrock								
VT51	Constant	10.4	10.3	10.3	10.3	10.3	10.3	10.3
	1	10.4	10.3	10.3	10.4	10.4	10.4	10.3
	2	10.4	10.3	10.3	10.4	10.4	10.4	10.3
	3	10.4	10.3	10.3	10.4	10.4	10.4	10.4
	4	10.4	10.3	10.3	10.4	10.4	10.4	10.4
VT60 (PINE)	Constant	10.5	10.5	10.5	10.5	10.5	10.4	10.4
	1	10.5	10.5	10.5	10.5	10.5	10.5	10.4
	2	10.5	10.5	10.5	10.5	10.5	10.5	10.5
	3	10.5	10.5	10.5	10.5	10.5	10.5	10.5
	4	10.5	10.5	10.5	10.5	10.5	10.5	10.5
VT61	Constant	10.6	10.6	10.6	10.6	10.6	10.6	10.6
	1	10.6	10.6	10.6	10.6	10.6	10.6	10.6
	2	10.6	10.6	10.6	10.6	10.6	10.6	10.6
	3	10.6	10.6	10.6	10.6	10.6	10.6	10.6
	4	10.6	10.6	10.6	10.6	10.6	10.6	10.6
VT66	Constant	10.3	10.3	10.3	10.3	10.3	10.3	10.3
	1	10.3	10.3	10.3	10.3	10.3	10.3	10.3
	2	10.3	10.3	10.3	10.3	10.3	10.3	10.3
	3	10.3	10.3	10.3	10.3	10.3	10.3	10.3
	4	10.3	10.3	10.3	10.3	10.3	10.3	10.3
VT75	Constant	10.3	10.2	10.2	10.2	10.2	10.2	10.2
	1	10.3	10.2	10.2	10.2	10.2	10.2	10.2
	2	10.3	10.2	10.2	10.2	10.2	10.2	10.2
	3	10.3	10.2	10.2	10.2	10.2	10.2	10.2
	4	10.3	10.2	10.2	10.2	10.2	10.2	10.2

[a] For stream names, see Table VI-2.

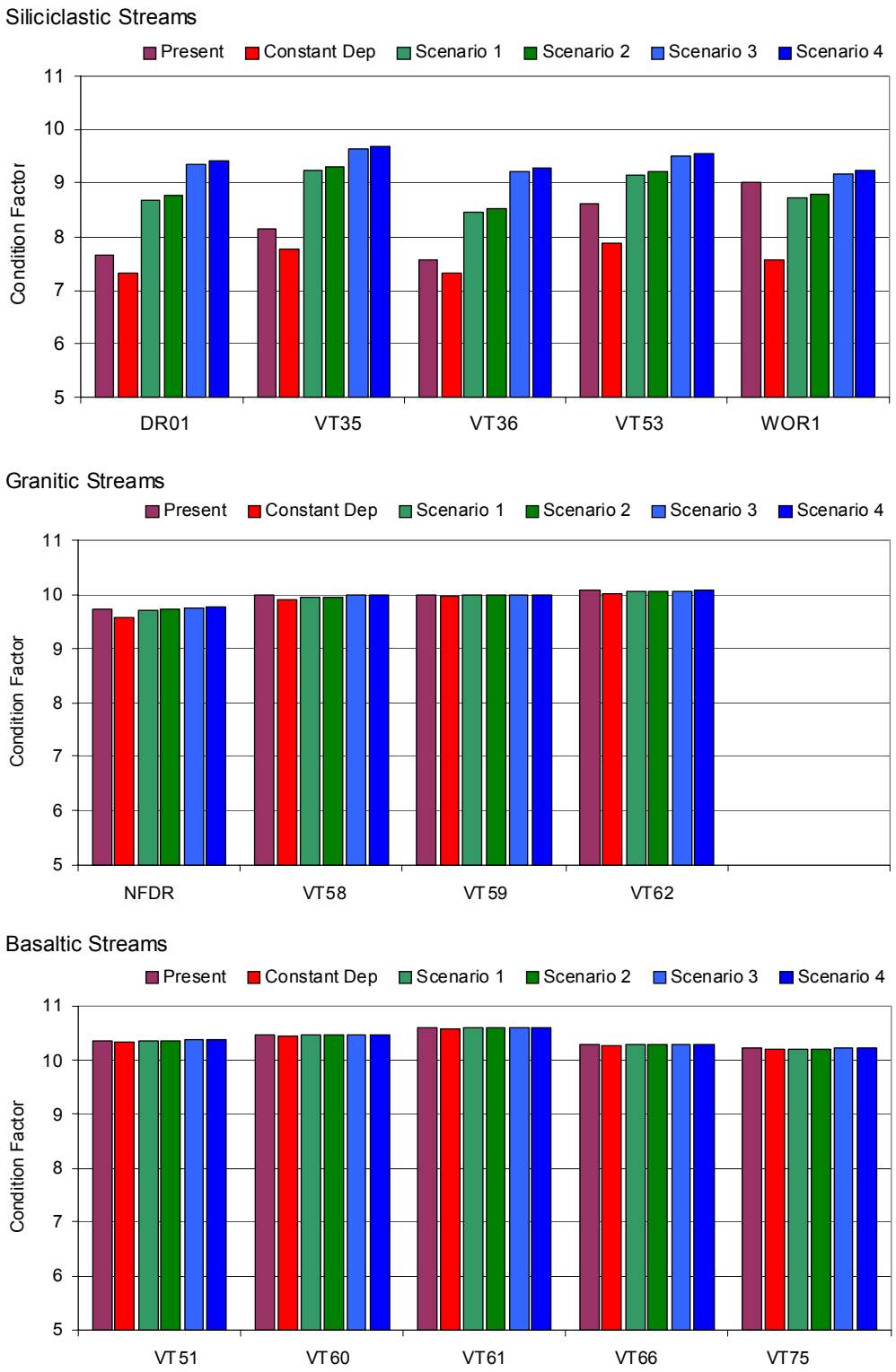

Figure VII-17. Projected condition factor for blacknose dace in 14 SHEN streams for the year 2040 in response to simulated constant deposition at 1990 levels and the four emissions control scenarios.

Species Presence/Absence

Although there are known differences in acid sensitivity among fish species, experimentally determined acid sensitivities are available for only a minority of freshwater fish species. For example, of 28 species of fish commonly found in SHEN, the critical pH range is known for only nine (see Table VI-8 and associated discussion). Critical pH can be defined as the threshold for significant adverse effects on fish populations. In general, there is no single pH threshold for a given species. Table VI-8 reports a range of pH values which represent the various investigators' estimates of uncertainty of this critical pH for any species. The range of response within species depends in part on differences in sensitivity among life stages, and on different exposure concentrations of calcium (Ca^{2+}) and Al. These ranges of critical pH can be used to predict the potential presence or absence of these species in a stream, given the streamwater pH.

In this section, we combine the pH ranges presented in Table VI-8 with predicted streamwater pH values (Table VII-9) to provide estimates of the expected presence or absence of nine fish species in each of the modeled streams for the past, present and future conditions simulated for the streams. The projections presented here concerning presence/absence ignore whether or not other habitat factors are suitable (temperature, food sources, etc.). As such, these projections are useful *only* as an *index*. This index allows the question to be asked "If other habitat factors are suitable, would the acid/base status of the streamwater (pH) be suitable for the presence of this species of fish in this stream?" When calculating the presence/absence, the range of critical pH values in Table VI-8 was explicitly considered by establishing three categories of prediction: 1) *suitable conditions* mean that the predicted pH was above the upper pH threshold for that species; 2) *marginal conditions* mean that predicted pH was between the upper and lower thresholds; and 3) *unsuitable conditions* for a species means that the predicted pH was below the lower threshold of the pH range.

The coupled geochemical and biological model projections were evaluated by comparing the predicted presence/absence of each species with observed presence/absence data (Table II-1). As can be seen (Figure VII-18), for the species considered in these predictions only four of the nine species actually appear in any the 14 modeled streams, regardless of the predicted pH. This re-emphasizes the use of this metric of biological response as an *index* of potential biological suitability for these streams. Lack of observed presence of many of the species may be due to inadequacy of habitat variables other than pH.

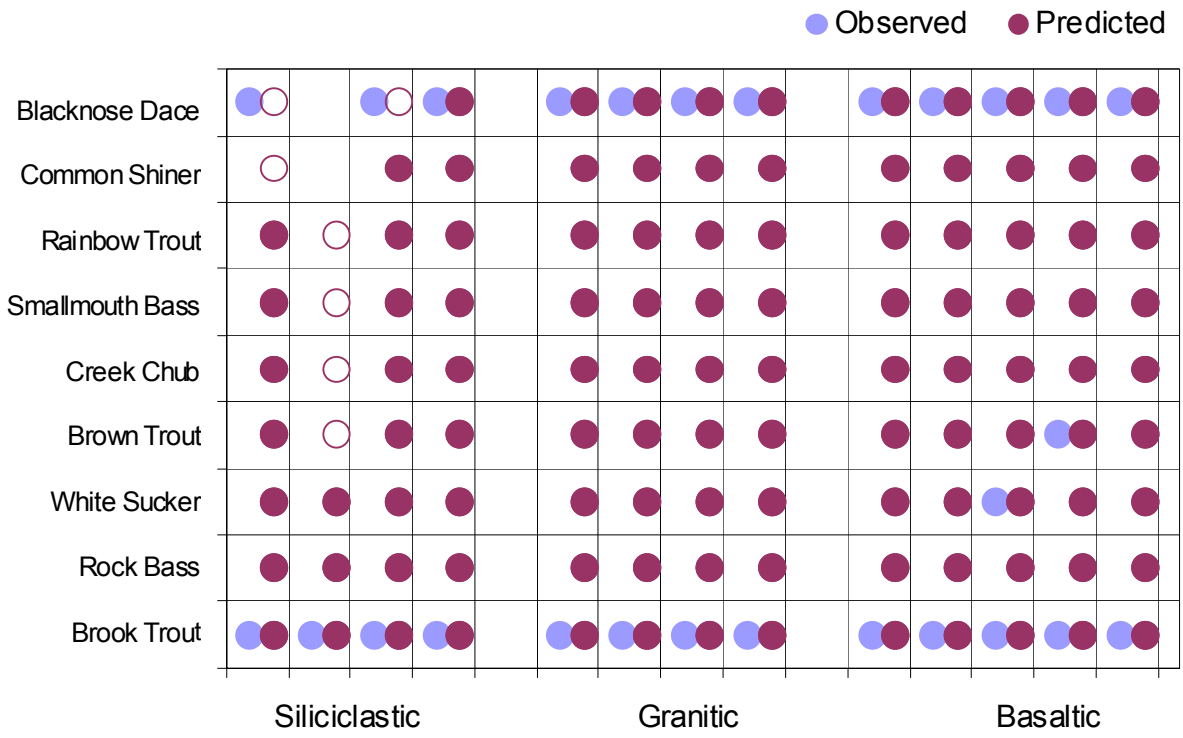

Figure VII-18. Projected suitability of streamwater pH for, and observed presence/absence of, nine fish species in 13 SHEN streams for the year 2000. For the projections (right side of each column), solid symbols indicate that streamwater pH is suitable; open symbols indicate that streamwater pH is marginal; no symbol indicates that streamwater pH is unsuitable. For the observations (left side of each column), presence is indicated by a solid symbol and absence is indicated by no symbol.

Model reconstructions of the past for these nine species (Figure VII-19) suggested that past streamwater pH should have produced suitable conditions for all species in all streams, and the decrease in suitability (both in terms of number of streams and number of species) has been greatest in the siliciclastic streams. Projections of the expected future presence/absence of the nine species in each of the streams for a selected year in each of the future deposition scenarios (Figure VII-20) showed that recovery of marginal or suitable conditions for all nine species in all streams is expected for all future scenarios except constant deposition.

Discussion of Biological Modeling Results

In order to make the projections described above of likely past and future responses of aquatic biota to changing deposition in SHEN, the geochemical model MAGIC was coupled

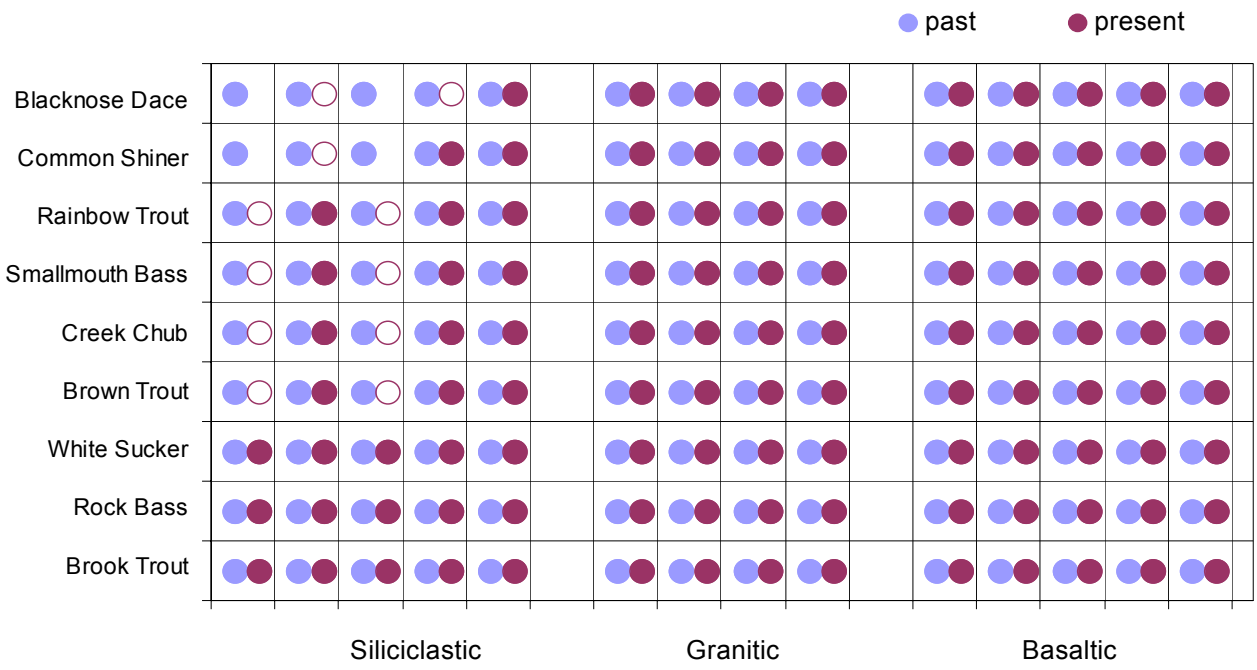

Figure VII-19. Projected suitability of streamwater pH for nine fish species in 14 SHEN streams for past (left side of column) and present (right side of column) conditions. Solid symbols indicate that streamwater pH is suitable; open symbols indicate that streamwater pH is marginal; no symbol indicates that streamwater pH is unsuitable.

with several empirical relationships which link biological response to water quality. The coupling of these models is straightforward from a procedural point of view. The interpretation and utility of the results, however, require consideration of a number of points that arise because of the different nature of the models that were coupled.

Unlike MAGIC which is a process-based model, the biological effects estimates are based on observed empirical relationships rooted in correlation and expressed as linear relationships. Correlation does not necessarily imply causality, but an observed pattern of co-variation between variables does provide a quantitative context for extrapolation. In this case, the projections being made do not require extrapolation beyond the observed ranges of observations, and therefore the projections are statistically robust. To the extent that the observed empirical relationships used in the coupled models do in fact reflect the effects of acid stress on aquatic biota, the projections are also biologically robust.

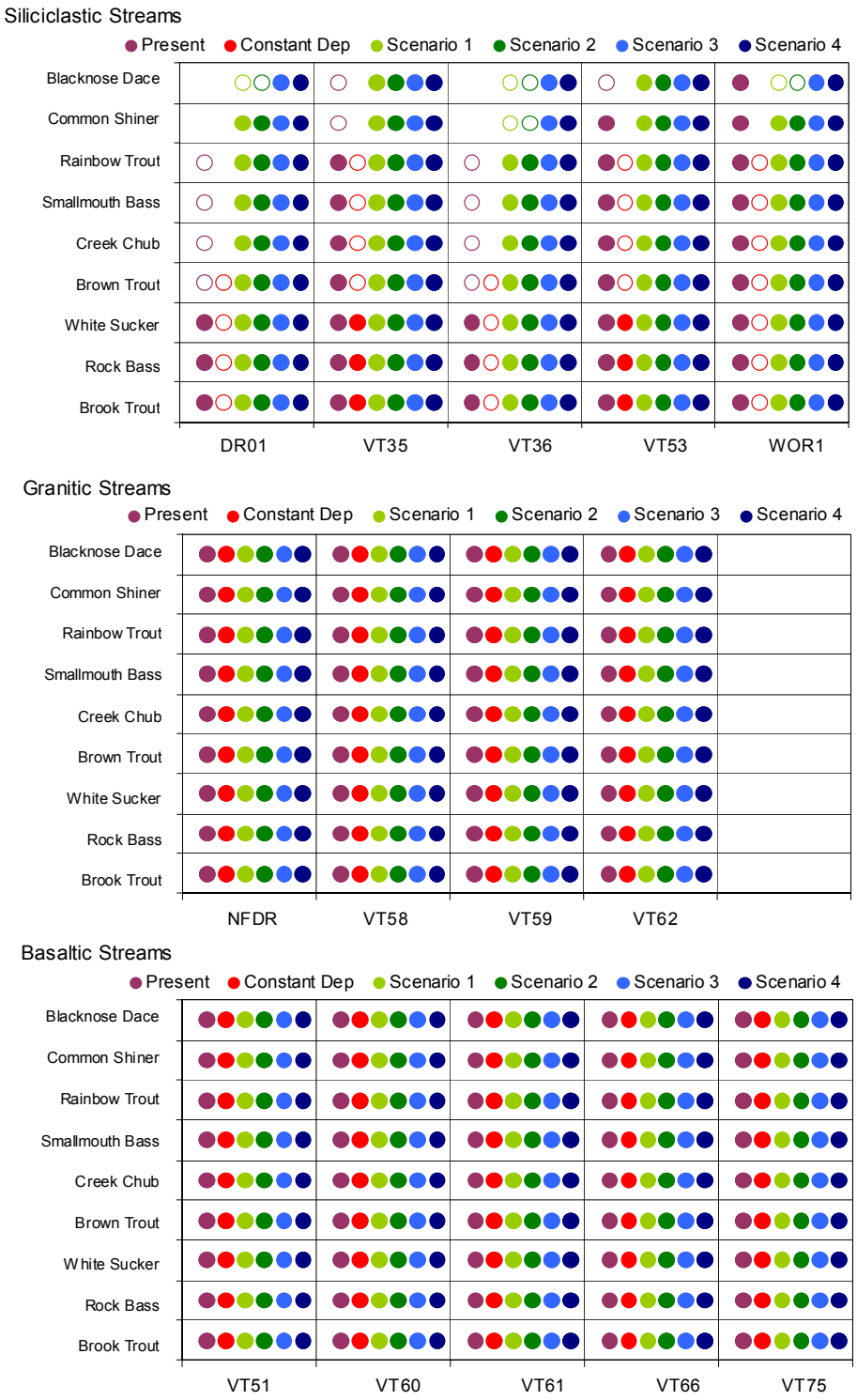

Figure VII-20. Projected suitability of streamwater pH for nine fish species in 14 SHEN streams for the year 2040 in response to simulated constant deposition at 1990 levels and the four emissions control scenarios. Solid symbols indicate that streamwater pH is suitable; open symbols indicate that streamwater pH is marginal; no symbol indicates that streamwater pH is unsuitable.

Besides the distinction between process-based and empirical models, the geochemical and biological response models differ in another way. MAGIC is a dynamic model and explicitly predicts the time-course of changing water quality. The empirical relationships used for the biological response models, however, are static. These relationships reflect a point in time (when the observations were made) and provide no information concerning the *dynamics* of biological response. That is, the empirical models predict a new biological status for a new water chemistry, but give no indication of the time required to achieve the biological status once the water quality change has occurred.

There are thus two considerations that must be kept in mind when interpreting the biological responses predicted in this section: the causality of the relationship between water quality and response, and the dynamics of biological response. With respect to the issue of causality, acidification is a disturbance, and disturbance always lowers species richness. Loss of species usually lowers productivity and stability of ecosystems. Fish biodiversity loss is a predictable and proven consequence of acidification, and there are abundant examples of this in North America and Europe (c.f., Bulger et al. 2000). Continued fish biodiversity loss is not sustainable, and carries significant ecological and economic costs.

With respect to the dynamics of biological recovery, there is no theoretical basis on which to predict the paths of biological recovery. At some scale, each stream or river is unique. The null hypothesis is that recovery will proceed in the same fashion as acidification, only backwards. Thus, for example, the last species lost (the most acid tolerant) would be the first to return. However, time lags are expected because of species recolonization times, which differ widely among species and among streams.

Stream macroinvertebrate communities are often dominated by immature life stages of flying insects, such as mayflies, dragonflies, and stoneflies. Such species have rather rapid colonization times, such that a functional stream macroinvertebrate community may return in about three years. However, fish community recovery is expected to be quite variable, depending on sources of colonists. In streams, fish could be introduced as soon as the water quality becomes suitable and/or the macroinvertebrate community becomes established. In streams which had simple fish communities in the past, a fish community might become rapidly established with species introductions, or might take many decades for complex communities

without species introductions. In SHEN, recolonization would be expected to be relatively rapid because of the interconnectivity of all of the rivers, which provides a ready supply of colonists.

e. Prognosis for Recovery of Aquatic Ecosystems

Background

As described above, available data, model projections, and the weight of scientific evidence suggest that air pollution and acidic deposition have caused environmental degradation of surface waters, forests, and visibility in SHEN. Recent emissions control efforts have focused on attempts to reduce air pollution and deposition sufficiently to permit ecosystem recovery, if not to pre-industrial levels, at least to levels that might allow some reduction in ecological damage. Key questions now facing scientists and policy-makers have to do with the degree in space and in time to which S, N, and volatile organic carbon emissions will need to be reduced in order to allow ecosystem recovery to proceed and to prevent further damage (c.f., Jenkins et al. 1998). A substantial body of scientific literature exists on this topic with respect to aquatic effects, and modeling approaches are available with which to specify the needed emissions reductions.

Public policy measures to reduce emissions should be based on an understanding of dose/response relationships which reflect the tolerance of natural ecosystems to various inputs of atmospheric pollutants. This need has given rise to the concepts of critical levels of pollutants and critical loads of deposition (e.g., Bull 1991, 1992), as well as interest in establishing and refining standards for ambient air pollution and acid deposition. A critical level or load can be defined as a quantitative estimate of an exposure (concentration or loading) to one or more pollutants below which significant harmful effects on specified sensitive elements of the environment do not occur according to present knowledge (e.g. Nilsson 1986, Gundersen 1992). Although such an approach to establishing a standard is intuitively satisfying, the assignment of a standard or critical load is difficult because a variety of natural processes and anthropogenic activities affect the status of sensitive resources, in addition to air pollution and atmospheric deposition of S and N. Furthermore, the pollutant concentrations or deposition loadings that may be required to protect *the most sensitive* elements of an ecosystem may be difficult to quantify.

The basic concept of critical load is relatively simple: the threshold concentration of pollutants at which harmful effects on sensitive receptors begin to occur. Implementation of the concept is, however, not at all simple or straight-forward. For example, the acid-base chemistry of surface waters typically exhibits substantial intra- and interannual variability. Seasonal variability in the concentration of key chemical parameters often varies by more than the amount of acidification that might occur in the future in response to acidic deposition. Such variability makes quantification of acidification and recovery responses difficult, and also complicates attempts to evaluate sensitivity to acidification based on "index" or annual average chemistry, as is typically collected in stream surveys.

Technical information required by the U.S. EPA for assessing the feasibility of adopting one or more acid deposition standards for the protection of aquatic resources was summarized by Sullivan and Eilers (1994), Van Sickle and Church (1995), and Church and Van Sickle (1999). Quantitative model-based analyses were conducted for areas of the United States intensively studied in EPA's model forecasting program, the Direct Delayed Response Project (DDRP, Church et al. 1989). The MAGIC model (Cosby et al. 1985a,b) was used to project changes in surface water chemistry for a range of S and N deposition scenarios, assuming a range of N retention efficiencies (Van Sickle and Church 1995). Subsequently, a report was prepared for Congress on the feasibility of adopting one or more acid deposition standards (U.S. EPA 1995). The report concluded that establishment of such standards for S and N deposition in the United States was technically feasible, but that two critical areas of uncertainty advised against the setting of national standards at that time. First, policy decisions regarding appropriate or desired goals for protecting sensitive systems were needed, especially with respect to the level of protection desired and the costs and benefits of such protection. Second, key scientific unknowns, particularly regarding watershed processes that govern N dynamics, limited the ability to recommend specific standards for N deposition at that time (EPA 1995a, Sullivan 2000).

Federal agencies have made progress regarding policy decisions on protection of sensitive systems; however decisions for some resources and locations are still needed. The more scientific data that is made available for Federal land managers to base these types of decisions on, the more robust the decisions are likely to be in the future.

Prior to and since publication of EPA's Acid Deposition Standards Feasibility Report (U.S. EPA 1995), considerable research has been conducted on the topics of N dynamics and the effects of atmospheric N deposition (c.f., Sullivan 1993, Emmett et al. 1997, Jenkins et al. 1997, Cosby et al. 1997, Aber et al. 1997, 1998). A variety of dynamic models are now available with which to estimate critical loads for N at the watershed scale. Nitrogen dynamics have recently been added to the MAGIC model (Cosby et al. 2001; see also Appendix F), thus allowing MAGIC to be used for assessment of critical loads for either S or N or a combination of the two.

The forest soils in SHEN currently retain virtually all atmospheric N except during and subsequent to insect infestation. A preliminary modeling study of a representative catchment in SHEN using the PnET model (Aber and Federer 1992, Aber et al. 1997) found that both the forests and the forest soils in SHEN are very actively aggrading N (Fievet 2001). The model output suggested that, at current levels of N deposition and barring pest outbreaks or substantial land use changes, more than 100 years will elapse before the forest ecosystem becomes "saturated" with N to the point that significant N losses in streamwater will occur. This result is similar to that found for aggrading temperate hardwood forests elsewhere (Aber et al. 1998). In the SHEN forests, the current levels of atmospheric N deposition are below threshold values commonly associated with forest N saturation (Sullivan, 2000). Also, the forests within the park are regenerating as a consequence of large-scale disturbances prior to the formation of the park, and therefore have relatively high N demand. For these reasons, the critical load of N deposition (at least with respect to N leaching and acidification) is not as important a consideration for this park as is the critical load of S deposition at the present time. Of course, this could change if N deposition dramatically increased in the future.

The adoption of acid deposition standards or thresholds for the protection of surface water quality from potential adverse effects of S and N deposition is a multifaceted problem. It requires that S and N be treated separately as potentially-acidifying agents. Appropriate criteria must be selected as being indicative of damaged water quality, for example ANC or pH. Once a criterion has been selected, a critical value must be estimated, below which the criterion should not fall. For example, if the selected criterion is surface water ANC, one could specify that ANC should not fall below, or should recover to, 0, 20, or 50 μeq/L in response to acidic deposition (e.g., Kämäri et al. 1992). Selection of critical values for ANC or pH is confounded by the existence of streams that are acidic or very low in pH or ANC due entirely to natural factors,

irrespective of acidic deposition (Sullivan 1990). In particular, low contributions of base cations in solution, due to low weathering rates and/or minimal contact between drainage waters and mineral soils, and high concentrations of organic acids contribute to naturally low pH and ANC in surface waters. Other factors also can be important in some cases, including watershed sources of S (Sullivan 2000).

Acid deposition standards or thresholds might be selected on the basis of protecting aquatic systems from either chronic or episodic acidification. Thus, selection of appropriate acidic deposition standards or thresholds involves consideration of a matrix of factors. Specification of numerical values for the protection of sensitive resources against adverse impacts associated with S and/or N deposition is dependent on a host of both scientific and policy decisions. These include, for example:

- scientific determination of the extent to which water chemistry will change in its acid-base character in response to various deposition loading rates (chemical dose-response relationship),
- scientific estimation of the biological responses associated with given changes in water chemistry (biological dose-response relationship),
- policy determination of the percent of sensitive resources within a given region that one wishes to protect against adverse changes, and
- policy determination of what biological changes must be protected against (Sullivan 2000).

It is now fairly straightforward to estimate the dose-response functions for a given watershed or group of watersheds within a region, although this does entail a moderate level of uncertainty (e.g., Turner et al. 1992, Sullivan and Eilers 1994, van Sickle and Church 1995, Sullivan 2000). Furthermore, there are generally well-accepted criteria for specifying biological response functions, both chronically and episodically (e.g., Section VII.C.1.d., Baker et al. 1990b, Wigington et al. 1993), based on observed empirical relationships and a general knowledge of the magnitude of episodic excursions from measured chronic chemistry and regional hydrology (e.g., Eshleman 1988, Webb et al. 1994).

Critical Loads Analysis for SHEN Streams

The principal objectives of the critical loads work reported here for aquatic ecosystems in SHEN were to determine, using the MAGIC model, threshold levels of sustained atmospheric

deposition of S below which adverse effects to sensitive aquatic receptors in SHEN will not occur, and to evaluate interactions between the critical ANC endpoint value specified and the time period over which the critical load is examined. Critical loads for S deposition were calculated using the MAGIC model for the 14 streams selected in SHEN for modeling, distributed into geological sensitivity classes as follows: 5 each on siliciclastic and basaltic bedrock, and 4 on granitic bedrock.

The MAGIC model was used in an iterative fashion to calculate the S deposition values that would cause the chemistry of each of the modeled streams to either increase or decrease streamwater ANC (depending on the current value) to reach the specified critical levels. For some analyses, the critical ANC levels were set at 0, 20, and 50 μeq/L, the first two of which are believed to approximately correspond with chronic and episodic damage to the relatively acid-tolerant brook trout populations in park streams (Bulger et al. 2000). Other more acid-sensitive species of aquatic biota may be impacted at higher ANC values. In order to conduct this critical loads analysis for S deposition, it was necessary to specify the corresponding levels of N deposition. Nitrogen deposition accounts, however, for only a minor component of the overall acidification response of streams in the park. For this analysis, future N deposition was held constant at 1990 levels (7.6 kg N/ha/yr). It was also necessary to specify the times in the future at which the critical ANC values would be reached. We selected the years 2020, 2040, and 2100. It must be recognized that streamwater chemistry will continue to change in the future for many decades subsequent to stabilization of deposition levels. This is mainly because soils will continue to change in the degree to which they adsorb incoming S and because some watersheds will have become depleted of base cations. The latter process can cause streamwater base cation concentrations and ANC to decrease over time while SO_4^{2-} and NO_3^- concentrations maintain relatively constant levels.

The levels of S deposition that were simulated to cause streamwater ANC to increase or decrease to the three specified critical levels (0, 20, and 50 μeq/L) are listed in Table VII-13 for each of the modeled streams. Estimated critical loads for S deposition ranged from less than zero (ANC objective not attainable) to several hundred kg/ha/yr, depending on the selected site, ANC endpoint, and evaluation year.

It is useful to put the results of this critical loads analysis into the perspective of the population of streams within the park. This cannot be done directly, however, because the

Table VII-13. Estimated critical load (kg/ha/yr) of sulfur[a] to achieve a variety of ANC (μeq/L) endpoints in a variety of future years for modeled streams in SHEN.[b]

Site[d]	Bedrock Class[e]	ANC (μeq/L)		Critical Load to Achieve ANC Value[c]								
				ANC = 0			ANC = 20			ANC = 50		
		1990	Pre-1900	2020	2040	2100	2020	2040	2100	2020	2040	2100
VT36	S	0	69	9	9	9	2	5	6	< 0	< 0	1
DR01	S	2	78	14	13	12	5	8	9	< 0	< 0	3
VT35[f]	S	7	91	16	15	14	11	11	11	1	4	6
VT53	S	16	81	20	17	15	11	12	11	< 0	1	5
WOR1	S	26	66	22	15	10	5	6	6	< 0	< 0	< 0
NFDR	G	60	82	53	33	17	43	26	13	15	10	7
VT58	G	88	98	119	59	29	109	53	25	83	40	18
VT59[f]	G	88	96	164	86	45	154	79	40	127	62	30
VT62	G	102	116	122	60	29	112	55	26	92	44	20
VT75	B	126	143	331	183	78	307	173	76	248	147	69
VT66	B	147	159	155	118	73	143	109	69	127	93	60
VT51	B	166	191	281	151	65	267	145	64	239	134	62
VT60[f]	B	204	218	241	147	72	230	142	70	211	134	67
VT61	B	258	277	502	281	124	487	276	122	459	265	119

[a] Deposition of sulfur in 1990 was about 13 kg/ha/yr
[b] All simulations based on straight-line ramp changes in deposition from 2000 to 2010, followed by constant deposition thereafter.
[c] <0 indicates that the ANC endpoint could not be achieved (no recovery) even if S deposition was reduced to zero.
[d] See Table VI-2 for stream names
[e] Siliciclastic, S; Granitic, G; Basaltic, B
[f] Intensively studied sites are VT35 (PAIN), VT59 (STAN), and VT60 (PINE)

modeled streams were not statistically selected. This can be done indirectly if the range of critical load estimates is relatively narrow within a given ANC class or geologic sensitivity class or if the critical load estimates vary in a predictable way as a function of some aspect of the current streamwater chemistry. Results of the estimated critical load values are summarized by ANC class and by geologic sensitivity class in Table VII-14. None of the granitic or basaltic streams exhibited critical loads values lower than the current S deposition level (13 kg/ha/yr), when evaluated for the year 2100 using ANC criterion values of either 0 or 20 μeq/L.

In marked contrast, all of the modeled siliciclastic streams exhibited critical loads ≤ 11 kg/ha/yr to protect against acidification to ANC ≤ 20 in the year 2100 (Table VII-14). The median modeled siliciclastic stream had a calculated critical load to protect against acidification to ANC ≤ 20 μeq/L that was about 31% lower than the 1990 deposition that was used as the baseline for the modeling analyses (13 kg S/ha/yr).

Table VII-14. Median and range of estimated critical load values for sulfur deposition, by principal geologic sensitivity class within the watershed.

Geologic Sensitivity Class	Number of Modeled Streams in Class (n)	Median (Range) Estimated Critical Load of Sulfur Deposition (kg/ha/yr) for the Year 2100		
		ANC = 0	ANC = 20 μeq/L	ANC = 50 μeq/L
Siliciclastic	5	12 (9-15)	9 (6-11)	3 (<0-6)
Granitic	4	29 (17-45)	26 (13-40)	20 (7-30)
Basaltic	5	73 (65-124)	70 (64-122)	67 (60-119)

The calculated S deposition critical load for streams in SHEN varied as a function of watershed sensitivity (as reflected in geologic sensitivity class, and soils and streamwater characteristics), the selected chemical criterion (critical ANC value), and the future year for which the evaluation was made. All of these criteria are important. For example, the modeled critical S load to protect the 14 modeled streams in SHEN from becoming acidic (ANC=0) in the year 2100 varied from 9 to 124 kg S/ha/yr (Table VII-13). Similarly, for site WOR1 (White Oak Run) in the year 2100, the critical load to protect against ANC=0 was 10 kg S/ha/yr, but this watershed could tolerate only 6 kg S/ha/yr to protect against acidification to ANC of 20 μeq/L within the same time period. The model suggested that it would not be possible to achieve ANC=50 μeq/L at this site by 2100, even if S deposition was reduced to zero. The estimated pre-1900 ANC of this stream was 66 μeq/L, which declined to 26 μeq/L by 1990.

Table VII-15 provides estimates of the percent change in S deposition required from 1990 loads to achieve ANC values of 0, 20, or 50 μeq/L by the years 2020, 2040, and 2100. Of the streams underlain by siliciclastic bedrock, only Meadow Run (VT36) and White Oak Run (WOR1) required decreased deposition to protect against acidification to ANC=0 in any of the projection year endpoints. However, all of the sites underlain by siliciclastic bedrock required reduced deposition in order to protect against acidification to ANC below 20 μeq/L in all three future evaluation years (Table VII-15). The required deposition reductions ranged from 9% (Twomile Run) to 55% (White Oak Run) for the evaluation year 2100. All except one (White Oak Run) of the siliciclastic sites were projected to be able to achieve ANC above 50 μeq/L in 2100, but S deposition would have to be reduced by 55 to 89% to realize that objective.

Table VII-15. Estimated percent change in 1990 sulfur deposition[a] required to produce a variety of ANC (μeq/L) endpoints in a variety of future years for streams in SHEN.[b]

Site[d]	Bedrock Class[e]	ANC (μeq/L)		Percent Change in 1990 Deposition to Achieve ANC Value[c]								
				ANC = 0			ANC = 20			ANC = 50		
		1990	Pre-1900	2020	2040	2100	2020	2040	2100	2020	2040	2100
VT36	S	0	69	-24	-25	-28	-84	-59	-50	< -100	< -100	-89
DR01	S	2	78	8	3	-2	-59	-35	-28	< -100	< -100	-73
VT35[f]	S	7	91	28	17	10	-16	-13	-15	-96	-67	-55
VT53	S	16	81	58	34	20	-14	-7	-9	< -100	-92	-61
WOR1	S	26	66	77	16	-18	-60	-56	-55	< -100	< -100	< -100
NFDR	G	60	82	321	162	33	245	111	7	18	-19	-45
VT59[f]	G	88	96	1210	583	262	1126	526	221	908	397	140
VT58	G	88	98	851	371	130	767	324	103	558	215	45
VT62	G	102	116	868	375	133	795	335	109	633	251	63
VT75	B	126	143	2535	1358	525	2344	1281	505	1880	1071	449
VT66	B	147	159	1138	840	484	1042	767	446	908	640	378
VT51	B	166	191	2136	1102	416	2028	1059	409	1808	970	392
VT60[f]	B	204	218	1821	1074	472	1737	1035	457	1584	965	431
VT61	B	258	277	3904	2140	890	3780	2104	876	3561	2016	851

[a] Current deposition of sulfur is 13 kg/ha/yr
[b] All simulations based on straight-line ramp changes in deposition from 2000 to 2010, followed by constant deposition thereafter.
[c] < 100% indicates that the ANC endpoint could not be achieved (no recovery) even if S deposition was reduced to zero.
[d] See Table VI-2 for stream names
[e] Siliciclastic, S; Granitic, G; Basaltic, B
[f] Intensively studied sites are VT35 (PAIN), VT59 (STAN), and VT60 (PINE)

The relationships between critical load, selection of ANC criterion value, and selection of evaluation year are illustrated in Figures VII-21 and VII-22. Higher critical loads can be tolerated if one only wishes to protect against acidification to the year 2020, as compared with more stringent deposition reductions required to protect systems against acidification for a longer period of time (Figure VII-21). Higher critical loads can be tolerated to prevent acidification to ANC = 0 (chronic acidification) than if one wishes to be more restrictive and prevent acidification to ANC below 20 μeq/L (possible episodic acidification; Figure VII-22).

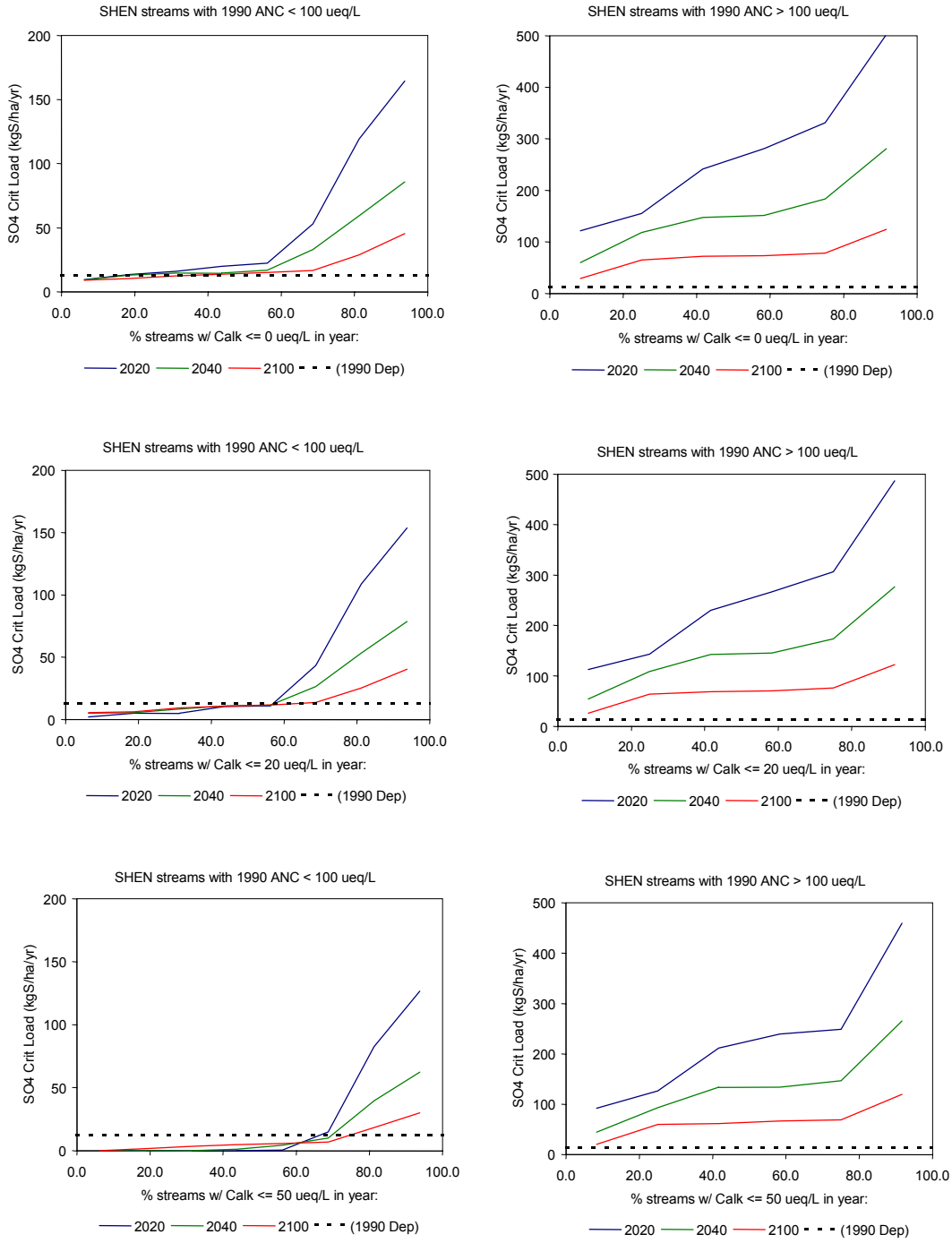

Figure VII-21. Relationship between the simulated sulfur deposition load and the percent of modeled streams in SHEN that have ANC less than or equal to a critical value (0, 20, or 50 µeq/L) in three different future years (2020, 2040, 2100). Deposition in 1990 is indicated as a dotted reference line. For ease of comparison, streams are grouped according to whether 1990 ANC was above or below 100 µeq/L.

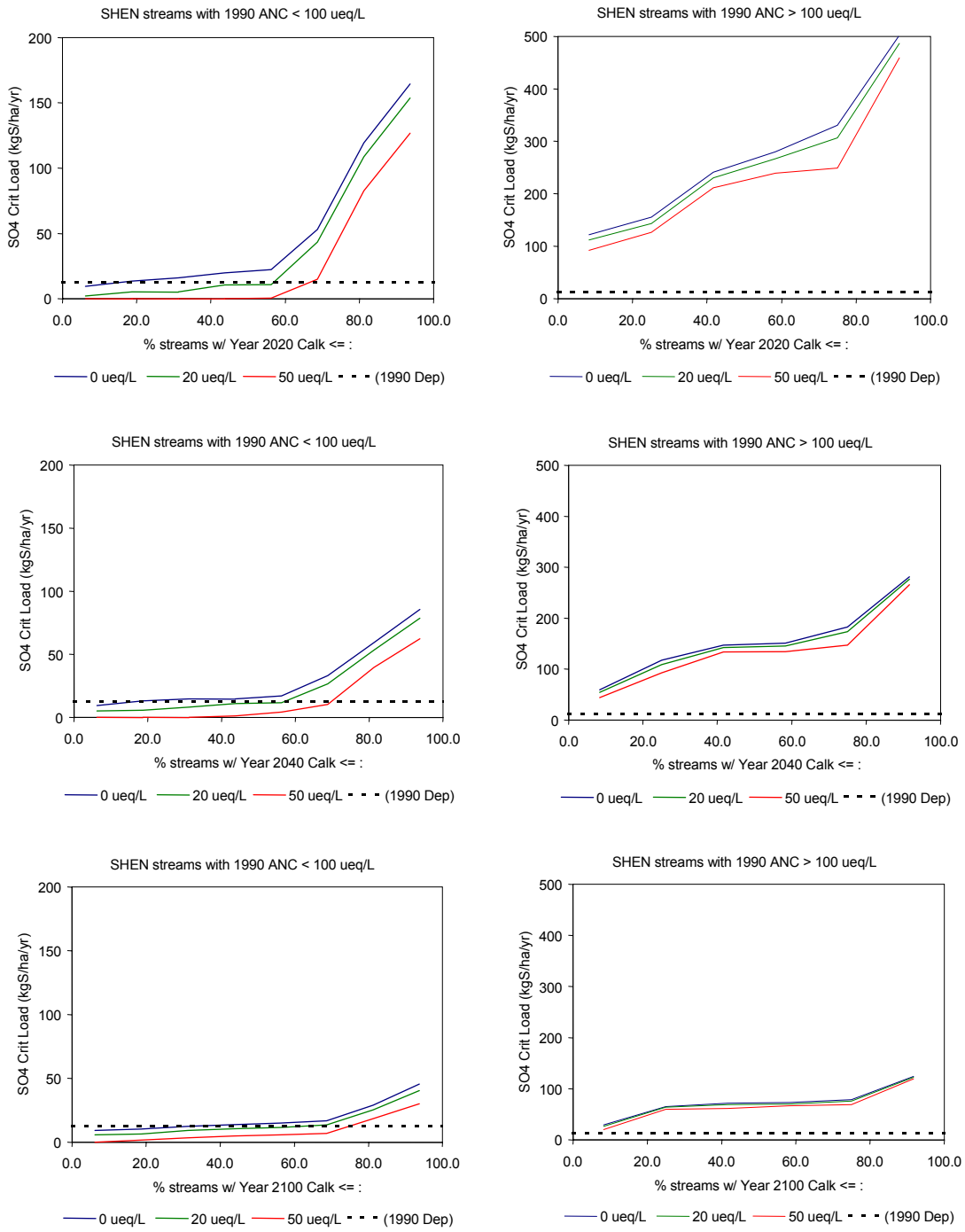

Figure VII-22. Relationship between the simulated sulfur deposition load and the percent of modeled streams in SHEN that have ANC less than or equal to a critical value (0, 20, or 50 µeq/L) in three different future years (2020, 2040, 2100). Deposition in 1990 is indicated as a dotted reference line. For ease of comparison, streams are grouped according to whether 1990 ANC was above or below 100 µeq/L.

The model suggested that it would not be possible to regain streamwater ANC values by the year 2100 that would be similar to pre-industrial ANC, at least for the most acid-sensitive systems, even if S deposition was reduced to zero. For example, of the modeled streams that had ANC < 100 μeq/L in 1990, only one (Staunton River) was projected to reach within 10% of its inferred pre-industrial ANC value anytime between now and 2100, regardless of how much S deposition was reduced.

The data presented in Tables VII-13 and VII-14 and in Figures VII-21 and VII-22, clearly illustrate that how you phrase the critical load question is extremely important. The estimated deposition change required to achieve certain benchmark streamwater chemistry endpoints can be highly variable depending on how and for what time period the endpoint is defined, and on the starting point chemistry of the watersheds that are selected for modeling.

The model estimates of critical loads of S deposition required to prevent streamwater acidification to ANC values below 0, 20, and 50 μeq/L varied consistently as a function of measured ANC in 1990, which in turn was separated into rather distinct groupings according to geologic sensitivity class (Figure VII-23). For example, these model output data suggested, based on the equation given in Figure VII-23, middle panel, that all streams within the park that had 1990 ANC ≤ 20 μeq/L would require critical load values between 2.5 and 14.4 kg S/ha/yr to maintain ANC above 20 μeq/L in the year 2040. Similarly, the model data suggested that a critical load of 7.3 kg S/ha/yr would protect all streams in the park that had positive ANC in 1990 from becoming chronically acidic by 2040; a critical load of 2.5 kg S/ha/yr would allow those same streams to achieve or maintain ANC above 20 μeq/L by 2040; but even with a reduction in S deposition to zero, some of those streams would not achieve or maintain ANC above 50 μeq/L by 2040.

The equations describing the relationships between MAGIC model estimates of S critical load and 1990 streamwater ANC values are given in Table VII-16 for the various ANC endpoints and end years considered. Once the desired ANC endpoint and end year are specified, these equations can be used to estimate the critical load of S deposition that would be required, based on MAGIC model projections, to achieve or maintain those ANC endpoint criteria values for any stream in the park. Note, however, that the model projections suggested that it would not be possible to achieve ANC = 50 μeq/L in any of the end years evaluated for at least some low-ANC streams.

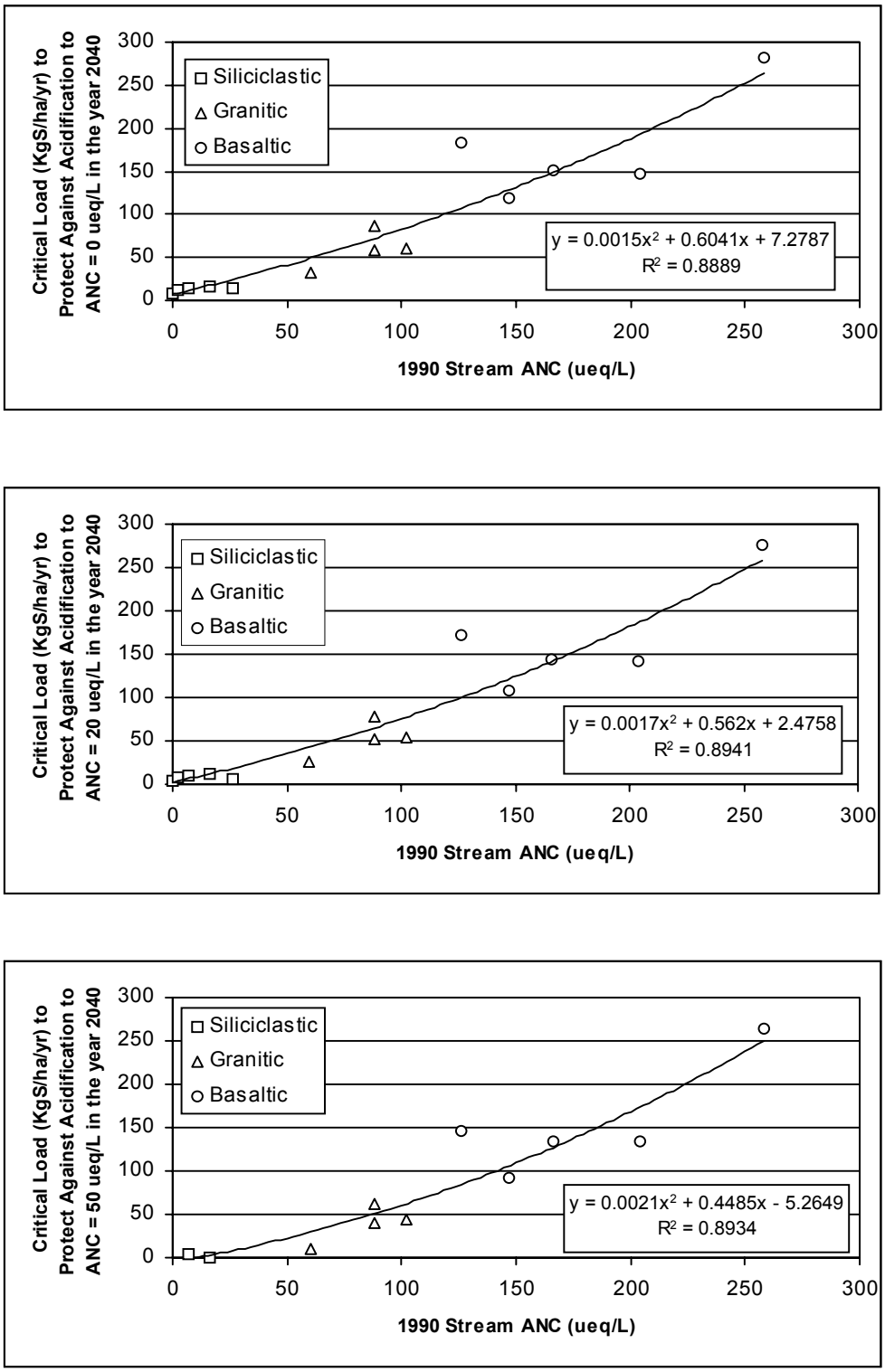

Figure VII-23. Sulfur critical load simulated by the MAGIC model to protect streams in SHEN against acidification to ANC below 0 (top panel), 20 µeq/L (middle panel), and 50 µeq/L (bottom panel) by the year 2040, as a function of 1990 ANC and geologic sensitivity class.

Table VII-16. Regression equations for estimating critical load of sulfur deposition to protect against having ANC below a given threshold in a given endpoint year, based on 14 modeled streams in SHEN.

ANC Threshold	Endpoint Year	Number of Sites (n)[a]	r-squared value	Equation to Estimate Critical Load of Sulfur Deposition (kg S/ha/yr) Given 1990 ANC (μeq/L)
0	2020	14	0.8567	$y = 0.0023x^2 + 1.1588x + 6.2184$
0	2040	14	0.8889	$y = 0.0015x^2 + 0.6041x + 7.2787$
0	2100	14	0.8989	$y = 0.0006x^2 + 0.2698x + 8.6056$
20	2020	14	0.8645	$y = 0.0025x^2 + 1.0949x - 1.9446$
20	2040	14	0.8941	$y = 0.0017x^2 + 0.562x + 2.4758$
20	2100	14	0.9016	$y = 0.0007x^2 + 0.2662x + 5.1181$
50	2020	10	0.9375	$y = 0.0327x^{1.7175}$
50	2040	11	0.8934	$y = 0.0021x^2 + 0.4485x - 5.2649$
50	2100	13	0.9135	$y = 0.0009x^2 + 0.2245x + 0.8005$

[a] For each ANC threshold and endpoint year, MAGIC model results were evaluated for 14 streams. However, output suggested that ANC = 50 μeq/L would not be achieved for some of these streams in some endpoint years even if S deposition was reduced to zero.

We did not attempt to estimate critical loads for N deposition in SHEN. Empirical studies in both Europe and the northeastern United States have suggested that N deposition must be higher than currently occurs at SHEN (7.8 kg N/ha/yr) before forest soils become saturated and begin to chronically leach NO_3^- to surface waters. Dise and Wright (1995) examined watershed and plot-scale input-output budgets for N across Europe and found elevated N leaching at sites that received in excess of about 10 kg/ha/yr of N, about one-fourth higher than the N deposition received at SHEN. Sullivan et al. (1997) found that the observed fall NO_3^- concentration in Adirondack Mountain lakes, New York, could largely be explained by NO_3^- deposition directly to the lake surface without the need for NO_3^- leaching from watershed soils. Those lakes that did show lakewater NO_3^- concentrations higher than would be predicted from direct NO_3^- deposition to the lake surface were generally among the most acid-sensitive of the study lakes (pH 4.7 to 5.3) and received generally high levels of N deposition (~ 10 to 12 kg N/ha/yr, Ollinger et al. 1993). Thus, the finding that watershed soils in SHEN take up essentially 100% of incoming N in the absence of major disturbance seems reasonable under current N deposition. If N deposition increases substantially in the future, then the possibility of N saturation of forest ecosystems in SHEN may become an important concern.

Target Loads

A target load (e.g. Henriksen and Brakke 1988) can be based on political, economic, or temporal considerations, and implies that the environment will be protected to a specified level (i.e. certain degree of allowable damage) and/or over a specified period of time. There has been a rapid acceptance of the concepts of critical and target loads throughout Europe and Canada for use in political negotiations concerning air pollution and development of abatement strategies to mitigate environmental damage (e.g., Posch et al. 1997).

Whereas a critical load is objectively determined, a target load is based on both science and policy. A target load is set on the basis of, in addition to model-based estimates of critical loads, such considerations as:

- desire to protect the ecosystem against chronic critical load exceedance
- temporal components of acidification/recovery processes, so that, for example, resources could be protected only for a specified period of time or allowed to recover within a designated window
- seasonal and episodic variability in water chemistry, and probable associated biological responses
- model, data, and knowledge uncertainty and any desire to err on the side of resource protection.

A target load is subjectively determined, but it is rooted in science and incorporates allowances for uncertainty and ecosystem variability.

Criteria of unacceptable change should be set in relation to known or expected effects on aquatic or terrestrial organisms. For protection of aquatic organisms, the ANC of surface water is most commonly used (Nilsson and Grennfelt 1988, Henriksen and Brakke 1988, Sverdrup et al. 1990). Concentrations below which ANC should not be permitted to fall have been set at 0, 20, and 50 ueq/L for various applications (e.g., Kämäri et al. 1992).

Selection of the best, or most appropriate, target load for protecting and restoring sensitive resources in SHEN is not a scientific issue. Model simulations such as those presented in this report will provide useful information for the decision process, although the final determination must be based on NPS policy judgment.

2. Vegetation

a. Background

The most important known threat from air pollution to vegetation resources in SHEN is the threat of O_3 damage to forest growth and health. Ozone is likely to be a long-term debilitating stress to the park's trees and forests. An O_3 effects modeling analysis was therefore conducted, with the following objectives:

- to use models of tree and forest stand response, individually and linked, to project the current impact of O_3 on the growth of forest trees and stands in SHEN
- to extrapolate the results of the simulations over the spatial extent of the species and stands within the park
- to project the impact of future O_3 scenarios on the growth and development of forest trees and stands in the park.

These simulation results are for O_3 alone, and do not consider interactions of O_3 with insects, diseases, drought, and other potentially exacerbating stresses, or cumulative stresses known to alter responses of trees to ozone.

This simulation analysis was not designed to predict the extent of visible injury to foliage. This type of injury is expected to continue at SHEN unless ambient O_3 levels decrease below current levels. Such visible injury is, however, unlikely to lead to large growth reductions of individual species or stand basal area.

b. Modeling Methods for Ground-level Ozone Effects

<u>Ozone and Meteorology Scenarios for Simulations</u>

Hourly O_3 data from the Big Meadows site were acquired from the Aerometric Information Retrieval System (AIRS) database for 1997-1999 and summarized to determine an average value for SUM06, the 5-month cumulative summation of hourly O_3 concentrations that equaled or exceeded 60 ppb between 8:00 AM and 8:00 PM. Additional hourly exposure regimes were then created for input into TREGRO (Weinstein et al. 1991) to create exposure-response functions relating simulated growth to O_3 exposure and precipitation and to generate growth modifiers for use in ZELIG (Urban 1980, Urban et al. 1991). Two sub-ambient and four above-ambient regimes were generated from hourly O_3 monitoring and are summarized in Tables VII-17 and

VII-18[2]. Table VII-17 provides the three-year exposure metrics, that is, the total exposure provided in the TREGRO simulations. Table VII-18 lists the year-by-year exposure, illustrating the variation between years. The three-year exposure regimes used for TREGRO simulations are illustrated in Figures VII-24 and VII-25. The lowest O_3 exposure (Ozone1) was used as a base for standardization of response.

Although summary metrics are used to characterize exposure regimes, TREGRO uses hourly O_3 concentrations as input data. To create the hourly exposure concentrations for use in TREGRO, a quadratic weighting of hourly O_3 concentrations was used:

$$Oz' = Oz * [1 - (1-f) * Oz / max(Oz)]$$

where max(Oz) = annual maximum hourly O_3 concentration and f is the scale adjustment of the max(Oz) (Tingey et al. 2001). For example, a 10% reduction of the maximum hourly O_3 concentration corresponds to f=0.9 and a 10% increase of the maximum concentration corresponds to f=1.1.

TREGRO Parameterizations

TREGRO, a physiologically-based model of the growth of individual trees (Weinstein et al. 1991) was used to study the response of large trees to O_3. TREGRO (Version 3.0.0.10)[3] was parameterized for large, mature individuals of 8 species for use in this study: basswood (*Tilia Americana* L.), black cherry (*Prunus serotina* Ehrh.), chestnut oak (*Quercus prinus* L.), red maple (*Acer rubrum* L.), red oak (*Quercus rubra* L.), sugar maple (*Acer saccharaum* L.), white ash (*Fraxinus americana* L.), and yellow poplar (*Liriodendron tulipifera* L.). Parameterizations for black cherry, red maple, red oak, sugar maple, and yellow poplar were available from the Plant Modeling Group at Boyce Thompson Institute, Ithaca, NY. These parameter sets were adjusted slightly so that the simulated growth under Big Meadows meteorological conditions

---

[2] There are many metrics to summarize O_3 exposures, with no clear favorite among the research and regulatory communities of North America and Europe. We chose a 5-month (May-September) 12-hour (8:00 AM - 8:00 PM) SUM06, which is a summation of all hours $\geq$0.06 ppm O_3 during those times. In Tables VII-1 and VII-2, other common metrics are presented as well so that exposures used in these studies may be related to other common measures, as desired, by users of this report.

[3] TREGRO is available from David A. Weinstein (daw5@cornell.edu), Boyce Thompson Institute, Cornell University, Ithaca, NY 14853

Table VII-17. Total three-year daylight (0800-2000) ozone exposure metrics[a] (ppm·hr) calculated from hourly concentrations used for TREGRO simulations.

	SUM 0			SUM 06[b]			W126			AOT 04		
Simulated Ozone Exposure	12 month	5 month	3 month	12 month	5 month	3 month	12 month	5 month	3 month	12 month	5 month	3 month
1	549	265	164	14	36	9	68	41	28	78	52	34
2	567	283	175	90	78	54	86	66	44	92	69	45
3[c]	630	322	199	220	182	123	170	132	87	145	106	69
4	660	340	211	266	214	144	213	164	108	171	123	78
5	719	375	234	369	282	185	302	227	149	225	158	102
6	778	410	255	465	343	221	393	288	188	2798	192	124
7	1,149	630	394	980	611	386	912	590	375	637	411	262

[a] SUM 0 is the sum of all O_3 concentrations; SUM 06 is the sum of all concentrations ≥0.06 ppm; W126 is a sigmoidally weighted summation of all concentrations, and AOT 04 is the sum of all hours after subtracting a threshold of up to 0.04 ppm. All summations are for the 1997-1999 period, from 0800 to 2000 EST, for the entire year (12 month), May-September (5 month), or June-August (3 month). These are summary statistics only—TREGRO uses the actual hourly data (SUM0).

[b] 25 ppm·hr, 3-month, 12-hour SUM06 is the metric recommended by EPA staff as the secondary standard to protect sensitive vegetation in Class I areas

[c] Simulated O_3 exposure #3 represents ambient 1997-1999 exposure at Big Meadows.

Table VII-18. Ozone exposure metrics[a], by year, calculated from hourly concentrations used for TREGRO simulations.

Simulated Ozone Exposure	SUM 0			SUM 06			W126			AOT 4		
	1997	1998	1999	1997	1998	1999	1997	1998	1999	1997	1998	1999
1	177	176	196	14	9	36	19	17	33	22	22	34
2	186	184	196	30	24	36	28	25	33	30	28	34
3[b]	195	217	218	46	96	78	38	70	61	37	56	53
4	204	227	229	63	111	92	50	86	77	44	65	62
5	223	246	250	93	142	134	76	116	110	61	82	82
6	242	266	271	128	168	169	104	146	143	77	100	102
7	358	386	405	303	321	356	305	334	273	188	216	232

[a] SUM 0 is the sum of all O_3 concentrations; SUM 06 is the sum of all concentrations ≥ 0.06 ppm; W126 is a sigmoidally weighted summation of all concentrations, and AOT 04 is the sum of all hours after subtracting a threshold of up to 0.04 ppm. All summations are for the 1997-1999 period, from 0800 to 2000 EST, for the June-August (3 month) period. These are summary statistics only; TREGRO uses the actual hourly data (SUM0).

[b] Simulated O_3 exposure #3 represents ambient 1997-1999 exposure at Big Meadows.

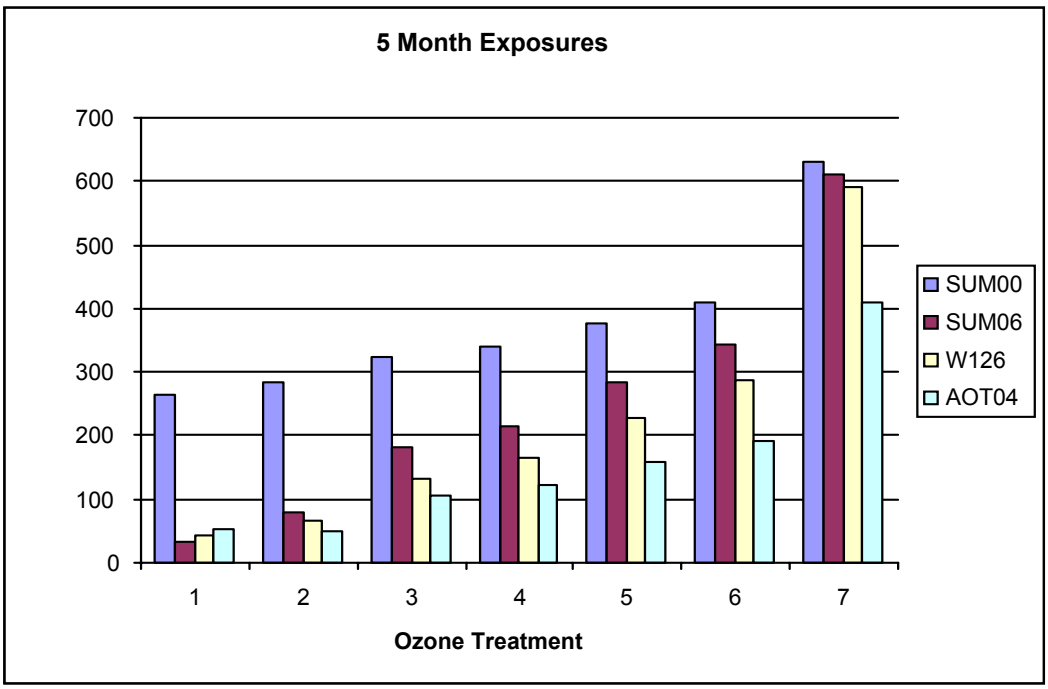

Figure VII-24. Ozone exposures (total for 1997-1999) used in TREGRO simulations. Treatment 3 is the 1997-1999 monitored ambient exposure at Big Meadows.

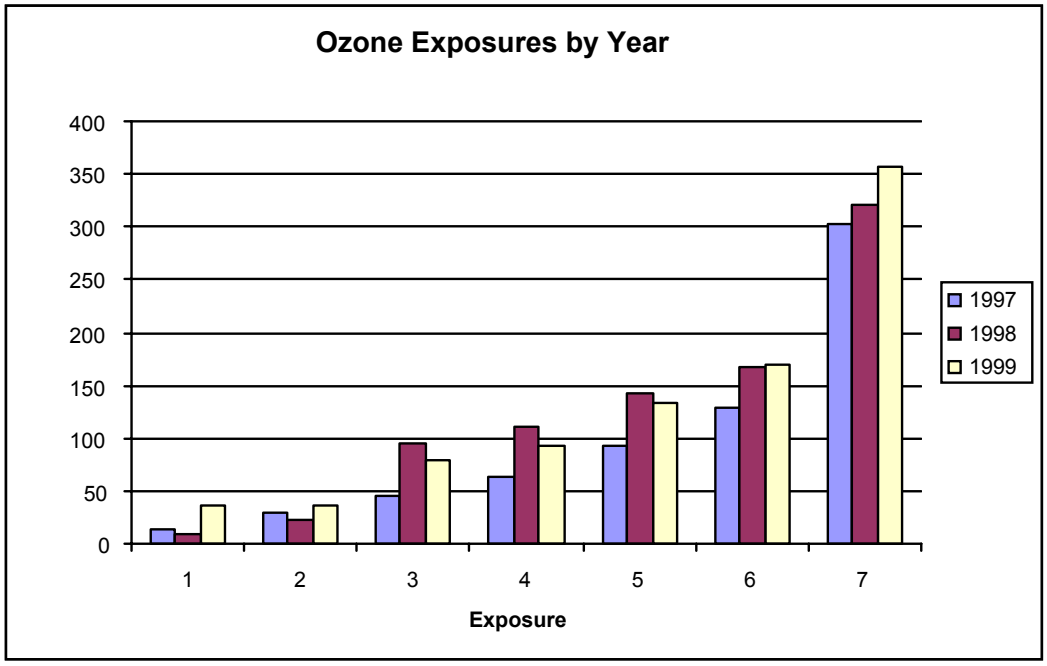

Figure VII-25. Ozone exposures (5 month SUM06) for each of the three simulation years. Treatment 3 is the 1997-1999 monitored ambient exposure at Big Meadows.

matched that of the original target tree (within at least ±10%). Basswood, chestnut oak, and white ash were parameterized for TREGRO for the first time in this study. Details of the parameterizations and growth rate targets are given in Appendix G.

Of the eight species used in this study, a large-tree O_3 response function has been reported in the literature for black cherry (Weinstein et al. 2001), red maple (Weinstein et al. 2001), red oak (Weinstein et al. 1998), sugar maple (Retzlaff et al. 1996), and yellow poplar (Weinstein et al. 2001). The O_3 response of basswood, chestnut oak, and white ash were set to those of red maple, red oak, and red maple, respectively, based upon their physiological and ecological similarities.

TREGRO Simulations

A three-year TREGRO simulation for each species was conducted using meteorological data for Big Meadows and the seven O_3 scenarios illustrated in Figure VII-24. At the end of the simulations, the results were standardized by expressing the final biomass as:

$$Y = \frac{[\text{Final Biomass(O Ozone)} - \text{Final Biomass(Ozone1)}]}{\text{Final Biomass(Ozone1)}}$$

where O Ozone is any given treatment level and Ozone1 is the first treatment level, the lowest simulated O_3 exposure.

Spline regression was used to fit a linear-linear model to % relative tissue mass (y) as a function of O_3 exposure index (x), as follows:

$$Y = a+bx \ (x \leq x_0)$$
$$= c+dx \ (x > x_0)$$

where x_0 is the join point. The parameter a represents the relative mass at zero exposure and was set to equal 0. Note that $x_0=c/(b-d)$.

All calculations were performed using SAS PROC NLIN (SAS Institute, Cary, NC) using several different initial parameter values. In most cases, the parameter values were not uniquely defined and the minimum RMSE criterion was used to select among several candidate models.

Linkage of TREGRO and ZELIG

In order to provide a physiological basis for the projection of O_3 effects at the stand level, TREGRO and ZELIG were linked through three output variables from the individual tree

simulations (Laurence et al. 2001, Weinstein et al. 2001). At the end of each growing season in each of the three-year TREGRO simulations, the value for total tree mass, leaf mass, and fine root mass to leaf mass ratio were output. The average of the three-year response was calculated and standardized for each treatment by dividing each O_3 treatment by the value for the Ozone 1 treatment. These values (modifiers) were used to scale particular processes in ZELIG, thus incorporating a physiological basis for reduced growth of trees in a stand. Modifiers calculated in this study are shown in Table VII-19. The modifiers were then input to ZELIG to alter (by multiplication) the growth rate, leaf area (and therefore shading), and nutrient and drought sensitivity of each of the species as they occurred in the three forest types. Thus, ZELIG results were all expressed relative to the lowest O_3 exposure (about 87% of monitored ambient Sum 0 and 18% of the ambient 5 month SUM06; Tables VII-17 and VII-18).

ZELIG Parameterizations

ZELIG, a model of forest stand dynamics and succession (Urban 1980, Urban et al. 1991), was used to estimate the effect of O_3 on productivity and composition of major forests in the park. The three forest types that comprise the majority of the forest at SHEN were simulated: Chestnut Oak, Cove Hardwood, and Yellow Poplar. The principal species included in each forest type are shown in Table VII-20.

Long-term weather data for Big Meadows were obtained from the EarthInfo database (EarthInfo 1992) and were used to calculate monthly 30-year means and standard deviations for temperature and precipitation.

ZELIG simulates the establishment of seedlings on the plot as a function of the average annual environmental conditions and the ability of selected species to withstand these conditions. The model produces a projection of the average basal area (m^2/ha) for each tree species for each year of simulation, calculated from a landscape containing 100 forest plots, each 600 m^2 in area.

A species parameter set for use with ZELIG was constructed for each of the three forest types. To assure that ZELIG reproduced the diameter growth rates of trees observed from this region, growth rates of trees reported in the Forest Inventory Analysis (FIA; Hansen et al. 1992) were calculated. Growth records from trees for each of the simulated species in or near SHEN were divided into 5 cm diameter size classes. The mean growth rate of all trees of a given species in a given size class was calculated. A polynomial regression was fitted through points representing the mean plus one standard deviation in each size class in order to estimate the

Table VII-19. Modifiers of ZELIG processes calculated from TREGRO simulations. Reductions in growth, leaf area, and root production are achieved by multiplying the calculated modifier and the appropriate variable in ZELIG for the appropriate ozone exposure treatment.

Species	Ozone Exposure[a]	Total Growth	Shoot	Root:Shoot[b]
Basswood	1	1.00000	1.00000	1.00000
	2	0.99893	1.00000	0.99404
	3	0.99632	1.00000	0.97912
	4	0.99525	1.00000	0.97144
	5	0.99306	1.00000	0.95552
	6	0.99088	1.00000	0.93989
	7	0.97140	0.99796	0.82469
Black Cherry	1	1.00000	1.00000	1.00000
	2	0.99995	1.00000	1.00000
	3	0.99980	1.00000	1.00000
	4	0.99974	1.00000	1.00000
	5	0.99966	1.00000	1.00000
	6	0.99955	1.00000	1.00000
	7	0.99064	0.99902	1.04930
Chestnut Oak	1	1.00000	1.00000	1.00000
	2	0.99893	1.00000	0.99404
	3	0.99632	1.00000	0.97912
	4	0.99525	1.00000	0.97144
	5	0.99306	1.00000	0.95552
	6	0.99088	1.00000	0.93989
	7	0.97140	0.99796	0.82469
Red Maple	1	1.00000	1.00000	1.00000
	2	0.99987	1.00000	1.00000
	3	0.99954	1.00000	1.00000
	4	0.99929	1.00000	1.00000
	5	0.99867	1.00000	1.00000
	6	0.99745	1.00000	1.00000
	7	0.97554	1.00082	0.91828
Red Oak	1	1.00000	1.00000	1.00000
	2	1.00000	1.00000	0.99998
	3	1.00001	1.00000	0.99997
	4	0.99996	1.00000	0.99912
	5	0.99986	1.00000	0.99740
	6	0.99976	1.00000	0.99568
	7	0.98766	0.99957	0.87844
Sugar Maple	1	1.00000	1.00000	1.00000
	2	0.99996	1.00000	1.00000
	3	0.99992	0.99998	1.00002
	4	0.99988	0.99998	1.00002
	5	0.99980	0.99997	1.00003
	6	0.99972	0.99996	1.00003
	7	0.99289	0.99812	1.09320

Table VII-19. Continued.

Species	Ozone Exposure[a]	Total Growth	Shoot	Root:Shoot[b]
White Ash	1	1.00000	1.00000	1.00000
	2	0.99809	1.00000	0.98249
	3	0.99385	1.00000	0.94723
	4	0.99201	1.00000	0.93099
	5	0.98832	1.00000	0.89927
	6	0.98455	1.00000	0.86869
	7	0.95750	1.00254	0.73567
Yellow Poplar	1	1.00000	1.00000	1.00000
	2	0.99986	1.00000	1.00000
	3	0.99965	1.00000	1.00000
	4	0.99950	1.00000	1.00000
	5	0.99913	1.00000	1.00000
	6	0.99840	1.00000	1.00000
	7	0.98031	1.00000	0.84447

[a] Ozone exposures based on 7 scenarios of future ozone concentrations
[b] Values of the root:shoot ratio less than 1.0 suggest an effect of ozone on plant growth

Table VII-20. Species included in three forest types simulated with ZELIG.

Chestnut Oak	*Acer rubrum*, *Carya glabra*, *Fraxinus americana, Quercus alba, Quercus coccinea, Quercus prinus*, *Quercus rubra*, *Pinus strobus*
Cove Hardwood	*Acer rubrum*, *Acer saccharum*, *Betula lenta*, *Fraxinus americana, Liriodendron tulipifera, Prunus serotina, Quercus prinus, Quercus rubra, Robinia pseudoacacia, Tilia americana, Tsuga canadensis*
Yellow Poplar	*Acer rubrum*, *Betula lenta*, *Liriodendron tulipifera, Quercus prinus, Quercus rubra, Robinia pseudoacacia, Tilia americana, Carya glabra, Cornus florida*

average growth rate of trees less likely to be suppressed by shade (in order to more accurately estimate an unstressed growth rate). For most species, the polynomial regression closely fit the points. The growth rates estimated in this fashion represent the actual growth reported from the early 1980s until the early 1990s under existing climatic conditions. Thus, if O_3, or other stresses, were suppressing growth during that time, the effect of the stress is included in the baseline growth for each species.

The parameters for the growth equation used in ZELIG were then estimated using the polynomial regression equation described above. The fitting process continued until the

projected mean growth rates deviated from estimates based on field data by less than 5% in any size class less than 50 cm in diameter. For most species, this process also produced reasonable projections of growth for larger trees as well. For a few species, the estimates of growth derived from the field data suggested that larger trees exhibited greater growth rates. Since this is not likely to be correct, the ZELIG growth equation parameters were set to produce a close calibration to the smaller trees. For these species, the growth equation projected diameter increment to follow a parabola, with highest growth in mid-sized classes, as the other species were found to follow.

To provide meteorologic parameter values for ZELIG, a profile of mean monthly temperature and precipitation was constructed from weather data from Big Meadows at 1,081 m elevation. This meteorology was used to simulate the Chestnut Oak forest type. Using an adiabatic lapse rate of 3°C per 1,000 m elevation, a data file was created for estimating equivalent mean monthly temperatures at 600 m — the elevation used for simulations of the Cove Hardwood and Yellow poplar forests. ZELIG simulates the year-to-year variation in annual weather by using the standard deviations in mean monthly temperature and precipitation calculated from observed long term weather records. These deviations were assumed to be the same at 600 m and 1,100 m.

ZELIG Simulations

The average age following farm abandonment for each forest type was calculated from analysis of the FIA plots from this region. ZELIG was then run for this number of years for each forest type, starting from a bare plot. The projected composition after this simulation period was compared to that observed from field plots in SHEN to assure that the model projected forest composition with reasonable accuracy. For a few species, adjustments were made in their rate of seedling production until their final species composition reproduced the field data as closely as possible. This forest then was used as the initial forest for all simulations involving O_3 exposure.

All further simulations were conducted for an additional 100 years, with the same O_3 modifiers applied for each year of the simulation. Thus, in the best case, the forest received no O_3-induced modification of growth, and in the worst case, the modifiers for the highest exposure were applied every year during the simulation.

Output from the simulations, including basal area of the stand, woody biomass of the stand, and the basal areas of the individual species were plotted for the time course of the simulation.

Spatial Interpolation

A Geographic Information System (GIS) was built in ArcInfo® (version 8.02, Environmental Systems Research Institute Inc., Redlands, CA 92373) in order to visualize the spatial distribution of tree species, forest types, and O_3 exposures within the park. Details of the regional O_3 interpolation are presented in Appendix H.

The forest cover spatial database that depicts the major forest types was obtained from the NPS web page (http://www.nps. gov/gis/park_gisdata/virginia/shen.htm). The forest types are designated based on the dominant tree species in an association of forest species. These polygon data are in the UTM zone 17 projection and have an estimated accuracy of 70%. The coverage metadata indicated the distribution data should not be used at a scale less than 1:12,000. The coverage contains eight forest types plus open areas and rock outcrops: Bear Oak, Black Locust, Chestnut Oak, Cove Hardwood, Hemlock, Pine, Red Oak, and Yellow Poplar. The three most prevalent types in the park were Chestnut Oak, Cove Hardwood, and Yellow Poplar, accounting for 49, 15, and 16% of the total area, respectively. This coverage was used to create the distribution of chestnut oak, red oak, and yellow poplar forests within the park. Since detailed species information was not available in all cases, a map of deciduous versus coniferous trees was made using these data to create TREGRO maps of black cherry, basswood, red maple, sugar maple, and white ash. Maps of ZELIG results were created using Cove Hardwood, Chestnut Oak, and Yellow Poplar coverages from the NPS forest type map.

The interpolated tropospheric O_3 exposures were converted from a tabular database to a GIS database. Then the data were converted to the UTM zone 17 projection using the NAD27 datum and re-sampled to 500-m resolution using ArcInfo® software.

Spatial coverages of tropospheric O_3 impacts on tree growth based on TREGRO model runs were created using the ArcInfo/GRID® software using regression equations reported in Appendix I. The growth change projected by ZELIG was estimated by developing linear regression equations between each reported point within the O_3 range reported at SHEN (150 to 182 ppm·hr). Linear regressions were used to construct lookup tables of values corresponding to the range of O_3 exposures that were applied to the spatial database of O_3 exposures.

c. Vegetation Modeling Results

Because of the design of the simulation study, it is possible to examine the projected response of both individual trees and forest stands. The results from TREGRO simulations provide an estimate of the relative sensitivity of the individual species and likely impact of O_3 on the growth of individuals. ZELIG simulations translate those individual effects into a projection of how entire stands will perform in response to varying levels of O_3 exposure. By studying the results from both sets of simulations, an evaluation of differences in individual and stand performance is possible.

TREGRO Simulations

The results of TREGRO simulations of O_3 effects on components of tree mass are illustrated in Figure VII-26 and discussed below. In addition, regression coefficients for equations describing the simulated effect of O_3 on the total mass of the tree and the masses of shoot, stem, and root are presented in Appendix I.

In general, the greatest simulated effects of O_3 were on the mass of root systems, as has been reported previously (U.S. EPA 1996). At the highest three-year O_3 exposure, the magnitude of the effect ranged from about a 2% increase in the mass of sugar maple roots to an 18% decrease in roots of white ash. Under ambient O_3 exposure, simulated current root mass reductions, compared with the lowest simulated O_3 exposure, were less than 2% for all species except white ash (4% reduction). Decreases in the simulated total mass of the trees ranged from about 0.5% in sugar maple to about 7% in white ash over the three-year simulation (Figure VII-26). Simulated current total mass reductions in response to ambient O_3 exposure compared to the lowest simulated O_3 exposure, were less than 1% for all species except white ash, which was < 2%. The species, in order of most sensitive to least sensitive were:

White ash>basswood=chestnut oak>red maple>yellow poplar>black cherry=red oak>sugar maple

In the regression analysis, the r^2 values were generally greater than 0.98, indicating that the models were adequate in describing the relationships. The r^2 values are simply measures of fit and should not be interpreted as the proportion of total variation explained by the model, since TREGRO has no stochastic component. The equations were incorporated into the GIS to project the likely effect of O_3 on growth of individual trees where the species occur.

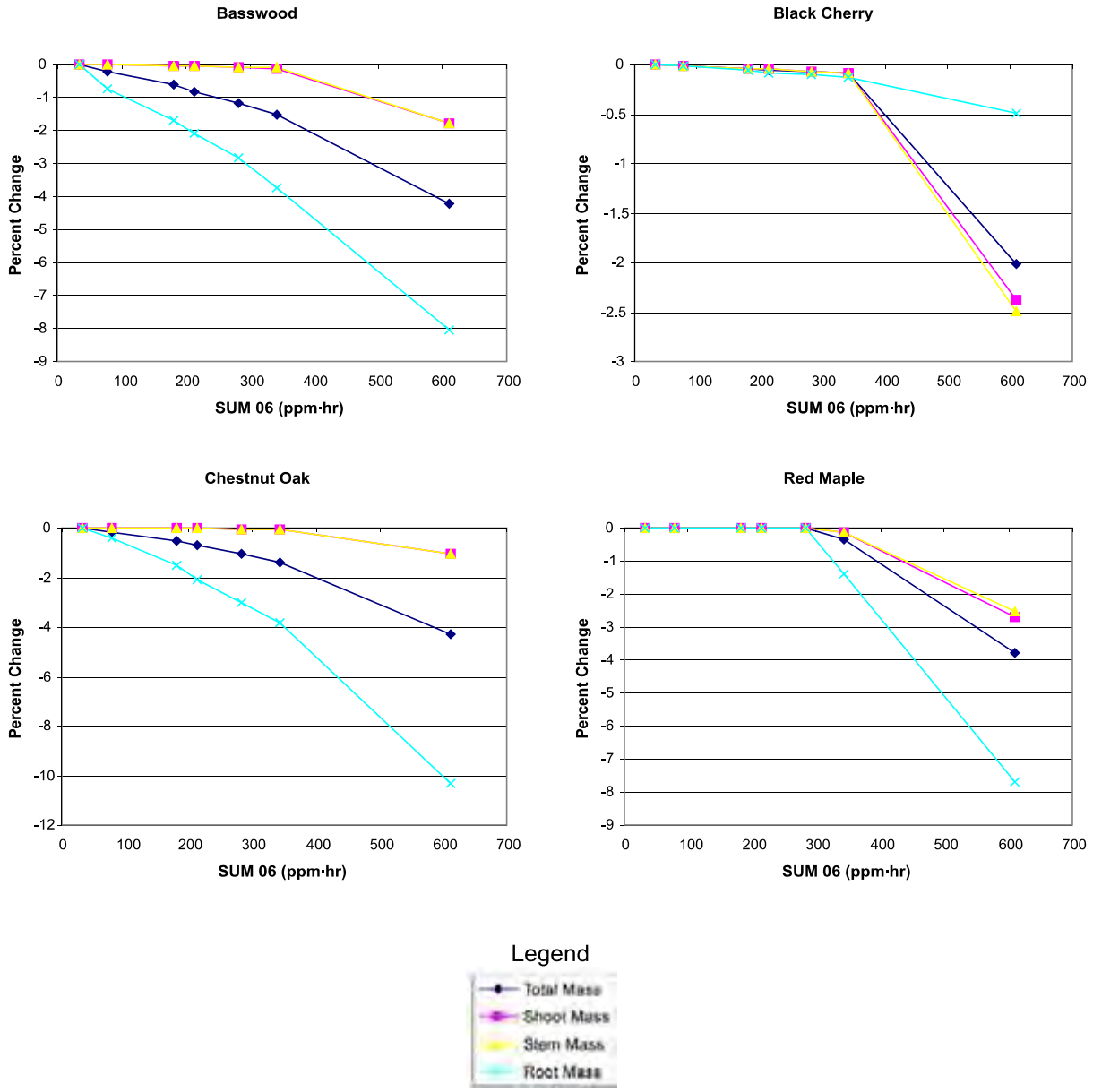

Figure VII-26. Percent change, compared to the lowest ozone exposure, in the mass of the total tree, shoot, stem, and root of basswood, black cherry, chestnut oak, red maple, red oak, sugar maple, white ash, and yellow poplar simulated by TREGRO. The ambient 5-month exposure (total for 1997-1999) was 192 ppm - hr over the three year period of the simulations.

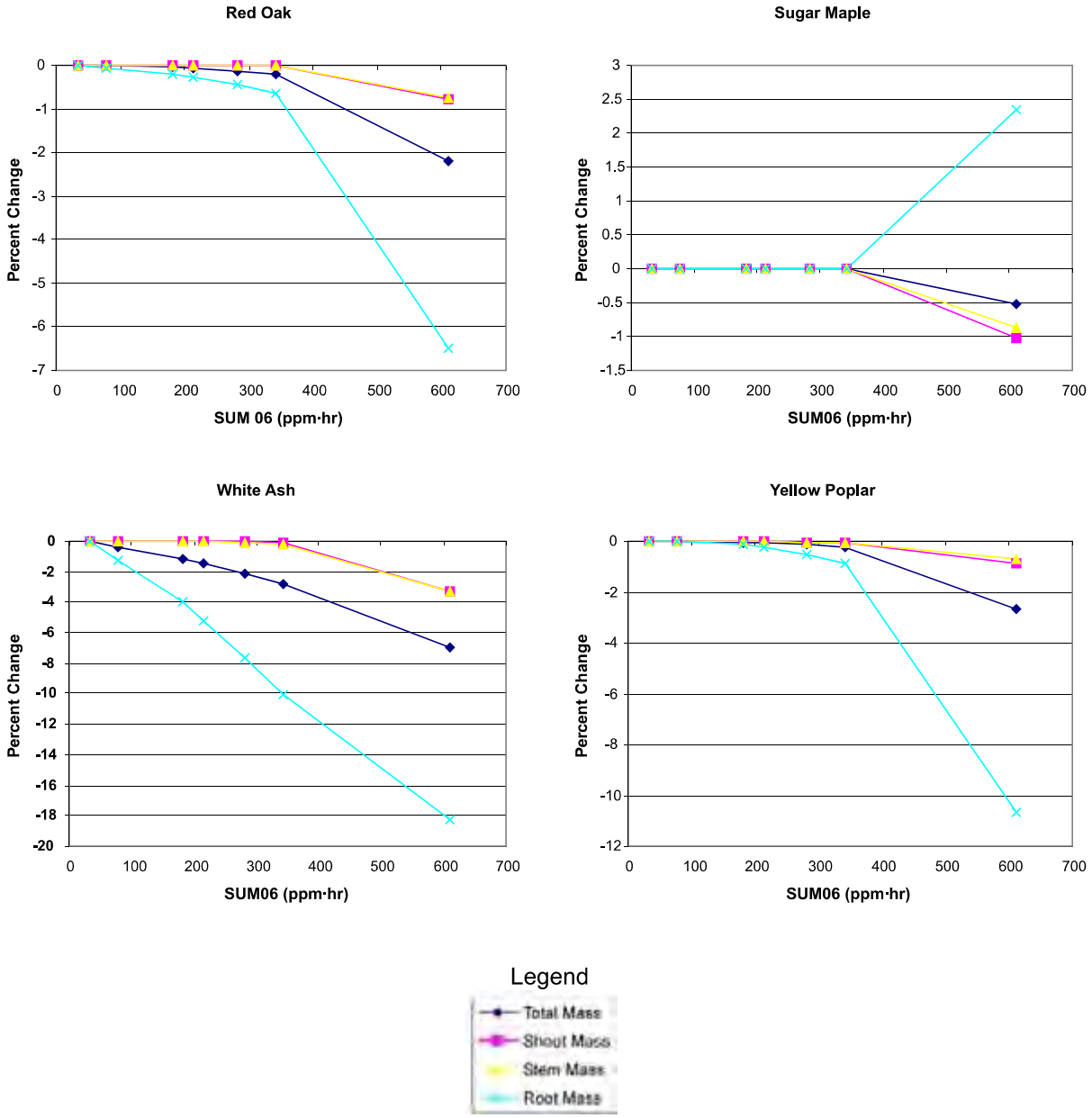

Figure VII-26. Continued.

ZELIG Simulations

The simulated responses of the three forest types to long-term O_3 exposures are illustrated in Figures VII-27 through VII-29. Because of the number of species used in the simulations, and the influence of competition, the results were highly variable, thus preventing the development of regression equations to describe an O_3 exposure-response function. In most cases, the projected effect of O_3 at a wide range of exposure levels on total stand growth and development was less than a 10% reduction in growth. However, some changes were noted in stand composition resulting from the sensitivity of individual species. These results are not surprising given that TREGRO simulated limited impacts of O_3 on growth and ZELIG allows for the possibility that stands will compensate for the loss of sensitive individuals.

The Chestnut Oak forest (Figure VII-27) showed little overall effect of O_3 exposure in terms of total basal area (<1%), woody biomass (<1%), or basal areas of most of the individual species (<10%). White ash, however, was reduced by up to 75% in the final forest due to O_3 exposure. Even at current ambient levels, the simulations indicated that white ash is reduced in growth over what might be expected at low O_3. White ash comprises about 6% of the Chestnut Oak forest in SHEN. Although the simulated impact on white ash growth does not substantially affect the overall growth and development of the chestnut oak forest, protecting sensitive species such as white ash is an important NPS concern.

Simulations of O_3 impact on the Cove Hardwood forest (Figure VII-28) projected a reduction in both total basal area and woody biomass of about 10% at the highest O_3 exposure. These simulated reductions were due primarily to changes in the basal area of yellow poplar and white ash. Yellow poplar and white ash comprise about 22 and 24% of the basal area of Cove Hardwood forests in SHEN, respectively. There was little simulated impact of O_3 at exposures less than the most severe, and stand basal area was not projected to decrease in response to continued ambient O_3 exposure.

There were few, if any differences in the productivity and composition of the Yellow Poplar forest type (Figure VII-29) associated with O_3 exposure. White ash comprises only about 2% of the basal area of Yellow Poplar forests in SHEN.

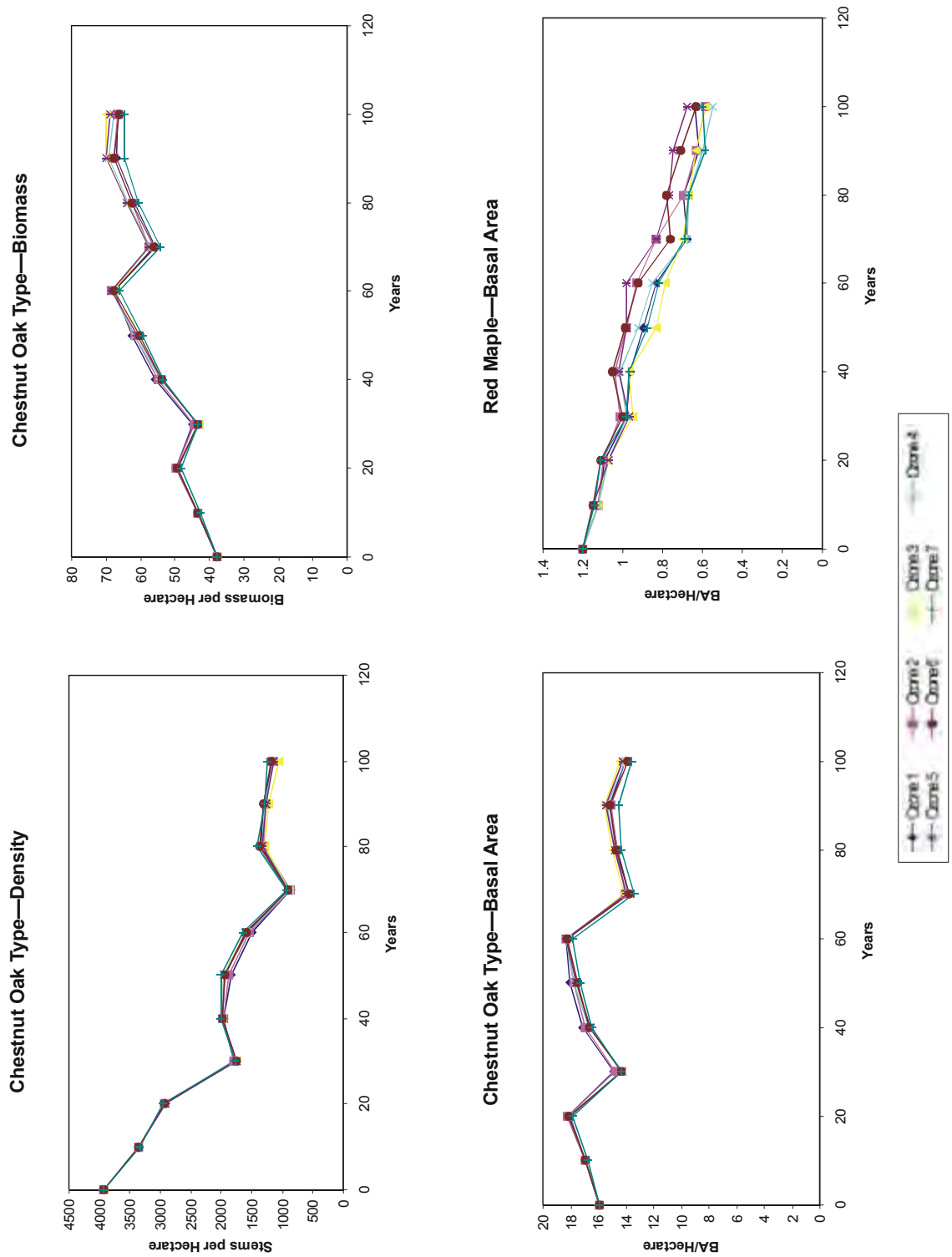

Figure VII-27. Simulated effects of ozone on the density of trees, total woody biomass, and basal area of the stand, and the growth of major species in the Chestnut Oak forest type as affected by ozone. Simulated ozone exposure levels 1-7 correspond to exposures listed in Table VII-17.

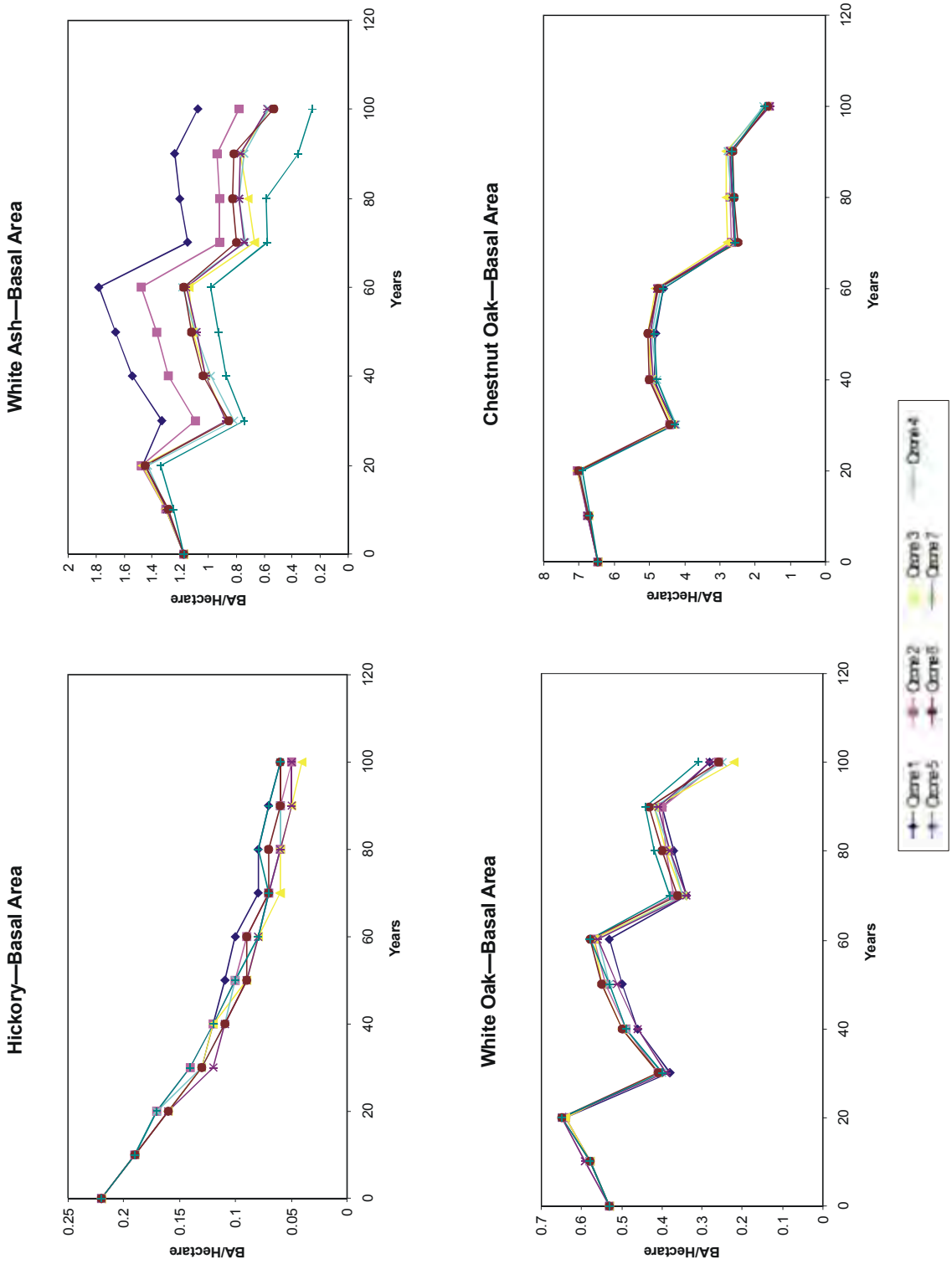

Figure VII-27. Continued.

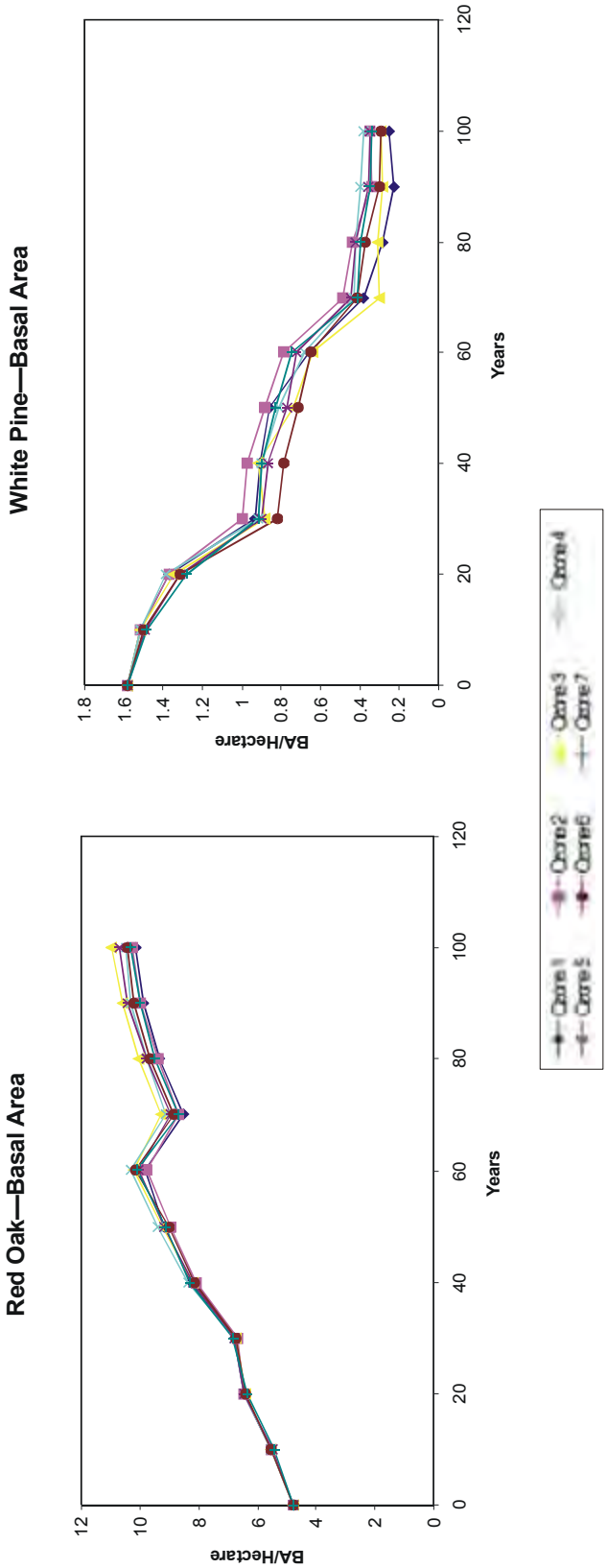

Figure VII-27. Continued.

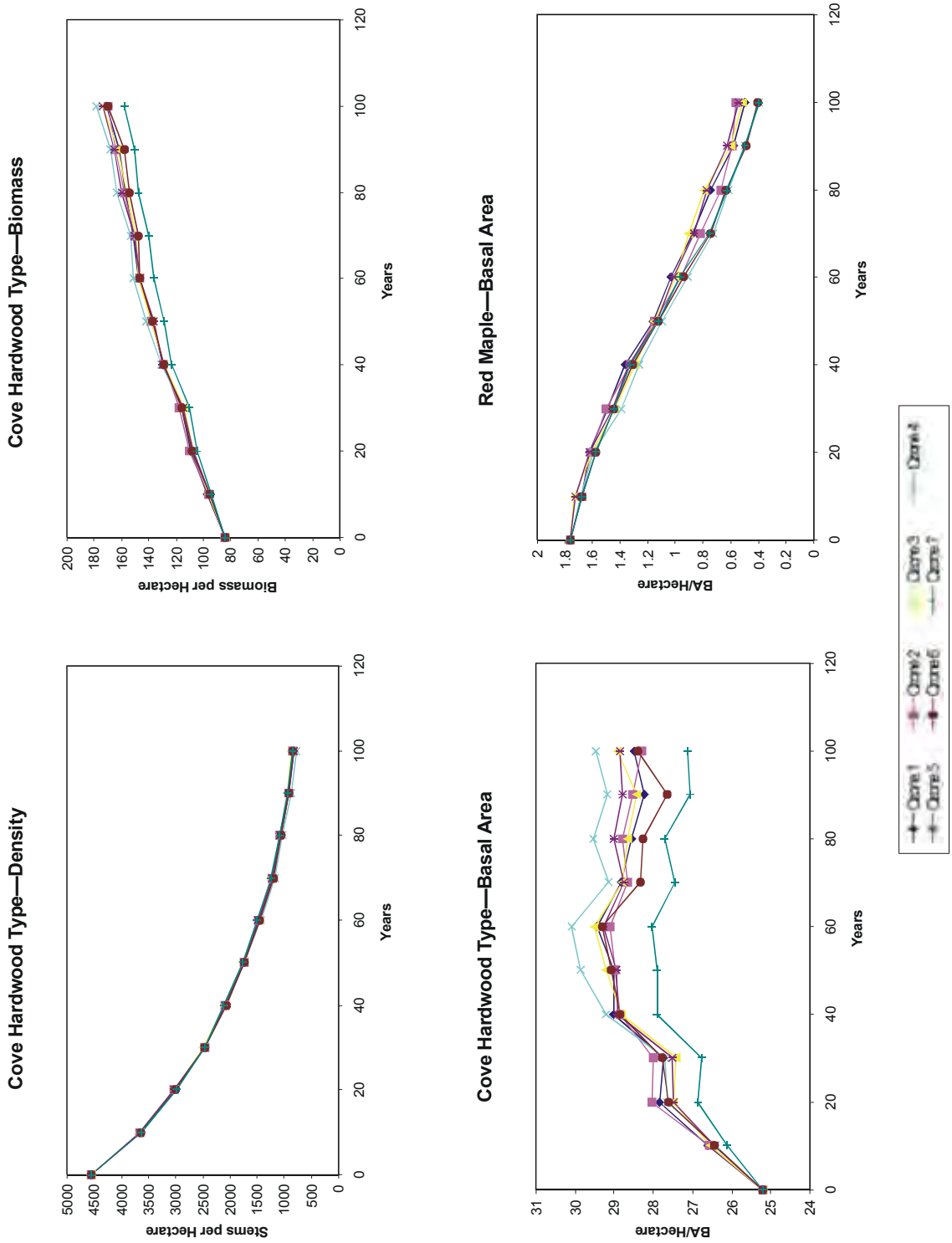

Figure VII-28. Simulated effects of ozone on the density of trees, total woody biomass, and basal area of the stand, and the growth of major species in the Cove Hardwood forest type as affected by ozone. Simulated ozone exposure levels 1-7 correspond to exposures listed in Table VII-17.

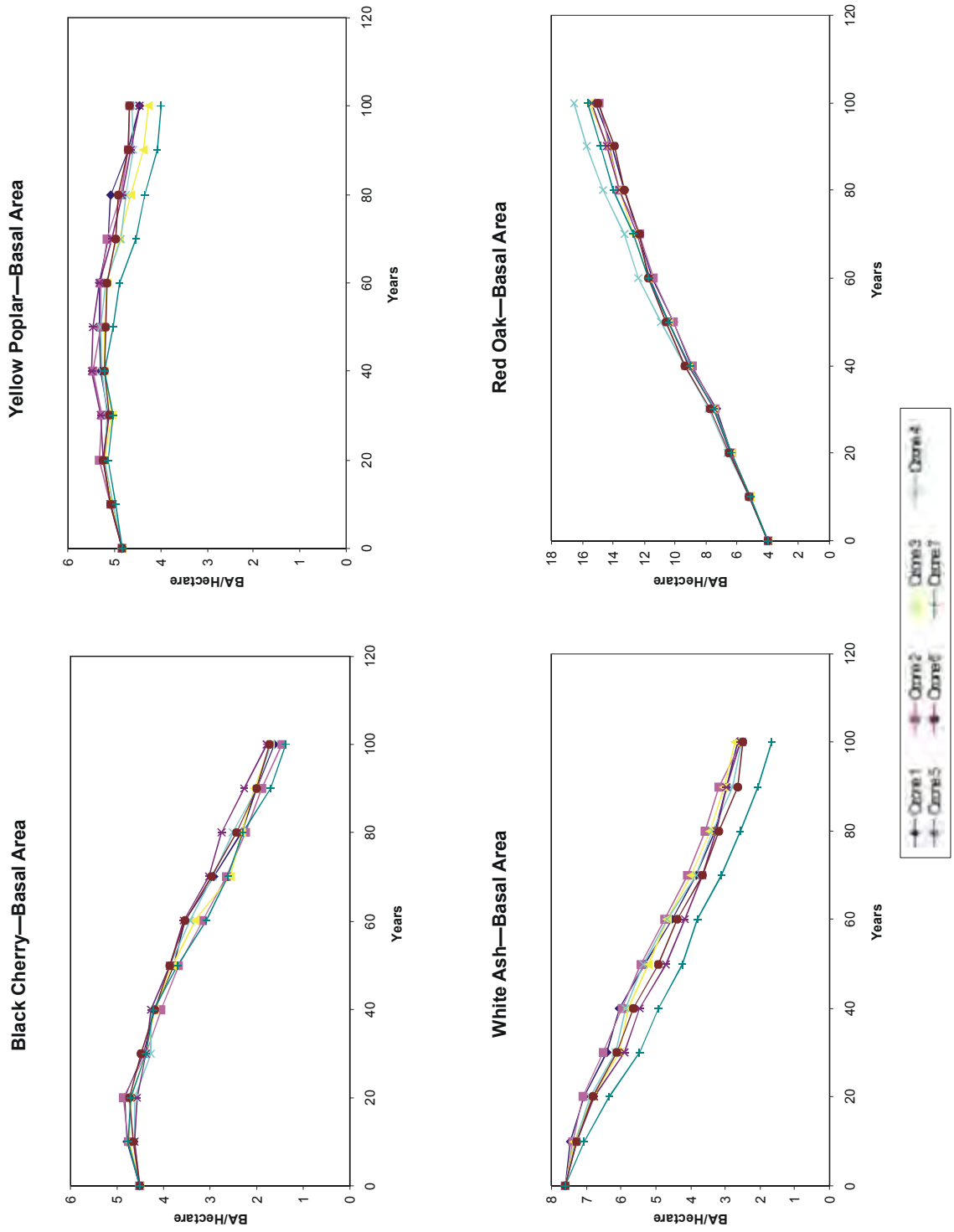

Figure VII-28. Continued.

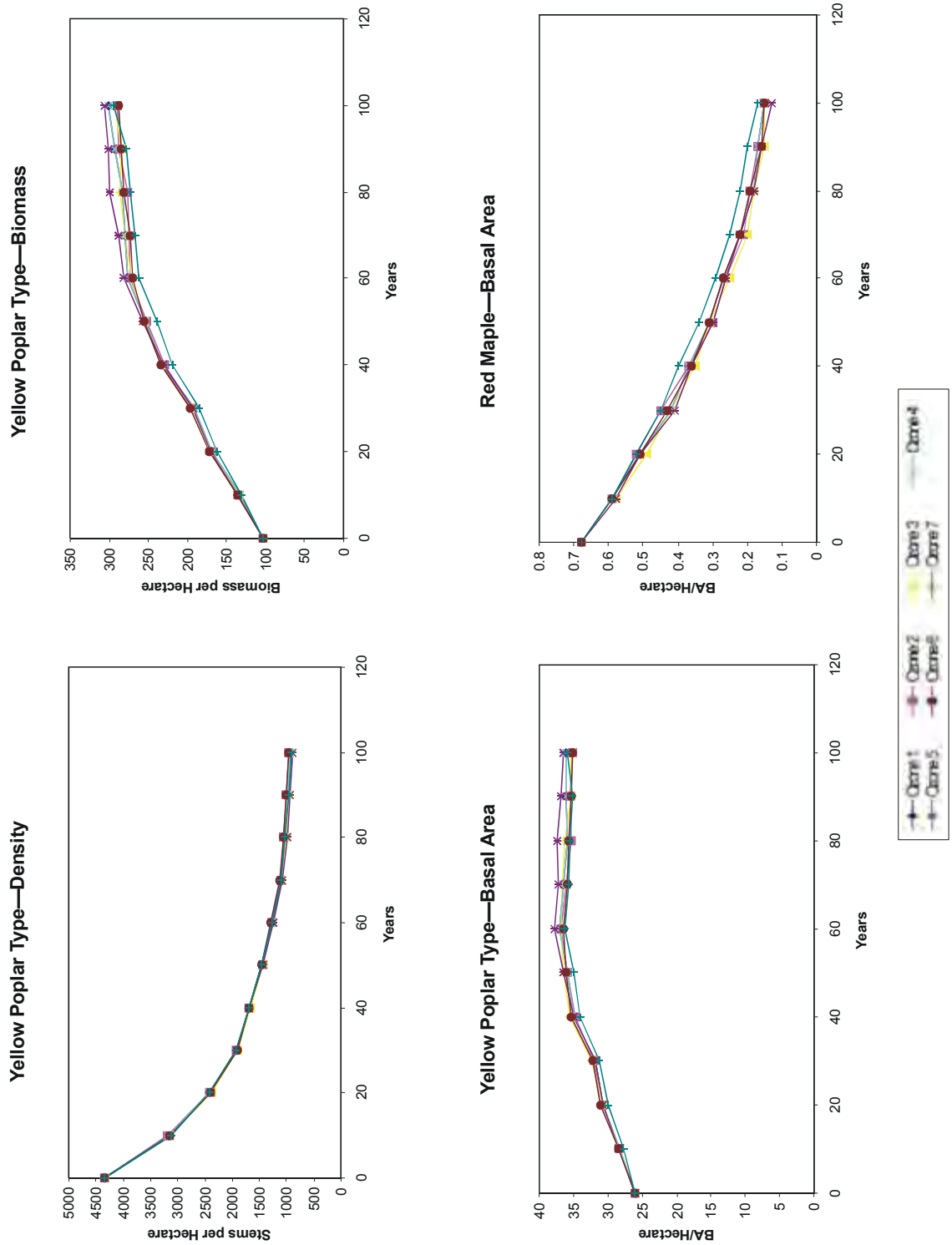

Figure VII-29. Simulated effects of ozone on the density of trees, total woody biomass, and basal area of the stand, and the growth of major species in the Yellow Poplar forest type as affected by ozone. Simulated ozone exposure levels 1-7 correspond to exposures listed in Table VII-17.

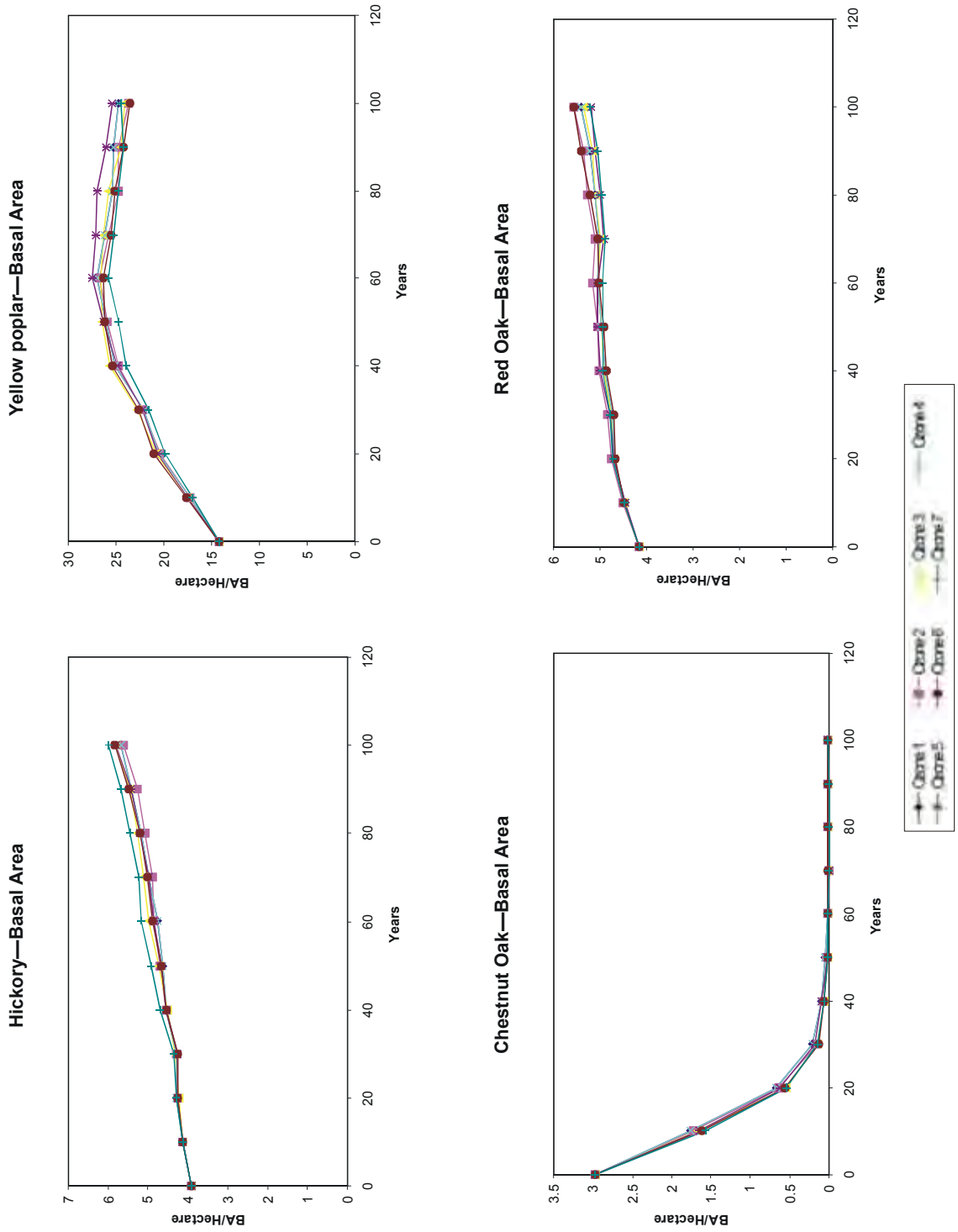

Figure VII-29. Continued.

Comparison of Individual Species versus Response in a Stand

Figure VII-30 illustrates the simulated response of species as individuals (TREGRO) compared to how the same species responded when growing in a stand (ZELIG). It is important to remember that although the responses were standardized, the TREGRO simulations lasted for 3 years whereas ZELIG simulations were for 100 years. Four general types of simulated response were identified. First, there may be a consistent response by the species, regardless of whether simulated as an individual or in a stand. This kind of response was simulated for white ash, which showed a reduction in growth due to O_3 both as an individual and in a stand. The stand response was much greater, illustrating the effect of long-term exposure.

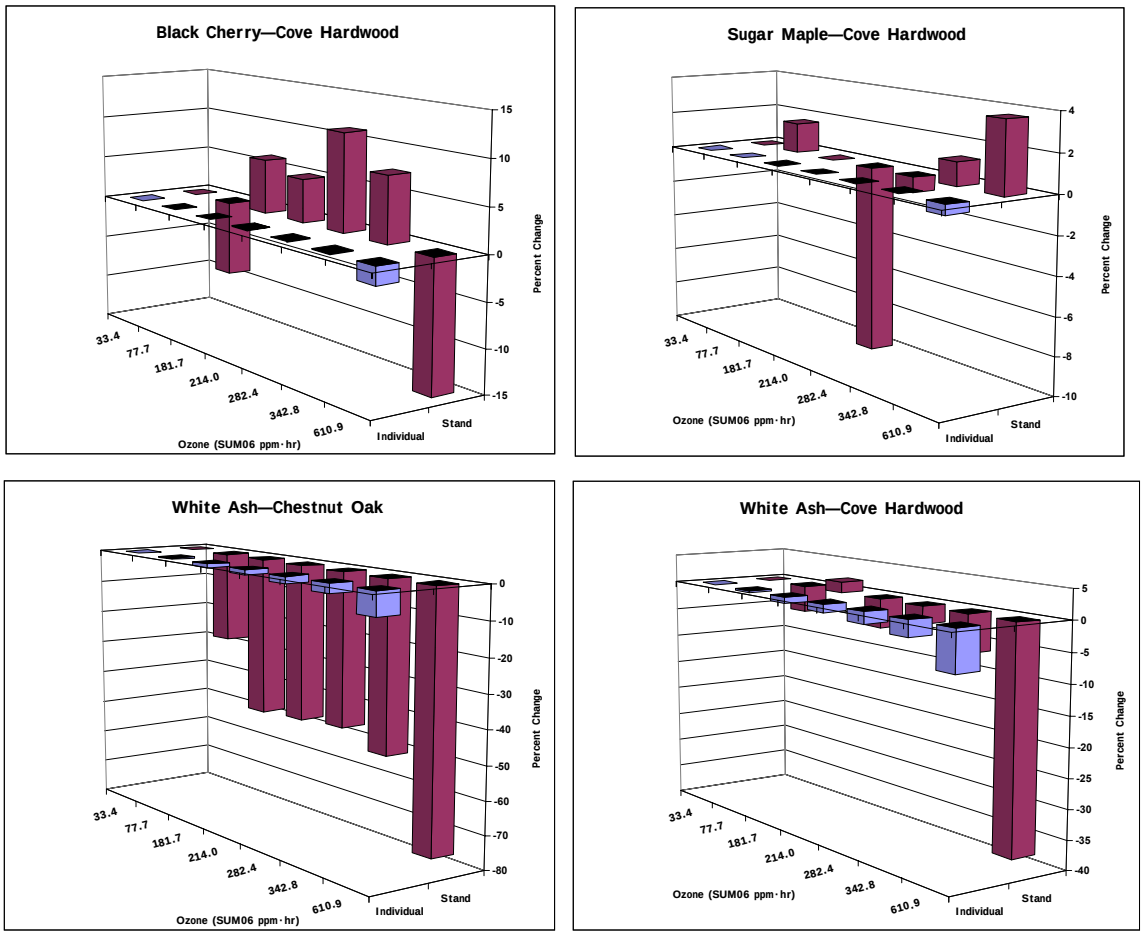

Figure VII-30. Comparison of the effects of ozone on the basal area of species simulated as individuals over three years (blue bars) versus as a member of a stand over 100 years (red bars).

Second, there may be a consistent decrease in growth as an individual, but a variable response in the stand. Such a response was illustrated by chestnut oak, red maple, and yellow poplar; the response in the stand depended upon the relative sensitivities of the other components of the forest and the level of the stress. Thus, growth in the stand may increase in some cases, taking advantage of the demise of other more sensitive species.

Third, a species that is dominant, or becoming so, may increase in growth consistently at the expense of other species, even though its own growth is impaired by O_3. This type of response was illustrated by red oak within the Chestnut Oak forest type.

Finally, some species may show the combined effects of competition and O_3. In the case of black cherry at low O_3, it is not able to compete as well as some other species in the stand. At high O_3, its own growth is diminished, preventing it from taking advantage of slower growth by other species.

The inconsistencies due to the interaction of O_3 with normal stand development would be exacerbated if other stresses such as drought or attack by insect and disease were considered.

Spatial Extrapolation

Maps illustrating the interpolation of O_3 exposures over the extent of the park for 1997-1999, and for the total exposure over three years, are shown in Figures VII-31 through VII-34. The patterns reflect primarily the differences in elevation within the park. These interpolations were used to extrapolate TREGRO and ZELIG projections over the park.

The spatial extrapolations of the effects of ambient levels of O_3 projected by TREGRO on growth of individuals are illustrated in Figure VII-35 and the figures in Appendix G. The simulated effects of current levels of O_3 on the growth of target species ranged from no change in growth to about a 1% decrease in total growth of white ash over the three year simulation. Based on these analyses, it seems likely that only the growth of white ash is significantly affected by O_3 at the present time. It is important to note, however, that although projected growth losses are small, they may accumulate over time. Furthermore, visible injury of leaves may be present at exposures less than those necessary to cause a reduction in growth. Results for white ash are shown in Figure VII-35. Results for other species, which were less pronounced, are shown in Appendix J.

The spatial extrapolations of ZELIG results are shown in Figures VII-36 through VII-38. Virtually no response of forest types to O_3 was projected over the park due to the relatively small

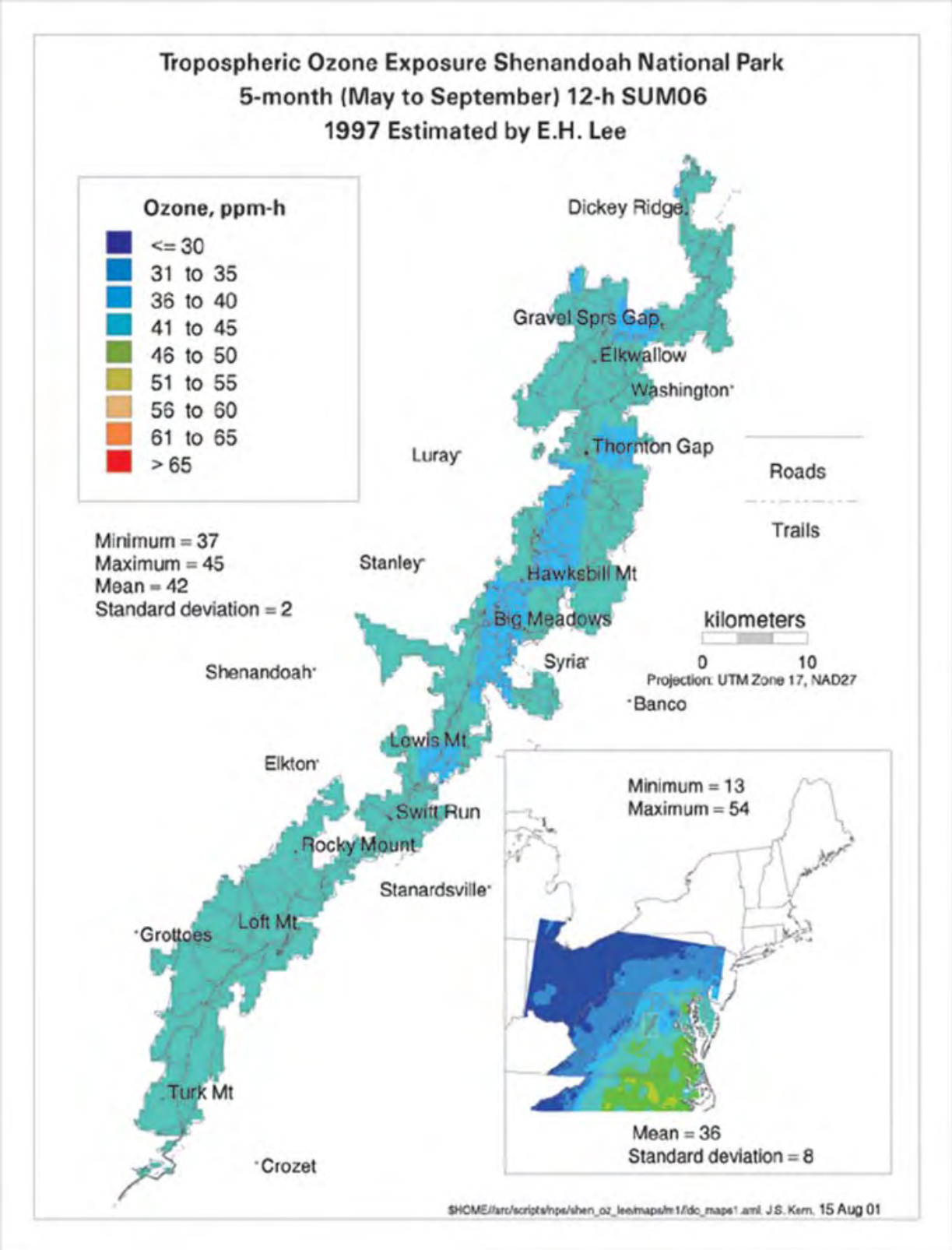

Figure VII-31. Interpolated ozone exposure (on a 4 km grid) for SHEN in 1997.

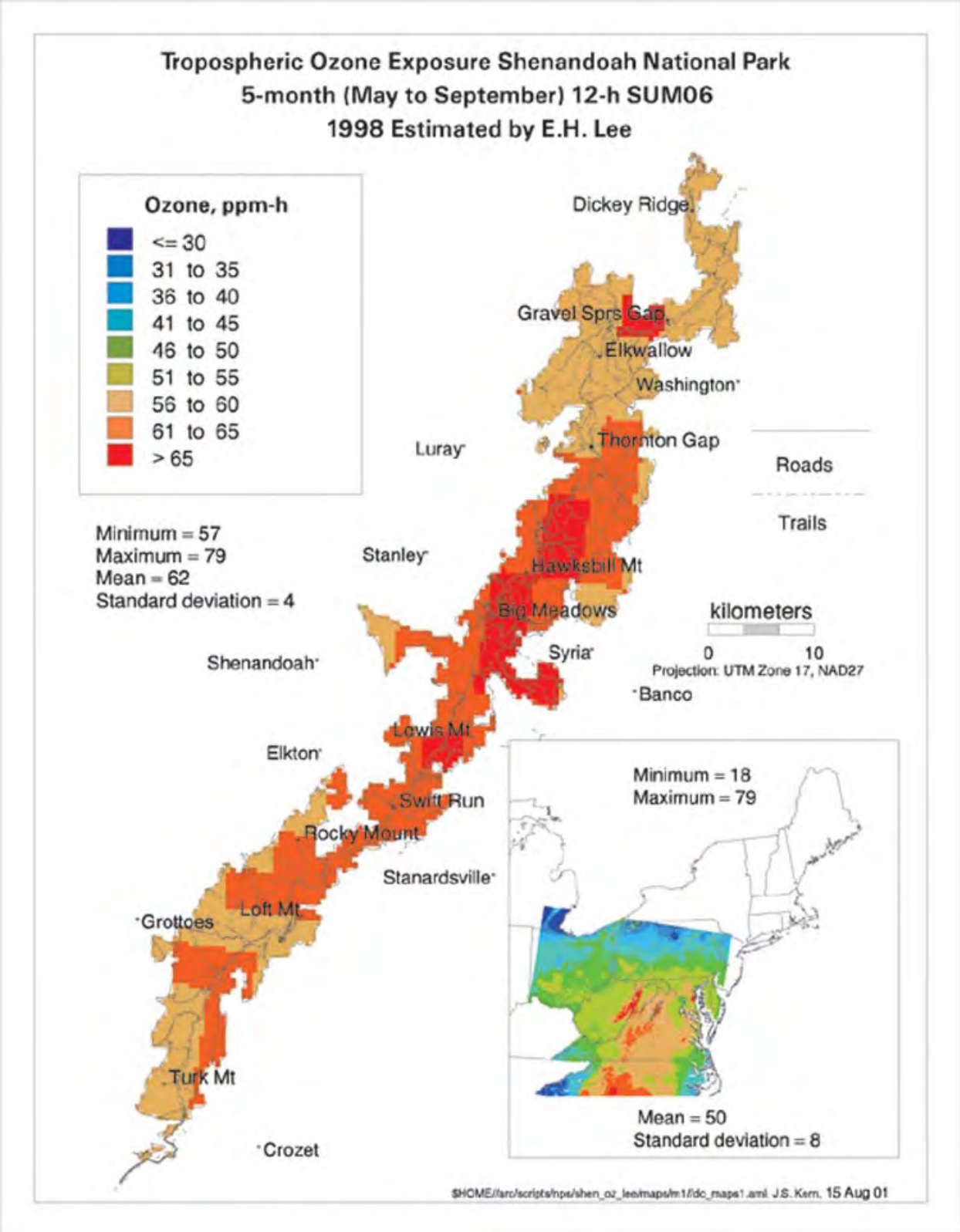

Figure VII-32. Interpolated ozone exposure (4 km grid) for SHEN in 1998.

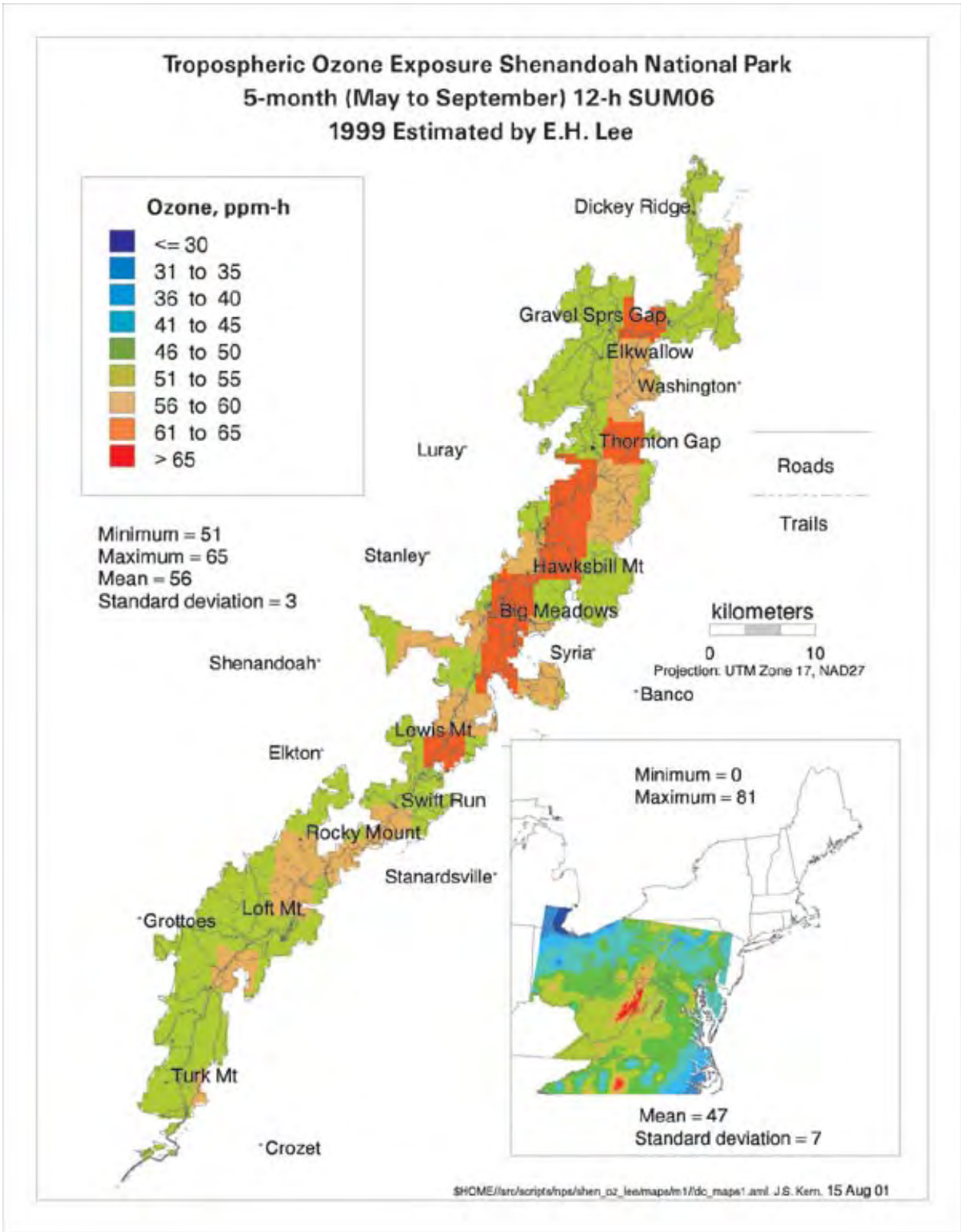

Figure VII-33. Interpolated ozone exposure (4 km grid) for SHEN in 1999.

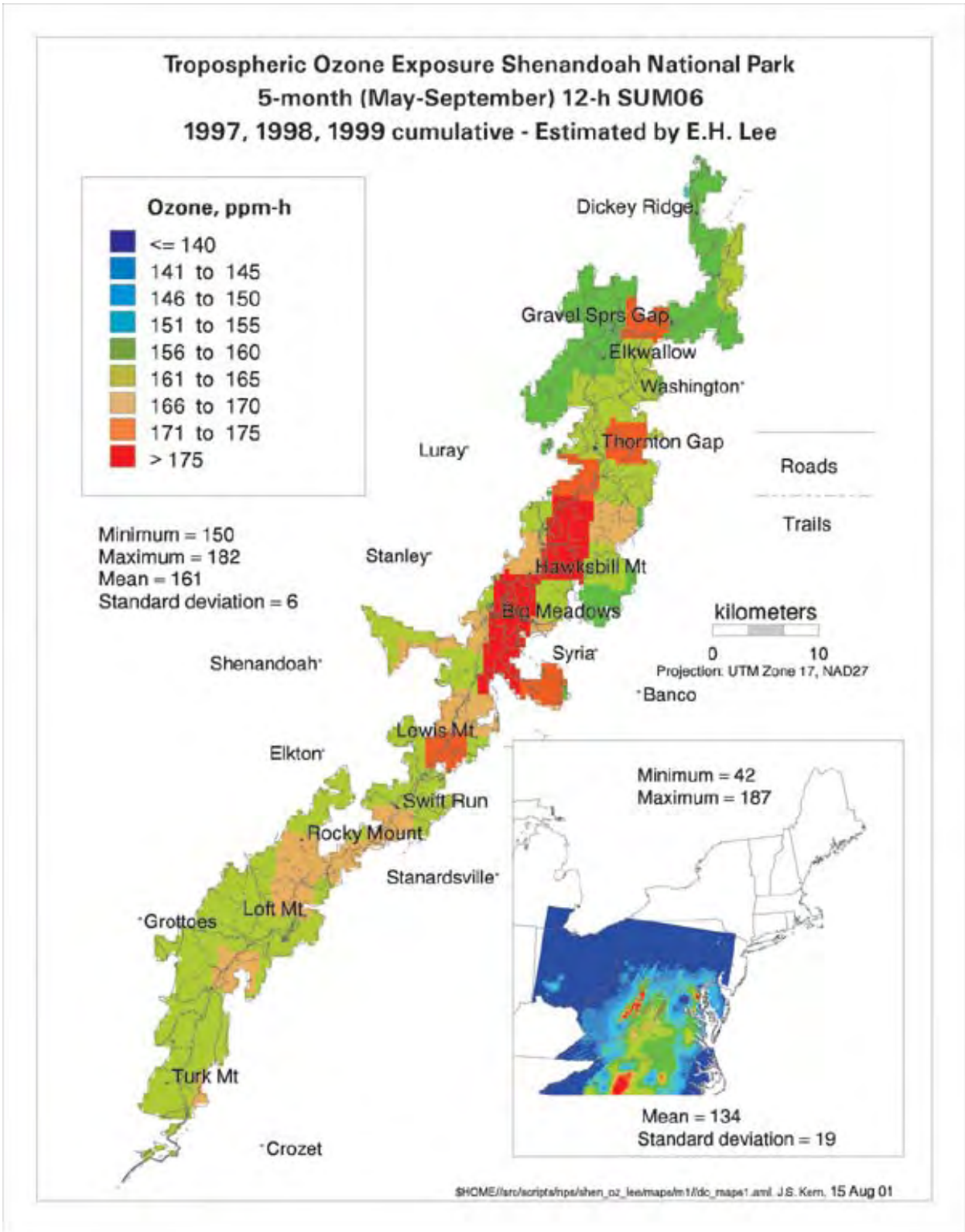

Figure VII-34. Interpolated total ozone exposure (4 km grid) for SHEN, 1997-1999.

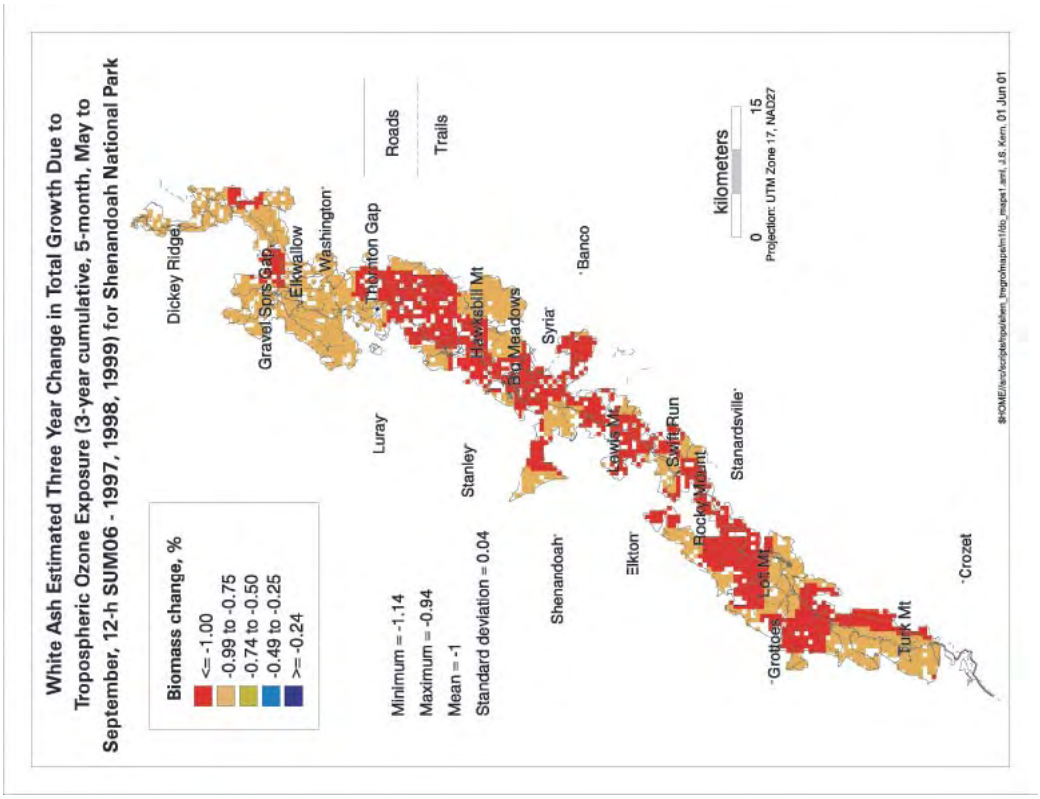

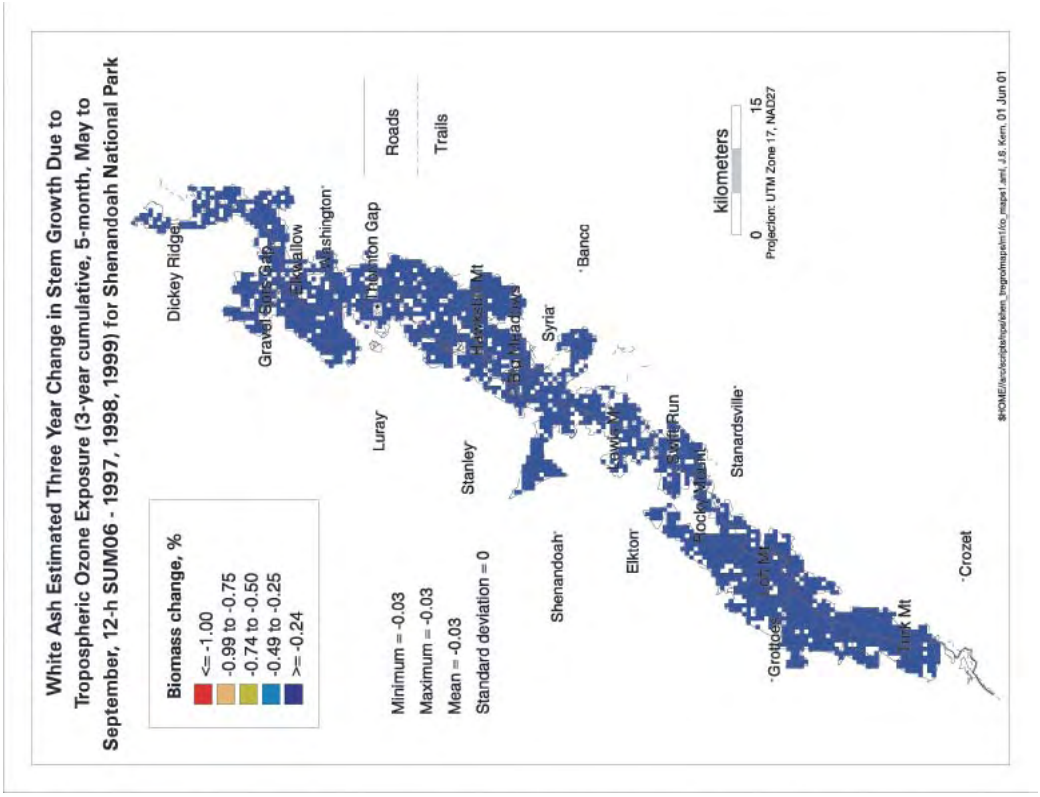

Figure VII-35. Projected change in stem (left) and total (right) mass of white ash in response to ozone exposures in 1997-1999.

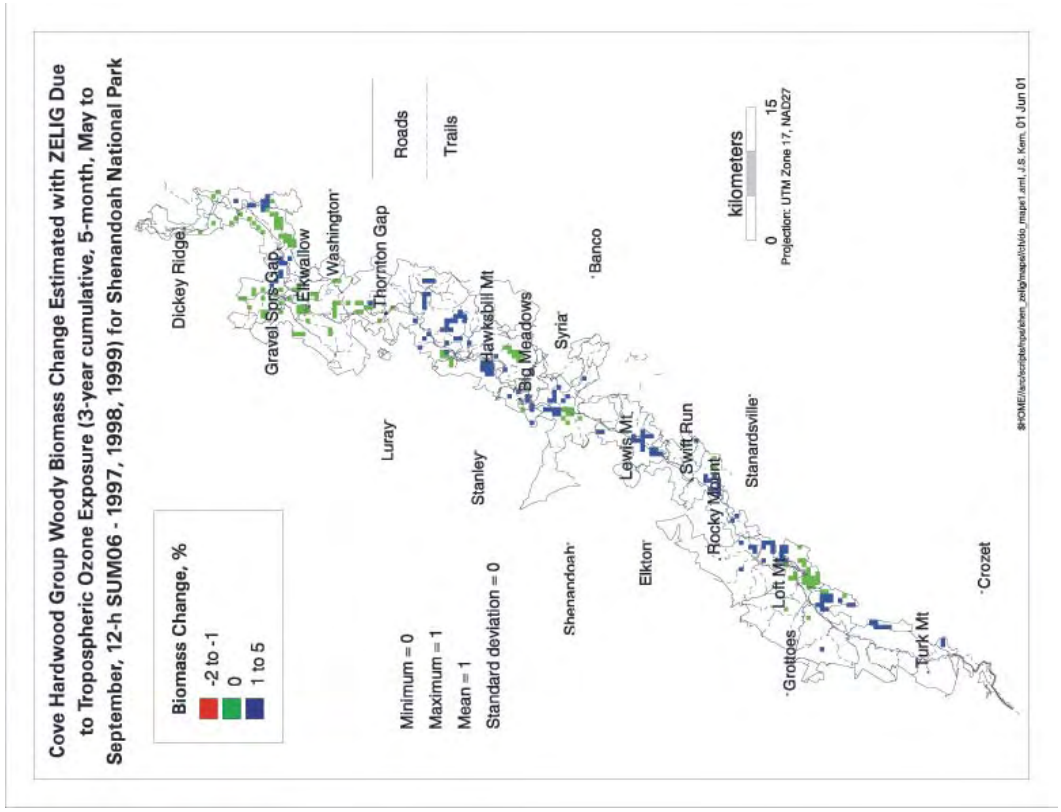

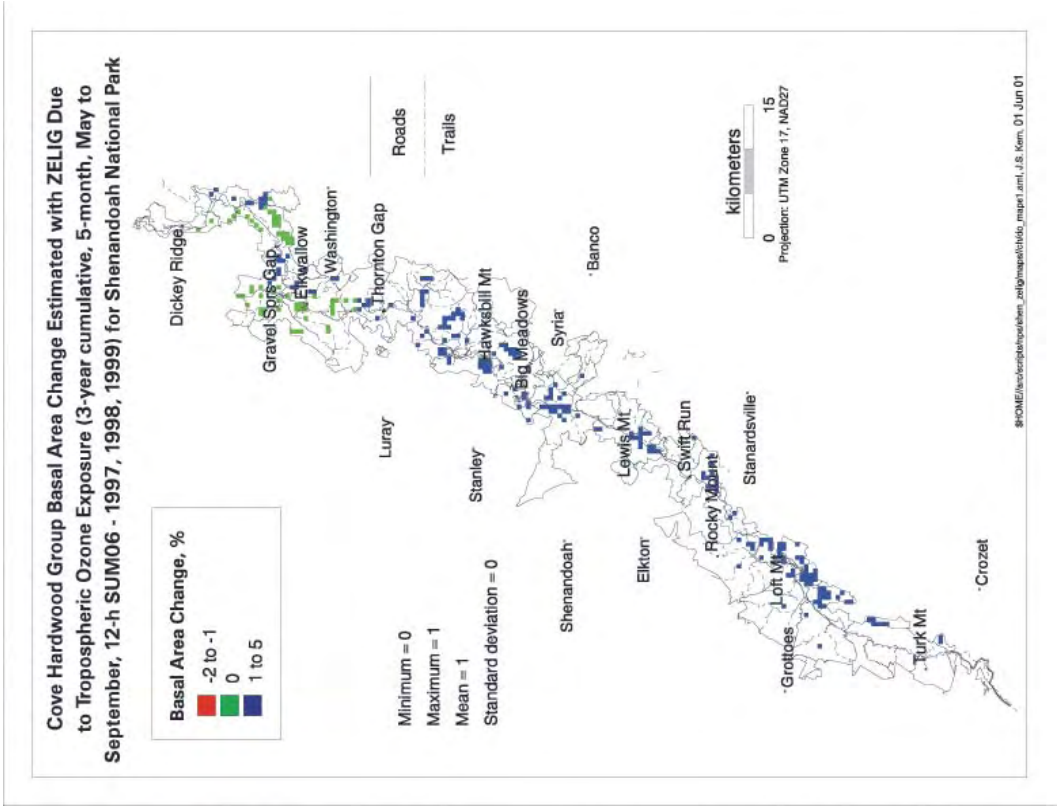

Figure VII-36. Projected change in basal area (left) and woody biomass (right) in Cove Hardwood forests in response to ozone over 100 years.

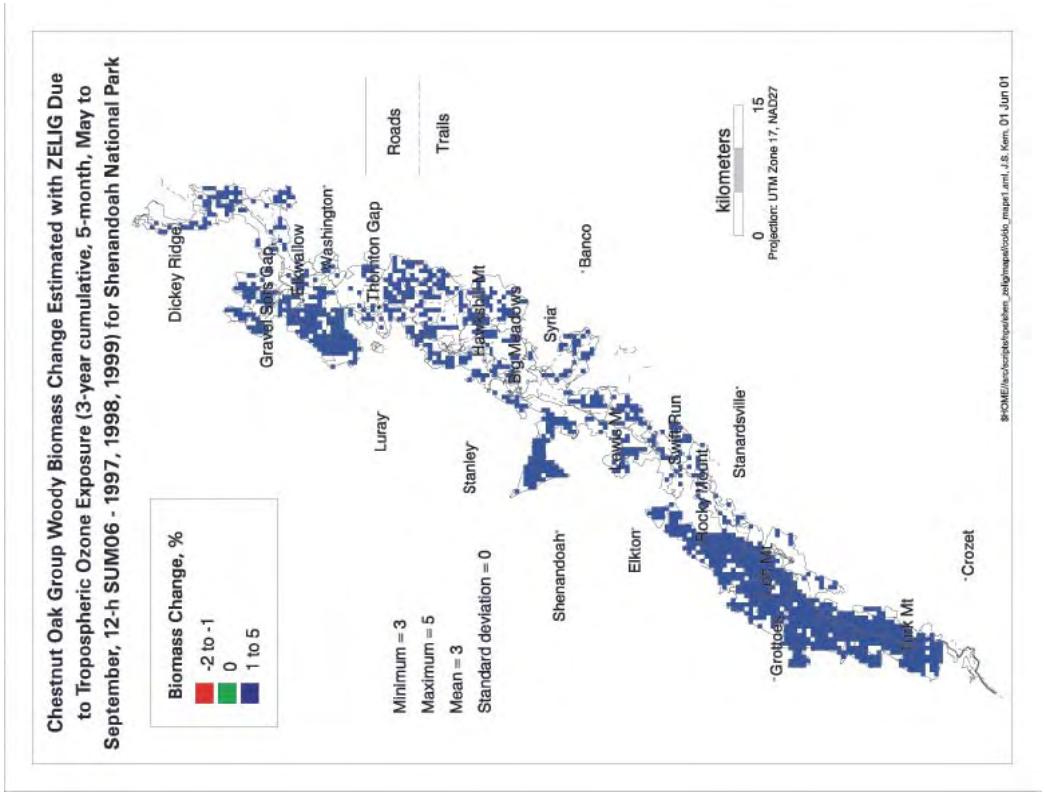

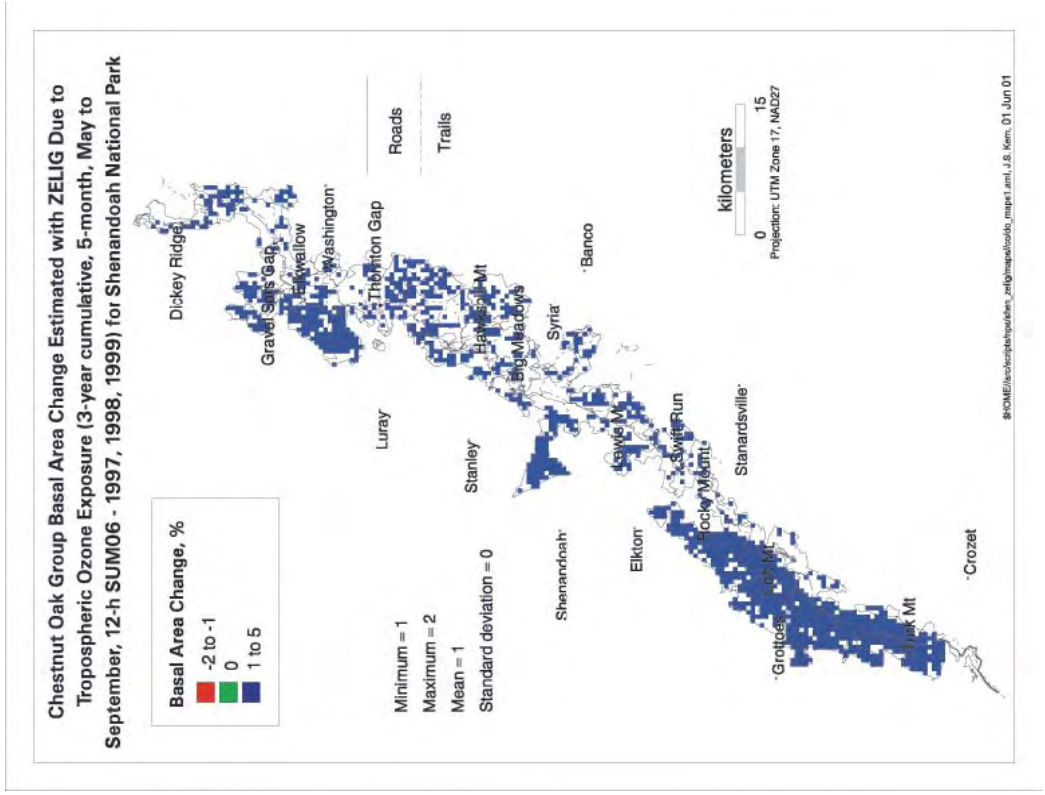

Figure VII-37. Projected change in basal area (left) and woody biomass (right) in Chestnut Oak forests in response to ozone over 100 years.

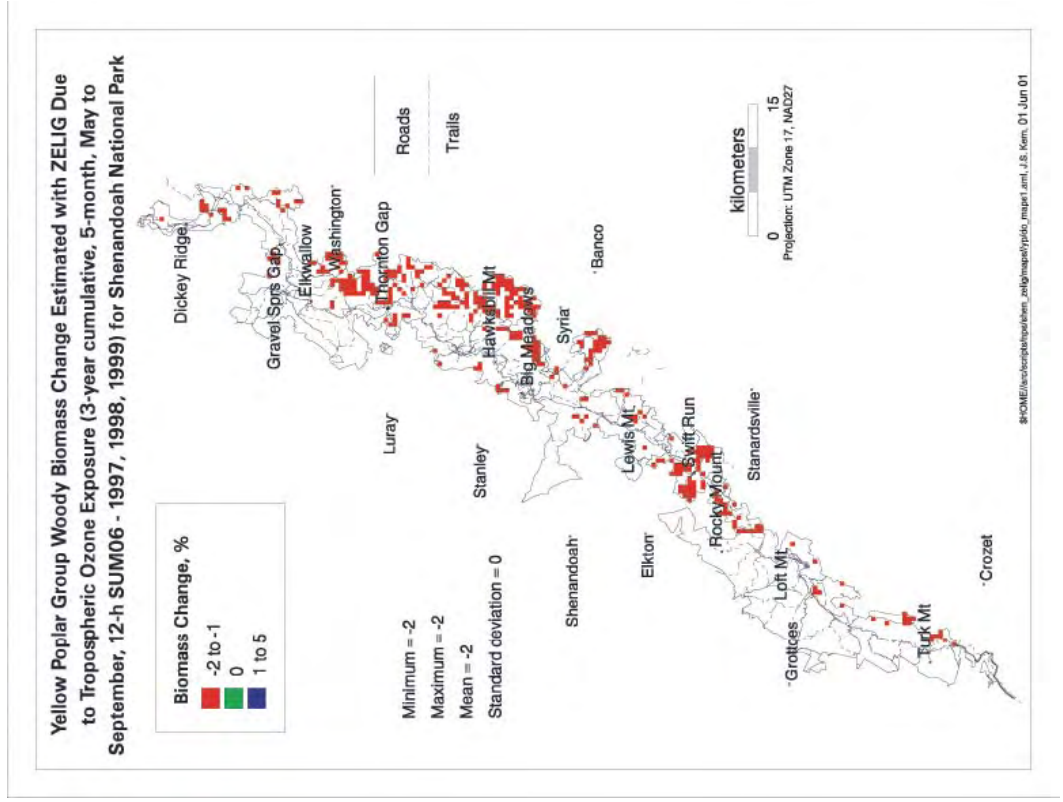

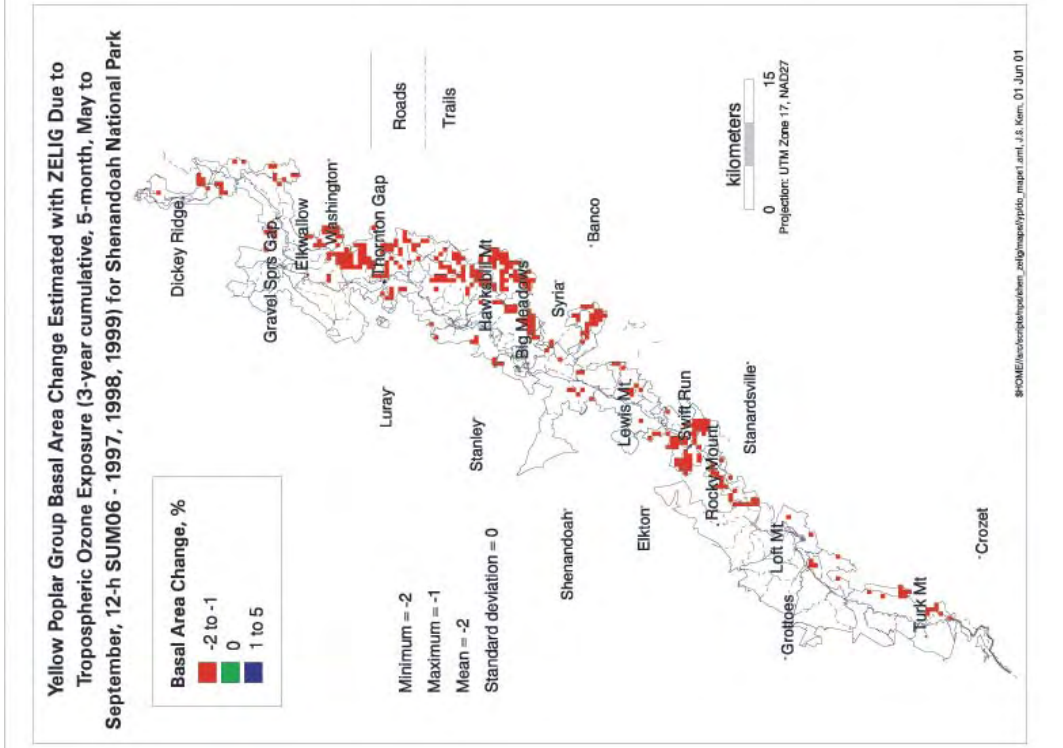

Figure VII-38. Projected change in basal area (left) and woody biomass (right) in Yellow Poplar forests in response to ozone over 100 years.

changes in growth and composition simulated by ZELIG at ambient O_3 concentrations. No changes were observed in the total projected productivity or composition of species or forests.

Uncertainties and Limitations in the Analysis

There are a number of recognized limitations in this analysis. The limitations fall into four general categories: species response, simulation methodology, model linkages, and extrapolation.

In this analysis, we assume that the species response to O_3 determined experimentally is correct, and further, that it applies to all mature individuals. We ignore potential genetic differences in sensitivity and possible influences of variable environmental conditions on the exposure-response relationships. To address this limitation, we conducted simulations at seven O_3 exposure levels. Potential differences in sensitivity can be addressed by assuming a greater or lesser exposure.

The simulation methodology has been tested and verified extensively. However, it must be remembered that simulation models are simplifications of reality, and we obviously do not simulate all processes that occur in trees and forest stands. Based upon years of use and comparisons with controlled experiments or known tree and forest growth, we believe the results reasonably reflect responses in the field.

In this assessment, we linked TREGRO to ZELIG using only three modifiers of stand processes. It would be possible to use many more linkages, but the research necessary to establish those linkages was beyond the scope of this project. The TREGRO-ZELIG linkage has been subjected to peer-review and we believe it is a reasonable approach to provide a physiological mechanism for estimating O_3 impact on stand growth.

Finally, we extrapolated the results of our simulations across SHEN. This extrapolation assumes that the O_3 exposures we hypothesize to occur do, in fact, occur; that the trees and forest types are found where the maps indicate they are found; that the exposure-response relationships developed from the simulations hold at all locations in the park; and that there are no interactions with other stresses. We do not believe these assumptions limit the validity and usefulness of the assessment. It is important to note, however, that pollutant stresses do not act individually. Trees and forest stands are exposed simultaneously to multiple air pollutants and also to multiple diseases, insects, and other disturbance mechanisms. Multiple stresses probably affect the structure and function of park ecosystems beyond the effects of one stressor in isolation.

d. Prognosis for Recovery of Terrestrial Ecosystems

Based on the results of this simulation study, it seems unlikely that reductions in the growth of forest trees in excess of about 1%, or in the composition of forest stands, are occurring as a result of O_3 exposure at SHEN. An exception to this is white ash, which seems to be more sensitive, both as an individual and in a stand, than the other species.

In general, these results are in agreement with other simulations of O_3 effects on the growth of mature trees and forests. For instance, Laurence et al. (2001) reported a simulated decrease in growth of about 0.7% for loblolly pine and 0.2% for yellow poplar over the southern United States. Woodbury et al. (1995) also reported relatively small growth reductions in loblolly pine using a different simulation system. Ollinger, in Laurence et al. (2000), found reductions in net primary productivity of about 5 to 9% over a five-year simulation of forests in the northeast United States. His analysis showed that drought stress had a greater impact on growth than O_3, and in the driest conditions, drought reduced the O_3 response by 25%.

On the other hand, large reductions in growth have been simulated in some studies elsewhere. Tingey et al. (2001) simulated reductions in growth of ponderosa pine (*Pinus ponderosa*) due to O_3 ranging from close to 0 to greater than 40% under the most severe conditions in southern California. Weinstein et al. (2001) reported no change in the simulated growth of black cherry in the Great Smoky Mountains, but large reductions in the growth of yellow poplar and red maple (>40% and 20%, respectively). Their simulations used essentially the same parameter values for the species as we used in this study.

There are two potential explanations for these differences in model output. First, we used three years of actual meteorological observations from Big Meadows whereas Weinstein et al. (2001) used the same weather (1992), repeated three times. We know that both 1998 and 1999 were warm years, which could reduce the effect of O_3 in the model (Tingey et al. 2001). The second difference relates to the construction of O_3 profiles. Our method increases the exposure in proportion to the annual maximum O_3 concentration. Weinstein et al. (2001) applied a multiplier to all concentrations; in their 0.5 x ambient profiles, the lowest concentrations were also decreased by 50% whereas our lowest exposure was reduced by only 13% of the total O_3 exposure. This makes a substantial difference in the "background exposure" that is used to calculate projected growth decrease. Differences in the elevated O_3 exposure, calculated using a constant multiplier versus proportional increase, could affect the dynamics of carbon gain,

particularly when there is heavy demand on stored carbohydrates for growth, and this could account for differences in our projections.

There are few field studies of the effects of O_3 on mature trees. McLaughlin and Downing (1995) projected circumference growth reductions due to the interaction of O_3 and soil moisture of from 0 to about 30%, depending on the year. For conditions similar to those in this study, the projected growth loss was 7% or less. Samuelson and Kelly (1996) compared the response of seedling and mature red oak to O_3 and found, in general, that mature trees had a greater uptake rate of O_3 than did seedlings. However, in a three-year study, they did not find the growth of mature trees to be reduced by ambient O_3 at Norris, Tennessee.

Duchelle et al. (1982) exposed seedlings of eight tree species to ambient and charcoal-filtered air in open-top chambers at Big Meadows. They reported a substantial decrease in height growth of yellow poplar seedlings under ambient O_3 conditions, but did not report total growth or foliar injury. Neufeld et al. (1995) exposed black cherry seedlings to O_3 in open-top chambers at Great Smoky Mountains National Park. They reported seasonal losses of 1-2% in growth at ambient O_3. Effects on seedlings do not necessarily translate to effects on mature trees, however.

Recently, Chappelka and Samuelson (1998) reviewed the literature and concluded that growth losses in the eastern United States from ambient O_3 are likely less than 10% and are affected by a multitude of factors. Intuitively, it seems unlikely that the growth reductions of up to 40% reported by Weinstein et al. (2001) for the Great Smoky Mountains could have been occurring over long periods of time without such differences being measured in forest inventories. We believe O_3 is more likely to be a long-term debilitating stress, causing relatively small changes in growth on an annual basis, but some potentially large changes in species composition, such as for white ash in SHEN.

Ozone causes visible injury on many plant species in SHEN, an endpoint that cannot be addressed in this simulation study. Hildebrand et al. (1996) reported that O_3, at approximately the same levels as reported for SHEN in this study, caused visible injury on yellow poplar, black cherry, and white ash. Although a high percentage of the trees had symptoms of O_3 exposure, the amount of leaf area injured was relatively small. They did not make measurements of growth that could be compared to our results.

Results of the analyses performed for this assessment suggest that further deterioration in air quality at SHEN would begin to take a toll on the growth of forest trees and the composition of

stands. In addition, whereas the current impacts of O_3 seem to be small, it is important to remember that O_3 does not act alone. The O_3 effects modeling analysis is an attempt to isolate the effects of O_3 from those of other stresses, but other stresses do occur, potentially exacerbating the relatively small, direct growth effects of O_3 at current concentrations.

The results of the O_3 effects modeling suggest that up to a 20% increase in current ambient O_3 could be tolerated in the absence of other significant stressors before substantial effects on tree growth and stand composition would occur. However, it is likely that some species, such as white ash, would begin to decline further in growth with any increase in ambient concentrations. We would also expect impacts to occur on stand composition, primarily through the effects on white ash. Visible foliar injury to sensitive species would certainly increase beyond what currently occurs. Given these results, it seems that the critical exposure level for sensitive species like white ash is likely below current ambient levels. Simulation results suggest that critical O_3 exposures ranging from about 15% less than current ambient levels to up to 20% greater that current ambient levels should protect against growth and species composition impacts to sensitive (e.g., white ash) and less sensitive (e.g., sugar maple) species, respectively. The critical level to protect against visible foliar O_3 injury or growth effects on tree seedlings would be substantially lower than current ambient exposure, probably in the range of 8 to 12 ppm·hr SUM06 (3 month, 12-hour) or 10 to 15 ppm·hr, respectively, as suggested by Heck and Cowling (1997).

3. Visibility

As shown in Section V, visibility at SHEN, while showing some indications of improvement, is presently much worse than estimated natural conditions. In order to assess the sensitivity of visibility to changes in emissions, future visibility conditions at the park were estimated from modeling analyses of expected and hypothetical emissions scenarios described in Section IV. Emissions and ambient conditions from 1990 were selected as the base case for this projection. The 1996 column in Table VII-21 reflects visibility improvements related to SO_2 emissions reductions mandated by Phase I of the Title IV Acid Rain Program of the CAAA of 1990.

The visibility condition associated with each emissions (modeling) scenario was calculated using the expected reduction in particle concentrations (see Table VII-21, top half) and the

Table VII-21. Degree of visibility improvement associated with the emission reductions scenarios given in Section IV, relative to the 1990 Base Case.

Attribute	1996	Scenario 1 2007/10	Scenario 2 2020	Scenario 3 2020	Scenario 4 2020
Combined Reduction of Fine Particle Ammonium Sulfate and Nitrate Relative to the 1990 Base Case					
Annual Mean	-6.9%	-15.7%	-17.5%	-41.7%	-50.4%
Warm Season Mean	-15.0%	-28.5%	-30.8%	-55.7%	-63.6%
Expected Visibility Improvement[a]					
Annual Mean	5.1%	11.7%	13.0%	31.0%	37.5%
Warm Season Mean	12.4%	23.5%	25.4%	45.9%	52.4%

[a] Relative humidity adjustment factors of 3.65 and 4.31 were used for annual and warm season means, respectively

corresponding change in light extinction coefficient (see Appendix B for calculation method). The observed 1990 annual mean and warm season mean visibility conditions at SHEN were 111 Mm^{-1} (35 km visual range) and 187 Mm^{-1} (21 km visual range), respectively. Expected improvements from this base case are presented in Table VII-21 (bottom half). The estimated annual mean improvement in atmospheric extinction ranged from 105 to 69 Mm^{-1} (visual ranges from 24 to 44 km). Although these visibility improvements represent progress toward the national visibility goal (Section I), they fall substantially short of the nearly 80% improvement in extinction needed to restore natural conditions (Section IV) as is required by the 1999 Regional Haze Rule. An interesting comparison can be made between the model projections of improvements for 1996 of 5.1 and 12.4% for the annual and warm season mean and the actual changes estimated from ambient data collected in the park in 1990 and 1996 of 12 and 10% for the same respective averaging times (Table V-11). The improvements estimated by the model for 1996 as compared to 1990 Base Case were generally similar to the actual differences in the "measured" extinction at the park for the years 1990 and 1996.

The encouraging recent trend in visibility at the park, notwithstanding, current visibility conditions still represent a significant departure from what a visitor could experience if natural conditions were more prevalent. The park certainly has benefitted (Malm et al. 2002), and should continue to benefit, from emission reductions contained in Scenario 1 (primarily Title IV emissions reductions at EGUs and Federal Tier II standards; Section IV). However, these conditions are forecasted to achieve only an 11.7 % improvement in annual average visibility (Table VII-21). Only emissions scenarios 3 and 4, which have more stringent controls

(including over 90% reductions for EGUs), would make significant progress towards the national visibility goal. For the warm season, the degree of needed improvement is nearly 85%, but even the most stringent scenario (4) was forecasted to achieve only a 52.4% improvement in visibility (Table VII-21).

VI. ENVIRONMENTAL RECEPTORS AND EFFECTS OF AIR QUALITY

A. PURPOSE

The purpose of this section is to describe the current status of air quality related values (AQRVs) in Shenandoah National Park (SHEN), trends in resource conditions, and available data regarding air pollution dose-response relationships. Information is presented for aquatic, vegetation, and visibility resources.

B. AQUATIC ECOSYSTEMS

1. Current Status of Streamwater Chemistry

Information concerning the status of streams within SHEN relative to acidic deposition was provided through the Shenandoah Watershed Study (SWAS), a cooperative program of the Department of Environmental Sciences at the University of Virginia and the National Park Service (NPS). The primary scientific objective of the SWAS program has been to improve understanding of watershed processes and hydro-biogeochemical conditions in forested watersheds in SHEN and within the larger central Appalachian Mountain region. The primary on-going resource management objective is to detect and assess hydro-biogeochemical changes that are occurring in relatively pristine ecosystems in response to acidic deposition.

The SWAS program was initiated in 1979, with the establishment of water quality monitoring on two streams (Webb et al. 1993). The current watershed data collection involves 14 primary study watersheds (Figure VI-1), including a combination of discharge gauging, routine quarterly and weekly water quality sampling, and high-frequency episodic, or storm-flow, sampling (Galloway et al. 1999). In addition, a number of extensive stream chemistry surveys, fish population surveys, and other watershed data collection efforts have been conducted throughout the park in support of various research efforts. The SWAS program is presently coordinated with the Virginia Trout Stream Sensitivity Study (VTSSS), which extends quarterly sampling to an additional 51 native brook trout (*Salvelinus fontinalis*) streams located on public lands throughout western Virginia (primarily in the George Washington and Jefferson National Forests).

Aquatic effects research at SHEN has contributed significantly to the development of scientific understanding of watershed processes that control aquatic effects of acidic deposition

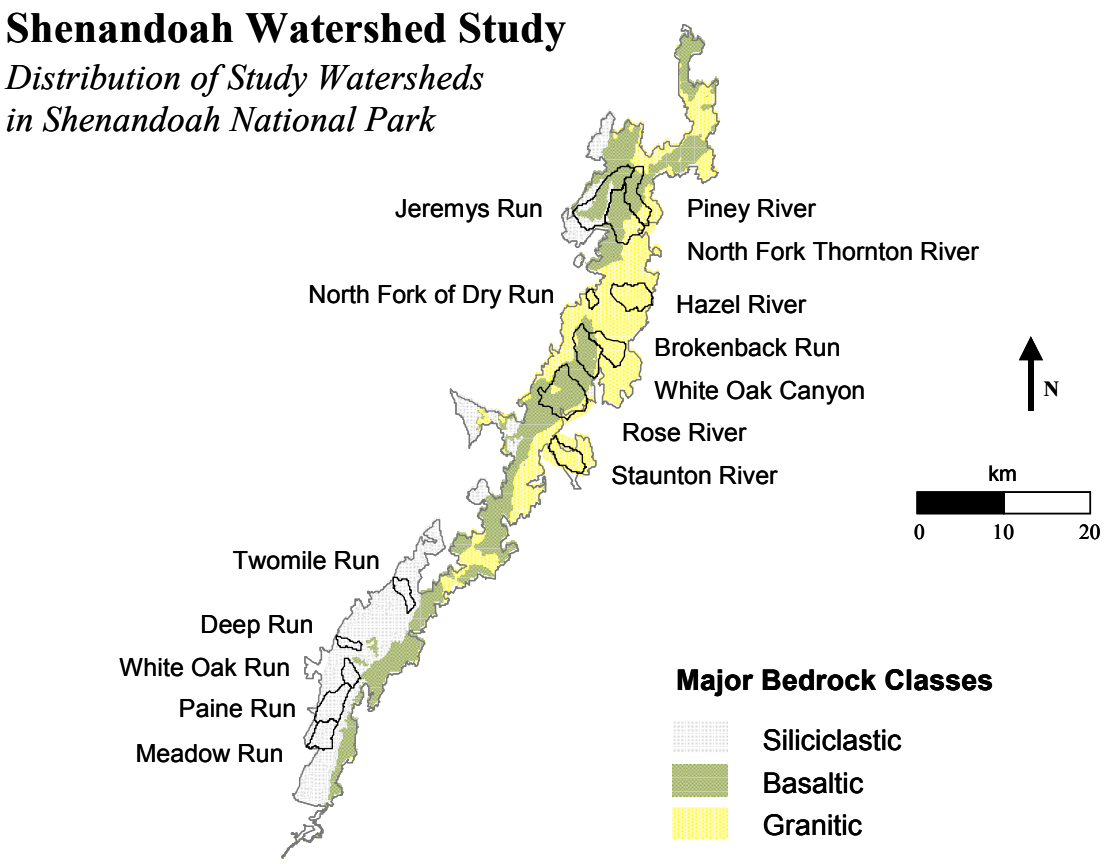

Figure VI-1. Primary study watersheds in SHEN shown in relation to the distribution of major bedrock types.

(c.f., Galloway et al. 1983, 1984). In particular, this research has contributed to our understanding of relationships between geology and sensitivity to acidification (Lynch and Dise 1985, Bricker and Rice 1989) and of the effects of forest insect infestation on episodic chemical processes (Webb et al. 1995, Eshleman et al. 2001). The MAGIC model (Cosby et al. 1985a,b,c) of watershed response was initially developed largely using data collected within SHEN. MAGIC was the principal model used by the National Acid Precipitation Assessment Program (NAPAP) to estimate future damage to lakes and streams in the eastern United States (Thornton et al. 1990, NAPAP 1991) and is now the most widely used acid-base chemistry model in the United States and Europe (Sullivan 2000).

During the past two decades, the SWAS program has developed a uniquely comprehensive watershed database for SHEN, while making major contributions to scientific understanding of surface water acidification and the biogeochemistry of forested mountain watersheds. Data and analyses provided through SWAS have contributed significantly to regional and national assessments of acidic deposition effects, including several that led to enactment of the Clean Air Act Amendments (CAAA) of 1990 (e.g., Baker et al. 1990b, NAPAP 1991, Cosby et al. 1991). More recently, the SWAS and VTSSS programs have provided some of the most comprehensive data available for use in the aquatic effects assessment conducted as part of the Southern Appalachian Mountain Initiative (SAMI), a multistate, multiagency effort to address the air pollution problem in the southern Appalachian region (Sullivan et al. 2002a). The combined SWAS and VTSSS programs presently contribute data to the U.S. Environmental Protection Agency (EPA) for use in Congressionally mandated evaluation of air pollution control program benefits relative to acidic-deposition effects on sensitive surface waters. As a consequence of this extensive monitoring, research, and assessment activity, SHEN is a leader among the national parks with respect to park-specific knowledge of acidic deposition effects and watershed ecosystem conditions in general.

Sulfur (S) is the primary determinant of precipitation acidity and sulfate (SO_4^{2-}) is the dominant acid anion associated with acidic streams, both in the central Appalachian Mountains region and within SHEN. Although a substantial proportion of atmospherically deposited S is retained in watershed soils, SO_4^{2-} concentrations in western Virginia mountain streams appear to have increased dramatically as a consequence of acidic deposition. Elevated streamwater SO_4^{2-} concentrations, low acid neutralizing capacity (ANC), and the base-poor status of watershed soils provide evidence of acidification of a substantial portion of the mountain streams in SHEN and among native brook trout streams throughout western Virginia. Such acidification is partly a consequence of past and current S deposition.

Nitrate (NO_3^-) concentrations measured in streamwater are generally negligible, except in association with forest defoliation by the gypsy moth (*Lymantria dispar*; Webb et al. 1995; Eshleman et al. 1998, 2001). In the absence of severe disturbance, nitrogen (N) is generally tightly cycled within SHEN watersheds and does not contribute significantly to streamwater acidification. This is likely a consequence of the 1) observation that levels of N deposition in SHEN are lower than in other forested areas with documented effects on streamwaters, 2) past

landscape disturbance, and 3) prevalence of deciduous forest types, which seem to have a higher N demand than coniferous forests.

The distributions of streamwater ANC, SO_4^{2-}, and sum of base cation concentrations for the streams that have been recently monitored in SHEN are given in Table VI-1. There are large differences (i.e., up to a factor of three among monitored sites) in median streamwater SO_4^{2-} concentrations. There are also distinct patterns in the distribution of sites having high versus low streamwater SO_4^{2-} concentration, despite the fact that S deposition appears to be relatively uniform across the park (Galloway et al. 1999). Data for all quarterly samples during all seasons are summarized in Table VI-1a. In the following tables (VI-1b through VI-1e), quarterly data for each season are presented separately. Sulfate concentrations tend to be higher and ANC values tend to be lower during winter and spring than during summer and fall. Site location information and ANC summary data for most of the streams (n = 297) sampled in SHEN through the SWAS program during the 1980-2001 water-year period are provided in Appendix D.

With the exception of three previously established weekly sampling sites, the primary SWAS watersheds shown in Figure VI-1 were selected for quarterly streamwater sampling following a near-census sampling survey (n = 344) of western Virginia's native brook trout streams conducted in 1987 through the VTSSS program. Results of the VTSSS survey were reported by Webb et al. (1989) and Cosby et al. (1991) and incorporated into regional analyses by Baker et al. (1990a) and Herlihy et al. (1993). In addition to providing a baseline against which to measure future change, the VTSSS survey revealed the sensitivity of many of the region's mountain headwater streams to the effects of acidic deposition. Following the survey, a subset of surveyed streams was selected for continued long-term water quality monitoring.

Selection of the long-term monitoring streams, including those presently maintained by the SWAS program in SHEN and by the VTSSS program in the larger western Virginia area, involved systematic identification of geologically-representative streams with minimal current watershed disturbance. The objective was to select the subset of second or third order streams that most closely represented the range of regional variation in watershed responsiveness to acidic deposition effects, while minimizing the confounding influence of other anthropogenic factors. Within SHEN, the process essentially involved selection of all the second or third order streams that met the disturbance criteria. That is, most of the park's larger streams were selected

Table VI-1 a. Interquartile distributions of ANC, sulfate and sum of base cations (Ca+Mg+Na+K) for SHEN study streams during the period 1988 to 2001 for ALL quarterly samples.[a]

Site ID	Watershed	Percent of Watershed Area			ANC (ueq/L)			SO4 (ueq/L)			SBC (ueq/L)		
		Siliciclastic	Granitic	Basaltic	25th	median	75th	25th	median	75th	25th	median	75th
Siliciclastic Bedrock Class													
DR01	Deep Run	100	0	0	0.3	1.9	5.1	88.8	102.0	107.3	129.7	132.7	137.4
PAIN	Paine Run	100	0	0	2.9	6.4	10.6	106.4	110.8	115.5	144.9	150.1	156.6
VT36	Meadow Run	100	0	0	-3.9	-1.3	1.0	78.3	87.3	92.6	108.3	113.1	118.3
VT53	Twomile Run	100	0	0	9.4	12.8	22.8	88.9	98.3	104.1	139.4	143.1	147.8
WOR1	White Oak Run	100	0	0	15.7	21.6	39.7	73.9	77.8	81.9	134.9	148.2	167.2
Granitic Bedrock Class													
NFDR	North Fork Dry Run	0	100	0	45.1	59.5	83.4	92.9	97.5	101.7	209.2	223.7	252.7
VT58	Brokenback Run	0	93	7	66.8	83.6	108.9	37.5	41.4	44.9	152.5	165.9	185.8
STAN	Staunton River	0	100	0	73.6	81.4	101.2	39.7	42.4	45.4	154.8	161.1	177.7
VT62	Hazel River	0	100	0	77.7	93.0	112.1	33.8	38.3	41.8	163.9	175.8	196.0
Basaltic Bedrock Class													
VT51	Jeremys Run	31	0	69	140.6	179.5	260.1	105.0	119.2	130.0	328.3	366.6	408.6
PINE	Piney River	0	31	69	166.2	207.4	300.4	54.0	62.5	69.4	311.7	341.3	396.5
VT61	North Fork Thornton River	5	27	68	217.3	266.5	363.6	67.5	78.8	92.4	381.0	416.1	478.0
VT66	Rose River	0	9	91	112.8	141.6	186.2	47.1	51.3	57.6	243.9	265.1	294.3
VT75	White Oak Canyon Run	0	14	86	101.7	130.4	172.7	45.4	51.4	58.3	221.9	247.8	275.2

[a] The data cover 14 water years except for VT75 (11 years)

Table VI-1 b. Interquartile distributions of ANC, sulfate and sum of base cations (Ca+Mg+Na+K) for SHEN study streams during the period 1988 to 2001 for WINTER quarterly samples (sampled in the last week of January). [a]

Site ID	Watershed	Percent of Watershed Area			ANC (ueq/L)			SO4 (ueq/L)			SBC (ueq/L)		
		Siliciclastic	Granitic	Basaltic	25th	median	75th	25th	median	75th	25th	median	75th
Siliciclastic Bedrock Class													
DR01	Deep Run	100	0	0	-0.4	0.3	1.7	105.3	108.9	111.2	133.8	137.4	137.7
PAIN	Paine Run	100	0	0	1.2	2.9	4.4	110.2	113.9	116.1	144.8	149.5	155.3
VT36	Meadow Run	100	0	0	-4.6	-2.4	-0.8	89.4	92.3	101.8	115.3	118.2	124.6
VT53	Twomile Run	100	0	0	4.6	7.8	10.3	100.3	105.7	108.6	141.1	143.9	147.5
WOR1	White Oak Run	100	0	0	13.1	15.3	17.1	74.1	79.6	82.5	132.1	133.9	148.0
Granitic Bedrock Class													
NFDR	North Fork Dry Run	0	100	0	32.4	35.3	44.1	96.8	101.1	110.1	194.4	207.4	225.5
VT58	Brokenback Run	0	93	7	49.4	57.9	65.6	42.7	45.3	51.4	140.7	146.2	156.8
STAN	Staunton River	0	100	0	68.0	71.2	74.4	42.3	47.0	50.0	152.2	153.3	157.4
VT62	Hazel River	0	100	0	59.5	65.8	75.7	39.4	42.5	46.4	152.4	155.6	173.4
Basaltic Bedrock Class													
VT51	Jeremys Run	31	0	69	110.5	120.8	137.8	128.6	133.6	138.6	313.5	320.7	328.3
PINE	Piney River	0	31	69	138.3	145.1	159.3	68.3	71.8	76.2	278.8	296.4	307.8
VT61	North Fork Thornton River	5	27	68	177.1	190.5	205.8	92.4	95.0	96.6	358.7	364.5	378.0
VT66	Rose River	0	9	91	96.1	102.8	108.0	56.1	58.4	61.3	230.0	231.6	245.3
VT75	White Oak Canyon Run	0	14	86	87.0	89.4	99.6	55.3	59.4	60.6	210.1	212.8	220.3

[a] The data cover 14 water years except for VT75 (11 years)

Table VI-1 c. Interquartile distributions of ANC, sulfate and sum of base cations (Ca+Mg+Na+K) for SHEN study streams during the period 1988 to 2001 for SPRING quarterly samples (sampled in the last week of April). [a]

Site ID	Watershed	Percent of Watershed Area			ANC (ueq/L)			SO_4 (ueq/L)			SBC (ueq/L)		
		Siliciclastic	Granitic	Basaltic	25th	median	75th	25th	median	75th	25th	median	75th
Siliciclastic Bedrock Class													
DR01	Deep Run	100	0	0	-0.4	0.3	1.2	101.1	103.8	107.7	129.8	131.1	132.4
PAIN	Paine Run	100	0	0	3.0	4.5	5.3	107.2	109.4	112.1	142.8	144.4	148.6
VT36	Meadow Run	100	0	0	-4.2	-1.8	-0.7	87.1	89.6	93.2	112.3	114.6	118.2
VT53	Twomile Run	100	0	0	8.9	10.8	12.8	94.9	98.5	100.9	138.1	140.4	144.5
WOR1	White Oak Run	100	0	0	15.1	19.0	23.3	72.5	77.8	81.6	131.0	139.8	145.0
Granitic Bedrock Class													
NFDR	North Fork Dry Run	0	100	0	44.8	48.3	51.0	93.3	97.5	101.8	201.5	211.7	216.0
VT58	Brokenback Run	0	93	7	71.8	77.0	81.9	37.3	40.7	42.1	152.3	156.1	163.2
STAN	Staunton River	0	100	0	74.6	76.1	81.4	40.9	43.0	45.5	155.6	157.5	160.9
VT62	Hazel River	0	100	0	79.5	87.3	91.8	35.5	37.1	38.6	162.4	167.8	174.6
Basaltic Bedrock Class													
VT51	Jeremys Run	31	0	69	151.5	161.6	171.9	121.9	126.8	132.2	328.3	340.7	358.2
PINE	Piney River	0	31	69	187.4	198.0	207.2	61.0	64.2	69.1	318.4	324.4	341.7
VT61	North Fork Thornton River	5	27	68	231.7	253.3	265.4	78.7	85.1	90.9	389.7	392.7	416.4
VT66	Rose River	0	9	91	132.5	135.0	142.2	50.0	52.2	58.5	247.9	256.9	270.7
VT75	White Oak Canyon Run	0	14	86	117.6	122.0	128.6	50.4	53.1	57.4	227.5	237.6	251.1

[a] The data cover 14 water years except for VT75 (11 years)

Table VI-1 d. Interquartile distributions of ANC, sulfate and sum of base cations (Ca+Mg+Na+K) for SHEN study streams during the period 1988 to 2001 for SUMMER quarterly samples (sampled in the last week of July). [a]

Site ID	Watershed	Percent of Watershed Area			ANC (ueq/L)			SO_4 (ueq/L)			SBC (ueq/L)		
		Siliciclastic	Granitic	Basaltic	25th	median	75th	25th	median	75th	25th	median	75th
Siliciclastic Bedrock Class													
DR01	Deep Run	100	0	0	1.9	4.4	7.0	82.6	82.9	87.6	125.5	129.7	134.3
PAIN	Paine Run	100	0	0	7.4	10.4	12.0	102.7	104.7	110.4	147.7	151.2	157.4
VT36	Meadow Run	100	0	0	-4.3	-1.6	0.1	72.8	74.9	81.0	107.1	108.3	111.3
VT53	Twomile Run	100	0	0	19.9	23.0	25.4	75.1	83.8	88.1	137.0	140.6	147.8
WOR1	White Oak Run	100	0	0	34.9	49.1	55.3	70.5	75.1	77.3	164.4	174.4	179.2
Granitic Bedrock Class													
NFDR	North Fork Dry Run	0	100	0	44.8	48.3	51.0	93.3	97.5	101.8	201.5	211.7	216.0
VT58	Brokenback Run	0	93	7	71.8	77.0	81.9	37.3	40.7	42.1	152.3	156.1	163.2
STAN	Staunton River	0	100	0	74.6	76.1	81.4	40.9	43.0	45.5	155.6	157.5	160.9
VT62	Hazel River	0	100	0	79.5	87.3	91.8	35.5	37.1	38.6	162.4	167.8	174.6
Basaltic Bedrock Class													
VT51	Jeremys Run	31	0	69	248.2	277.0	347.2	90.3	94.5	103.4	399.8	414.5	483.5
PINE	Piney River	0	31	69	304.2	317.4	330.8	49.7	52.5	54.5	403.2	409.1	420.9
VT61	North Fork Thornton River	5	27	68	358.7	386.0	411.0	57.9	63.4	68.6	472.4	488.8	505.4
VT66	Rose River	0	9	91	179.0	188.6	205.0	41.1	46.9	53.2	294.0	299.2	312.0
VT75	White Oak Canyon Run	0	14	86	168.2	177.8	198.6	42.2	49.8	52.7	273.6	286.3	313.0

[a] The data cover 14 water years except for VT75 (11 years)

Table VI-1 e. Interquartile distributions of ANC, sulfate and sum of base cations (Ca+Mg+Na+K) for SHEN study streams during the period 1988 to 2001 for FALL quarterly samples (sampled in the last week of October). [a]

Site ID	Watershed	Percent of Watershed Area			ANC (ueq/L)			SO_4 (ueq/L)			SBC (ueq/L)		
		Siliciclastic	Granitic	Basaltic	25th	median	75th	25th	median	75th	25th	median	75th
Siliciclastic Bedrock Class													
DR01	Deep Run	100	0	0	2.8	4.5	6.2	88.0	94.6	104.0	129.5	133.3	137.5
PAIN	Paine Run	100	0	0	6.9	12.6	16.5	110.1	114.2	117.1	150.3	152.3	156.4
VT36	Meadow Run	100	0	0	-0.3	1.2	5.4	72.1	79.6	90.2	103.6	109.1	116.1
VT53	Twomile Run	100	0	0	13.2	21.1	24.4	92.5	98.6	103.6	142.3	146.3	149.4
WOR1	White Oak Run	100	0	0	24.7	34.5	50.0	77.8	81.0	83.1	142.7	159.6	179.1
Granitic Bedrock Class													
NFDR	North Fork Dry Run	0	100	0	59.3	73.2	87.8	94.2	98.1	101.2	221.5	226.0	246.5
VT58	Brokenback Run	0	93	7	87.9	95.7	119.4	37.4	40.2	42.8	166.8	171.2	198.1
STAN	Staunton River	0	100	0	81.3	87.4	102.5	36.8	38.6	41.5	165.7	169.6	181.5
VT62	Hazel River	0	100	0	97.4	106.6	131.1	33.0	35.9	39.0	173.9	190.0	208.5
Basaltic Bedrock Class													
VT51	Jeremys Run	31	0	69	194.6	248.0	341.4	105.2	110.6	115.0	367.7	401.5	504.7
PINE	Piney River	0	31	69	214.2	244.2	281.9	53.7	59.8	63.1	336.6	357.0	383.0
VT61	North Fork Thornton River	5	27	68	295.2	309.7	367.7	63.6	73.8	82.8	416.9	439.7	488.6
VT66	Rose River	0	9	91	146.0	170.4	202.9	44.6	47.4	50.4	256.2	270.2	294.6
VT75	White Oak Canyon Run	0	14	86	134.1	146.2	170.2	44.5	45.4	49.1	235.9	253.0	280.8

[a] The data cover 14 water years except for VT75 (11 years)

except those that had significant disturbance factors within the watersheds such as campgrounds, restaurants, visitor centers, waste-water treatment facilities, or roads subject to salt treatment. An additional small number of streams were not selected due to access problems.

The selection of long-term monitoring streams provided a reasonably unbiased representation of streams on the three major bedrock types in SHEN. As indicated in Table VI-2, the proportional representation of bedrock type by the primary SWAS study watersheds closely corresponded to the proportional distribution of bedrock types in SHEN. In addition, it has been shown that streamwater ANC distributions for the SWAS study watersheds, classified by predominant bedrock type, generally correspond to the distribution of observed ANC concentrations for the three major SHEN bedrock types (Webb et al. 1993, Galloway et al. 1999).

Table VI-2. Bedrock distribution in SHEN and SWAS watersheds.

Site ID	Stream	Watershed Area (km^2)	Percent Bedrock Coverage[a]		
			Siliciclastic	Granitic	Basaltic
VT51	Jeremys Run	22.0	31.0	0.0	69.0
VT61	North Fork Thornton River	19.1	5.2	27.0	67.8
VT60	Piney River (PINE)	12.4	0.0	31.3	68.7
VT58	Brokenback Run	9.9	0.0	93.4	6.6
VT62	Hazel River	13.2	0.0	100.0	0.0
NFDR	North Fork Dry Run	2.3	0.0	100.0	0.0
VT66	Rose River	23.7	0.0	9.1	90.9
VT59	Staunton River (STAN)	10.5	0.0	100.0	0.0
VT75	Whiteoak Canyon (Robinson River)	14.1	0.0	14.1	85.9
DR01	Deep Run	3.1	100.0	0.0	0.0
VT36	Meadow Run	8.9	100.0	0.0	0.0
VT35	Paine Run (PAIN)	12.4	100.0	0.0	0.0
VT53	Twomile Run	5.6	100.0	0.0	0.0
WOR1	White Oak Run	5.1	100.0	0.0	0.0
Total SWAS Watersheds		162.3	26.4	29.8	43.7
Total Shenandoah National Park		797.0	28.8	32.4	38.8

[a] percent of the watershed area underlain by bedrock within each of the major geologic sensitivity classes

Additional water quality data were collected in a spatially-intensive water chemistry survey conducted within 11 of the 14 primary SWAS study watersheds during March of 1992 in association with the Shenandoah National Park:Fish in Sensitive Habitats (FISH) project. The spatial distribution of measured streamwater ANC determined for all sites (n = 220) sampled in the 1992 survey is illustrated in Figure VI-2.

a. Relationships between Geology and Streamwater Chemistry

The SHEN landscape includes three major geologic sensitivity types: siliciclastic (quartzite and sandstone), granitic, and basaltic (Figure VI-1). Each of these bedrock types influences about one-third of the stream length in the park.

All of the primary SWAS streams on siliciclastic bedrock monitored during the period 1988 to 1999 had relatively high median SO_4^{2-} concentration (76-109 μeq/L), whereas three of four streams monitored on granitic bedrock had SO_4^{2-} concentration < 43 μeq/L. Sulfate concentrations in streams draining basaltic bedrock were more variable, ranging from 52 to 127 μeq/L. Streamwater base cation concentrations and ANC also varied dramatically from site to site. Median streamwater base cation concentrations were generally lowest in the watersheds on siliciclastic bedrock, and this could reflect lower base cation supply from watershed soils and/or greater base cation depletion of soils caused by leaching of SO_4^{2-} to streams. Base cation concentrations were substantially higher (median > 235 μeq/L) in watersheds on basaltic bedrock.

There are many streams on siliciclastic bedrock in the park that have chronic ANC in the range where adverse effects are likely to occur on sensitive aquatic biota and where episodic acidification to ANC values near or below zero frequently occur during hydrological events. The streams that are most susceptible to adverse chronic or episodic effects on in-stream biota are those having chronic ANC less than about 50 μeq/L, especially those having chronic ANC less than about 20 μeq/L. These are also primarily on siliciclastic bedrock (Table VI-1).

The observed patterns in streamwater chemistry are strongly related to patterns in bedrock geology within the park (Figure VI-1). In fact, geological type, soils conditions that developed from underlying geology, and water chemistry conditions are all closely interrelated within SHEN. This is partly because rock and soils materials in SHEN and elsewhere in the Southeast were not transported from place to place (and thereby mixed) by the process of glaciation.

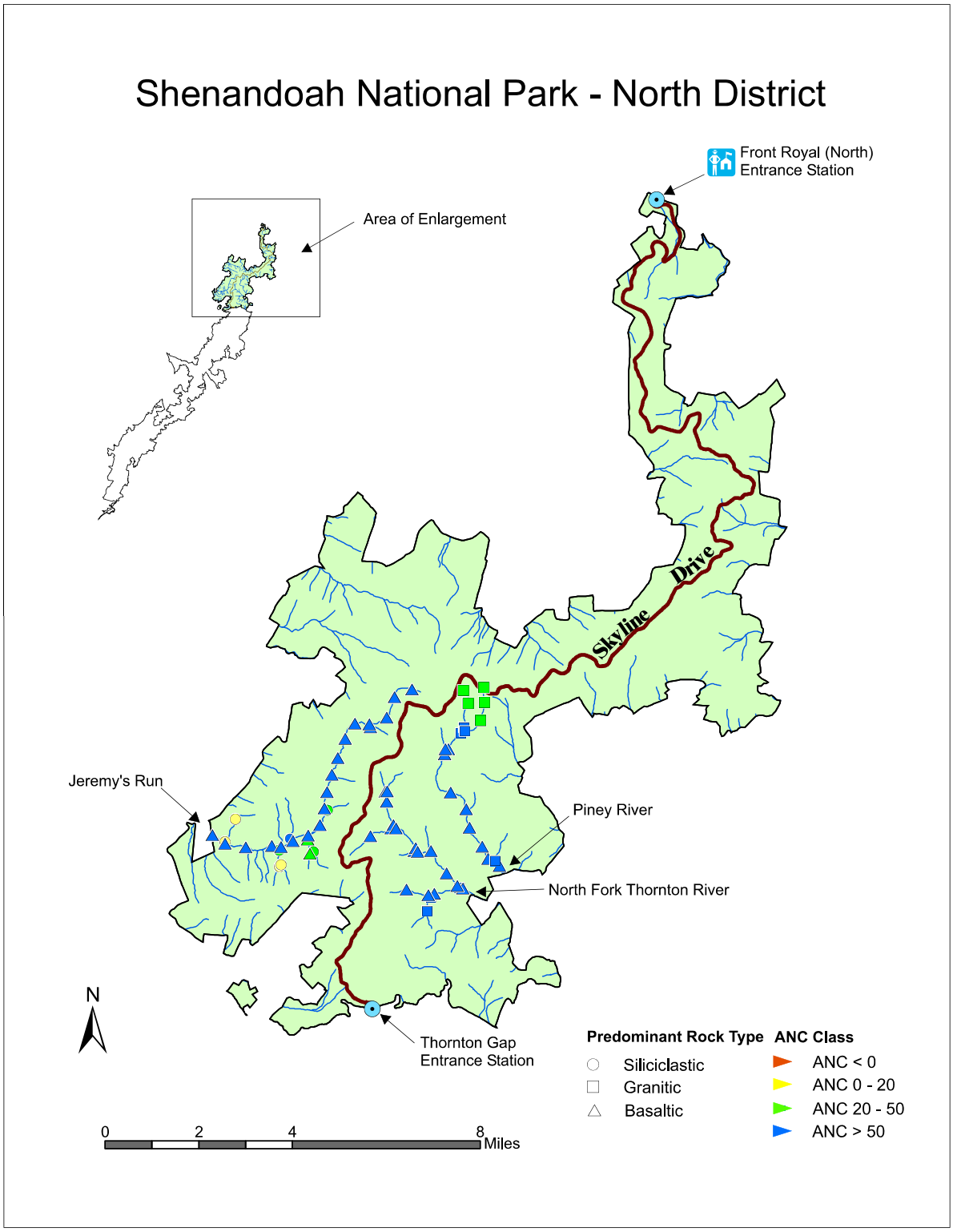

Figure VI-2. Distribution of streamwater ANC determined in the 1992 spring survey of water chemistry within 11 watersheds in SHEN. Stream sampling sites are coded according to ANC class (colors) and geologic sensitivity class (symbol shape).

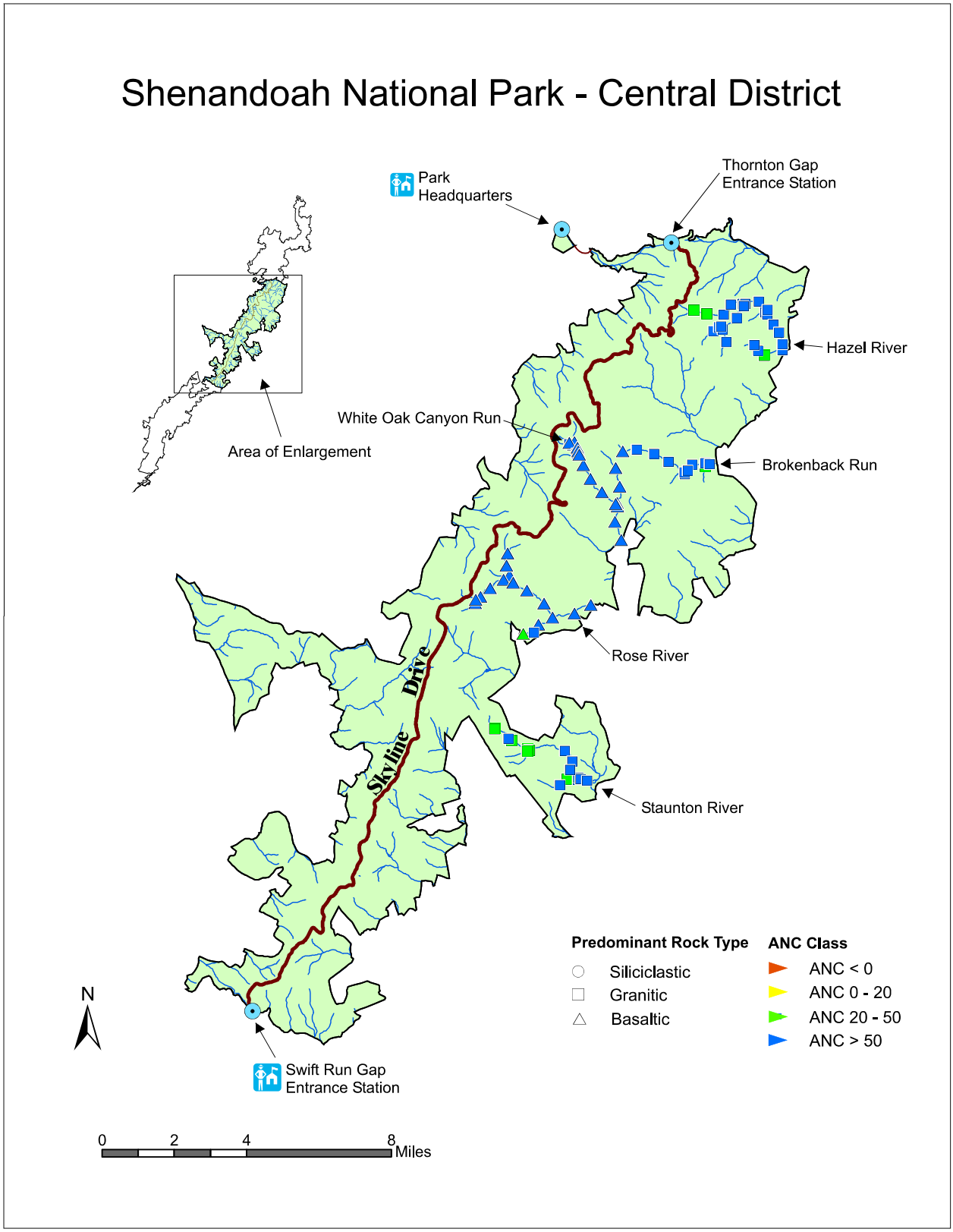

Figure VI-2. Continued.

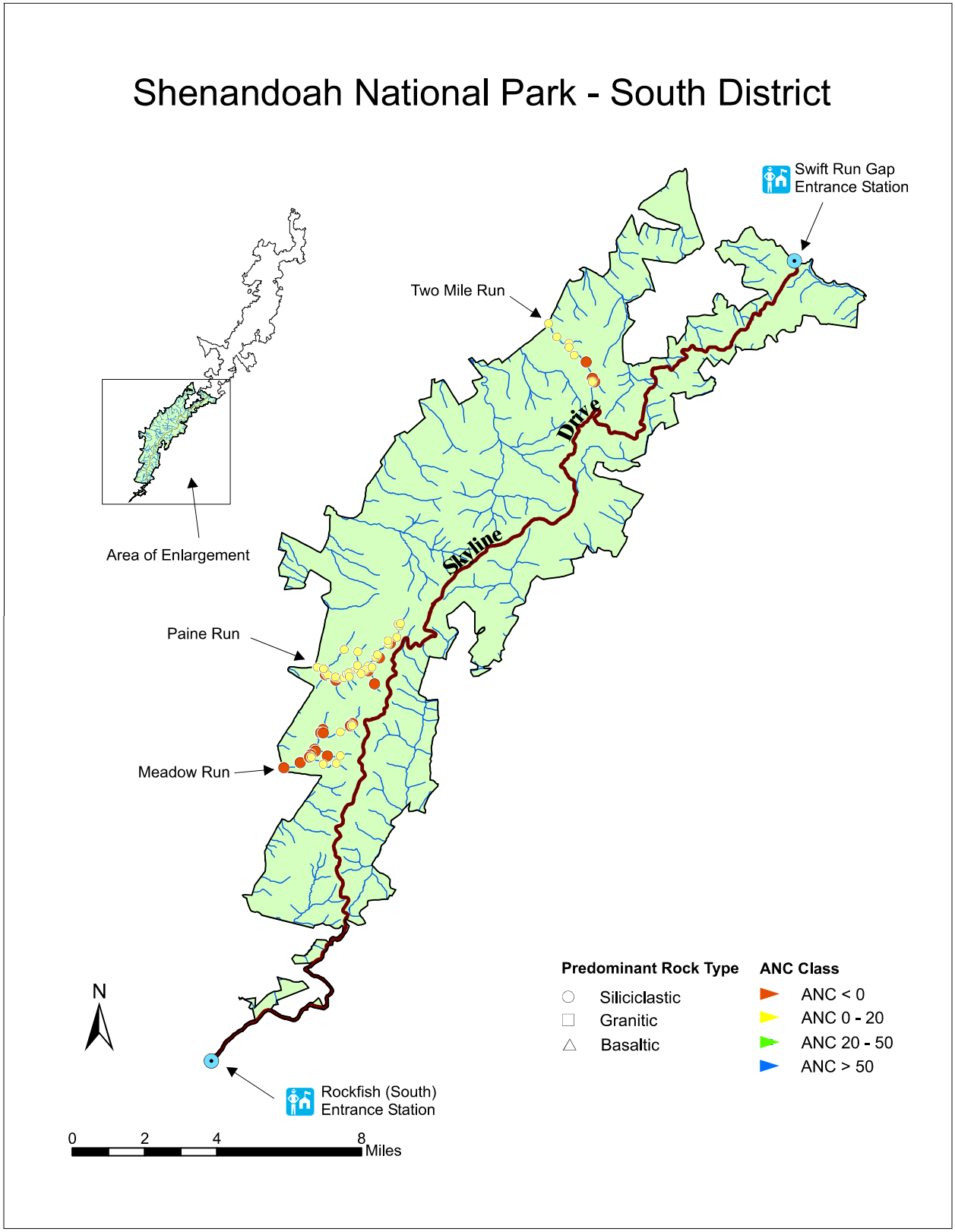

Figure VI-2. Continued.

Relationships between water chemistry and geology within SHEN have been known for some time. Lynch and Dise (1985) reported results from six synoptic surveys of 56 streams that drain SHEN. Concentrations of silica, base cations, and ANC were strongly related to the distribution of geologic formations. The effects of acidification were often greatest in watersheds underlain by the Antietam Formation (Figure II-4), which had streamwater pH averaging 5.0 and ANC averaging -7 μeq/L. Lynch and Dise (1985) found that flow-weighted streamwater ANC decreased in order of the underlying geologic formation as follows:

> basaltic (Catoctin formation) > granitic (Pedlar and Old Rag formations) > siliciclastic (Hampton and Antietam formations)

Regression relationships suggested that streamwater ANC would generally range from about 175 μeq/L on the Catoctin Formation to -7 μeq/L on the Antietam Formation. After accounting for variations in streamwater chemistry with geology, Lynch and Dise (1985) further found lower streamwater ANC on the western side of the park, as compared with the eastern side. The authors speculated that this could be due to the upwind sources of acidic deposition being in closer proximity to the park's western border, which results in greater S deposition on west-facing slopes. However, there are also soils differences between east- and west-facing slopes (Figures II-5 and VI-2), which might be important.

Additional perspective concerning the relationship between streamwater chemistry and geology in SHEN is provided by the 1992 survey of sub-watersheds within the primary study watersheds. Whereas Lynch and Dise (1985) derived regression models to predict streamwater composition as function of multiple bedrock types, the 1992 survey provides an opportunity to examine the composition of streamwaters associated with single bedrock types. From the relatively large number of small watersheds sampled in the survey, subsets of 62 siliciclastic, 46 granitic, and 15 basaltic subwatersheds were identified. Table VI-3 presents descriptive statistics for measurements of ANC, pH, sum of base cations, and SO_4^{2-} concentrations obtained for the subset of the 1992 survey samples (n = 123) associated with single bedrock types. The bedrock-related differences in ANC and pH distributions are consistent with expectations based on the earlier Lynch and Dise (1985) analysis.

As indicated in Table VI-3, streamwater ANC and pH values were lowest for the surveyed siliciclastic subwatersheds and highest for basaltic subwatersheds. Almost half of the sampled streams in siliciclastic subwatersheds had ANC in the chronically acidic range (< 0 μeq/L) in

Table VI-3. Range and distribution of streamwater concentrations within SHEN associated with major bedrock classes: Spring 1992 Synoptic Survey (Galloway et al. 1999).

	n	Minimum	25%	Median	75%	Maximum
ANC (µeq/L)						
Siliciclastic	62	-18.1	-1.0	1.2	3.7	12.8
Granitic	46	22.0	47.2	58.7	67.0	130.4
Basaltic	15	33.7	97.0	149.2	179.0	226.7
pH						
Siliciclastic	62	4.8	5.4	5.6	5.7	6.0
Granitic	46	6.0	6.7	6.8	6.8	7.1
Basaltic	15	6.6	6.9	7.1	7.2	7.3
Sum of Base Cations (µeq/L)						
Siliciclastic	62	92.1	138.1	168.2	190.4	272.1
Granitic	46	89.5	136.7	147.7	161.3	243.5
Basaltic	15	138.0	232.0	369.5	381.1	450.9
Sulfate (µeq/L)						
Siliciclastic	62	67.2	88.5	97.2	104.8	177.8
Granitic	46	13.4	30.1	36.6	42.1	96.3
Basaltic	15	12.3	36.2	62.2	97.9	164.3

Notes: (1) The data were obtained for watersheds underlain by a single bedrock type.
(2) 25% and 75% refer to the 25th and 75th percentile values. 50 percent of all the values are within the interquartile range, as bounded by the 25th and 75th percentile values.

which lethal effects on brook trout are probable (see Section VI.B.3). The balance of the streams associated with siliciclastic bedrock had ANC in the episodically acidic range (having chronic ANC in the range 0-20 µeq/L) in which sub-lethal or lethal effects are possible. Many of the streams associated with the granitic bedrock type were in the indeterminate range (20-50 µeq/L). In contrast, the streams associated with the basaltic bedrock type had ANC values that were well within the suitable range for brook trout.

The pH values for the streams in the 1992 survey displayed a similar relationship with bedrock type, with the streams having lowest pH being associated with siliciclastic bedrock and those having highest pH associated with basaltic bedrock. All of the streams on siliciclastic bedrock had pH < 6, identified by Baker and Christiansen (1991) as too acidic for some acid-sensitive fish species.

Sulfate concentration values for streams in the 1992 survey also differed among bedrock types. This difference is critically important with respect to the observed streamwater ANC,

which is determined by the relative concentrations of base cations and acid anions. Whereas both the siliciclastic and basaltic bedrock types were associated with relatively high streamwater SO_4^{2-} concentrations, the siliciclastic bedrock type was associated with much lower base cation concentrations, and therefore lower streamwater ANC. In contrast, streams on granitic bedrock exhibited both low base cation and low SO_4^{2-} concentrations, with resulting intermediate ANC.

The observed differences in streamwater SO_4^{2-} concentrations for the major bedrock types in SHEN primarily reflect differences in SO_4^{2-} retention properties of the associated soils. Watersheds in the southeastern United States commonly retain more than 50% of deposited S (Rochelle and Church 1987, Turner et al. 1990). This S retention is attributed to SO_4^{2-} adsorption in the old and highly-weathered southeastern soils (Galloway et al. 1983, Baker et al. 1991). Although there are other mechanisms of S retention or immobilization in watersheds, including S reduction and biological uptake, these are generally considered less important on regional or park-specific scales than is adsorption, particularly in upland forests (Turner et al. 1990). Regardless of mechanism, S retention in watersheds reduces the potential for the acidification of surface waters that is associated with increasing concentrations and mobility of SO_4^{2-}. However, S retention by adsorption is a capacity-limited process. As the finite adsorption capacity of watershed soils is exhausted, SO_4^{2-} concentrations can increase in surface waters, potentially contributing to greater acidification (Johnson and Cole 1980, Munson and Gherini 1991, Church et al. 1992). Moreover, as indicated by the available soil and water quality data for SHEN, there can be substantial variation in S retention capacity among watersheds in close geographic proximity.

Figure VI-3 illustrates the effect of varying S retention capacity on the estimated historic increase in SO_4^{2-} concentrations in SHEN streamwaters. Median SO_4^{2-} concentrations in 1992 are shown for streams on the major bedrock types in SHEN (Table VI-3) in relation to estimated background SO_4^{2-} concentrations for low-ANC surface waters in the eastern United States (Brakke et al. 1989, Cosby et al. 1991). Whereas streamwater SO_4^{2-} concentrations have increased by a factor of about 4.4 in streams on siliciclastic bedrock, SO_4^{2-} concentrations have only increased by a factor of about 1.7 in streams on granitic bedrock. These differences are consistent with direct measurements of adsorption properties obtained by Webb (1988) and Ingersol (1994) for SHEN soils.

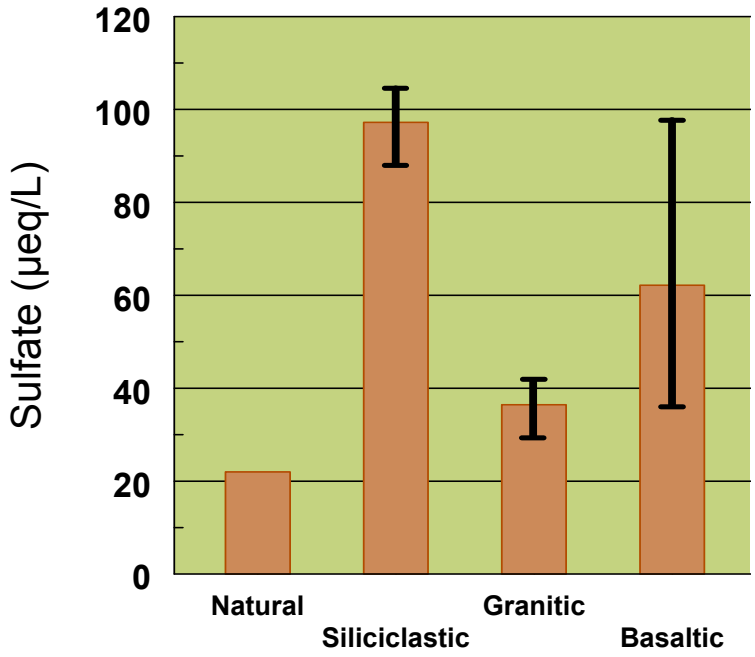

Figure VI-3. Comparison of estimated natural background and current median sulfate concentrations among streams located on major bedrock types in SHEN. Error bars delimit interquartile ranges for current conditions. (Current concentrations based on 1992 survey data; see Table VI-3.)

Comparison of current median streamwater SO_4^{2-} concentrations with steady-state concentration values calculated from current precipitation, evapotranspiration, and deposition provides an estimate of percent S retention values. Based on estimated deposition and runoff values for 1990, the average steady-state SO_4^{2-} concentration for streamwaters in SHEN was 120 µeq/L. Comparison of this value with the median SO_4^{2-} concentration values in Table VI-3 provides S retention estimates for siliciclastic watersheds of 19%, for granitic watersheds of 70%, and for basaltic watersheds of 49%. Given the resulting effect of SO_4^{2-} leaching on streamwater ANC, this is a difference with significant geochemical and biological implications.

b. Relationships between Soils and Streamwater Chemistry

A common measure of base availability in soils is the percent base saturation, which represents the fraction of exchange sites (or cation exchange capacity [CEC]) occupied by base cations. Base saturation values in the range of 10–20% have been cited as threshold values for incomplete acid neutralization and leaching of aluminum (Al) from soil to surface waters (Reuss

and Johnson 1986, Binkley et al. 1989, Cronan and Schofield 1990). Data from the 2000 soil survey conducted by the University of Virginia (Welsch et al. 2001) are summarized in Table VI-4 for each of the study watersheds, stratified by the predominant bedrock class present in each watershed. As indicated in Figure VI-4, median base saturation was generally less than 10% for mineral soils associated with siliciclastic bedrock and less than about 14% for mineral soils associated with granitic bedrock in the park. The present low base cation availability in soils of watersheds underlain by siliciclastic or granitic bedrock is probably due to a combination of low base cation content of the parent bedrock and depletion by previous land use and decades of accelerated leaching by acidic deposition. The relative importance of these factors is not known. This low base cation availability suggests the potential for leaching of Al to streams.

Table VI-4. Interquartile distribution of pH, cation exchange capacity (CEC), and percent base saturation for soil samples[a] collected in SHEN study watersheds during the 2000 soil survey.

			pH			CEC (cmol/kg)			Percent Base Saturation		
Site ID	Watershed	n	25th	Med	75th	25th	Med	75th	25th	Med	75th
Siliciclastic Bedrock Class[b]											
PAIN	Paine Run	6	4.4	4.5	4.7	3.7	5.7	5.7	7.1	10.0	24.9
WOR1	White Oak Run	6	4.3	4.4	4.4	4.8	7.5	7.8	5.3	7.5	8.5
DR01	Deep Run	5	4.3	4.4	4.5	3.9	5.0	5.8	7.2	8.9	10.8
VT36	Meadow Run	6	4.4	4.4	4.5	3.1	3.5	7.6	7.8	8.7	11.3
VT53	Twomile Run	5	4.3	4.5	4.5	4.6	6.0	6.9	11.7	12.3	13.6
Granitic Bedrock Class											
STAN	Staunton River	6	4.7	4.8	4.9	6.5	7.5	9.2	9.1	13.9	29.5
NFDR	NF of Dry Run	5	4.4	4.5	4.7	7.3	8.0	9.2	7.5	10.8	12.4
VT58	Brokenback Run	5	4.6	4.7	4.7	7.3	8.4	9.6	6.0	6.7	9.7
VT62	Hazel River	4	4.5	4.7	4.8	5.3	5.3	6.5	12.3	12.8	21.6
Basaltic Bedrock Class											
PINE	Piney River	6	4.7	5.0	5.3	7.3	7.7	10.0	17.0	24.0	57.0
VT66	Rose River	8	4.8	5.0	5.3	7.3	10.1	10.7	19.1	38.0	63.5
VT75	White Oak Canyon	6	4.9	5.1	5.5	7.1	7.5	9.3	15.6	32.8	43.4
VT61	NF of Thornton River	7	5.1	5.2	5.3	7.7	9.6	10.8	35.6	54.4	71.2
VT51	Jeremys Run	4	4.7	5.0	5.3	6.3	7.6	7.7	15.0	22.8	46.1

[a] Samples collected from mineral soil >20cm depth
[b] Watersheds are stratified according to the predominant bedrock class present in each watershed.

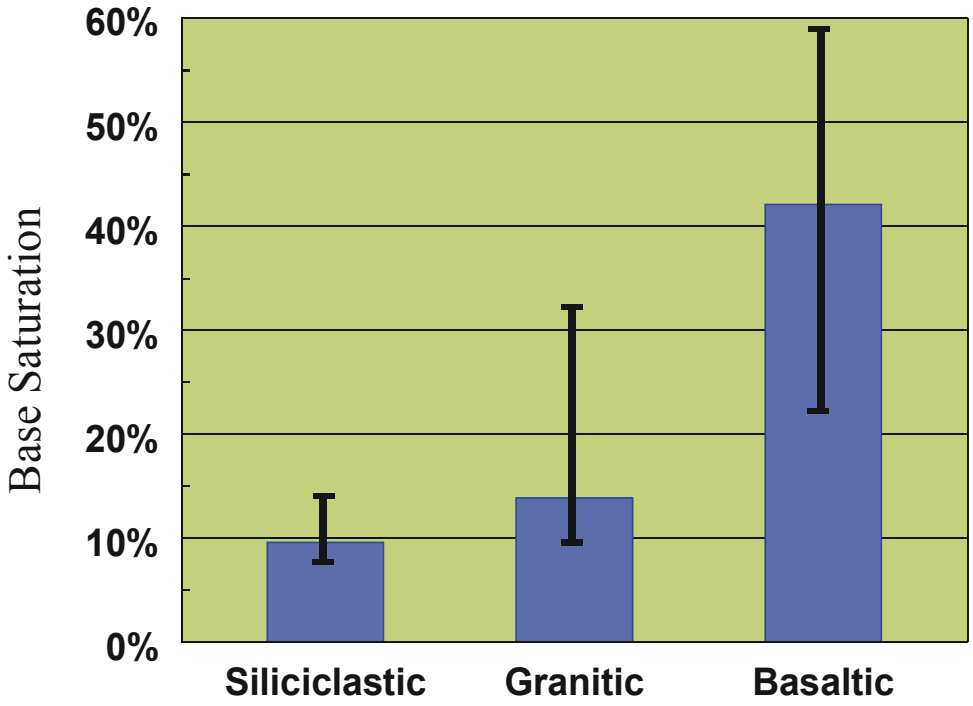

Figure VI-4. Median percent base saturation for soils associated with SHEN's three bedrock types. Brackets delimit interquartile ranges. The base saturation of soils derived from siliciclastic and granitic bedrock is too low for effective buffering of acidic deposition in many watersheds. The data were obtained for mineral-horizon soil samples collected in the summer of 2000 at 79 geologically distributed sites in SHEN (Welsch et al. 2001).

A clear relationship was found between streamwater ANC and measured soil base saturation among the SWAS watersheds (Figure VI-5). All watersheds that were characterized by soil base saturation less than 15% had average streamwater ANC < 100 μeq/L. Watersheds that had higher soil base saturation (all of which were > 22%) were dominated by the basaltic bedrock type and had average streamwater ANC > 100 μeq/L. Lowest base saturation values (7 to 14%) were found in the siliciclastic and granitic watersheds, with much higher values in the basaltic watersheds. We do not advocate using the relationship between streamwater ANC and soil base saturation, shown in Figure VI-5, for predictive purposes, however. Within a particular bedrock class, soil base saturation is not a good predictor of streamwater ANC. In addition, the ranges of base saturation among the study watersheds were similar for the siliciclastic and granitic types, despite the clear separation in streamwater ANC (Figure VI-5).

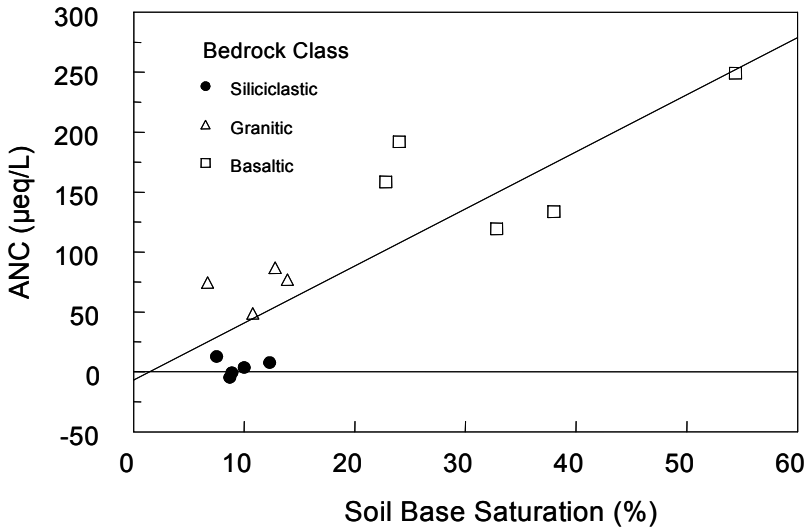

Figure VI-5. Median spring ANC of streams in SWAS watersheds during the period 1988 to 1999 versus median base saturation of watershed soils. Soils data were collected by the University of Virginia during the summer of 2000 (Welsch et al. 2001).

The data presented in Table VI-4 are based on soils data stratified by watershed, and each watershed was geologically classified based on the predominant bedrock type found within the watershed. However, a watershed that was primarily underlain by granitic bedrock may have included, for example, one or more soil pits located over basaltic bedrock. We therefore reanalyzed the soils data by classifying all soil pits according to the underlying bedrock type, irrespective of the predominant bedrock class within the watershed in which the soil pit was located. The results of this analysis, shown in Table VI-5, illustrate a more distinct separation of soils characteristics across bedrock types, especially for the mineral soil layer (> 20 cm depth). For example, the interquartile ranges (25th to 75th percentile) for base saturation in the mineral soil were 8 to 14%, 10 to 32%, and 22 to 59% for the siliciclastic, granitic, and basaltic classes, respectively. Soil pH showed almost a complete interquartile separation, with interquartile ranges in the mineral soil of 4.4 to 4.6, 4.7 to 5.0, and 4.9 to 5.3 for the three respective bedrock types. Cation exchange capacity values were lower in the siliciclastic soils (interquartile range in the mineral soil of 3.7 to 7.5) than in the other two bedrock types, which showed similar CEC values (Table VI-5).

Table VI-5. Interquartile distributions for each bedrock class of pH, cation exchange capacity (CEC), and percent base saturation for all soil pits excavated within the 2000 soil survey.

Bedrock Class and Soil Layer[a]	N	pH			CEC (cmol/kg)			Percent Base Saturation		
		25th	Med	75th	25th	Med	75th	25th	Med	75th
Siliciclastic Bedrock Class										
Surface soil	28	4.1	4.2	4.4	6.9	10.5	13.5	9.9	15.3	28.3
Mineral soil	28	4.4	4.5	4.6	3.7	5.7	7.5	7.5	9.6	13.7
Granitic Bedrock Class										
Surface soil	26	4.3	4.6	4.9	6.9	10.1	13.2	17.2	31.1	46.0
Mineral soil	26	4.7	4.8	5.0	6.9	8.1	10.5	10.1	13.9	32.3
Basaltic Bedrock Class										
Surface soil	25	4.7	5.3	5.6	9.5	10.3	15.1	29.0	46.6	74.5
Mineral soil	25	4.9	5.1	5.3	7.4	8.1	10.1	22.0	42.1	58.8

[a] Surface soil collected from depth $\leq$20 cm; mineral soil collected from depth >20 cm. Each soil pit was classified into a bedrock class based on the location of the soil pit, irrespective of the predominant bedrock class within the watershed in which the soil pit was located.

c. Influence of Forest Defoliation on Streamwater Chemistry

Between the mid-1980s and the early 1990s, the southward expanding range of the European gypsy moth traversed SHEN and affected all of the SWAS study watersheds (Webb 1999). Some areas of the park were heavily defoliated two to three years in a row. The White Oak Run watershed, for example, was more than 90% defoliated in both 1991 and 1992. The gypsy moth population in White Oak Run then collapsed due to pathogen outbreak and there was no further heavy defoliation in subsequent years. This insect infestation of forest ecosystems in SHEN resulted in substantial impacts on streamwater chemistry. The most notable effects of the defoliation on park streams were dramatic increases in the concentration and export of N and base cations in streamwater. Figure VI-6 shows the increase in NO_3^- export that occurred in White Oak Run. Following defoliation, NO_3^- export increased to previously unobserved levels and remained high for over six years before returning to predefoliation levels. Eshleman et al. (2001) estimated that park-wide export of NO_3^- in 1992, the year of peak defoliation, increased 1700% from a predefoliation baseline of about 0.1 kg/ha/yr. The very low levels of NO_3^- export in park streams were consistent with expectations for N-limited, regenerating forests (e.g., Aber et al. 1989, Stoddard 1994). Release of NO_3^- to surface waters following defoliation was

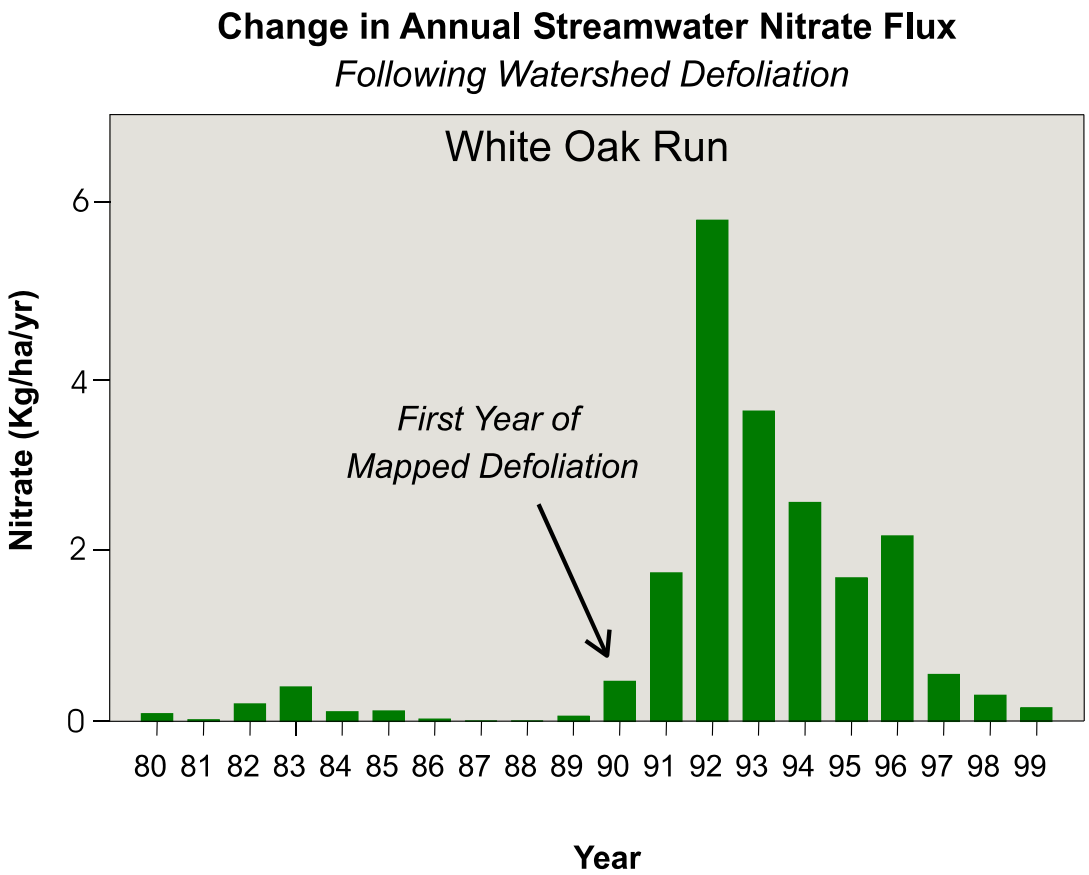

Figure VI-6. Effect of watershed defoliation by the gypsy moth caterpillar on nitrate flux in streamwater. White Oak Run was heavily defoliated for three consecutive years. The watershed area defoliated was 46.5% in 1990, 92.9% in 1991, and 90.4% in 1992. In 1993, the gypsy moth population collapsed and there was no further defoliation.

likewise consistent with previous observations of increased N export due to forest disturbance (e.g., Likens et al. 1970, Swank 1988). The exact mechanisms have not been determined, but it is evident that the repeated consumption and processing of foliage by the gypsy moth larva disrupted the ordinarily tight cycling of N in SHEN forests.

Although N is thought to play an important role in the chronic acidification of surface waters in some areas (c.f., Sullivan et al. 1997), the elevated concentrations of NO_3^- in SHEN streams following defoliation did not appear to contribute to baseflow acidification in White Oak Run. This was due to a concurrent increase in concentrations of base cations in streamwater (Webb et al. 1995). Both NO_3^- and base cation concentrations increased during high-runoff conditions, although the increase in base cations did not fully compensate for the episodic

increase in NO_3^-. Episodic acidification following defoliation thus became more frequent and more extreme in terms of observed minimum ANC (Webb et al. 1995).

The full effect of the gypsy moth on aquatic resources in SHEN is not well understood. One consequence may be a reduction in the supply of available soil base cations and associated effects on streamwater ANC. Repeated periods of defoliation would probably increase the impact of episodic acidification on sensitive aquatic fauna and may determine the conditions under which some species are lost. Ultimately such effects may depend upon both the severity of future gypsy moth or other insect outbreaks and possibly on the amount of atmospheric N deposition. Gypsy moth populations typically display a pattern of periodic outbreaks and collapse (Cambell 1981). It remains to be seen what the long-term pattern will be.

d. Regional Context

In a regional context, SHEN is a major focal point of aquatic effects of S deposition, due largely to the prevalence of siliciclastic bedrock geology. Based on the two extensive probability sampling programs for streamwater chemistry within the region (National Stream Survey [NSS, Herlihy et al. 1993] and Environmental Monitoring and Assessment Program [EMAP, Herlihy et al. 2000]), there are about 11,300 km of wadeable stream in western Virginia. Data collected in EMAP showed about 10% of this stream length with ANC ≤ 50 μeq/L, and 5% with ANC ≤ 20 μeq/L. Many of these low-ANC streams are located in and around SHEN. The median value of streamwater ANC within the SAMI region was 172 μeq/L, based on an extrapolation of data from 154 NSS upstream reach sample sites to a population of 19,940 streams (Sullivan et al. 2002a). In contrast, the median ANC for 47 streams within SHEN was 82 μeq/L (Herlihy et al. 1996).

2. Trends in Streamwater Chemistry

Although SHEN has the longest continuous record of streamwater composition in a national park and among the longest anywhere in the United States, the record only goes back to 1979. The 14 SWAS streams that are located in the park (Figure VI-1) have quarterly water quality data extending back to 1988. These streams are used here to examine the trends in streamwater chemistry in the park over the period 1988 to 2001 (data actually cover the 14 water years from Oct. 1987 to Sept. 2001). Trends within the park are placed in a regional context by comparing

results with trends calculated for the 65 VTSSS long-term monitoring streams which cover the western part of Virginia. The VTSSS trends are also based on quarterly streamwater samples, which were taken contemporaneously with the SWAS stream samples.

a. Methods and Data

Trends were calculated for individual ions in streamwater using all quarterly samples for all 14 years of the data record using two techniques: 1) simple linear regressions (SLR) of changes in ionic concentration over time; and 2) the seasonal Kendal tau test (SKT; Hirsch et al. 1982, Hirsch and Slack 1984), a commonly applied nonparametric test for monotonic trends in seasonally-varying water quality data. The slope estimates from the SKT and the SLR were compared and found to be essentially the same for all solutes and streams analyzed (Appendix E). In the discussion that follows, all trends are derived from the slope of the SLR technique and are in units of ueq/L/year, unless otherwise specified. Significance of trends, where expressed, are based on statistically significant deviations of the regression slope from a value of zero (the standard test of significance in simple linear regression analyses).

The 14 SWAS streams and 65 VTSSS streams cover a range of bedrock geology and occur within two physiographic provinces in western Virginia. This allows examination of the patterns of trends on different parts of the landscape. The quarterly nature of the data allows examination of seasonal trends in solute concentrations by performing the SLR analyses separately on winter, spring, summer and fall quarter samples. In these seasonal analyses, there will be 14 data points in the regressions as opposed to 56 data points (4x14) in the regression analyses when all quarters are used for annual trend estimation. Time series plots of the quarterly data for all solutes for the 14 SWAS streams, along with the SLR regression line, are presented in Appendix E.

Given that trend estimates are available for a number of streams in the park (or in western Virginia, or on a particular bedrock type, or in a particular physiographic province), it is sometimes useful to have a single measure of streamwater solute behavior for a region or group of streams. In such cases, the median value of the trend estimates for a solute for all streams within a group is used. The use of the median trend to summarize the regional response is common. For instance, median trends were used in the most recent EPA report to Congress concerning surface water responses to acidic deposition (Stoddard et al. 2003). The statistical

significance of regional trends as represented by the median of a population of trend estimates is determined by calculating confidence limits about the median value in the distribution of all slopes in the analysis (SAS Institute Inc. 1988; Altman et al. 2000). Plots of the full distributions of annual trends for all solutes for all of the 65 VTSSS streams and all of the 14 SHEN streams are provided in Appendix E for comparison with the medians used in the discussions below.

b. Results

The utility of using the median trend for the 14 monitored streams in the park can be illustrated by examining the individual trends for all streams for a given solute (Figure VI-7). For example, ANC increased during the period of record at most streams, whereas SO_4^{2-} and NO_3^- concentrations generally decreased. Using the median provides a summary of the direction and magnitude of change in the population of streams. It is important to note that for a given solute and group of streams all trends may be in the same direction and of the same magnitude as the median trend. However, it is frequently the case that the magnitudes and even the directions of trends in some streams may be very different from the medians. An examination of plots for all of the ranked slope distributions for all solutes, partitioned by season, physiography or lithology, would be at best tedious and at worst confusing. In order to elucidate and understand the general patterns in the trends of streamwater chemistry, and their relationship to season and to the landscape, the median slope values (median trends) for each solute will be used to discuss the patterns in trends in streamwater chemistry in SHEN.

The median trends for each solute in the 14 SWAS streams are summarized in Table VI-6 along with the median trends for the 65 VTSSS streams for the same solutes and period. Note that the 14 SWAS streams are also included in the analyses of the 65 VTSSS streams. Median trends were also calculated for the basic streamwater chemistry data disaggregated by season and physiographic province or bedrock geology (Table VI-6).

The general trends in streamwater chemistry in the park can be understood by considering the behavior of SO_4^{2-}, the sum of the base cations (SBC = Ca + Mg + Na + K), and ANC. Median annual and seasonal trends for ANC, SO_4^{2-}, and SBC determined for streams within geographically and lithologically defined classes are displayed in Figures VI-8 through VI-10. These median trends are extracted from Table VI-6 and presented graphically to aid discussion. The significance of any of the trends in the figures can be determined by reference to Table VI-

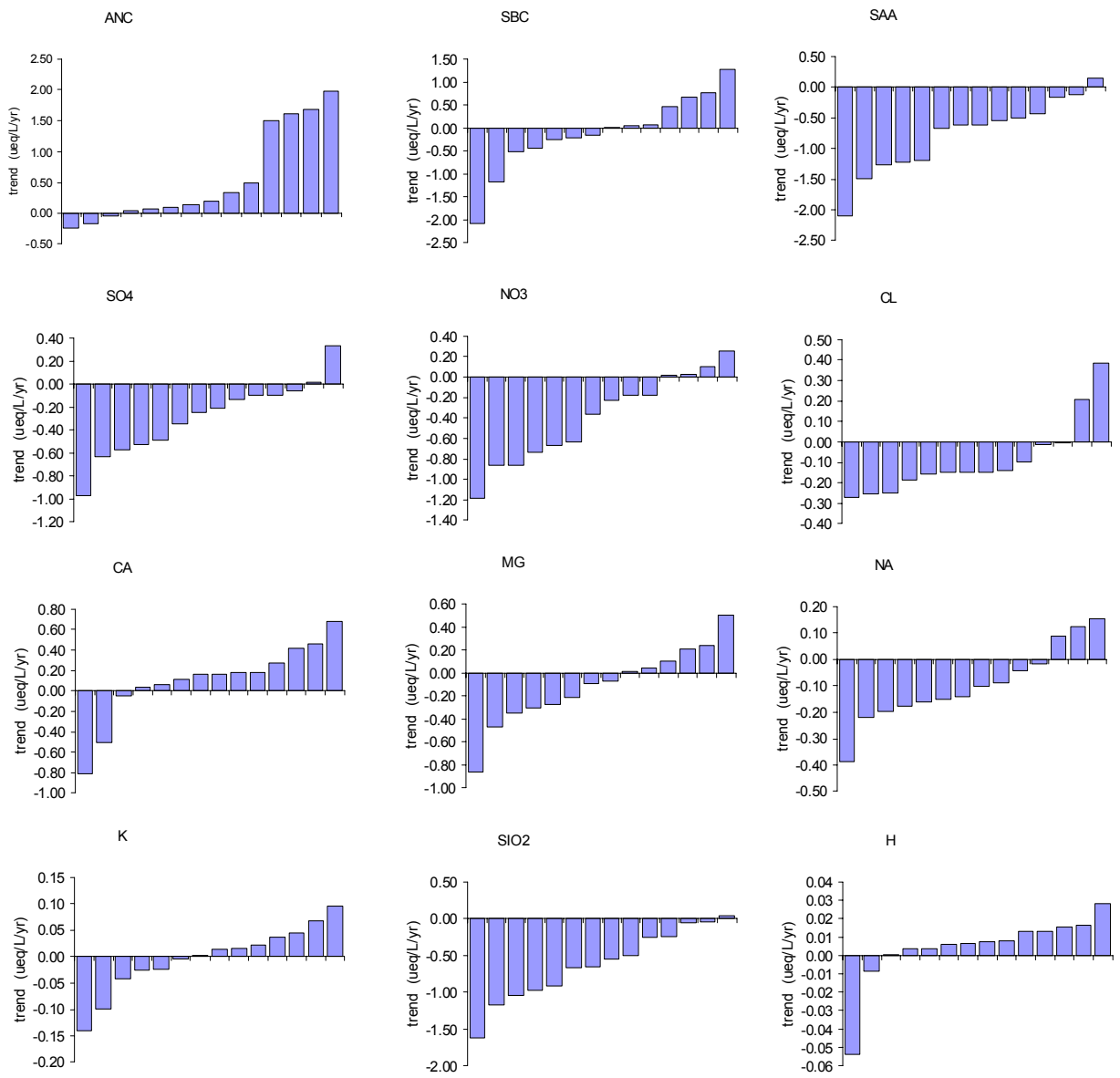

Figure VI-7. Trends in solute concentrations for the 14 SWAS streams in SHEN (ueq/L/yr). The trends are the slopes of simple linear regressions on all quarterly data for 14 years (1988 to 2001; n=56). For each solute, the trends have been sorted from lowest to highest to display the range of estimated trends in a given solute across the 14 streams. Each bar represents one stream.

Table VI-6. Median trends in solute concentrations within geographically or lithologically defined classes for the 14-year period 1988-2001 (water years). The median trends were derived from the slopes of simple linear regressions on all quarterly data for annual trends (n=56), or on individual quarterly values for seasonal trends (n=14). Significant trends ($p < .05$) are indicated in bold.

Sites	N sites	Annual Trends	Seasonal Trends			
			Winter	Spring	Summer	Fall
ANC (µeq/L)						
All Virginia Sites	65	-0.015	-0.138	-0.015	0.084	0.287
Blue Ridge Sites	37	0.071	-0.130	0.169	0.316	0.395
Valley and Ridge Sites	28	-0.056	-0.217	-0.099	-0.129	0.228
All SNP Sites	14	**0.168**	-0.036	**0.969**	0.512	0.195
SNP Siliciclastic Sites	5	0.142	-0.136	0.049	0.475	0.081
SNP Granitic Sites	4	0.076	-0.223	0.969	-0.170	0.107
SNP Basaltic Sites	5	1.612	**0.535**	**2.300**	1.818	0.612
Sulfate (µeq/L)						
All Virginia Sites	65	0.028	**0.333**	0.021	**-0.164**	**-0.143**
Blue Ridge Sites	37	0.013	0.258	-0.040	-0.164	**-0.244**
Valley and Ridge Sites	28	0.109	**0.429**	0.152	-0.179	-0.134
All SNP Sites	14	**-0.229**	0.006	-0.193	-0.389	**-0.395**
SNP Siliciclastic Sites	5	-0.349	-0.096	**-0.214**	-0.775	-0.361
SNP Granitic Sites	4	-0.115	0.040	-0.052	-0.153	-0.326
SNP Basaltic Sites	5	**-0.246**	0.107	-0.151	-0.381	**-0.452**
Sum of Base Cations (µeq/L/yr)						
All Virginia Sites	65	0.044	0.085	-0.184	0.082	0.057
Blue Ridge Sites	37	0.007	-0.002	-0.221	0.221	0.037
Valley and Ridge Sites	28	0.064	0.294	-0.130	0.016	0.151
All SNP Sites	14	-0.073	-0.115	-0.023	0.120	-0.525
SNP Siliciclastic Sites	5	-0.212	-0.026	-0.420	-0.443	**-0.274**
SNP Granitic Sites	4	-0.128	-0.065	-0.025	0.294	**-0.550**
SNP Basaltic Sites	5	0.675	-0.656	0.585	1.798	-0.105

Table VI-6. Continued.

Sites	N sites	Annual Trends	Seasonal Trends			
			Winter	Spring	Summer	Fall
Nitrate (µeq/L/yr)						
All Virginia Sites	65	0.035	0.044	**-0.021**	**0.086**	**-0.012**
Blue Ridge Sites	37	0.005	0.025	**-0.043**	-0.007	**-0.014**
Valley and Ridge Sites	28	0.091	0.150	-0.003	0.230	-0.010
All SNP Sites	14	-0.298	-0.127	**-0.430**	-0.124	**-0.382**
SNP Siliciclastic Sites	5	0.017	0.028	-0.127	0.086	-0.029
SNP Granitic Sites	4	-0.205	-0.237	**-0.242**	**-0.150**	**-0.031**
SNP Basaltic Sites	5	**-0.867**	**-1.089**	**-1.165**	-0.151	**-0.947**
Chloride (µeq/L/yr)						
All Virginia Sites	65	-0.014	0.022	-0.011	0.025	-0.015
Blue Ridge Sites	37	-0.014	0.008	0.005	0.031	-0.028
Valley and Ridge Sites	28	-0.018	0.037	-0.033	0.020	0.010
All SNP Sites	14	**-0.147**	-0.121	-0.163	-0.092	-0.129
SNP Siliciclastic Sites	5	**-0.147**	-0.119	**-0.170**	**-0.123**	-0.129
SNP Granitic Sites	4	**-0.172**	-0.172	-0.129	-0.092	-0.190
SNP Basaltic Sites	5	-0.095	-0.078	-0.052	0.032	-0.093
Sum of Acid Anions (µeq/L/yr)						
All Virginia Sites	65	0.094	**0.490**	-0.021	0.086	**-0.251**
Blue Ridge Sites	37	-0.084	0.367	**-0.255**	-0.227	**-0.355**
Valley and Ridge Sites	28	0.197	**0.717**	0.197	0.305	-0.080
All SNP Sites	14	**-0.619**	-0.411	**-0.814**	-0.559	**-0.655**
SNP Siliciclastic Sites	5	-0.613	-0.148	**-0.717**	**-0.343**	**-0.624**
SNP Granitic Sites	4	**-0.302**	-0.046	-0.324	-0.721	-0.556
SNP Basaltic Sites	5	**-1.228**	**-1.445**	**-1.726**	-0.554	**-1.572**
Hydrogen Ion (µeq/L/yr)						
All Virginia Sites	65	**0.007**	**0.016**	0.010	0.006	**-0.004**
Blue Ridge Sites	37	0.007	**0.010**	**0.008**	0.005	-0.003
Valley and Ridge Sites	28	**0.008**	**0.032**	0.011	**0.006**	-0.012
All SNP Sites	14	**0.007**	**0.015**	**0.004**	0.000	0.000

Table VI-6. Continued.

Sites	N sites	Annual Trends	Seasonal Trends			
			Winter	Spring	Summer	Fall
SNP Siliciclastic Sites	5	0.015	0.043	0.006	**-0.038**	-0.054
SNP Granitic Sites	4	**0.010**	**0.020**	**0.005**	0.010	-0.004
SNP Basaltic Sites	5	**0.006**	**0.008**	**0.003**	0.004	0.003
Calcium Ion (µeq/L/yr)						
All Virginia Sites	65	0.078	0.151	0.031	0.076	0.048
Blue Ridge Sites	37	0.125	0.128	0.047	0.163	0.062
Valley and Ridge Sites	28	0.066	0.218	0.024	0.033	0.008
All SNP Sites	14	**0.163**	0.215	0.220	0.156	0.005
SNP Siliciclastic Sites	5	**0.161**	**0.314**	0.053	0.088	**0.062**
SNP Granitic Sites	4	-0.008	0.161	0.098	0.025	**-0.261**
SNP Basaltic Sites	5	0.422	-0.084	**0.413**	0.972	0.009
Magnesium Ion (µeq/L/yr)						
All Virginia Sites	65	0.007	0.030	**-0.041**	0-082	0.024
Blue Ridge Sites	37	-0.015	0.008	**-0.048**	0.004	-0.004
Valley and Ridge Sites	28	0.041	0.114	-0.033	0.112	0.127
All SNP Sites	14	-0.082	-0.033	-0.107	-0.075	**-0.179**
SNP Siliciclastic Sites	5	**-0.273**	-0.057	**-0.283**	-0.270	**-0.256**
SNP Granitic Sites	4	-0.103	-0.004	0.017	-0.020	**-0.116**
SNP Basaltic Sites	5	0.204	-0.356	0.057	0.625	-0.026
Sodium Ion (µeq/L/yr)						
All Virginia Sites	65	-0.020	-0.043	**-0.076**	-0.005	0.025
Blue Ridge Sites	37	-0.018	-0.103	**-0.086**	0.168	0.034
Valley and Ridge Sites	28	**-0.030**	-0.026	**-0.073**	-0.012	0.016
All SNP Sites	14	-0.121	**-0.226**	-0.188	0.039	-0.123
SNP Siliciclastic Sites	5	**-0.163**	**-0.226**	**-0.234**	**-0.063**	**-0.112**
SNP Granitic Sites	4	**-0.127**	**-0.352**	**-0.209**	0.274	-0.219
SNP Basaltic Sites	5	0.086	-0.214	0.002	0.208	-0.058

Table VI-6. Continued.

Sites	N sites	Annual Trends	Seasonal Trends			
			Winter	Spring	Summer	Fall
Potassium Ion (µeq/L/yr)						
All Virginia Sites	65	**-0.043**	-0.013	**-0.040**	**-0.070**	**-0.095**
Blue Ridge Sites	37	-0.034	-0.019	-0.018	-0.025	**-0.085**
Valley and Ridge Sites	28	**-0.067**	-0.007	**-0.067**	**-0.087**	**-0.103**
All SNP Sites	14	0.007	0.048	0.019	0.020	**-0.075**
SNP Siliciclastic Sites	5	-0.006	0.074	0.031	-0.105	**-0.207**
SNP Granitic Sites	4	**0.033**	0.048	0.059	**0.089**	**-0.047**
SNP Basaltic Sites	5	-0.025	0.043	0.006	0.009	**-0.085**
Silica (µm/L/yr)						
All Virginia Sites	65	**-0.079**	-0.107	**-0.120**	**-0.151**	0.115
Blue Ridge Sites	37	**-0.130**	-0.171	**-0.285**	**-0.151**	0.104
Valley and Ridge Sites	28	**-0.057**	**-0.083**	-0.017	-0.169	0.157
All SNP Sites	14	**-0.601**	**-0.472**	**-0.340**	**-0.863**	**-0.639**
SNP Siliciclastic Sites	5	**-0.242**	-0.098	-0.307	-0.097	-0.218
SNP Granitic Sites	4	**-0.705**	**-0.647**	**-0.340**	-1.096	**-0.639**
SNP Basaltic Sites	5	**-0.972**	**-0.607**	-0.404	**-1.384**	-1.623
CALK[a] (µeq/L/yr)						
All Virginia Sites	65	0.042	-0.302	-0.104	0.138	0.294
Blue Ridge Sites	37	0.177	-0.290	0.116	0.602	0.295
Valley and Ridge Sites	28	-0.171	-0.347	-0.317	-0.380	0.258
All SNP Sites	14	**0.294**	**0.164**	**0.439**	0.668	0.076
SNP Siliciclastic Sites	5	0.177	0.131	**0.309**	0.206	0.007
SNP Granitic Sites	4	0.211	-0.128	0.270	0.623	0.006
SNP Basaltic Sites	5	**1.805**	**0.911**	**2.311**	2.352	1.141

[a] CALK is calculated ANC (CALK=SBC-SAA)

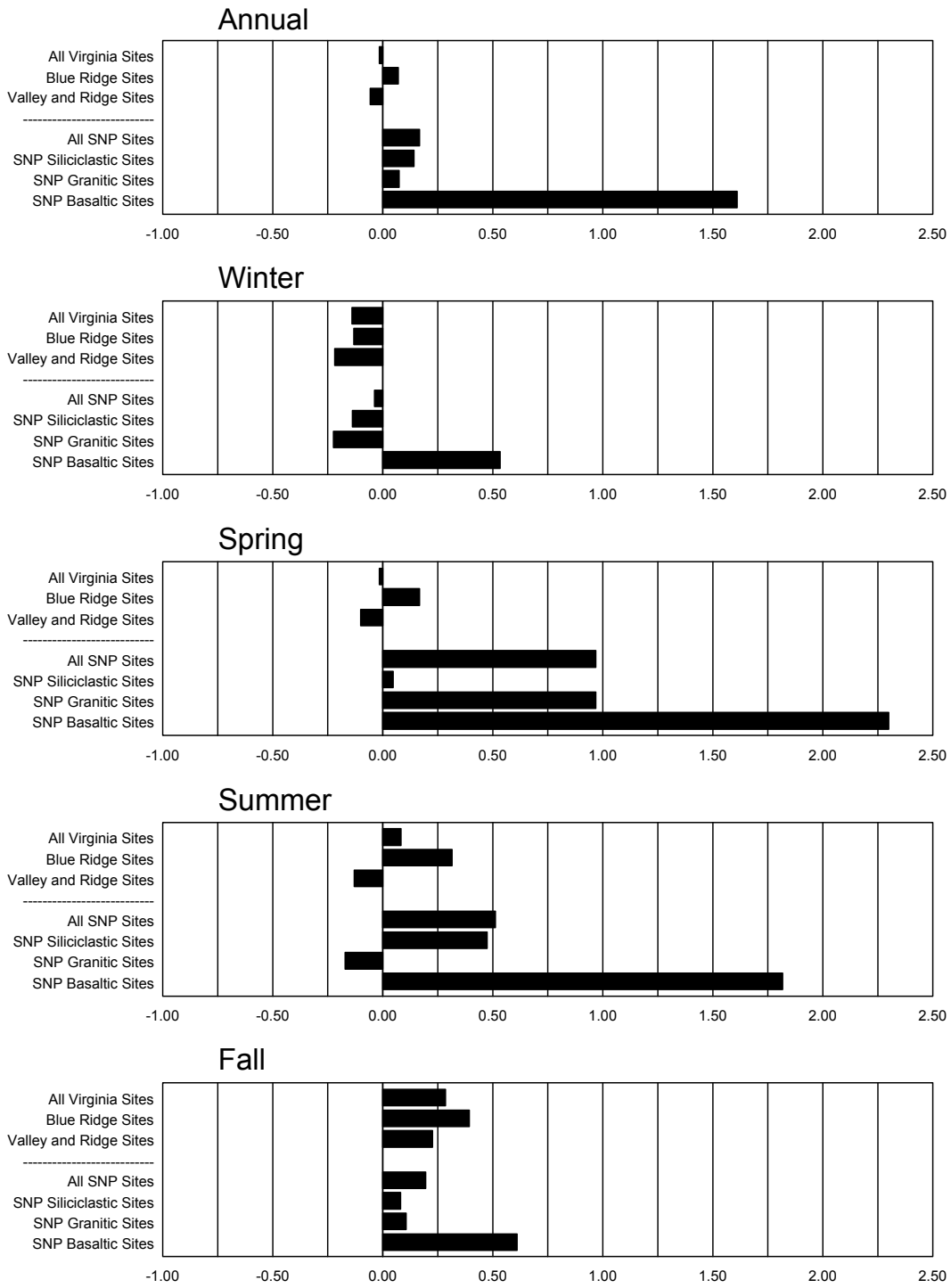

Figure VI-8. Median values of annual and seasonal trends (in µeq/L) in streamwater ANC concentrations among VTSSS and SWAS watersheds: 1988-2001. The median values are from distributions of ANC trends determined for streams within classes defined by physiography or lithology. The annual trends are based on simple linear regressions on all quarterly data for 14 years (n=56). Seasonal trends are based on individual quarterly values for 14 years (n=14).

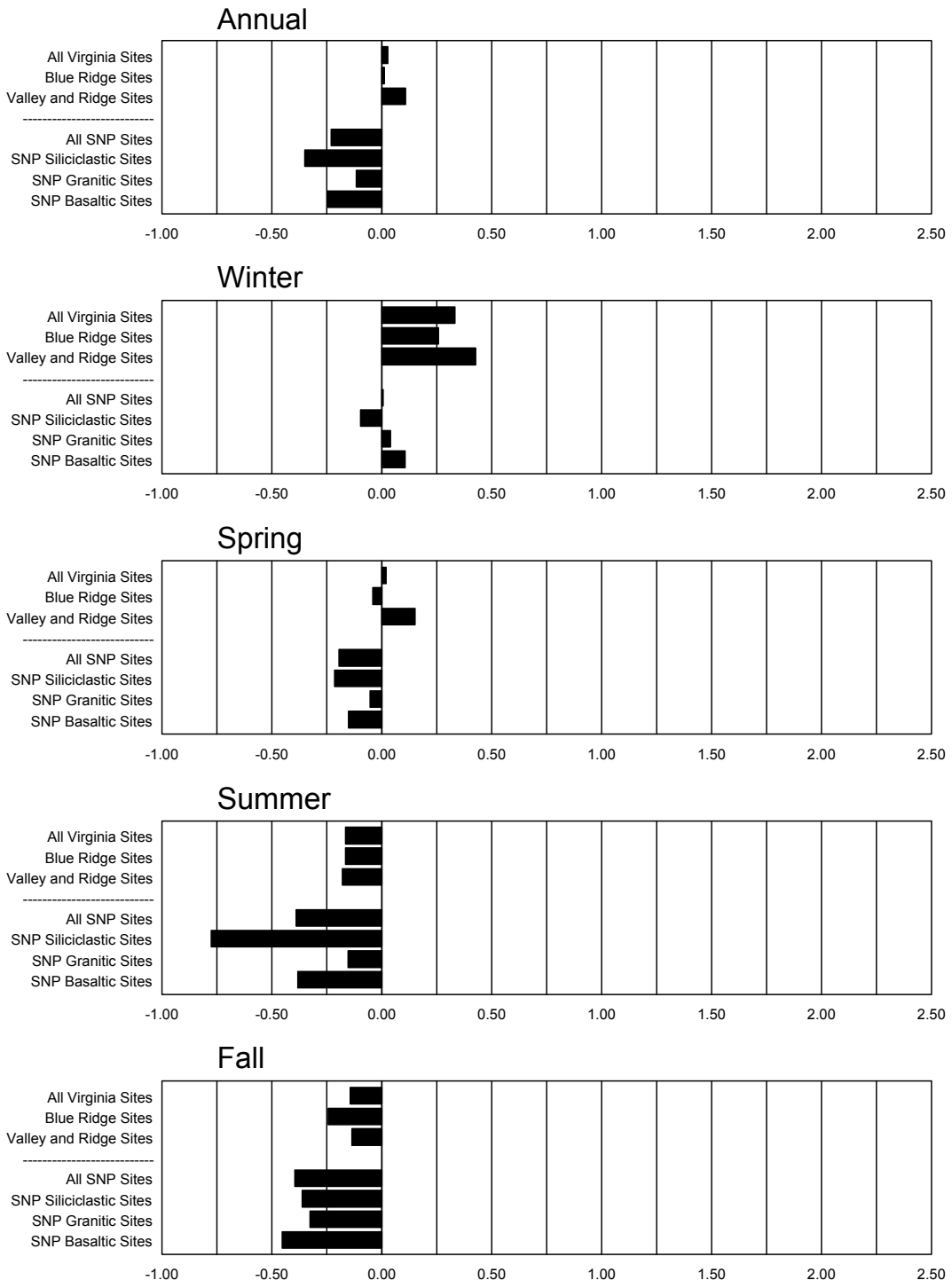

Figure VI-9. Median values of annual and seasonal trends in streamwater SO_4^{2-} concentrations (in µeq/L) among VTSSS and SWAS watersheds: 1988-2001. The median values are from distributions of ANC trends determined for streams within classes defined by physiography or lithology. The annual trends are based on simple linear regressions on all quarterly data for 14 years (n=56). Seasonal trends are based on individual quarterly values for 14 years (n=14).

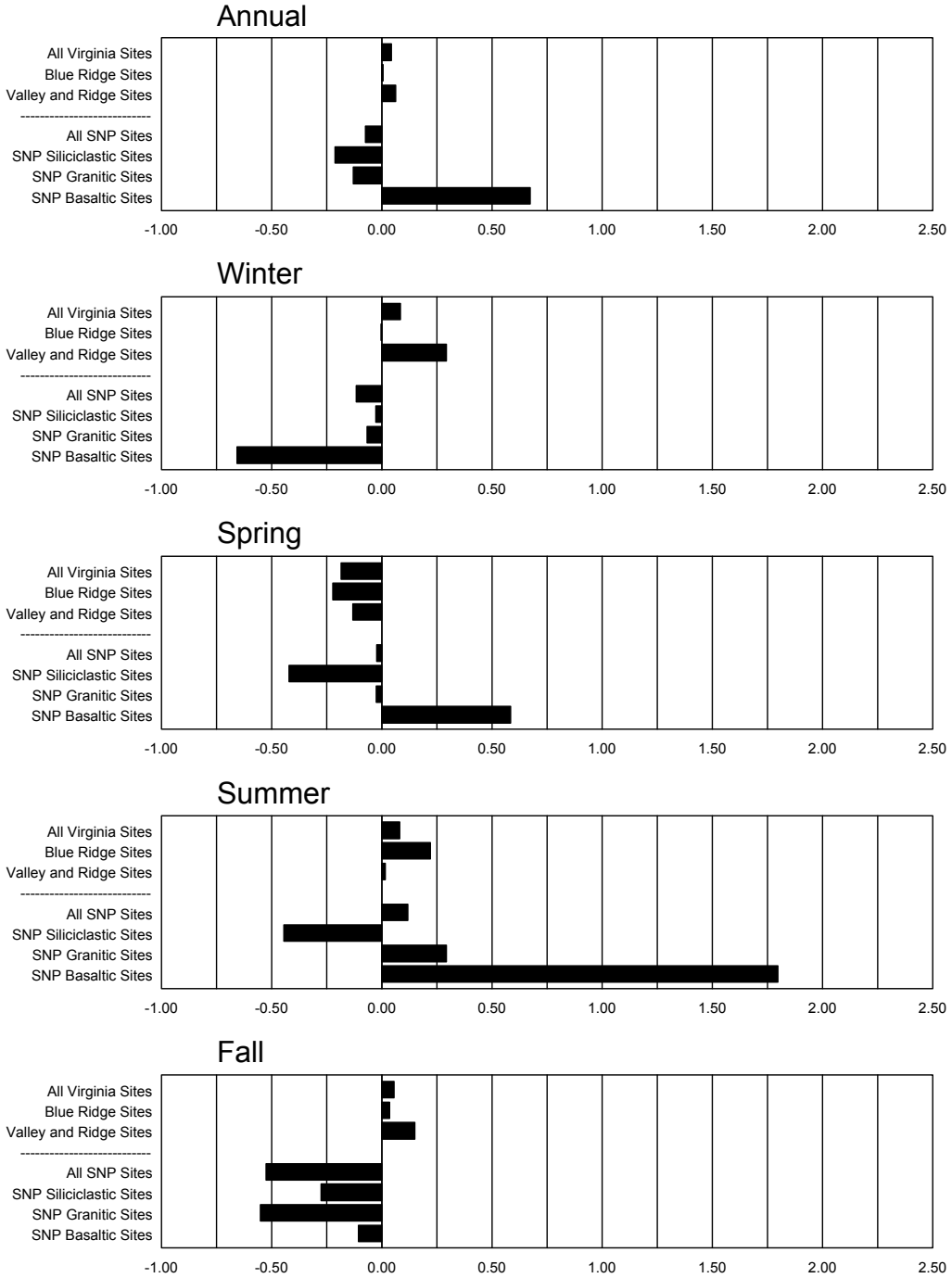

Figure VI-10. Median values of annual and seasonal trends in streamwater SBC concentrations (in µeq/L) among VTSSS and SWAS watersheds: 1988-2001. The median values are from distributions of ANC trends determined for streams within classes defined by physiography or lithology. The annual trends are based on simple linear regressions on all quarterly data for 14 years (n=56). Seasonal trends are based on individual quarterly values for 14 years (n=14).

6. Although most of the observed median trend values for these key parameters are small and generally not significant, geographic, lithologic, and seasonal patterns are evident.

ANC Trends

The median annual trend in ANC was positive for the group of 14 study streams in SHEN, as well as for all of the lithologically defined subsets of streams (Figure VI-8). In contrast, the median ANC decreased on an annual basis for the 65 study streams in western Virginia. Thus, although there is some evidence for some recovery from acidification effects on streamwater composition among the SHEN streams, there is evidence for continuing acidification among streams in the larger region, which encompasses those in SHEN. This observation of continuing acidification among the study streams in the larger western Virginia region is consistent with trend results reported by Stoddard et al. (2003), who evaluated trends among the same set of streams for the 1990-2000 period. It should be noted that the observed median annual trends in ANC in both SHEN and the western Virginia region are quite small; when considered over the 14-year period, the median ANC change in streamwaters is only +2.4 μeq/L in SHEN and –0.2 μeq/L in western Virginia.

It should also be noted that the observed median annual trends differ for western Virginia streams classified by physiographic province. Median trends were negative for streams in the Valley and Ridge province and positive for streams in the Blue Ridge province, which includes the SHEN area. Thus, there is some evidence for a recovery gradient between the two provinces, as well as between the park and western Virginia as a whole.

Additional patterns in ANC trends were evident among the different seasons. Most notably, the median trend values in winter contrasted with those of the other seasons, generally showing a negative trend in median ANC. Only the SHEN streams associated with basaltic bedrock showed a positive value for median ANC trend in winter. In contrast, the median trend values for the fall season were positive for all of the defined classes of streams. These observed seasonal differences in median ANC trends may have biological significance because winter is the period of the year when the most acid-sensitive life stages of the brook trout (eggs and fry) are present in the streams of SHEN and western Virginia (Figure VI-11).

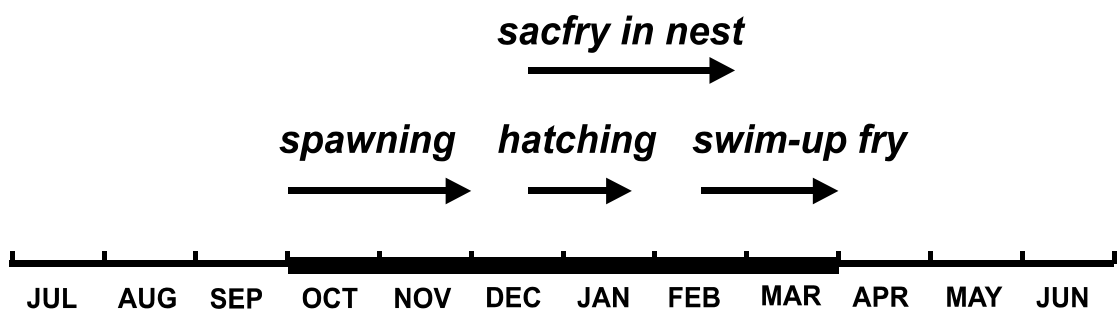

Figure VI-11. Life stages of brook trout.

Sulfate Trends

The level of SO_4^{2-} leaching, which is the principal acidifying process, and the availability of exchangeable base cations, which serve to neutralize acidity, determine both acidification and recovery of streams in the central Appalachian region. Plots of median trends in streamwater SO_4^{2-} (Figure VI-9) are consistent with the observation that changes in SO_4^{2-} mobility are largely driving both the acidification and recovery processes in the streams of SHEN and the adjacent mountainous region. The median annual trend in SO_4^{2-} concentration was negative for all the streams in SHEN, including each of the lithologically-defined subgroups. A negative median annual trend in SO_4^{2-} concentration was associated with a positive median annual trend in ANC.

Again, a different pattern is evident for the median annual trends in SO_4^{2-} among the streams in the larger western Virginia region. The observed median annual trend in SO_4^{2-} concentration was positive for the regional streams. For the Virginia streams, as well as the streams in the Valley and Ridge province, a positive median annual trend in SO_4^{2-} concentration was associated with a negative median annual trend in ANC. It thus appears that recent differences in streamwater ANC trends between SHEN and the larger western Virginia region, although

relatively small in terms of absolute magnitude, may be largely attributed to differences in streamwater SO_4^{2-} trends between the two defined areas.

A plot of SO_4^{2-} trends for individual study streams in the western Virginia region (Figure VI-12) suggests that these observed differences in SO_4^{2-} trends can be explained as a consequence of S retention dynamics. As indicated in Figure VI-12, the streams with the largest negative trends in SO_4^{2-} concentration over the 14-year period, including many in the park, were generally those with higher median SO_4^{2-} concentrations. This observation is consistent with the expectation that streamwater SO_4^{2-} concentrations in the southern Appalachian Mountains in general are determined by the S adsorption properties of watershed soils and the level of watershed exposure to S deposition. For watersheds with high S deposition and relatively little retention, streamwater SO_4^{2-} concentrations will be high. Decreases in S deposition may then result in decreases in streamwater SO_4^{2-} concentrations. For watersheds that more strongly retain S, streamwater SO_4^{2-} concentrations will be lower. Decreases in S deposition may then either result in no change in streamwater SO_4^{2-} concentrations or SO_4^{2-} concentrations may actually continue to increase as the retention capacity of watershed soils is depleted.

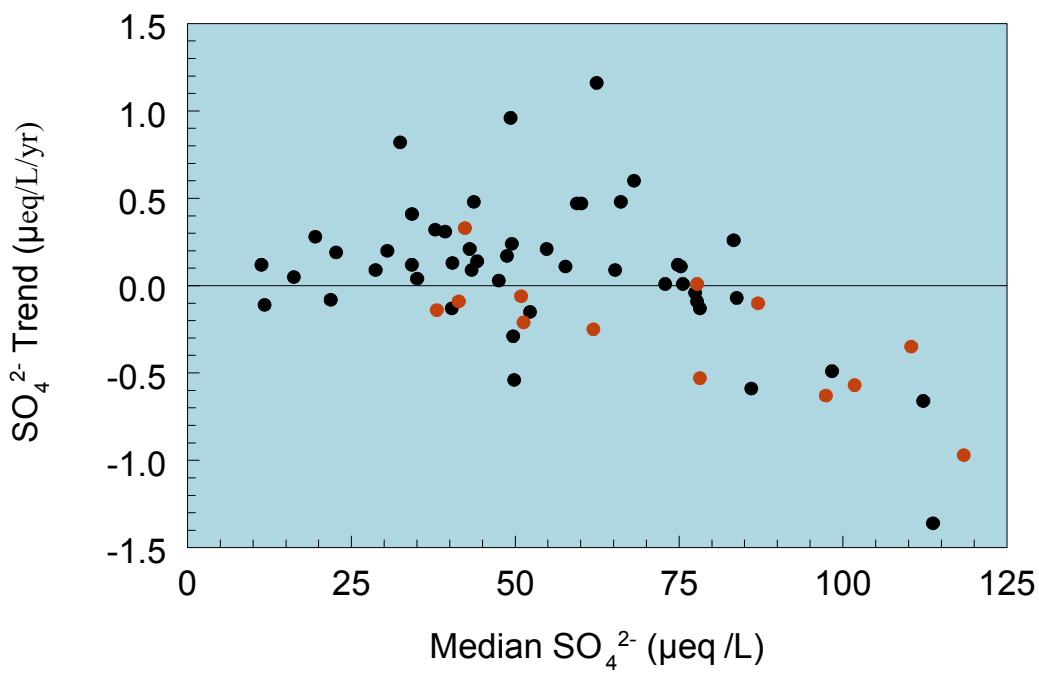

Figure VI-12. Trends in streamwater SO_4^{2-} concentrations in relation to median SO_4^{2-} concentrations for VTSSS and SWAS streams. Trends and medians are based on quarterly sampling data (1988-2001). SWAS study streams (located in SHEN) are indicated with red symbols.

Seasonal patterns in median SO_4^{2-} concentration trends indicate that the difference in ANC change between winter and the rest of the year is also largely a function of SO_4^{2-} trends. The largest and most general increases in median SO_4^{2-} concentrations were observed during winter. Sulfate concentration trends were generally negative in other seasons.

SBC Trends

The plots of median trends in the sum of base cation concentrations are also informative (Figure VI-10), and suggest that base cation availability is a limiting factor with respect to recovery of streams in SHEN and western Virginia. The median annual trends in the sum of base cations were decreasing in all SHEN streams except streams associated with basaltic bedrock. As indicated in Table VI-1 and Figure VI-4, streams on basaltic bedrock had relatively high base cation concentrations and soils on basaltic bedrock had relatively high base cation availability. For the streams on relatively base-poor siliciclastic or granitic bedrock, the observed decrease in the sum of base cations coincident with the decrease in SO_4^{2-} concentrations suggested that low availability of base cations limited recovery of ANC.

It is also notable that although there was much seasonal variation in median trends in the sum of base cations, the SHEN streams with the most consistently negative trends were on siliciclastic bedrock. This may be an indication of base cation depletion in watershed soils, given that the soils on siliciclastic bedrock had notably low base cation availability (see Figure VI-4). For this subset of streams in particular, ANC recovery may be limited by base cation availability and additional acidification may be expected to occur as the watershed base cation supplies are further depleted, especially if S deposition remains relatively high.

c. Summary of Trends in Streamwater Chemistry in SHEN

In summary, it appears that the streams in SHEN are showing signs of recovery, whereas the streams in the larger western Virginia region are not. Moreover, the patterns of trends in ANC and SO_4^{2-} are consistent with expectations for recovery. Considered in relation to the regional-scale analysis of Stoddard et al. (2003), these observations suggest that evidence for decreasing SO_4^{2-} concentrations and increasing ANC in SHEN streams may reflect a north-to-south recovery gradient in the eastern United States. It should be noted, however, that the changes in both ANC and SO_4^{2-} concentrations in SHEN and western Virginia are small

compared to those reported for other regions by Stoddard et al. (2003), are confounded by seasonal differences, and in many cases are not statistically significant.

3. Biological Effects

Extensive information is available on the effects of acidification on aquatic communities in general. In addition, some studies have been conducted within SHEN and throughout western Virginia. Whole system experiments, mesocosm experiments, and field surveys have demonstrated major shifts in species composition and decreases in species richness with increasing acidity. The range of sensitivity to acidification varies among fish species, and to a greater extent among invertebrate species. Some sensitive species are lost at even moderate pH levels, around pH 6.0. In lakes, some important zooplankton predators are affected at pH 5.6-5.9. Some sensitive mayflies and fish (e.g. fathead minnow [*Baetis lapponicus*]) are lost at pH 5.6- 6.0 (Baker and Christensen 1991). Toxic mechanisms are well established for fish, and for invertebrates to a lesser degree (Baker et al. 1991).

a. Acidification Effects on Aquatic Invertebrates in SHEN

Benthic macroinvertebrates have been monitored in SHEN streams since 1986 as part of the Long-Term Ecological Monitoring System (LTEMS). Moeykens and Voshell (2002) recently examined these data, comparing them with streamwater chemistry in the park. Their analysis was based on interpretation of 10 chemical and physical variables measured at 89 sites in SHEN (28 low-ANC sites and 61 higher-ANC sites) for which macroinvertebrate data were available. They compared their results for SHEN streams with similar analyses for 45 sites (13 low-ANC sites and 32 higher-ANC sites) elsewhere in the Blue Ridge ecoregion of Virginia. The macroinvertebrate communities in both data sets were characterized with 12 robust variables thought to represent the ecological function and composition of these communities. Moeykens and Voshell (2002) concluded that the higher-ANC streams in SHEN had "superior ecological condition" which was comparable to the best that can be found among the streams in the broader Blue Ridge ecoregion. However, they also concluded that acidification of streamwater causes the only conspicuous degradation of macroinvertebrate communities in some low-ANC SHEN streams. Other disturbances, such as fire and flood, did not appear to have had noticeable long-term effects on the streams. Moeykens and Voshell (2002) concluded that acidified streams in

SHEN host fewer invertebrate taxa and fewer functional groups than streams with higher pH and ANC. Similar findings were reported earlier for SHEN streams by Feldman and Connor (1992).

Though not part of SHEN, the proximity of the St. Mary's River (30 km south of SHEN) makes the recent analyses of changes in macroinvertebrate communities in that stream pertinent to this analysis for SHEN streams. As described by Kauffman et al. (1999), the record for St. Mary's River provides a unique opportunity to compare reliable macroinvertebrate data on an acidified stream over a 60-year time span. Surber (1951) collected the earliest benthic data for St. Mary's River. Starting in August of 1935, and continuing for two years, he collected 20 samples per month from the river's main stem. Subsequent data were collected by the Virginia Department of Game and Inland Fisheries (VDGIF) in 1976 and then biennially beginning in 1986 (Kauffman et al. 1999) using methods comparable to those used for the 1930s collections. The VDGIF data were collected at six evenly spaced locations extending the length of the main stem above the Wilderness boundary. The later collections were made in June, and only June data are used in the following comparisons.

As summarized by Kauffman et al. (1999), changes in the St. Mary's River benthic community are consistent with streamwater acidification. Whereas 29-32 benthic taxa were documented in the 1930s, no more than 22 benthic taxa were observed in the 1990s. Acid-sensitive taxa have generally declined in abundance and some may have been extirpated. In contrast, certain acid-tolerant taxa have increased in abundance, apparently due to less competition from acid-sensitive taxa.

The total abundance of mayfly (Ephemeroptera) larva in the St. Mary's River has dramatically decreased over the 60-year period, and two of the mayfly genera, Paraleptophlebia and Epeorus, were last collected in 1976. Mayflies are known to decline in species abundance and richness with increasing acidity (Peterson and Van Eeckhautz 1992, Kobuszewski and Perry 1993). The total abundance of caddisfly (Trichoptera) larva also declined dramatically over the 60-year period of record. Baker et al. (1990b) indicated that caddisflies exhibit a wide range of response to acidity, with some species affected by even moderate acidity levels. The total abundance of the larva of the stonefly (Plecoptera) genera Leuctra/Alloperla has dramatically increased over the 60-year period. Increased abundance of these stoneflies in acidified waters has been well documented (Kimmel and Murphy 1985). Another insect family that has prospered in St. Mary's River is the midge (Chironomidae), whose larval population has

increased ten fold since the 1930s collections. Increased midge abundance in acidified waters has also been well documented (Kimmel and Murphy 1985, Baker et al. 1990b).

Many stream invertebrate communities are dominated by early life stages of insects that have great dispersal abilities as flying adults. Thus, with many local sources of colonists and the possibility of continual re-colonization, invertebrate biodiversity in affected streams in SHEN is probably continually suppressed by acidity levels. In all likelihood (by analogy to the St. Mary's study), currently acidified SHEN streams hosted more diverse invertebrate communities in pre-industrial times. Given the relatively rapid recovery time (about 3 years) of stream invertebrate communities from disturbance, more productive and diverse invertebrate communities might be among the first positive results of lower acid deposition. On the other hand, if streamwater ANC declines further, we can expect macroinvertebrate diversity to decrease.

Species – ANC Relationships for Aquatic Invertebrates in SHEN Streams

In light of this previous work, the quantitative relationships between invertebrate communities and streamwater quality in SHEN streams were analyzed. The data from the SHEN-LTEMS aquatic macroinvertebrate data base (summarized in Section II.D.2) and the quarterly streamwater data (described in Section VI.B.1) were used in this analysis. The objective was to describe and quantify the correlations between streamwater chemistry (primarily ANC) and various measures of invertebrate community status in the streams.

The 14 SWAS streams in the park (Figure VI-1) have quarterly water quality data extending back to 1988. The means, maxima, and minima of solute concentrations in these streams were calculated for the period 1988 to 2001 for use in the analyses (Table VI-7). Interquartile values for these streamwater chemistry samples are given in Table (VI-1). Note that the quarterly samples actually cover the 14 water years from Oct. 1987 to Sept. 2001.

The LTEMS benthic invertebrate data for the period June 1988 through June 2000 were selected for comparison with water quality data. There are five phyla of benthic macroinvertebrates represented in the samples from SHEN streams (Annelida, Arthropoda, Mollusca, Nematoda, and Platyhelminthes). Because of their importance to park streams and known sensitivity of many taxa to acidification, this analysis was limited to the data collected on aquatic insects (class Insecta of the phylum Arthropoda).

Table VI-7. Minimum, average and maximum ANC values in the 14 SHEN study streams during the period 1988 to 2001 for all quarterly samples. The data cover 14 water years except for VT75 (11 years).

Site ID	Watershed	ANC (ueq/L)		
		Minima	Mean	Maxima
Siliciclastic Bedrock Class				
DR01	Deep Run	-9.5	2.9	24.4
VT35 (PAIN)	Paine Run	-1.3	7.0	19.5
VT36	Meadow Run	-11.4	-1.3	6.2
VT53	Twomile Creek	2.8	15.2	38.6
WOR1	White Oak Run	3.6	27.7	58.6
Granitic Bedrock Class				
NFDR	North Fork Dry Run	22.5	65.6	187.8
VT58	Brokenback Run	44.0	87.9	155.4
VT59 (STAN)	Staunton River	46.1	87.3	189.4
VT62	Hazel River	54.4	95.6	163.6
Basaltic Bedrock Class				
VT51	Jeremys Run	93.7	217.2	542.5
VT60 (PINE)	Piney River	118.7	228.4	382.9
VT61	North Fork Thornton River	156.2	286.6	452.9
VT66	Rose River	94.4	150.2	229.2
VT75	White Oak Canyon Run	81.2	138.6	237.2

There are nine orders of aquatic insects present in the SHEN LTEMS samples: Coleoptera, Collembola, Diptera, Ephemeroptera, Hemiptera, Megaloptera, Odonata, Plecoptera, and Trichoptera. From these nine orders of aquatic insects, 79 families have been collected in SHEN streams. Not all families are present in each stream. The total number of insect families found in a given stream during the sampling period varied from 21 to 56 (Table II-2). Of the nine orders of aquatic insects found in SHEN streams, there were three which were most abundant both in terms of frequency of occurrence in samples and total numbers of individuals collected: Ephemeroptera (mayflies); Plecoptera (stoneflies); and Trichoptera (caddisflies). The use of these three orders as indicators of acidification response in streams is well established. A combined metric based on all three families, the Ephemeroptera-Plecoptera-Trichoptera (EPT) index, is one measure of stream macroinvertebrate community integrity. This is the total number of families in the three insect orders present in a collection. These orders contain families of varying acid sensitivity so the index value (the number of families) is lower at acidified sites (c.f., Section III.C.2, SAMAB, 1996).

Strong relationships for all three orders were observed between mean and minimum streamwater ANC and the number of families in each order (Figure VI-13). The total numbers of individuals in each order was also related strongly to the mean and minimum ANC values of the 14 streams (Figure VI-14). The EPT index provides a single measure of all three orders and was, as expected, also strongly related to mean and minimum streamwater ANC (Figure VI-15).

b. Acidification Effects on Fish in SHEN

Although there are known differences in acid sensitivity among fish species, experimentally-determined acid sensitivities are available for only a minority of freshwater fish species. For example, of 30 species of fish found in SHEN, the critical pH is known for only nine (Table VI-8). Baker and Christensen (1991) reported critical pH values for 25 species of fish. They defined critical pH as the threshold for significant adverse effects on fish populations. The reported range of pH values represents the authors' estimate of the uncertainty of this threshold. The range of response within species depends on differences in sensitivity among life stages, and on different exposure concentrations of calcium (Ca^{2+}) and Al. These ranges, based on multiple studies for each species, are shown in Table VI-8. To cite a few examples, blacknose dace (*Rhinichthys atratulus*) is regarded as very sensitive to acid stress, because population loss due to acidification has been documented in this species at pH values as high as 6.1; in field bioassays, embryo mortality has been attributed to acid stress at pH values as high as 5.9. Embryo mortality has occurred in common shiner (*Luxilus cornutus*) at pH values as high as 6.0. Although the critical pH range for rainbow trout (*Oncorhynchus mykiss*) is designated as 4.9-5.6, adult and juvenile mortality have occurred at pH values as high as 5.9. Brown trout (*Salmo trutta*) population loss has occurred over the pH range of 4.8-6.0, and brook trout fry mortality has occurred over the range of 4.8-5.9 (Baker and Christensen 1991). Relative sensitivities can be suggested by regional surveys as well, although interpretation of such data is complicated by factors that correlate with elevation. Such factors, including habitat complexity and refugia from high-flow conditions, often vary with elevation in parallel with acid sensitivity. It is noteworthy, however that about half of the 53 fish species found in Adirondack Mountain waters in New York never occur at pH values below 6.0 (Kretzer et al. 1989, Driscoll et al. 2001a); for those species whose acid tolerances are unknown, it is likely that acid sensitivity is responsible for at least some of these absences. It is the difference in acid tolerance among

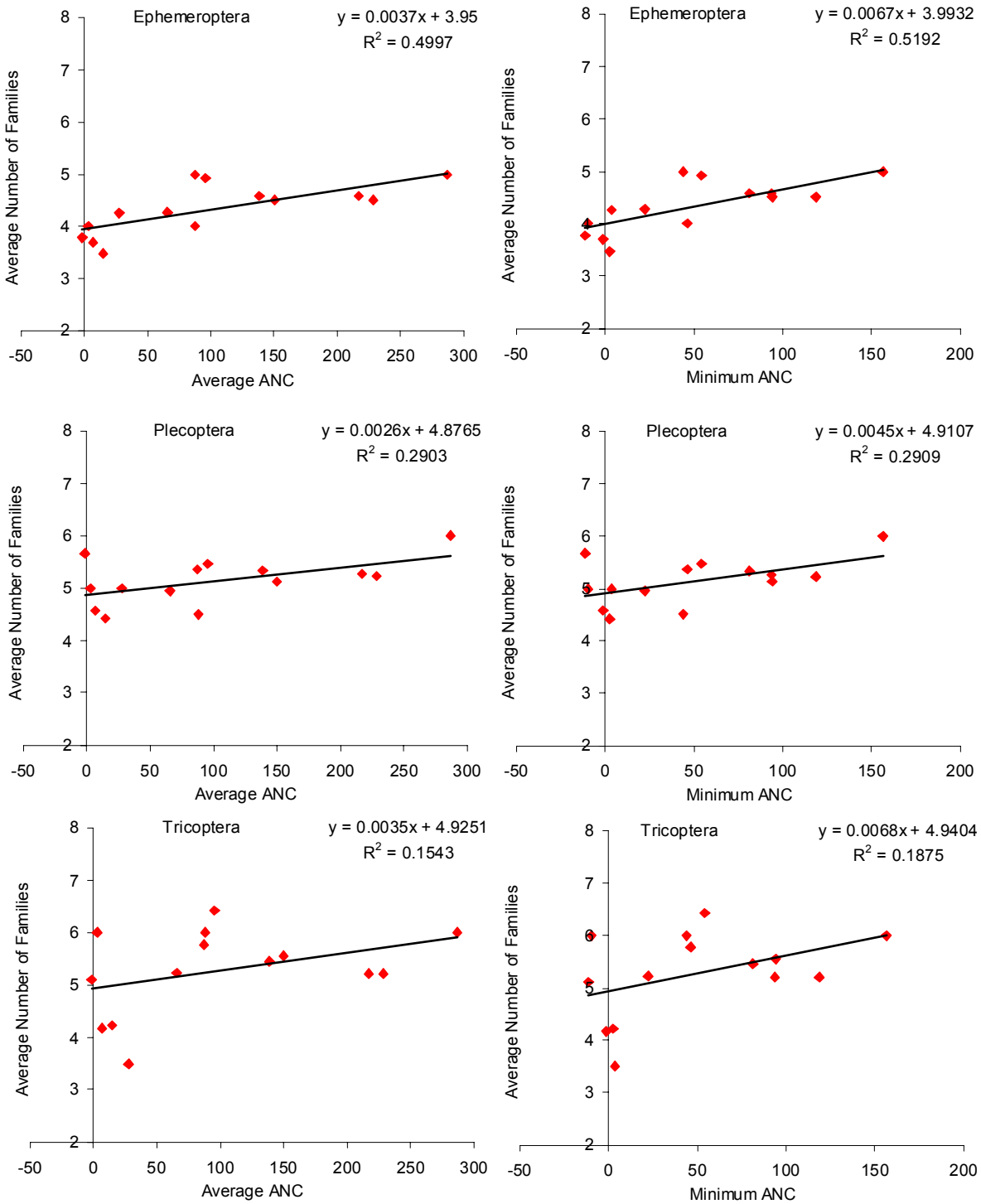

Figure VI-13. Average number of families of aquatic insects in a sample for each of 14 streams in SHEN versus the mean (left) or minimum (right) ANC of each stream. The stream ANC values are based on quarterly samples from 1988 to 2001. The invertebrate samples are contemporaneous. Results are presented for the orders Ephemeroptera (top), Plecoptera (center), and Tricoptera (bottom). The regression relationship and correlation are given on each diagram.

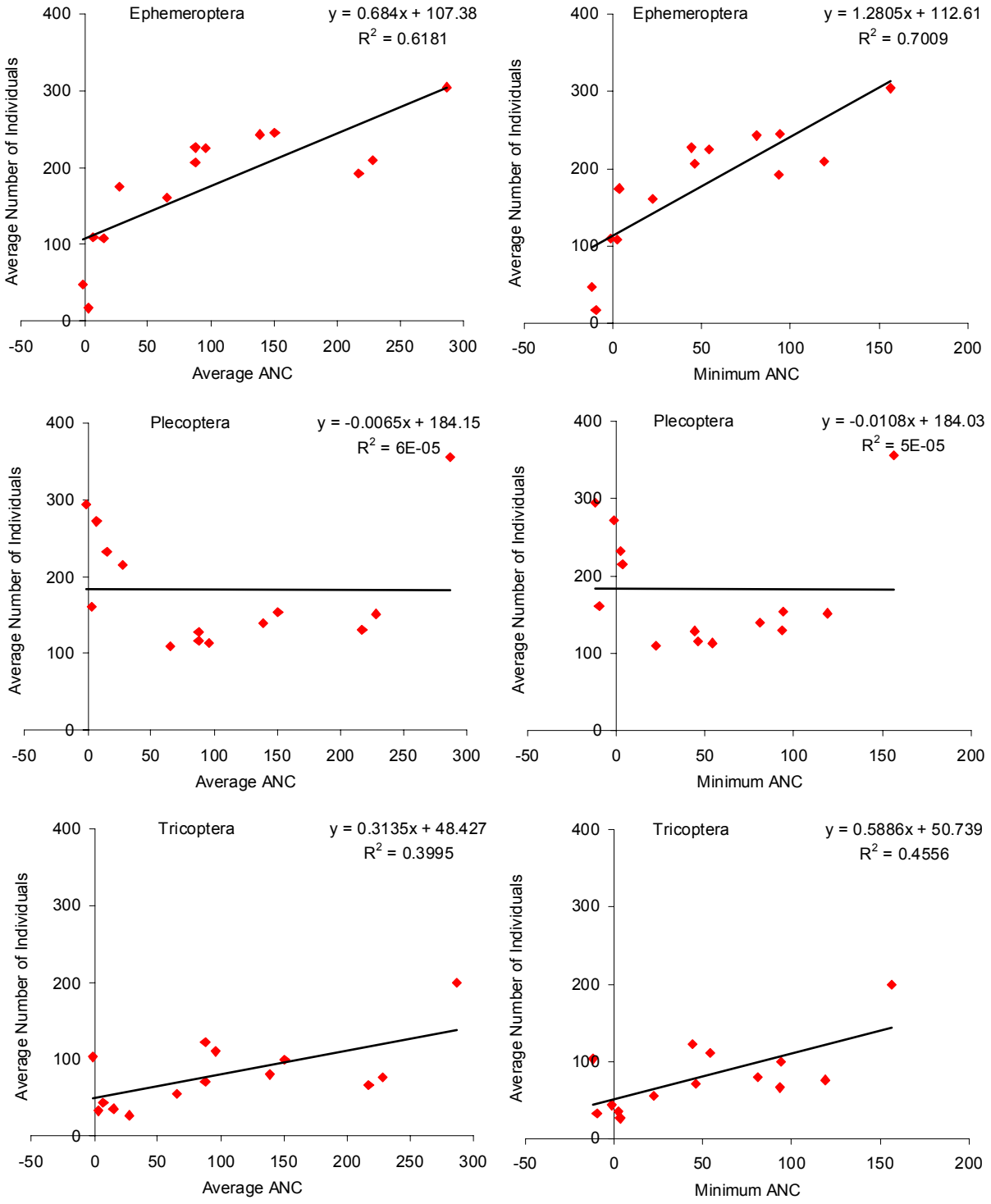

Figure VI-14. Average total number of individuals of aquatic insects in a sample for each of 14 streams in SHEN versus the mean (left) or minimum (right) ANC of each stream. The stream ANC values are based on quarterly samples from 1988 to 2001. The invertebrate samples are contemporaneous. Results are presented for the orders Ephemeroptera (top), Plecoptera (center), and Tricoptera (bottom). The regression relationship and correlation are given on each diagram.

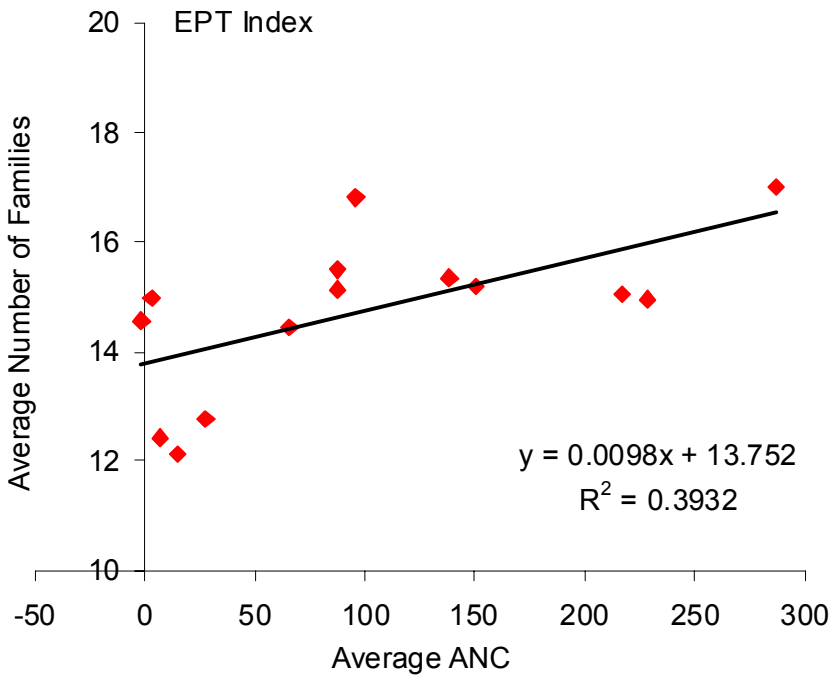

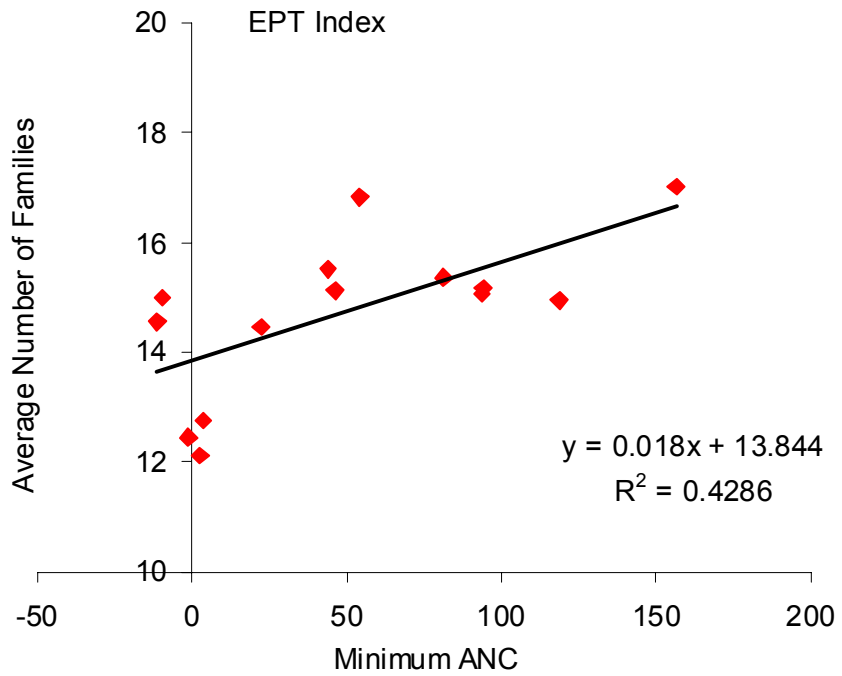

Figure VI-15. Average EPT index in a sample for each of 14 streams in SHEN versus the mean (top) or minimum (bottom) ANC of each stream. The stream ANC values are based on quarterly samples from 1988 to 2001. The invertebrate samples are contemporaneous. The regression relationship and correlation are given on each diagram.

Table VI-8. Critical pH thresholds for fish species of SHEN. (Source: Bulger et al. 1999)

Common Name	Latin Name	Family	Critical pH[a] Threshold
American Eel	*Anguilla rostrata*	Anguillidae	
Mtn. Redbelly Dace	*Phoxinus oreas*	Cyprinidae	
Rosyside Dace	*Clinostomus funduloides*	Cyprinidae	
Longnose Dace	*Rhinichthys cataractae*	Cyprinidae	
Blacknose Dace	*Rhinichthys atratulus*	Cyprinidae	5.6 to 6.2
Central Stoneroller	*Campostoma anomalum*	Cyprinidae	
Fallfish	*Semotilus corporalis*	Cyprinidae	
Creek Chub	*Semotilus atromaculatus*	Cyprinidae	5.0 to 5.4
Cutlips Minnow	*Exoglossum maxillingua*	Cyprinidae	
River Chub	*Nocomis micropogon*	Cyprinidae	
Bluehead Chub	*Nocomis leptocephalus*	Cyprinidae	
Common Shiner	*Luxilus cornutus*	Cyprinidae	5.4 to 6.0
Potomac Sculpin	*Cottus girardi*	Cottidae	
Northern Hogsucker	*Hypentelium nigricans*	Catostomidae	
Torrent Sucker	*Thoburnia rhothocea*	Catostomidae	
White Sucker	*Catastomus commersoni*	Catostomidae	4.7 to 5.2
Margined Madtom	*Noturus insignis*	Ictaluridae	
Brook Trout	*Salvelinus fontinalis*	Salmonidae	4.7 to 5.2
Brown Trout	*Salmo trutta*	Salmonidae	4.8 to 5.4
Tiger Trout[b]	*Salmo X Salvelinus*	Salmonidae	
Rainbow Trout	*Oncorhynchus mykiss*	Salmonidae	4.9 to 5.6
Mottled Sculpin	*Cottus bairdi*	Cottidae	
Bluntnose Minnow	*Pimephales notatus*	Cyprinidae	
Rock Bass	*Ambloplites rupestris*	Centrarchidae	4.7 to 5.2
Smallmouth Bass	*Micropterus dolomieui*	Centrarchidae	5.0 to 5.5
Largemouth Bass	*Micropterus salmoides*	Centrarchidae	
Redbreast Sunfish	*Lepomis auritus*	Centrarchidae	
Pumpkinseed	*Lepomis gibbosus*	Centrarchidae	
Johnny Darter	*Etheostoma nigrum*	Percidae	
Tesselated Darter	*Etheostoma olmstedi*	Percidae	
Fantail Darter	*Etheostoma flabellare*	Percidae	
Greenside Darter[b]	*Etheostoma blennioides*	Percidae	

[a] threshold for serious adverse effects on populations (from Baker & Christensen 1991)
[b] rare (6-10 individuals)

species that produces a gradual decline in species richness as acidification progresses, with the most sensitive species lost first. Some Blue Ridge streams can become too acidic even for brook trout, as evidenced by the absence of the species from streams with mean pH < 5.0 in Great Smoky Mountains National Park (Elwood et al. 1991).

A direct outcome of fish population loss as a result of acidification is a decline in species richness (the total number of species in a lake or stream). This appears to be a highly predictable outcome of regional acidification, although the pattern and rate of species loss varies from region to region. Baker et al. (1990a) discussed 10 selected studies which documented this phenomenon, with sample sizes ranging from 12 to nearly 3,000 lakes and streams analyzed per study. An excellent example occurs in the Adirondacks. Fully 346 of 1469 lakes surveyed supported no fish at all. These lakes were significantly lower in pH, dissolved Ca^{2+}, and ANC than lakes hosting one or more species of fish. Among lakes with fish, there was an unambiguous relationship between the number of fish species and lake pH, ranging from about one species per lake for lakes having pH less than 4.5 to about six species per lake for lakes having pH > 6.5 (Kretzer et al. 1989, Driscoll et al. 2001b).

Relatively less is known about changes in fish biomass, density and condition (robustness of individual fish) which occur in the course of acidification. Such changes result in part from both indirect and direct interactions within the fish community. Loss of sensitive individuals within species (such as early life stages) may reduce competition for food among the survivors, resulting in better growth rates, survival, or condition. Similarly, competitive release (increase in growth or abundance subsequent to removal of a competitor) may result from the loss of a sensitive species, with positive effects on the density, growth, or survival of competitor population(s) of other species (Baker et al. 1990b). In some cases where acidification continued, transient positive effects on size of surviving fish were shortly followed by extirpation (Bulger et al. 1993).

ANC criteria have been used for evaluation of potential acidification effects on fish communities. The utility of these criteria lies in the association between ANC and the surface water constituents that directly contribute to or ameliorate acidity-related stress, in particular pH, Ca^{2+}, and Al. Bulger et al. (2000) developed ANC thresholds for brook trout response to acidification in forested headwater catchments in western Virginia (Table VI-9). Note that because brook trout are comparatively acid tolerant, adverse effects on many other fish species should be expected at relatively higher ANC values.

Table VI-9. Streamwater acid neutralizing capacity (ANC) categories for brook trout response (Bulger et al. 2000).			
Response Category	ANC Class	ANC Range µeq/L	Brook Trout Response
Suitable	Not acidic	>50	Reproducing brook trout populations expected where habitat suitable
Indeterminate	Indeterminate	20-50	Extremely sensitive to acidification; brook trout response variable
Marginal	Episodically acidic	0-20	Sub-lethal and/or lethal effects on brook trout possible
Unsuitable	Chronically acidic	<0	Lethal effects on brook trout probable
Note: ANC range based on volume-weighted annual mean.			

The early life stages of brook trout are most sensitive to adverse impacts from acidification (Bulger et al. 2000). These early life stages occur in SHEN throughout the cold season in general, and the winter in particular (Figure VI-11). For this reason, data presented in Section VI.B.2 suggesting ongoing winter season acidification trends for streams within SHEN are of particular concern.

Adult brook trout in SHEN streams are more tolerant of acidity than are adult blacknose dace. For both species, the early life stages are more sensitive than the adults, and brook trout young are actually more sensitive than blacknose dace adults (Bulger et al. 1999). Blacknose dace spawn during summer and the eggs and very young fry are therefore somewhat insulated from the most acidic episodes, which typically occur during cold-season, high-flow conditions.

The recent three-year FISH study of stream acidification in SHEN demonstrated negative effects on fish from both chronic and episodic acidification (Bulger et al. 1999). Biological differences in low- versus high-ANC streams included species richness, population density, condition factor (a measure of robustness in individual fish), age, size, and field bioassay survival. Of particular note is that both episodic and chronic mortality occurred in young brook trout exposed in a low-ANC stream, but not in a high-ANC stream (MacAvoy and Bulger 1995), and that blacknose dace in low-ANC streams were in poor condition relative to blacknose dace in higher-ANC streams (Dennis et al 1995, Dennis and Bulger 1995).

A statistically-robust relationship between acid-base status of streamwater and fish species richness was shown in SHEN as well. As an element of the FISH project (Bulger et al. 1999),

numbers of fish species were compared among 13 SHEN streams spanning a range of pH/ANC conditions. There was a highly significant ($p<0.0001$) relationship between stream acid-base status (during the seven-year period of record) and fish species richness among the 13 streams, such that the streams having the lowest ANC hosted the fewest species (Figure VI-16). Although the number of streams in the study was small, the results were consistent with other studies (Baker et al. 1990a); this is the first, however, to provide a statistically-robust analysis among multiple streams in the southeastern United States.

In addition to acid-base status, stream size and drainage area are very important for fish diversity for a number of reasons. In this regard the FISH project streams appeared to be similar. The study streams in the FISH project were all first or second order streams within SHEN. They all may be regarded as high-gradient, well-oxygenated streams having large pebble/cobble substrates. All were shaded by riparian vegetation across their width during the study, although a later flood denuded the banks of one stream. Long riffles typically alternate with deeper pools; there are occasional small cascades. Width and depth vary with discharge, but all are wadeable at their widest point (typically at or near the park boundary) and upstream in summer.

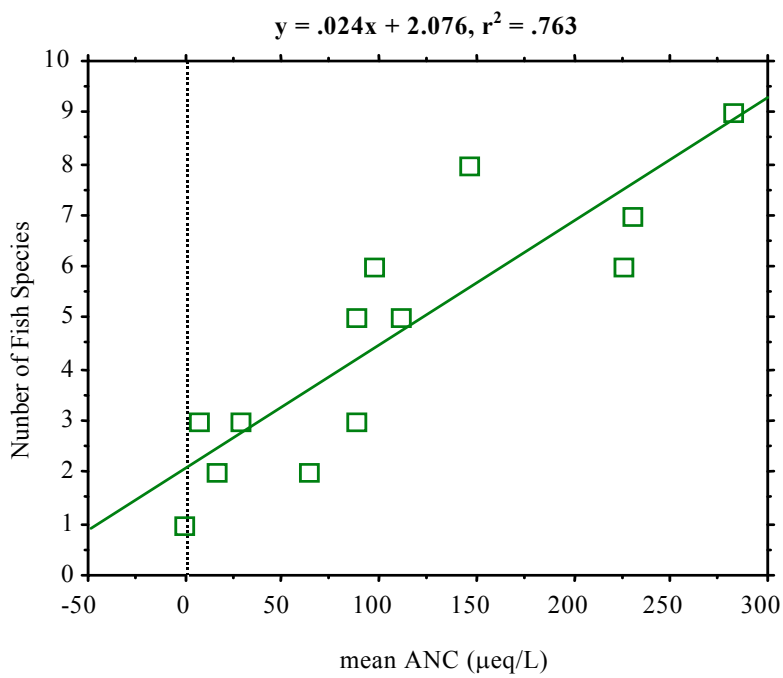

Figure VI-16. Number of fish species among 13 streams in SHEN. Values of ANC are means based on quarterly measurements, 1987-94. The regression analysis showed a highly significant relationship ($p \leq 0.0001$) between mean stream ANC and number of fish species. Streams having ANC consistently < 75 µeq/L had three or fewer species.

Median streamwater ANC values and watershed areas are shown in Table VI-10 for the 13 streams used by Bulger et al. (1999) to develop the relationship between ANC and fish species richness shown in Figure VI-16. Despite the overall similarities, these study streams vary in watershed area by a factor of 10. The streams that have larger watershed areas generally have more fish species than the streams having smaller watershed areas. All of the "rivers" have watersheds larger than 10 km^2 and ANC higher than 75 μeq/L. In contrast, the majority (but not all) of the "runs" have watershed area smaller than 10 km^2 and ANC less than 20 μeq/L. All of the streams that have watershed areas smaller than 10 km^2 have three or fewer known species of fish present. The ANC of the smaller streams is determined largely by the underlying geology. All of the streams having larger watersheds (> 10 km^2) have three or more known fish species; seven of nine have five or more species; and the average number of fish species is six. One of the streams in the larger-watershed category that had fewer than five species of fish (Paine Run, three species) had very low ANC. There is no clear distinction between river and run, but it is clear that as small streams in SHEN combine and flow into larger streams and eventually to

Table VI-10. Median streamwater ANC and watershed area of streams in SHEN that have water chemistry and fish species richness data.

Site ID	Watershed Area (km^2)	Median ANC (μeq/L)	Number of Fish Species
Smaller Watersheds (< 10 km^2)			
North Fork Dry Run	2.3	48.7	2
Deep Run	3.6	0.3	N.D.[a]
White Oak Run	4.9	16.2	3
Two Mile Run	5.4	10.0	2
Meadow Run	8.8	-3.1	1
Larger Watersheds (>10 km^2)			
Brokenback Run	10.1	74.4	3
Staunton River	10.6	76.8	5
Piney River	12.4	191.9	7
Paine Run	12.7	3.7	3
Hazel River	13.2	86.8	6
White Oak Canyon	14.0	119.3	7
N. Fork Thornton River	18.9	249.1	9
Jeremy's Run	22.0	158.5	6
Rose River	23.6	133.6	8

[a] No data were available regarding the number of fish species in Deep Run.

rivers, two things happen: acid-sensitivity *generally* declines, and habitat *generally* becomes suitable for additional fish species.

This does not imply that either acid-base status or fish species richness is controlled solely by either acidic deposition or watershed area. It appears that fish species richness is controlled by multiple factors, of which both acidification and watershed area can be important. Watershed area might be important in this context because smaller watersheds may contain smaller streams having less diversity of habitat, more pronounced impacts on fish from high flow periods, or lower food availability. Such issues interact with other stresses, including acidification, to determine overall habitat suitability.

As another component of the FISH project, condition factor was compared in populations of blacknose dace in SHEN in 11 streams spanning a range of pH/ANC conditions (Bulger et al. 1999). Figure VI-17 shows the highly significant relationship between mean stream pH and condition factor in blacknose dace. Note that the four populations represented on the left side of the figure all have mean pH values within or below the range of critical pH values, at which negative populations effects are likely for the species (Baker and Christensen 1991). That poor condition is related to population survival is suggested by the extirpation in 1997 of the blacknose dace population from the stream (Meadow Run) with the lowest pH and ANC (J. Atkinson, pers. comm.; Figure VI-17).

The results of the condition factor comparisons among the 11 streams indicated that the mean length-adjusted condition factor of fish from the stream with the lowest ANC was about 20% lower than that of the fish in best condition. No previous studies have reported changes in condition factor of blacknose dace during acidification. Comparisons with the work of Schofield and Driscoll (1987) and Kretser et al. (1989) suggest that pH in the low-pH SHEN streams is near or below the limit of occurrence for blacknose dace populations in the Adirondack region of New York.

As with reduced growth rates observed for acid-stressed populations of invertebrates, smaller blacknose dace body size could result from direct toxicity (e.g., elevated energy use to compensate for sublethal ionoregulatory stress) or from reduced access to food or lower food quality (Baker et al. 1990a). Primary productivity is low in headwater streams and lower still in softwater headwaters, which are more likely to be acidified. Production of invertebrates is likely to be low in such streams as well, even though terrestrial inputs of food are much more

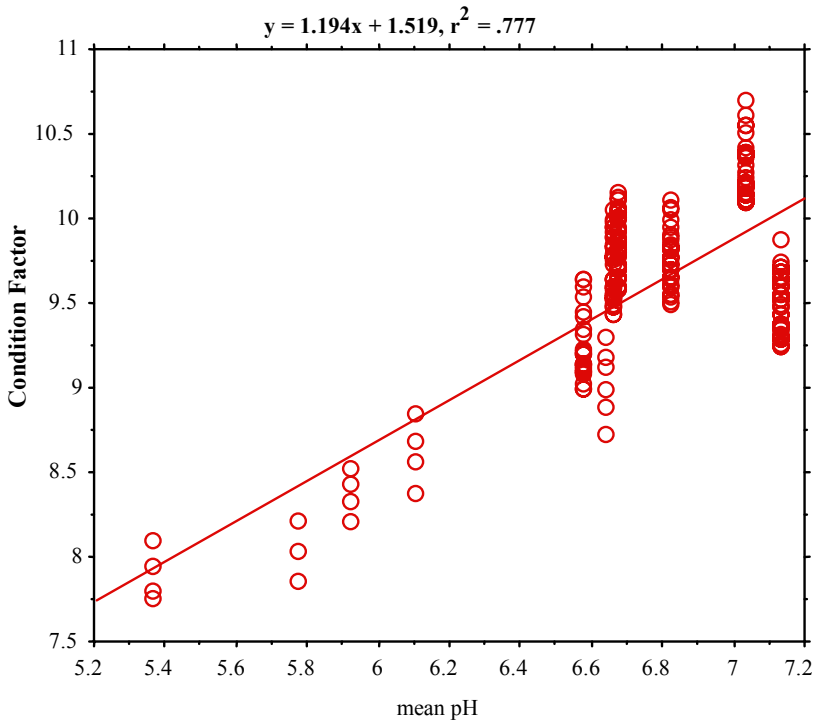

Figure VI-17. Length-adjusted condition factor (K), a measure of body size in blacknose dace (*Rhinichthys atratulus*) among 11 populations (n=442) in SHEN. Values of pH are means based on quarterly measurements, 1991-94; K was measured in 1994. The regression analysis showed a highly significant relationship ($p \leq 0.0001$) between mean stream pH and body size, such that fish from acidified streams were smaller than fish from circumneutral streams.

important for insect productivity in forested catchments than in-stream production (Wallace et al. 1992). Thus, lower food availability cannot be ruled out as a potential contributor to lowered condition in SHEN blacknose dace populations. Nevertheless, reduced growth rates have been attributed to acid stress in a number of other fish species, including Atlantic salmon, chinook salmon, lake trout, rainbow trout, brook trout, brown trout, and Arctic char. Furthermore, the blacknose dace population in poorest condition in SHEN occurred in a stream with mean pH below the minimum recorded for blacknose dace populations in Vermont, New Hampshire, Maine and New York (Baker et al. 1990a). The four blacknose dace populations in poorest condition in SHEN occurred in streams at or below the critical pH for the species, where adverse effects due to acidification are likely to be detectable at the population level (Baker et al 1990a). Consequently, acid stress is probably at least partly responsible for the lower condition of

blacknose dace populations in SHEN, though lower food availability, either resulting from the nature of softwater streams or exacerbated by acidification, cannot be ruled out.

It is possible that smaller body size in blacknose dace (and the lake trout cited above) is the result of energy transfer from somatic growth to physiological maintenance, secondary to chronic sublethal acidification stress. It is well known that chronic sublethal stress reduces growth in fish, as well as reproductive success (Wedemeyer et al. 1990). Chronic sublethal stress caused by pH levels up to 6.0 may have serious effects on wild trout populations. There is an energy cost in maintaining physiological homeostasis; the calories used to respond to stress are a part of the fish's total energy budget and are unavailable for other functions, such as growth (Schreck 1981, 1982).

The energy costs to fish for active iono-osmoregulation can be substantial (Farmer and Beamish 1969, Bulger 1986). The concentrations of serum electrolytes (such as sodium [Na^+] and chloride [Cl^-]) are many times higher (often 100-fold higher) in fish blood than in the freshwaters in which they live. The active uptake of these ions occurs at the gills. Because of the steep gradient in Na^+ and Cl^- concentrations between the blood and freshwater, there is constant diffusional loss of these ions, which must be replaced by energy-requiring active transport. Low pH increases the rate of passive loss of blood electrolytes (especially Na^+ and Cl^-); and Al elevates losses of Na^+ and Cl^- above the levels due to acid stress alone (Wood 1989). Since dace in an acidified stream maintain whole-body Na^+ at levels similar to dace in a high-ANC stream (Dennis and Bulger 1995), despite probable higher gill losses of electrolytes due to acid/Al stress, then the homeostatic mechanisms at the gill responsible for maintaining blood electrolyte levels must work harder and use more energy to maintain these levels.

An additional component of the FISH project used multiple bioassays over three years in one of the low-ANC streams to determine the effect of stream baseflow and acid episode stream chemistry on the survival of brook trout eggs and fry (MacAvoy and Bulger 1995). Simultaneous bioassays took place in mid- and higher-ANC reference streams. Acid episodes (with associated low pH and elevated Al concentrations, and high streamwater discharge) induced rapid mortality in the low-ANC stream, while the test fish in the higher-ANC stream, experiencing only the high streamwater discharge, survived (Bulger et al. 1999).

The effects of acidification on fish have been well documented for the St. Mary's River (Bugas et al. 1999). Fourteen fish species have been collected in St. Mary's River since 1976;

only four remained as of 1998. Rosyside dace (*Clinostomus funduloides*) and torrent sucker (*Thoburnia rhothocea*) were last present in 1996; Johnny darter (*Etheostoma nigrum*) and brown trout were last present in 1994; rainbow trout and longnose dace (*Rhinichthys cataractae*) were last present in 1992; bluehead chub (*Nocomis leptocephalus*) and smallmouth bass (*Micropterus dolomieui*) were last present in 1990 and 1988, respectively; white sucker (*Catastomus commersoni*) and central stoneroller (*Campostoma anomalum*) were last present in 1986. Of the four remaining species, three (blacknose dace, fantail darter [Etheostoma flabellare]), and mottled sculpin [*Cottus bairdi*]) have declined in density and/or biomass; the fourth remaining species is brook trout, the region's most acid tolerant species; this population has fluctuated, and reproductive success has been sporadic. Blacknose dace, once abundant throughout the river, remain only at the lowest sampling station, which has the highest pH, and at such low numbers (five individuals in 1998) that they might be strays from downstream. For some of the species (smallmouth bass, white sucker, the three trout, and blacknose dace) the critical pH is known (see Table VI-8), and their decline and/or extirpation, given the pH of the river, is not surprising. Based on trend analysis over the period 1987-1997, the St. Mary's River, near SHEN, is continuing to acidify (Webb and Deviney 1999).

Recent analyses (Bulger et al. 1998, 2000) divided Virginia's streams into four categories of acid-base status, to compare the number of streams in each category at present with estimated numbers in pre-industrial times and in the future. Within SHEN, streams that are chronically or episodically acidic are the most likely to have experienced adverse biological effects from acidic deposition to date. They are also the streams most at risk for future damage. These streams are found primarily on siliciclastic bedrock. See listing of known acidic and low-ANC streams within the park in Appendix D.

4. Episodic Acidification Effects

Values of annual average or spring season average water chemistry are typically used to represent conditions at a given site for purposes of characterization. However, streamwater chemistry undergoes substantial temporal variability, especially in association with hydrological episodes. During such episodes, which are driven by rainstorms and/or snowmelt events, both discharge (streamflow volume per unit time) and water chemistry change, sometimes dramatically. This is important because streams may in some cases exhibit chronic chemistry

that is suitable for aquatic biota, but experience occasional episodic acidification with lethal consequences (c.f., Wigington et al. 1993).

Data regarding episodic variability in streamwater ANC for six intensively-studied sites within SHEN for the period 1993 to 1999 are presented in Figure VI-18. The minimum measured ANC each year at each site (which generally is recorded during a large hydrological episode) is plotted against the median spring ANC for that year at that site. Sites that exhibited median spring ANC below about 20 μeq/L (Paine Run, White Oak Run, Deep Run) generally had minimum measured ANC about 10 μeq/L lower than median spring ANC. In contrast, at the high-ANC Piney River site (median spring ANC > 150 μeq/L), the minimum measured ANC was generally more than about 40 μeq/L lower than the respective median spring ANC. At sites

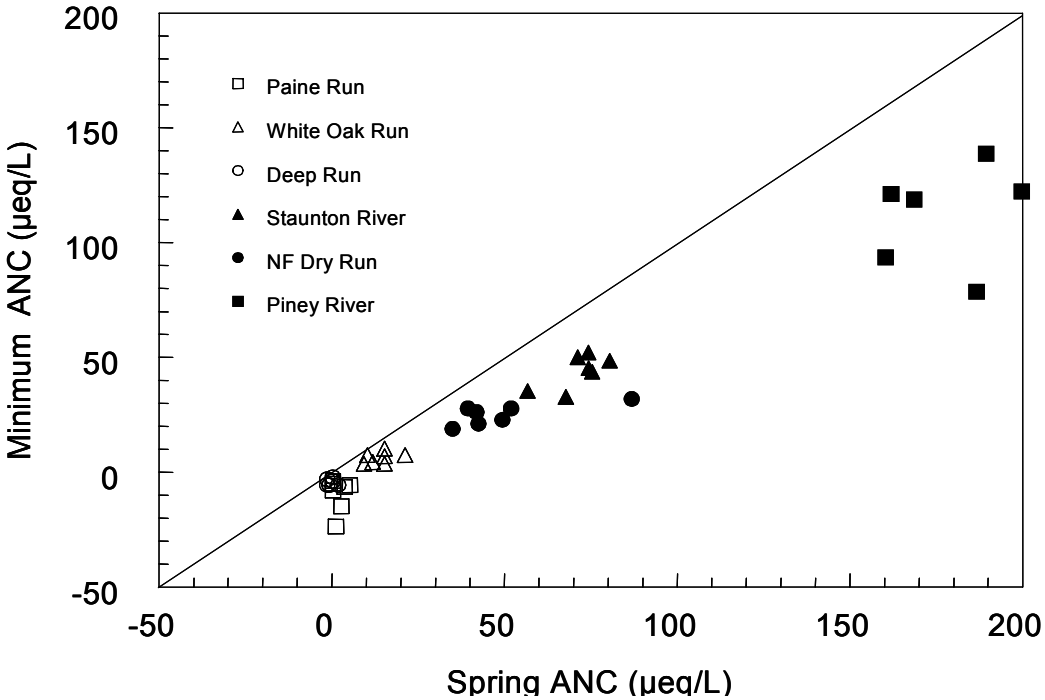

Figure VI-18. Minimum streamwater ANC sampled at each site during each year versus median spring ANC for all samples collected at that site during that spring season. Data are provided for all intensively-studied streams within SHEN during the period 1993-1999. A 1:1 line is provided for reference. The vertical distance from each sample point upwards to the 1:1 line indicates the ANC difference between the median spring value and the lowest sample value for each site and year.

having intermediate ANC values, with median spring ANC in the range of about 30 to 90 μeq/L, the minimum ANC measured each year was generally about 20 to 30 μeq/L lower than the respective median spring ANC. Thus, there is a rather clear pattern of larger episodic ANC depressions in streams having higher median ANC and smaller episodic ANC depressions in streams having lower median ANC. The two sites that had median spring ANC between about 0 and 10 μeq/L consistently showed minimum measured values below 0. Streams having low chronic ANC can be expected to experience relatively small episodic ANC depressions. However, those depressions often result in minimum ANC values that are associated with toxicity to aquatic biota.

The routing of water as it flows through a watershed determines the degree of contact with acidifying or neutralizing materials and therefore influences (along with soils and bedrock characteristics) the amount of episodic acidification that occurs. In any given watershed, surface water ANC may vary in time depending upon the proportion of the flow that has contact with deep versus shallow soil horizons; the more subsurface contact, the higher the surface water ANC (Turner et al. 1990). This can be attributed in part to higher base saturation and greater SO_4^{2-} adsorption capacity in subsurface soils. It may also be related to the accumulation in the upper soil horizons of acidic material derived from atmospheric deposition and decay processes (Lynch and Corbett 1989, Turner et al. 1990). Storm flow and snowmelt are often associated with episodes of extreme surface water acidity due to an increase in the proportion of flow derived from water that has moved laterally through the surface soil without infiltration to deeper soil horizons (Wigington et al. 1990). Episodic acidification may be the limiting condition for aquatic organisms in central Appalachian streams that are marginally suitable for aquatic life under baseflow conditions.

A number of studies of episodic acidification have been conducted in streams within SHEN. Miller-Marshall (1993) analyzed data from the SWAS for the period 1988-1991 for White Oak Run, North Fork Dry Run, Deep Run, and Madison Run, and also conducted a field experiment in 1992 at White Oak Run and North Fork Dry Run. Acid anion flushing was the predominant acidification mechanism during hydrological episodes. Base cation dilution frequently also played a large role, depending on the underlying bedrock geology and baseflow ANC. The ratio of ΔSBC/ΔANC varied from 0.5 at Madison Run (median spring baseflow ANC = 63 μeq/L) to -1.4 at Deep Run (median spring baseflow ANC = 1 μeq/L). Ratios were intermediate (0.2 and

0.3, respectively) at North Fork Dry Run (median spring baseflow ANC = 40 μeq/L) and White Oak Run (median spring baseflow ANC = 16 μeq/L). Thus, at the site exhibiting the lowest baseflow ANC (Deep Run), base cations increased during episodes. At the other sites, base cation concentrations were diluted during episodes, with the greatest dilution occurring in the streams that were highest in baseflow ANC (Miller-Marshall 1993).

There are several different mechanisms of episodic acidification in operation in the streams in SHEN, depending at least in part on the bedrock geology of the stream. Eshleman and Hyer (2000) estimated the contribution of each major ion to observed episodic ANC depressions in Paine Run, Staunton River, and Piney River during a three-year period. During the study, 33 discrete storm events were sampled and water chemistry values were compared between antecedent baseflow and the point of minimum measured ANC (near peak discharge). The relative contribution of each ion to the ANC depressions was estimated using the method of Molot et al. (1989), which normalized the change in ion concentration by the overall change in ANC during the episode. At the low-ANC (≈ 0) Paine Run site on siliciclastic bedrock, increases in NO_3^- and SO_4^{2-}, and to a lesser extent organic acid anions, were the primary causes of episodic acidification. Base cations tended to compensate for most of the increases in acid anion concentration. ANC declined by 3 to 21 μeq/L (median 7 μeq/L) during the episodes studied. At the intermediate-ANC (≈ 60 to 120 μeq/L) Staunton River site on granitic bedrock, increases in SO_4^{2-} and organic acid anions, and to a lesser extent NO_3^-, were the primary causes of episodic acidification. Base cation increases compensated these changes to a large degree, and ANC declined by 2 to 68 μeq/L during the episodes (median decrease in ANC was 21 μeq/L). At the high-ANC (≈150 to 200 μeq/L) Piney River site on basaltic (69%) and granitic (31%) bedrock, base cation concentrations declined during episodes (in contrast with the other two sites where base cation concentrations increased). Sulfate and NO_3^- usually increased. The change in ANC during the episodes studied ranged from 9 to 163 μeq/L (median 57 μeq/L; Eshleman and Hyer 2000). Changes in base cation concentrations during episodes contributed to the ANC of Paine Run, had little impact in Staunton River, and consumed ANC in Piney River (Hyer 1997).

The relative importance of the major processes that contribute to episodic acidification varies among the streams within SHEN, in part as a function of bedrock geology and baseflow streamwater ANC. Sulfur-driven acidification was an important contributor to episodic loss of

ANC at all three sites, probably because S adsorption by soils occurs to a lesser extent during high-flow periods. This is due, at least in part, to diminished contact between drainage water and potentially adsorbing soils surfaces. Dilution of base cation concentrations was most important at the high-ANC site.

Similar conclusions were reached by Miller-Marshall (1993). Acid anion flushing was the predominant acidification mechanism during episodic acidification. Base cation dilution also played a large role for most of the watersheds, but the extent of its importance depended largely on the underlying bedrock.

The importance of NO_3^- to episodic acidification is a relatively recent development, attributed to the effects of gypsy moth infestation in many watersheds within the park (Webb et al. 1995, Eshleman et al. 1999). Consumption of foliage by the moth larvae converted foliar N, which is normally tied up in long-term N cycling processes, into more labile N forms on the forest floor.

Eshleman et al. (1999) concluded that episodic acidification of streams in SHEN is controlled by a complex set of natural, anthropogenic, and disturbance factors that together produce a transient response that varies dramatically from watershed to watershed. They further hypothesized that the results of recent studies in the park can be largely explained by a biogeochemical response to forest disturbance by gypsy moth larvae, which temporarily overwhelmed the normal controls on N and base cation dynamics.

The most acidic conditions in SHEN streams occur during high-flow periods, in conjunction with storm or snowmelt runoff. The general relationship between flow level and ANC is evident in Figure VI-19, which plots ANC measurements against flow for three intensively-studied streams representing the major bedrock types in the park. The response of all three streams is similar in that most of the lower ANC values occur in the upper range of flows levels. However, consistent with observations by Eshleman (1988), the minimum ANC values that occur in response to high flow are related to baseflow ANC values. Paine Run (siliciclastic bedrock) had a mean weekly ANC value of about 6 μeq/L and often had high-flow ANC values that were less than 0 μeq/L. Staunton River (granitic bedrock) had a mean weekly ANC value of about 82 μeq/L and had only a few high-flow ANC values less than 50 μeq/L. Piney River (basaltic bedrock) had a mean weekly ANC value of 217 μeq/L and no values as low as 50 μeq/L.

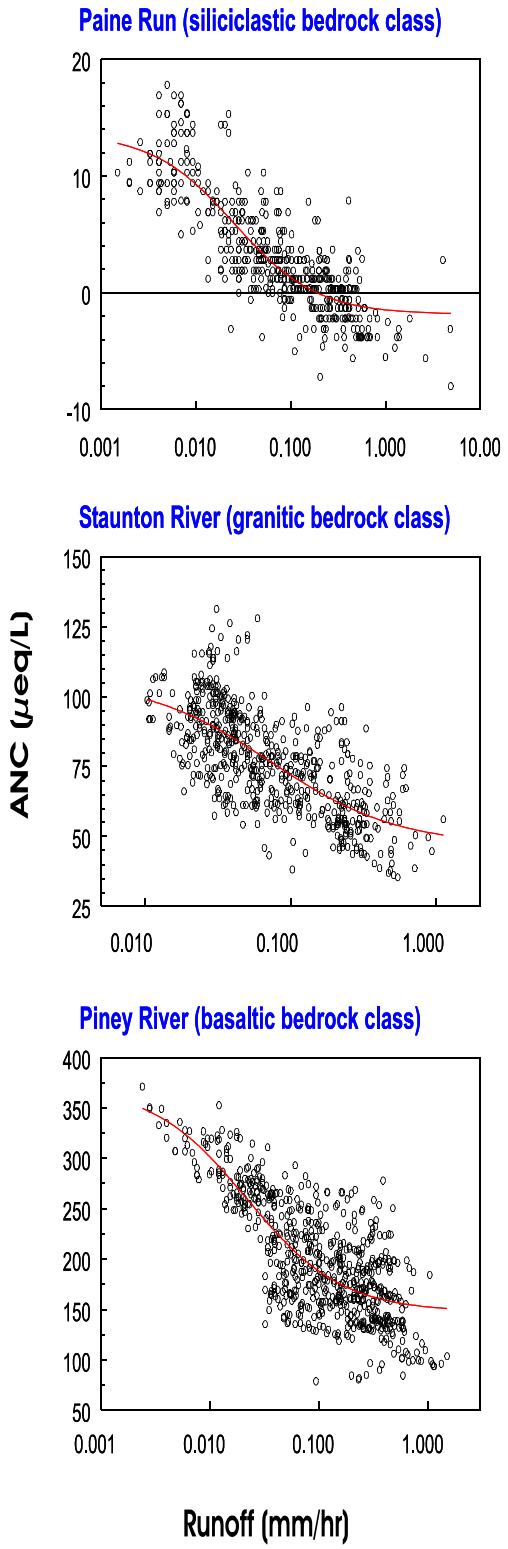

Figure VI-19. Relationship between ANC and runoff for streamwater samples collected at intensively-studied sites in SHEN. The data represent samples collected during the 1992-1997 period.

Previous studies have shown that mobilization of dissolved Al during episodic acidification is a primary cause of fish mortality in streams that have low ANC under baseflow conditions (Wigington et al. 1993). Streams with higher ANC during baseflow are less likely to become sufficiently acidic during episodes to bring much Al into solution. Figure VI-20 provides an example of changes in ANC, pH, and dissolved Al that occurred in Paine Run, Staunton River, and Piney River during a high-flow episode in January 1995. Under baseflow conditions, ANC at the Paine Run site was above 0 μeq/L, pH was above 5.5, and Al concentration was less than 25 μg/L. Discharge levels increased dramatically during the episode, resulting in depression of ANC to less than 0 μeq/L, pH values less than 5.5, and an increase in Al concentration to near 75 μg/L, above the threshold for adverse effects on some species of aquatic biota. That same episode also resulted in substantial declines in ANC in the granitic (Staunton River) and basaltic (Piney River) watersheds. However, ANC values at these two sites were relatively high prior to the episode (about 75 and 175 μeq/L, respectively) and did not decline to below about 50 μeq/L during the episode at either site, and pH values remained above 6.0 and 6.5, respectively (Figure VI-20).

It is notable, however, that Al concentrations at the Staunton River site increased from less than 10 μg/L to about 25 μg/L during the episode. This is somewhat surprising given that Al has very low solubility at pH values above 6.0. Similarly elevated Al concentrations at relatively high pH values have been observed during other high-runoff events in Staunton River (e.g., Bulger et al.1999). This may simply indicate that the sampling frequency has been insufficient to capture the pH extremes that occur during the high-runoff episodes. Another explanation is that Al may be mobilized in more acidic parts of the watershed and then remain in solution at the sampling location despite the higher pH. If so, the range of Al concentrations in streamwater within the watershed probably include higher values than are observed at the sampling site. This latter explanation is supported by the observation that lower streamwater ANC and pH values generally occur at upstream locations within the primary study watersheds (see Tables VI-1 and VI-3). For Staunton River, in particular, the observed within-watershed variation in streamwater ANC during the 1992 survey (see Figure VI-2) was substantial; although ANC was 67 μeq/L at the downstream sampling site, ANC was below 50 μeq/L at 41% of the upstream sampling sites.

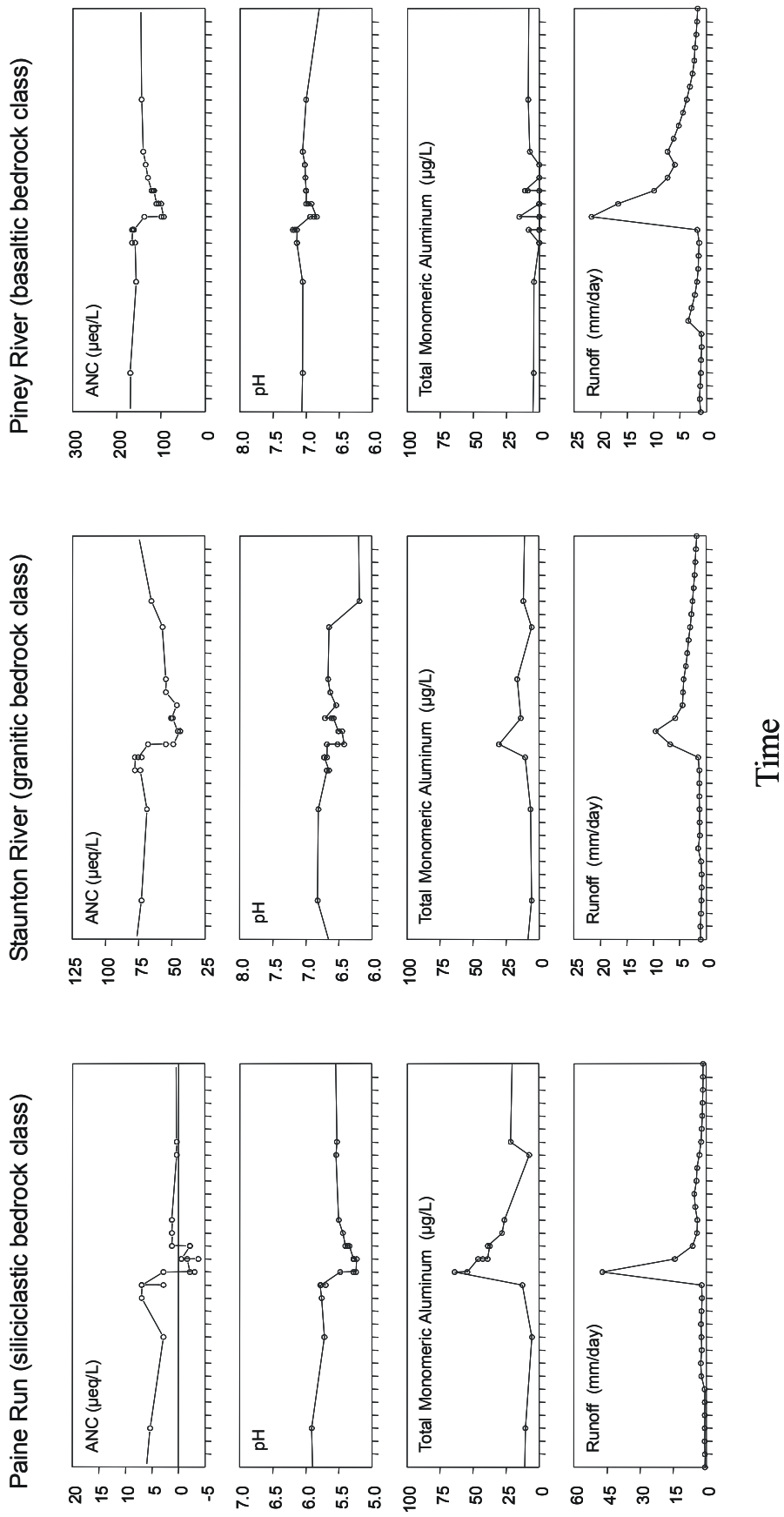

Figure VI-20. Decrease in ANC and pH and increase in dissolved aluminum in response to a sharp increase in streamflow in three watersheds within SHEN during a hydrological episode in 1995. The watersheds were selected to be representative of the three geologic sensitivity classes within the park. Data are shown for the month of January, 1995.

This spatial pattern in streamwater ANC variability within the SWAS watersheds is similar for streams on all three major bedrock types. The implications may be greatest, however, for streams on granitic bedrock. Although these streams usually have ANC and pH values above the range of values commonly associated with harm to fish and other aquatic life, adverse effects may occur periodically due to episodic mobilization of Al from the more acidic portions of the watersheds.

In general, pre-episode ANC is a good predictor of minimum episodic ANC and also a reasonable predictor of episodic ΔANC. Higher values of pre-episode ANC lead to larger ΔANC values, but minimum ANC values of such streams are generally not especially low. Lowest minimum ANC values are reached in streams that have low pre-episode ANC, but the ΔANC values for such streams are generally small.

Webb et al. (1994) developed an approach to calibration of an episodic acidification model for VTSSS long-term monitoring streams in western Virginia that was based on the regression method described by Eshleman (1988). Median, spring quarter ANC concentrations for the period 1988 to 1993 were used to represent chronic ANC, from which episodic ANC was predicted. Regression results were very similar for the four lowest ANC watershed classes, and they were therefore combined to yield a single regression model to predict the minimum measured ANC from the chronic ANC. Extreme ANC values were about 20% lower than chronic values, based on the regression equation:

$$ANC_{min} = 0.79\ ANC_{chronic} - 5.88 \quad (r^2=0.97;\ \text{se of slope}=0.02,\ p \leq 0.001)$$

Because the model was based on estimation of the minimum ANC measured in the quarterly sampling program, it is likely that the true minimum ANC values were actually somewhat lower than 20% below the measured chronic ANC. Nevertheless, regression approaches for estimation of the minimum episodic ANC of surface waters, such as was employed by Webb et al. (1994) for western Virginia, provide a basis for predicting future episodic acidification. It must be recognized, however, that future episodic behavior might vary from current behavior if chronic conditions change dramatically.

Results from the U.S. EPA's Episodic Response Project demonstrated that episodic acidification can have long-term adverse effects on fish populations. Streams with suitable

chemistry during low-flow, but low pH and high Al levels during high flow, had substantially lower numbers and biomass of brook trout than were found in non-acidic streams (Wigington et al. 1996). Streams having acidic episodes showed significant mortality of fish. Some brook trout avoided exposure to stressful chemical conditions during episodes by moving downstream or into areas with higher pH and lower Al. This movement of brook trout only partially mitigated the adverse effects of episodic acidification, however, and was not sufficient to sustain fish biomass or species composition at levels that would be expected in the absence of acidic episodes. These findings suggested that stream assessments based solely on chemical measurements during low-flow conditions will not accurately predict the status of fish populations and communities in small mountain streams unless some adjustment is made for episodic processes (Baker et al. 1990b, Baker et al. 1996, Wigington et al. 1996, Sullivan 2000).

Thus, episodic acidification of streams in SHEN can be attributed to a number of causes, including dilution of base cations and increased concentrations of sulfuric, nitric, and organic acids (Eshleman et al. 1995, Hyer et al. 1995). For streams having low pre-episodic ANC, episodic decreases in pH and ANC and increases in toxic Al concentrations can have adverse impacts on fish populations. Not all of the causes of episodic acidification are related to acidic deposition. Base-cation dilution and increase in organic acid anions during high-flow conditions are natural processes. The contribution of nitric acid, indicated by increased NO_3^- concentrations, has evidently been (at least for streams in the park) related to forest defoliation by the gypsy moth (Webb et al. 1995, Eshleman et al. 1998). However, significant contributions of sulfuric acid, indicated by increased SO_4^{2-} concentrations during episodes in some streams, is an effect of atmospheric deposition and the dynamics of S adsorption on soils (Eshleman and Hyer 2000).

C. VEGETATION

1. Effects of Ground-level Ozone and Other Gaseous Pollutants

Ozone (O_3) is a photochemical oxidant that occurs naturally in the earth's troposphere. Concentrations of O_3 generally increase during the day in a pattern that parallels photosynthetic activity of plants, although this may not be true at high elevation or under conditions of long-range transport. Ozone enters the leaf through stomata during the normal uptake of carbon dioxide and loss of water. Inside the leaf, O_3 catalyzes the formation of free radicals which oxidize membranes and damage the photosynthetic apparatus. Although repair of injured tissues

takes place, plants are generally unable to completely reverse the effects of exposure to high concentrations of O_3, and visible injury and/or growth losses frequently occur.

In 1996, after a review of the scientific literature (U.S. EPA 1996a), the staff of the EPA Office of Air Quality Planning and Standards concluded that the existing secondary National Ambient Air Quality Standards (NAAQS) for O_3 did not provide adequate protection for vegetation (U.S. EPA 1996b). They recommended that if the EPA Administrator found that additional protection provided by the proposed change to the primary NAAQS was not sufficient to protect vegetation, that a secondary standard of 25 to 38 ppm·hr (parts per million per hour) 3-month, 12-hour SUM06 be considered[1]. They stated that the lower end of the range would "provide increased protection against effects to vegetation and ecosystem resources in Class I and other areas" (U.S. EPA 1996b). In 1997-1999, the 3-month, 12-hour SUM06 at Big Meadows in SHEN was 28, 52, and 43 ppm·hr respectively, in all cases above the most protective level recommended, and in two of three years, greater than the upper limit recommended by EPA staff. After consideration, the EPA Administrator determined that additional protection, above and beyond that provided by a new, more stringent primary standard to protect human health, was not needed.

a. Visible Injury Caused by Ground-level Ozone

Ozone injury is commonly observed on sensitive vegetation in the eastern United States and in southern California. It takes on a special significance in national parks where it is an obvious sign of adverse impact due to air pollution. However, visible injury has rarely been related to quantitative changes in growth or function of a plant, so questions regarding the importance of visible injury to the health and vitality of the forest remain unanswered.

Some plants, such as milkweed (*Asclepias* spp.), black cherry (*Prunus serotina* Ehrh.), and yellow poplar (*Liriodendron tulipifera* L.), are sensitive to O_3 and may be injured at exposure to less than 15 ppm·hr, 3-month SUM06. The injury generally is manifested as a purple to brown stipple on the upper surface of the leaf (Figure VI-21). Under severe conditions, the injury may become necrotic and cause flecking on the leaf. The current NAAQS for O_3 will not protect all

[1] To calculate this metric, all ozone concentrations $\geq$0.06 parts per million (ppm) that occur during 0800-2000 local time in the months of June, July, and August are summed. The 5 month SUM06 used later in this report is calculated in the same manner, but over the growing season months May through September.

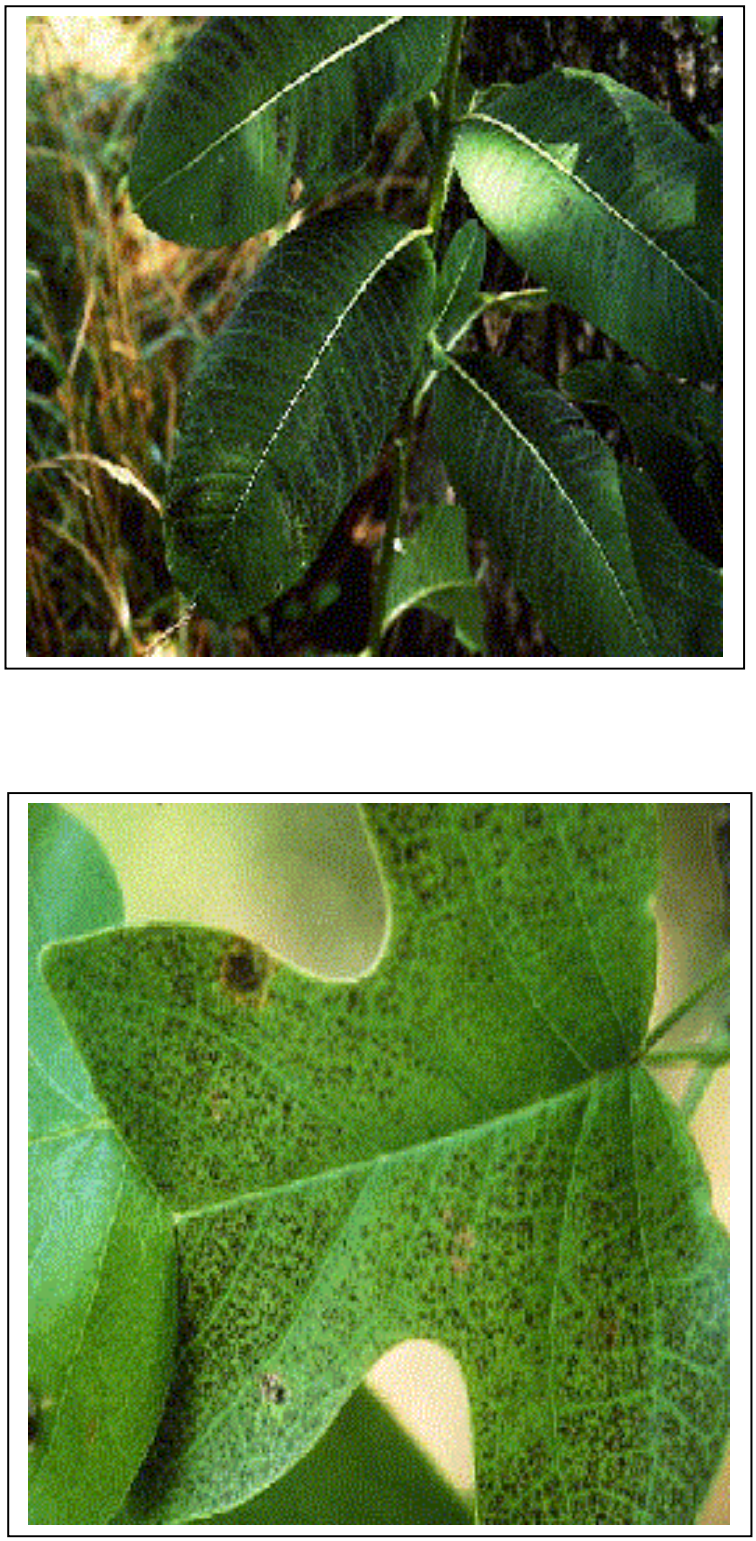

Figure VI-21. Visible injury (purple stippling) caused by ozone on milkweed (top) and yellow poplar (bottom) at SHEN.

sensitive plants from visible injury caused by O_3. Sensitive plants in SHEN are likely to continue to show injury well into the future.

In general, visible injury is directly related to the level of O_3 exposure (Skelly et al. 2001). If exposures decrease under future air pollution control scenarios, there should be some amelioration of current levels of visible injury. However, if O_3 concentrations increase in the lower atmosphere, one would expect not only an increase in the severity of injury to sensitive species but also an increase in the number of species injured. In addition, based on the modeling results reported in Section VII, increased effects on growth might also be expected for some species.

b. Effects of Sulfur and Nitrogen Oxides

Some species of plants that occur at SHEN, including raspberry, ragweed, aster, and birch, are reported to be sensitive to SO_2 (National Academy of Sciences [NAS] 1978), but it is unlikely that phytotoxic concentrations of the pollutant exist in the park. Similarly, it is unlikely that phytotoxic concentrations of gaseous N occur in SHEN.

Direct vegetation effects of oxides of N in a gaseous form are rare because the toxicities of these compounds are less than those of other pollutants. By far the most important effects of these compounds in SHEN are as precursors to O_3 and other photochemical oxidants (c.f., NAS 1977), as fertilizers, and as components of acidic deposition.

2. Sensitivity of Plant Species in SHEN

There are a number of plant species that occur within SHEN that are known to be sensitive to O_3 effects on foliage at O_3 concentrations found within the park (Table VI-11). However, not much is known about the effects of O_3 on the growth of trees in SHEN, primarily because it is difficult to work with large trees and the response of seedlings may not be indicative of the response of mature trees (see the discussion below of effects on seedlings). Generally, sugar maple is considered insensitive (Laurence et al. 1996) whereas yellow poplar, red maple (*Acer rubrum*), and red oak (*Quercus rubra* L.) might be considered intermediate (U.S. EPA 1996b). Black cherry is considered to be sensitive in terms of visible injury, but may be less so when evaluating growth responses (Weinstein et al. 2001). Little experimental data is available

Table VI-11. List of plant species in SHEN known to be sensitive to visible injury on foliage from ozone exposure levels found within the park.[a] This list is for general guidance only and does not provide an indication of relative sensitivity to ozone effects on plant growth and vigor.

Scientific Name	Common Name
SPECIES VERY SENSITIVE TO OZONE EXPOSURE PRESENT AT THIS SITE	
Ailanthus altissima (P. Mill.) Swingle	tree of heaven
Apocynum androsaemifolium L.	spreading dogbane
Asclepias exaltata L.	poke milkweed
Asclepias quadrifolia Jacq.	fourleaf milkweed
Asclepias syriaca L.	common milkweed
Aster acuminatus Michx.	Oclemena acuminata
Aster macrophyllus L.	bigleaf aster
Aster puniceus L.	purplestem aster
Aster umbellatus P. Mill.	Doellingeria umbellata
Fraxinus americana L.	white ash
Fraxinus pennsylvanica Marsh.	green ash
Liquidambar styraciflua L.	sweetgum
Liriodendron tulipifera L.	tuliptree
Parthenocissus quinquefolia (L.) Planch.	Virginia creeper
Pinus pungens Lamb.	table mountain pine
Platanus occidentalis L.	American sycamore
Populus tremuloides Michx.	quaking aspen
Prunus pensylvanica L. f.	pin cherry
Prunus serotina Ehrh.	black cherry
Rhus copallina L.	dwarf sumac
Rubus allegheniensis Porter	Allegheny blackberry
Rudbeckia hirta L.	blackeyed Susan
Rudbeckia laciniata L.	cutleaf coneflower
Sambucus canadensis L.	Sambucus nigra ssp. canadensis
Sassafras albidum (Nutt.) Nees	sassafras
Vitis labrusca L.	fox grape
SPECIES SLIGHTLY SENSITIVE TO OZONE EXPOSURE PRESENT AT THIS SITE	
Acer negundo L.	boxelder
Acer rubrum L.	red maple
Betula alleghaniensis Britt.	yellow birch
Betula populifolia Marsh.	gray birch
Bromus tectorum L.	cheatgrass
Cercis canadensis L.	eastern redbud
Cornus florida L.	flowering dogwood
Pinus virginiana P. Mill.	Virginia pine
Rhus glabra L.	smooth sumac
Rhus typhina L.	Rhus hirta
Robinia pseudoacacia L.	black locust
Symphoricarpos albus (L.) Blake	common snowberry
Tilia americana L.	American basswood
Verbesina occidentalis (L.) Walt.	yellow crownbeard

[a] This information was provided by Bruce Nash, NPS Natural Resources Information Division, 1999

regarding the response of white ash (*Fraxinus americana*; reported sensitive based on visible injury in the 1960s), chestnut oak (*Quercus prinus* L.), or basswood (*Tilia americana* L.).

In a recent report, Skelly et al. (2001) estimated the extent of visible foliar injury on black cherry, red maple, yellow poplar, and white ash growing in open-top chambers with ambient air in Pennsylvania. In general, they found black cherry to be most sensitive, with injury also occurring on yellow poplar and red maple. White ash was not injured. They were not able to detect O_3-induced changes in radial growth of the trees.

Field plots and open-top chambers were established in Big Meadows in SHEN in 1979 to investigate the effects of O_3 on tree seedlings. Studies conducted from 1979 to 1981 suggested that ambient levels of O_3 caused foliar injury on seedlings of yellow poplar, green ash (*Fraxinus pennsylvanica*), and sweetgum (*Liquidambar styraciflua*), as well as reduced average height growth of yellow poplar, green ash, black locust (*Robinia pseudoacacia*), Virginia pine (*Pinus virginiana*), Eastern white pine (*Pinus strobus*), table mountain pine, (*Pinus pungens*), and Eastern hemlock (*Tsuga canadensis*; Duchelle et al. 1982). It must be recognized, however, that open-top chambers might result in better height growth due to reduced wind stress, so the results of such experiments may not necessarily reflect O_3 exposure effects. A concurrent study found that ambient O_3 concentrations reduced above-ground biomass production of native vegetation compared to charcoal-filtered air (Duchelle et al. 1983).

Foliar injury surveys were conducted on five native plant species in SHEN in 1982. Three of the five species (virgin's bower [*Clematis virginiana*], black locust, and wild grape [*Vitis* sp.]) displayed increased injury with increased elevation (Winner et al. 1989).

In 1991, trend plots of the O_3-sensitive hardwoods yellow poplar, black cherry, and white ash were established near the ambient O_3 monitors at Dickey Ridge, Big Meadows, and Sawmill Run in the park. Marked trees in each plot were evaluated for foliar O_3 injury in 1991, 1992, and 1993 (Hildebrand et al. 1996). Black cherry and white ash exhibited increased foliar injury with increased O_3 exposure across all three sites and at each site across all years of study. Whereas the amount of foliar injury on yellow poplar at Dickey Ridge corresponded well with O_3 exposure, there was no correlation for this species at the Big Meadows or Sawmill Run sites. The authors speculated the lack of correlation for yellow poplar at Big Meadows and Sawmill Run may have been due to extremes in moisture availability at the two sites. Hildebrand et al. (1996) concluded that cumulative O_3 statistics, such as SUM06 and W126 (the sum of hourly

average O_3 concentrations using a sigmoidal weighting function), best represented foliar injury observations, particularly for black cherry, during the period of study.

Thus, O_3-induced foliar injury has been observed on a number of species in SHEN since the early 1980s. The amount of foliar injury on black cherry, in particular, correlated well with cumulative O_3 exposures. Subsequent data showed that O_3 concentrations generally increased in the park throughout the 1990s, which suggests that O_3 injury continued.

3. Acidification Effects

Deposition of both S and N are of concern with respect to potential acidification effects on forest vegetation throughout the Appalachian Mountains, including within SHEN. However, the forest resource in this region at greatest risk is the spruce-fir ecosystem that is found at high elevation, and that has limited occurrence within SHEN. This resource is of greatest concern because it:

1) contains a tree species (red spruce [*Picea rubens*]) that is highly sensitive to damage by acidification,

2) exhibits soil properties that render it particularly sensitive to soil acidification, including low pH and base saturation, and shallow rooting zone, and

3) receives very high levels of cloud deposition, and therefore total deposition, of S and N at some locations.

Potentially sensitive spruce-fir forest resources are found at high elevation (generally above about 1,370 m) in the southern Appalachian Mountains, including some areas of West Virginia and Virginia. There are small (~18 ha) relic populations of red spruce in SHEN at Limberlost and Hawksbill Peak (NPS 1981). These populations are likely under considerable natural stress and may be more susceptible to the effects of high S and/or N deposition than other forest types in SHEN.

In general, deciduous forest stands in the eastern United States do not progress toward N-saturation as rapidly or as far as coniferous stands. Decreased growth and increased mortality have more commonly been observed in coniferous stands (Aber et al. 1998). There is no evidence to suggest that the levels of N deposition observed in SHEN should lead to forest decline in the deciduous forests of the park. However, the complex relationships between atmospheric inputs and forest health are nevertheless of concern, especially in view of the

demonstrated effects of acidic deposition in some situations on soil acidity, nutrient supply, metal toxicity, and tree growth. It is also not known whether forest ecosystems at SHEN are experiencing subtle effects of elevated N-deposition, and whether, for example, some plant species are favored by the relatively high-N environment at the expense of other species.

Possible mechanisms for acidification impacts on terrestrial ecosystems include soil acidification, increased concentration of Al in soil solution, and decreased availability of base cations. These mechanisms can be inter-related. For example, Lawrence et al. (1995) proposed that the dissolution of Al in the mineral soil by mineral acid anions supplied by acidic deposition (SO_4^{2-}, NO_3^-) can decrease the availability of Ca^{2+} in the overlying forest floor. This conclusion was based on the results of a survey in 1992 and 1993 of soils in red spruce forests that had been acidified to varying degrees throughout the northeastern United States. The proposed mechanism for Ca^{2+} depletion is as follows. Acidic deposition lowers the pH in the mineral soil, thereby increasing the concentration of dissolved Al in soil solution. Some of the Al is then taken up by tree roots and transported throughout the trees, eventually to be recycled to the forest floor in leaves and branches. Additional dissolved Al is transported to the forest floor by rising water table during wet periods and by capillary movement during dry periods. Because Al^{3+} has a higher affinity for negatively-charged soil surfaces than Ca^{2+}, introduction of Al into the forest floor, where root-uptake of nutrients is greatest, causes Ca^{2+} to be displaced from the cation exchange complex, and therefore more easily leached with drainage water (Lawrence et al. 1995, Lawrence and Huntington 1999).

Aluminum is not only toxic to aquatic biota. Aqueous Al is also toxic to tree roots, although much higher concentrations of Al in soil solution are required in order to elicit a toxic response as compared with the toxicity of Al to fish in surface water. Plants affected by high levels of Al in soil solution typically exhibit reduced root growth. Stunting of the root system restricts the ability of the plant to take up water and nutrients (Parker et al. 1989). Calcium is well known as an ameliorant for Al toxicity to roots, as well as to fish. Magnesium, and to a lesser extent the monovalent base cations, Na^+ and K^+, have also been associated with reduced Al toxicity. Neither the molecular basis for Al toxicity to plant roots nor the basis for the reduction in toxicity found for base cations is well understood. Efforts to estimate critical levels of atmospheric S or N deposition that will protect sensitive forest resources from damage often use the molar ratio of Ca^{2+} to Al in soil solution as an indicator of potential toxic effects. It has

been suggested that damaged forest stands often exhibit Ca:Al < 1.0 (Ulrich 1983, Schulze 1989, Sverdrup et al. 1992).

The adverse, soil-mediated effects of acidic deposition are believed to result from increased toxic Al in soil solution and concomitant decreased Ca^{2+} or other base cation concentrations (Ulrich 1983, Sverdrup et al. 1992, Cronan and Grigal 1995). A reduction in the Ca:Al ratio in soil solution has been proposed as an indicator reflecting increased probability of Al toxicity and nutrient imbalances in sensitive tree species. This topic was reviewed in detail by Cronan and Grigal (1995), who concluded that the Ca:Al molar ratio provides a valuable measurement endpoint for identification of approximate thresholds beyond which the risk of forest damage from Al stress and nutrient imbalances increases. Base cation removal in forest harvesting can have a similar effect and can exacerbate the adverse effects of acidic deposition. Based on a critical review of the literature, Cronan and Grigal (1995) estimated that there is a 50% risk of adverse impacts on tree growth or nutrition where soil solution Ca:Al $\leq$ 1.0. Aluminum toxicity to tree roots and associated nutrient deficiency problems are largely restricted to soils having low base saturation. The Ca:Al ratio indicator was recommended for assessment of forest health risks at sites or in geographic regions where the soil base saturation is < 15%, such as is found in siliciclastic and many granitic watersheds in SHEN.

Based on published research findings, it is unlikely that terrestrial ecosystems in SHEN have experienced sufficiently high deposition of S or N so as to cause substantial adverse acidification-related impacts to forests. There are several reasons why such impacts are unlikely. First, the vegetation type that appears to be most susceptible to damage from acidic deposition, spruce-fir forest, is largely absent from SHEN, although there are small relic populations of red spruce. Second, the highest point in the park is only 1,234 m, which is below the elevation at which cloud deposition of S and N has been shown to be a large contributor to total S and N deposition. For example, Sigmon et al. (1989) estimated total warm season cloud deposition at the Pinnacles of SHEN (1,014 m elevation) equal to 0.9, 0.7, and 0.2 kg/ha/mo, respectively, for SO_4^{2-}, NO_3^-, and NH_4^+. These cloud deposition estimates contrast with the estimates by Lindberg et al. (1988) at Great Smoky Mountains National Park (1,740 m elevation) that were more than three-fold higher for NO_3^-, eight-fold higher for SO_4^{2-}, and five-fold higher for NH_4^+ (c.f., Vong et al. 1991). Due to high cloud deposition, total S and N deposition levels are therefore much higher at Great Smoky Mountains than at SHEN. Third, total deposition levels of both S and N

are below levels that have been shown to cause adverse impacts on forest ecosystems elsewhere (Tietema and Beier 1995, Dise and Wright 1995, Dise et al. 1998). Fourth, because the forests in SHEN are almost exclusively second growth, subsequent to large-scale timber harvesting and localized agricultural land use prior to park creation, the N-demand of the regrowing forest is likely to be high. This precludes NO_3^- leaching at current N deposition levels in the absence of significant disturbance such as was seen with gypsy moth infestation. Fifth, it is likely that the lower elevation deciduous forests of SHEN, as compared with the high-elevation spruce-fir forests of Great Smoky Mountains, have higher base saturation and soil pH and would therefore not be expected to show the same level of cation deficiency and inorganic Al stress that sometimes characterize the higher elevation sites (Eagar et al. 1996).

Thus, although there is some evidence that spruce forests in the Great Smoky Mountains have experienced adverse effects from N deposition, it is important to note that total N (wet, dry, cloud) deposition at high elevation in the Great Smoky Mountains is considerably higher than is found in SHEN. In addition, the deciduous forests at SHEN are less sensitive to adverse impacts of N deposition. The very high levels of N deposition at some locations in the Great Smoky Mountains are mostly attributable to the high amounts of cloud deposition received in those high elevation areas. As a consequence, the streams that drain undisturbed watersheds in the Great Smoky Mountains exhibit some of the highest recorded NO_3^- concentrations in the United States and also NO_3^- concentrations that can be comparable to or higher than SO_4^{2-} concentrations (U.S. EPA 1993). In contrast, NO_3^- concentrations in SHEN streams are negligible in the absence of insect infestation.

Thus, with respect to the risk factors generally associated with acidification effects on forest vegetation in other areas of the southern Appalachian Mountains, it appears that forests in SHEN are relatively less susceptible to harm. Nonetheless, examination of the available soils information for SHEN watersheds suggests that there may be some risk of adverse effects and that the degree of risk varies spatially within the park. Some acid-base chemistry measurements for soils on siliciclastic bedrock, and to a lesser extent for soils on granitic bedrock, approach or exceed values that have been suggested as thresholds for identification of acid-sensitive forest soils (e.g., base saturation less than 20%, pH less than 4.5; Table VI-4). It is not clear whether forest soils at SHEN will ultimately develop Ca^{2+} deficiency. Soils may stop changing their base

cation status before deficiencies develop as deposition levels decline, or weathering rates may be sufficient to maintain adequate cation nutrient supplies.

As discussed previously, Tables VI-4 and VI-5 provide summary data for soils sampled in 2000 at 79 geologically distributed sites in SHEN (Welsch et al. 2001). The range of base saturation values obtained for soils associated with both siliciclastic and granitic bedrock include values in the 10-20% range cited as possible threshold values for incomplete acid neutralization and leaching of Al (Reuss and Johnson 1986, Binkley et al. 1989, Cronan and Schofield 1990). Moreover, the measured soil pH for soils associated with both siliciclastic and granitic bedrock include values in the highly acidic range (pH < 4.5) in which the more-toxic forms of Al often predominate (Binkley et al. 1989).

Elevated Al concentrations in streamwater are often observed during high-runoff conditions in intensively monitored streams (for example, see Figure VI-20), suggesting probable Al mobilization from soils to soil water, although the hydrologic routing of the increased Al is not well understood. As expected, levels of increased Al reflect the observed bedrock-related gradient in soil pH, suggesting that episodically elevated Al concentrations occur in soil water, especially soil water associated with siliciclastic and to a lesser extent granitic bedrock.

Direct measurements of solute composition in SHEN soil waters were obtained using soil water lysimeters installed during 1999-2000 in lower portions of the Paine Run, Staunton River, and Piney River watersheds, representing the park's three major bedrock types (Rice et al. 2001). Table VI-12 provides a summary of the obtained Ca^{2+} and Al concentration data, as well as Ca:Al soil solution molar ratios. In considering this information it should be noted that: (1) the data were not obtained as part of a regular monitoring program, and thus are not expected to account for spatial and temporal variance in park soils; and (2) lysimeter data are highly dependent upon lysimeter design and installation method, which raises questions about data comparability. However, the data do provide preliminary perspective in relation to indices that have been proposed for evaluation of potential soil acidification impacts on vegetation. Binkley et al. (1989) estimated that soil water Al concentrations of 10 to 50 µm/L may affect the growth of sensitive plant species. Median soil solution Al concentrations were well below this range at all sampling locations, although a maximum value of 20.8 µM was reported for the 35 cm depth site in the Paine River watershed (Table VI-12). It has also been observed that uptake of nutrient

Table VI-12. Calcium and aluminum data[a] collected for soil water samples from three watersheds in SHEN[b] during the period 1999-2000.

Stream	Sample Depth (cm)	n	Ca^{2+} Concentration		Al Concentration		Ca:Al Molar Ratio	
			Min.	Median	Median	Max	Min	Median
PAIN	35	8	10.8	49.3	5.4	20.8	2.7	4.1
	66	6	32.7	46.8	1.4	4.4	11.4	33.5
	97	10	12.3	25.2	1.4	9.1	3.6	19.1
STAN	35	8	67.2	89.9	0.1	0.8	133.8	503.0
	66	9	69.5	79.7	0.1	0.6	210.2	626.0
	97	4	48.8	55.2	0.0	0.2	355.2	489.0
PINE	35	11	42.8	74.8	0.7	4.5	9.5	110.6
	66	7	72.9	93.5	0.1	1.4	410.9	930.0
	97	12	36.2	150.3	0.5	1.9	143.0	336.0

[a] Units are µM
[b] Source of data: Rice et al. 2001

cations can be diminished somewhat at Al concentrations below those required to reduce growth (Binkley et al. 1989).

Examination of the soil lysimeter data for SHEN in relation to the Ca:Al molar ratio threshold of 1.0 (c.f., Cronan and Griegal 1995) suggests that soil water solute concentrations collected in all three watersheds were always above the threshold, and the minimum reported value was 2.7 (Table VI-12). Additional study would be needed to determine the extent to which this response threshold is meaningful and/or might be exceeded for the park's forest soils. However, the mixed hardwood forests that predominate in SHEN are evidently less sensitive to harm from soil acidification than the higher elevation spruce-fir forests located elsewhere in the southern Appalachian Mountains. Nevertheless, in view of the limited available soil and soil water data, the potential for harm in SHEN cannot be ruled-out.

V. AIR QUALITY AND DEPOSITION

A. BACKGROUND ON MONITORING EFFORTS

The Shenandoah National Park (SHEN) air quality monitoring and research program has acquired information about key air pollutants that can degrade visibility, injure or impact growth and vitality of plant species sensitive to ground-level (tropospheric) ozone (O_3), acidify streams, impact aquatic biota, leach nutrients from soils, erode buildings and materials, or harm human health. Table V-1 summarizes the park's comprehensive visibility, ambient air quality, and deposition monitoring and research program.

Table V-1. Visibility, air quality and atmospheric deposition monitoring at SHEN.

Monitoring Parameter	Program	Location	Years
Visibility/Particulate Matter			
Teleradiometer and manual 35mm camera	National Park Service (NPS)	Loft Mountain (Rocky Mountain Vista)	1980-1986
Automatic 35 mm camera	NPS	Pinnacles (Laird's Knob Vista)	1986-1991
Transmissometer	Interagency Monitoring of Protected Visual Environments (IMPROVE)	Big Meadows	1987-1991
Transmissometer – Long	IMPROVE	Big Meadows	1991-present
Nephelometer	IMPROVE Research	Big Meadows	1991 summer
Nephelometer	IMPROVE Research	Big Meadows	1992 (July-Aug)
Nephelometer	IMPROVE	Big Meadows	1996-present
Time-lapse 8mm camera	NPS	Skyland (WNW Vista)	1991-1992
Automatic 35 mm camera	IMPROVE	Skyland (WNW Vista)	1991-1995
Automatic 35 mm camera and 8mm camera	IMPROVE	Dickey Ridge (SW Vista)	1991
Particulate Matter (PM_{10} & $PM_{2.5}$) – Stacked Filter Unit	IMPROVE	Big Meadows	1982-1987
Particulate Matter (PM_{10} & $PM_{2.5}$)	IMPROVE	Big Meadows	1988-1999
Particulate Matter (PM_{10} & $PM_{2.5}$) - Version II Sampler	IMPROVE	Big Meadows	2000-present
Ammonium	IMPROVE Research	Big Meadows	1997-present
Visibility Study – additional IMPROVE sampler, Ammonia & Ammonium	IMPROVE Research	Big Meadows	1991 (summer)
Comparison Study – additional IMPROVE sampler	IMPROVE Research	Big Meadows	1996 (summer)

Table V-1. Continued.

Monitoring Parameter	Program	Location	Years
Mass-Independent Sulfur Isotopic Compositions in Sulfate Aerosols	Special Research	Big Meadows	2001
Monitor and study aerosol optical properties	Aerosol Robotic Network	Big Meadows	2001-present
Ambient Air Quality			
Ozone	NPS	Big Meadows	1983-present
Ozone – Passive Samplers	NPS Research	Big Meadows	1995
Ozone, Sulfur Dioxide	NPS	Dickey Ridge	1983-1994 (summers)
Ozone	NPS	Sawmill Run	1983-1994 (summers)
Sulfur Dioxide	NPS	Sawmill Run	1984-1994 (summers)
Meteorology	NPS	Big Meadows	1988-present
Meteorology	NPS	Sawmill Run	1987-1994 (summers)
Meteorology	NPS	Dickey Ridge	1989-1994 (summers)
Low Level Sulfur Dioxide, Carbon Monoxide	Enhanced Ozone Monitoring Research	Big Meadows	1995-present
Volatile Organic Compounds, Nitrogen Oxides	Enhanced Ozone Monitoring Research	Big Meadows	1995-2000
Atmospheric Chlorofluorocarbons	US Geological Survey (USGS) Groundwater Studies	Big Meadows	1996-present
Volatile Organic Compounds, ozone, meteorology	Environmental Protection Agency (EPA) Funded Research	Big Meadows, Loft Mountain, Hogback Mountain	1998-1999
Ultraviolet Radiation	Park Research and Intensive Monitoring Network	Big Meadows	1997-present
Atmospheric Deposition			
Wet Acid Deposition	National Atmospheric Deposition Program	Big Meadows	1981-present
Wet Acid Deposition	University of Virginia	North Fork Dry Run (Pinnacles)	1986-present
Wet Acid Deposition	University of Virginia	White Oak Run	1980-present
Wet Acid Deposition	USGS	Weakley Hollow	1982-present
Dry Acid Deposition, Nitric Acid, Sulfate, Nitrate, Sulfur Dioxide	Clean Air Status and Trends Network	Big Meadows	1988-present
Cloud Chemistry	Cloud Water Project	Loft Mounain	1984-1985
Cloud Chemistry	EPA Mountain Cloud Chemistry Program	North Fork Dry Run Watershed – 3 locations	1986-1988
Cloud Chemistry	Shenandoah Cloud and Photochemistry Experiment	Pinnacles	1990
Mercury in Precipitation	Mercury Deposition Network	Big Meadows	2002-present
Precipitation Sulfur Isotopes	USGS Groundwater Studies	Big Meadows	1989-present

The purpose of this chapter is to characterize past, current, and future air quality and deposition within SHEN. Natural background conditions are estimated for O_3, visibility, and deposition of sulfur (S) and nitrogen (N). Current conditions and recent trends are summarized. Finally, modeled future changes in air quality and deposition are presented in response to each of the emissions control scenarios described in Section IV.

B. ESTIMATED NATURAL CONDITIONS

1. Ground-level Ozone

There are factors not controlled or influenced by human activity that contribute to a variable background concentration of ground-level O_3. There are also some O_3-enhancing human activities that are generally not considered subject to control. Thus, there may be both a "natural" background and a "practical" background level of O_3. Examples of indirect influences include hemispheric very-long-range transport of O_3 or its precursors, changes in land use, and changes in vegetation. There is some indication that O_3 background concentrations may have increased from near 5 to 10 ppb (parts per billion) in the nineteenth century (Beck and Grennfelt 1994, Kasibhatla et al. 1996) to an estimated 20 to 45 ppb during summer in the United States today (Fiore et al. 2002). Increases of a few ppb have likely occurred over the United States during the past two decades (Oltmans et al. 1998, Lin et al. 2000).

The spatial and temporal distribution of background O_3 varies with season, climate, landmass, elevation, vegetation, and latitude. Annual variation in O_3 concentration, with a maximum in spring, is the natural expected pattern. Only locations remote from anthropogenic emissions sources still exhibit this pattern. Continental areas are well known to have higher background O_3 than remote oceanic areas. This is partly due to deeper convective activity over the landmasses which transport stratospheric and lightning-produced O_3 from above the boundary layer down to the surface. The large amount of thunderstorm activity along the equator produces O_3 that is transported progressively towards the poles. Higher elevation sites are more likely to have higher background O_3 because they are more frequently above the surface mixing layer and are more likely to intercept free-tropospheric air that contains stratospheric O_3 and lightning-produced O_3. Thus, location will also affect the expected background.

Four techniques have been used to estimate background O_3 from observed data. Each is described below.

a. Average Observed Ground-level Ozone Concentrations at Remote Locations

The remote mid-latitude Atlantic Ocean has average O_3 concentrations of 15- 25 ppb (Ray et al. 1990, Kasibhatla et al. 1996). Especially in the summer, meteorology in the eastern United States is dominated by a circular flow around the Bermuda High that carries Atlantic air masses over the continent. This low background is sometimes observed in Florida and along the southeastern coastline, and SHEN is influenced by this oceanic flow periodically. An extreme case was observed during hurricane Hugo when O_3 concentrations of 19 ppb were observed at Big Meadows (Doddridge et al. 1991)

Aircraft and surface measurements indicate an average O_3 concentration from 5 to 20 ppb over the Pacific Ocean (Oltmans, et al. 1998). Measured concentrations at western coastal sites subject to clean air inflows from the ocean have been 10-20 ppb at Olympic NP and 21-23 ppb at Redwoods NP (Altshuller and Lefohn 1996).

Measurements from long-term National Oceanic and Atmospheric Administration (NOAA) monitoring stations located at high elevation and often influenced by free tropospheric air have mean annual O_3 values of 35-42 ppb at Whiteface Mountain, NY and about 40 ppb at Mauna Loa, HI. Both sites have seen small increases in O_3 since 1975 (Oltmans et al. 1998).

b. Probability Distribution Methods

The 25th percentile of the probability distribution (36 ppb) was used at Harvard Forest, MA to estimate the background O_3 level for the eastern United States, which was compared to other locations (45 ppb and 50 ppb in western Tennessee and at the Grand Canyon in Arizona, respectively; Lin et al. 2000, Fiore et al. 2002). Other percentiles could be chosen. For example, Altshuller and Lefohn (1966) summarized 10th and 30th percentile data from several inland monitoring stations (Table V-2). SHEN data for 1983-1990 are given in the table for comparison, as reported in the National Park Service (NPS) Quick Look Report, Volume II (Joseph and Flores 1993) for the 10th and 25th percentiles. There appears to be an elevational gradient in O_3 concentration in the park, based on results from the three monitoring sites. The 25th percentile values for background O_3 of 26 to 39 ppb were within the ranges for other remote locations and the Harvard Forest site.

Table V-2. Values for the 10th and 30th percentile O_3 measurements at remote inland locations compared with generally comparable data from SHEN.

Location	State	10th Percentile	30th Percentile
Badlands NP[a]	SD	20	24
Yellowstone NP[a]	WY	18	28
Theodore-Roosevelt NP[a]	ND	19	27
Great Sand Dunes NP[a]	CO	30	37
Arches NP[a]	UT	26	33
Montgomery Co.[a]	AR	5	15
		10th Percentile	25th Percentile
SHEN - Big Meadows [b]	VA	30	39
SHEN - Dickey Ridge[b]	VA	28	37
SHEN - Sawmill Run [b]	VA	17	26

[a] Altshuller and Lefohn (1966)

[b] Joseph and Flores (1993). Measurement elevations were: Big Meadows, 1074 m; Dickey Ridge, 610 m; and Sawmill Run, 445 m

c. Correlation Methods with Ground-level Ozone Precursors

Regression models for O_3 vs $[NO_y - NO_x]$ provide a useful context for the question of background O_3 concentration. The regression intercept provides an estimate of the background O_3 concentration because at zero nitrogen oxide (NO_x) concentration the photochemical formation of O_3 would cease. Using this approach, 1995 data from Harvard Forest suggested background O_3 of 30 ppb (Fiore et al. 2002). Typical values from Harvard Forest were 20 to 40 ppb for background O_3 (Hirsch et al. 1996). For a location in Giles County, TN, 110 km SSW of Nashville, a summer 1991 study estimated a background of 36 to 42 ppb (Olszyna et al. 1994).

Detailed studies of O_3 and reactive oxides of N (NO_y) have been conducted at Big Meadows in SHEN (Hallock-Waters 2000). A background intercept of 39 ppb was found for three years of O_3 and NO_y data, although it must be noted that the slope and correlation varied strongly by season. The summertime intercept estimate of background O_3 was about 20 ppb. This may reflect cleaner air from the Atlantic Ocean region that is carried in by the flow around the

Bermuda High that develops each summer. Back trajectory analysis indicated that highest O_3 values at SHEN occur when air flow is from the west and northwest. A weighted climatological average based on air flow would define the annual average background.

d. Computer Simulation Modeling

Ozone production in the North American boundary layer includes about 50% surface afternoon O_3. Most of the remainder is from tropospheric production outside the region. Stratospheric injection is not believed to contribute more than 2 ppb to the background. Mean summer afternoon O_3 concentrations derived from transportation from outside the boundary layer were estimated to range from 15 to 35 ppb, with the highest values in the western United States. The higher background in the West can be explained by the higher average O_3 lifetime of three to five days in the West as compared with less than two days in the East. The West also has a higher mixing layer (2 km) and lower average O_3 deposition (0.4 cm/sec) than the East (Fiore et al. 2002).

In a modeling study, Jacob et al. (1993) estimated that background North American O_3 concentration was regulated by horizontal transport and deposition and ranged from 30 to 40 ppb. For much of the eastern United States, the estimated background was 35 to 40 ppb. About half of the average summertime O_3 concentration at the surface over the continental United States was estimated to be background O_3 originating from outside the continent.

In summary, the background O_3 concentration is not known with a high degree of certainty, partly because of different ways of defining it and partly because it is not a measurable condition. Human activities now influence O_3 concentration throughout the Northern Hemisphere. Changes not normally associated with air pollution, such as widespread agriculture and landscape vegetation changes, have also altered the natural components of the background O_3. The O_3 background concentration over the eastern United States likely ranges from approximately 20 to 40 ppb.

2. Visibility

As was discussed in Section III.F, there are natural causes for visibility degradation. For example:

- The scattering of light by oxygen (O) and N molecules in the air limits visibility and causes the sky to appear blue.

- Particles associated with natural processes (e.g., biogenic emissions, volcanic activity, oceanic hazes, or windblown dust) can become suspended in the air, thus causing visibility impairment.

- If suspended particles are hygroscopic, their effect on visibility will be exacerbated by high relative humidity.

A simplified, general approach was used to establish a benchmark of natural visibility conditions for assessing current visibility conditions and trends throughout the United States and more specifically within SHEN. The approach relied on estimates of the natural concentrations of particulate matter that are known to contribute to visibility impairment and the calculated contribution to light extinction that can be attributed to these assumed background concentrations.

The estimates of annual average concentrations for natural levels presented in Table V-3 for the key particulate species were adapted from Trijonis (1990) and the U.S. EPA guidance document on estimating natural conditions (U.S. EPA 2001b). The calculated contribution to visibility degradation of each of these key species is based on the Interagency Monitoring of Protected Visual Environments Program (IMPROVE) algorithm (Appendix B) which applies the dry extinction efficiencies and appropriate adjustment for relative humidity to these

Table V-3. Estimated natural background particulate concentrations and light extinction.

	Annual Average Mass Concentrations (mg/m^3)		Dry Extinction Efficiencies (m^2/gm)	Estimated Average Annual Natural Conditions (Mm^{-1})	
	East	West		East	West
Fine Particles					
Ammonium Sulfate	0.23	0.11	3.0	2.83	0.73
Organic Material	1.4	0.47	4.0	5.60	1.88
Light-absorbing Carbon	0.02	0.02	10.0	0.20	0.20
Ammonium Nitrate	0.1	0.1	3.0	1.23	0.66
Soil	0.5	0.5	1.0	0.50	0.50
Coarse Mass	3.0	3.0	0.6	1.80	1.80
Clear Sky (Rayleigh)				10.00	10.00
Light Extinction Coefficient (Haziness)				22.2 (8.0 dv)	15.8 (4.6 dv)
Visual Range				176 km (109 miles)	248 km (154 miles)
Relative Humidity Factors				4.1 (87%RH)	2.2 (70%RH)

concentrations, to calculate the total light extinction due to assumed natural conditions. For concentrations, to calculate the total light extinction due to assumed natural conditions. For illustrative purposes, nominal relative humidity adjustments for the eastern and western United States of 4.1 and 2.2, respectively (Malm 2000), have been applied to give a rough comparison of the two geographical areas.

These estimates are generally accepted as reasonable first approximations to annual average background conditions. They are, however, rough estimates and could easily be off by a factor of two or more. The estimates are summarized graphically in Figure V-1. In the East, natural visual range is estimated to be 176 km (109 mi) whereas in the West it is 248 km (154 mi). Under natural conditions, carbon (C)-based particles are responsible for most of the non-Rayleigh visibility reduction, with all other particle species contributing significantly less. Clear sky scatter (Rayleigh) is the largest contributing factor to the reduction of visual range, at about 45% in the East.

Estimates have also been derived for the distribution of natural conditions at SHEN (U.S. EPA 2001b). The estimated average natural background standard visual range at SHEN is ~184 km (~115 mi) (U.S. EPA 2001b). The standard visual range is estimated to be ~270 km (~170 mi) for the best natural conditions (mean of the 20% best days) and ~125 km (~78 mi) for the mean of the worst 20% days. The corresponding light extinction values under natural conditions are 21.2, 14.5, and 31.2 Mm^{-1}, respectively; and the corresponding haziness values under natural conditions are 7.5, 3.7, and 11.4 dv, respectively.

3. Deposition

Historical levels of S and N deposition prior to about 1980 in and near SHEN are not well known. However, Shannon (1998) provided estimates of historical deposition during the period 1900 to 1990 at SHEN, as part of the Southern Appalachian Mountains Initiative (SAMI) assessment (Sullivan et al. 2002a). These estimates (Table V-4) were based on historical emissions data and were constructed with the Advanced Statistical Trajectory Regional Air Pollution (ASTRAP) model (Shannon 1981, 1985), including wet, dry, and cloud forms of deposition. Estimates of pre-industrial (i.e., pre-1850) deposition of S and N are not available, but are assumed to have been substantially lower than Shannon's (1998) estimates for 1900.

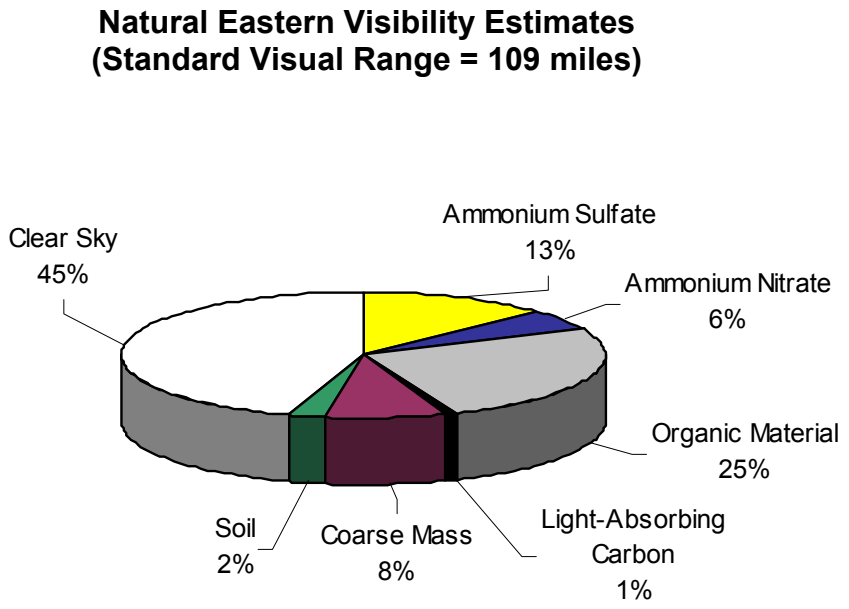

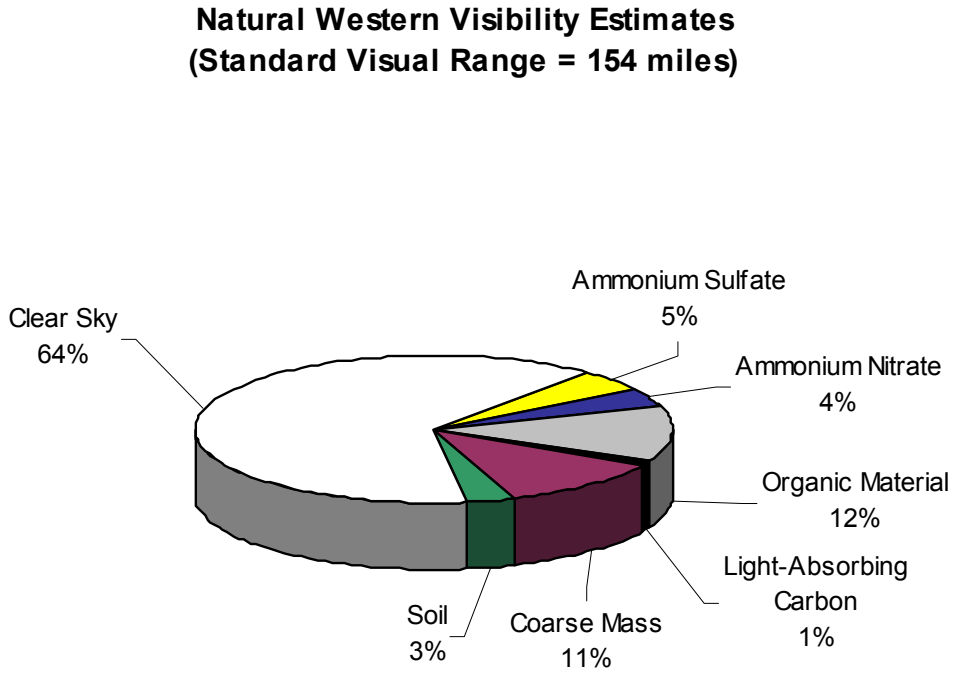

Figure V-1. Estimated natural background particle contributions to visibility reduction in the eastern and western United States.

Table V-4. Estimates of historical deposition in SHEN of sulfur and oxidized nitrogen at five year intervals, normalized to 1990 and expressed as a percentage of the 1990 values (Shannon 1998).

Year	S Deposition (Percent of 1990 Value)[a]				Nitrate-N Deposition (Percent of 1990 Value)[a]			
	Wet	Dry	Cloud	Total	Wet	Dry	Cloud	Total
1900	30	33	42	34	14	14	13	14
1905	42	47	60	47	18	18	18	18
1910	52	58	75	59	22	24	24	23
1915	62	69	90	70	25	27	28	26
1920	66	73	98	75	27	29	30	28
1925	72	79	106	81	36	36	35	36
1930	65	72	98	74	40	38	37	39
1935	53	58	82	60	32	31	30	31
1940	64	69	97	72	36	36	37	36
1945	83	90	132	96	48	46	48	48
1950	78	83	126	90	53	52	54	53
1955	78	83	114	87	60	60	61	61
1960	87	90	125	96	71	70	72	71
1965	92	102	102	96	79	78	72	77
1970	113	121	116	116	92	90	84	90
1975	116	118	102	113	98	94	86	94
1980	104	104	90	100	102	97	90	97
1985	97	96	86	95	97	96	96	97
1990	100	100	100	100	100	100	100	100

[a] For reference, five-year average values, centered on 1990, of total deposition of S and N were 13 and 7.6 kg/ha/yr, respectively

C. CURRENT CONDITIONS AND TRENDS

1. Air Quality

a. Ambient Conditions

The NPS maintains a network of O_3 monitors, using ultraviolet absorption photometric analyzers, at about 30 park units across the country. Monitoring has occurred in SHEN since 1983, although data collection was spotty prior to 1988. SHEN's monitoring locations are shown in Figure V-2. Two of the monitoring locations, Dickey Ridge and Sawmill Run, were closed after the 1994 O_3 season, but the Big Meadows site (U.S. EPA AIRS Site No. 51-113-0003, Madison County, Virginia) continues in operation. Meteorological parameters and O_3 measurements were collected at all three sites. Also shown in Figure V-2 are state O_3 monitoring locations near SHEN. Monitoring methods and quality assurance procedures used in the NPS monitoring network meet the applicable 40 CFR Part 58 EPA requirements, allowing

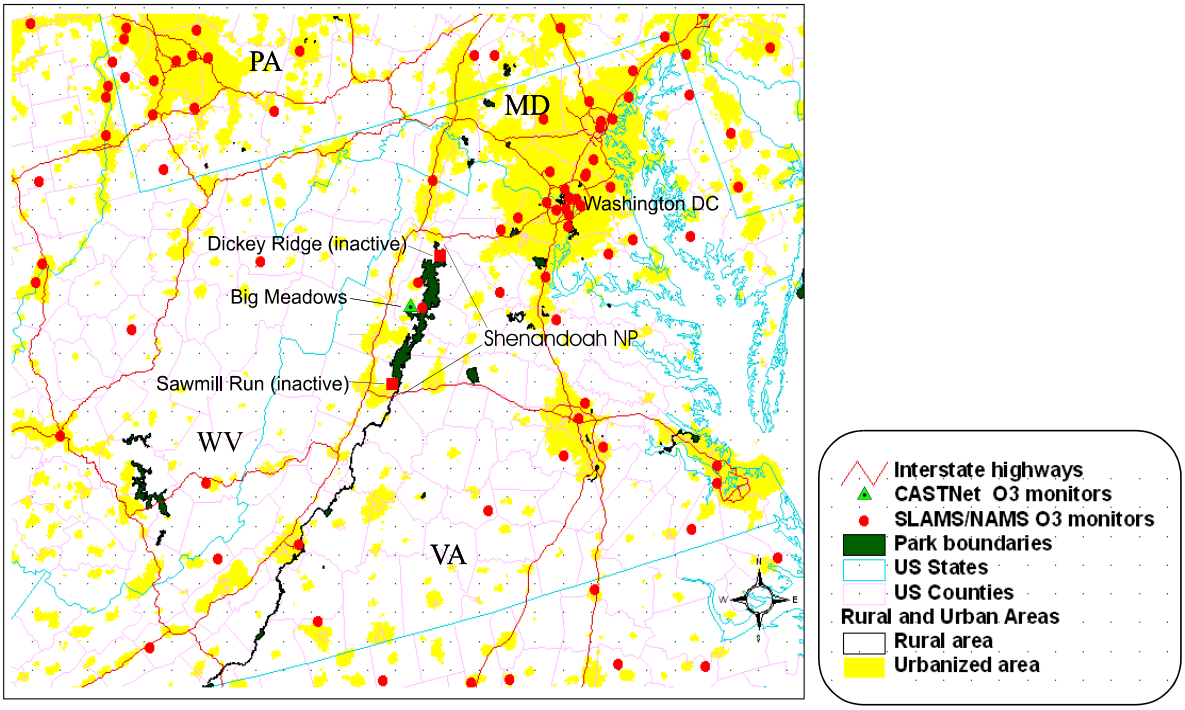

Figure V-2. Ozone monitoring locations in and near SHEN.

for the direct comparison of NPS-collected data with those collected by the EPA and state and local air pollution control agencies. Hourly average O_3 concentrations are recorded by on-site data loggers and transferred to a central database located at Air Resource Specialists, Inc., in Fort Collins, Colorado, where the data are validated.

Based on back trajectory modeling, Big Meadows is mostly removed from strong local anthropogenic sources of air pollution and is largely representative of regional O_3 levels (Poulida et al. 1991, Hallock-Waters 2000, Cooper and Moody 2000). It should be noted, however, that back trajectory models have limited capability to estimate the contributions of local sources to O_3 exposures at a given sensitive receptor (J. Moody, pers. comm., May 2003; K. Gebhart, pers. comm., April 2003). In addition to O_3, measurements of other trace gases have been made at the Big Meadows site from 1995 to 2000. These trace gases include sulfur dioxide (SO_2), carbon monoxide (CO), and NO_y. Reactive oxides of N encompass a range of compounds including NO, NO_2, NO_3, nitric acid (HNO_3), and peroxyacetylnitrate (PAN), as well as other oxides of nitrogen. Examination of the concentrations of trace gases can provide insight into the origins of these pollutants. More detailed analyses of these data can be found elsewhere (e.g., Hallock-

Waters 2000, Kang et al. 2001), so only the major conclusions from these analyses are summarized here.

High O_3 concentrations often occur during periods of warm temperatures, high atmospheric pressure, stagnant air masses, and high solar insolation. As a result, O_3 levels frequently exhibit strong seasonal trends. Two Virginia O_3 sites located outside the park in Frederick County (U.S. EPA AIRS site no. 51-069-0010) and Fauquier County (U.S. EPA AIRS site no. 51-061-0002) are included in the O_3 data analyses for illustrative purposes to compare high (SHEN-Big Meadows) and low elevation O_3 data. Figure V-3 shows the monthly maximum 1-hour O_3 concentrations measured at Big Meadows from 1995 through 1997. The higher values generally occurred in the summer season of May through September. Peak O_3 values were most often recorded in July or August. The lowest monthly maximum 1-hour concentrations generally occurred in November through January.

The three-year averages of the annual fourth-highest daily maximum 8-hour O_3 concentrations at Big Meadows, Frederick County, and Fauquier County are shown in Table V-5 and plotted in Figure V-4 for 1992-2000. Only April through October data were used to generate these averages. Three-year averages are shown for all periods that met the EPA's completeness criteria. Values not meeting the EPA standard are indicated in bold. The current primary NAAQS for O_3 provides that the fourth highest annual daily maximum 8-hour average O_3 concentration cannot exceed 0.08 ppm over three years. Thus, a site is in compliance if there are fewer than 4 days with a maximum daily 8-hour average O_3 concentration greater than, or equal to, 0.085 ppm (resulting in a rounded average of 0.08 ppm) over three years. An analysis of the monitoring data showed that the number of times that a maximum 8-hour average exceeded 0.085 ppm (85 ppb) in 1997-1999 were 6, 22, and 15, respectively. Based on this standard, Big Meadows was not in compliance during the study period. The previous primary and secondary NAAQS for O_3 was 0.125 ppm (rounded to 0.12), not to be exceeded more than once per year. Under this older standard, Big Meadows was not in compliance in 1998, but did not violate the standard in 1997, when the maximum monitored concentration was 0.104 ppm, or in 1999, when the maximum monitored concentration was 0.111 ppm. For comparison, the Fauquier County monitoring site exceeded the standard in 1993, 1999, and 2000, and the Frederick County site exceeded the standard in 1998-2000. Also shown in Table V-5 are the number of individual days at each site with a maximum 8-hour O_3 average greater than or equal to 85 ppb. At all three sites, at least one such day occurred in each year listed.

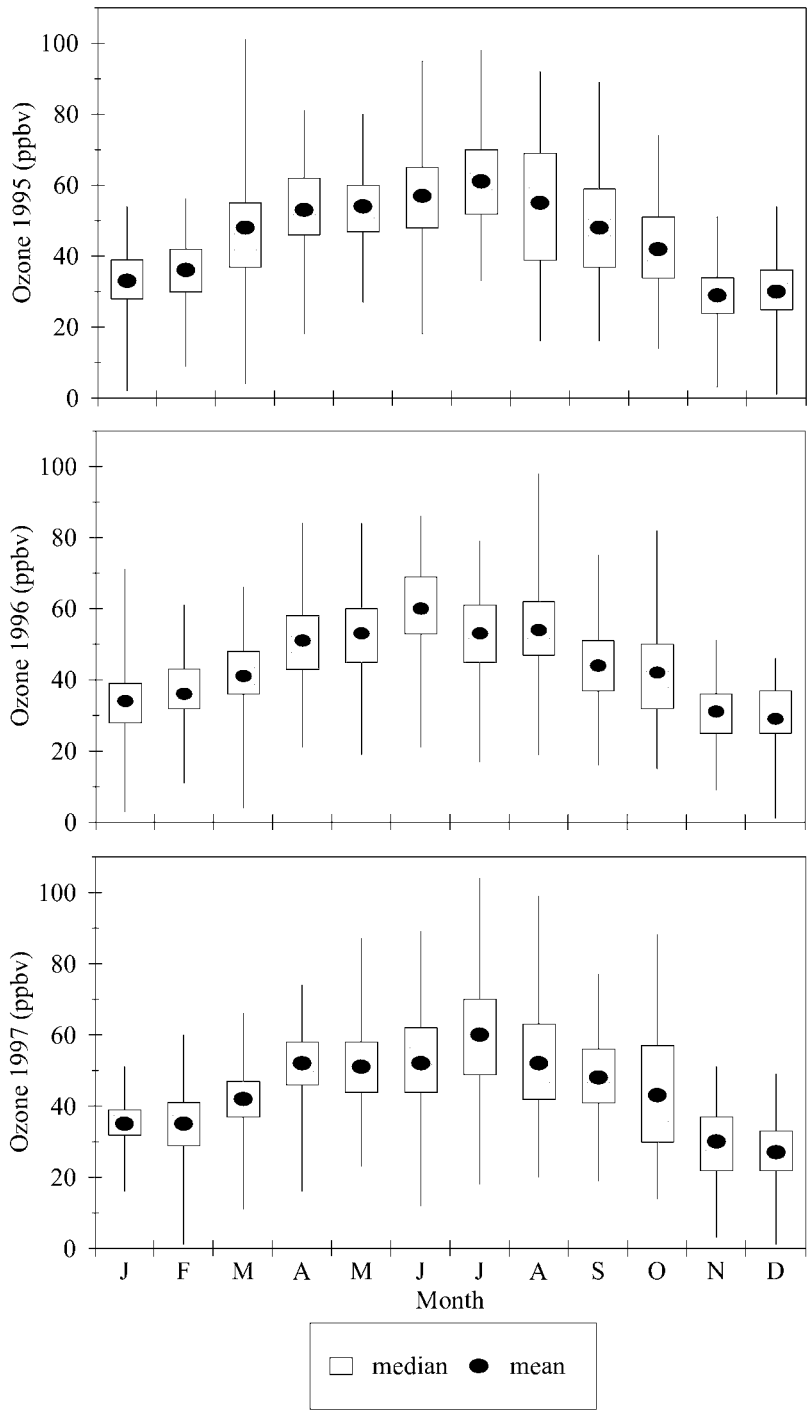

Figure V-3. Box and whisker plot showing the monthly maximum 1-hour ozone averages at Big Meadows for the period 1995 to 1997. The rectangle signifies the quartile values and the whiskers reflect the range. (Source: Hallock-Waters 2000)

Table V-5. Three-year averages of annual 4th highest daily maximum 8-hr ozone concentrations and annual exceedances. (Ozone season defined as April through October.) Values in bold exceed the level of the 1997 National Ambient Air Quality Standard for Ozone.

	SHEN--Big Meadows		Fauquier County		Frederick County	
	3-Year Average of the 4th High Daily Max 8-hr O_3 ppb [a]	Number of Days with Maximum 8-Hour Ozone Concentration ≥ 85 ppb	3-Year Average of the 4th High Daily Max 8-hr O_3 ppb [a]	Number of Days with Maximum 8-Hour Ozone Concentration ≥85 ppb	3-Year Average of the 4th High Daily Max 8-hr O_3 ppb [a]	Number of Days with Maximum 8-Hour Ozone Concentration ≥ 85 ppb
1992	b	1	84	2	c	1
1993	b	2	**85**	6	c	1
1994	81	2	82	2	80	2
1995	84	7	82	1	83	4
1996	83	1	79	2	82	1
1997	**85**	6	81	3	84	4
1998	**92**	22	84	12	**88**	10
1999	**96**	15	**88**	9	**90**	5
2000	**93**	1	**86**	1	**87**	2

[a] Year indicates the ending year of the 3-year average
[b] Did not meet EPA's completeness criteria for computing 3-year average
[c] Data collection began 1992

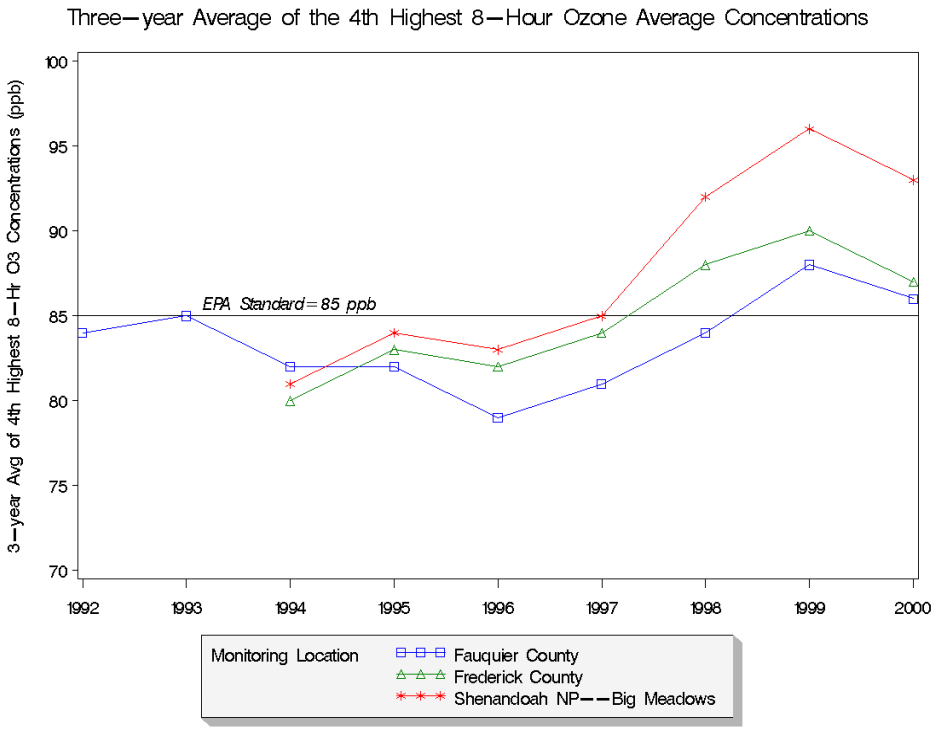

Figure V-4. Three-year average of the 4th highest 8-hour ozone average concentrations.

Urban areas typically experience strong diurnal trends in ambient O_3 concentrations. Ozone concentrations begin increasing after sunrise and peak in the late afternoon or early evening. At night, as photochemical activity ceases, O_3 reacts with fresh NO and is removed from the atmosphere. This is not the case, however, for Big Meadows. Situated at a relatively high elevation (1,073 m), it is generally above the inversion layers that trap nighttime pollution. It is also located in a rural setting and is mostly removed from strong local sources of fresh NO. As a result, removal of O_3 by NO at night does not occur to any significant degree and thus the diurnal pattern at this location does not exhibit the range of variation typical of urban areas. Figure V-5 shows hourly O_3 averages plotted against each hour of the day during each of the four seasons during the period 1995 to 1999. The mean 1-hour average varied only slightly during the course of the day. Maximum hourly values also exhibited relatively little diurnal variation, with the

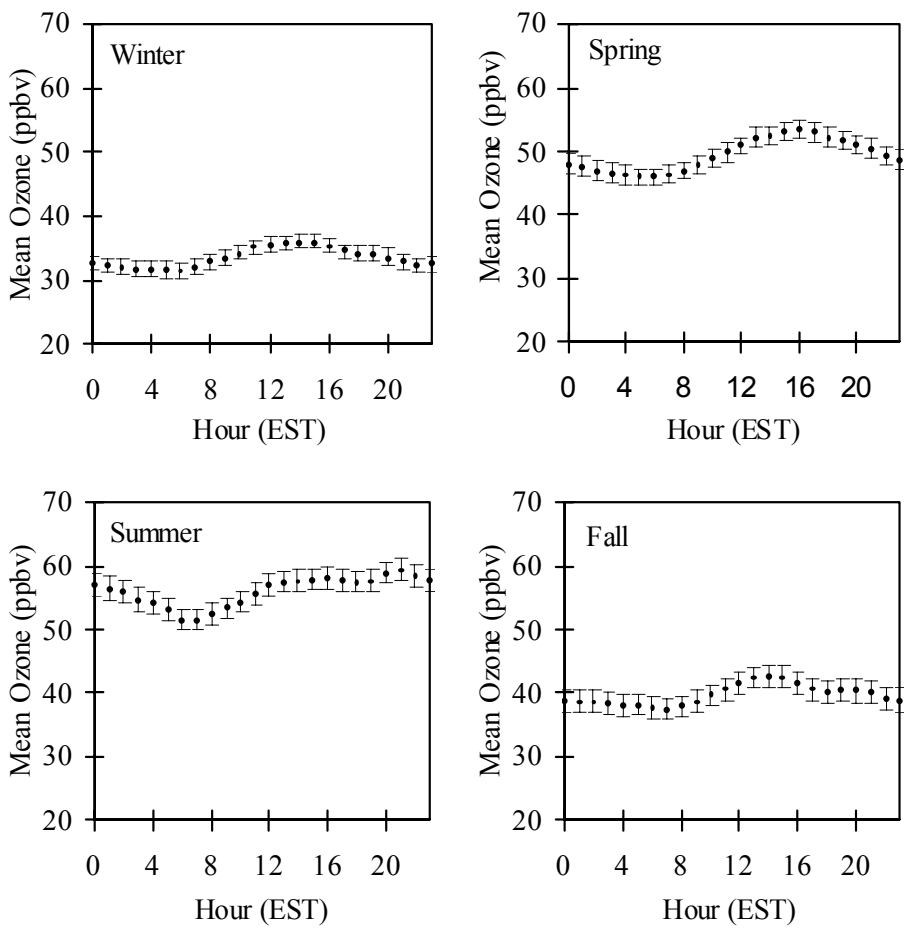

Figure V-5. Diurnal hourly ozone patterns at Big Meadows during each of the four seasons during the period 1995 to 1999. (Source: Hallock-Waters 2000)

highest values occurring during late afternoon or early evening for all seasons except summer, when the daily peak values tended to occur during evening or night time. This suggests that insufficient NO is generally available during the nighttime hours to significantly lower O_3 concentrations, or during the day to boost O_3 concentrations locally. This lack of strong diurnal variation contrasts with urban locations such as Washington, DC (Figure V-6), where peak hourly O_3 concentrations occur between noon and 1 p.m.

Table V-6 contains means, minima, and maxima of the annual May-September values of the SUM06 and W126 O_3 exposure indices, which are particularly relevant for vegetation, calculated for all three SHEN monitoring sites and the nearby monitoring sites in Frederick and Fauquier Counties. Because all O_3 values are added to the W126 index, and every O_3 value 0.06 ppm (60 ppb) and higher is added to the SUM06 index, these indices are particularly sensitive to missing data. Ozone data completeness during some years, particularly for Dickey Ridge and Sawmill Run, was less than during other years, making comparisons between years particularly difficult. For this reason, the raw index values were adjusted by dividing by the percentage of data completeness. For example, in 1991 at Dickey Ridge 76.6% of hourly values from 8 AM to 8

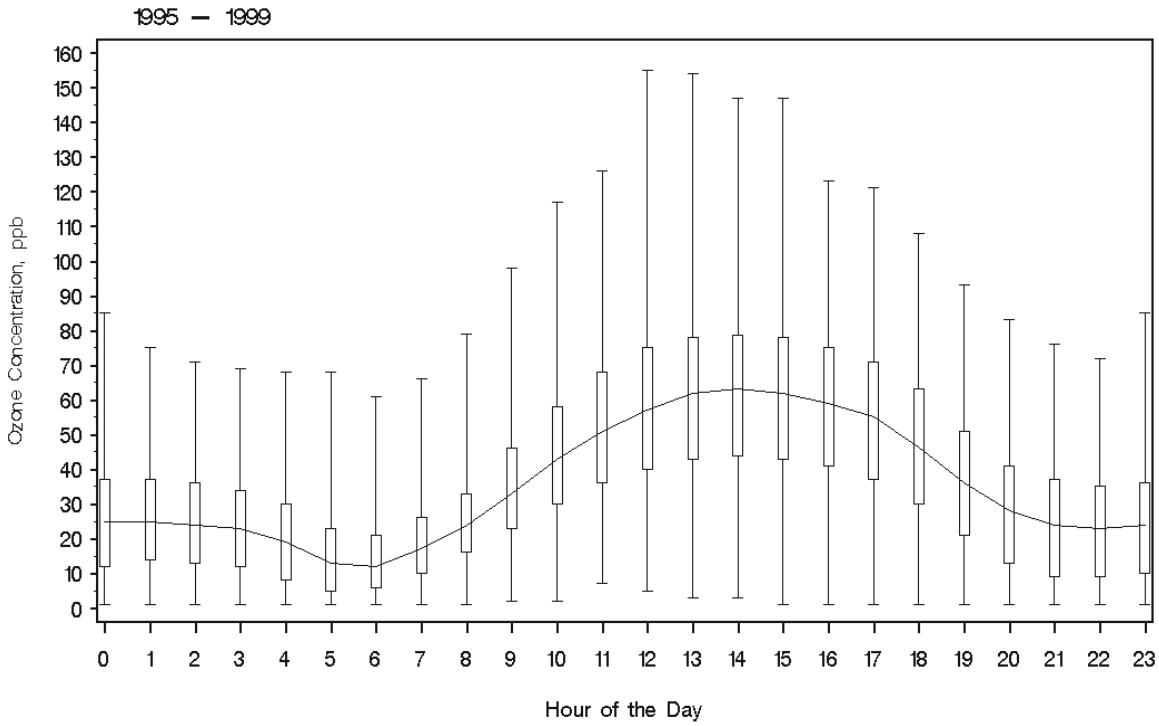

Figure V-6. May-September diurnal ozone patterns at Washington, DC for the period 1995 to 1999 (AIRS Site No. 11-001-0043). The range of concentration values is provided by hour.

Table V-6. May Through September SUM06 and W126 ozone exposure values, for the period 8AM-8PM, adjusted by percent of data completeness.

Site	May-Sep SUM06 Exposure (ppm-hr)			May-Sep W126 Exposure (ppm-hr)		
	Mean	Minimum	Maximum	Mean	Minimum	Maximum
Fauquier County 1990-2000	35.5	21.4	49.1	26.9	16.5	38.4
Frederick County 1992-2000	35.3	19.9	55.9	26.5	16.0	42.1
SHEN-Big Meadows 1990-2000	46.9	31.1	83.4	34.1	22.5	60.1
SHEN-Dickey Ridge 1989-1994	27.3	16.2	41.8	20.9	14.1	30.3
SHEN-Sawmill Run 1989-1994	25.5	13.2	36.4	20.2	11.6	28.7

PM during May through September were available, so the O_3 exposure indices were divided by 0.766. In no case was the percentage of data completeness less than 60%.

Adjusted SUM06 values from the Big Meadows, Fauquier County, and Frederick County monitoring locations are plotted in Figure V-7. The highest values generally occur at the Big Meadows site, which has the highest elevation, but all three sites follow similar patterns. Particularly noticeable is a large increase in the SUM06 index in 1998, followed in 1999 by much lower exposures, and in 2000 by the lowest values in the 11-year period. Adjusted W126 values are plotted in Figure V-8. Patterns here are similar to the SUM06 plot, and again the highest W126 exposures were recorded at Big Meadows.

b. Trends in Air Quality

The adjusted SUM06 and W126 index values were tested for trends using the method described by Theil (1950). In this analysis, slopes were first calculated between all possible pairs of points, where each point is the value of the May-September 8 AM-8 PM SUM06 or W126 exposure index in a given year. These slopes were then sorted from smallest to largest. The slope of the overall trend line was estimated to be the median of the individual slopes. The significance of the Theil slope is found by assuming that the "true" slope is zero, then calculating the probability that the estimated slope occurred by chance. The results obtained by this technique are not affected by unusually high or low values (Sisler and Malm 1998).

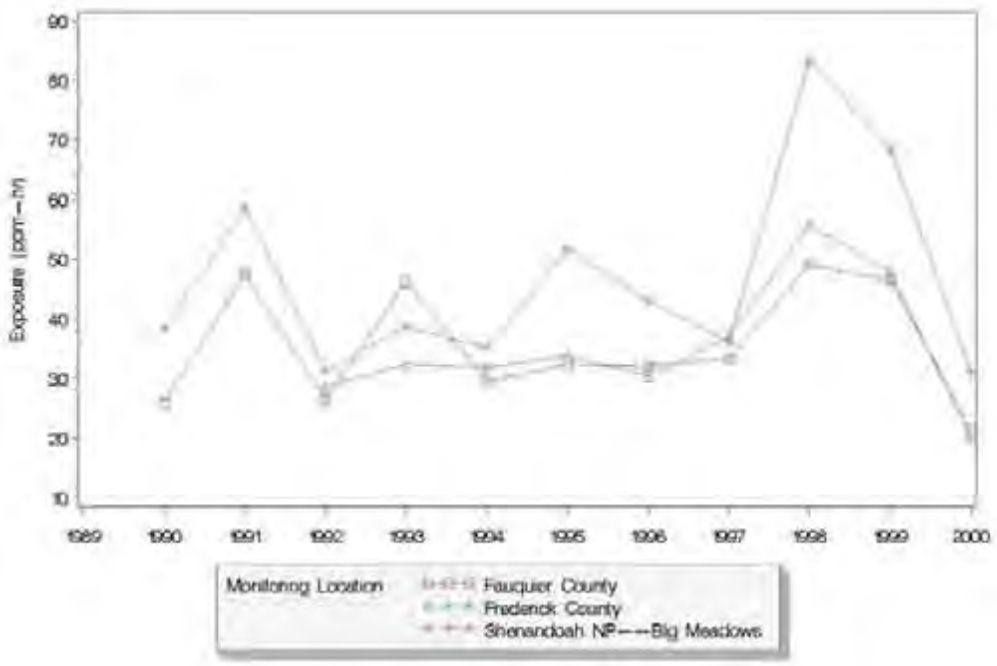

Figure V-7. Adjusted SUM06 values for Fauquier County, Frederick County, and Big Meadows monitoring sites for the period 1990 through 2000.

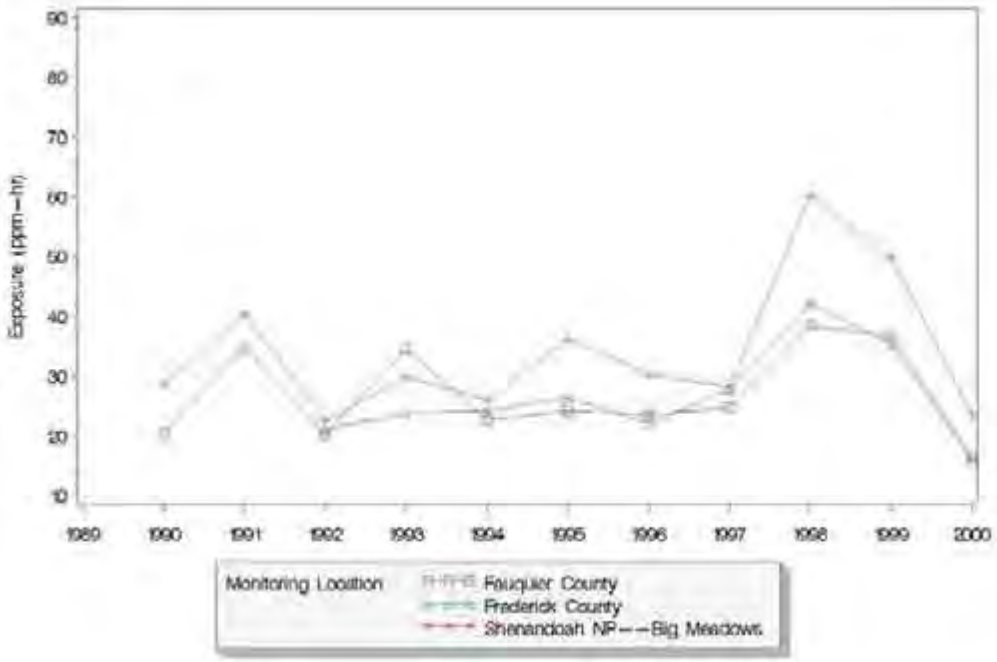

Figure V-8. Adjusted W126 values for Fauquier County, Frederick County, and Big Meadows monitoring sites for the period 1990 through 2000.

Trends in SUM06 and W126 at the Big Meadows, Frederick County, and Fauquier County monitoring sites are shown in Table V-7. Sawmill Run and Dickey Ridge are not included since they closed in 1994. Trends were calculated from 1990 (1992 for Frederick County) through 2000. A positive slope indicates increasing O_3 exposure, and thus deteriorating air quality; a negative slope indicates improving air quality. Slopes of the trend lines were all positive, but they were not statistically significant, with the exception of the Frederick County W126 index which had a positive slope of 1.29 ppm-hr/year ($p \leq 0.15$). A significance level of 0.15 is used in order to maintain consistency with NPS trend reporting under the Government Performance and Results Act (GPRA; www2.nature.nps.gov/ard/GPRA/index.html).

Table V-7. Trends in May through September (8 AM-8 PM) ozone exposure in and around SHEN during the period 1990-2000.

Site	SUM06		W126	
	Annual Slope (ppm-hr/yr)	p-value	Annual Slope (ppm-hr/yr)	p-value
SHEN--Big Meadows	+0.70	0.38	+0.74	0.32
Fauquier County	+0.68	0.27	+0.57	0.27
Frederick County	+1.56	0.18	+1.29	0.13

Trends in O_3 concentration are routinely calculated by the NPS for all of its monitoring locations for reporting under GPRA. The O_3 statistic used for this purpose is the average daily maximum 1-hour O_3 value from May through September, where each day's maximum is the maximum of all 24 1-hour values (as opposed to using only those from 8 AM to 8 PM). The resulting trends are shown in Table V-8. For purposes of GPRA reporting, a sliding ten-year window is used. The trend estimate for Big Meadows over 1991-2000 was not statistically significant ($p=0.36$). Also included in the table for comparison are the same trends for Fauquier and Frederick Counties. The slope determined for Frederick County was 0.80 ppb/yr ($p=0.13$); the slope for Fauquier County was not statistically significant.

GPRA trends for the previous 10-year sliding window are also included in the table. The period 1990-1999 was used to estimate trend, except for the Frederick County site where the period was 1992-1999. The trend estimates for this time period were statistically significant and increasing at Big Meadows and the Frederick County site ($p=0.08$ and $p=0.01$, respectively),

Table V-8. Trends in May through September daily maximum 1-hour average ozone concentration.

Site	Time Period	Average Daily Maximum	
		Annual Slope (ppb/yr)	p-value
SHEN--Big Meadows	1991-2000	+0.43	0.36
Fauquier County	1991-2000	-0.29	0.30
Frederick County	1992-2000	+0.80	0.13
SHEN--Big Meadows	1990-1999	+0.94	0.08
Fauquier County	1990-1999	+0.31	0.24
Frederick County	1992-1999	+0.99	0.01

with slopes of almost 1 ppb per year at both locations. The 1990-1999 trend estimate for Fauquier County was not statistically significant. Overall, the available data suggest that the May through September average daily maximum 1-hour average O_3 concentration appears to have been increasing at Big Meadows and Frederick County through 1999, but not at the Fauquier County site. The trend estimate was sensitive to the low O_3 in 2000 and the 10-year period of evaluation that was selected.

c. Ground-level Ozone Formation

The relationship between O_3, NO_x, and volatile organic compound (VOC) concentrations is non-linear. It is possible, depending upon the initial concentrations of these gases, that decreases in either NO_x or VOC concentrations will not decrease O_3 concentrations, and may actually increase them. Production of O_3 may be limited by the availability of either NO_x or VOCs, depending upon the NO_x to VOC ratio. Research by Hallock-Waters (2000) using 1995-1997 Big Meadows data indicated that O_3 production is NO_x-limited over SHEN during the summertime, when production of VOCs by vegetation is high, and VOC-limited during the winter. Autumn is a period of transition from NO_x-limited to VOC-limited O_3 production. These results confirm earlier modeling work by Jacob et al. (1995).

Nitrogen oxides are emitted in large quantities from anthropogenic sources such as industrial processes, coal-fired utilities, and vehicles. These emissions are generally in the form of NO, which is rapidly oxidized to NO_2. The sum of these two compounds is generally referred to as NO_x. Hallock-Waters (2000) found that NO concentrations at SHEN were generally below detection limits at night, when the lack of sunlight prevented photolysis of NO_2 to create NO.

NO concentrations were highest during the winter, when photochemical activity and O_3 concentrations were lowest. Based on the oxidation rate of NO to NO_2, Hallock-Waters (2000) concluded that most NO_x in air parcels at SHEN resulted from long-range transport.

Similarly, the NO_x/NO_y ratio is also indicative of the degree of photochemical aging experienced by an air parcel. NO_x represents the most photochemically active fraction of NO_y. For relatively fresh emissions, nearly all of the nitrogen oxides would be in the form of NO_x, since time is required for NO_x to convert to other nitrogen oxide compounds. This would result in a NO_x/NO_y ratio near one. Ratios of one were, in fact, observed at times, suggesting fresh plumes arrived on those occasions. More often, however, the ratio was much lower—around 0.25 to 0.5 in summer, and 0.45 to 0.6 in winter. This is consistent with the idea that Big Meadows is mainly removed from strong local sources of NO_x, and generally receives air parcels that have undergone photochemical processing during long-range transport before arriving at the site (Hallock-Waters 2000).

Cooper and Moody (2000) examined back trajectories for air masses arriving at Big Meadows from 1989-1994 during periods of relatively high and relatively low O_3. They found that in springtime, air masses associated with low O_3 concentrations were more likely to arrive from the north, whereas air masses associated with higher O_3 concentrations were more likely to arrive from the southwest. During the summertime, air masses associated with low O_3 concentrations were more likely to have originated to the south of Big Meadows, while air masses associated with high O_3 concentrations were most likely to have come from the west. In addition, air masses arriving at Big Meadows with high O_3 concentrations during both seasons were generally associated with high pressure systems and often descended from higher altitudes. In contrast, air masses arriving at Big Meadows with lower O_3 concentrations were generally associated with low pressure systems and approached the site from low elevations.

Sources of NO_x include both stationary and mobile sources. Sulfur dioxide and CO can be used as tracers of these sources, since stationary sources emit large quantities of SO_2 but relatively little CO, while mobile sources emit large amounts of CO but little SO_2. Stehr et al. (2000) used two approaches to examine the relationship between NO_x, CO, and SO_2 at Big Meadows. Data used in the study were collected from September through December, 1996. The first approach involved using U.S. EPA emissions data to estimate the SO_2/NO_y ratio for stationary sources and the CO/NO_y ratio for mobile sources. These ratios were used along with the measured concentrations of CO and SO_2 at Big Meadows to estimate the fraction of NO_y

attributable to mobile and point sources. The second approach used linear regression to fit the concentrations of NO_y as functions of SO_2 and CO. Both approaches yielded similar results. Based upon the results of these two analysis methods, Stehr et al. (2000) estimated that approximately 34% of NO_y at SHEN resulted from point sources. Hallock-Waters (2000) also examined the correlation between NO_y and both CO and SO_2, finding NO_y correlated reasonably well with both; this also suggested that sources of NO_y at Big Meadows include both stationary and mobile sources.

The observed O_3 concentration at Big Meadows is the result of several atmospheric processes, including horizontal transport, vertical mixing, and local O_3 production. During transport, both formation and destruction of O_3 occurs; the extent of each is dependent on the source regions and transport path. VOC and CO measurements at Big Meadows can help infer the local O_3 production component. Biogenic emissions of isoprene and other very reactive VOCs typically constitute the dominant precursors for O_3 formation in rural environments (Goldan et al. 2000). At Big Meadows, the measured biogenic fraction of VOC accounted for approximately 70% of the O_3 formation potential. However, air mass aging, dilution, and prior O_3 formation have reduced the overall anthropogenic VOC concentration to fairly low O_3 formation potential at SHEN. Based on model projections, the local production of O_3 accounts for only about 43% of the observed O_3, whereas 50% of daytime O_3 in SHEN is attributable to transport from other areas (Kang et al. 2001). Several VOCs have been measured at SHEN at concentrations greater than those often reported in urban areas. In addition, there is evidence for an anthropogenic VOC source to the southwest of the park that emits several chlorinated organics (Zika 2001).

Often overlooked in the discussion of O_3 formation is the contribution of CO, which is a precursor of relatively low reactivity, but which often occurs at high concentrations (160 to 180 ppb average during summer) compared to the other VOC species. Thus, when more reactive VOC species are not available and when O_3 formation occurs over periods of several days, the O_3 formed from CO can be important to the total observed. Overall, 29% of the variance in summer season O_3 at SHEN is associated with CO (Hallock-Waters 2000). At Big Meadows, CO has weak diurnal and weak seasonal variation. However, the O_3 to CO correlation has a seasonal variation that is positive in summer (O_3 formation) and negative in winter (O_3 destruction). Over the period from 1988 to 1997, CO concentrations were observed to decrease by 5 ppb/year (-22.9% change) at Big Meadows (Hallock-Waters et al. 1999). This is similar to

the 18.3% decrease in emissions reported by EPA for the entire United States (U.S. EPA 1998b) and the 21% decrease reported at Big Meadows in 1999. Thus, the Big Meadows site appears to be regionally representative. The fact that O_3 showed little or no statistical decrease at Big Meadows during this period, yet both CO and VOC emissions decreased in the 1995-1999 period, suggests that NO_x is more likely to be controlling in summertime O_3 events (Hallock-Waters 2000, Poulida et al. 1991).

Computer Modeling of VOC Photochemical Reactions and Ozone Formation

Computer modeling was used to assess the effects of VOC concentrations at SHEN on local production of O_3. Extensive data were collected over a five year period at SHEN (Big Meadows) and at locations in two other eastern parks (Great Smoky Mountains [GRSM] and Mammoth Cave [MACA]) that can be used for comparison and model evaluation. Observational data were compared to output from the Multiscale Air Quality Simulation Platform (MAQSIP) model, an emissions-based comprehensive Eulerian grid model (Kang et al. in review, Mathur et al. in review).

The modeling domain was chosen so as to adequately represent conditions at the three subject eastern national parks (Kang et al. 2001). The subdomain of this modeling system consisted of 35 x 43 cells using 36-km horizontal resolution. The vertical domain varied from the surface to the stratosphere and was separated into layers. Only concentration fields in the lower 12 layers nearest the surface were extracted from the model output for this evaluation. The time period chosen for the model exercise was 12:00 pm July 14 to 12:00 pm July 29, 1995, to take advantage of the greater VOC sampling frequency during that period and because photochemical activity is at a maximum in July (Kang et al. 2001). Several scenarios were run with different emissions levels to estimate the effects of emissions changes on O_3 formation. Since our primary concerns were rural areas and the characteristics of biogenic hydrocarbons, represented by isoprene, rather than anthropogenic hydrocarbons, emissions of isoprene were varied in the scenarios more than other VOCs.

The model provided an estimate of the overall O_3 production and the extent to which the observed O_3 at Big Meadows was produced locally. Input to the model included emissions inventory and meteorological data plus emissions levels of biogenic isoprenes, which were estimated using the Biogenic Emissions Inventory System (BEIS3) model. Model output was compared to measured O_3, anthropogenic VOC, and isoprene concentrations at the three parks.

The observed O_3 at Big Meadows was a combination of transported and locally-produced O_3, as described in the previous section.

The mean daily total O_3 production (P_{O3}) through photochemical reactions within the model domain is shown in Figure V-9. This parameter was evaluated as the average of hourly O_3 production from 10 AM to 5 PM for each day during the modeling period. Of the three locations, MACA consistently was simulated to have the largest P_{O3}, GRSM the least, and SHEN intermediate. Ozone production rates at SHEN and GRSM were substantially (about one-fourth) less than those in and immediately downwind of urban areas. Variations across the scenarios suggested that O_3 production is significant when total VOC levels increase up to the highest VOC level observed at MACA, but simulated O_3 production was not sensitive to VOC emissions increases at GRSM and SHEN.

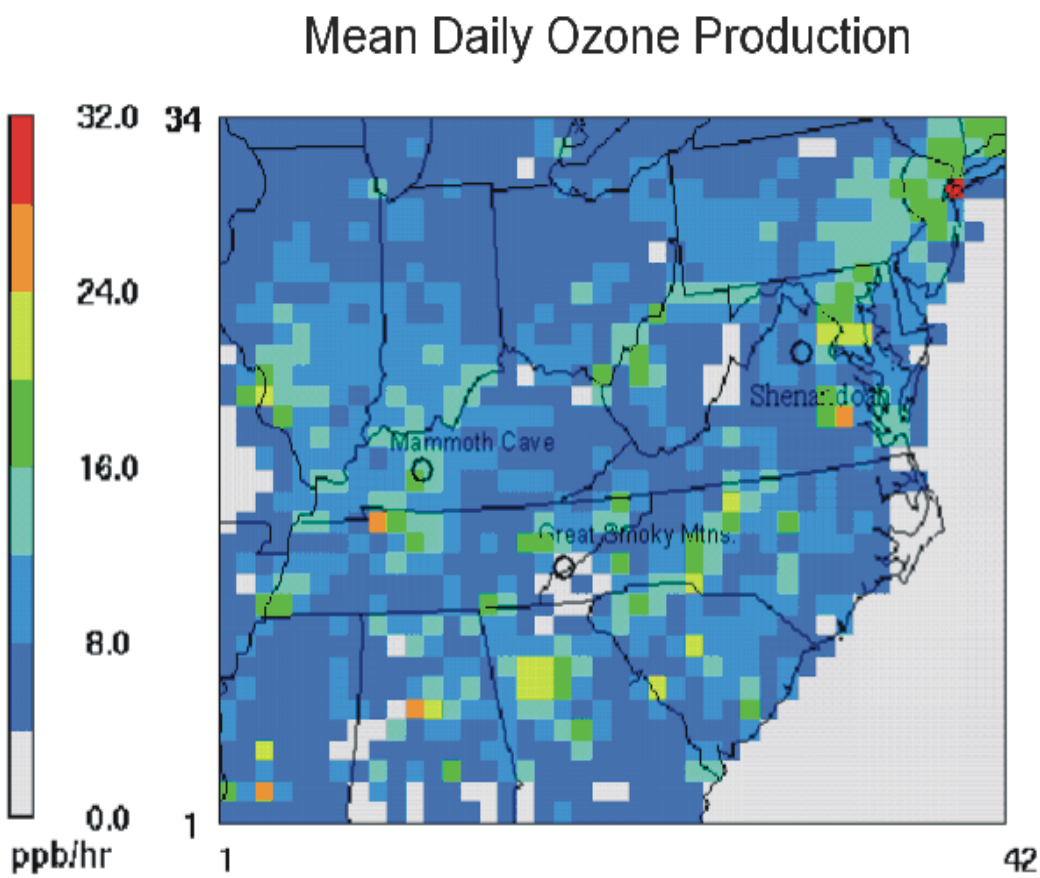

Figure V-9. Mean daily ozone production rates during the modeling period in 1995. Production rates are coded for each cell in the modeling domain. Largest production rates are near urban centers. The area around SHEN had a fairly low simulated ozone production rate.

The average simulated VOC loss (L_{VOC}) due to photochemistry during the photochemically active period of each day over the entire modeling period is presented in Figure V-10. It is interesting to note that, unlike O_3 chemistry in which MACA was always simulated to have the largest P_{O3}, the largest simulated L_{VOC} always appeared at SHEN. Reactive VOCs react not only with hydroxide (OH^-) to produce O_3, but also directly with O_3 as well. One possible explanation for the simulated higher VOC photochemistry but lower O_3 production due to photochemistry at SHEN lies in the fact that reactive VOC species (i.e., isoprene) constitute a larger share of total VOCs at this location. The reactive part of the VOCs reacts with O_3 readily, leading to O_3 removal rather than O_3 formation. Isoprene concentrations at SHEN (mean mid-day concentration: 3.36 ppbv) were much higher than those at MACA (mean mid-day concentration: 0.78 ppbv). Thus, although more VOC is undergoing reaction at SHEN, the net O_3 production is lower than at MACA.

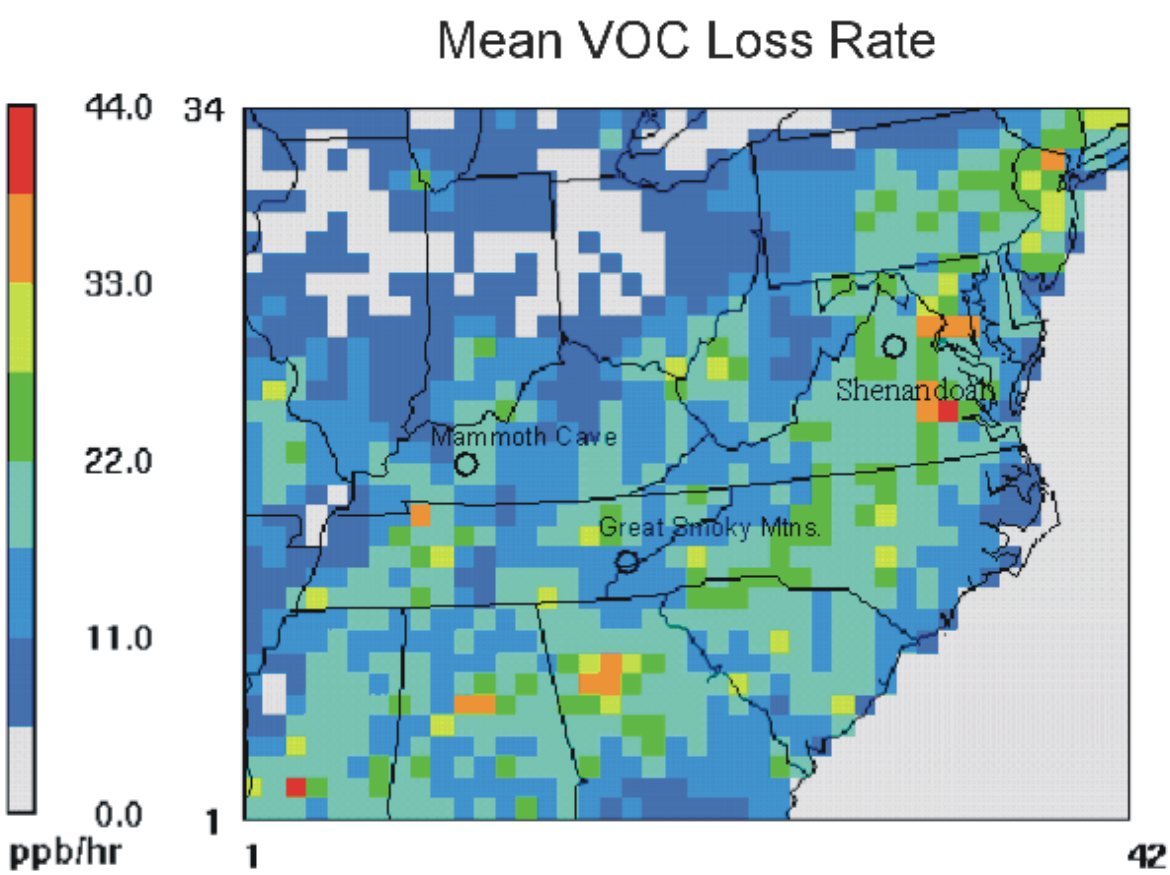

Figure V-10. Domain plot of the simulated average VOC loss (L_{VOC}) due to photochemistry.

The relationship between net O_3 production (P_{O3}) and VOC loss by reaction (L_{VOC}) at the three locations is presented in Figure V-11. Note that VOCs are consumed as O_3 is produced by the photochemical reactions. (For convenience's sake, the negative sign of the VOC chemistry term is changed to positive). Model output suggested that the consumption of VOCs contributed to an approximately linear production of O_3 at all three locations, but the actual relationship between simulated O_3 production and VOC consumption varied from location to location.

The ozone production efficiency can be expressed by the ratio of the ozone production to the VOC loss. Thus the potential for O_3 production (VPOP) is defined as:

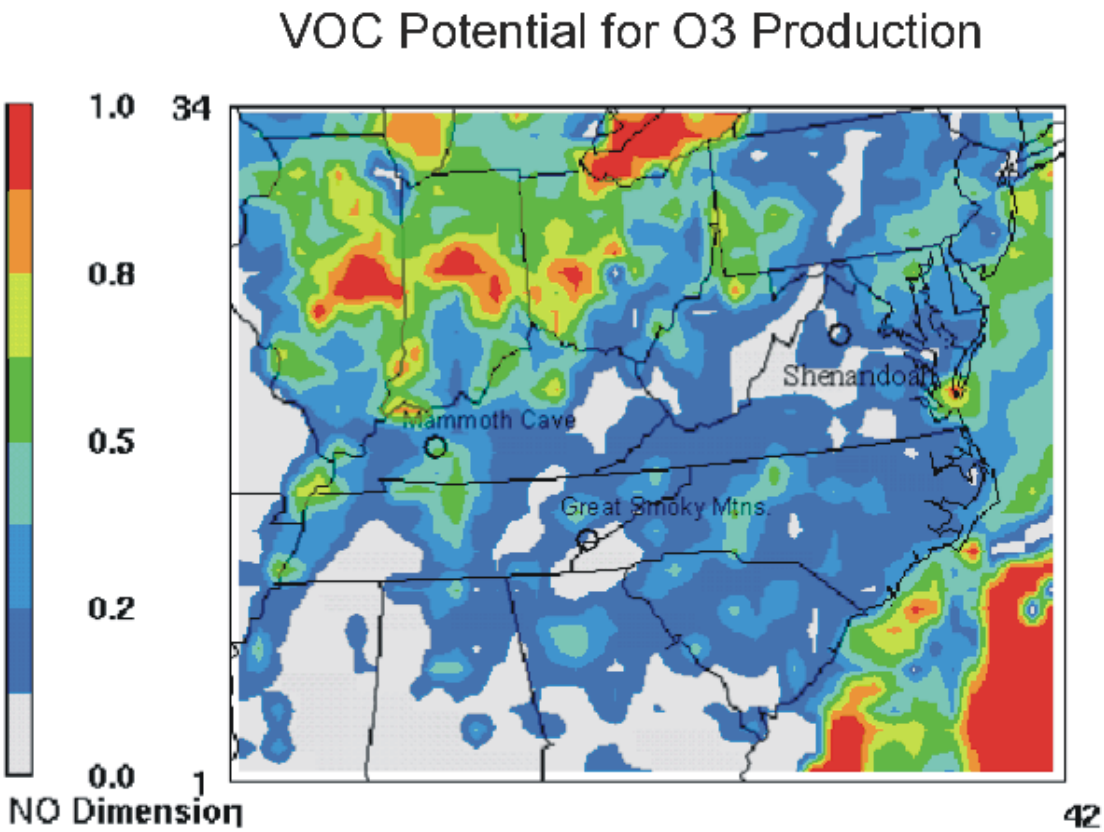

Figure V-11. Simulated values of VPOP, the O_3 production efficiency of VOC photochemistry. Areas in the Midwest were simulated to have high VPOP and therefore may be more sensitive to changes in VOC concentration. SHEN is located in a region that appears to be relatively insensitive to VOC change.

$$VPOP = \frac{d\,[O_3\ chemistry]}{d\,[VOC\ chemistry]}$$

VPOP is a measure of how much O_3 is produced per unit of VOCs consumed or, in other words, the O_3 production efficiency of VOC chemistry.

As shown in Figure V-11 for the modeling domain, the ratios (in ppbv) of O_3 production to VOC consumption, were 0.065 (GRSM), 0.11 (SHEN), and 0.36 (MACA). The model output suggested that local O_3 production from VOC photochemistry is inefficient at SHEN during summer. It is interesting to note that if VOC chemistry is set to zero, values for O_3 production due to photochemistry are similar at all three locations (3.1 to 4.4 ppbv/hr). These values may represent background O_3 production from inorganic reactions such as, for example, with CO and methane (CH_4) plus contributions from very-long range transport and from stratospheric exchange.

The sensitivity of net O_3 production to additional VOC can be expressed relative to the base scenario which was selected to represent existing conditions. If we define the maximum VOC capacity point (MVCP; the point at which any further addition of VOCs reduces O_3 concentrations) as:

$$\text{MVCP} = \text{VOC emission (kgC/km}^2\text{hr) when } \frac{d\,[O_3]}{d\,[VOC]_e} = 0$$

where $[O_3]$ is O_3 concentration, and $[VOC]_e$ is VOC emissions (kgC/km^{2}hr), then the simulated MVCPs are 1.59 (GRSM), 2.61 (MACA), and 2.02 (SHEN) kgC/km^{2}hr (Figure V-12). Both MACA and SHEN in the base scenario have not reached their MVCPs, so any additional VOC emissions at these two locations may increase O_3 concentrations. Therefore, the MVCP, combined with the emissions data, can be used as a measure to determine if a location is NO_X-limited. In older models that used O_3 isopleths, when VOC concentrations are increased within a NO_X-limited area, the O_3 concentration usually levels off, with no such capacity points as MVCP. However, at all three locations, the model results reported here suggested the existence of MVCP. This condition is expected to occur primarily during summer when biogenic organic emissions produce a local abundance of VOC in rural areas. When isoprene emissions are increased by three-fold in the model, the estimated increase in O_3 at SHEN is relatively small (0-5%). In contrast, the estimated increases at GRSM are up to 10% and at MACA up to 15%.

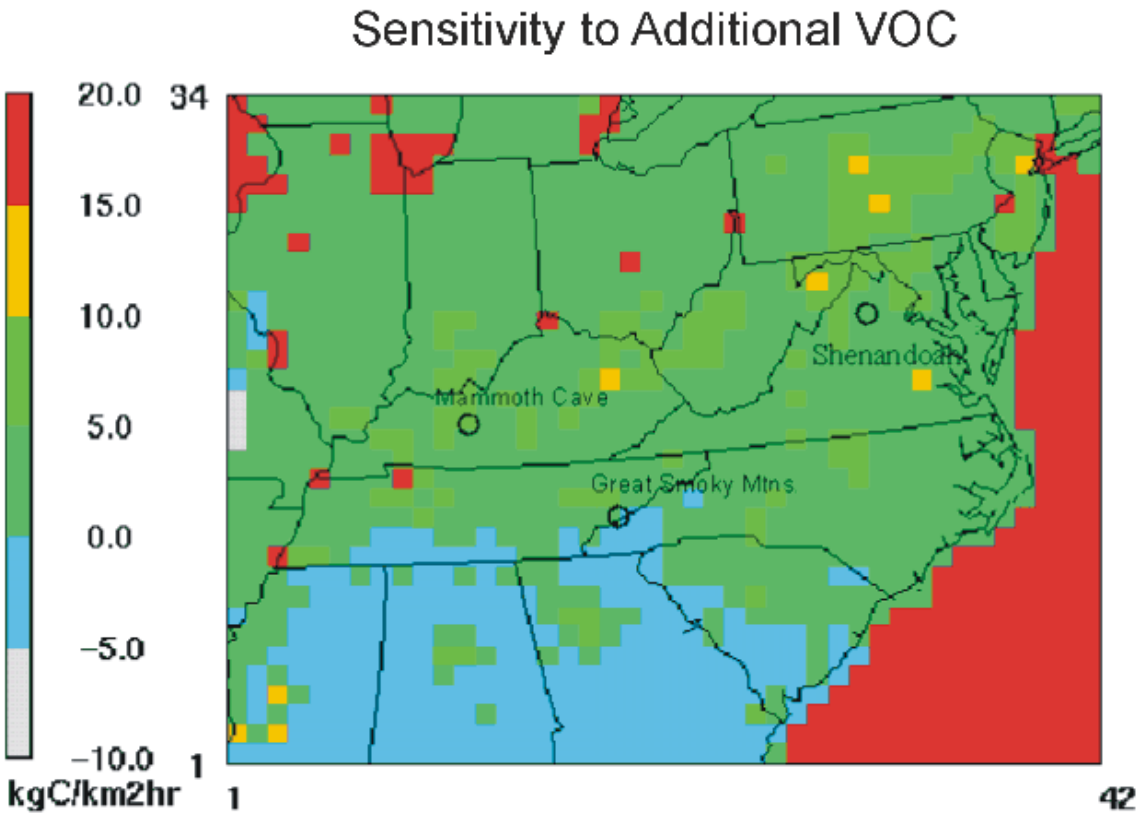

Figure V-12. Sensitivity to added VOC. Positive values suggest that with an increase of VOC emissions above the Base Scenario, O_3 concentrations will increase. Negative values suggest that the MVCP point has been reached before the emissions level for the Base Scenario, and at the Base Scenario emissions rate O_3 concentration will decrease. The MVCP points are never reached within the designed emissions perturbation scheme in the red areas.

The results of this analysis suggest that there are distinctive characteristics of O_3 distribution, transport, and production at different locations, perhaps partly in response to different elevations. At SHEN, the model output suggested that reducing anthropogenic VOC emissions will not reduce O_3 concentrations. Since transport dominates local O_3 concentrations at high-elevation sites, the most effective O_3 reduction strategy is to reduce O_3 levels in the source areas from which it is transported. The apparent existence of MVCP implies that the large amounts of reactive biogenic VOCs that are often found in densely vegetated environments during summer may help moderate local production of O_3 under NO_X-limited conditions.

2. Visibility

Visitors come to national parks in part to experience the breathtaking views of mountains, valleys, clear skies, and unique geologic features. Air pollution interferes with this experience to some degree in virtually all national parks, particularly in the eastern United States. Visibility is an especially important resource at SHEN. The Southern Appalachian National Park Committee's Report to Congress of 1924 emphasized the importance of the views from a "possible sky-line drive along the mountain top" in evaluating the suitability of the Shenandoah area for establishment of a national park. Shenandoah's Skyline Drive is on the National Register of Historic Places and features 69 historic overlooks that span the Park's 170-km length. Skyline Drive and the nearby Appalachian National Scenic Trail are designated SHEN cultural landscapes. Skyline Drive is also a designated Virginia State Scenic Highway. SHEN is one of three parks that are considered "regionally representative parks" where visibility is considered an important preservation value by the public (Chestnut and Rowe 1990). However, the views that gave the Blue Ridge its name are often obscured by human-caused haze.

The following sections describe first the current visibility conditions and recent trends throughout the United States and then the conditions and trends within SHEN. The visibility metric most often used in this discussion will be the light extinction coefficient (b_{ext}) , with parenthetical references to the corresponding visual range (VR). The reader is referred to Section III.F.1c and Appendix B for the definitions and relationships among visibility metrics.

a. National Conditions and Trends

In 1987, the IMPROVE visibility monitoring network was established as a cooperative effort between EPA, NPS, USDA Forest Service, Bureau of Land Management, U.S. Fish & Wildlife Service, NOAA, and state governments. The objectives of the network are to establish current conditions, to track progress toward the national visibility goal by documenting long-term trends, and to provide information for determining the types of pollutants and sources primarily responsible for visibility degradation.

Current National Conditions

Chemical analysis of particle measurements provides ambient concentrations and associated light extinction for PM_{10}, $PM_{2.5}$, sulfates, nitrates[1], organic and light absorbing carbon (LAC), soil, and a number of other elements. The data summaries from EPA, NPS, and IMPROVE that follow are based on data from the IMPROVE network. Figure V-13 provides a graphic view of all the IMPROVE deployed sites in operation as of December 1999 (Malm et al. 2000). The network has undergone a significant expansion in 2001 and these data will be available for future assessments.

Figure V-14 shows isopleths of current annual average visibility conditions calculated from March 1996 - February 1999 IMPROVE particle data (CIRA 2001). The same data are presented on all three maps but are represented in terms of the indices: b_{ext} (Mm^{-1}), haziness

Figure V-13. IMPROVE Monitoring Sites.

[1] In May 2001, the NPS and other participants of the IMPROVE Program identified technical concerns about measured nitrate concentrations at all IMPROVE sites prior to June 1996, and about estimates of sulfate, primarily at eastern IMPROVE sites prior to 1995. A discussion of the technical concerns can be found on the IMPROVE Web site, http://vista.cira.colostate.edu/IMPROVE/Data/QA_QC/issues.htm.

Figure V-14.

Average 3-year visibility (March 1996 - February 1999) reconstructed from IMPROVE aerosol data and represented as:

(a) Light extinction coefficient (Mm^{-1})

(b) Haziness (deciview)

(c) Standard visual range (km)

(deciview [dc]), and standard visual range (SVR; km). Because only a few IMPROVE monitoring sites exist in the eastern United States, isopleths cannot be drawn with a high degree of accuracy. The poorest visibility, highest light extinction (more than 120 Mm^{-1}, about 25 dv, or 33 km SVR) occurs in the eastern United States, whereas the best visibility, lowest light extinction (less than 22 Mm^{-1}, about 8 dv, or 178 km SVR) occurs in the Great Basin, central Rocky Mountains, and non-urban southwest. Comparison of current conditions with the natural conditions given in Section V.B (8.1 dv and 4.7 dv for the East and West, respectively) indicates a high degree of current degradation.

In order to remedy existing visibility impairment, the EPA promulgated the Regional Haze Regulations that require states to adopt plans that achieve progress toward a national goal of no human-caused impairment. The regulations specifically call for improvement of the haziest days (mean of the "worst" 20%) and no degradation of the clearest days (mean of the "best" 20%). Figures V-15a to V-15c (U.S. EPA 2001c) illustrate current levels of visibility impairment, in terms of deciviews, for the clearest, middle (typical), and haziest 20% days based on IMPROVE data from 1997-1999.

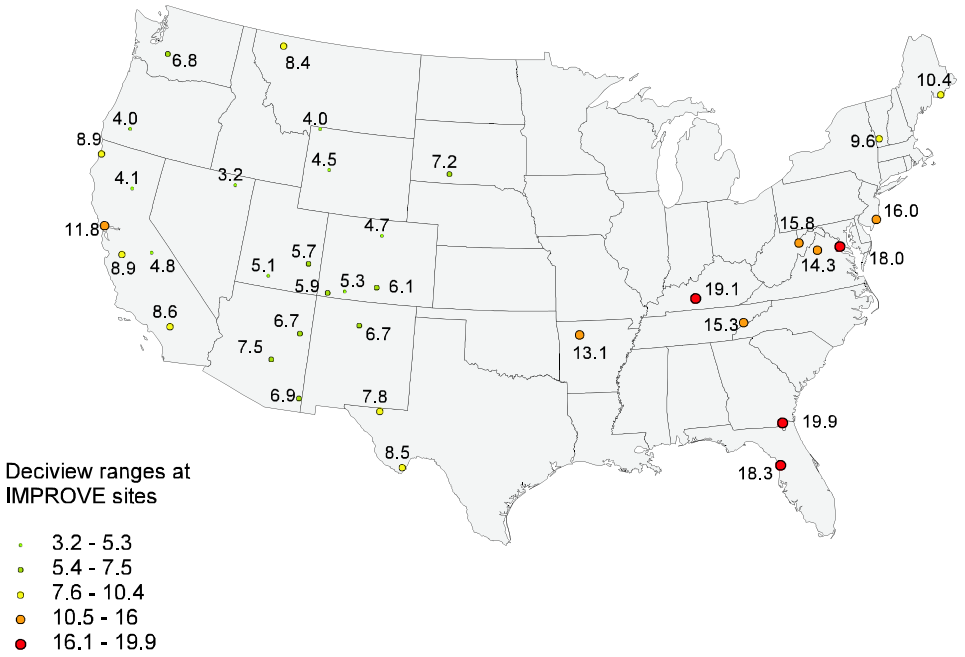

Figure V-15a. Current visibility impairment expressed in deciviews for the clearest 20 percent days based on 1997-1999 IMPROVE data.

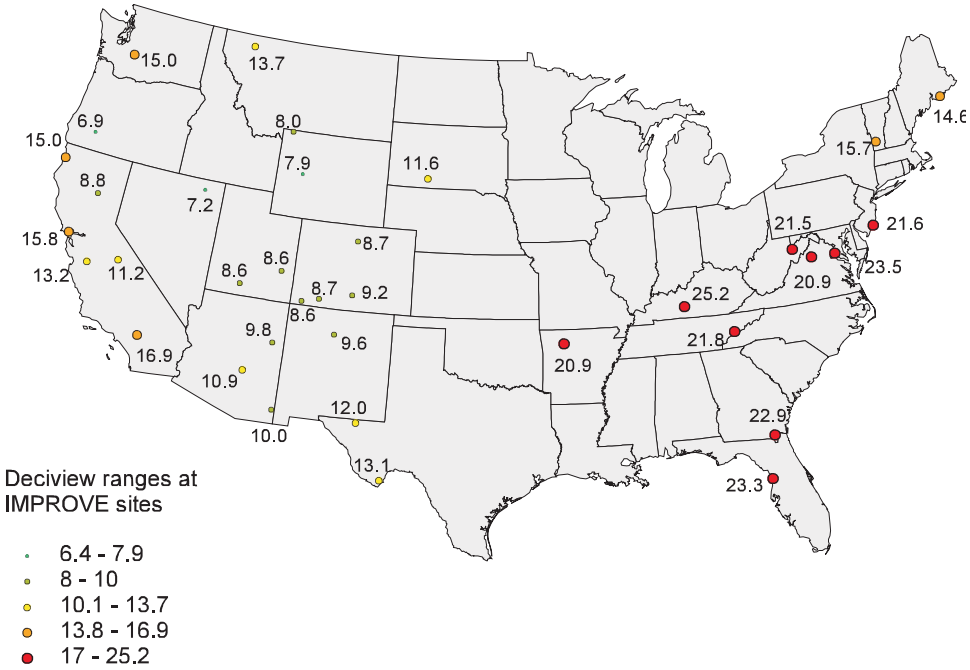

Figure V-15b. Current visibility impairment expressed in deciviews for the middle 20 percent days based on 1997-1999 IMPROVE data.

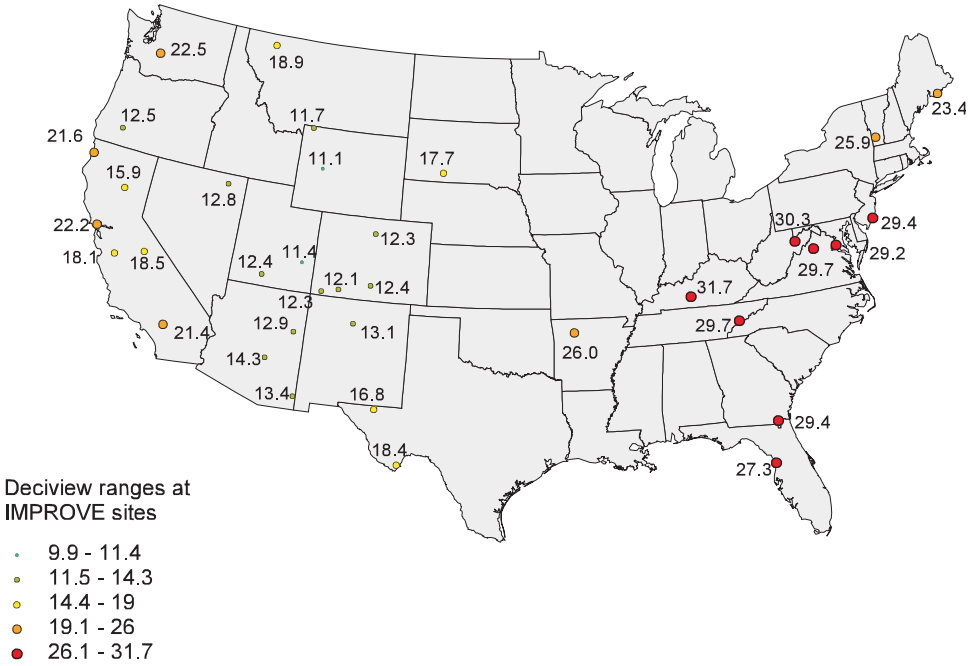

Figure V-15c. Current visibility impairment expressed in deciviews for the haziest 20 percent days based on 1997-1999 IMPROVE data.

Historical Trends

Since the late 1940s, there have been a number of particle and visibility monitoring programs implemented in the United States, most notably the National Weather Service (NWS) and IMPROVE Programs. Trends in visibility degradation can be inferred from these long-term records of visual range. Figures V-16 through V-19 describe long-term visibility degradation trends derived from such data.

Airport Observations

The isopleths of the 75th percentile visual range, shown in Figure V-16, were derived from airport data from 1950 through 1994 (Schichtel et al. 2001). Winter includes January, February, and March; spring includes April, May, and June; summer includes July, August, and September; and autumn includes October, November, and December. The reference scale

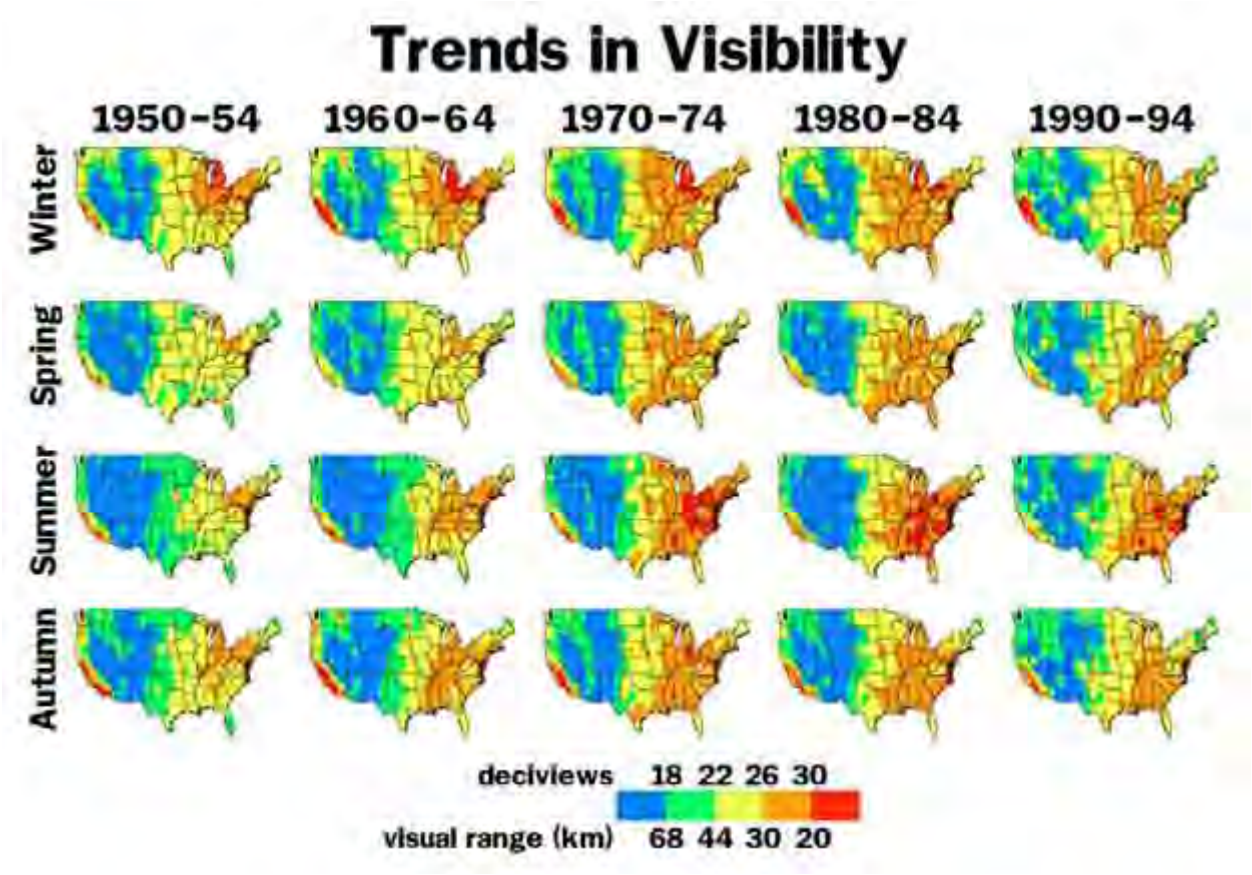

Figure V-16. Trends in 75th percentile visual range over the United States from 1950 through 1994. These data have been filtered for weather and adjusted to a relative humidity of 60% (Schichtel et al. 2001).

takes into account site-specific target considerations and human-eye sensitivity (red being worst, blue being best). The prominent nationwide features are fairly apparent. For example, visibility is generally better in the west (southern California excepted) and poorer in the East and the summer season provides the worst visibility in the East and the best in the West. Historical trends of generally decreasing visibility in the eastern portion of the country are quite evident in Figure V-16. The poorest visibility occurs in summer, and the winter months have somewhat better visibility. There have also been changes observed over time:

- In winter, there was some improvement in visibility in the north-central United States from the period 1950-54 to the period 1990-1994. However, during the 1960s and 1970s, the winter season showed decreased visibility in the Southeast.
- The spring season showed a degradation of visibility throughout the entire eastern United States, especially along the Gulf Coast and the south and central East Coast.
- In summer, a region of poor visibility in the eastern United States during 1950 to 1954 steadily expanded and became worse, until the entire eastern United States was substantially degraded. By the 1970s, summer was the haziest season in the eastern United States.
- The autumn season showed some improvement in the north central industrial areas in recent years, with little change in the remainder of the east.

IMPROVE Data

IMPROVE seasonal patterns are graphically portrayed in Figure V-17 (Malm et al. 2000). (Note that this figure includes only particle extinction and does not include the Rayleigh scattering effect.) The summer extinction coefficient is the greatest in the East, with the greatest seasonal differences also occurring in the East. In the West, the worst visibility conditions can occur in any season, and the seasonal differences are not as pronounced as they are in the East. These East-West differences are due in part to the greater pollutant emissions (particularly SO_2) and high relative humidity in the East. Annually, SO_4^{2-} species comprise over 70% of the measured visibility impacts in the East.

IMPROVE data from the 36 Class I area monitoring sites across the United States that have a minimum of 10 years of monitoring data each, were analyzed for upward and downward light extinction trends using nonparametric regression methodology (U.S. EPA 2001c). Table V-9 summarizes the trends analysis performed on these 36 sites for haziness (expressed in deciviews)

Figure V-17. Summary plot of calculated light extinction and the fractional contribution of each species for the 20 monitoring regions in the IMPROVE network (Washington, D.C. is not shown).

Table V-9. Summary of Class I area extinction trend analysis[a].

Parameter	Number of Sites With Significant[b] Upward Haziness (Deteriorating Visibility) Trends		Number of Sites With Significant[b] Downward Haziness (Improving Visibility) Trends	
	West	East	West	East
Deciviews, worst 20% [c]	4	0	1	2
Deciviews, middle 20% [c]	0	0	6	2
Deciviews, best 20% [c]	0	0	9	1
Light extinction due to sulfate, worst 20%	4	0	4	2
Light extinction due to sulfate, middle 20%	1	1	6	4
Light extinction due to sulfate, best 20%	0	1	14	0

[a] Based on a total of 36 monitored sites with at least 10 years of data in the West and eight years of data in the East: 26 sites in the West, 10 sites in the East.
[b] Statistically significant at the 5-percent level.
[c] For deciview trends changes in nitrate concentrations were not considered in the trend analysis. A constant value based on mean 1997 – 1999 extinction associated with nitrates was substituted for all years.

and light extinction due to sulfates on an area-by-area basis. Figures V-18 and V-19 graphically depict the significant trends for the Class I areas as summarized in Table V-9. A solid dot indicates the IMPROVE monitoring site location. An up-arrow indicates increasing haziness and therefore a deteriorating visibility trend, and a down-arrow indicates an improving visibility trend. The different color arrows represent the cleanest 20% of days, middle 20% of days, and haziest 20% of days. As shown in Figure V-18, several sites in the eastern United States with improving trends show improvement in more than one of the three quintiles. Figure V-19 also shows there are improving trends associated with aerosol b_{ext} due to SO_4^{2-} in the East.

b. Current Conditions and Trends in SHEN

As part of the IMPROVE monitoring network, visual air quality at SHEN has been monitored using an aerosol sampler, nephelometer, transmissometer, and camera. The aerosol sampler has operated from 1982 through the present. The IMPROVE network upgraded the

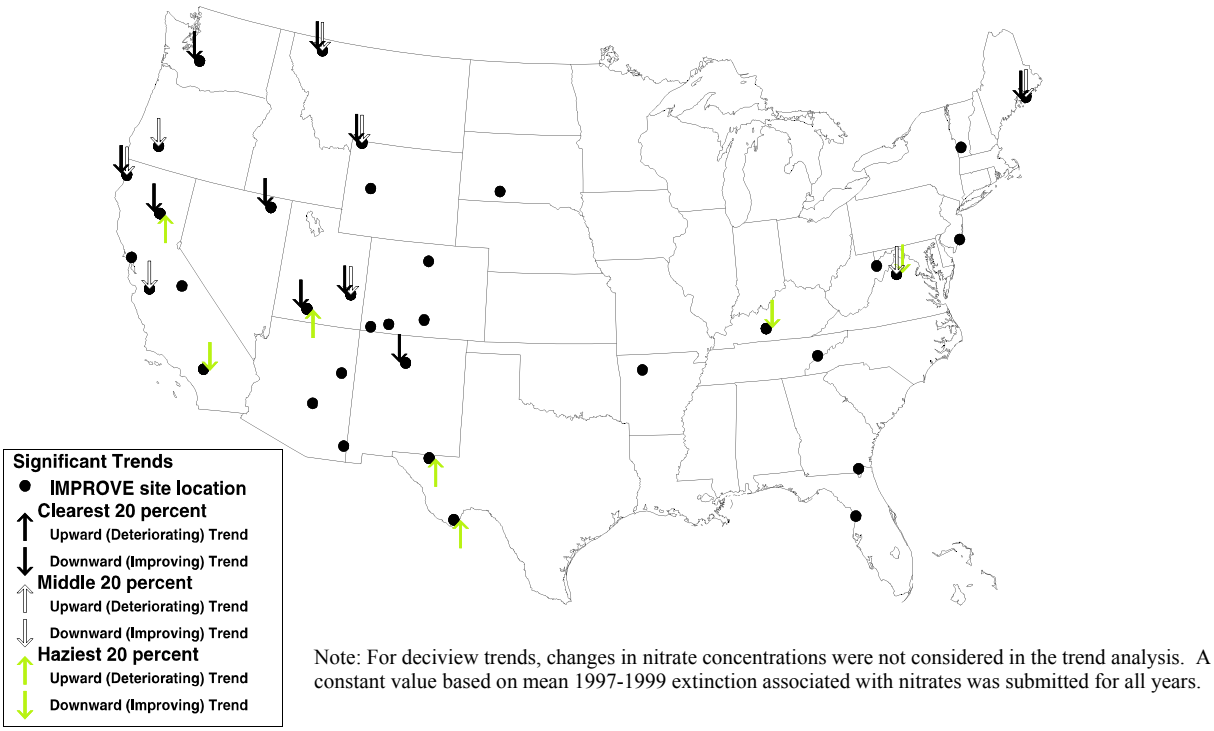

Figure V-18. Class I area significant trends in haziness for the clearest 20%, middle 20%, and haziest 20% days, as summarized in Table V-9.

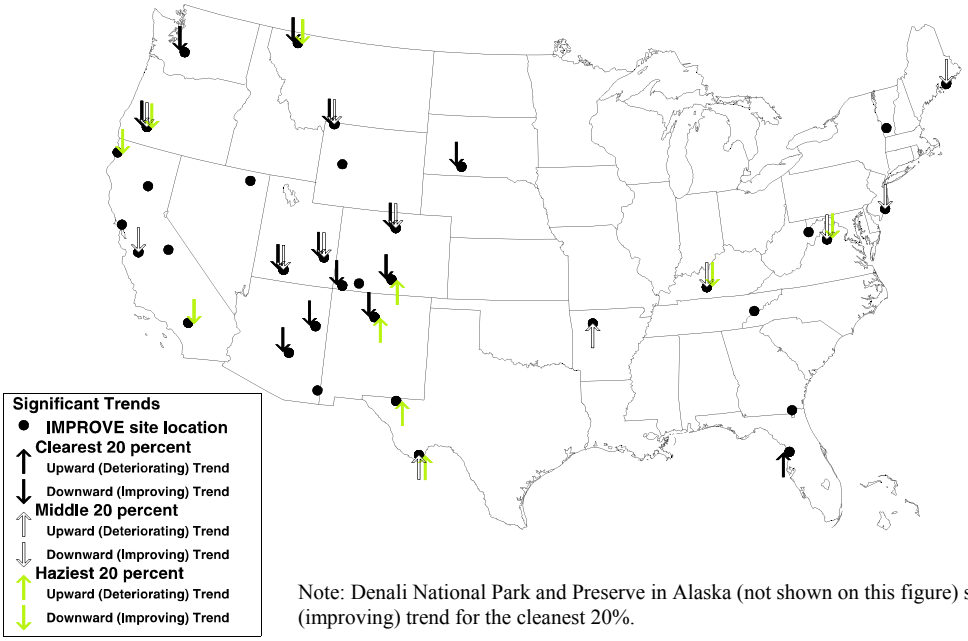

Note: Denali National Park and Preserve in Alaska (not shown on this figure) showed a downward (improving) trend for the cleanest 20%.

Figure V-19. Class I area significant trends in light extinction due to sulfate for the clearest 20%, middle 20%, and haziest 20% days as summarized in Table V-9.

SHEN sampler to an IMPROVE Version II sampler in January 2000. The transmissometer has been operating from December 1988 to the present. The nephelometer has been operating from September 1996 to the present. An automatic 35mm camera was operated at Skyland from July 1991 through April 1995, viewing west-northwest. Another automatic 35mm camera was operated at Dickey Ridge as part of an intercomparison study from July of 1991 through November 1991, viewing southwest.

Particle Monitoring

Particle data from the SHEN IMPROVE site have been summarized to characterize the full range of visibility conditions for March 1988 through February 2000, based on seasonal periods (spring: March, April, May; summer: June, July, August; autumn: September, October, November; and winter: December, January, February) and annual periods (March through February of the following year, (e.g., the annual period of 1998 includes March 1998 through February 1999).

The composition and concentration of visibility-reducing pollutants are generally quantified by aerosol sampling. Aerosol sampling provides a time-integrated (generally 24-hour average) measurement of the size, concentration, and chemical composition of visibility-related aerosols.

Prior to the calculation of multi-year average, yearly aerosol sampler data were checked for completeness using the criteria that:

- No more than nine samples in a row were missing at any time; and
- No less than 75% of all possible samples during a year had at least some data available.

SHEN data for 1995 did not meet these criteria, but because all missing data occurred in the winter, the other three seasons are displayed. No annual data are reported for this year.

Observed Concentrations

Table V-10 shows the mass concentrations ($\mu g/m^3$) of fine and coarse aerosol, and the chemical composition (mass budgets) of the fine aerosol for SHEN for the period March 1988 through February 2000. Note that these concentrations, particularly ammonium sulfate, exceed the natural conditions estimates given in Table V-3. Fine mass budgets for the mean of the cleanest, middle, and haziest 20 percent days are presented in Figure V-20.

Table V-10. Measured fine and coarse aerosol mass concentrations (in $\mu g/m^3$) for SHEN (March 1988 - February 2000).

Season	Fine Mass	Ammonium Sulfate	Ammonium Nitrate	Organics	Light Absorbing Carbon	Fine Soil	Coarse Mass
Spring	9.3	5.8	0.5	2.0	0.4	0.5	4.8
Summer	17.1	11.9	0.5	3.6	0.4	0.7	5.8
Autumn	9.9	6.2	0.5	2.3	0.4	0.4	4.9
Winter	5.7	3.1	0.5	1.5	0.3	0.2	3.0
Annual	10.5	6.8	0.5	2.4	0.4	0.5	4.7

Calculated Light Extinction Coefficients

Atmospheric b_{ext} (see Appendix B) generated from aerosol sampler data apportion the extinction at SHEN to specific aerosol species, Rayleigh scattering (the natural scattering of light by atmospheric gases), ammonium sulfate ($[NH_4]_2SO_4$) , ammonium nitrate (NH_4NO_3), organics, elemental (light absorbing) C, and coarse mass. The effects of relative humidity on extinction by $(NH_4)_2SO_4$ and NH_4NO_3 were based on monthly climatological averages. Common sources contributing to each aerosol species are as follows:

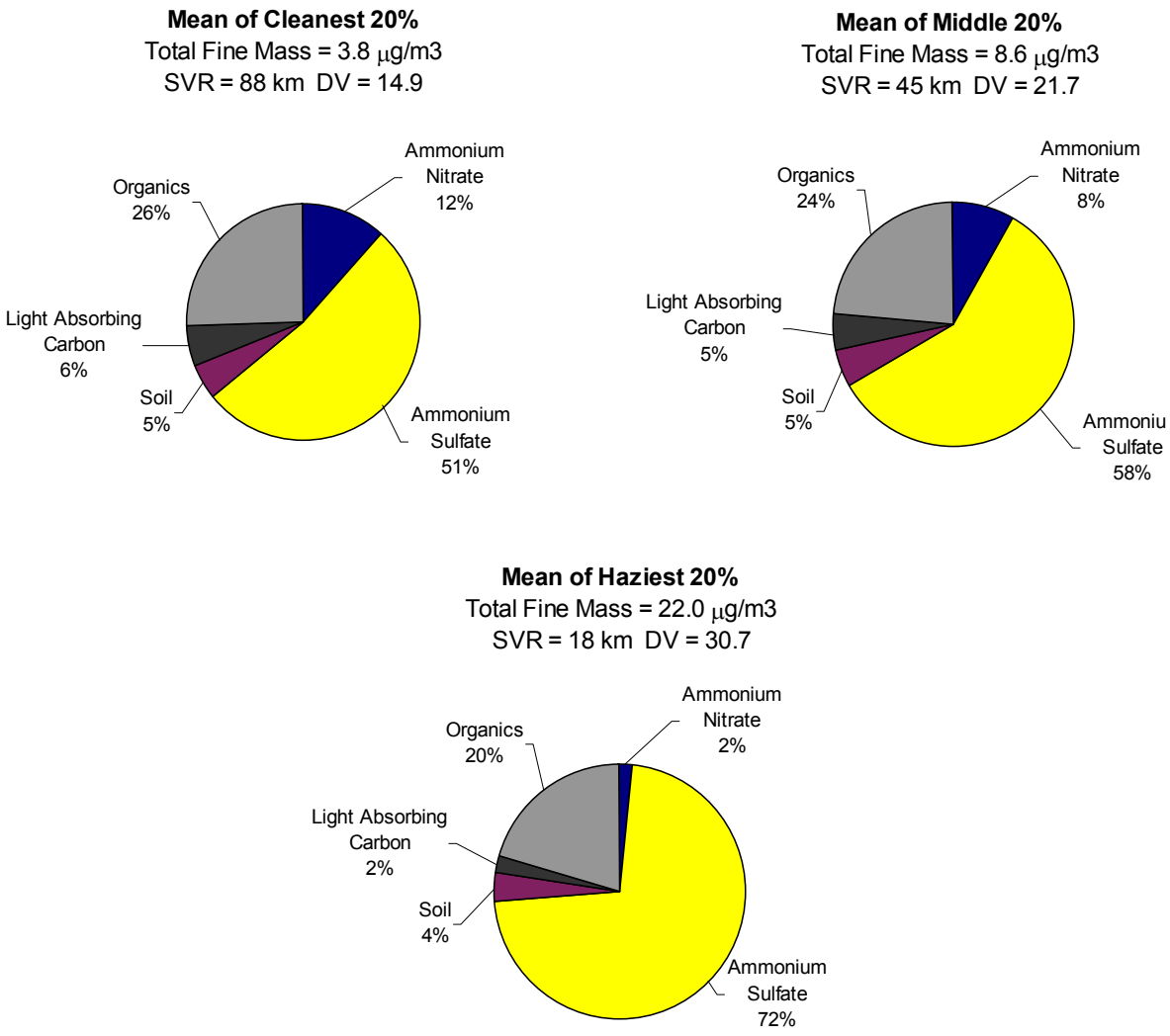

Figure V-20. Fine mass budgets (in percent) for the mean of the cleanest, middle, and haziest 20% of days for SHEN (March 1988 - February 2000). SVR refers to standard visual range and DV refers to the haziness index in deciviews.

Sulfate: Coal/oil fired power plants, refining and smelting activities;

Nitrate: Automobiles, combustion sources;

Organics: Biogenics (natural emissions), smoke, industrial solvents;

Light absorbing carbon: diesel exhaust, smoke;

Fine soil: Wind-blown dust, agricultural activities, off-road traffic;

Coarse particles: Dust, smoke, pollen.

This list is not complete and does not necessarily represent sources of pollution at SHEN. The sum of these species accounts for the majority of non-weather related visibility degradation. Figure V-21 depicts graphically the seasonal and annual variation in extinction budgets for the mean of the cleanest, middle, and haziest 20 percent. The "cleanest" and the "haziest" signify lowest fine mass concentrations and highest fine mass concentrations respectively, with "middle" representing the 20% of days with fine mass concentrations in the middle of the distribution. Each budget includes the corresponding b_{ext}, SVR, and dv. The segment at the bottom of each stacked bar in Figure V-21 represents Rayleigh scattering, which is assumed to be a constant 10 Mm^{-1} at all sites during all seasons. Higher fractions of extinction due to Rayleigh scattering indicate cleaner conditions. Comparisons of calculated extinctions for the 1988-2000 period (Figure V-21) to estimated natural conditions discussed in Section V.B.2 demonstrate that visibility in and near the park has been severely degraded. The average visual range for the cleanest days (Figure V-21) is presently about 90 km, or about 30% of what it was estimated to have been in the absence of anthropogenic air pollution (270 km). Figure V-22 further identifies average contributions of SO_4^{2-}, NO_3^-, organics, LAC, and coarse particles (including fine soil) by month for the period 1996-1998.

A tabular and graphic summary of average calculated extinction coefficient values by season and year for the March 1988 - February 2000 period are provided in Table V-11 and Figure V-23, respectively.

Trends

Data from other IMPROVE visibility sites around the country have been presented graphically (Section V.C.2.a) so that spatial, historical, and seasonal trends in visual air quality for SHEN can be understood in perspective. Figures V-20 through V-21, as well as Tables V-10 and V-11, have been provided to summarize visual air quality in SHEN during the March 1988 - February 2000 period. Seasonal variability in the mean of the haziest 20% fractions is driven primarily by $(NH_4)_2SO_4$ extinctions. Non-Rayleigh atmospheric light extinction at SHEN is largely due to organics and $(NH_4)_2SO_4$. Historically, visibility varied with patterns in weather, wind (and the effects of wind on coarse particles), and smoke from fires.

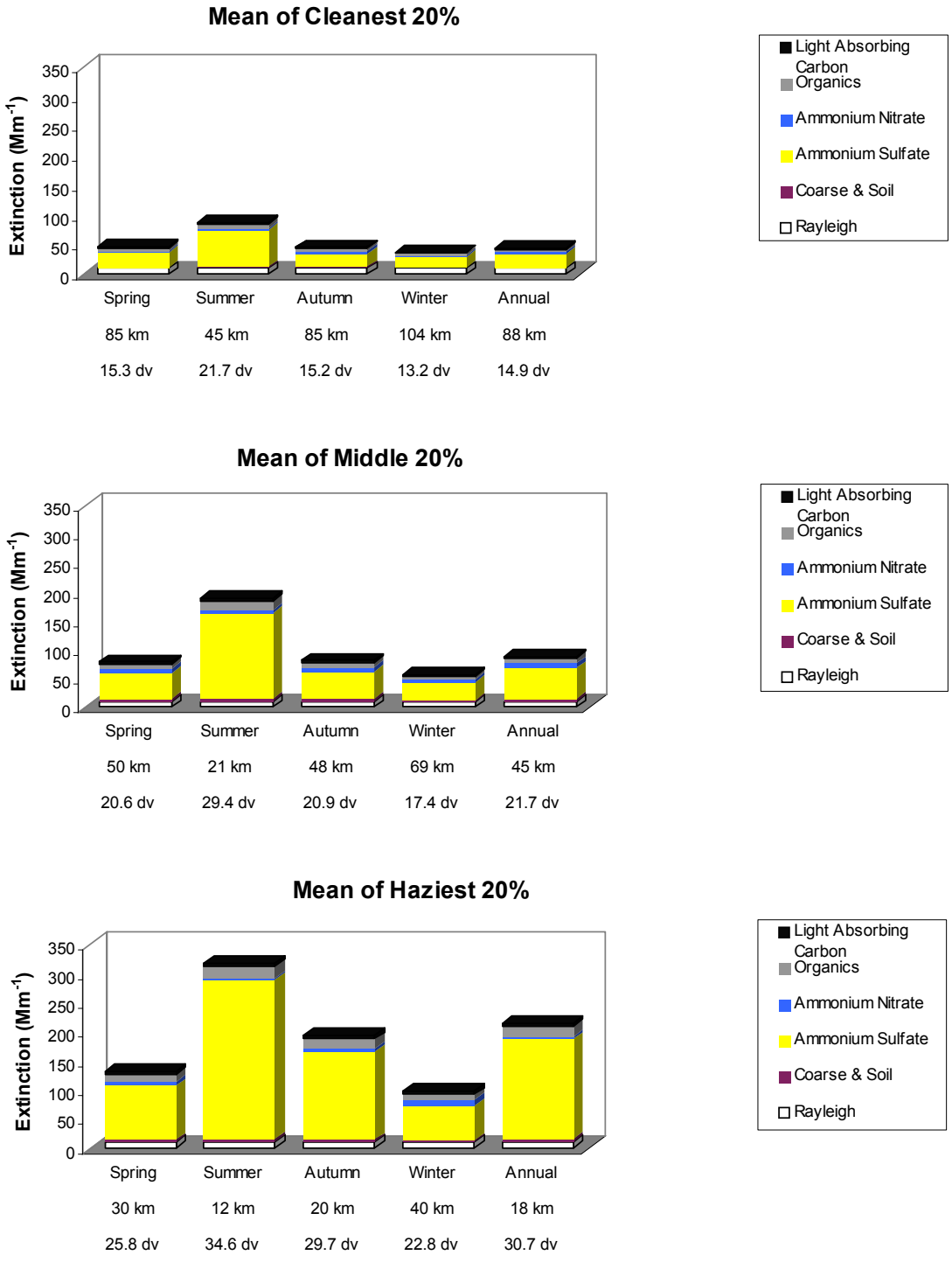

Figure V-21. Calculated extinction coefficient budgets for SHEN, March 1988-February 2000.

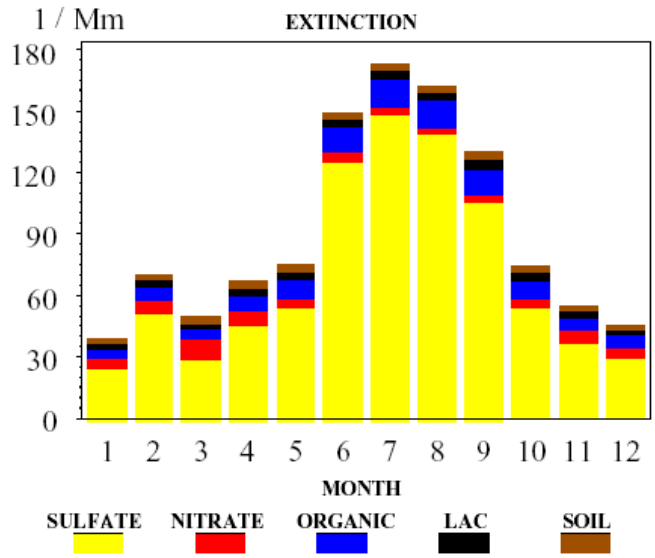

Figure V-22. Monthly contributions of total light extinction (excluding Rayleigh) contributed by sulfate, nitrate, organics, light absorbing carbon (LAC), and soil for SHEN (1996 – 1998).

Table V-11. Seasonal and annual average standard visual range (SVR; km) and calculated extinction (Mm^{-1}) at SHEN, March 1988 - February 2000.

Year	Spring (Mar, Apr, May)		Summer (Jun, Jul, Aug)		Autumn (Sep, Oct, Nov)		Winter (Dec, Jan, Feb)		Annual (Feb-Mar)[a]	
	SVR (km)	b_{ext} (Mm^{-1})	SVR (km)	b_{ext} (Mm^{-1})	SVR (km)	b_{ext} (Mm^{-1})	SVR (km)	b_{ext} (Mm^{-1})	SVR (km)	b_{ext} (Mm^{-1})
1988	40	98.1	30	132.4	39	100.7	70	56.1	39	100.2
1989	43	90.1	20	192.6	37	105.7	56	70.0	36	108.7
1990	44	88.6	19	202.2	38	104.3	67	57.9	35	110.8
1991	41	95.3	17	236.3	31	124.8	63	61.6	31	124.8
1992	45	87.5	20	199.0	36	107.5	54	72.4	34	113.7
1993	46	85.8	17	235.1	35	113.0	67	58.5	33	119.4
1994	54	73.0	17	223.9	40	98.1	75	52.0	36	108.9
1995	48	81.7	19	201.1	43	90.5	NA[c]	NA[c]	NA[c]	NA[c]
1996	54	72.3	21	181.9	46	84.7	59	66.2	40	98.0
1997	55	70.6	22	174.1	40	98.1	76	51.4	39	99.6
1998	51	76.7	23	173.0	39	101.5	63	61.7	39	101.4
1999	56	69.6	23	170.2	45	86.0	62	63.3	43	91.2
Mean[b]	47	82.4	20	193.5	39	101.2	64	61.0	36.8	107.0 [d]

[a] Annual period data represent the mean of all data for each March through February annual period.
[b] Combined season data represent the mean of all seasonal means for each season of the March 1988 through February 2000 period.
[c] Winter and annual average values are not available for 1995 because of missing data.
[d] Combined annual period data represent the mean of all combined season means.

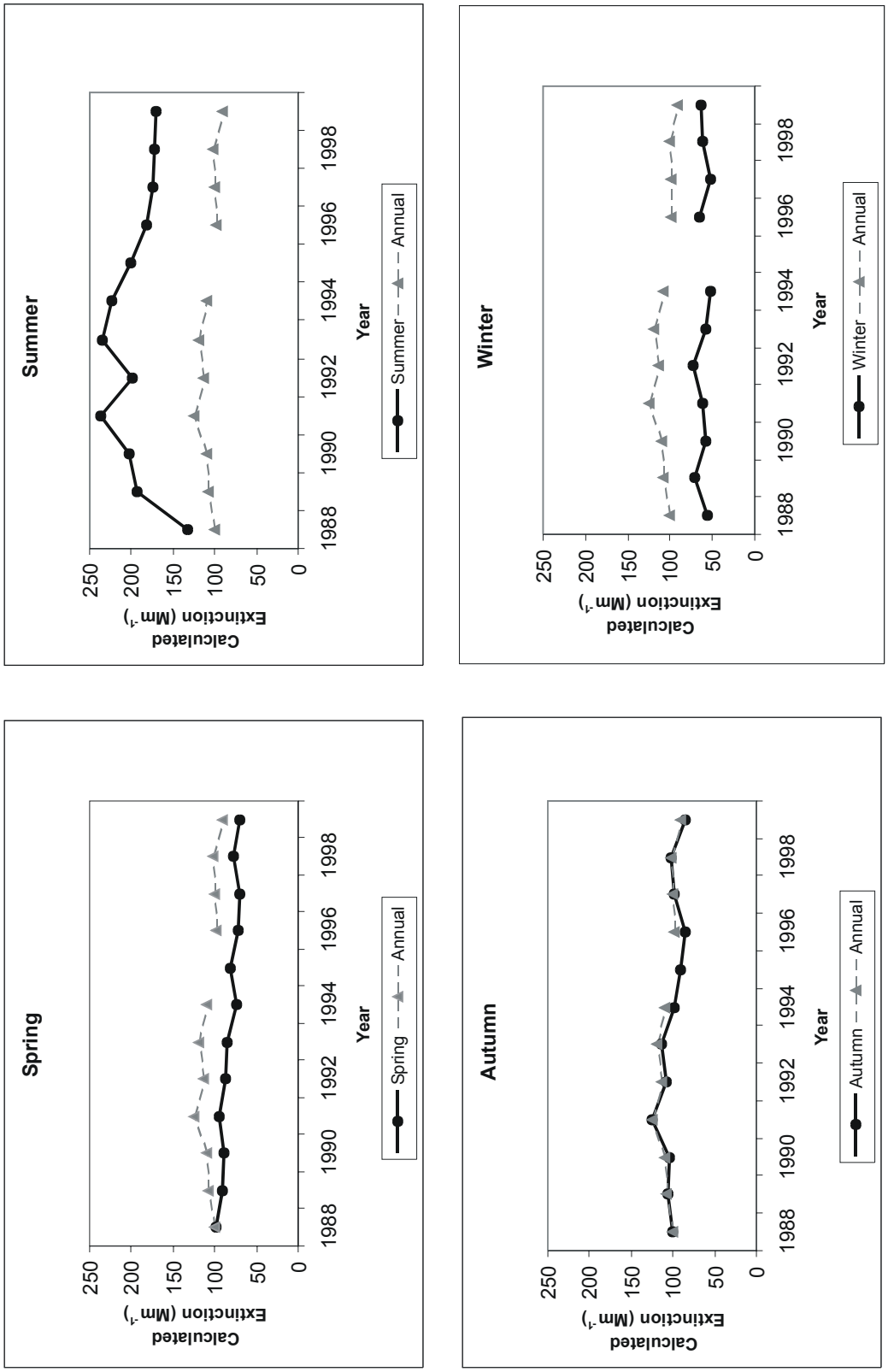

Figure V-23. Seasonal and annual average calculated extinction (Mm^{-1}) for SHEN, March 1988 – February 2000.

The characterization of long-term trends can be a highly subjective exercise in that slopes and their significance can vary depending on the technique employed. Recently the IMPROVE aerosol network, initiated in March 1988, matured to a point where long-term trends of average ambient aerosol concentrations and calculated extinction can be assessed. In the IMPROVE report (Malm et al. 2000), the Theil (1950) approach was applied to describe trends for IMPROVE sites with 11 years of data. The distribution of $PM_{2.5}$ mass concentrations, calculated extinction expressed as dv, and associated constituents were examined for each site. The data were sorted into three groups based on the cumulative frequency of occurrence of $PM_{2.5}$: lowest fine mass days, 0%-20%; median fine mass days, 40%-60%; and highest fine mass days, 80%-100%. After sorting each group's average concentrations of $PM_{2.5}$ and selecting the associated principal aerosol species, scattering and/or absorption of each species, calculated light extinction and dv were estimated.

Figure V-24 plots the relative contribution to aerosol light extinction by the five principal particulate matter constituents for the cleanest 20%, middle 20%, and haziest 20% groups at SHEN from 1988 to 2000. Figure V-25 shows plots of the trends in annual average calculated light extinction for the cleanest 20%, middle 20% and haziest 20% groups at SHEN. Extinction is also presented in units of SVR (km) and dv.

Optical/View Monitoring

IMPROVE optical monitoring provides a continuous quantitative ambient measurement (generally hourly averages) of light extinction or its components. Optical data document the dynamics of the visual air quality, including diurnal variation or specific events. Optical data cannot identify the cause (pollutant composition) of visibility degradation. However, if optical and aerosol data are taken at the same location, measured visibility and aerosol-based estimates of visibility (calculated extinction) can be compared to refine and/or verify the assumptions applied to compute visibility parameters from aerosol measurements.

SHEN is one of three national parks that use both transmissometer and nephelometer monitoring instruments to measure light extinction or its components. As described in Section III.F, light extinction represents the attenuation of light per unit distance of travel in the atmosphere, due to scattering and absorption of light by particles and gases in the air (aerosols). The transmissometer instrument measures light extinction over a short path length (~5km). The nephelometer instrument measures light scattering (b_{scat}) at a given point. Nephelometers are

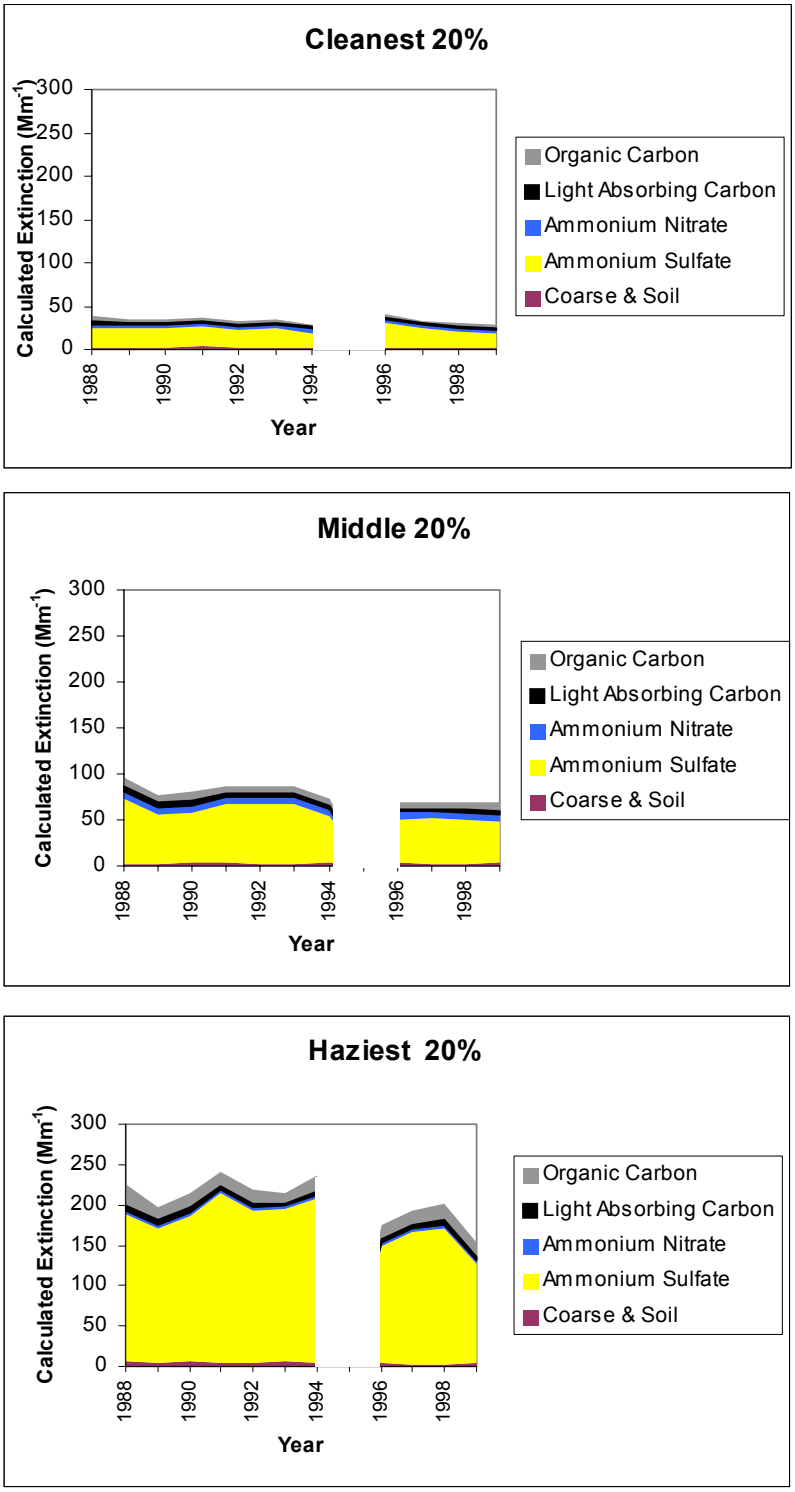

Figure V-24. Calculated aerosol light extinction in SHEN for the cleanest 20%, middle 20%, and haziest 20% of the days in the distribution, February 1988 - March 2000.

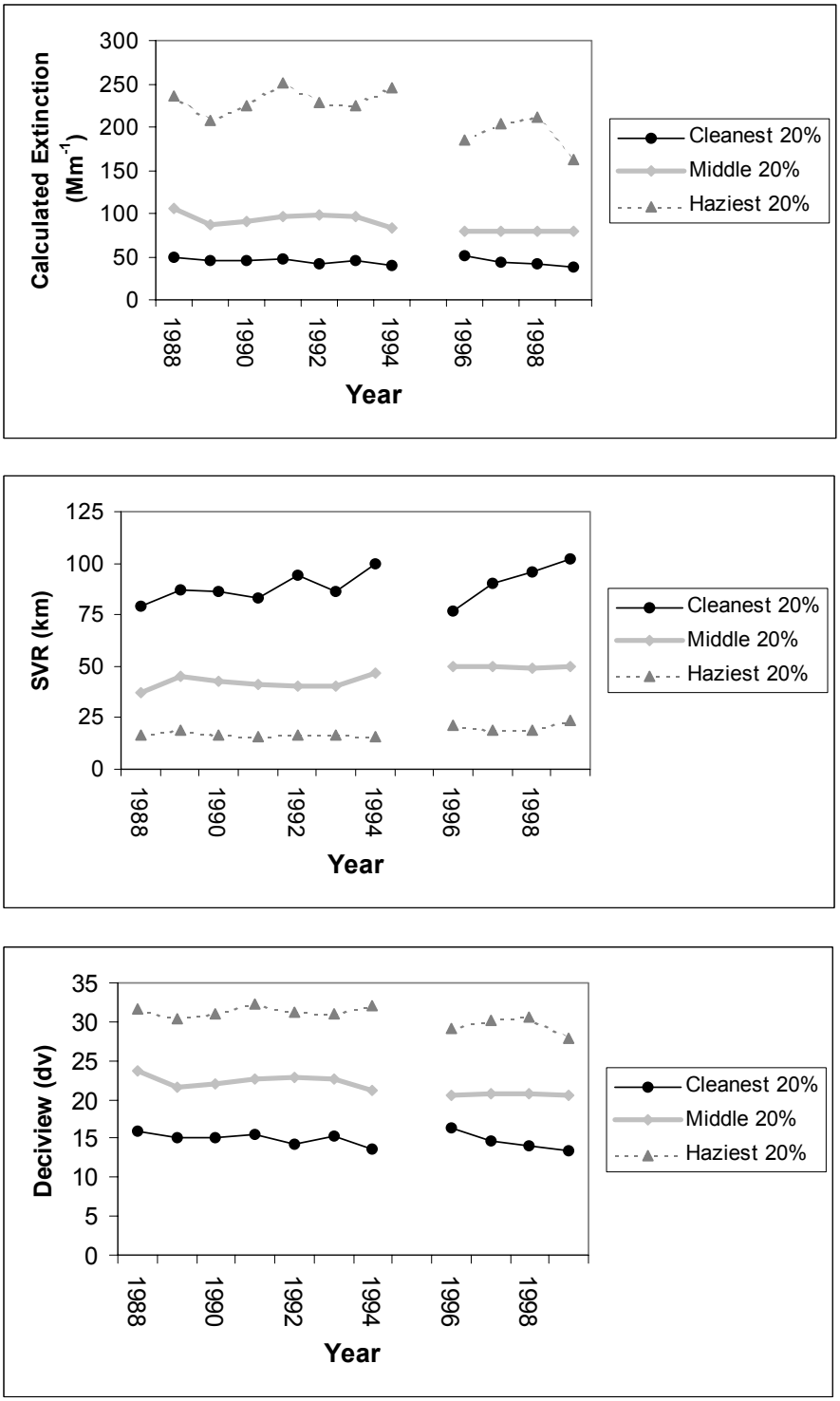

Figure V-25. Trends in annual averages for aerosol extinction (Mm^{-1}), standard visual range (SVR; km), and dv, February 1988 - March 2000.

often co-located with aerosol samplers, which provide the absorption component needed to calculate b_{ext} for the point location. By incorporating both types of optical monitoring instrumentation, SHEN includes both continuous path measurements of atmospheric extinction and continuous point measurements of the scattering component of extinction, for comparison to co-located aerosol measurements. Having both forms of optical monitoring provides a greater understanding of the temporal dynamics of visibility and additional cross checks of measured extinction (from transmissometers) and calculated extinction measurements (from aerosol samplers).

The goal of view monitoring is to use still-frame or time-lapse imagery to provide a qualitative representation of the visual quality of a scene of interest under a variety of air quality and illumination conditions at different times of day throughout the year. View monitoring images can be used to document how vistas appear under various air quality, meteorological, and seasonal conditions; record the frequency that various visual conditions occur, provide a quality assurance reference for collocated aerosol or optical measurements, and provide quality media for visually presenting program goals, objectives, and results to decision-makers and the public.

Transmissometer Data

The transmissometer system consists of two individually housed primary components: a transmitter (light source) and a receiver (detector). The b_{ext} can be calculated based on the intensity of light emitted from the source and the amount of light measured by the receiver (along with the path length between the two). Transmissometers provide continuous, hourly b_{ext} measurements. Meteorological or optical interference factors (such as fog, rain, or a dirty optical surface) can affect transmissometer measurements. Collected data that may be affected by such interferences are flagged, and the resultant data are designated "filtered". Detailed descriptions of the transmissometer system and data reduction and validation procedures used can be found in Standard Operating Procedures and Technical Instructions for Optec LPV-2 Transmissometer Systems (ARS 1996a).

Caution should be used when relying on transmissometer data without examining concurrent co-located nephelometer and/or speciated aerosol data. Relying solely on transmissometer data to represent visibility-related trends can often result in misleading conclusions, due to the following concerns: sight path interference (such as rain, airborne insect swarms, fogged or dirty optical surfaces), inadequate transmissometer calibration methods, and

insufficient manual and automatic hourly data validation analysis. Caution should also be used when comparing calculated (aerosol and/or nephelometer) and measured (transmissometer) extinction. Given differences in measurement periods and averaging methods, as well as relative humidity filtering methods and effects on light extinction efficiencies, the ratio of calculated extinction to measured extinction is seldom greater than 0.8.

Table V-12 provides a tabular summary of the "filtered" seasonal and annual mean extinction values. Combined season data represent the mean of all valid data for the combined seasons. Extinction values are also presented in units of SVR (in km) and dv. Tables V-13 and V-14 summarize the 20% cleanest and 20% haziest visibility metric statistics respectively. Data are represented according to the following conditions:

- No data are reported for seasons when the percentage of valid hourly averages (including weather) compared to total possible hourly averages was less than 50%.
- Annual data represent the mean of all valid data for each March through February annual period. No data are reported for years that had one or more invalid seasons.
- Combined season data represent the mean of all valid data for each season (spring, summer, autumn, winter) of the December 1988 through February 2000 period.
- Combined annual period data represent the mean of all combined data values for the period December 1988 through February 2000.

Figure V-26 provides a graphic representation of the "filtered" seasonal and annual means. No data are reported for annual periods with one or more invalid seasons.

Nephelometer Data

The nephelometer consists of a sampling chamber and a light source confined to a small volume so that the instrument may directly measure the light scattered by aerosols and gases at a fixed point. Nephelometers provide continuous, five-minute measurements of particle scattering (b_{sp}). The atmospheric scattering coefficient, b_{scat}, can be directly estimated from this measurement. Nephelometer measurements can be influenced by weather-related factors such as fog. Therefore, the data are "filtered" by flagging data points with relative humidities greater that 95%. Detailed descriptions of the nephelometer system and data reduction and validation procedures used can be found in Standard Operating Procedures and Technical Instructions for Nephelometer Systems (ARS 1996b).

Table V-12. Seasonal and annual arithmetic means, SHEN, transmissometer data (filtered), December 1988 through February 2000.

YEAR	Spring (Mar, Apr, May)			Summer (Jun, Jul, Aug)			Autumn (Sep, Oct, Nov)			Winter (Dec, Jan, Feb)			Annual (March - February)[a]		
	SVR[b] (km)	b_{ext} (Mm^{-1})	dv	SVR (km)	b_{ext} (Mm^{-1})	dv	SVR (km)	b_{ext} (Mm^{-1})	dv	SVR (km)	b_{ext} (Mm^{-1})	dv	SVR[b] (km)	b_{ext} (Mm^{-1})	dv
1988							---	---	---	65	61	18.1	***	***	***
1989	21	185	29.2	--	--	--	--	--	--	--	--	--	***	***	***
1990	--	--	--	19	202	30.1	42	93	22.3	--	--	--	***	***	***
1991	--	--	--	18	221	31.0	37	107	23.7	57	69	19.3	***	***	***
1992	49	80	20.8	--	--	--	45	88	21.7	43	92	22.2	***	***	***
1993	38	104	23.4	23	170	28.3	47	84	21.3	82	48	15.7	37	107	23.7
1994	49	80	20.8	24	166	28.1	43	92	22.2	73	54	16.9	45	88	21.7
1995	41	95	22.5	24	162	27.9	33	119	24.8	--	--	--	***	***	***
1996	56	70	19.5	26	152	27.2	46	85	21.4	39	102	23.2	40	98	22.8
1997	60	66	18.9	28	140	26.4	40	99	22.9	47	83	21.2	41	96	22.6
1998	30	132	25.8	18	219	30.9	28	138	26.2	31	128	25.5	26	153	27.3
1999	42	94	22.4	29	137	26.2	46	85	21.4	40	98	22.8	39	101	23.1
Mean[c]	40	98	22.8	22	176	28.7	40	98	22.8	44	89	21.9	35[d]	111[d]	24.1[d]

-- No data are reported for seasons with <50% valid data.
*** No annual data are reported for periods with one or more invalid seasons.
a Annual period data represent the mean of all valid data for each March through February annual period.
b The estimated natural visual range is about 185 km (115 mi; U.S. EPA 2001b).
c Combined season data represent the mean of all valid data for each season of the December 1988 through February 2000 period.
d Combined annual period data represent the mean of all combined valid data between December 1988 and February 2000.

Table V-13. Seasonal and annual 20% cleanest visibility metric statistics, SHEN, transmissometer data (filtered), December 1988 through February 2000.

YEAR	Spring (Mar, Apr, May)			Summer (Jun, Jul, Aug)			Autumn (Sep, Oct, Nov)			Winter (Dec, Jan, Feb)			Annual (March - February)[a]		
	SVR (km)	b_{ext} (Mm^{-1})	dv	SVR (km)	b_{ext} (Mm^{-1})	dv	SVR (km)	b_{ext} (Mm^{-1})	dv	SVR (km)	b_{ext} (Mm^{-1})	dv	SVR[b] (km)	b_{ext} (Mm^{-1})	dv
1988							---	---	---	191	21	7.4	***	***	***
1989	32	122	25.0	--	--	--	--	--	--	--	--	--	***	***	***
1990	--	--	--	49	81	20.9	133	30	11.0	--	--	--	***	***	***
1991	--	--	--	63	63	18.4	64.7	61	18.1	87.9	45	15.0	***	***	***
1992	102	39	13.6	--	--	--	91	43	14.7	76	52	16.5	***	***	***
1993	63	63	18.4	57	69	19.3	127	31	11.4	150	27	9.8	107	37	13.1
1994	108	37	13.0	61	64	18.6	120	33	12.0	179	22	8.1	129	31	11.2
1995	102	39	13.5	55	71	19.6	62	64	18.5	--	--	--	***	***	***
1996	104	38	13.4	67	59	17.8	129	31	11.3	85	46	15.4	100	39	13.7
1997	118	34	12.1	75	53	16.6	91	44	14.7	97	41	14.1	101	39	13.7
1998	46	86	21.5	35	114	24.3	51	78	20.5	45	87	21.6	46	86	21.5
1999	71	56	17.2	81	49	15.9	105	38	13.3	90	44	14.8	87	45	15.1
Mean[c]	94	42	14.4	63	63	18.4	102	39	13.6	110	36	12.8	94[d]	42[d]	14.4[d]

-- No data are reported for seasons with <50% valid data.
*** No annual data are reported for periods with one or more invalid seasons.
a Annual period data represent the mean of all valid data for each March through February annual period.
b The estimated natural visual range is about 185 km (115 mi; U.S. EPA 2001b).
c Combined season data represent the mean of all valid data for each season of the December 1988 through February 2000 period.
d Combined annual period data represent the mean of all combined valid data between December 1988 and February 2000.

Table V-14. Seasonal and annual 20% haziest visibility metric statistics, SHEN, transmissometer data (filtered), December 1988 through February 2000.

YEAR	Spring (Mar, Apr, May)			Summer (Jun, Jul, Aug)			Autumn (Sep, Oct, Nov)			Winter (Dec, Jan, Feb)			Annual (March - February)[a]		
	SVR (km)	b_{ext} (Mm^{-1})	dv	SVR (km)	b_{ext} (Mm^{-1})	dv	SVR (km)	b_{ext} (Mm^{-1})	dv	SVR (km)	b_{ext} (Mm^{-1})	dv	SVR[b] (km)	b_{ext} (Mm^{-1})	dv
1988							---	---	---	28	142	26.5	***	***	***
1989	15	259	32.5	--	--	--	--	--	--	--	--	--	***	***	***
1990	--	--	--	11	344	35.3	18	217	30.8	--	--	--	***	***	***
1991	--	--	--	8	478	38.7	19	202	30.1	37	105	23.5	***	***	***
1992	28	142	26.5	--	--	--	23	171	28.4	24	161	27.8	***	***	***
1993	22	182	29.0	12	340	35.3	22	179	28.8	49	80	20.8	17	234	31.5
1994	25	156	27.5	12	324	34.8	22	181	29.0	38	103	23.3	21	190	29.4
1995	21	184	29.1	13	310	34.3	16	241	31.8	--	--	--	***	***	***
1996	31	127	25.4	13	298	34.0	22	175	28.6	17	234	31.5	18	220	30.9
1997	32	121	24.9	13	292	33.7	19	202	30.1	25	159	27.7	19	208	30.3
1998	19	209	30.4	11	361	35.9	15	262	32.6	20	199	29.9	14	277	33.2
1999	26	149	27.0	15	258	32.5	25	160	27.7	23	170	28.3	21	185	29.2
Mean[c]	21	187	29.3	11	351	35.6	20	198	29.9	23	173	28.5	17[d]	237[d]	31.7[d]

-- No data are reported for seasons with <50% valid data.
*** No annual data are reported for periods with one or more invalid seasons.
a Annual period data represent the mean of all valid data for each March through February annual period.
b The estimated natural visual range is about 185 km (115 mi; U.S. EPA 2001b).
c Combined season data represent the mean of all valid data for each season of the December 1988 through February 2000 period.
d Combined annual period data represent the mean of all combined valid data between December 1988 and February 2000.

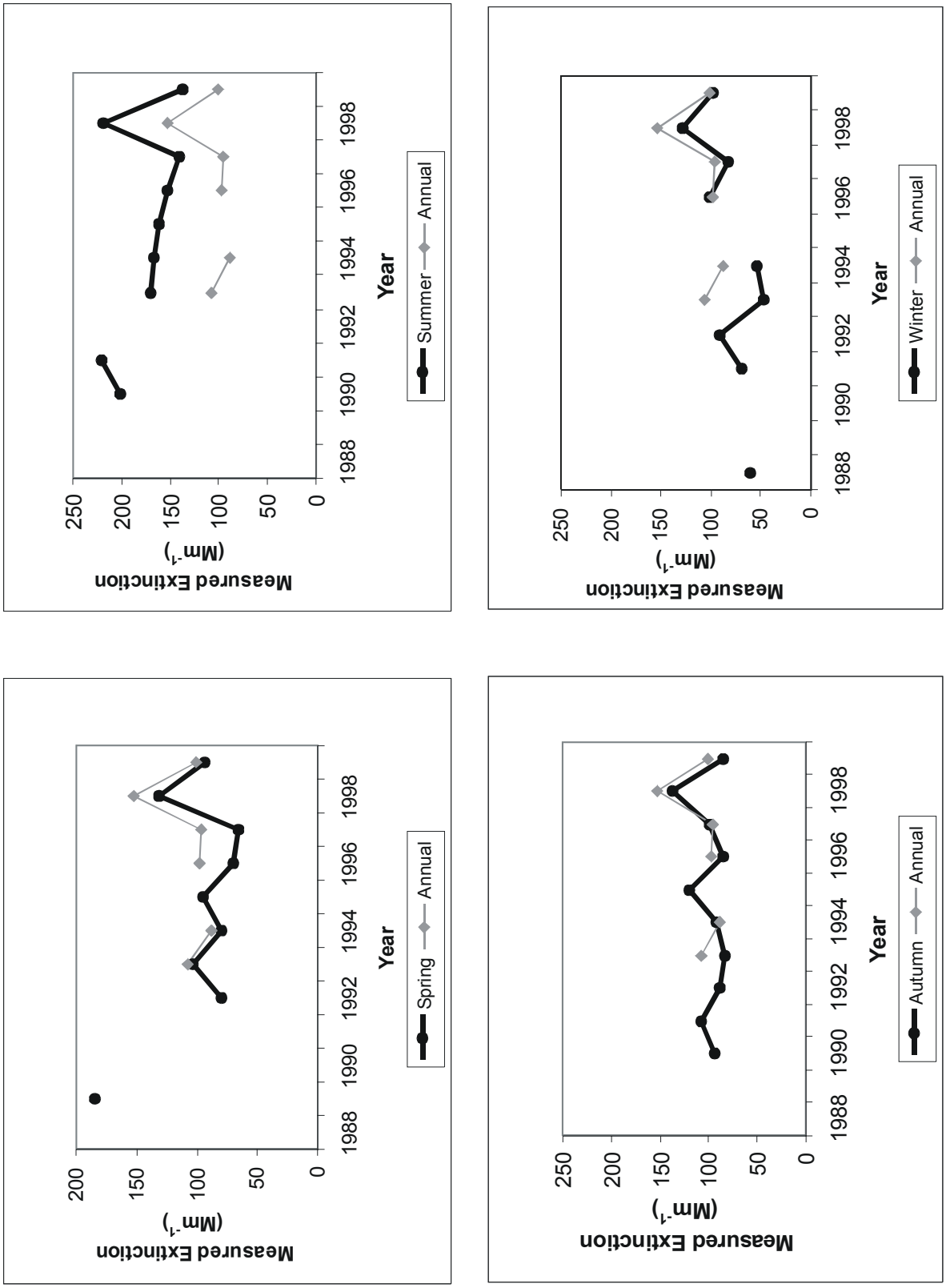

Figure V-26. Seasonal and annual arithmetic means for transmissometer data (filtered) at SHEN during the period 1988 to 2000.

Measurements of nephelometer b_{scat} are combined with estimates of aerosol absorption (b_{abs}) obtained from IMPROVE aerosol sampler measurements to calculate the total light extinction. Table V-15 provides a tabular summary of the "filtered" seasonal and annual mean scattering, absorption and extinction values. Extinction values are also presented in units of SVR (in km) and dv. Since nephelometer data rely on seasonal mean aerosol measurements of b_{abs} in order to reconstruct b_{ext}, no 20% cleanest or 20% haziest visibility metric statistics are provided. No data are reported for seasons when the percentage of valid hourly averages (including weather) compared to total possible hourly averages, was less than 50%. Figure V-27 provides a graphic

Table V-15. Seasonal and annual arithmetic means, SHEN, nephelometer data (filtered), September 1996 through February 2000.

Season	Year	b_{scat} Mean	b_{abs} Mean	b_{ext} [a]	dv	SVR
Spring	1996	--	--	--	--	–
	1997	43	3.1	46	15.3	85
	1998	47	3.5	51	16.2	78
	1999	38	4.3	42	14.4	94
Summer	1996	--	--	--	--	–
	1997	101	3.5	104	23.5	38
	1998	97	4.4	102	23.2	39
	1999	90	3.9	93	22.4	42
Autumn	1996	49	3.6	53	16.7	75
	1997	61	4.1	65	18.8	60
	1998	85	4.8	90	21.9	44
	1999	46	3.5	49	15.9	81
Winter	1996	43	3.1	46	15.3	86
	1997	40	2.8	43	14.6	92
	1998	43	3.4	47	15.4	85
	1999	39	2.8	42	14.4	94
Annual	1996	***	***	***	***	***
	1997	61	3.5	65	18.7	61
	1998	66	4.0	70	19.5	56
	1999	50	3.6	54	16.9	73

[a] Estimation based on the combined b_{scat} measurement (mean) and mean aerosol absorption coefficient (b_{abs}).
-- No data are reported for seasons with <50% valid data.
*** No annual data are reported for periods with one or more missing or invalid seasons.

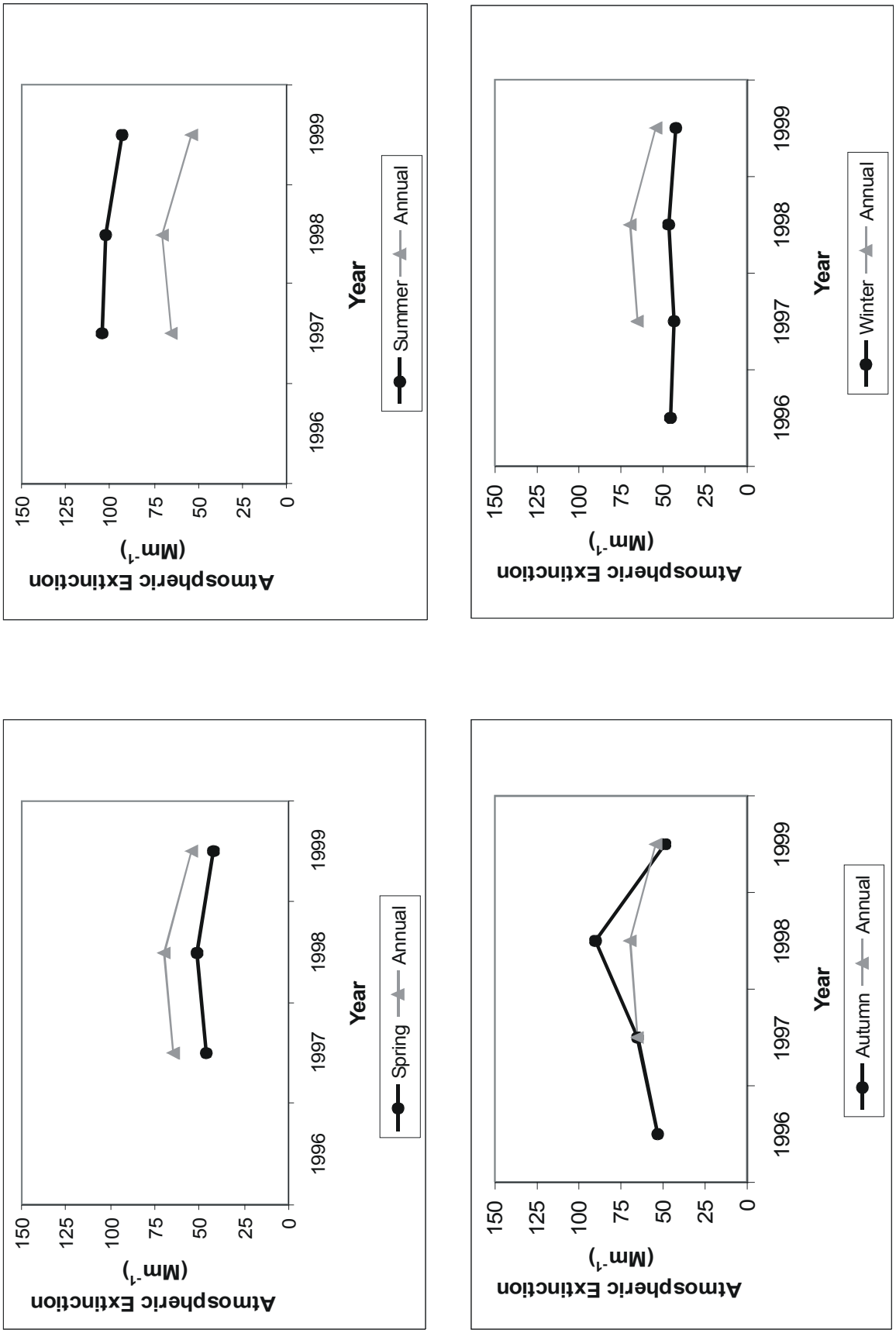

Figure V-27. Seasonal and annual arithmetic means, SHEN, nephelometer data (filtered), 1996 to 1999.

representation of the "filtered" seasonal and annual means of the nephelometer data. No data are reported for annual periods with one or more invalid seasons.

Camera Data

The NPS operated an automatic 35mm camera system at the Skyland-WNW vista in the Central District from July 1991 through April 1995. Color 35mm photographs of New Market Gap in the Massanutten Mountain were taken three times per day at 9:00 a.m., 12:00 p.m., and 3:00 p.m. In the summer of 1991, a second camera was temporarily set up at the Dickey Ridge-SW vista in order to do an intercomparison study of the Shenandoah Valley. This camera operated from July 1991 through November 1991. Color 35mm photographs were taken daily at 9:00 a.m., 12:00 p.m., and 3:00 p.m., and hourly from 7:00 am to 5:00 pm for a short time. The Skyland and Dickey Ridge vista photographs presented in Figures V-28 and V-29 were chosen to provide a feel for the range of visibility conditions possible and to help relate extinction, SVR, and deciview (haziness) data to the visual sense.

Optical/View Summary

Aerosol data at SHEN were presented in Section V-C.2.a so that the composition and concentrations of visibility reducing pollutants could be understood. For comparison, Figures V-24 and V-25 and Tables V-12 through V-15 have been provided to summarize optical data (measured and calculated extinction) at SHEN during the December 1988 through February 2000 period.

Caution should be used when comparing calculated (aerosol and nephelometer) extinction (Tables V-11 and V-15) with measured (transmissometer) extinction (Table V-12). The following differences and similarities should be considered:

- Data Collection - Calculated aerosol extinction measurements represent 24-hour samples collected twice per week from 1988 through 1999 and every three days since January 2000. Nephelometer scattering and transmissometer extinction estimates represent continuous measurements summarized as hourly means, 24 hours per day, seven days per week.

- Point versus Path Measurements - Calculated aerosol and nephelometer extinction represents an indirect measure of extinction at a fixed point. The transmissometer directly measures the irradiance of light (which calculated gives a direct measure of extinction) over a finite atmospheric path.

SHEN
on an "Excellent" day

Estimated Visibility Conditions:
Visual Range: 275-325 km
B_{ext}: 14-12 Mm^{-1}
Haziness: 4-2 dv

(a)

SHEN
on an "Average" day

Estimated Visibility Conditions:
Visual Range: 100-110 km
B_{ext}: 39-36 Mm^{-1}
Haziness: 14-13 dv

(b)

SHEN
on a "Poor" day

Estimated Visibility Conditions:
Visual Range: 20-25 km
B_{ext}: 156-196 Mm^{-1}
Haziness: 30-28 dv

(c)

Figure V-28. Photographs illustrating visibility conditions at Skyland in SHEN.

SHEN
on an "Excellent" day

Estimated Visibility Conditions:
Visual Range: 275-325 km
B_{ext}: 14-12 Mm^{-1}
Haziness: 4-2 dv

(a)

SHEN
on an "Average" day

Estimated Visibility Conditions:
Visual Range: 70-80 km
B_{ext}: 17-16 Mm^{-1}
Haziness: 56-49 dv

(b)

SHEN
on a "Poor" day

Estimated Visibility Conditions:
Visual Range: 5-6 km
B_{ext}: 782-652 Mm^{-1}
Haziness: 44-42 dv

(c)

Figure V-29. Photographs illustrating visibility conditions at SHEN, Dickey Ridge vista.

3. Deposition

a. Ambient Deposition

Some data are available regarding all forms of deposition in SHEN. An NADP/NTN wet deposition monitoring station has been in operation at Big Meadows (elevation 1,074 m) since 1981. Precipitation volume and the concentrations of major ions in precipitation are reported. Wet deposition of each ion is calculated as the product of the precipitation volume and ionic concentration in precipitation.

Annual wet deposition measurements and interpolated isopleths of SO_4^{2-}, NO_3^-, and inorganic N (NH_4^+ plus NO_3^-, as N) for the year 2001 are shown for the eastern United States in Figures V-30 to V-32. These are the most recent annual data available from the NADP/NTN monitoring program. Compared with other locations in the eastern United States, SHEN and the rest of western Virginia receive relatively high wet deposition of S (expressed on the map as SO_4^{2-}), and moderately high wet deposition of NH_4^+ and NO_3^-. Among Class I national parks, SHEN and GRSM receive the highest S and NO_3-N deposition. In general, S and N wet deposition values tend to be higher to the west and north of SHEN, but lower to the southeast of the park.

The concentrations of major ions measured in precipitation and measured precipitation amounts within SHEN are given in Table V-16. Data are available for three monitoring stations within the park: Big Meadows (1981-2000), White Oak Run (1980-2000) and North Fork Dry Run (1987-2000). Locations are shown in Figures II-1 and VI-1. Annual average precipitation at the monitoring stations, over the period of record, ranged from 91 cm at White Oak Run to 135 cm at Big Meadows. The Big Meadows site generally showed lower concentrations of major ions in precipitation than did the other two sites, with average SO_4^{2-}, NO_3^-, and sum of base cation concentrations equal to 31, 14, and 9 μeq/L, respectively (Table V-16).

Wet deposition fluxes (kg/ha/yr) were determined at each of the three wet deposition monitoring stations in the park for each year of available data. Annual average wet S deposition at Big Meadows varied over the period of record from about 2 to 10 kg/ha/yr, with an average of 6.7 kg/ha/yr (Table V-17). Both NH_4^+ and NO_3^- wet deposition varied during most years between 1 and about 3 kg N/ha/yr, with averages of 2.0 and 2.6 kg N/ha/yr, respectively at Big Meadows. The annual average total wet N deposition levels at Big Meadows, White Oak Run, and North Fork Dry Run during the periods of record were generally similar: 4.6, 3.8, and 4.8,

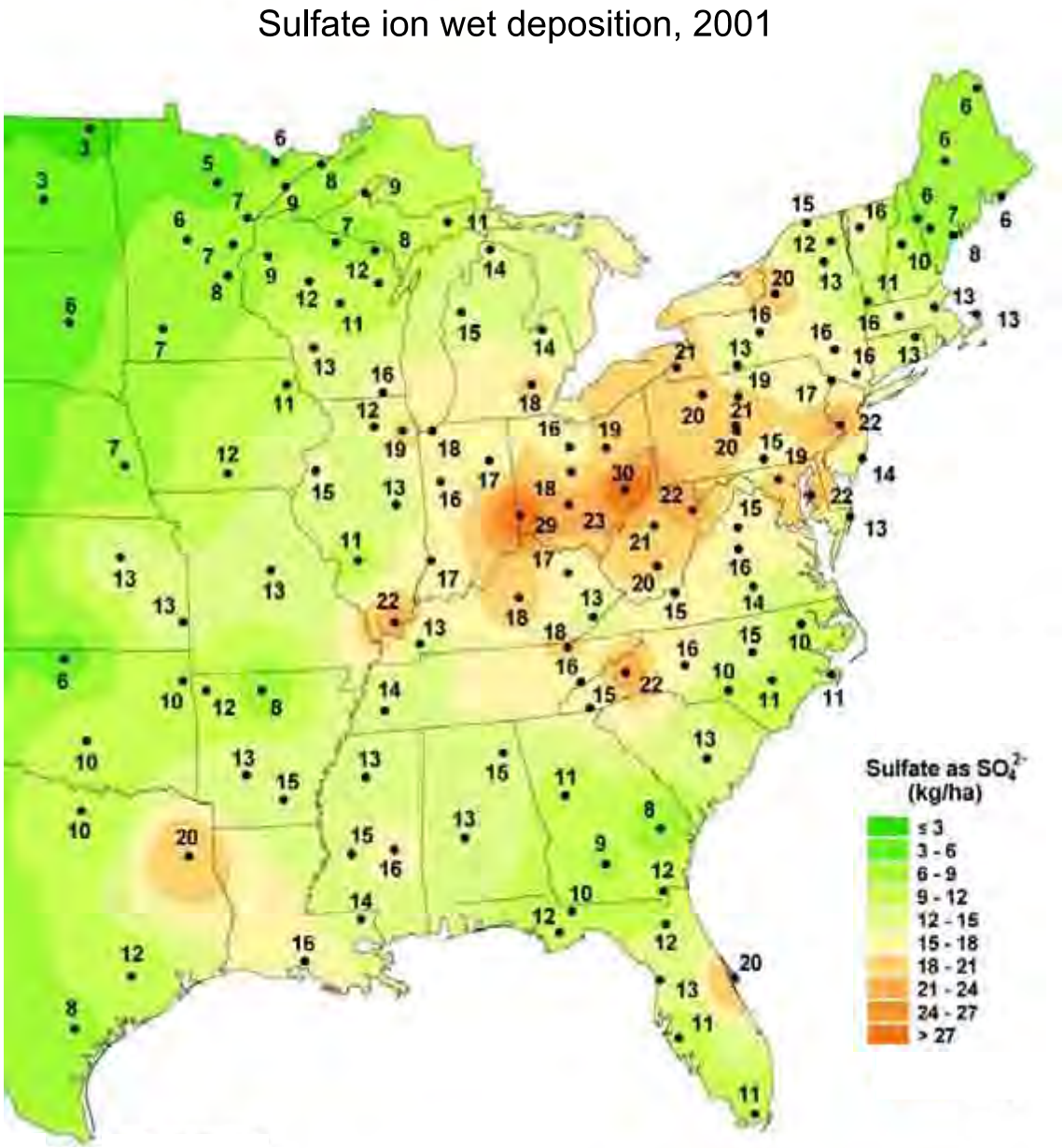

Figure V-30. Annual wet deposition of sulfate throughout the eastern United States during the most recent year of record. Note that sulfur deposition (as used elsewhere in this report) is one-third of sulfate deposition (as shown on this map). Source: http://nadp.sws.uiuc.edu

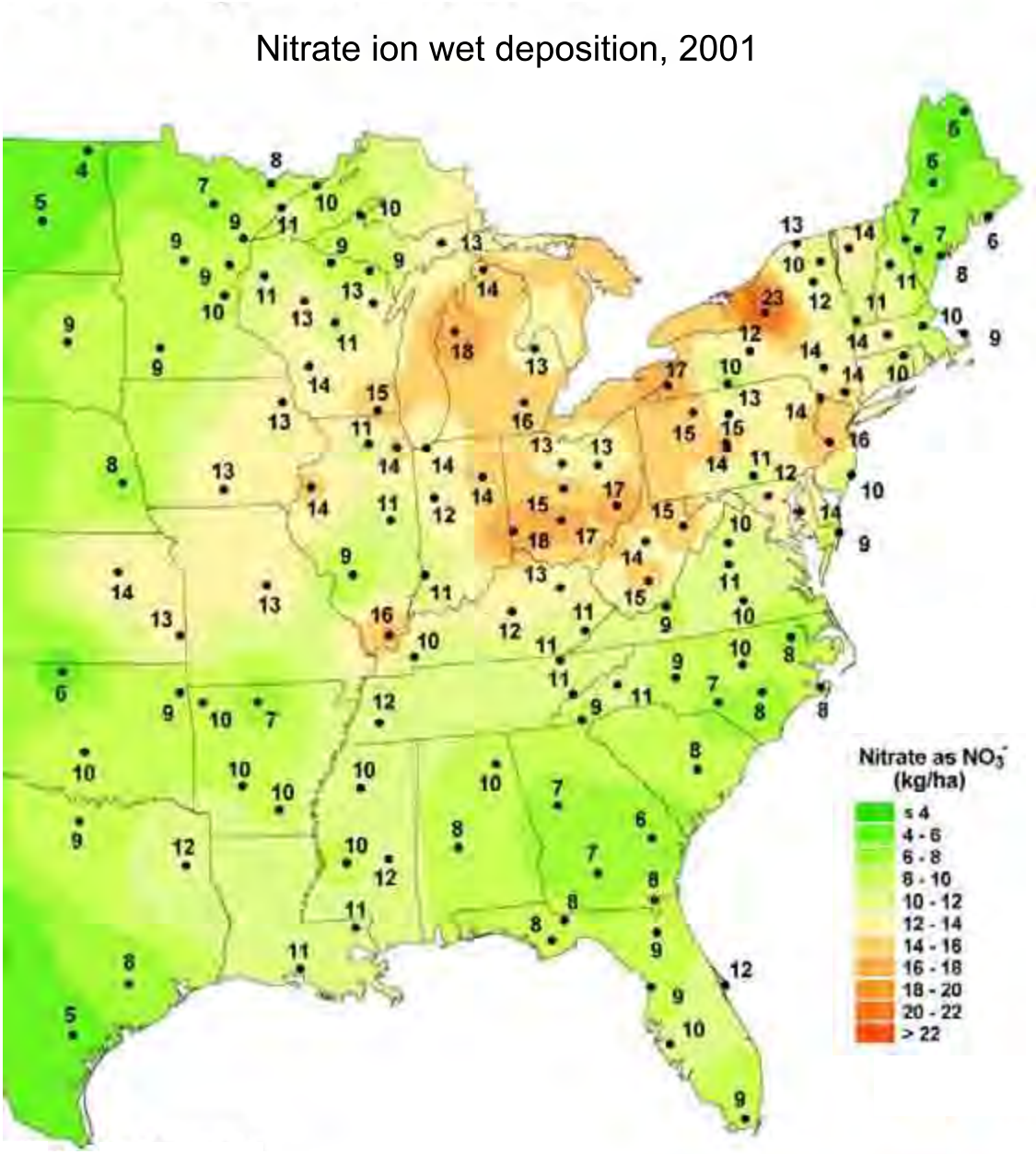

Figure V-31. Annual wet deposition of nitrate throughout the eastern United States during the most recent year of record. Note that nitrogen deposition as nitrate-nitrogen is equal to 22.58% of nitrate deposition (as shown on this map). Source: http://nadp.sws.uiuc.edu

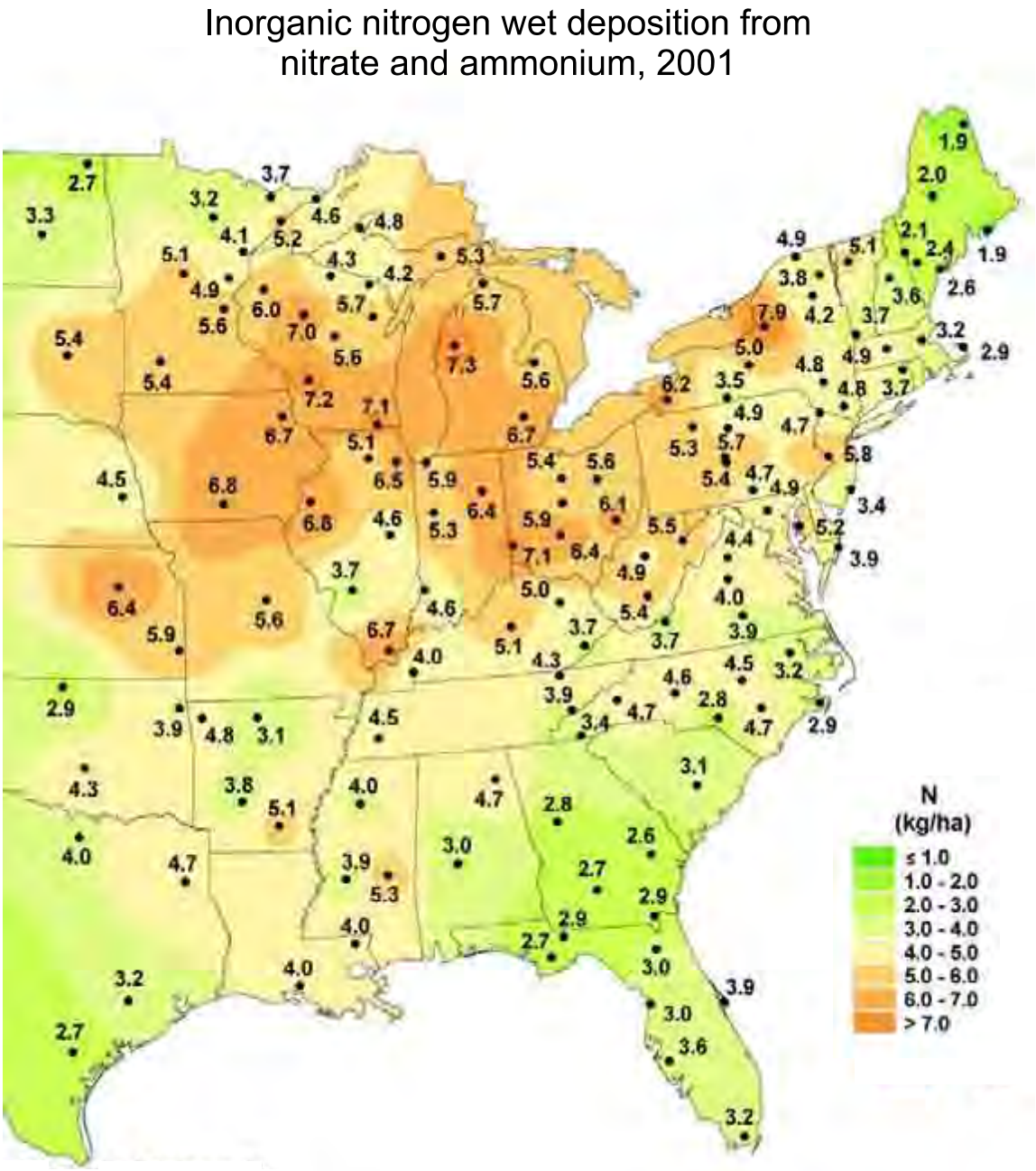

Figure V-32. Annual wet deposition of inorganic nitrogen throughout the eastern United States during the most recent year of record. Source: http://nadp.sws.uiuc.edu

Table V-16. Precipitation volume and measured concentrations of major ions in precipitation at monitoring sites within SHEN.

Year	Precipitation Amount (cm)	Concentration of Ion in Precipitation								pH
		Ca	Mg	Na	K	NH_4	SO_4	NO_3	Cl	
		----------(μeq/L)----------								
Big Meadows[a] (Center of Central District, 1074 m)										
1981	93.3	6.1	4.2	5.6	0.7	10.7	40.2	13.7	5.3	4.5
1982	122.6	6.1	2.6	5.8	1.4	13.0	49.6	18.5	4.3	4.4
1983	183.4	3.1	2.0	5.2	0.5	8.7	29.4	11.9	7.1	4.6
1984	144.2	3.6	1.6	3.4	2.2	16.6	37.0	13.1	4.9	4.6
1985	151.0	3.0	1.6	2.2	0.3	6.5	34.0	11.5	3.0	4.5
1986	104.5	2.7	1.3	2.6	0.3	9.6	40.1	15.4	2.9	4.4
1987	51.7	2.5	1.1	3.0	0.2	4.6	19.6	9.9	3.4	4.7
1988	108.2	3.4	1.6	3.0	0.3	7.0	31.2	14.3	3.4	4.6
1989	150.7	3.1	1.5	4.3	0.4	13.9	40.4	17.5	5.9	4.4
1990	157.5	2.6	1.4	4.2	0.4	10.9	31.2	12.9	5.4	4.6
1991	107.5	2.6	0.9	2.6	0.7	12.1	34.5	15.0	3.8	4.5
1992	169.1	1.7	1.1	4.3	0.3	8.0	23.0	9.9	4.9	4.7
1993	150.8	1.8	0.7	2.0	0.2	10.9	30.9	13.2	2.5	4.5
1994	137.6	3.1	1.0	2.6	0.4	12.0	29.2	14.0	3.0	4.6
1995	193.5	2.1	2.1	11.4	0.3	8.1	17.0	10.1	9.6	4.8
1996	171.2	2.9	1.2	4.4	0.3	11.5	28.4	15.9	4.8	4.5
1997	126.5	2.3	0.8	2.3	0.2	11.2	29.3	14.7	2.9	4.6
1998	131.6	2.5	0.9	2.7	0.4	12.3	27.0	13.6	3.5	4.6
1999	141.1	3.4	1.7	4.1	0.4	10.4	27.7	12.7	5.2	4.6
2000	110.7	2.9	0.9	2.1	0.3	11.2	26.3	13.8	2.9	4.6
Average	135.3	3.1	1.5	3.9	0.5	10.5	31.3	13.6	4.4	4.6
White Oak Run[a] (South District, 387 m)										
1980	75.1	11.8	3.7	4.3	1.5	16.1	60.2	27.0	7.0	4.2
1981	71.9	10.2	3.2	6.1	1.8	11.1	55.6	21.7	8.1	4.3
1982	109.6	5.4	1.9	3.0	1.1	10.9	49.0	19.5	4.1	4.2
1983	106.5	6.0	1.5	5.2	1.3	15.1	61.8	21.2	5.9	4.3
1984	103.7	6.9	10.2	3.9	1.5	12.9	64.9	19.5	4.2	4.3
1985	102.1	6.1	2.4	6.1	2.4	13.3	42.3	19.6	7.7	4.3
1986	66.5	9.1	3.0	7.1	3.4	11.3	51.4	21.7	12.0	4.3
1987	88.9	7.7	2.2	2.9	2.0	14.4	74.2	26.1	6.0	4.1
1988	79.1	13.2	3.7	4.1	4.5	5.1	49.3	19.9	7.0	4.3
1989	125.3	7.4	2.3	2.2	1.8	5.1	48.3	16.0	5.1	4.3
1990	89.9	8.1	3.1	4.9	2.9	7.1	41.2	16.2	7.9	4.3

Table V-16. Continued.

Year	Precipitation Amount (cm)	Concentration of Ion in Precipitation								pH
		Ca	Mg	Na	K	NH_4	SO_4	NO_3	Cl	
		----------(μeq/L)----------								
White Oak Run (continued)										
1991	97.0	8.0	2.0	2.3	1.8	12.4	48.4	20.3	4.6	4.3
1992	105.2	4.7	2.1	4.5	1.6	8.3	40.6	17.1	6.7	4.3
1993	95.6	5.6	1.9	2.6	2.0	7.6	43.5	17.6	5.0	4.3
1994	68.1	7.1	2.5	3.2	2.6	10.9	45.1	21.3	5.8	4.3
1995	70.5	7.1	3.4	8.4	1.9	6.8	28.8	14.8	11.4	4.5
1996	105.3	8.5	2.8	6.0	1.8	9.9	32.9	24.4	8.5	4.4
1997	86.9	7.1	2.2	4.0	2.3	10.9	36.7	15.6	5.6	4.4
1998	100.1	6.0	1.8	1.9	1.4	9.3	28.9	16.1	4.1	4.5
1999	86.9	8.5	2.6	4.1	1.5	9.2	39.2	19.7	7.3	4.3
2000	79.0	9.1	2.7	2.4	2.5	9.3	36.9	20.0	4.0	4.4
Average	91.1	7.8	2.9	4.2	2.1	10.5	46.8	19.9	6.6	4.3
North Fork Dry Run[a] (North End of Central District, 1014 m)										
1987	121.8	4.6	2.3	4.1	4.3	17.4	52.8	19.6	5.7	4.4
1988	88.4	9.2	3.9	3.9	3.6	17.5	52.3	20.8	5.2	4.4
1989	132.3	5.7	3.1	3.0	3.1	11.9	29.2	18.8	4.9	4.5
1990	135.5	6.4	2.5	4.5	5.3	15.0	36.2	15.9	5.9	4.5
1991	85.9	7.2	2.2	3.1	5.0	15.8	51.1	19.6	5.3	4.3
1992	129.5	4.3	2.4	4.9	3.9	8.0	30.6	13.0	6.6	4.5
1993	100.6	9.1	3.1	3.5	7.0	11.8	49.1	21.7	6.0	4.3
1994	97.6	9.0	3.1	3.3	5.6	14.5	47.7	21.2	5.4	4.4
1995	123.2	6.5	3.2	6.5	3.7	9.0	35.7	17.3	9.2	4.5
1996	125.7	6.9	2.8	4.3	6.2	8.2	33.3	17.9	6.3	4.5
1997	110.3	4.9	1.8	2.2	3.0	12.7	38.3	15.9	4.4	4.4
1998	118.6	3.3	1.2	2.9	0.8	10.3	30.4	17.0	4.5	4.5
1999	115.4	3.9	1.8	4.6	1.4	11.5	34.9	15.7	6.9	4.5
2000	113.3	4.3	1.5	2.4	1.0	12.7	31.1	17.5	3.5	4.5
Average	114.1	6.1	2.5	3.8	3.9	12.6	39.5	18.0	5.7	4.5

[a] Data were collected at Big Meadows by the National Atmospheric Deposition Program (http://nadp.sws.uiuc.edu) and at White Oak Run and North Fork Dry Run by the SWAS (University of Virginia, Department of Environmental Sciences)

Table V-17. Measured wet deposition fluxes at monitoring sites within SHEN.

Year	Wet Deposition (kg/ha/yr)									
	Ca	Mg	Na	K	H	Cl	SO_4-S	NH_4-N	NO_3-N	Total N
Big Meadows[a]										
1981	1.1	0.5	2.0	0.1	0.3	1.8	6.0	1.4	1.8	3.2
1982	1.5	0.4	2.8	0.4	0.4	1.9	9.7	2.2	3.2	5.4
1983	1.1	0.4	3.7	0.2	0.5	4.6	8.6	2.2	3.0	5.3
1984	1.0	0.3	1.9	0.7	0.3	2.5	8.5	3.3	2.6	6.0
1985	0.9	0.3	1.3	0.1	0.5	1.6	8.2	1.4	2.4	3.8
1986	0.6	0.2	1.0	0.1	0.4	1.1	6.7	1.4	2.3	3.7
1987	0.3	0.1	0.6	0.0	0.1	0.6	1.6	0.3	0.7	1.0
1988	0.7	0.2	1.3	0.1	0.3	1.3	5.4	1.1	2.2	3.2
1989	0.9	0.3	2.6	0.1	0.5	3.1	9.7	2.9	3.7	6.6
1990	0.8	0.3	2.6	0.1	0.4	3.0	7.9	2.4	2.8	5.2
1991	0.6	0.1	1.1	0.2	0.3	1.4	5.9	1.8	2.3	4.1
1992	0.6	0.2	2.8	0.1	0.4	3.0	6.2	1.9	2.4	4.3
1993	0.5	0.1	1.2	0.1	0.4	1.3	7.5	2.3	2.8	5.1
1994	0.9	0.2	1.4	0.1	0.4	1.5	6.4	2.3	2.7	5.0
1995	0.8	0.5	8.7	0.1	0.3	6.6	5.3	2.2	2.7	4.9
1996	1.0	0.3	2.9	0.1	0.5	2.9	7.8	2.8	3.8	6.6
1997	0.6	0.1	1.1	0.1	0.4	1.3	5.9	2.0	2.6	4.6
1998	0.7	0.1	1.4	0.1	0.3	1.6	5.7	2.3	2.5	4.8
1999	1.0	0.3	2.3	0.1	0.3	2.6	6.2	2.1	2.5	4.6
2000	0.6	0.1	0.9	0.1	0.3	1.1	4.7	1.7	2.1	3.9
Average	0.8	0.2	2.2	0.2	0.4	2.2	6.7	2.0	2.6	4.6
White Oak Run[a]										
1980	1.8	0.3	1.3	0.3	0.4	1.9	7.2	1.7	2.8	4.5
1981	1.5	0.3	1.7	0.3	0.4	2.1	6.4	1.1	2.2	3.3
1982	1.2	0.3	1.3	0.3	0.6	1.6	8.6	1.7	3.0	4.7
1983	1.3	0.2	2.2	0.3	0.5	2.2	10.5	2.2	3.2	5.4
1984	1.4	1.3	1.6	0.4	0.5	1.5	10.8	1.9	2.8	4.7
1985	1.3	0.3	2.4	0.6	0.5	2.8	6.9	1.9	2.8	4.7
1986	1.2	0.2	1.9	0.5	0.3	2.8	5.5	1.1	2.0	3.1
1987	1.4	0.2	1.0	0.4	0.7	1.9	10.6	1.8	3.2	5.0
1988	2.1	0.4	1.3	0.8	0.4	2.0	6.2	0.6	2.2	2.8
1989	1.9	0.3	1.1	0.5	0.6	2.2	9.7	0.9	2.8	3.7
1990	1.5	0.3	1.7	0.6	0.4	2.5	5.9	0.9	2.0	2.9
1991	1.6	0.2	0.9	0.4	0.5	1.6	7.5	1.7	2.8	4.4
1992	1.0	0.3	1.8	0.4	0.5	2.5	6.8	1.2	2.5	3.7
1993	1.1	0.2	1.0	0.4	0.5	1.7	6.6	1.0	2.4	3.4
1994	1.0	0.2	0.8	0.4	0.4	1.4	4.9	1.0	2.0	3.1
1995	1.0	0.3	2.3	0.3	0.2	2.8	3.2	0.7	1.5	2.1
1996	1.8	0.4	2.5	0.4	0.5	3.2	5.5	1.5	3.6	5.1
1997	1.2	0.2	1.3	0.5	0.4	1.7	5.1	1.3	1.9	3.2

Table V-17. Continued.

Year	Wet Deposition (kg/ha/yr)									
	Ca	Mg	Na	K	H	Cl	SO_4-S	NH_4-N	NO_3-N	Total N
1998	1.2	0.2	0.8	0.3	0.3	1.4	4.6	1.3	2.3	3.6
1999	1.5	0.3	1.4	0.3	0.4	2.3	5.5	1.1	2.4	3.5
2000	1.4	0.3	0.7	0.4	0.3	1.1	4.7	1.0	2.2	3.2
Average	1.4	0.3	1.5	0.4	0.4	2.1	7.0	1.5	2.6	3.8
North Fork Dry Run[a]										
1987	1.1	0.3	2.0	1.2	0.5	2.5	10.3	3.0	3.3	6.3
1988	1.6	0.4	1.4	0.7	0.4	1.6	7.4	2.2	2.6	4.7
1989	1.5	0.5	1.6	0.9	0.4	2.3	6.2	2.2	3.5	5.7
1990	1.7	0.4	2.4	1.7	0.4	2.8	7.8	2.9	3.0	5.9
1991	1.2	0.2	1.0	1.0	0.4	1.6	7.0	1.9	2.4	4.3
1992	1.1	0.4	2.5	1.2	0.4	3.0	6.3	1.5	2.3	3.8
1993	1.8	0.4	1.4	1.6	0.5	2.1	7.9	1.7	3.1	4.7
1994	1.8	0.4	1.3	1.3	0.4	1.9	7.5	2.0	2.9	4.9
1995	1.6	0.5	3.1	1.1	0.4	4.0	7.0	1.6	3.0	4.6
1996	1.7	0.4	2.1	1.8	0.4	2.8	6.7	1.4	3.1	4.6
1997	1.1	0.2	1.0	0.8	0.4	1.7	6.8	2.0	2.5	4.4
1998	0.8	0.2	1.3	0.2	0.4	1.9	5.8	1.7	2.8	4.5
1999	0.9	0.3	2.1	0.4	0.4	2.8	6.5	1.9	2.5	4.4
2000	1.0	0.2	1.1	0.3	0.3	1.4	5.6	2.0	2.8	4.8
Average	1.4	0.3	1.7	1.0	0.4	2.3	7.1	2.0	2.8	4.8

[a] Data were collected at Big Meadows by the National Atmospheric Deposition Program (http://nadp.sws.uiuc.edu) and at White Oak Run and North Fork Dry Run by the SWAS (University of Virginia, Department of Environmental Sciences)

respectively (Table V-17). Average annual wet S deposition was also similar among sites (6.7 to 7.1 kg S/ha/yr).

Dry deposition fluxes were estimated at Big Meadows by CASTNet for the period 1991 through 1998, although data were incomplete for 1994 (Table V-18). Dry deposition estimates for S and N were slightly lower than the respective wet deposition estimates (about 73% and 70% for S and N, respectively), in agreement with ASTRAP model estimates provided by Shannon (1998) for use in the SAMI assessment (Sullivan et al. 2002a).

Cloud deposition can be substantial in some cases, particularly at high-elevation sites that are immersed in clouds more than 25% of the time (Mohnen 1988a,b; Lovett and Kinsman 1990). The percent of total S deposition contributed by cloud deposition has been estimated to range from near zero for lower-elevation sites (< 1,000 m) to over 50% at higher elevation (Lovett and Kinsman 1990). At SHEN, most of the park lies below 1,000 m elevation. Cloud

Table V-18. Estimated dry deposition fluxes at Big Meadows, based on data and calculations from CASTNet (http://www.epa.gov/castnet/)

Year[a]	Dry deposition (kg/ha/yr)						
	SO_2	SO_4	HNO_3	NO_3	NH_4	Total S	Total N
1991	4.0	0.8	2.6	0.0	0.1	4.8	2.8
1992	5.1	0.8	2.7	0.0	0.1	5.8	2.9
1993	5.3	0.9	3.0	0.0	0.2	6.2	3.2
1995	3.4	0.7	3.3	0.1	0.2	4.1	3.5
1996	3.3	0.7	2.8	0.0	0.1	4.0	3.0
1997	3.5	0.7	3.1	0.0	0.2	4.2	3.3
1998	4.3	0.8	3.3	0.0	0.2	5.1	3.6
Average	4.4	1.3	3.4	0.5	0.7	4.9	3.2

[a] Data were not available for all four quarters for 1994.

deposition is therefore not expected to constitute a sizeable component of total deposition to acid-sensitive watersheds within the park. This assumption is in agreement with measured (Mohren 1988b, Weathers et al. 1988) and modeled (Shannon 1998) values for cloud deposition of S in SHEN.

Estes (1990) collected and analyzed cloud water samples in the North Fork Dry Run watershed in SHEN (1,014 m) during the period 1986-1987. Highly concentrated cloudwater events (those having H^+ plus SO_4^{2-} concentration greater than 400 μeq/L) were more likely to be associated with NW or ESE wind trajectories than with other trajectories, were most common in summer, and were likely to occur in the presence of a stagnant high pressure system. Such highly concentrated acidic cloudwater events tended to be of relatively short duration, typically less than 20 hours long.

Cloud water data had also been collected earlier, during the Cloud Water Project (Weathers et al. 1988) at Loft Mountain in SHEN (~ 1,000 m), yielding similar median concentrations of major ions in cloud water at the North Fork Dry Run and Loft Mountain sites ($SO_4^{2-} \approx$ 200-300 μeq/L, $NO_3^- \approx$ 120 μeq/L). Mean concentrations of SO_4^{2-} in cloudwater collected during the Mountain Cloud Chemistry Project (MCCP) at Mt. Mitchell, NC (2,006 m) and Whitetop Mt., VA (1,680 m) were more than double those found at the SHEN sites, and concentrations of NO_3^-, NH_4^+, and H^+ were also considerably higher at the Mt. Mitchell and Whitetop Mt. sites (Estes 1990). Elevations within SHEN are considerably lower than the sites included in the MCCP; many peaks in SHEN are above 900 m elevation, but the highest point in the park is only 1,234 m, at Hawksbill Mountain.

During the period 1995 to 1998, average total S deposition was 10.5 kg/ha/yr and average total N deposition was 8.6 kg/ha/yr at Big Meadows, the only site in SHEN for which both wet and dry deposition estimates are available directly from monitoring station data. The S deposition varies, based on the RADM simulation, decreasing from north to south within the park by less than 12%. East-west differences would be expected to be larger due to elevational changes and orographic effects, but the meteorological model resolution (80-km native prediction interpolated to a 20-km grid) was too coarse to resolve the Shenandoah topography, making it impossible to differentiate within-park east-west variability.

b. Trends in Deposition

Reductions in the S component of acidic deposition have generally followed the recent reductions in SO_2 emissions. Preliminary analysis for the eastern United States indicates that total S deposition, which includes dissolved, particulate, and gaseous forms, declined by an average of 26% between 1989 and 1998 (U.S. EPA 2000a). Of more specific relevance to SHEN, wet deposition of S in the mid-Appalachian area (West Virginia and Virginia, as well as areas to the north), declined by 23% between the periods of 1983-94 and 1995-98 (USGAO 2000). Legislated reductions in SO_2 emissions were largely responsible for these reductions in S deposition, and additional, albeit smaller, reductions can be anticipated though 2010.

NADP wet deposition monitoring data are available for Big Meadows since 1981. Annual average wet deposition has declined at many sites in the eastern United States, including Big Meadows (Figure V-33). Lynch et al. (1996) noted substantial decreases since 1995 in the concentration of SO_4^{2-} in precipitation and in wet S deposition at some NADP stations in and immediately downwind of the Ohio River Valley. These decreases were attributed by Lynch et al. (1996) to implementation of Phase I of the CAAA, Title IV.

Data from the wet deposition monitoring stations at White Oak Run and North Fork Dry Run showed generally declining patterns in wet deposition of S (Figure V-33), total N (Figure V-34), NH_4^+-N (Figure V-35), and NO_3^--N (Figure V-36) throughout the period of record. At each site, however, year-to-year variability was generally high. There is an indication of pronounced consistent variability in wet S deposition among the three sites, despite the substantial year-to-year variation at each site. The overall patterns of annual S deposition values at these sites were generally within 10 to 15% of each other throughout the period of record. At the Big Meadows

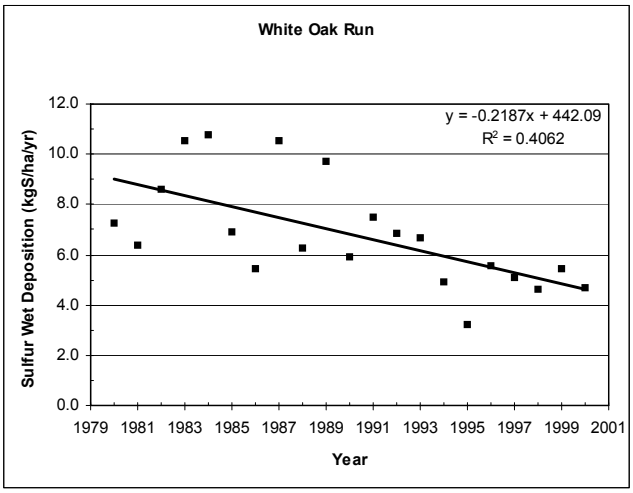

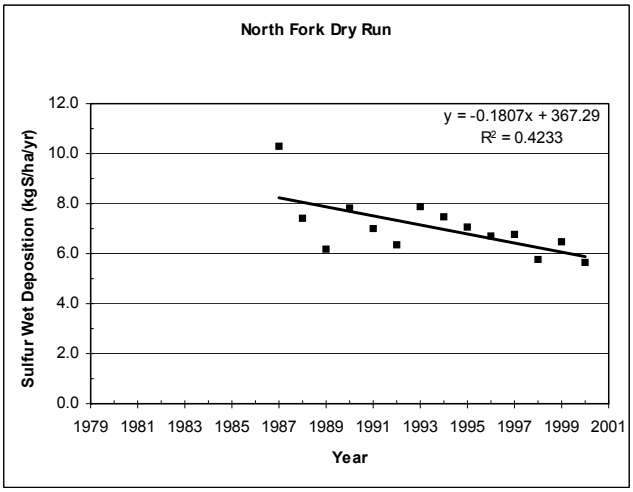

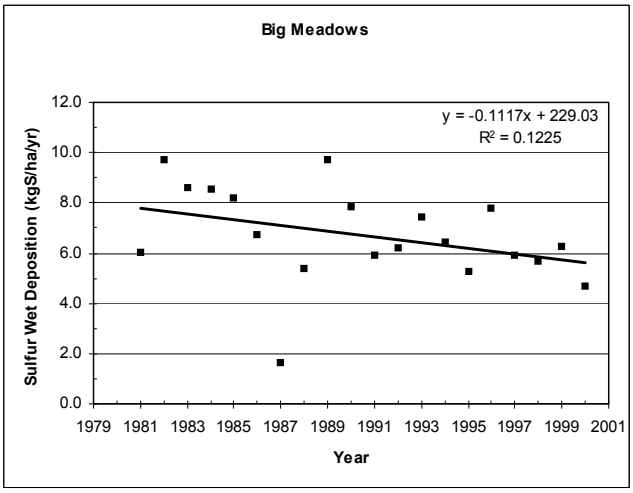

Figure V-33. Wet sulfur deposition for the period of record at three monitoring sites in SHEN. Best-fit regression lines are added. (Data obtained from NADP website and from the University of Virginia.)

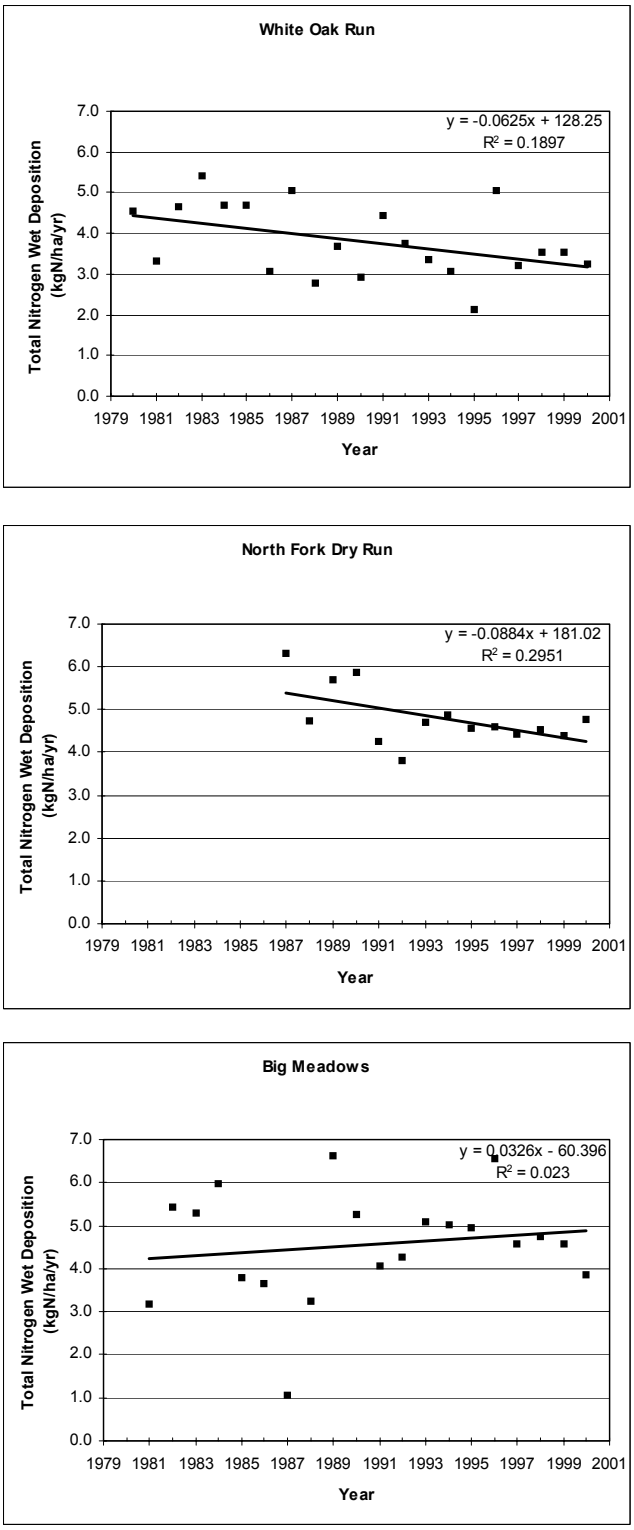

Figure V-34. Wet inorganic nitrogen deposition for the period of record at three monitoring sites in SHEN. Best-fit regression lines are added. (Data obtained from NADP website and from the University of Virginia.)

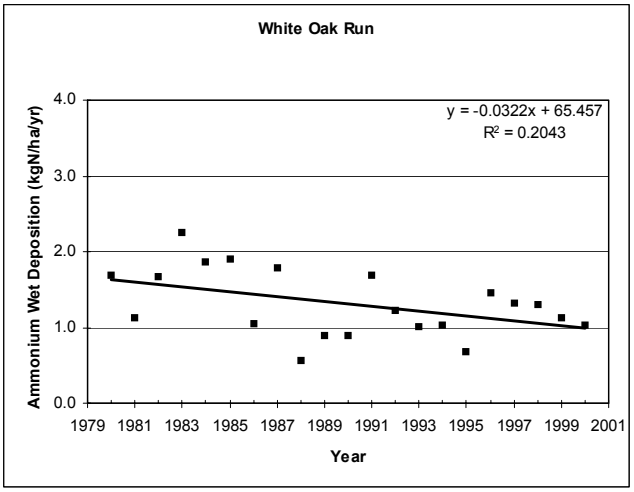

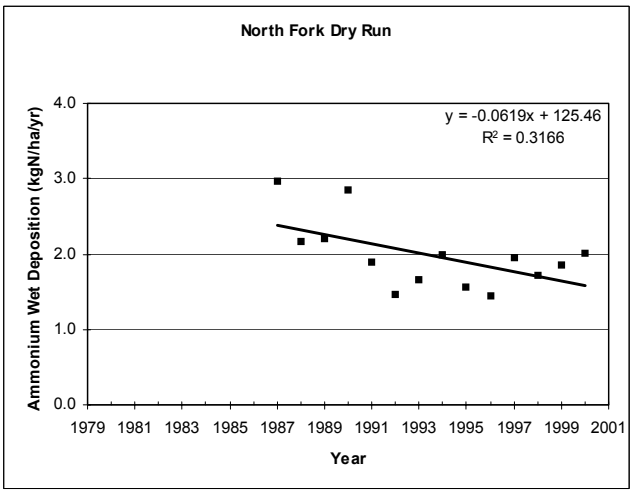

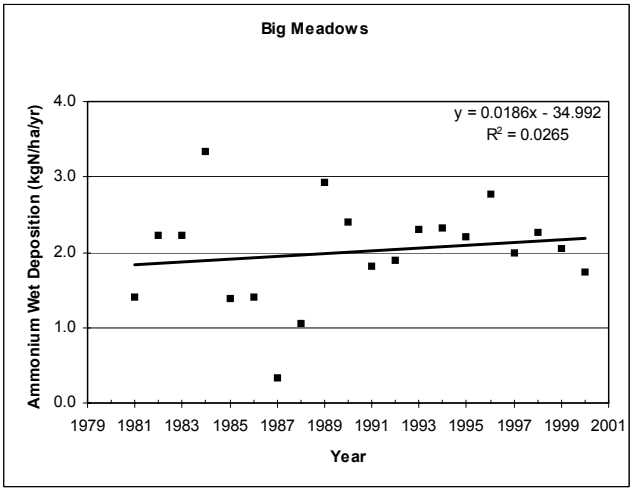

Figure V-35. Wet ammonium deposition for the period of record at three monitoring sites in SHEN. Best-fit regression lines are added. (Data obtained from NADP website and from the University of Virginia.)

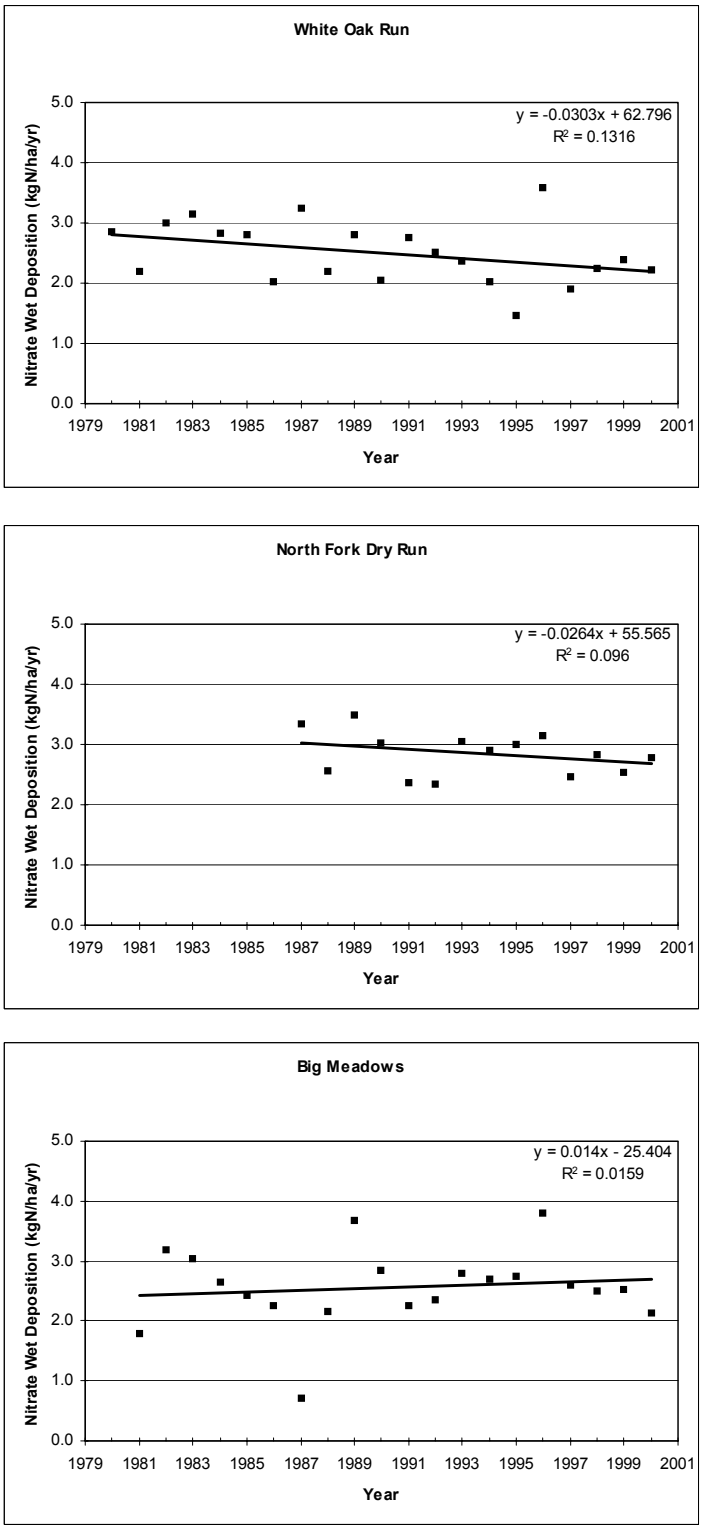

Figure V-36. Wet nitrate deposition for the period of record at three monitoring sites in SHEN. Best-fit regression lines are added. (Data obtained from NADP website and from the University of Virginia.)

monitoring station, S wet deposition data suggested a declining pattern since 1981, but N wet deposition data (total N, NO_3^--N, NH_4^+-N) did not (Figures V-33 through V-36).

Over the 1981 to 2000 period of record, wet N deposition at Big Meadows has varied substantially, generally between about 3 and 7 kg N/ha/yr. There is no indication of large long-term increases or decreases in wet N deposition, although there has been a relatively consistent short-term decline over the last five years at Big Meadows (Figure V-34 and V-36). Additional data will be required to determine whether this apparent downward trend is meaningful.

D. PROJECTED CHANGES IN FUTURE AIR QUALITY AND DEPOSITION

The RADM was developed with grids that are 80-km on a side (Figure V-37). More recently, a 20-km grid covering the northeastern U.S. was created as a one-way nest within the 80-km grid. The 20-km grid was the principal grid used for this assessment. The model was extended or enhanced by adding the capability to represent SO_4^{2-}-NO_3^--NH_4^+-water aerosol composition based on equilibrium thermodynamics by incorporating into RADM a module from the Regional Particulate Model (Binkowski and Shankar 1995). The Extended RADM is described in Appendix C.

RADM is very computationally intensive because it predicts hourly photochemistry. A statistical approach, termed aggregation (Dennis et al. 1990), was developed as part of NAPAP to create annual estimates of acidic deposition without having to model an entire year. Meteorological cases of five-day duration were grouped by large-scale wind flow pattern through cluster analysis and sampled proportionate to their frequency of occurrence across a seven-year period of the early 1980s (Brook et al. 1995a,b). A total of 30 cases constitute the aggregation sample. The precipitation predicted for each cluster was adjusted to the long-term mean precipitation for that cluster to estimate average deposition. The aggregation method produced a climatological average of transport and deposition representative of the transport of the 1980s and the seven-year average precipitation of that period. The precipitation average approximated well the 30-year normal precipitation. Although developed to represent an annual average, the 30 aggregation cases naturally divide into a warm and a cold season. Thus, broad seasonality can be accommodated with the aggregation method which matches well with the seasonally-oriented O_3 control approaches, such as the NO_X SIP Call.

For the Base Case and the scenario projections, the meteorology was held constant, retaining the same climatology of transport, temperature, cloudiness and precipitation. Only the

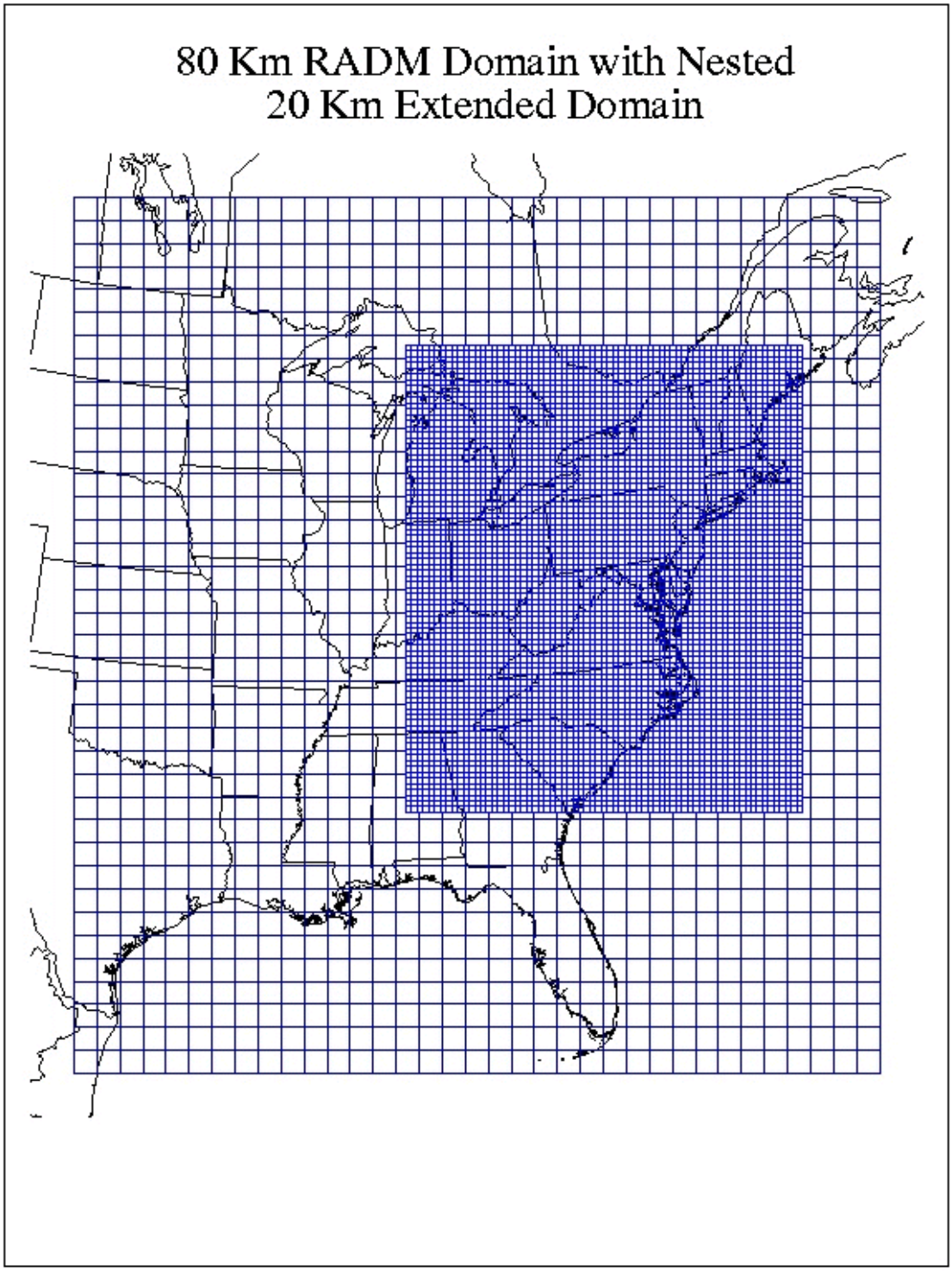

Figure V-37. Representation of the 80-km grid domain of the RADM model, with the nested 20-km grid that was created for this assessment.

emissions were changed for the emissions scenarios. Gridded, hourly emissions were regenerated from the county-level emissions inventory for each of the 30 five-day aggregation cases, using the emissions processing models. The Extended RADM was run in two steps for each of the 30 cases: first the 80-km grid domain and then the 20-km domain nested within it. The 30 cases from each grid domain were aggregated into the corresponding annual (or warm- or cold-season) average for use in the analysis of changes in air quality and deposition metrics associated with the changes in emissions.

The changes in the pollution metrics predicted by the Extended RADM air quality model relative to the 1990 Base Case are given in Table V-19. Each major pollution metric is discussed in turn.

Ozone - The percent change in O_3 concentrations of the upper two-thirds of the O_3 distribution is well illustrated by the changes in the 70th percentile. The percent change in this percentile is consistent with the NO_X emission changes and the corresponding percent changes in NO_x deposition. The projected O_3 change was about one-third of the projected NO_x deposition change, which is consistent with and typical of other regional O_3 modeling results. The growing season SUM06 O_3 exposure metric using a 60 ppb threshold is best represented in its hours-per-day stratification by the Extended RADM with an exposure calculated using a model threshold of 65 ppb O_3 (see Appendix C). The change in the O_3 growing season exposure metric (Exposure above threshold) was projected to change much more than the O_3 concentration. The much larger projected change in exposure above threshold was due to the fact that an increasing number of days/hours during the summer dropped below the threshold. The change in hours above the threshold was large: +7.8%, -27.8%, -49.1%, -58.8%, and -87.6% for 1996, Scenario 1, Scenario 2, Scenario 3, and Scenario 4, respectively. The two factors, the change in O_3 concentration and the change in hours above threshold, together explain the change in the Extended RADM representation of the SUM06 O_3 exposure metric, and that change was dominated by the change in the number of hours above the threshold. For example, in Scenario 2 the O_3 concentration change was -15.7%, the change in hours above threshold was -49.1% and the resulting change in the O_3 exposure metric was -55.5%.

Total sulfur deposition - The estimated changes in annual S deposition were smaller than the estimated changes in annual SO_2 emissions. For example, Scenario 3 had a 90% reduction in EGU SO_2 emissions, which translates into 74% and 77% reduction in total SO_2 emissions for the Top 10 States and Top 5 States, respectively (Table IV-4). The change in median annual SO_2 air

Table V-19. Percent changes in pollutants and pollutant metrics relative to the 1990 Base Case as predicted by the Extended RADM (20-km Grid) model.

Attribute	1996	Scenario 1 2007/10	Scenario 2 2020	Scenario 3 2020	Scenario 4 2020
O_3 - growing season Exposure above threshold	9.9%	-35.4%	-55.5%	-63.2%	-89.7%
O_3 - 70th Percentile	2.0%	-10.0%	-15.7%	-17.1%	-22.4%
O_3 - Hours above threshold (65 ppm)	7.8%	-27.9%	-49.1%	-58.8%	-87.6%
Total sulfur deposition (annual)	-20.2%	-33.2%	-36.7%	-68.7%	-74.9%
Total oxidized nitrogen deposition (annual)	2.7%	-35.2%	-50.3%	-59.0%	-66.8%
Ratio total ox-N/total red-N deposition[a] (where ammonia emissions are kept constant)	2.9 (2.5)	1.9 (1.6)	1.4 (1.3)	1.2 (1.0)	1.0 (0.8)
SO_4+NO_3+NH_4 fine particle air concentrations					
Annual 50th Percentile	-6.9%	-15.7%	-17.5%	-41.7%	-50.4%
Warm Season 50th Percentile	-15.0%	-28.5%	-30.8%	-55.7%	-63.6%
SO_4 fine particle air concentrations					
SO_4 annual 50th Percentile	-10.6%	-21.7%	-23.1%	-54.6%	-61.6%
SO_4 warm season 50th Percentile	-18.0%	-29.5%	-32.0%	-59.1%	-66.4%
SO_2 air concentrations					
SO_2 annual 50th Percentile	-23.2%	-44.5%	-48.8%	-77.1%	-82.6%

[a] Ratio in parenthesis is based on 1990-centered Shenandoah average oxidized and reduced nitrogen deposition estimated from NADP and UVa wet deposition, NADP and CASTNet (ox-N wet-to-dry ratio), and NADP and Extended RADM (red-N wet-to-dry ratio).

concentrations was 77%, consistent with the emissions reduction, while the resulting reduction in S deposition was 69%, about 10% smaller than the air concentration reduction. The S deposition reductions were smaller because of the expected nonlinearity in S wet deposition due to oxidant limitation. The degree of nonlinearity was consistent with estimates made during the NAPAP study.

Total oxidized nitrogen deposition - The projected changes in oxidized nitrogen deposition were somewhat larger than estimated changes in the Top 10 state NO_X emissions. The main reason for this is that the local, top 3 state estimated changes in NO_X emissions were larger than the Top 10 state emission changes and much closer to the change in oxidized nitrogen deposition. The nearby states had a strong influence on projected oxidized nitrogen deposition at SHEN. A quantitatively unimportant effect was the increase in the ratio of particulate NO_3^- partitioned to total NO_3^-. It increased because of the strong reductions in SO_4^{2-}. Particulate NO_3^- dry deposition was an order of magnitude smaller than nitric acid dry deposition; hence, the estimated total rate of oxidized nitrogen dry deposition decreased. However, this effect on the dry deposition rate was offset by the result that the total NO_3^- budget increased, thereby increasing the rate of wet deposition. There was only a small percentage point difference in the projected changes in overall oxidized nitrogen wet and dry deposition.

Inorganic fine particles - The estimated changes in SO_4^{2-} fine particles were smaller than the estimated changes in SO_2 air concentrations. For example, in Scenario 3 the median annual SO_2 air concentrations declined 77%, whereas the median annual SO_4^{2-} air concentrations declined 55%. This was the result of oxidant limitation effects in the aqueous-phase production of SO_4^{2-}. Four of the 5 top source regions affecting SO_4^{2-} air concentrations in SHEN are in the Ohio River Valley (Figure IV-9) where the nonlinearity in SO_4^{2-} production is strongest. The estimated changes in total inorganic fine particles were smaller than even the SO_4^{2-} air concentration changes. The reductions in total inorganic fine particles were influenced toward smaller reductions because of the NO_3^-. Sulfate, and the NH_4^+ associated with it, is currently the largest component of inorganic fine particulate. Major reductions in SO_2 emissions with no reduction in NH_3 emissions would be expected to leave more NH_3 in the atmosphere to bind with nitric acid and form particulate NH_3. Ammonia binds preferentially with sulfuric acid to produce SO_4^{2-}. The eastern U.S. is presently NH_3-limited, the available SO_4^{2-} is not completely neutralized by NH_3, and there is abundant nitric acid. The formation of NO_3^- is determined by "left-over" NH_3 availability. As SO_4^{2-} is reduced, the ratio of particulate NO_3^- to total NO_3^- will increase due to the increase in availability of NH_3, greatly moderating decreases in NO_3^- concentrations and mitigating or offsetting a portion of the SO_4^{2-} reductions.

IV. EMISSIONS AND AIR POLLUTANT TRANSPORT

A. PURPOSE

Ambient and visual air quality degradation and acidic deposition in Shenandoah National Park (SHEN) are the result of distant and local (including in-park) pollutant emissions. Based upon pollutant transformations and lifetimes in the atmosphere and on regional climatology, the various emissions sources contribute in varying degree to pollutant loading or exposure in the park. The purpose of this section is to summarize regional and local emissions and assess the effects of atmospheric transport processes. Major air pollution source regions and states affecting the park are identified. Several scenarios of future emissions controls are described, providing the foundation for evaluation of possible resource recovery in the future.

B. RECENT AND PROJECTED FUTURE REGIONAL EMISSIONS

The emissions from two base years, 1990 and 1996, are analyzed in this assessment. Four estimates of future emissions were developed and analyzed as well. These future emissions scenarios were developed by applying growth and emissions control assumptions to the 1996 base year inventory. The development of these emission inventories is discussed here.

State-level sulfur (S) and nitrogen (N) 1990 emissions data were compiled for this project from the annual National Emissions Trend inventory, as revised in October 2000 by the U.S. Environmental Protection Agency (EPA). The area source emissions were taken from version 3.01a, the mobile source emissions from version 3.00, and the point source emissions from version 2.00. In all cases, mobile (e.g., on-highway cars, light trucks and heavy trucks), area-stationary (e.g., commercial and residential heating and vented emissions from commercial buildings), and area-nonroad (off-road vehicles, tractors, construction equipment, locomotives, and ships) emissions were developed at the county level, whereas point source locations were defined in terms of their latitude and longitude.

In addition, 1996 emissions data were derived from the annual National Emissions Trend inventory (U.S. EPA 2000a). The point source emissions for electricity generating units (EGUs) and non-EGUs were taken from version 3.12, and the stationary area-source emissions from version 3.11. Other 1996 emissions were developed by EPA as part of their regulatory analysis of heavy-duty engine and vehicle standards and highway diesel fuel rulemaking. The majority of the mobile nonroad source emissions were developed using EPA's draft NONROAD model, while aircraft, commercial marine, and locomotives (not in NONROAD) were estimated separately (U.S. EPA 2000b). The combined categories of all nonroad emissions are termed here area-nonroad emissions. For 1996 mobile source emissions, the on-highway vehicle emission

inventory created in 1998 was updated. In particular, a new vehicle miles traveled (VMT) mapping from the Highway Performance Monitoring System data to MOBILE5b was developed by EPA and the latest information on 1996 control programs was used, including Inspection and Maintenance programs, Reformulated Gasoline use, Oxygenated Gasoline use, and the Low Emission Vehicle program. Details are provided in U.S. EPA (2000b). The 1996 Case reflects 1990 Clean Air Act Amendments (CAAA) Title IV Phase I implementation of EGU sulfur dioxide (SO_2) and nitrogen oxide (NO_x) emission reductions.

The airsheds of SHEN contain numerous major stationary sources of air pollution. Emissions from mobile sources and many stationary sources are expected to increase with substantial population and industrial growth in Virginia and other airshed states (Shenandoah National Park 1998b). More Prevention of Significant Deterioration (PSD) air permit applications have been reviewed by the National Park Service (NPS) Air Resources Division (ARD) for SHEN than for any other NPS area (Figure IV-1). In addition, SHEN and Great Smoky Mountains National Park are two Class I parks where the NPS has been able to compile an overwhelming amount of data indicating that resources are damaged by human-caused air pollution (NPS 1990, NPS 2000c).

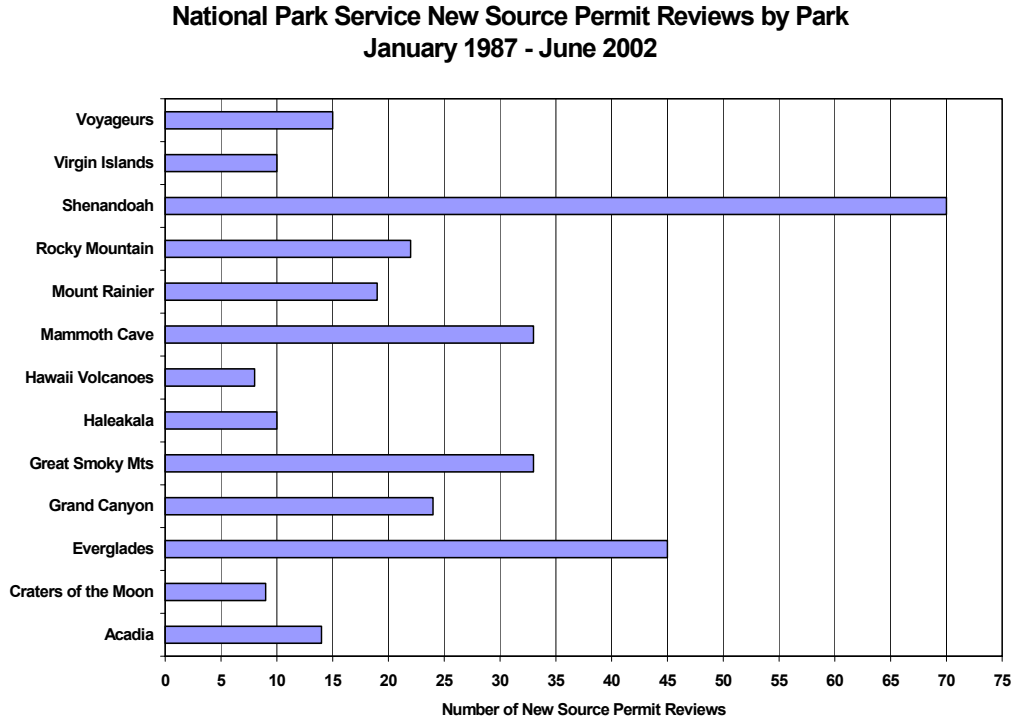

Figure IV-1. New source permit reviews during the period January 1987 to June 2002. In addition, there have been about 6 additional Virginia/ Shenandoah new source permit reviews since June 2002.

A brief description is given here of the four future emissions scenarios selected for this assessment. State-level emissions for fifteen states surrounding SHEN are listed in Tables IV-1 and IV-2 for the 1990 Base Case, the 1996 case, and the four scenarios for future SO_2 and NO_x emissions, respectively. The top four states for both SO_2 and NO_x Base Case emissions were Ohio, Indiana, Pennsylvania, and Illinois. Each of the scenarios is described below.

Scenario 1. 2007/2010 Base with NO_x State Implementation Plan (SIP) Call

Scenario 1 provides our best estimate of emissions expected for the 2010 time frame. This scenario represents the base 1990 CAAA effect on emissions due to control programs already in place, with projections provided to 2010. Scenario 1 consists of projected emissions for all source categories assuming a reasonable amount of economic growth as projected by the Bureau of Economic Analysis (BEA) in the Department of Labor, and emissions limitations due to existing 1990 CAAA air pollution emissions control programs that have been codified in law, with rules promulgated and any litigation settled as of summer 2000[1]. The emissions limitations

Table IV-1. State-level annual emissions totals of SO_2 for the 1990 Base Case, the 1996 case, and the four scenarios (tons/year). The top five states are shaded for each scenario.

	1990 Base	1996	Scenario 1	Scenario 2	Scenario 3	Scenario 4
Delaware	100,000	97,303	86,676	96,403	62,826	52,167
Georgia	1,000,330	594,127	720,507	719,843	204,996	156,647
Illinois	1,261,534	1,070,104	836,073	863,813	543,451	333,329
Indiana	1,920,416	1,116,166	729,283	689,224	397,407	289,683
Kentucky	1,034,272	767,112	570,764	512,412	232,278	210,750
Maryland	435,774	298,151	257,244	233,549	73,650	70,394
Michigan	726,298	572,744	565,822	536,399	300,129	250,124
New York	867,415	627,866	522,022	405,096	359,902	234,217
North Carolina	487,616	577,874	693,293	663,277	250,218	191,850
Ohio	2,736,237	1,974,126	1,380,563	1,224,841	577,144	401,665
Pennsylvania	1,517,739	1,291,592	886,909	866,065	333,294	250,912
South Carolina	292,567	285,982	285,136	297,850	143,150	107,738
Tennessee	1,077,345	753,602	505,268	425,899	265,951	167,749
Virginia	403,610	341,015	353,543	347,235	232,967	170,651
West Virginia	1,074,715	773,282	606,655	530,000	196,623	164,911

[1] This implies the NO_x SIP call in the eastern states is based upon implementation of a one hour standard and does not take into account the final decision handed down by the DC Circuit Court March 26, 2002.

Table IV-2. State-level annual emissions totals of NO_x for the 1990 Base Case, the 1996 case, and the four scenarios (tons/year). The top five states are shaded for each scenario.

	1990 Base	1996	Scenario 1	Scenario 2	Scenario 3	Scenario 4
Delaware	102,989	84,705	65,833	51,747	44,038	36,379
Georgia	687,001	756,961	675,430	531,896	370,390	298,698
Illinois	922,261	1,135,766	836,627	671,787	565,381	441,999
Indiana	905,979	881,712	598,377	456,076	328,825	276,648
Kentucky	674,772	752,302	510,432	425,022	295,271	260,610
Maryland	354,842	354,692	240,890	180,155	143,809	126,394
Michigan	887,552	904,068	708,591	579,000	511,067	394,655
New York	844,656	765,350	523,248	346,138	324,112	276,303
North Carolina	577,599	732,552	523,519	402,401	319,437	257,449
Ohio	1,156,094	1,310,664	793,495	614,480	479,899	396,716
Pennsylvania	1,081,534	1,086,095	847,346	661,327	542,779	397,475
South Carolina	353,655	401,430	298,566	232,078	193,871	146,594
Tennessee	727,134	816,578	557,305	420,384	357,456	285,032
Virginia	564,357	609,972	456,249	331,008	296,699	239,502
West Virginia	568,976	514,532	366,492	308,767	201,437	159,869

expected from existing programs currently "on the books" as of the year 2000 include Federal, state and local emissions control programs. The major programs included in this base emissions projection are the Federal CAAA Title IV limits on electricity generation for SO_2 and NO_x, designed to address the problem of acid deposition; Federal Tier II vehicle standards, designed to help alleviate problems related to urban smog; the Federal NO_x SIP Call in approximately twenty states located east of the Mississippi River, designed to address tropospheric O_3 attainment problems under the Federal National Ambient Air Quality Standards (NAAQS); and the Federal Heavy Duty Diesel Vehicle (HDDV) Standards program. Details regarding the future year projections are specified in the technical support document for the HDDV rule (U.S. EPA 2000b). The two programs accounting for the great majority of the emissions reductions by 2010 are the Title IV limits and the Federal NO_x SIP Call. Scenario 1 was constructed by using the 2007 HDDV inventory for point, area, and mobile source emissions, and a 2010 Integrated Planning Model (IPM) projection for electricity generation emissions as revised to reflect the result of litigation decisions finalized in the summer of 2000.

Scenario 2. 2020 CAAA with Tier II and Heavy Duty Diesel Regulations

Scenario 2 provides the current best estimate of emissions expected for the 2020 time frame due to CAA regulations that are now in place. This scenario has the same basic set of control programs as described above, but with their effects on emissions now projected to the year 2020. The reduction in mobile source emissions due to the new Tier II Vehicle Standards is becoming more evident due to great penetration of the control technology over time into the fleet of vehicles actually on the road. It typically takes 15 years for the effect of new mobile source emissions reductions to be fully actualized. In addition, the HDDV standards have been implemented and are resulting in noticeable improvements in emissions from heavy duty diesels. Finally, CAAA Title IV acid rain controls on EGUs are being seen near the level of the cap, having nearly exhausted the banked allowances from reductions beyond required amounts in earlier years. The Tier II and HDDV standards are responsible for a large majority of the emissions reductions between 2010 and 2020, i.e., differences between Scenario 1 and Scenario 2.

Scenario 3. 2020 CAAA with the Addition of Stringent Utility Controls

The objective of Scenario 3 is to assess the potential for ambient and visual air quality and acidic deposition improvements beyond current plans if additional, maximally-feasible controls were applied to EGUs only. This scenario, and Scenario 4 (described below) were devised because current plans are not expected to produce air quality and acidic deposition levels low enough to be considered protective of all sensitive receptors (e.g., visibility, acid-sensitive streams and biota, O_3-sensitive plants). This scenario takes the projected emissions levels in 2020 for all sectors as identified above and adds additional controls to EGUs. This case imposes a nationwide 90% reduction in EGU SO_2 emissions beyond Title IV acid rain emission control levels. The controls in this scenario are imposed starting in the year 2005. The existing allowance bank for SO_2 allowances due to excess reductions in earlier years is not discounted[2]. The EGU NO_x emissions are constrained starting in 2005 at an annual national emission rate of 0.10 lb NO_x (as nitrogen dioxide) per million BTU of heat input. This NO_x scenario is a cap and trade scenario operating annually and nationally (in the contiguous 48 States and Washington,

[2] This means that any and all allowances banked in years prior to 2005 as part of CAAA Title IV acid rain program compliance are available in subsequent years. The analysis indicates, however, that the bank is essentially used up by the year 2020.

DC). Any existing banked allowances from excess reductions beyond the required reduction, due to existing NO_x control programs (such as the Ozone Transport Commission and any cap and trade SIP Call programs), are available for use in years 2005 and beyond[3].

Scenario 4. 2020 CAAA with the Addition of Stringent Controls on Utility, Industry-Point, and Mobile Sources

The purpose of Scenario 4 is to assess the levels of air quality and acidic deposition that might be attained through additional, stringent controls of EGU (same as Scenario 3), non-EGU and mobile source emissions. The objective was to determine if air quality levels could be achieved that would be considered protective of the park's visibility and aquatic and terrestrial ecosystems. This scenario incorporates additional reductions from sources other than electricity generation to the limit of currently available commercial reduction technology. These additional reductions are combined with the stringent EGU reductions modeled in Scenario 3. The target level for this analysis of control strategies was to achieve 50% SO_2 and NO_x emissions reductions in 2020 nationwide from point sources other than electricity generation and mobile sources. The baseline for non-EGU point source and mobile source reductions was the suite of emissions projections that were prepared for the HDDV rulemaking. Methods used to prepare the baseline emissions projections used in this analysis are described in Pechan and Associates (2001). Non-utility (non-EGU) sources were analyzed to determine the control technology predicted to be in place in 2020 for the HDDV analysis. Given the base 2020 technologies, estimates were made of the maximum amount of emissions reduction possible, with the technologies that are currently commercially available, that can be applied to the specific sources as listed in the inventory. Complete description of the analysis was provided in Pechan and Associates (2001). Light duty mobile vehicles emissions were adjusted to reflect super-ultra-low emissions vehicles consistent with the California Clean Car alternatives (CARB 2001), thereby achieving additional reductions beyond the Federal or state rules in place in the rest of the country as of the summer of 2000.

Using the definition of each of the four scenarios, future emissions were projected for each scenario. The base emissions inventories for 2007 (Scenario 1) and 2020 (Scenario 2) were developed by applying growth and control assumptions to the 1996 Base Year inventory. The

---

[3] It should be noted, however, that the control level is sufficiently stringent that banking of NO_x allowances is not significant and can essentially be considered zero by 2020.

IPM model (U.S. EPA 2002a,b) was used to project unit-level emissions for EGU point sources. New units were incorporated in the simulation where needed to meet projected generation demands. Complete implementation of the 1990 CAAA Title IV limits on electricity generation emissions, set for 2010, were assumed for EGU point sources. For the non-EGU sources and non-mobile emissions, 1995 BEA Gross State Product growth projections (BEA 1995) at the state level were utilized to estimate changes in activity factors and industrial mix from 1996 to 2007 and 2020. For mobile emissions, the number of VMT was projected from 1996 using VMT projection data (at the county, vehicle type, and roadway type level of detail) from EPA's Tier 2 rulemaking (U.S. EPA 1999). Fleet emissions were estimated based on the MOBILE5b emission factor model with some additional adjustments. The growth and control assumptions are documented in U.S. EPA (2000b). For the emissions control scenarios, ammonia (NH_3) emissions were kept constant at the mass emissions rates of the early 1990s. After applying the changes in activity and VMT, together with the effect of existing emissions control programs, to create future Base Cases, additional controls were added to reflect the alternative scenarios for 2020. Estimates of major emissions were developed at the county level for mobile highway, stationary non-road, EGU, non-EGU, and stationary area sources. These mass emissions inventories were developed for winter and summer months for input to the emissions processing models used to create the gridded inputs for the air quality model.

Emissions summaries for 1990, 1996, and the future projections were combined into five source categories for the modeling analysis: Area Stationary, Area Nonroad, Mobile, EGU-Point and non-EGU Point Sources. To provide an overview of the changes in emissions associated with each scenario, Area Stationary, Area Nonroad and Mobile Sources were grouped and termed Surface Sources whereas EGU-Point Sources and non-EGU Point Sources were grouped and termed Point Sources. In addition, the emissions for the top 10 and top 5 states affecting SHEN were summed for the overview. The annual emissions for the top 10 and top 5 states for the two groups are given in Table IV-3 for the 1990 Base Case, the 1996 Case and the 4 future scenarios. Bar charts in Figures IV-2 and IV-3 show the annual SO_2 and NO_x emissions, respectively, from Table IV-3 for the top 10 states. The percent changes from the 1990 Base Case are given in Table IV-4. Major reductions in emissions are anticipated as the result of current rules and regulatory plans, represented by Scenario 2. Under the current set of rules that exist or are being promulgated, nationwide SO_2 emissions would be reduced by 47% from 1990

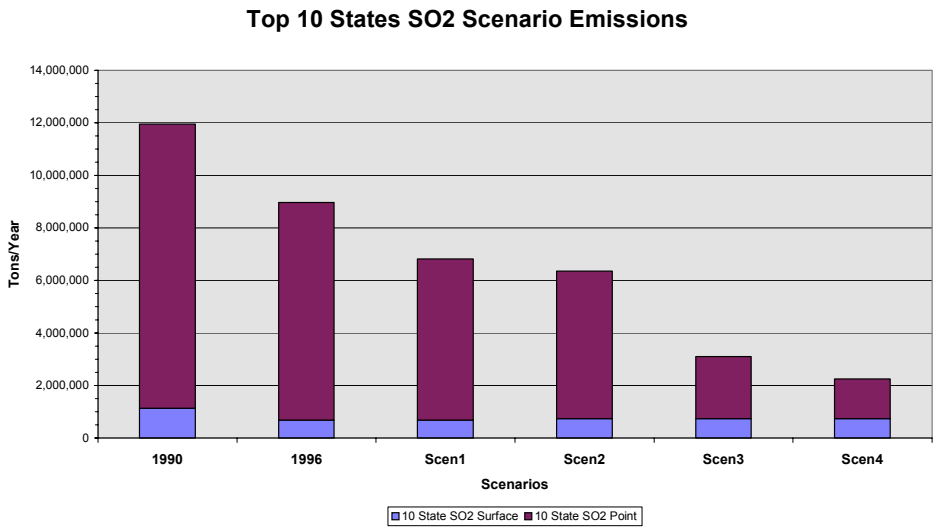

Figure IV-2. Bar chart of SO_2 emissions showing Surface and Point emissions for the top 10 states in 1990, 1996, and each of the scenarios.

Table IV-3. Summary of annual SO_2 and NO_x emissions subdivided into Surface and Point Sources for the 1990 Base, 1996 and the four scenarios.

	1990	1996	Scenario 1	Scenario 2	Scenario 3	Scenario 4
Emissions for Top 10 States Tons/Year (000s)						
SOx - Surface	1,131	684	676	742	742	742
SOx - Point	10,818	8,279	6,143	5,615	2,361	1,510
SOx - Total	11,949	8,963	6,820	6,356	3,103	2,252
NOx - Surface	3,759	4,510	3,416	2,198	2,198	1,952
NOx - Point	3,774	3,685	2,315	2,273	1,333	889
NOx - Total	7,534	8,195	5,731	4,471	3,531	2,842
Emissions for Top 5 States Tons/Year (000s)						
SOx - Surface	569	411	395	423	423	423
SOx - Point	6,198	4,736	3,403	3,058	1,150	776
SOx - Total	6,767	5,147	3,798	3,481	1,572	1,199
NOx - Surface	1,876	2,309	1,727	1,082	1,082	951
NOx - Point	2,073	1,945	1,260	1,236	758	500
NOx - Total	3,949	4,254	2,987	2,318	1,840	1,451

Surface = Area-Stationary + Area-Nonroad + Mobile
Point = EGU-Point Sources + non-EGU-Point Sources

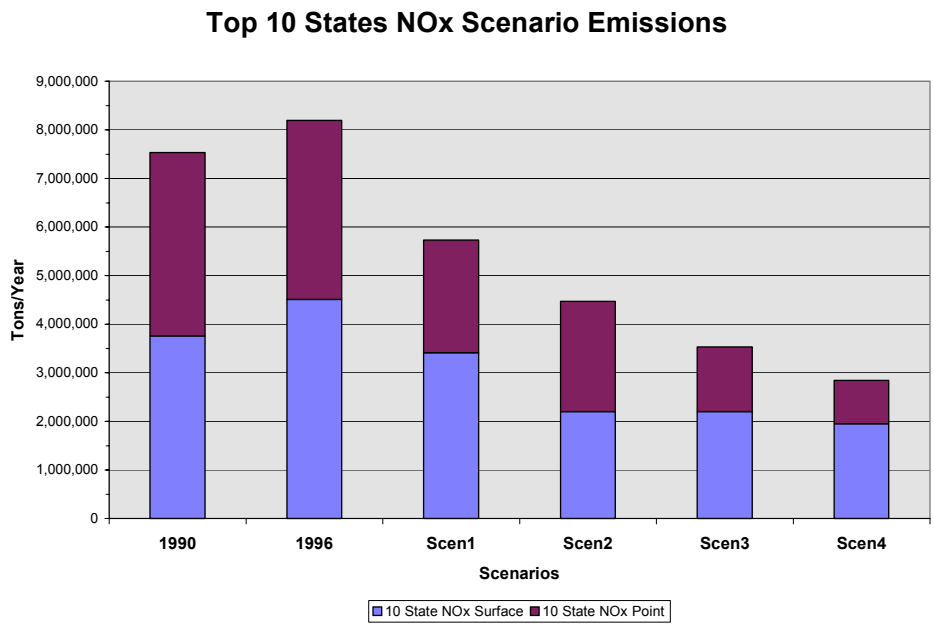

Figure IV-3. Bar chart of NO_x emissions for Surface and Point Source emissions for the top 10 states in 1990, 1996, and each of the scenarios.

Table IV-4. Summary of the percent changes in annual SO_2 and NO_x emissions from the 1990 Base Case to 1996 and the four future scenarios for the Surface and Point Source categories.

	1996	Scenario 1	Scenario 2	Scenario 3	Scenario 4
Percent Change Top 10 States[a]					
SOx - Surface[b]	-39.6%	-40.2%	-34.4%	-34.4%	-34.4%
SOx - Point[c]	-23.5%	-43.2%	-48.1%	-78.2%	-86.0%
SOx - Total	-25.0%	-42.9%	-46.8%	-74.0%	-81.2%
NOx - Surface	20.0%	-9.1%	-41.5%	-41.5%	-48.1%
NOx - Point	-2.4%	-38.7%	-39.8%	-64.7%	-76.4%
NOx - Total	8.8%	-23.9%	-40.7%	-53.1%	-62.3%
Percent Change Top 5 States					
SOx - Surface	-27.8%	-30.6%	-25.7%	-25.7%	-25.7%
SOx - Point	-23.6%	-45.1%	-50.7%	-81.5%	-87.5%
SOx - Total	-23.9%	-43.9%	-48.6%	-76.8%	-82.3%
NOx - Surface	23.1%	-7.9%	-42.3%	-42.3%	-49.3%
NOx - Point	-6.1%	-39.2%	-40.4%	63.4%	-75.9%
NOx - Total	7.7%	-24.4%	-41.3%	-53.4%	-63.3%

[a] To identify which are the Top 5 or the Top 10 states, as emissions sources for SHEN, see Tables IV-1 and IV-2
[b] Surface = Area-Stationary + Area-Nonroad + Mobile
[c] Point = EGU-Point Sources + non-EGU-Point Sources

levels and NO_x emissions reduced by 41% relative to 1990. Scenarios 3 and 4 represent significant reductions beyond current plans.

Compared to the levels of emissions anticipated for Scenario 2, Scenario 4 would further reduce nationwide SO_2 emissions by 64%. The largest SO_2 reduction occurs between Scenarios 2 and 3. For nationwide NO_x emissions, the reductions are important but less dramatic; between Scenario 2 and 4 they are 36%. The NO_x reduction from Scenario 2 to 3 is 21% and from Scenario 3 to 4 is 18%. The trend in the magnitude of SO_2 emissions from 1990 over the scenarios is shown in Figure IV-2. There were fairly large reductions in SO_2 emissions from 1990 to 1996 and then from 1996 to Scenario 1 that are the result of the 1990 CAAA Title IV Phase 1 (1996) and Phase 2 (Scenario 1) controls, approximately 3 million and 2 million tons of SO_2, respectively. There is only a small additional reduction of SO_2 emissions with Scenario 2 because SO_2 is not targeted in the emissions controls specified for this scenario. There is more than a 3 million ton reduction of SO_2 between Scenario 2 and 3, a significant additional reduction. An additional 800,000 tons of SO_2 is assumed to be removed in going from Scenario 3 to 4. The vast bulk of the additional SO_2 reductions between 1990 and Scenario 4 come from the EGUs, approximately 9.3 million tons out of the total of 9.7 million tons for the top 10 states.

The proportion of emissions in each source category changes dramatically for SO_2 between 1990, Scenario 3, and Scenario 4. This is shown in the pie charts of Figure IV-4 for the top 10 states. In 1990, EGU point sources made up 79% of the SO_2 emissions, while the EGU and non-EGU point sources together made up 91%. After the significant reductions in EGU SO_2 emissions for Scenario 3, their estimated proportion was reduced to 29% and the non-EGU point source proportion expanded to 48%. Together, they still accounted for approximately three-quarters of the SO_2 emissions. With the major non-EGU point reduction in SO_2 emissions for Scenario 4, point sources still accounted for 67% of the SO_2 emissions and the area-stationary and area-nonroad sources quadrupled from 8% in 1990 to 33% in Scenario 4. It took the strong focus on reducing SO_2 point source emissions, 86% reduction for point sources compared to the 34% reduction for surface sources, to achieve this dramatic shift in proportions of SO_2 emissions attributed to each sector.

The trend in the magnitude of NO_x emissions from 1990 over the scenarios is shown in Figure IV-3. There was an increase in NO_x emissions from 1990 to 1996, then continual reductions for each scenario step after 1996. Compared to 1990, the additional increment in the percent reductions becomes progressively smaller, about two thirds as large as the previous

(a)

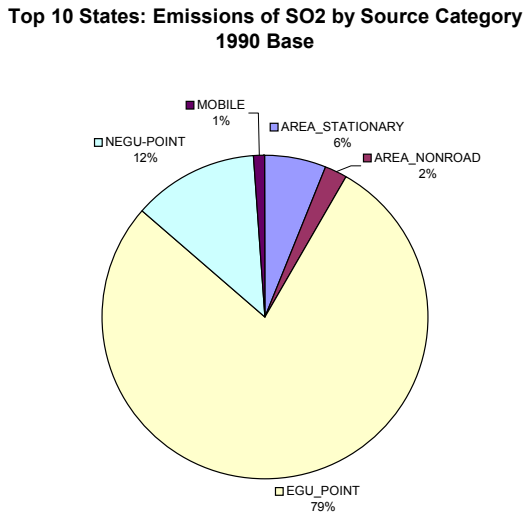

(b)

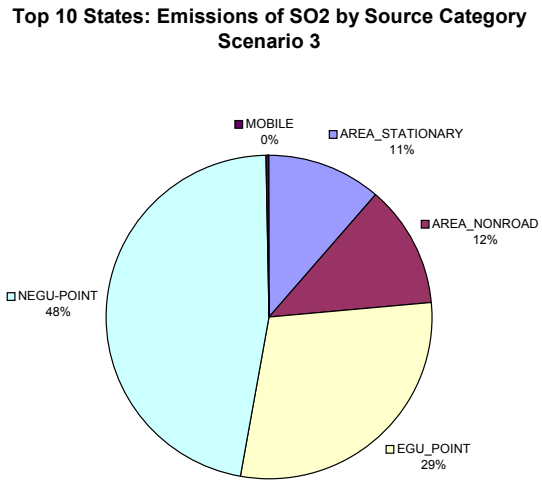

(c)

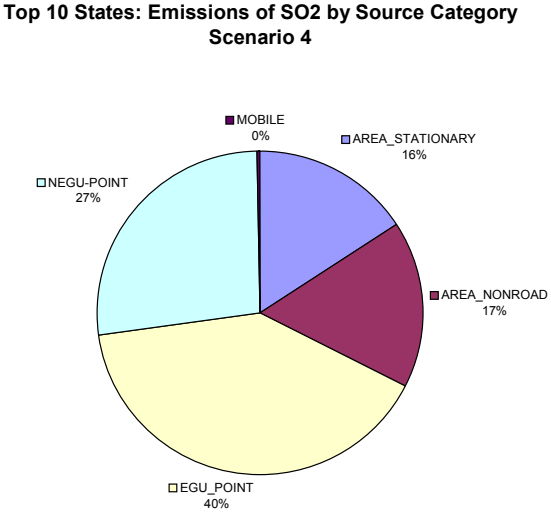

Figure IV-4. Pie chart of SO_2 emissions broken down by five source categories comparing (a) 1990, (b) Scenario 3, and (c) Scenario 4.

scenario increment for each successive scenario percent change (24%, 17%, 13% and 8% for Scenarios 1-4). If each scenario is compared only to the previous one, such as the reduction from Scenario 1 to 2, then the percent reductions are more even, being 23%, 21%, 18% for Scenario 1-to-Scenario 2, Scenario 2-to-Scenario 3, and Scenario 3-to-Scenario 4, respectively. For simulated NO_x emissions reductions, both the surface sources (mobile) and the point sources are important. From 1996 to Scenario 1, surface emissions are reduced by 1.1 million tons. More than half of the 4.7 million ton NO_x emissions reduction between the 1990 Base and Scenario 4 comes from the EGUs. Non-EGU reductions contribute 440,000 tons, increasing the point source contribution to 2.9 million tons. Mobile source reductions are important at 1.8 million tons.

As shown in Figure IV-5 for the top 10 states, mobile plus all point sources accounted for 75% of the NO_x emissions in 1990, with the two largest sectors being EGU point sources (39%) and mobile sources (25%). More of a balance is achieved by Scenario 3, where mobile plus all point sources accounted for just over half of the NO_x emissions (53%). In Scenario 4, roles were reversed and area-stationary plus area-nonroad accounted for over half (58%). In Scenario 4, area-nonroad was the largest NO_x sector at 36%, with area-stationary second at 22%. Mobile was the smallest NO_x sector at 10% and EGU point sources was third at 20%. The shifts and role reversal occurred because major NO_x emissions reductions were projected for both mobile and EGU point sources, 84% and 81%, respectively, with very little reduction in area-stationary NO_x (4%) and area-nonroad (15%) sources.

C. PATTERNS OF AIR POLLUTANT TRANSPORT

1. Source Areas

Long-range transport is involved with each of the pollutants of concern affecting SHEN, especially the pollutants responsible for acidic deposition and visibility degradation, but also for O_3. Sources can have a reach of many hundred kilometers (km) in the prevailing wind direction. The regional reach of these pollutant emissions has been well established by the acid rain programs in North America and Europe (Binkowski et al. 1990, Dennis et al. 1990, Langner and Rodhe 1991, NAPAP 1991, Hov and Hjøllo 1994, U.S. EPA 1995, Wojcik and Chang 1997). The regional reach of O_3 was established in the mid-1990s by the Ozone Transport Assessment Group and further established by the NARSTO O_3 assessment (NARSTO 2000).

(a)

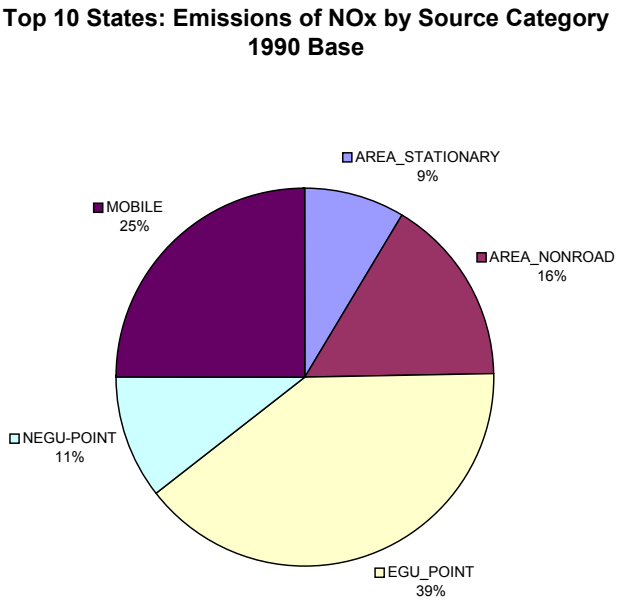

(b)

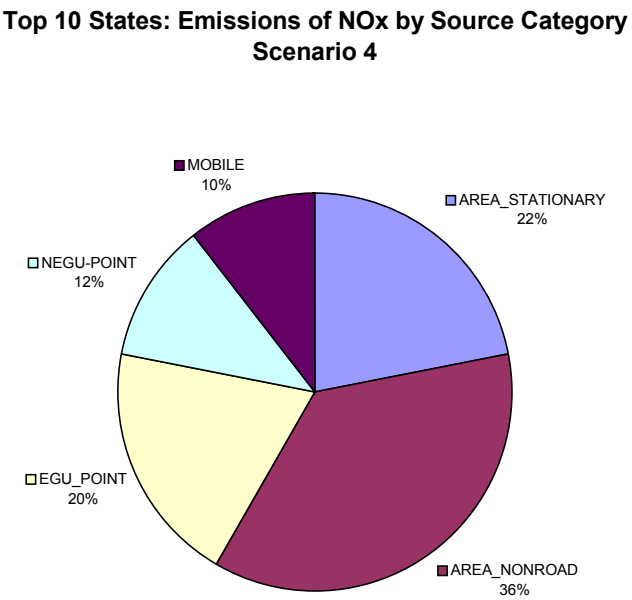

Figure IV-5. Pie chart of NO_x emissions by five-source categories comparing (a) 1990 and (b) Scenario 4.

An extended version of the Regional Acid Deposition Model (RADM; Chang et al. 1987), termed the Extended RADM (Dennis and Mathur 2001), was used to model air pollution transport and deposition in this assessment. The RADM is an Eulerian (fixed-grid) model that was developed under the National Acidic Precipitation Assessment Program as a state-of-the-science model to address regional gas-photochemistry, aqueous chemistry, cloud processes, transport, and wet and dry deposition (Chang et al. 1990). See Section V.D and Appendix C for additional information regarding the model and how it was used for this assessment.

Figure IV-6 shows examples of the reach of emission source subregions responsible for S deposition, oxidized N deposition, reduced N deposition and haze-forming SO_4^{2-} air concentrations, as determined by RADM. The emissions are from a 160x160 km square centered at the joining of the state boundaries of West Virginia, Kentucky and Ohio in the Ohio River Valley. The contour divisions show the distance from the sources to which one must travel to count up one-fourth, one-half, etc. of the total ground-level pollution contributed by the source over the entire eastern North American domain of the model. The deposition loads (kg/ha) or pollutant concentrations ($\mu g/m^3$) along each contour are constrained to have the same magnitude, which sets the shape of the contour. Thus, the shape of the contours about each source subregion shows how the pollutant lifetimes and the climatological mix of wind directions that results in a "prevailing" wind direction combine to produce the overall pattern of pollutant loading or exposure. The contours go farthest away from the source region in the direction of the "prevailing winds" and are closest to the source region in directions "against" the "prevailing" wind.

For all three pollutants, the 25% contour, the area nearest the source with the highest deposition and concentration, is shifted eastward with a tilt to the east-northeast. The 50% contour is further shifted and tilted to the northeast. This is the result of the "prevailing" winds. They tend to transport the pollutant mostly in an arc from the north-northeast to the east. What we see for this particular source subregion in the Ohio River Valley is that the same level of pollution ends up three times farther to the east than to the west. The SO_4^{2-} air concentrations show two main influences: the direction of the "prevailing" winds and the latitudinal variation in the frequency of cloud cover (increasing to the south).

The "reach" of SO_4^{2-} air concentrations, stemming from SO_2, is longest (650-950 km). The reach of NH_3 emissions or reduced N relative to nutrient deposition is the shortest (around 400 km), and the oxides of N and S in terms of acidic deposition have a reach that is in-between

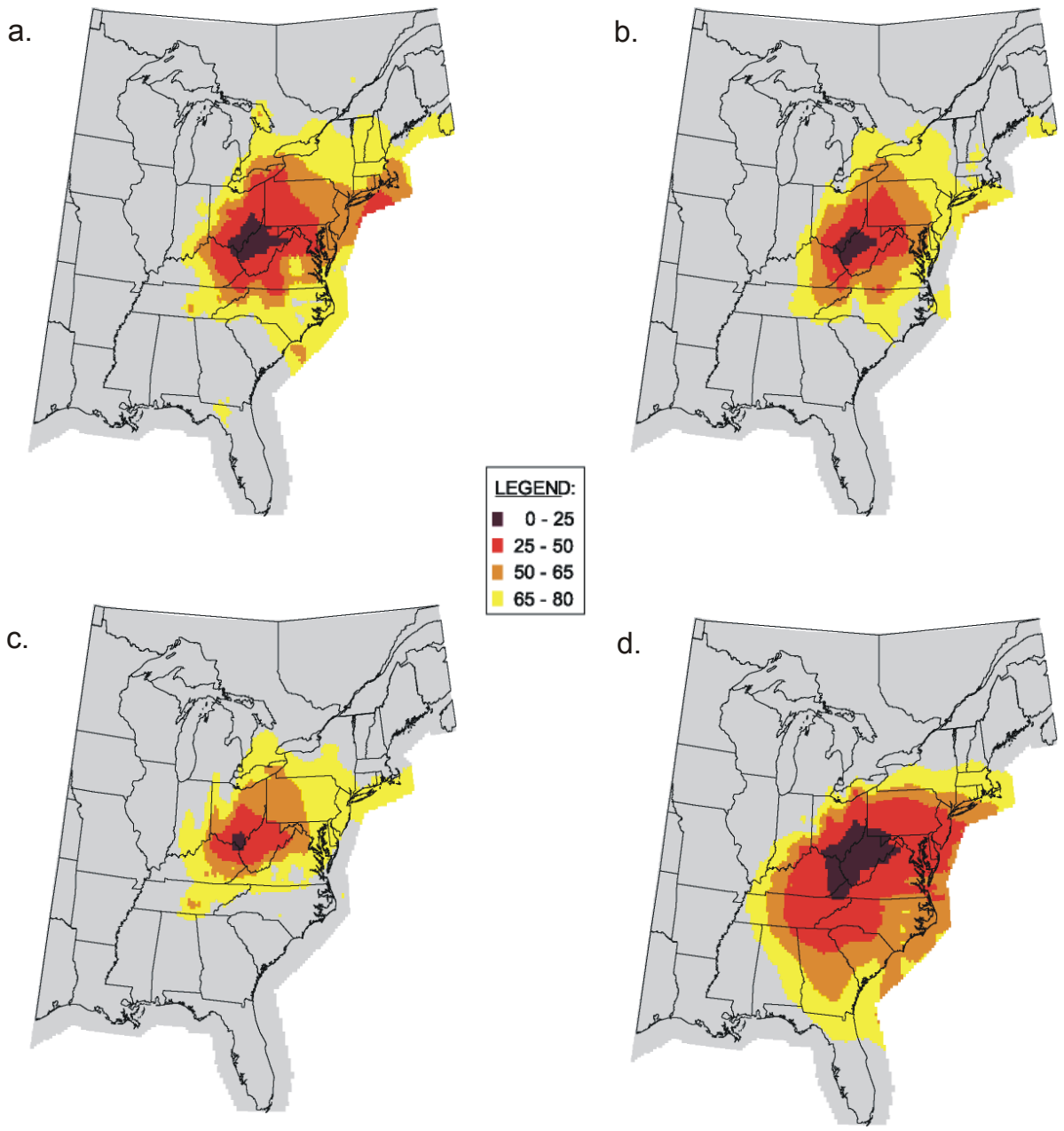

Figure IV-6. Range of influence of (a) sulfur deposition, (b) oxidized nitrogen deposition, (c) reduced nitrogen deposition, (d) sulfate air concentrations expressed as the percent contribution from Subregion 20, a 160x160 km square centered at the joining of the state boundaries of WV, KY, and OH in the Ohio River Valley.

(550-650 km and 600-700 km, respectively). Comparing Figure IV-6(a) with IV-6(d), SO_4^{2-} air concentrations also occur much farther to the southeast, compared to S deposition, because SO_2 is very efficiently converted to SO_4^{2-} in clouds and the frequency of clouds is higher in the south. The effect of clouds influences the shape and apparent "reach" of SO_4^{2-} air concentrations produced from SO_2 emissions from a particular source region.

Hence, we expect pollutants that are emitted within a few hundred km (generally 200 km but up to 300 km for very large sources) of a receptor area (the park) of concern to be very important to the existence of pollution in the receptor area. We also expect pollutants that are emitted within several hundred km still to be important enough to need to consider their responsibility for a portion of the pollution.

We have explored the relative responsibility of regional sources of emissions to air pollution and deposition in SHEN from the perspective of the major airshed contributing pollution to the park. We focused on two main species of emissions: NO_x, responsible for oxidized N deposition (in the form of nitric acid and particulate nitrate), O_3 production, and (beyond scope of this analysis) NO_3^- air concentrations; and SO_2, responsible for S deposition and SO_4^{2-} air concentrations. The geographic pattern of emissions was based on data from the early 1990s, due to the availability of model studies to support this analysis. The airshed view is irrespective of political boundaries and only considers the climatological patterns of transport, transformation and loading/exposure to the end point of interest (the park). We have also explored the relative importance of emissions from several states surrounding SHEN as contributors to the pollution levels in the park. States included were those identified in the airshed analysis as generally being "upwind" of, or in close proximity to, SHEN. Each viewpoint regarding the sources of pollution affecting the park for the 1990 conditions is discussed.

2. Airsheds

Airsheds are more difficult to define than watersheds, because there are no clear boundaries in the atmosphere as there are for surface hydrology. Pollutant concentrations in the atmosphere progressively diminish after they are formed or after they are emitted from a source as they travel downwind, until they become effectively unimportant. The drawing of a major airshed around a geographic region of interest depicts the boundary within which sources of emissions are deemed to contribute substantially to the pollution in the region and outside of which sources

are deemed to play a less important role. The approach used to develop the airsheds for this project was based on analyses presented by Dennis (1997).

The panels in Figure IV-7 show the boundaries (in black) of the major airsheds for SHEN for oxidized N deposition (wet + dry), S deposition (wet + dry) and SO_4^{2-} air concentrations, respectively. The major airsheds are very large compared to the park. As presented in Table IV-5, all three major airsheds of SHEN are approximately a million square kilometers in area. The airsheds for oxidized N and S deposition are the same size and nominally cover 13 states. The airshed for SO_4^{2-} air concentrations is slightly smaller, has a different shape and nominally covers 12 states. The shape of the airsheds is determined by the multi-year climatology of pollutant transport, transformation and loss. The boundary is farthest away from SHEN in the

Table IV-5. Characteristics of major airsheds that contribute air pollution to SHEN.

Oxidized-Nitrogen Deposition Major Airshed	
Size	1,100,800 km^2
States Included	DE, GA, IN, KY, MD, NC, NJ, OH, PA, SC, TN, VA, WV (13 States)
Percent of Deposition Explained by Emissions from within Boundary	85.6%
Percent of Eastern North American Emissions Contained within Boundary	38.9%
Sulfur Deposition Major Airshed	
Size	1,100,800 km^2
States Included	DE, GA, IN, KY, MD, NC, NJ, OH, PA, SC, TN, VA, WV (13 States)
Percent of Deposition Explained by Emissions from within Boundary	83.3%
Percent of Eastern North American Emissions Contained within Boundary	55.8%
Sulfate Air Concentration Major Airshed	
Size	985,600 km^2
States Included	DE, IN, IL, KY, MD, MI, NC, OH, PA, TN, VA, WV (12 States)
Percent of Air Concentration Explained by Emissions from within Boundary	80.4%
Percent of Eastern North American Emissions Contained within Boundary	59.3%

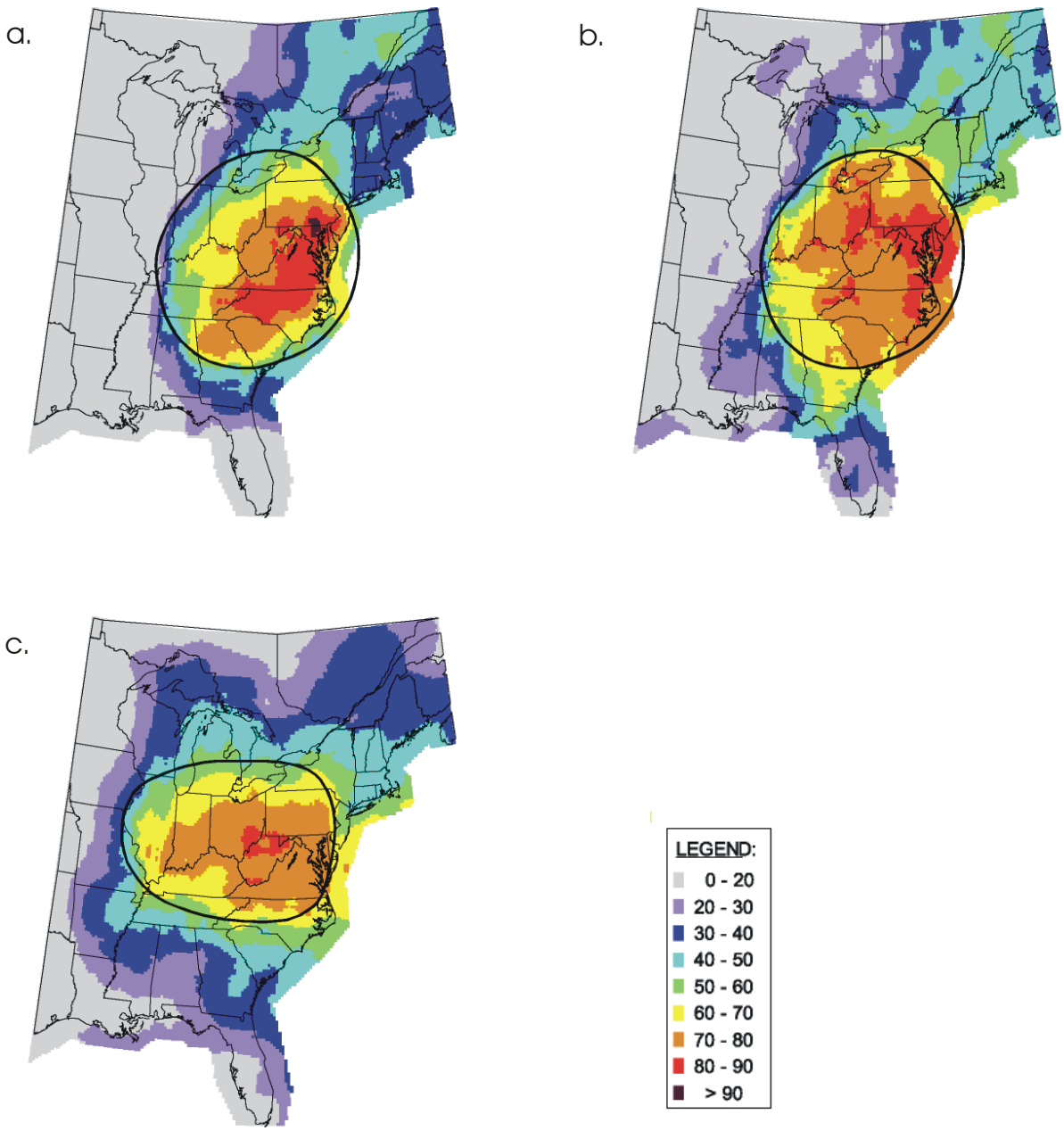

Figure IV-7. Major airsheds for SHEN for (a) oxidized nitrogen deposition, (b) sulfur deposition, (c) sulfate air concentrations. Contours show the percent contribution areas.

direction from which the climatological mix of synoptic meteorological patterns are most conducive to long-range transport in the direction of SHEN (the western or southwestern side). The boundary is closest to SHEN in the direction from which the synoptic patterns are least-conducive to transport towards SHEN (on the eastern side). As noted for Figure IV-7, air pollution travels farthest in the direction of the "prevailing" wind. The SO_4^{2-} airshed boundary does not reach as far to the southeast as does the S deposition airshed because the greater rainfall in the south cleanses the air more of particles while augmenting S deposition.

The contours of percent contribution to deposition or air concentration accounted for by the emissions derived from within the airshed are also depicted in Figure IV-7. SHEN is near to, or in the contour of, the maximum percent explained. This is because the shape of the airshed reflects the climatology of winds bringing pollution to the park from each of the directions, as designed. SHEN is not exactly in the center of the contour of maximum percent explained because the emissions are not distributed uniformly across the airshed. The contours show that the effects of the emissions in terms of deposition or air concentrations tend to continue spreading out well past the airshed boundary in the direction of the "prevailing" wind (to the northeast and out over the ocean). As given in Table IV-5, the percent of oxidized N deposition in SHEN accounted for within the major airshed is 86%. These airshed emissions, on the other hand, represent just 39% of the NO_x emissions of eastern North America. This means that the majority of oxidized N deposition in SHEN (86%) is linked to a relatively small component (39%) of the overall regional emissions. Therefore, NO_x sources within the airshed are very important to N deposition within the park. Similarly, the percentages of S deposition and SO_4^{2-} air concentrations accounted for by SO_2 emissions from within the major airsheds are 83% and 80%, respectively. The SO_2 airshed emissions represent 59% of the eastern North American sulfur oxide (SO_x) emissions.

Table IV-6 gives the emissions of the 15 states nominally covered by any of the airsheds plus one state (New York) included in the analyses of the next section. Because they are included in the SHEN airsheds, these are the states whose emissions have the greatest bearing on the air quality conditions and deposition in SHEN. The emissions of the 13 states included within the S and N deposition airsheds and the 12 states included within the SO_4^{2-} airshed are also summed in the table. Even though the assembly of airshed emissions does not follow state boundaries, the percent of the eastern North American emissions accounted for by the 13-state

Table IV-6. 1990 emissions for the states nominally covered by the SHEN airsheds.

State	SO_2 (tons/yr)	NO_x (tons/yr)	VOC (tons/yr)	CO (tons/yr)
Delaware	100,000	102,989	62,194	269,066
Georgia	1,000,330	687,001	547,448	3,534,801
Illinois	1,261,534	922,261	716,925	3,122,795
Indiana	1,920,416	905,979	541,288	2,301,532
Kentucky	1,034,272	674,772	394,980	1,413,270
Maryland	435,774	354,842	271,811	1,472,063
Michigan	726,298	887,552	868,822	3,481,743
New Jersey	310,629	542,496	540,420	1,841,841
New York	867,415	844,656	996,945	3,892,413
North Carolina	487,616	577,599	673,225	2,755,837
Ohio	2,736,237	1,156,094	849,155	4,138,869
Pennsylvania	1,517,739	1,081,534	827,894	4,180,528
South Carolina	292,567	353,655	369,211	1,598,653
Tennessee	1,077,345	727,134	569,692	2,076,405
Virginia	403,610	564,357	570,977	2,443,994
West Virginia	1,074,715	568,976	200,413	843,463
13-State S&N Deposition Airshed Set	12,391,250	8,297,428	6,418,708	28,870,322
% No. American Emissions	56.3%	40.3%	30.6%	37.5%
12-State SO_4^{2-} Airshed Set	12,775,556	8,524,089	6,547,376	28,499,565
% No. American Emissions	58.1%	41.4%	31.2%	37.1%
Total All 16 States	15,246,497	10,951,897	9,001,400	39,367,273

and 12-state totals given in Table IV-6 are very close to the percentages for the airshed emissions given in Table IV-5.

Not all of the emissions within the airshed contribute equally to the deposition or air concentrations in SHEN. Emissions closer to the park contribute relatively more. Larger emissions sources also contribute relatively more, but proximity is very important. The three airsheds were subdivided into 4 geographic domains, as shown in Figure IV-8. The subdivisions are: local domain, inner domain, middle annulus, and outer annulus. The subdivisions for the oxidized N and S deposition airsheds are comparable. The local domain is the source region that includes SHEN, the receptor region of interest. The inner domain represents the climatologically next most important group of emissions after the local domain in terms of potential importance of emissions affecting SHEN. The inner domain is asymmetric to the west of the park because that is the direction of the influential "prevailing" winds. The middle and outer annuluses

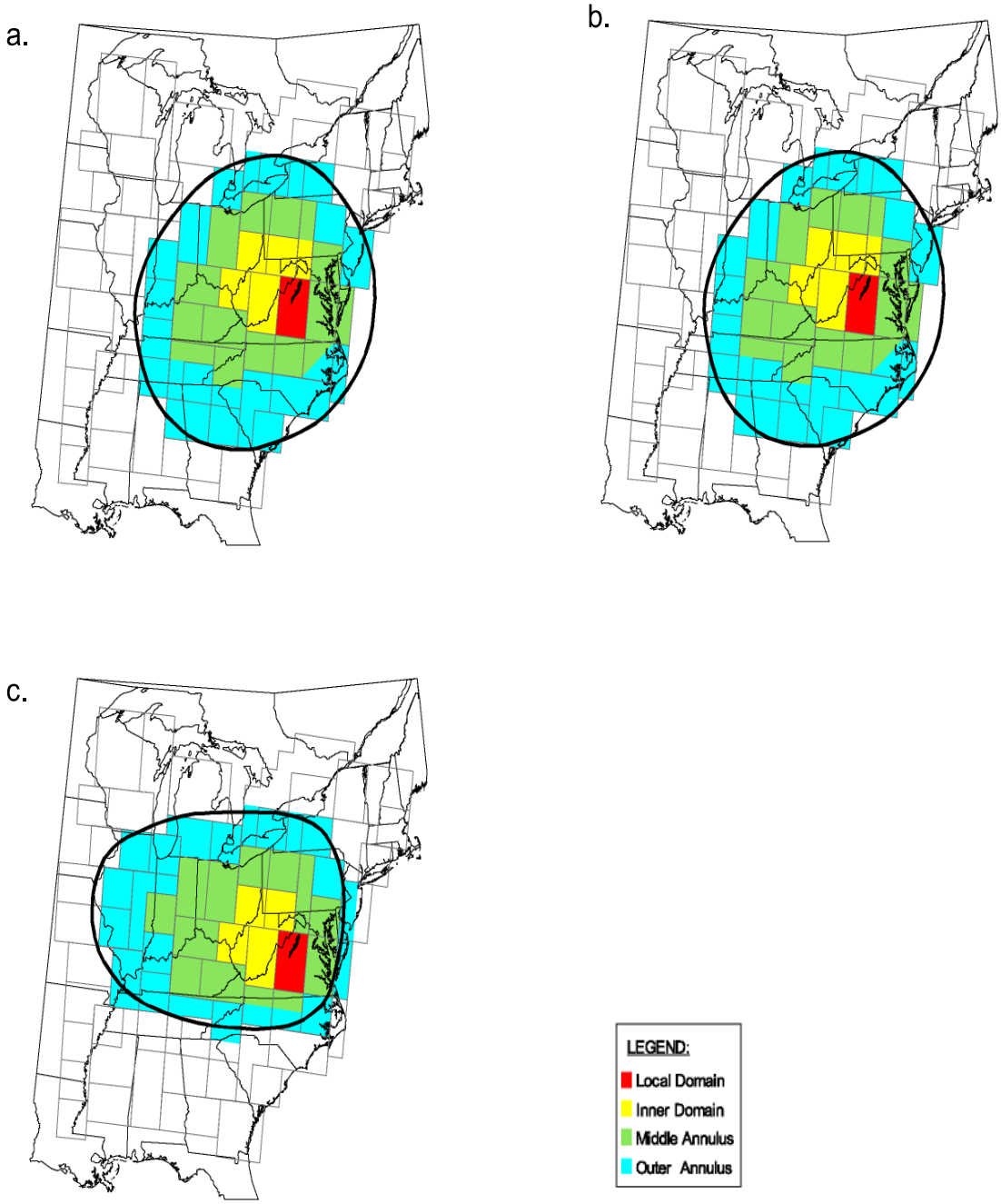

Figure IV-8. Geographic subdivision of the Shenandoah major airsheds: (a) oxidized nitrogen deposition, (b) sulfur deposition, (c) sulfate air concentrations.

subdivide the rest of the airshed in a climatologically consistent manner. The percent of the deposition or air concentrations in SHEN explained by the emissions from each geographic subdivision is given in Table IV-7, along with the percent of eastern North American emissions within each subdivision. The relative efficiency with which a unit of emissions will produce an effect at SHEN is represented by dividing the % Deposition or % Air Concentration number by the % Emissions number. The relative efficiency is given in the last column of Table IV-7.

The effectiveness of the local domain emissions on pollution in SHEN is very high, even though the local emissions are quite low relative to other, more distant emissions sources. The emissions of the next most important geographic subdivision, the Inner Domain, are much less effective at contributing to SHEN's pollution. For deposition, the farther away the geographic subdivision is from the park, the less efficient its emissions are at causing an effect at SHEN.

Table IV-7. Contributions from geographic subdivisions of SHEN major airsheds and efficiency for causing pollution in the park.

Geographic Subdivision	% Deposition/Air Concentration	% Emissions	Efficiency
Local Domain			
Ox-Nitrogen Dep	10.3	0.39	26.4
Sulfur Dep	4.8	0.16	30.0
Sulfate Air Conc.	5.5	0.16	34.4
Inner Domain			
Ox-Nitrogen Dep	26.4	6.3	4.2
Sulfur Dep	34.8	14.4	2.4
Sulfate Air Conc.	25.8	14.3	1.8
Middle Annulus			
Ox-Nitrogen Dep	32.6	13.7	2.4
Sulfur Dep	27.1	17.0	1.6
Sulfate Air Conc.	24.1	17.3	1.4
Outer Annulus			
Ox-Nitrogen Dep	16.3	18.5	0.88
Sulfur Dep	16.6	24.2	0.69
Sulfate Air Conc.	25.0	27.6	0.91
Outside Major Airshed			
Ox-Nitrogen Dep	14.4	61.1	0.24
Sulfur Dep	16.7	44.2	0.38
Sulfate Air Conc.	19.6	40.7	0.48

Efficiency = (%Deposition or %Air Concentration)/(%Emissions)

From the Inner Domain to the Outer Annulus, the efficiency decreases by factors of 4.8 and 3.5 for oxidized N and S deposition, respectively. For SO_4^{2-} air concentrations, because SO_4^{2-} has a longer lifetime and is produced in transit from SO_2 at an overall moderate rate, the efficiency of emissions for producing SO_4^{2-} particles over SHEN only decreases by a factor of two from the Inner Domain to the Outer Annulus. The in-transit production can replenish some of the SO_4^{2-} lost to dilution, deposition and transport into the upper troposphere. As a result, the percent contributed to SO_4^{2-} at SHEN from the three non-local domains is the same, in contrast to the results found for deposition. As shown in Table IV-8, for the constellation of 1990 emissions, about 60% of the deposition and 50% of the air concentrations in SHEN come from the Inner plus Middle Domains. A clear majority comes from the three innermost domains (including Local).

Table IV-8. Percent of the pollution in SHEN explained by accumulating geographic subdivisions of the major airsheds.

	Oxidized Nitrogen Deposition	Sulfur Deposition	Sulfate Air Concentration
Local	10.3 %	4.8 %	5.5 %
Local + Inner	36.7 %	39.6 %	31.3 %
Inner + Middle	59.0%	61.9%	49.9%
Local + Inner + Middle	69.3 %	66.7 %	55.4 %
Local + Inner + Middle + Outer	85.6 %	83.3 %	80.4 %

In summary, the major airsheds for SHEN are large and they cover many states. Emissions from within the major airsheds account for a large fraction of the pollution in the park. The shape of the airshed is asymmetric to account for the climatology of transport ("prevailing" winds). Not all emissions are equal; local, nearby emissions are exceedingly important and, generally, emissions within about 200 km are much more efficient in producing pollution in SHEN (on a per ton emitted basis) than those from farther away (Table IV-7).

3. Top Five Air Pollutant Source Subregions for SHEN

To provide a sense of the importance of the size of the emissions together with proximity, we labeled the top five source subregions based on the percent of pollution at SHEN explained by each (Figure IV-9). The top five source regions together account for 40%, 46%, and 35% of

the oxidized N deposition, S deposition and SO_4^{2-} air concentrations, respectively. The top 5 source subregions for oxidized N deposition cluster around and include the SHEN local domain, which is labeled number 1 in Figure IV-9. For S deposition, the fact that significant nearby (non-local domain) emissions exist together with very large emissions from sources along the Ohio River Valley determines the top five source subregions. The source subregion centered on the joint intersection of the boundaries of Ohio, West Virginia and Kentucky is number 1. This is the same source subregion presented in Figure IV-6. For SO_4^{2-} air concentrations, local sources and long-range transport from the northwest and west are most important, with the source subregions spreading out to the west. The same source subregion is most important for SO_4^{2-} air concentrations as for S deposition.

4. Relative Contributions by State

Table IV-9 gives the breakdown of relative contributions of emissions to air pollution or deposition within SHEN by state, of the 13 states included in the analysis. The list of states began with the 12 states associated with the SHEN SO_4^{2-} airshed. New York was added because its emissions were large and were roughly similar in distance from SHEN as those from New Jersey. Differences in importance of New York and New Jersey as contributors to air pollution in SHEN highlight the importance of the directional effect of the climatology of transport to SHEN. The states are presented in rank order of contribution for each pollutant. The overall percent explained by the 13 states is consistent with the percent explained by the emissions from within the airsheds. Color contour maps of the percent contribution of the number 1 ranked state are shown in Figures IV-10a, b, and c for S deposition (West Virginia), oxidized N deposition (Virginia) and SO_4^{2-} air concentrations (Ohio), respectively.

The top three states are the same for all three pollutants but the order is different. For S deposition, West Virginia is the top contributor, while for oxidized N deposition Virginia is number one, and for SO_4^{2-} air concentrations Ohio is number one. However, for SO_4^{2-} air concentrations the contribution from the top 3 states are so close as to basically be the same. The top five states are the same for S deposition and SO_4^{2-} air concentrations, with a different order. The top five differ by one state for oxidized N deposition - Kentucky is replaced by North Carolina. In all cases, the top three states account for more than a third of the deposition/air concentrations and the top five states account for more than half. It is interesting

Figure IV-9. Top 5 source regions contributing air pollution in SHEN: (a) oxidized nitrogen deposition, (b) sulfur deposition, (c) sulfate air concentrations. The most important contributing subregion for each constituent is numbered 1, followed systematically by the next 4 most important contributors.

Table IV-9. Percent of the pollution in SHEN explained by state emissions, expressed as the individual state (adjusted) contributions to deposition and atmospheric concentrations (with sulfur nonlinearity adjustment).

State	Sulfur Deposition	State	NO_x Deposition	State	SO_4 Air Concentrations
West Virginia	16.8%	Virginia	14.4%	Ohio	11.9%
Ohio	15.5%	West Virginia	12.3%	Virginia	11.8%
Virginia	10.1%	Ohio	10.9%	West Virginia	11.7%
Pennsylvania	9.9%	Pennsylvania	10.7%	Pennsylvania	10.6%
Kentucky	6.9%	North Carolina	7.8%	Kentucky	7.0%
Tennessee	5.4%	Maryland	7.4%	Indiana	5.8%
Maryland	4.6%	Kentucky	7.0%	Tennessee	5.6%
Indiana	4.4%	Tennessee	4.5%	North Carolina	5.1%
North Carolina	3.8%	Indiana	3.4%	Illinois	3.8%
Illinois	2.9%	Illinois	2.9%	Maryland	3.5%
Michigan	1.1%	Michigan	2.1%	New York	1.7%
New York	0.8%	New York	1.6%	Michigan	1.3%
Delaware	0.4%	Delaware	0.5%	Delaware	0.5%
Top 3 States	**42.4%**	**Top 3 States**	**37.6%**	**Top 3 States**	**35.4%**
Top 5 States	**59.2%**	**Top 5 States**	**56.0%**	**Top 5 States**	**53.0%**
Top 10 States	**80.3%**	**Top 10 States**	**81.2%**	**Top 10 States**	**76.8%**
All States*	**82.6%**	**All States**	**85.4%**	**All States**	**80.3%**

* Includes the 13 states that were part of this analysis

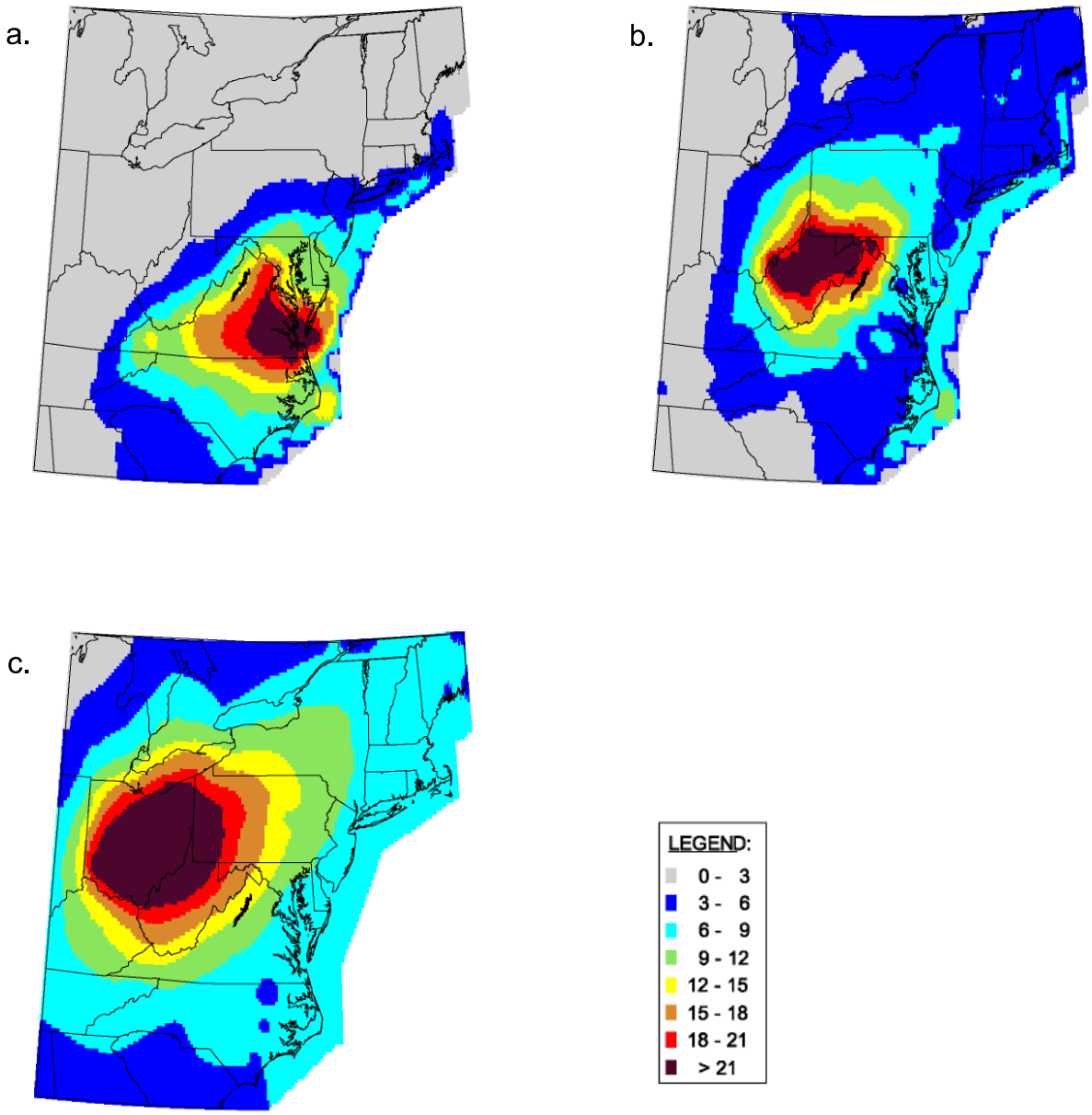

Figure IV-10. First-ranked state percent contribution contour for (a) oxidized nitrogen deposition (VA), (b) sulfur deposition (WV), (c) sulfate air concentrations (OH).

to note that while New York has a fair amount of emissions, it ranks well down on the list of contributing states, even lower than Illinois which is much farther away, because New York is located in a direction opposite the "prevailing" winds for SHEN.

D. IN-PARK EMISSIONS

An air emissions inventory was completed for SHEN by the NPS ARD in July, 2002. Table IV-10 provides a summary of in-park emissions. Prescribed burning, fireplaces and campfires, and mobile sources are the largest contributors to air pollutant emissions in SHEN. Stationary sources contribute very little to the overall park emissions.

The park is surrounded by the counties of Albermarle, Augusta, Greene, Page, Madison, Rappahannock, Rockingham, and Warren. Emission estimates for these counties, and for the Commonwealth of Virginia, were obtained by the NPS ARD from the 1999 National Emissions Inventory (NEI) maintained by the U.S. EPA. It is important to note that differences may exist between the methodologies used to generate the park emissions inventory and those stationary sources, whereas the NEI treats them as area sources. Table IV-11 provides a comparison among SHEN emissions and those from surrounding counties and the state. For all pollutants, SHEN emissions account for less than 1% of the surrounding county emissions. Figure IV-11 displays the contribution of in-park emissions relative to the surrounding counties.

Table IV-10. SHEN 1999 emissions (tons) summary. (Source: Aaron Worstell, NPS Denver)

	VOC	NO_x	SO_2	PM_{10}	CO
Stationary Sources					
Generators	0.1	0.6	0.0	0.0	0.8
External Combustion	0.0	0.0	0.0	0.0	0.0
Wastewater Treatment Plants	0.1	–	–	–	–
Gasoline Tanks	0.5	–	–	–	–
Subtotal	0.7	0.6	0.0	0.0	0.8
Mobile Sources					
All Vehicles	32.8	31.3	–	40.8	343.5
Area Sources					
Prescribed Burning	41.4	25.8	–	77.5	723.7
Fireplaces and Campfires	62.4	0.7	0.1	9.4	68.8
Subtotal	103.8	26.6	0.1	87.0	792.6
OVERALL TOTAL	137.3	58.4	0.1	127.8	1136.9

Table IV-11. Annual emissions totals (tons) from within SHEN and comparison with surrounding counties. (Source: Aaron Worstell, NPS Air Resources Division, Denver)

	VOC	NOx	SO_2	PM_{10}	CO
Area and Mobile Source					
SHEN	136.6	57.8	0.1	127.8	1136.0
Albermarle Co.	6655.0	8035.0	591.0	6005.0	47313.0
Augusta Co.	6248.0	6943.0	462.0	6512.0	36487.0
Greene Co.	906.0	812.0	62.0	1450.0	5128.0
Madison Co.	1100.0	944.0	70.0	1788.0	5733.0
Page Co.	1570.0	1568.0	112.0	2086.0	9974.0
Rappahannock Co.	562.0	490.0	36.0	989.0	2661.0
Rockingham Co.	5640.0	7214.0	488.0	7286.0	31925.0
Warren Co.	2232.0	2550.0	166.0	1930.0	15440.0
Surrounding County Total	24913.0	28556.0	1987.0	28046.0	154661.0
VA State Total	437462.0	406884.0	40106.0	344603.0	2452333.0
Point Source					
SHEN	0.7	0.6	0.0	0.0	0.8
Albermarle Co.	167.0	289.0	563.0	96.0	121.0
Augusta Co.	379.0	1067.0	1732.0	156.0	78.0
Greene Co.	13.0	20.0	0.5	2.0	17.0
Madison Co.	14.0	3.0	13.0	1.0	1.0
Page Co.	44.0	41.0	19.0	4.0	11.0
Rappahannock Co.	0.5	1.0	1.0	1.0	1.0
Rockingham Co.	633.0	568.0	1073.0	196.0	205.0
Warren Co.	57.0	39.0	109.0	18.0	4.0
Surrounding County Total	1307.5	2028.0	3510.5	474.0	438.0
VA State Total	59144.0	168416.0	334941.0	19550.0	66873.0
All Sources					
SHEN	137.3	58.4	0.1	127.8	1136.9
Albermarle Co.	6822.0	8324.0	1154.0	6101.0	47434.0
Augusta Co.	6627.0	8010.0	2194.0	6668.0	36565.0
Greene Co.	919.0	832.0	62.5	1452.0	5145.0
Madison Co.	1114.0	947.0	83.0	1789.0	5734.0
Page Co.	1614.0	1609.0	131.0	2090.0	9985.0
Rappahannock Co.	562.5	491.0	37.0	990.0	2662.0
Rockingham Co.	6273.0	7782.0	1561.0	7482.0	32130.0
Warren Co.	2289.0	2589.0	275.0	1948.0	15444.0
Surrounding County Total	26220.5	30584.0	5497.5	28520.0	155099.0
VA State Total	496606.0	575300.0	375047.0	364153.0	2519206.0

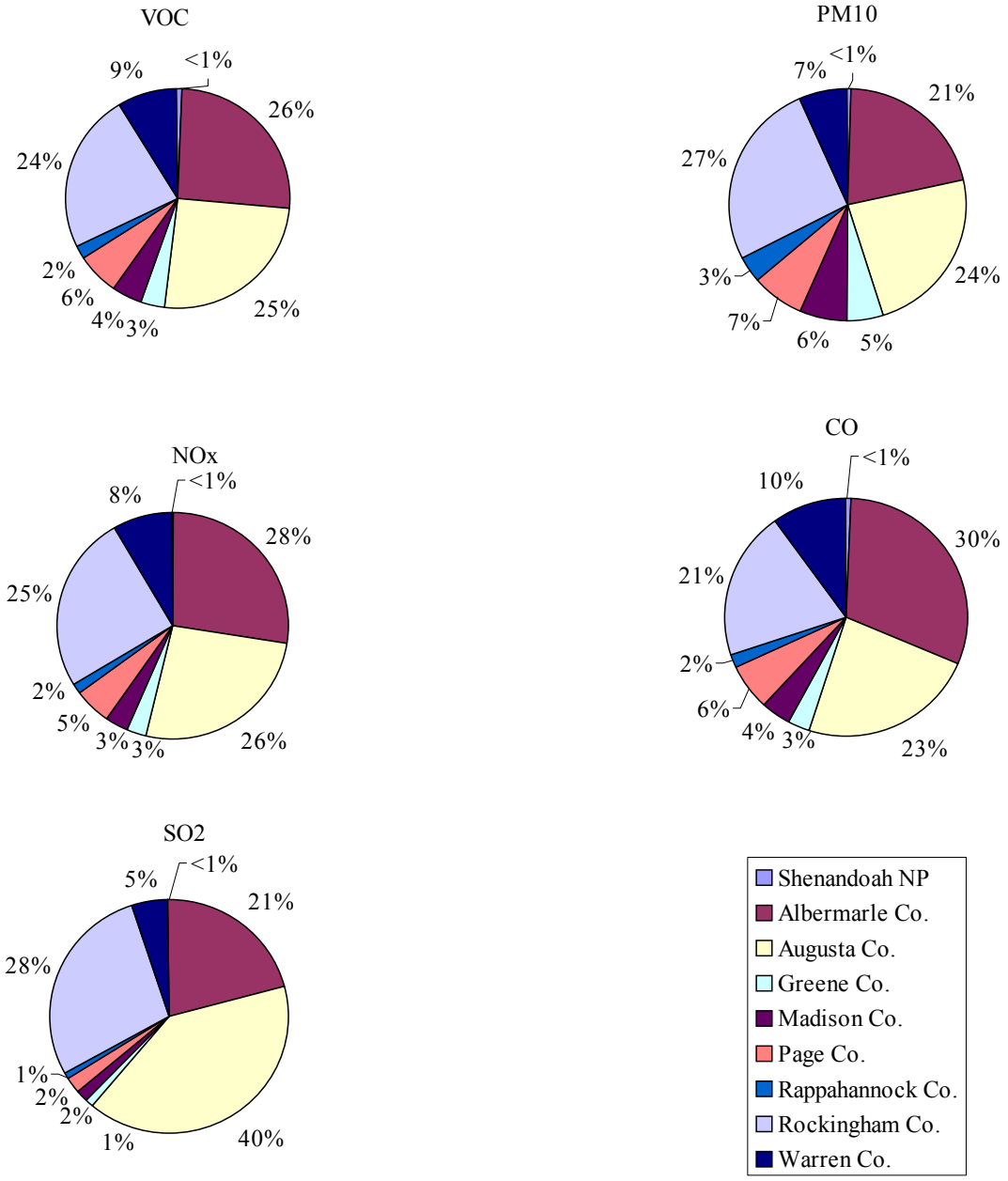

Figure IV-11. In-park SHEN emissions relative to emissions from surrounding counties. (Source: Aaron Worstell, NPS Air Resources Division, Denver)

III. SCIENTIFIC BACKGROUND

A. PURPOSE

The purpose of this section is to provide general scientific background information needed to understand some of the material presented and discussed elsewhere in this report. Information is provided for air pollutants, deposition of air pollutants from the atmosphere to terrestrial and aquatic ecosystems, aquatic receptors, terrestrial receptors that are sensitive to air pollutant effects, and finally visibility. Each topic is discussed in general terms. Shenandoah National Park (SHEN)-specific information is presented in subsequent sections of the report.

B. GASEOUS POLLUTANTS

1. Ground-level Ozone

Ground-level (tropospheric) ozone (O_3) is a particular concern for national park lands, including SHEN, because remote forested areas can experience greater cumulative O_3 exposure, higher minimum values, and higher maximum concentrations than the upwind urban and industrial areas where most of the pollutant sources are located. In many places, O_3 concentrations tend to increase with elevation (Brace and Peterson 1998, Cooper and Peterson 2000), although there are some exceptions (Bytnerowicz et al. 1999). This can lead to elevated values in mountainous locations (Aneja et al. 1991).

Ground-level ozone is a secondary pollutant formed by the photo-oxidation of nitrogen oxides (NO_x) and volatile organic compounds (VOCs). Ozone is a colorless gas and is a component of smog, which can develop during the clear warm weather associated with high pressure systems. It is an important regional pollutant because it forms during transport of its precursors and can occur at high concentrations in areas remote from precursor sources. The level of O_3 in a "pristine" area may have a weekly average as low as 10 to 25 parts per billion by volume (ppbv; Altshuller and Lefohn 1996, Cooper and Peterson 2000), with maximum hourly O_3 concentrations generally less than about 50 to 80 ppbv. Ozone is injurious to human health as well as to vegetation. It is an eye, nose, and lung irritant and causes damage to plants. Ozone is a potential threat to high-elevation plant species because concentrations and total exposure can be higher at higher elevations under appropriate atmospheric conditions (Loibl et al. 1994; Sandroni et al. 1994; Brace and Peterson 1996, 1998). Dispersion and transport of pollutants vary locally, but there are clearly periods of high O_3 exposure in and around SHEN every

summer. The challenge is to quantify the spatial distribution of this exposure relative to the location of sensitive receptors.

In order to protect human health and welfare, the U. S. EPA has established primary and secondary O_3 National Ambient Air Quality Standards for maximum allowable O_3 concentration levels. Prior to 1997, these standards were based upon 1-hour average O_3 measurements. They were revised in 1997, when the EPA promulgated new standards, both primary and secondary, based upon an 8-hour average value. Under this rule, the annual fourth-highest daily maximum 8-hour O_3 concentration, averaged over three years, must not exceed 0.08 ppm (parts per million; 80 ppbv, which can be rounded up to 85 ppbv). This average is computed by first determining the highest 8-hour average O_3 value for each day of the year, and then identifying the 4th-highest of all daily maximum 8-hour O_3 values that occurred during the year. These 4th-highest values are then averaged over three successive years to determine the final concentration value that is compared to the standard. Because of rounding procedures, EPA has indicated that 85 ppbv is the lowest concentration that would exceed the 80 ppbv standard. The new secondary standard is identical to the primary standard.

The decision by the U.S. EPA to transition from an O_3 standard based upon a 1-hour average to a standard based upon an 8-hour average was prompted by research indicating that prolonged exposure to O_3 at concentrations lower than the 1-hour standard can have significant impacts upon human health. There is also research indicating that prolonged exposure to O_3 is particularly harmful to vegetation. The EPA has recognized the potential usefulness of some type of exposure index in setting the secondary O_3 standard to protect agricultural crops and native vegetation (U.S. EPA 1997). In its final ruling on the new O_3 standard, the EPA recognized that a cumulative index measuring long-term O_3 exposure is very likely to be more relevant to vegetation than the 8-hour standard that was chosen, but concluded that there were not yet enough data to specify a new secondary standard based upon such an index. It did, however, indicate that it would focus additional research on this issue and reevaluate the need for a seasonal cumulative index in the next review of the O_3 standard.

Two such indices of O_3 exposure are presented here. The first is the SUM06. This index is computed by adding all hourly O_3 concentration values greater than or equal to 0.06 ppm. Because plants are most active photosynthetically during daylight hours in the summer time, and thus most likely to take in O_3 and other gases during these hours, the index was calculated here using values measured during the 12 hours from 8 AM to 8 PM in the months of May through

September of each year. A similar index is the W126 index. This index is the sum of all hourly O_3 concentrations where each concentration is weighted by a function that gives greater emphasis to the higher hourly concentrations while still including the lower ones (Appendix A).

2. Sulfur Dioxide

Sulfur dioxide (SO_2) is a product of fossil fuel, primarily coal and oil, combustion. Some of the largest emitters are coal-fired electric power plants and smelters. Although more stringent regulations have reduced emissions over the last 30 years, SO_2 continues to be a pollutant of concern in many areas of the United States, including throughout the Southeast. SO_2 is a precursor of pollutants which cause acidic deposition and visibility degradation.

Like O_3, SO_2 is a gas and enters the leaf through the stomata. Inside the leaf it disrupts mesophyll cell functioning, causing reduced productivity of the leaf. SO_2 injury in plants is characterized by leaf bleaching and chlorosis, necrotic lesions, and early senescence. Prolonged exposure can weaken a plant, making it susceptible to pathogens and other organisms. Some species are sensitive to chronic exposures as low as 25 ppbv (Treshow and Anderson 1989).

There are few data on the effects of sulfur (S) compounds on mature trees or other native plants, and there is a wide range of sensitivities to ambient S compounds (Davis and Wilhour 1976, Smith 1990). Limited data on tree seedlings (Hogsett et al. 1985) suggest that SO_2 concentrations below 20 ppbv (24-hour mean) do not produce visible injury symptoms (Peterson and Sullivan 1998). In addition to potential direct effects on vegetation, atmospheric S compounds contribute to visibility degradation and to S deposition that has been associated with effects on aquatic ecosystems.

3. Volatile Organic Compounds and Nitrogen Oxides

Volatile organic compounds and NO_x are important precursors of O_3. Several VOCs fall under the Hazardous Air Pollutant section of the Clean Air Act and VOCs must be addressed as precursors to O_3 under State Implementation Plans. NO_x is also a precursor for pollutants that cause acidic deposition and visibility degradation. VOCs can also contribute to visibility degradation.

All high-temperature combustion processes emit NO_x. Automobiles and stationary fossil fuel burning systems are the major anthropogenic (human-caused) sources of NO_x emissions in

the United States. Naturally-occurring NO_x compounds originate from soils, wildfire, lightning and decomposition.

Anthropogenic sources of VOCs include motor vehicle exhaust, gasoline vapors, stationary fuel combustion, commercial and industrial processes, and emissions from solid wastes (Smith 1990). Natural systems, particularly soils and vegetation, produce VOCs and emit them to the atmosphere; trees in particular emit the highly reactive hydrocarbons isoprene and terpene. Globally, biogenic sources of VOCs exceed anthropogenic sources, although anthropogenic sources typically dominate in localized, urban areas. VOCs include a large number of hydrocarbons which vary greatly in reactivity.

Ozone is formed from the reaction of NO_x in the presence of sunlight and VOCs. In unpolluted air, reactions involving NO, nitrogen dioxide (NO_2), and O_3 form a chemical cycle that does not lead to net loss or production of O_3. VOCs, both human-made and natural, interfere with this cycle, allowing for the buildup of O_3. Emitted NO rapidly converts to NO_2 in the atmosphere. The latter is a criteria pollutant. Both NO_x (the sum of NO and NO_2) and VOCs are thus precursors to O_3 formation. This buildup proceeds during the daytime when ultraviolet radiation from the sun is available to drive the required reactions, and ceases at night. When fresh NO is available at night, it reacts with O_3 and removes it from the atmosphere. This creates a pronounced diurnal cycle in O_3 concentrations in many areas.

C. ATMOSPHERIC DEPOSITION

Given the structural complexity of landforms and the broad distribution of major pollution source areas, a network of air quality and atmospheric deposition monitors in or near Class I areas is needed to fully evaluate the spatial patterns of air quality and atmospheric deposition within SHEN, or any other Class I area. Most existing air quality and deposition data are short-term and/or are from urban areas remote from wildland locations, although general patterns of nitrogen (N) and S deposition can be inferred from state and national databases. It is known that air pollution and deposition in some areas have increased considerably during the last 30 to 40 years, while decreasing in others.

The estimation of deposition of atmospheric pollutants in remote areas is especially difficult because all components of the deposition (rain, snow, cloudwater, dryfall and gases) have seldom been measured concurrently. Even measurement of wet deposition remains a problem in some areas because of the logistical difficulties in operating a site at remote locations. Portions

of the wetfall have been measured by using snow cores (or snow pits), bulk deposition (open containers), and automated sampling devices such as those used at the National Atmospheric Deposition Program/National Trends Network (NADP/NTN) sites. All of these approaches suffer from limitations that cause problems with respect to developing annual deposition estimates. The snow sampling includes results for only a portion of the year and may seriously underestimate the load for that period if there is a major rain-on-snow event. Bulk deposition samplers are subject to contamination problems from birds and litterfall. Weekly data on dry deposition are available at some sites (including Big Meadows within SHEN), collected within the Clean Air Status and Trends Network (CASTNet). Dryfall from wind-borne soil can constitute major input to the annual deposition load, particularly in arid environments. Aeolian inputs from dryfall can provide a major source of acid neutralization not generally measured in other forms of deposition. Gaseous deposition is calculated from the product of ambient air concentrations and estimated deposition velocities. However, the derivation of deposition velocities is subject to considerable debate.

The need to measure or estimate different forms of atmospheric deposition complicates the difficult task of measuring and monitoring total deposition. Cloudwater can be an important portion of the hydrologic budget in coastal areas and some high-elevation forests (Harr 1982, Lovett and Kinsman 1990), and failure to capture this portion of the deposition input could lead to underestimation of annual deposition. Furthermore, cloudwater chemistry has the potential to be more acidic than rainfall (Weathers et al. 1988). Due to these limitations, there is considerable uncertainty regarding the amount of current deposition (wet, dry, cloud) of atmospheric pollutants in any of the Class I areas in the United States.

Dry deposition approximates, or is slightly less than, wet deposition for most ions at most sites; for example, dry deposition constituted 30 to 50% of total deposition of most ions at most Integrated Forest Study (IFS) sites throughout the eastern United States (Johnson and Lindberg 1992). Cloud water deposition contributed substantially to total ionic deposition at only two high-elevation IFS sites: Whiteface Mt., NY (1,000 m) and near Clingman's Dome, NC (1,740 m), ranging from about 20% of total for base cations at Whiteface Mt. to 50% of total for sulfate (SO_4^{2-}) at the North Carolina site. Estimates of wet, dry, and cloud deposition were generated by Shannon (1998) at multiple sites throughout the southeastern United States using the Advanced Statistical Trajectory Regional Air Pollution (ASTRAP) model, suggesting that the sum of dry plus cloud deposition was approximately equal to wet deposition, for both S and N, throughout

the region (Sullivan et al. 2002a). These model estimates are in general agreement with data derived from NADP and CASTNet monitoring at Big Meadows in SHEN (Section V).

D. AQUATIC RESOURCES AND SENSITIVE INDICATORS

1. Water Chemistry

Water bodies are regarded by residents of the southern Appalachian Mountains region as extremely important (SAMAB 1996), and multiple uses include drinking water, fishing, other aquatic recreation, transportation, livestock watering, irrigation, flood control, hydroelectric power, wildlife observation, and waterfront human habitation. There is general agreement that water quality has improved in the southern Appalachians since the adoption of the Clean Water Act in 1972. However, the rate of improvement has recently slowed since most municipal and industrial discharges now control point source pollution, and the remaining nonpoint sources (storm water runoff, sediment contamination, acid deposition, and spills) are more difficult and expensive to control. Future water quality in some areas is likely to be challenged by population growth (Wallace et al. 1992, SAMAB 1996).

Stream concentrations of major ions depend on atmospheric inputs, soil pools of elements, in-stream processing, and weathering rates of rocks, including mechanical breakage of rocks and chemical processes that alter minerals by adding or removing elements. Chemical weathering is more important than mechanical weathering as a source of base cations for the soil cation exchange pool because chemical processes are more effective on smaller particles, which have greater overall surface area than do larger particles (Isphording and Fitzpatrick 1992).

The potential effects of S deposition on surface water quality have been well studied throughout the United States, particularly within the EPA's Aquatic Effects Research Program, a component of the National Acid Precipitation Assessment Program (NAPAP). Major findings were summarized in a series of State of Science and Technology Reports (e.g., Baker et al. 1990a,b; Sullivan 1990; Turner et al. 1990) and the final NAPAP policy report, the Integrated Assessment (NAPAP 1991). More recent findings were summarized in Church and Van Sickle (1999) and in the review of Sullivan (2000), which provides the basis for much of the material presented in the remainder of this section. Although aquatic effects from N deposition have not been studied as thoroughly as those from S deposition, concern has been expressed regarding the role of nitrate (NO_3^-) in acidification of surface waters (particularly during hydrologic episodes), the role of NO_3^- in the long-term acidification process, the contribution of ammonium (NH_4^+)

from agricultural sources to surface water acidification, and the potential for anthropogenic N deposition to stimulate eutrophication of freshwaters and estuaries (e.g., Sullivan 1993, 2000; Wigington et al. 1993; Sullivan et al. 1997; NAPAP 1998)

Computer models can be used to predict pollution effects on aquatic ecosystems and to perform simulations of future ecosystem response (c.f., Cosby et al. 1985a,b,c). The Model of Acidification of Groundwater in Catchments (MAGIC), a lumped-parameter mechanistic model, has been used throughout North America and Europe and extensively tested against the results of diatom reconstructions of historic water chemistry and ecosystem manipulation experiments (e.g., Wright et al. 1986; Sullivan et al. 1992, 1996; Sullivan and Cosby 1995; Cosby et al. 1995, 1996; Sullivan 2000). MAGIC provided the basis for aquatic effects modeling for this assessment, although other models are also available (c.f., Christophersen et al. 1982; Liu et al. 1991, 1992; Aber et al. 1997). Watershed models are valuable to management agencies which require quantitative predictions of air pollutant impacts and the likely future benefits of emissions control programs. Nitrogen dynamics have more recently been added to the MAGIC model (Jenkins et al. 1997).

Atmospheric deposition of S and N (as NO_3^- and as NH_4^+, which can be quickly nitrified to NO_3^-) often cause increased concentrations of SO_4^{2-} in drainage waters and can, in some cases, cause increased concentrations of NO_3^-. An increase in the concentration of either of these mineral acid anions will generally result in a number of additional changes in water chemistry. These can include:

- increased concentration of base cations (Ca^{2+}, Mg^{2+}, K^+, Na^+)
- decreased acid neutralizing capacity (ANC)
- increased concentration of hydrogen ion (H^+; decreased pH)
- increased concentration of dissolved aluminum (Al)

Increased leaching of base cations along with SO_4^{2-} and/or NO_3^- can lead to base cation depletion in base-poor watershed soils. In such cases, base cation concentrations in drainage waters will eventually decrease, sometimes to levels below those found prior to the initiation of acidic deposition. Increased concentrations of H^+ and/or Al in surface water occur only in response to higher concentrations of SO_4^{2-} or NO_3^- when ANC has decreased to less than about 50 to 100 μeq/L. At higher ANC values, contributions of SO_4^{2-} or NO_3^- are mainly balanced by increasing base cation concentrations in runoff and some decrease in ANC. High concentrations of H^+ or Al can be toxic to fish and other aquatic biota.

If NO_3^- leaches into stream or lakewater as a result of increased N deposition, the result can be eutrophication or acidification. If N is limiting for aquatic primary production, the added NO_3^- can result in increased algal productivity, which can cause disruption of aquatic community dynamics. If N is not limiting, then the added NO_3^- will remain in solution. If the added NO_3^- is not balanced by an increase in base cation concentration, acidification will occur.

The Southeast was not glaciated during the last glacial period (about 100,000 to 10,000 years ago). As a result, the soils of the Southeast are largely residual, relatively deep, and highly structured vertically, versus those in glaciated areas. The lower horizons of southeastern soils are also rich in iron and Al, which can strongly affect stream chemistry via efficient retention of many negatively charged solutes, of which SO_4^{2-} is of major interest in the context of acidification. Ultisols represent one of the dominant soil groups in the Southeast; these are characterized by surface and subsurface horizons that are loamy or clayey in texture. They are typically acidic soils low in base saturation (Adams and Hackney 1992).

Although NO_3^- is also associated with precipitation acidity, NO_3^- concentrations in upland surface waters are commonly low due to demand for N as a nutrient, especially in regenerating forests (Aber et al. 1989, 1998; Johnson and Lindberg 1992). The deposition and fate of S in watersheds has accordingly received most of the attention in regional-scale assessments of acidic-deposition effects on aquatic ecosystems (e.g., NAPAP 1991, Church et al. 1992, Sullivan et al. 2002a).

Surface waters that are sensitive to acidification from acidic deposition of S or N typically exhibit a number of characteristics. Such characteristics either predispose the waters to acidification and/or correlate with other parameters that predispose the waters to acidification. Although precise guidelines are not widely accepted, general ranges of parameter values that reflect sensitivity are as follows (c.f., Sullivan 2000):

<u>Dilute</u> - Waters have low concentrations of all major ions, and therefore specific conductance is low (< 25 µS/cm). Dilute waters are low in base cation concentrations, suggesting small cation pools in watershed soils.

<u>Acid neutralizing capacity</u> - ANC is low. Acidification sensitivity has long been defined as ANC<200 µeq/L, although more recent research has shown this criterion to be too inclusive. Waters sensitive to chronic acidification generally have ANC<50 µeq/L, and waters sensitive to episodic acidification generally have ANC<100 µeq/L.

<u>Base cations</u> - Concentrations are low in non-acidified waters, but can increase substantially in response to acidic deposition. In relatively pristine areas, the concentration of base

cations (Ca^{2+} + Mg^{2+} + Na^{+} + K^{+}) in sensitive waters will generally be less than about 50 to 100 μeq/L.

Organic acids - Concentrations are low in waters sensitive to the effects of acidic deposition. Dissolved organic carbon (DOC) and associated organic acids cause water to be naturally low in pH and ANC, or even to be acidic (ANC<0), but also impart substantial pH buffering at these low pH values.

pH - pH is low, generally less than 6.0 to 6.5 in acid-sensitive waters. In areas that have received substantial acidic deposition, paleolimnological studies have shown that acidified lakes are generally those that had pre-industrial pH between 5 and 6.

Acid anions - Sensitive waters generally do not have large contributions of mineral acid anions (e.g., SO_4^{2-}, F^-, Cl^-) from geological or geothermal sources. In particular, the concentration of SO_4^{2-} in drainage waters would not be substantially higher than could reasonably be attributed to atmospheric inputs, after accounting for probable dry deposition and evapotranspiration.

Physical characteristics - Sensitive waters are usually found at moderate to high elevation, in areas of high relief, with flashy hydrology and minimal contact between drainage waters and soils or geologic material that may contribute weathering products to solution. Sensitive streams are generally low order.

After passage of the Clean Air Act in 1970 and subsequent Amendments in 1977 and 1990, emissions and deposition of S were reduced and the concentrations of SO_4^{2-} in lake and streamwater in many areas in the eastern United States and Canada decreased (Dillon et al. 1987, Driscoll et al. 1989, Sisterson et al. 1990). Long-term monitoring data confirmed that much of the decrease in surface water SO_4^{2-} concentration was accompanied by rather small pH and ANC recoveries (Driscoll and van Dreason 1993, Kahl et al. 1993, Driscoll et al. 1995, Likens et al. 1996). The most significant response, on a quantitative basis, was decreased concentrations of calcium (Ca^{2+}) and other base cations. More recent data suggest increased surface water ANC during the 1990s in the Adirondack Mountains, Appalachian Plateau, and Upper Midwest, but not in the Ridge and Valley and Blue Ridge region of western Virginia (Stoddard et al. 2003).

As SO_4^{2-} concentrations in lakes and streams have declined, so too have the concentrations of Ca^{2+} and other base cations. There are several apparent reasons for this. First, the atmospheric deposition of base cations has decreased in recent decades (Hedin et al. 1994), likely due to a combination of air pollution controls, changing agricultural practices, and the paving of roads (the latter two affect generation of dust which is rich in base cations). Second, decreased movement of SO_4^{2-} through watershed soils causes reduced leaching of base cations

from soil surfaces. Third, soils in some sensitive areas have experienced prolonged base cation leaching to such an extent that soils may have been depleted of their base cation reserves. Such depletion greatly prolongs the acidification recovery time of watersheds and may adversely impact forest productivity (Kirchner and Lyderson 1995, Likens et al. 1996).

As aquatic effects researchers have revised their understanding of the quantitative importance of the various acidification processes, terrestrial effects researchers have also turned greater attention to the importance of the response of base cations to acidic deposition and the interactions between base cations (especially Ca^{2+} and Mg^{2+}) and Al. Likens et al. (1996) concluded that acidic deposition enhanced the release of base cations from forest soils at Hubbard Brook Experimental Forest (HBEF) in New Hampshire from the mid-1950s until the early 1970s, but that, as the labile pool of base cations in soil became depleted, the concentrations in streamwater decreased from 1970 through 1994 by about one-third. The marked decrease in base cation inputs and concomitant increase in net soil release of base cations at HBEF have likely depleted soil pools to the point where ecosystem recovery from decreased S deposition will be seriously delayed. Moreover, Likens et al. (1996) suggested that recently-observed declines in forest biomass accumulation at HBEF might be attributable to Ca^{2+} limitation or Al-toxicity, which can be expressed by the Ca^{2+} to Al^{n+} ratio in soil solution (Cronan and Grigal 1995).

Nitrate plays an important role in surface water acidification in some areas, especially with respect to episodic acidification during snowmelt or rainfall events (Wigington et al. 1993). This generally occurs in regions in which N deposition is sufficiently high that N supply exceeds the N demands of the forest vegetation and other biota, either chronically or episodically. Although most forests retain the majority of N inputs that they receive, some forested ecosystems leach significant amounts of NO_3^- to drainage water, and this occurs under a range of N deposition input levels. At some sites in the United States, relatively high levels of N deposition (10-30 kg N/ha/yr) have been shown to result in high N leaching losses (7-26 kg N/ha/yr). Good examples include watersheds in Great Smoky Mountains National Park in Tennessee (Johnson et al. 1991) and the San Bernardino Mountains in southern California (Fenn et al. 1996). At Fernow, West Virginia, high N loading (15-20 kg N/ha/yr) has caused moderate N leaching losses (~ 6 kg N/ha/yr; Gilliam et al. 1996, Peterjohn et al. 1996). Despite the observed variability in ecosystem response, a number of generalizations can be made (c.f., Sullivan 2000). Coniferous forests and alpine ecosystems seem to be more prone to N-saturation than deciduous forests

(Aber et al. 1995a, 1998; Williams et al. 1996). Young and successional forests, with their greater nutrient demand, are less prone to N-saturation than mature stands (Peet 1992). Climate, soil N pool size, and land use dramatically alter biological N-demand (Cole et al. 1992, van Miegroet et al. 1992, Feger 1992, Magill et al. 1996, Fenn et al. 1998). Because N is so critical to ecosystem primary productivity, other factors that influence plant and microbial growth (e.g., water availability, temperature) or the abundance or availability of other nutrients (e.g., Ca, Mg, P) will have significant effects on the ability of plants and microbes to utilize N and therefore the extent to which N will leach in drainage waters.

The relationship between measured wet deposition of N and streamwater output of NO_3^- was evaluated by Driscoll et al. (1989a) for sites in North America (mostly eastern areas), and augmented by Stoddard (1994). The resulting data showed a pattern of N leaching at wet-inputs greater than approximately 400 eq/ha (5.6 kg N/ha). This is about 22% higher than the 20-year average wet N deposition at Big Meadows in SHEN (4.6 kg N/ha), although wet N deposition at Big Meadows exceeded this amount in one year (6.6 kg N/ha in 1996) during the past decade and in three years over the period of record since 1981 (see Section V.C.3).

Stoddard (1994) presented a geographical analysis of patterns of watershed loss of N throughout the northeastern United States. He identified approximately 100 surface water sites in the region with sufficiently intensive data to determine their N status. Sites were coded according to their presumed stage of N retention, and sites ranged from Stage 0 through Stage 2. The geographic pattern in watershed N retention depicted by Stoddard (1994) followed the geographic pattern of N deposition. Sites in the Adirondack and Catskill Mountains in New York, where N deposition was about 11 to 13 kg/ha/yr, were typically identified as Stage 1 or Stage 2. Sites in Maine, where N deposition was about half as high, were nearly all Stage 0. Sites in New Hampshire and Vermont, which received intermediate levels of N deposition, were identified as primarily Stage 0, with some Stage 1 sites. Based on this analysis, a possible threshold of N deposition for transforming a northeastern site from the "natural" Stage 0 condition to Stage 1 would correspond to the deposition levels found throughout New Hampshire and Vermont, approximately 8 kg N/ha/yr. This agreed with Driscoll et al.'s (1989a) interpretation, which suggested N leaching at wet inputs above about 5.6 kg/N/ha/yr, which would likely correspond to total N inputs near 10 kg N/ha/yr. This is likely the approximate level at which episodic aquatic effects of N deposition would become apparent in many

watersheds of the eastern United States. It is about 28% higher than the estimated total (wet + dry) N deposition at Big Meadows, which is about 7.8 kg N/ha/yr.

Comparable results were found in a survey of N outputs from 65 forested plots and catchments throughout Europe by Dise and Wright (1995). Below throughfall inputs (estimate of wet plus dry deposition) of about 10 kg N/ha/yr, there was very little N leaching at any of the study sites. At throughfall inputs greater than 25 kg N/ha/yr, the study catchments consistently leached high concentrations of inorganic N. At deposition values of 10 to 25 kg N/ha/yr, Dise and Wright (1995) observed a broad range of watershed responses. Nitrogen output was most highly correlated with input N (r^2=0.69), but also significantly correlated with input S, soil pH, percent slope, bedrock type, and latitude. A combination of input N (positive correlation) and soil pH (negative correlation) explained 87% of the variation in output N at 20 sites (Dise and Wright 1995). Thus, total N deposition of about 7.8 kg N/ha/yr at SHEN might be considered close to the adverse loading rates seen in other parts of North American and Europe.

2. Aquatic Fauna

Regional aquatic biodiversity in the southern Appalachian region is very high. Southern Appalachian streams contain a rich diversity of invertebrate, fish, and salamander species. Local species richness depends on thermal regime, water chemistry, patterns of discharge, plus substrate type and geomorphology (Wallace et al. 1992).

Acidification of waters in the Southern Appalachian Mountains region occurs against a backdrop of highly modified streams and rivers. About 98% of the free-flowing freshwater communities in the United States have been drastically altered, and only about 20% are of high enough quality to warrant Federal protection. To date, only about 1,600 km of streams and rivers have been given conservation status; only about 10% of these are east of the Mississippi River. Despite the highest national biological diversity in aquatic communities, southeastern streams have been afforded little protection. Geographic distributions of fish species have been greatly altered by humans, in part by inter-basin exchanges of water and especially by fish introductions, whether intentional or not. Logging and mining have been especially detrimental to fish, particularly brook trout (*Salvelinus fontinalis*). Many relatively healthy streams in second growth forests remain, but most large rivers have been dammed. Although biodiversity remains very high, it has likely been reduced in most aquatic communities in the Southeast. The

inability of flowing-water species to survive in the slow or still water habitats of lakes and ponds has caused much of this loss of diversity. Flowing-water species are specialized and very diverse, whereas lake communities are generalized and supplemented by introduced species. Human populations are growing in all southeastern states, and aquatic environments will be subject to increasing pressure. The streams in national parks and wilderness areas, including SHEN, may become increasingly important as biological refugia in the southern Appalachians.

Macroinvertebrates are defined as animals without backbones, which can be seen with the unaided eye, usually larger than 0.025 cm (0.01 inches) in at least one dimension. Aquatic benthic macroinvertebrates occur on the bottoms of streams or lakes, in or among substrates such as stones (gravel, cobble, etc.), plants, or wood. In lower order streams, the immature aquatic insects represent most of the macroinvertebrates, together with mollusks and crustaceans. The community contains many species of known sensitivity to stresses such as acidification or sedimentation. As with other groups, counts of taxa (such as families, genera or species) at impacted versus unimpacted sites are often lower due to loss of sensitive taxa, so lower species richness or absence of specific taxa is often taken to indicate impacts (SAMAB 1996).

Macroinvertebrate ecological roles in aquatic communities are diverse. Invertebrate species richness in the region is probably the greatest in North America, with many endemic species. Indeed, the regional invertebrate fauna includes many as yet undescribed species. The cool, high mountain streams in the region contain species that are usually only found further north. Many regional taxa have evolved rather elaborate morphological and behavioral adaptations for maintaining their positions in high-gradient streams with high current velocity (Wallace et al. 1992).

Benthic invertebrates play important roles in the breakdown of terrestrial and detrital material in streams and in nutrient regeneration. Many fish, waterfowl and other bird species rely on benthic invertebrates as their primary food source. Acidification, and consequent impacts of acidification on acid-sensitive benthic invertebrate species, can therefore affect structure, function, and trophic relations in stream ecosystems. Because benthic invertebrates are diverse, relatively easy to collect (though time-consuming to identify), and have short generation times, they are used as indicator species for a number of potential pollutants. This is true in the case of acidification and recovery from acidification, because communities typically contain species with known acid sensitivities (Baker et. al. 1990). While regional diversity of stream invertebrates is high, standing stocks are typically low in high-gradient, low-order streams

(Elwood et al. 1991). Production is also low (for example, 0.5-9.2 g dry weight /m^2/yr), especially compared to very high production rates in regional rivers, which can be as high as 427.6 g dry mass/m^2/year in the New River below Bluestone Dam in Virginia. Secondary production is a measure of the rate at which animal biomass is produced, regardless of its fate (e.g., loss to predators, natural mortality, emigration). Its units are biomass or energy per unit area, per unit time. Most studies of stream secondary production have been limited to a few taxa, and in high-gradient streams have focused on species with clearly discernable life cycles. Few studies have attempted to measure total macroinvertebrate production within a stream.

There are currently few data suggesting that acidification has produced significant changes in the invertebrate biota of southern Appalachian streams. This likely reflects the scarcity of long-term data, however, more than the absence of effects (Wallace et al. 1992).

The Ephemeroptera-Plecoptera-Trichoptera (EPT) index is one measure of stream macroinvertebrate community integrity. This is the total number of families in the three insect orders Ephemeroptera (mayflies), Plecoptera (stoneflies), and Trichoptera (caddisflies) present in a collection. These orders contain families of varying acid sensitivity so the index value (the number of families) is lower at acidified sites. SAMAB (1996) used the work of Mark Hudy in the George Washington and Jefferson National Forests (Virginia) to illustrate the effects of acidification on macroinvertebrates. EPT indices were calculated for 110 sites in George Washington and Jefferson National Forests based on collections made between 1992 and 1995. Among the 27 sites which had low EPT scores (eight or fewer families, EPT= 8 or less), about 60% had ANC values less than 100 µeq/L. The remaining stream sites with low EPT scores had other impacts. Sites with EPT scores of 14 or more had no conspicuous impacts.

Other common impacts might include sedimentation and pesticides. Excess fine sediments are detrimental to aquatic macroinvertebrates, as they are to fish, because they clog the interstices among bottom stones where macroinvertebrates take refuge. Excess fine sediments therefore may deprive organisms of food, as well as clogging the gravel nests where many species lay eggs. Aquatic insects are often sensitive to insecticides used in agriculture or silviculture. Low elevation stream sites in the southern Appalachians are often surrounded by agricultural land, often with no riparian forest buffer.

Known recent impacts other than acidification are absent in the case of the St. Marys River, located 30 km south of SHEN, which is unique in Virginia in having historical records of both water quality and benthic macroinvertebrates (SAMAB 1996). Indeed, it is the first clearly

documented case of biodiversity loss over time due to acidification in a southeastern U. S. stream (Kauffman et al. 1999). The St. Marys River is in the St. Marys Wilderness, George Washington and Jefferson National Forests in Augusta County, VA. This stream was sampled in the 1930s by E. W. Surber and in the 1970s-1990s by the Virginia Department of Game and Inland Fisheries. The stream has been acidified by atmospheric deposition, with pH declining from 6.8 in 1936 to 5.2 in 1988. Over the same time period, acid-sensitive insects declined or disappeared, with the number of taxa dropping from 31 to 18. The EPT index (based on genera in this case) declined from 17 to 10 (SAMAB 1996). Since 1988, the invertebrate species richness has continued to decline. The Shannon diversity index for benthic macroinvertebrates was 3.94 in 1936, 2.02 in 1988, and 1.8 in 1998; this index is usually between 3 and 4 for unpolluted streams. The observed declines in invertebrate taxa are consistent with those reported in the literature for streams with low pH. These taxa include *Epeorus, Ephemerella, Paraleptophebia* and *Stenonema*. Taxa known to be acid-tolerant (*Leuctra* and Chironomidae) have replaced them. This clearly reflects community degradation due to acidification, which may have occurred simultaneously in many similar streams in the southern Appalachians for which there are no historical records (Kaufmann et al. 1988).

The southern Appalachian area is widely regarded as one of the most diverse landscapes in the Temperate Zone (SAMAB 1996). Fish diversity is quite high. There are about 950 freshwater fish species in North America (Jenkins and Burkhead 1993), of which about 485 species can be found in the Southeast, about 210 species in Virginia (Jenkins and Burkhead 1993), and more than 30 species in SHEN. Regional habitat diversity and intraspecific genetic diversity are also regarded as high. Thus, the Southeast is a unique national biodiversity resource for fish. Unfortunately, the Southern Appalachian Assessment concluded that 70% of sampled stream locations showed moderate to severe fish community degradation, and that about 50% of the stream length in West Virginia and Virginia showed habitat impairment (SAMAB 1996).

Fish communities of high-gradient southern Appalachian streams may contain a variety of species, but are often dominated by trout, especially brook trout. Of the 15.1 million ha (37.4 million ac) in the southern Appalachian region (as defined by SAMAB 1996), 5.9 million ha (14.6 million ac [39%]) are in the range of native brook trout, with up to 53,000 km (33,000 mi) of potential native brook trout streams. This includes over 19,000 km (12,000 mi) of trout streams in Virginia (SAMAB 1996). There has been little regional ecological research on other species except in biogeographic and systematic studies, although Jenkins and Burkhead (1993)

provided much ecological information on the fish species of Virginia. There are, nevertheless, clear patterns in species distribution from headwaters to rivers, which can also be seen in community comparisons among reaches at different elevations; the clearest pattern is that species richness increases in a downstream direction. This is thought to result from the rather small number of upstream species, which must tolerate simultaneously highest current velocities and lowest pH values. Fish are absent from the highest headwaters, where they are replaced by salamanders. The highest-elevation fish species is usually brook trout, typically joined downstream by dace (e.g., blacknose dace, *Rhinichthys atratulus*), a sculpin (e.g. mottled sculpin, *Cottus bairdi*) and a darter (e.g. fantail darter, *Etheostoma flabellare*), and perhaps by introduced brown (*Salmo trutta*) or rainbow (*Oncorhynchus mykiss*) trout (Wallace et al. 1992). In the context of acidification, the introduced trout are both more acid-sensitive than brook trout, and will not be present in acidified waters.

Proceeding downstream, other dace, darters, chubs, shiners, suckers and others are often present. In larger downstream reaches, still regarded as high-gradient, the important gamefish smallmouth bass (*Salmoides dolomieu*) is most abundant in riffles over substrate which is about 40% clean gravel, boulder or bedrock, and at gradients of 0.8-4.8 m/km and depth at least 1.2 m (Wallace et al. 1992).

The fish of the southern Appalachians are all primarily insect predators. Trout, some dace, and some chubs are midwater and surface feeders, catching drifting aquatic invertebrates and terrestrial insects. Sculpins, darters, most chubs and minnows, and some dace feed primarily on benthic invertebrates, searching on and in the rock and gravel streambed, and some overturn rocks in their search. Because of limited primary production in such streams (due to shading across their entire width in summer), herbivores such as stonerollers occur only in somewhat larger streams with open canopy and lower gradient. Detritivore fish are uncommon in high-gradient streams in the region (Wallace et al. 1992).

Estimates of fish predation pressure on stream invertebrates suggest that pressure is substantial, but not more than invertebrate production. The fish community as a whole and brook trout in particular depend heavily on allochthonous (terrestrial) production, and terrestrial insects may make up 50% of trout diets. This terrestrial connection is direct in the case of fish feeding on terrestrial insects, and indirect in the case of stream invertebrate prey feeding on terrestrial detritus. Thus, effects on fish resources can be attributed in part to the alterations of water quality (acidification, sedimentation) and also to removal of terrestrial energy and food

additions through activities such as forest removal. Most small, high-gradient southern Appalachian streams, especially those that drain crystalline bedrock, have very low invertebrate production. A considerable portion of this production goes to predaceous invertebrates. In small, fishless, headwater streams, production of salamanders is similar to fish production in larger downstream reaches. Secondary production of carnivorous invertebrates is likely to be strongly influenced by local availability of food resources (Wallace et al. 1992).

In addition to stream chemistry, four factors are related to patterns of distribution and abundance of aquatic biota: temperature, gradient, stream order, and flow regime. Streams are divided into cold versus warm water; cold water streams have temperatures that rarely exceed 24-26° C for extended periods, and are characterized by the presence of trout and sculpin. Even at low temperatures, trout have relatively high metabolic rates, and are more active than most fish. They can use food resources more effectively than other fish at cold or cool temperatures (Moyle and Cech 2000).

Whereas temperature is of great importance in determining broad distribution patterns, gradient (number of meters drop per kilometer of stream) is often of greater local importance. This is because gradient has great influence on water velocity, substrate size, number and size of pools, and oxygen content. High-gradient streams may have little slow water, with bottoms of bedrock, boulders and cobbles, and few deep pools (Moyle and Cech 2000).

Stream gradient and temperature both vary with stream order, a classification of streams based on branching patterns. In most river systems, first order streams are the highest, smallest, coldest, highest-gradient streams, with fewest species of fish. As stream order increases, species richness also increases, usually as a consequence of increase in habitat diversity; turbidity, temperature, and stream size increase as well. As stream order increases, usually new species of fish are added at a higher rate than upstream fish are subtracted from the community (Moyle and Cech 2000). The trophic structure of the fish community also changes with stream order. In first order streams, the dominant fish (e.g. trout) usually feed on insects that drop into the water from the overhanging vegetation or on detritus. In higher-order streams, predators of aquatic insects are added, then piscivores. However, most stream fish are opportunistic feeders and may feed on a wide variety of foods (Moyle and Cech 2000).

The flow regime has an overriding influence on fish communities with respect to temperature, stream order, and gradient. Extreme fluctuations in flow regime (droughts to floods) can reduce or eliminate fish species or communities. However, extirpation by flood is

extremely rare, since adults, at least of most native species, appear to be able to find refuge. Floods are a common cause of missing year classes in populations, causing larvae or young to be washed downstream. Periods of low water may eliminate species through lowered oxygen levels, higher temperature, or aquatic vegetation growth, and the pre-drought community returns only gradually after typical conditions return (Moyle and Cech 2000).

There is a general pattern of increasing fish species richness and abundance from lower-order to higher-order streams, probably resulting in part from a greater variety of habitat types (including spawning and nursery areas) and food sources downstream. Perhaps because of the greater possibility of isolation, low-order streams are more likely to host species unique to each drainage (Adams and Hackney 1992).

Streams change continuously in physical and chemical characteristics from headwaters to river mouth. Changes include shift from primarily terrestrial to in-stream organic matter contributions, nutrient and water retention times, water volume and velocity, oxygen content, substrate size, gradient, and temperature. These shifts play important roles in determining the communities in different river sections. For example, localized differences in gradient have great effects on fish and invertebrate occurrences, and may result in markedly discontinuous distributions of individual species (Adams and Hackney 1992).

Physical complexity in streams affects biological processes chiefly through the availability of stable substrates that provide habitat and attachment surfaces. For example, in low-order streams, plankton are virtually non-existent, with consumers dependent on detrital materials or periphyton production on immobile substrates. In addition, rocks and woody debris provide the majority of physical complexity. In contrast, lower-order streams often exhibit high within-stream spatial variability in habitat conditions (Adams and Hackney 1992).

The physical characteristics related to basin morphology often affect biological processes in many ways, the most important of which relate to light and nutrients. In the continuum from headwater to river, headwater streams have the greatest interconnections with the terrestrial environment, and allochthonous (originating outside the stream system) energy sources typically dominate energy budgets; the majority of allochthonous material enters headwater streams as direct leaf litter, which is processed in place or downstream by macroinvertebrates. Autochthonous (in-stream) production is limited in these streams by dense shading by riparian vegetation, and nutrient limitation (Adams and Hackney 1992).

Wallace et al. (1992) reviewed rates of in-stream primary productivity in high-gradient streams in the Southeast and concluded that the most important controlling variables were stream order, season, degree of shading, and nutrients. It is clear that these variables can be intercorrelated, i.e., low-order streams are likely to be shaded across their entire width in forested catchments, and have lower nutrient content than downstream habitats, which are the beneficiaries of more weathering products. They found that unshaded reaches within high-gradient streams had three times higher primary productivity than did shaded reaches. Rates were 1.3 to 9 g $C/m^2/yr$ in several forested second- and third-order streams in Virginia and North Carolina including both soft (low Ca^{2+} and Mg^{2+}) and hardwater (high Ca^{2+} and Mg^{2+}) streams. Periphyton production in a hardwater (high base cations) Tennessee stream was found to be about 2.6 times higher than in a similar-sized softwater (low base cations) stream in North Carolina. While these differences in algal productivity are likely to be important, they are dwarfed by rates of periphyton production in the broad, sixth order New River in Virginia, where rates were up to 1059 g $C/m^2/yr$ in hardwater reaches, which were three to five times the rates in softwater reaches. Thus, whereas softwaters have lower in-stream production rates, both hardwater and softwater mountain streams have rather low rates of production compared with larger streams.

E. TERRESTRIAL INDICATORS

Bioindicators are those species for which pollutant sensitivity has been documented and for which data exist on their dose-response to pollutants and/or on symptomatology. In some cases, bioindicators detect exposure to a pollutant at a site where air quality monitoring data are not available. Ozone and SO_2 are the most extensively studied pollutants regarding impacts on vegetation. However, identifying symptoms of air pollutant injury is difficult, because visual symptoms are generally poorly documented, and only a small fraction of the thousands of native plant species have been screened for sensitivity to air pollutants.

Gaseous air pollutants can reduce photosynthesis, growth, and productivity of sensitive plant species (Treshow and Anderson 1989, Smith 1990, Runeckles and Chevone 1992, Chappelka and Chevone 1992), even at relatively low exposure levels (c.f., Reich and Amundson 1985). Some species are sensitive to episodes of high ambient exposure, while others are sensitive to lower chronic exposure over an extended period of time. Plants that are

physiologically stressed from air pollutants can have reduced vigor, which in turn can lead to greater susceptibility to additional stresses such as insect attack (Innes 1993, Pronos et al. 1999).

1. Plant Symptomatology

Pollutants can cause injury to various plant tissues including leaves, stems, and roots. Foliar injury is the most visible form of damage, although it often can be confused with other biophysical injuries, including abrasion, desiccation, insect herbivory, and fungal pathogens.

Ozone symptoms in conifer, hardwood, and herbaceous foliage that could be considered "typical" include chlorosis, stipple (change in color of epidermal cells, usually brown or purple, with no necrosis), and accelerated needle and leaf loss (Miller et al. 1983; Thompson et al. 1984a,b; Hogsett et al. 1989; Treshow and Anderson 1989; Stolte 1996; Brace et al. 1999). Common symptoms of O_3-induced foliar injury are summarized in Table III-1 (Krupa and Manning 1988, Krupa et al. 1998, Sullivan et al. 2001).

Ozone causes injury to highly-sensitive species of plants at concentrations as low as 60 ppbv (Treshow and Anderson 1989). Ozone enters plant leaves as a gas and dissolves in the presence of water. The resulting free radicals oxidize proteins of cell membranes, including those of the thylakoid membranes where photosynthesis takes place. Injury includes leaf discoloration, reduced photosynthetic rates, lowered sugar production, reduced growth, and possibly death (Sullivan et al. 2001).

Acute injury, such as visible injury on leaves, usually occurs after exposure to high concentrations of O_3. Moderate concentrations of O_3 (similar to ambient levels in much of the eastern United States) for several days to several months can cause chronic injury, accelerated aging, premature casting of foliage, or growth loss without other symptoms (Pell et al. 1994a,b; U.S. EPA 1996a,b). Accelerated aging may result in premature color change and loss of foliage, an effect of considerable importance at SHEN since park visitation levels are relatively higher during the fall color season. Growth reductions at ambient levels of O_3 are often difficult to measure, although a cumulative stress over multiple growing seasons may significantly reduce the growth and productivity of trees and understory vegetation (Reich and Amundson 1985, U.S. EPA 1996b).

There is considerable genetic variability, both within and among species, in response to O_3 (Miller et al. 1982). The most sensitive plants are injured by exposure to concentrations of 0.06 ppm or less for several days and can often be used as biological indicators of O_3 exposure (U.S.

Table III-1. Common symptoms of O_3-induced foliar injury (from Krupa and Manning 1988, Krupa et al. 1998, Sullivan et al. 2001).

Acute Injury	Chronic Injury
<u>Conifers</u>	
• Banding; clear bands of chlorotic tissue develop on semi-mature needle tissue following O_3 episodes. • Tipburn; characterized by dying tips of young elongating needles. At first reddish-brown in color later turning brown, injury spreading	• Flecking[a] and mottling[b] ; flecking is the earliest symptom on the older needles of conifers. Mottling is generally associated with diffuse chlorotic areas interspersed with green tissue on first-year needles. • Premature senescence; early loss of needles.
<u>Broad-leaved plants (hardwood trees, herbaceous plants)</u>	
• Bleaching (unifacial or bifacial); small unpigmented necrotic spots or more general upper surface bleaching. Palisade cells and, where injury is more severe, upper epidermal cells collapse and become bleached. • Flecking; small necrotic areas due to death of palisade cells, metallic or brown, fading to tan, gray or white. • Stippling; small punctate spots where a few palisade cells are dead or injured, may be white, black, red, or red-purple. • Bifacial necrosis; when the entire tissue through the leaf is killed, bifacial dead areas develop, ranging in color from white to dark orange-red. While small veins are usually killed along with the other tissue, larger veins frequently survive	• Pigmentation (bronzing); leaves turn red-brown to brown as phenolic pigments accumulate. • Chlorosis; may result from pigmentation or may occur alone as chlorophyll breakdown. • Premature senescence; early loss of leaves, flowers, or fruit.

[a] Flecking is necrosis of tissue in small areas that may coalesce
[b] Mottling is variation in chlorosis over the leaf surface, without necrosis

EPA 1996b). Conversely, some plants are very tolerant of O_3 and are unaffected, even in severe exposures. Plants generally respond to lower O_3 concentrations than do people (U.S. EPA 1996b).

The timing of the O_3 exposure *vis-à-vis* the life cycle of the plant is important in determining response. For instance, in an annual plant before flowering, exposure to O_3 may reduce the growth of the root system; as the plant repairs injury in the leaves and maintains photosynthesis there is less carbon available to grow roots (U.S. EPA 1996b). In fact, root systems may be reduced in growth long before deleterious effects are manifested on above-ground portions of the plant. In perennial plants, the process is complex, as stored reserves are

usually available for growth and the effect of an exposure may not be manifested for several growing seasons (Hogsett et al. 1989, Andersen et al. 1991, Laurence et al. 1994). However, in the most sensitive species, a single season of exposure can be sufficient to reduce growth significantly (Wang et al. 1986, Woodbury et al. 1994).

Ozone may also affect the growth of plants indirectly through interactions with pests and pathogens (Laurence 1981), or by altering the symbiotic relations between plants and associated organisms (McCool 1988; Stroo et al. 1988; Andersen and Rygiewicz 1991, 1995; Rygiewicz and Andersen 1994). The resulting changes in nutrient availability or uptake may also result in altered plant growth, in this case mediated by O_3 exposure (Weinstein et al. 1991, Andersen and Scagel 1997, Weinstein and Yanai 1994).

Simulation modeling may be used to study the impact of O_3 on forest ecosystems, to establish the bounds of expected changes in growth, and to project shifts in ecosystem composition and structure (Laurence et al. 2001). While simulation modeling is unlikely to project exactly the response of any particular stand, the results, along with estimates of uncertainty in the projections, can be used to characterize potential changes and indicate the possible severity of effects (Woodbury et al. 1998).

Sulfur dioxide (SO_2) is a primary pollutant, given off during the combustion of fossil fuels, particularly coal, for the generation of electricity. The past three decades have seen tremendous advancements in control technologies and subsequent reductions in the emissions of this pollutant. For the most part, direct impacts of SO_2 on vegetation are a problem of the past in the United States. Indirect effects, through acidification of rain and deposition to forest ecosystems, while reduced, are still important. See Section VI.B.

Sulfur is an essential element for plant metabolism, and there are metabolic pathways for transformation of S. Plants generally take up S as SO_4^{2-} from the soil, not in a gaseous form. If SO_2 enters the leaf, it is converted to SO_4^{2-}. During the transformation, sulfite, a compound highly toxic to plants, is produced. If the atmospheric concentrations of SO_2 are high (>about 0.5 ppm for 3 hours), toxic concentrations of sulfite may accumulate and cause injury before they are transformed to SO_4^{2-}. If the exposure occurs over an extended period, SO_4^{2-} may also accumulate to toxic levels in the leaf.

Injury induced by SO_2 includes interveinal necrosis, dieback of leaf and needle tips, and necrotic spots (Thompson et al. 1980, 1984a,b; Treshow and Anderson 1989; Legge et al. 1998).

Unless a major S emissions source is located nearby, SO_2 rarely occurs in sufficiently high concentrations to cause direct damage to vegetation (Garner et al. 1989, Johnson et al. 1992).

There are few data or descriptions of the direct effects of NO_x on plant species, with the best description of symptomatology in Bytnerowicz et al. (1998). Concentrations of NO and NO_2 at locations remote from point sources are rarely high enough to cause visible injury symptoms. Experiments have been conducted to determine the relative sensitivity of plants to both nitrogen dioxide and nitric oxide, but the concentrations necessary to induce injury are far greater than those typically reported for ambient air quality, even in urban environments (NAS 1977). The adverse effects from long-term exposures can be reduced photosynthesis and growth in the absence of visible injury (Taylor 1968, Saxe 1994). At moderate levels, deposited N generally stimulates plant growth.

2. Physiological Effects

Considerable variation in the response of trees to air pollutants is caused by differences in the pollutant dose, phenological stage, age of leaves exposed, seed source, nutritional status of plants, and the integrated effects of multiple stresses (Bytnerowicz and Grulke 1992). There are several mechanisms for phytotoxicity, depending on the type of air pollutant. Physiological effects at the cellular and subcellular level can significantly affect plant function in the absence of visible symptoms of injury.

Gaseous air pollutants typically enter the plant through stomata, so the duration of stomatal opening greatly affects the pollutant dose assimilated. Once a pollutant enters a plant cell, there are many biochemical processes that are potentially affected (Wellburn 1988, Heath and Taylor 1997). Ozone increases the potential for the formation of harmful free radicals. Many of these free radicals are highly reactive and disrupt various metabolic processes through oxidation, substitution for other compounds, and toxicity. Disruption of photosynthetic processes (including damage to mesophyll cells and degradation of chlorophyll and chloroplasts [Grulke et al. 1996]) is one of the most deleterious effects of air pollutants, because it results in lower photosynthetic rates (Patterson and Rundel 1989, Grulke 1999), rapidly reduces plant vigor and productivity, and can affect internal resource allocation in the absence of visible symptoms (Matyssek and Innes 1999).

The degree of pollutant injury depends on the effective dose, which is a function of concentration, length of exposure, and stomatal aperture (Kozlowski and Constantinidou 1986).

Ozone injury of cells and tissues is essentially the same in woody and herbaceous plants (Bytnerowicz and Grulke 1992). Injury generally occurs first in the most photosynthetically active tissues, with disruption of chloroplasts in the palisade and mesophyll tissue. The loss of photosynthetic tissue results in visible chlorosis and necrosis.

Injury development in plants subjected to elevated concentrations of N compounds is not well understood, although it has been shown that acidic precipitation, particularly nitric acid vapor, can injure the cuticular layer and substomatal cavities. The contact time of acidic droplets or films on the leaf surface determines the degree of damage (Wellburn 1988). Acid-induced injury under experimental conditions typically requires exposure to very acidic solutions (pH < 3; Temple 1988, Turner et al. 1989), and injury in the field is rarely observed.

Photochemical reactions involving the absorption of sunlight and interactions with hydrocarbons and oxygen cause atmospheric NO_x to be consumed in the production of O_3, with peroxyacyl nitrates (PANs) given off as secondary pollutants (Taylor et al. 1975). PANs have been shown to be highly phytotoxic (Mudd 1975). They can cause glazing or bronzing of the lower surface of leaves, indicating damage of the mesophyll cells around the stomatal cavity. Sensitive species have been shown to be injured by levels as low as 20 ppbv for two to four hour exposure periods.

The relationship of pollutant exposure to seasonal variation in physiological activity can have a significant influence on physiological effects and visible injury in plants (Grulke 1999). Gaseous uptake generally is higher during periods when soil water potential is high. The potential for pollutant uptake is higher during periods when soil moisture is high and plants are most metabolically active. Therefore, injury is more likely to be manifested by O_3 exposure during the spring when gaseous uptake is higher. This finding has implications for how O_3 exposure indices are quantitatively compared to O_3 injury measurements. Interactions with insects, pathogens, and other pollutants can accentuate the stress complex for plants exposed to a particular pollutant (Bytnerowicz and Grulke 1992, Sullivan et al. 2001).

3. Nitrogen Saturation and Forest Decline

Nitrogen is an essential nutrient for both aquatic and terrestrial organisms, and is a growth-limiting nutrient in many ecosystems. For each ecosystem, there is an input level of N which will increase ecosystem productivity without causing significant changes in species distribution

or abundance. Above that input level, adverse effects can occur in both aquatic and terrestrial ecosystem compartments (Gunderson 1992, Stoddard 1994, Aber et al. 1998).

The N cycle is extremely complex and controlled by many factors besides atmospheric emissions and deposition. Also, N inputs that may be beneficial to some species or ecosystems may be harmful to others. Nitrogen inputs to forested ecosystems are typically derived from the atmosphere, either through natural N-fixation or from atmospheric deposition. However, the pool of available N used by plants and microbes within the watershed can originate either from an external (atmospheric) source or an internal source, via decomposition and mineralization of stored organic N. The amount of inorganic N released through mineralization is affected by both the size and quality of the soil N pool (Aber et al. 1998), which in turn can be affected by disturbance and land use.

Increased atmospheric deposition of N does not necessarily cause adverse environmental impacts. In most areas, added N is taken up by terrestrial biota and the most significant effect seems to be an increase in forest productivity (Kauppi et al. 1992). However, under certain circumstances, atmospherically-deposited N can exceed the capacity of forest ecosystems to take up N. In some areas terrestrial ecosystems have become N-saturated[1] and high levels of N deposition have caused elevated levels of NO_3^- in drainage waters (Aber et al. 1989, 1991; Stoddard 1994). This enhanced leaching of NO_3^- causes depletion of Ca^{2+} and other base cations from forest soils and can cause acidification of soils and drainage waters in areas of base-poor soils (Reuss and Johnson 1986).

Increased levels of N also have the potential to increase foliar N content, alter N metabolism in plants (including winter hardiness), alter soil chemistry and N cycling, affect mycorrhizae, modify soil microbial dynamics, and alter plant growth (Takemoto 2000, Takemoto et al. 2001). Furthermore, litter decomposition rates are higher in areas with highest N deposition, presumably because of lower C:N ratios in the forest-floor litter (Fenn and Dunn 1989, Fenn et al. 1998). This is a significant change in an ecosystem process that has implications for biogeochemical cycling in general.

There is concern that excess N deposition could cause long-term terrestrial ecosystem damage that may be difficult to detect. In particular, both empirical and theoretical evidence

---

[1] The term N-saturation has been defined in a variety of ways, all reflecting a condition whereby the input of N (e.g., as NO_3^-, NH_4^+) to the ecosystem exceeds the requirements of terrestrial biota and a substantial fraction of the incoming N leaches out of the ecosystem as NO_3^- in groundwater and surface water.

suggest that lost species diversity may result from excess N inputs (Galloway et al. 1995). Increased N inputs may favor some species over others, thus changing successional dynamics. Acid (including N) deposition appears to make red spruce (*Picea rubens*) more susceptible to winter damage (NAPAP 1991, Johnson et al. 1992), at least in the northern part of its range. High SO_4^{2-} and NO_3^- levels can contribute to Al toxicity in red spruce populations. In addition, acidic cloudwater at high elevations can damage red spruce foliage, for example by reduced photosynthesis and reduced growth.

The end results of N-saturation can include forest decline, reduced forest growth, increased forest susceptibility to disease and insect infestation, eutrophication of estuaries and near-shore oceans, freshwater and soil acidification, loss of fish and other aquatic life, and changes in terrestrial and aquatic biodiversity. Fortunately, atmospheric N inputs to most forests are not high enough to cause such problems. Because of the severity of the potential effects, however, it is important that we understand the N cycle and the extent to which it is being perturbed by atmospheric emissions (Aber et al. 1998, Sullivan 2000).

N cycling is also regulated to a significant degree by climate, disturbance, and land management. Such factors are believed to have both short and relatively long-lasting (i.e., decadal to century) effects on the response of forest ecosystems to atmospheric N deposition (Aber et al. 1989, 1995b, 1998; Mitchell et al. 1996; Fenn et al. 1998). The extent to which the land was logged, burned, or used for agricultural production in the past can profoundly affect the N-status of the soils and therefore the extent to which N deposition will or will not cause environmental degradation.

It has recently been hypothesized that prior land use history, extending back 100 years or more, can have a major effect on forest response to N deposition (Aber and Driscoll 1997; Foster et al. 1997; Aber et al. 1997, 1998). The greater the previous extraction of N from the site by agricultural conversion, fire, logging, or other disturbance, the more N the forest will be able to absorb without becoming N-saturated. Aber et al. (1998) contended that previous land use is more important than either current or total accumulated N deposition as a controlling factor for N-saturation in the northeastern United States.

Forest stand age has also been found to be associated with N retention by the forest system. Watersheds having older trees seem more likely to leach N to a higher degree than forests having younger trees (c.f., Vitousek 1977, Elwood et al. 1991, Emmett et al. 1993).

4. Soil Acidification

Calcium and other base cations are major components of surface water acid-base chemistry, and are also important nutrients that are taken up through plant roots in dissolved form. Base cations are typically found in abundance in rocks and soils, but a large fraction of the base cation stores are bound in mineral structures and are unavailable to plants. The pool of dissolved base cations resides in the soil as cations that are adsorbed to negatively-charged exchange sites. They can become desorbed in exchange for H^+ or Al^{n+}, and are thus termed exchangeable cations. The process of weathering gradually breaks down rocks and minerals, returning their stored base cations to the soil in dissolved form and thereby contributing to the pool of adsorbed base cations. Base cation reserves are gradually leached from the soils in drainage water, but are constantly being resupplied through weathering.

An increase in the concentration of SO_4^{2-} or other strong-acid anions in soil water will be balanced by an equivalent increase in the concentration of cations. Depending upon the availability of exchangeable base cations in the soil (primarily Ca^{2+}, Mg^{2+}, and K^+ ions), the cations associated with increasing concentrations of strong-acid anions in soil water can be either acidic or basic. The export of acidic cations (primarily H^+ and Al^{n+} ions) may contribute directly to loss of ANC, or soil water acidification. Although the export of base cations serves to reduce direct soil water and surface water acidification, it may also contribute to depletion of the base cation supply in the soil. Figure III-1 illustrates the process whereby S deposition leaches base cations from watershed soils. As the base-cation supply is reduced, the soil becomes more acidic and an

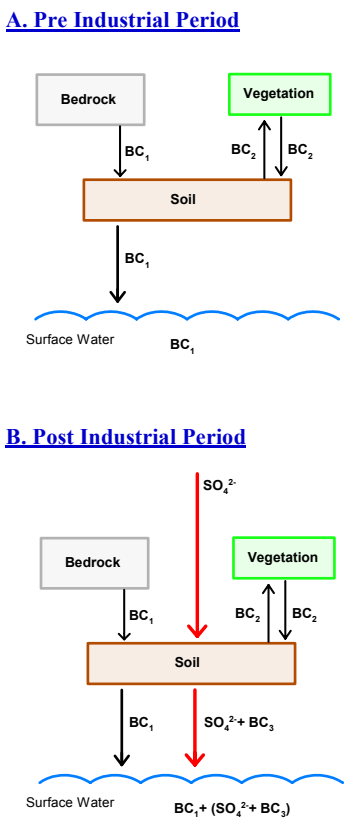

Figure III-1. Export of base cations (BC) from watershed soils.

A. Pre-Industrial Period: The base-cation supply in the soil is stable; losses to surface water are replaced by release from bedrock. Base cations taken up by vegetation are recycled.

B. Post-Industrial Period: Sulfate (SO_4^{2-}) moving through the soil leaches base cations. Acidity is buffered at the expense of the base-cation supply. In time, base-poor soils are dominated by the acidic cations H^+ and Al^{n+}.

increasing proportion of the cation supply that is released from soils to soil water and surface water consists of H^+ and Al^{n+} ions (Reuss and Johnson 1986).

The supply of base cations to watershed soils can be external or internal. External sources include atmospheric deposition of base cations. Internal watershed sources are the main sources of base cations in most upland drainage waters of the eastern United States (Baker 1991). The primary internal sources of base cations in most watersheds are weathering and soil exchange. By comparison with exchange reactions, weathering occurs at relatively slow and constant rates (Turner et al. 1990, Munson and Gherini 1991). Thus, the main source of cations for acid neutralization in most watersheds is the accumulated supply of exchangeable base cations in the soil. However, the size of this supply, and thus the degree to which soil and surface water acidification occurs, is ultimately determined in large part by the weathering of base cations in watershed bedrock. As reflected in the low ANC and low base cation concentrations of streamwaters, most of the ridges in the central Appalachian Mountain region are underlain by base-poor bedrock (Webb et al. 1989, Church et al. 1992, Herlihy et al. 1993).

It is well known that elevated leaching of base cations by acidic deposition might deplete the soil of exchangeable bases faster than they are resupplied via weathering (Cowling and Dochinger 1980). However, scientific appreciation of the importance of this response has increased with the realization that watersheds are generally not exhibiting much ANC and pH recovery in response to recent decreases in S deposition (Lawrence and Huntington 1999, Driscoll et al. 2001a). In many areas this low level of recovery can be at least partially attributed to decreased base cation concentrations in surface water, which may indicate base cation depletion from soils.

There are few hardwood forests in which actual soil changes have been measured in association with acidic deposition (Raynal et al. 1992). Acidification and/or nutrient loss can be inferred, however, from studies of elemental budgets (c.f., Binkley and Richter 1987). There is a general tendency for some hardwood trees to accumulate Ca^{2+}, especially oak and hickory species, and this can cause Ca^{2+} depletion and soil acidification. Such effects can be exacerbated by both tree harvesting and acidic deposition (Johnson et al. 1988). Calcium limitation has not been shown to be significant in eastern hardwood forests to date, but several studies have suggested impending Ca^{2+} depletion with intensive harvesting (Johnson et al. 1988, Federer et al. 1989, Johnson and Todd 1990). The issue therefore merits continued monitoring.

Sulfur retention in watershed soils delays and/or reduces the potential for soil and surface water acidification in response to S deposition. This is particularly the case in the southeastern United States, where watersheds commonly retain more than 50% of deposited S (Rochelle and Church 1987, Turner et al. 1990), largely due to S adsorption on watershed soils. However, such S adsorption is capacity-limited, and as the adsorption capacity of soils becomes diminished, SO_4^{2-} concentration in soil waters and surface waters can increase, contributing to further acidification (Munson and Gherini 1991, Church et al. 1992).

Although soil acidification can occur in response to acidic deposition, soil acidification is also a natural process (Binkley 1989). The magnitude of the soil base saturation (an indicator of soil acid-base status, calculated as the portion of the cation exchange capacity that is comprised of base cations, as opposed to H^+ and Al^{n+}) is determined by the relative magnitude of base cation sources (weathering and atmospheric deposition) and sinks (leaching and plant uptake). If base saturation is low, or is observed to decline over time, this does not necessarily indicate an impact from acidic deposition.

F. VISIBILITY

The NPS monitors visibility conditions and supports studies to determine the causes of visibility degradation (haze) at many parks and wilderness areas nationwide. The purpose of this monitoring is to characterize current visibility conditions, identify the specific pollutants and their sources that contribute to visibility degradation, and document long-term trends to assess the effects of changes in pollutant emissions. The NPS cooperates and shares resources with other Federal land management agencies, states, and the U.S. EPA in the Interagency Monitoring of Protected Visual Environments (IMPROVE) Program.

1. Visibility Degradation

a. Sources of Visibility Degradation

Visibility can be altered by a variety of naturally occurring events, such as inclement weather, wildfire, or blowing dust, although visibility degradation as considered here excludes the effects of obscuration by weather. Visibility degradation results from the scattering and absorption of visible light by gases and particles in the atmosphere. If there are no suspended particles in the air, the clean-limit of natural visibility is determined by the amount of light scattered by “air molecules.” Scattering of visible light from “air molecules” falls within the

Rayleigh scattering regime, which means that the light is scattered evenly in both the forward and backward direction, with a preferential scattering of shorter wavelengths (blue light); this scattering is responsible for the blueness of the sky. The value of the Rayleigh scattering is a function of air density and elevation.

Particles in the atmosphere, derived from both natural and human sources, also scatter light. The amount of particle light scattering depends on the size and concentration of the particles, which in turn is affected by their physical and chemical properties. Fine particles (particles less than 2.5 μm in diameter) have a greater scattering efficiency, on a per mass basis, than coarse particles (particles between 2.5 and 10.0 μm in diameter). Particles with sizes near the wavelength of visible light (0.4 μm to 0.7 μm) scatter most efficiently.

Chemical composition of particles also plays a role in their relative scattering efficiencies. Categories generally used to differentiate between fine particle chemical species that scatter light are sulfates, nitrates, organics, and soil. Sulfate and nitrate aerosols are hygroscopic, that is, they absorb water at higher relative humidity conditions. Growth of these aerosols at higher relative humidity conditions can dramatically enhance their effect on scattering. Coarse particles are generally not speciated and are generally lumped together in terms of their scattering efficiency.

Some gases and particles can also absorb light. Nitrogen dioxide is the only major visible light-absorbing gas in the lower atmosphere. It usually does not occur in sufficient concentration in remote areas to make a major contribution to absorption. Elemental carbon (C; soot) is the dominant light-absorbing particle in the lower atmosphere.

b. Types of Visibility Degradation

Visibility degradation from atmospheric pollutants can generally be classified as 1) uniform haze, 2) layered haze, or 3) plume. A uniform haze generally obscures the appearance of landscape features or the sky, causes changes in the color or the contrast among landscape features, or causes features of a view to disappear altogether. Pollutants suspended in a section of the atmosphere can become visible, by the contrast or color difference between a layer or plume and a viewed background, such as a landscape feature or the sky. The view through a layered haze or plume will be altered in similar fashion to a uniform haze, but layered hazes and plumes are distinguished by a discernable boundary between the haze layer or plume and the adjacent cleaner atmosphere.

Pollutants mixed through the planetary boundary layer cause uniform hazes. This mixing typically occurs over several diurnal cycles and the resulting haze can extend for hundreds of kilometers. This condition is shown schematically in Figure III-2a. Pollutants observed far from an emissions source typically appear as elevated haze layers. Pollutants observed near the source of emissions often cause plume impacts (Figure III-2b). Plumes can occur under any wind and stability conditions, but are usually most severe with light wind speeds and stable thermal stratification. When plumes are emitted from elevated sources into a stable layer aloft, they can be transported for long distances with little vertical dispersion. Pollutants emitted into a stable layer at the earth's surface can form a ground-based layered haze (Figure III-2c). Layered hazes are usually associated with emissions that are more local in nature as opposed to pollutants that are transported over hundreds of kilometers. An observer positioned within a layered haze may perceive it as a uniform haze because layered haze boundaries can only be observed from an elevated position.

Figure III-2a. Uniform haze: one of three ways that air pollution can visually degrade a scenic vista.

Figure III-2b. Coherent plume: one of three ways that air pollution can visually degrade a scenic vista.

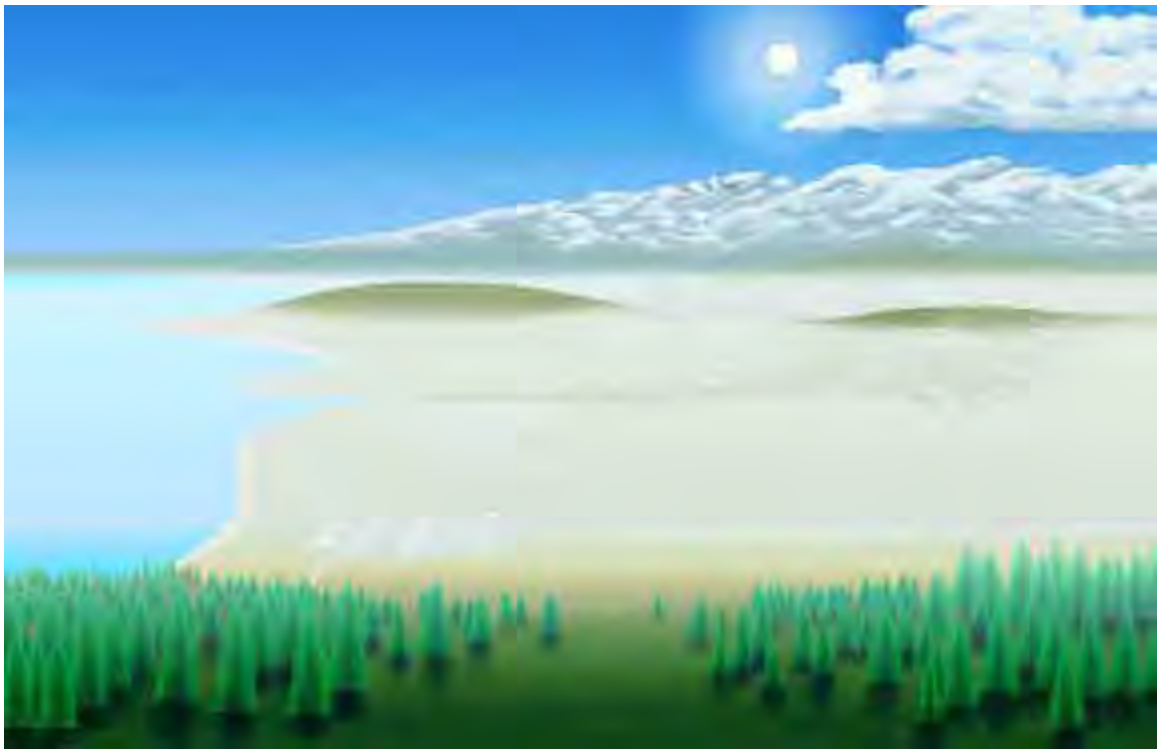

Figure III-2c. Layered haze: one of three ways that air pollution can visually degrade a scenic vista.

c. Visibility Scales/Metrics

To quantify visibility conditions and estimate the degree of degradation, several visibility scales/metrics can be employed. Depending on the application, metrics may include contrast and color difference index, light extinction coefficient (b_{ext}), visual range (VR), or degree of haziness.

For uniform haze circumstances, as depicted in Figure III-2a, where the pollutant loading becomes visible by contrast or color difference between the object luminance and the viewed background luminance, contrast or color difference metrics are generally used.

Light extinction coefficient, commonly called extinction, represents the attenuation of light per unit distance of travel in some medium, such as air, and is measured in inverse length (e.g., inverse kilometers [km^{-1}] or inverse mega meters [Mm^{-1}]). In the atmosphere, the b_{ext} comprises attenuation of light due to scattering and absorption of light by particles and gases in the air (aerosols).

Visual range is simply the greatest distance that a large, black object can be seen against a viewing background and is expressed as a distance (e.g., km or mi). Though easily understood and valuable for airport safety considerations, VR does not relate well to the perceived visual quality of a scene. A related metric is the Standard Visual Range (SVR). This metric is indexed to Rayleigh conditions at 1,800 m elevation rather than actual Rayleigh conditions at a specific location.

Visual range and the light extinction coefficient are inversely related (as VR decreases, b_{ext} increases) for certain assumed viewing conditions; a VR of 391 km signifies the best possible visibility (particle-free air, or Rayleigh conditions) and corresponds to a b_{ext} of 10 Mm^{-1}. These two metrics are usually used to quantify the level of degradation associated with uniform or ground-based layered hazes (Figures III.2a and c).

Neither VR nor b_{ext} is linear with respect to increases or decreases in perceived visual air quality. For example, a 15 km change in VR can result in a scene change either unnoticeably small or very apparent depending on the baseline visibility conditions. Therefore, another visibility metric, the haziness index (expressed as deciview [dv]), was defined to index a constant fractional change in the b_{ext} to visual perception (Pitchford and Malm 1994). The advantage of this characterization is that equal changes in dv are equally perceptible across different baseline conditions. Higher haziness index values signify poorer visibility. A zero dv corresponds to Rayleigh scattering (clean air), a VR of 391 km or a b_{ext} of 10 Mm^{-1}.

Of the three visibility metrics, the b_{ext} is the characterization most used by scientists concerned with the assessment of the causes of visibility degradation. Extinction can be directly calculated from light transmittance measurements (measured extinction) or derived from measured particle concentrations using linear relationships between the concentrations of particles and gases and their contribution to the extinction coefficient (calculated extinction). Understanding these relationships provides a method of estimating how visibility would change with changes in the concentrations of these atmospheric constituents. This methodology, known as "extinction budget analysis", is important for assessing the visibility consequences of proposed pollutant emissions sources, or for determining the extent of pollution control required to meet a desired visibility condition. Extinction, both measured and calculated, is the primary visibility characterization provided in this report. The functional relationship among the three scales/metrics can be found in Appendix B.

2. Background on the Visibility Monitoring Program

The assessment of current visibility conditions in the eastern region for this report will focus on visibility degradation attributable to cumulative air pollutant emissions from numerous sources over a wide geographic area. Visibility degradation can, of course, be caused by local sources and specific meteorological conditions. However, robust data sets on individual coherent plumes or layered hazes in remote areas are generally not available. Such plumes or layered hazes must usually be evaluated on a case-by-case basis. Therefore, this assessment will focus on the conditions associated with regional or uniform haze.

In 1977, Congress established a national goal of no human-caused visibility impairment in Class I areas, and in 1999 promulgated a rule requiring states to develop and implement plans to make continuous progress toward that goal. The rule directs the states to use the b_{ext} coefficient as the scale/metric with which to demonstrate their progress. In particular, the states are to use the light extinction coefficient derived from measured particle concentrations and estimated specific extinction efficiencies for relevant particle species (calculated extinction, see discussion in Appendix B). The EPA has provided detailed guidance for assessing regional haze using this metric (U.S. EPA 2001a). Clearly, assessment of progress toward the national goal requires long-term particle monitoring on which to base estimates of natural and current visibility conditions. This long-term monitoring is available from the IMPROVE Program.

The IMPROVE Program is a cooperative monitoring effort that is governed by a steering committee composed of representatives from Federal and regional-state organizations. It was established in 1985 to aid the creation of Federal and state implementation plans for the protection of visibility in mandatory Class I areas, as stipulated in the 1977 amendments to the Clean Air Act. The objectives of IMPROVE are to:

1. establish current visibility and aerosol conditions in Class I areas,
2. identify chemical species and emission sources responsible for existing human-caused visibility impairment,
3. document long-term trends for assessing progress toward the national visibility goal, and
4. provide regional haze monitoring representing all mandatory Federal Class I areas included within the Regional Haze Regulations.

Ideally, a fully complemented IMPROVE monitoring station would include fine and coarse particle monitoring, optical monitoring, and view monitoring with photography. Each type of monitoring is briefly described below.

a. Particle Monitoring

Particle monitoring provides concentration measurements of atmospheric constituents that contribute to visibility impairment. Four independent IMPROVE sampling modules are used to automatically collect 24-hour samples of suspended particles every Wednesday and Saturday[2] by drawing in air and collecting suspended particles on filters. The filters are later analyzed to determine the chemical makeup of the suspended particles. Three of the four samplers (modules A, B, and C) collect fine particles with diameters <2.5 µm. The fourth sampler (module D) collects particles with diameters up to 10 µm. Module A filters are analyzed to determine the gravimetric mass and elemental composition of the collected particles. Module B filters are analyzed specifically for SO_4^{2-}, NO_3^-, and chloride (Cl^-) ions (at SHEN, analysis for NH_4^+ has also been conducted since 1997). Module C filters are analyzed for organic material and light absorbing C. The gravimetric mass of coarse particles (2.5 to 10.0 µm) is determined by subtracting the Module A gravimetric mass from the Module D gravimetric mass.

---

[2] IMPROVE sampling schedules changed to a 1-in-3 day (EPA) schedule in 2000.

b. Optical Monitoring

Optical monitoring provides a direct quantitative measure of light extinction to represent visibility conditions. Water vapor in combination with suspended particles can affect visibility, so optical stations also record temperature and relative humidity. Optical monitoring uses ambient, long-path transmissometers or ambient nephelometers to collect hourly-averaged data. Transmissometers measure the amount of light transmitted through the atmosphere over a known distance (between 0.5 and 10.0 km) between a light source of known intensity (transmitter) and a light measurement device (receiver). The transmission measurements are electronically converted to hourly averaged light extinction (b_{ext}, scattering plus absorption). Ambient nephelometers draw air into a chamber and measure the scattering component of light extinction. Data from both of these instruments are recovered at a central location for storage and analyses. Optical measurements of extinction and scattering include meteorological events such as cloud cover and rain, but the data are "filtered" by flagging as invalid data points with high relative humidity (RH>90%). This filtering process is assumed to remove the largest effects of weather from the data set. Optical data also fulfill an important need by providing concurrent, independent measurement of extinction to compare with extinction coefficient calculations made using particle data.

c. View Monitoring

View monitoring is accomplished with automated 35 mm or digital camera systems. Cameras typically take three photographs a day (9:00, 12:00, and 15:00) of selected scenes. The resulting slides are used to facilitate data interpretation, and form a photographic record of characteristic visibility conditions. Based on April 1995 recommendations of the IMPROVE Steering Committee, view monitoring has been discontinued at all NPS Class I areas that have a five-year (or greater) photographic monitoring record. View monitoring has not been conducted at any of the NPS visibility monitoring sites in the Appalachian Region since October 1999.

II. ENVIRONMENTAL SETTING

A. BACKGROUND

Shenandoah National Park (SHEN) is an excellent example of the Blue Ridge/Central Appalachian biome. Figure II-1 shows the park boundary and its division into three management districts. Also indicated are the locations of Federally-designated wilderness areas and air quality monitoring stations. Figure II-2 shows the location of roads, trails, streams, and scenic historic overlooks within the park. SHEN is known for its scenic beauty, outstanding natural features and biota, and historic sites. There have been significant changes in land use prior to and since the establishment of the park. Formerly the location of farmsteads and other industry, land in the park has been allowed to revert to a more natural state since park formation in 1935. However, extensive evidence still remains of the long history of human use of the land.

Significant park features include the following:

1. Skyline Drive. This scenic 165 km drive, shown in Figure II-2, provides the opportunity for views of the Blue Ridge Mountains and surrounding areas. The road was designed and constructed in the 1930s to provide scenic views into the Piedmont Plateau to the east and the Shenandoah Valley to the west. Overlooks were constructed so that motorists could stop at intervals along the drive and enjoy the scenic vistas (Shenandoah National Park 2001).

2. Appalachian National Scenic Trail. The segment of the Appalachian National Scenic Trail that runs through SHEN (shown as the trail that generally parallels Skyline Drive in Figure II-2) is the backbone of the park's trail system.

3. Natural resources. The natural features and biota of the park include well-exposed rock strata of the Appalachians, which is one of the oldest mountain ranges in the world. The park comprises one of the nation's most diverse botanical reserves and diverse wildlife habitats.

4. Wilderness. Congressionally-designated wilderness area within the park is the largest in the Mid-Atlantic states and provides a comparatively accessible opportunity for solitude, study, and experience in a natural area (Shenandoah National Park 1998a).

5. Historic resources. There are over 135 buildings listed on the National Register of Historic Places.

The park is characterized by rounded hills and gently to steeply sloping valleys with near total vegetation coverage. The mountainous ridge of the park grades into the Valley and Ridge Province to the west and the Piedmont Province to the east. The montane-upland Blue Ridge Province extends from Pennsylvania to northern Georgia. Most physiographers apply the Blue

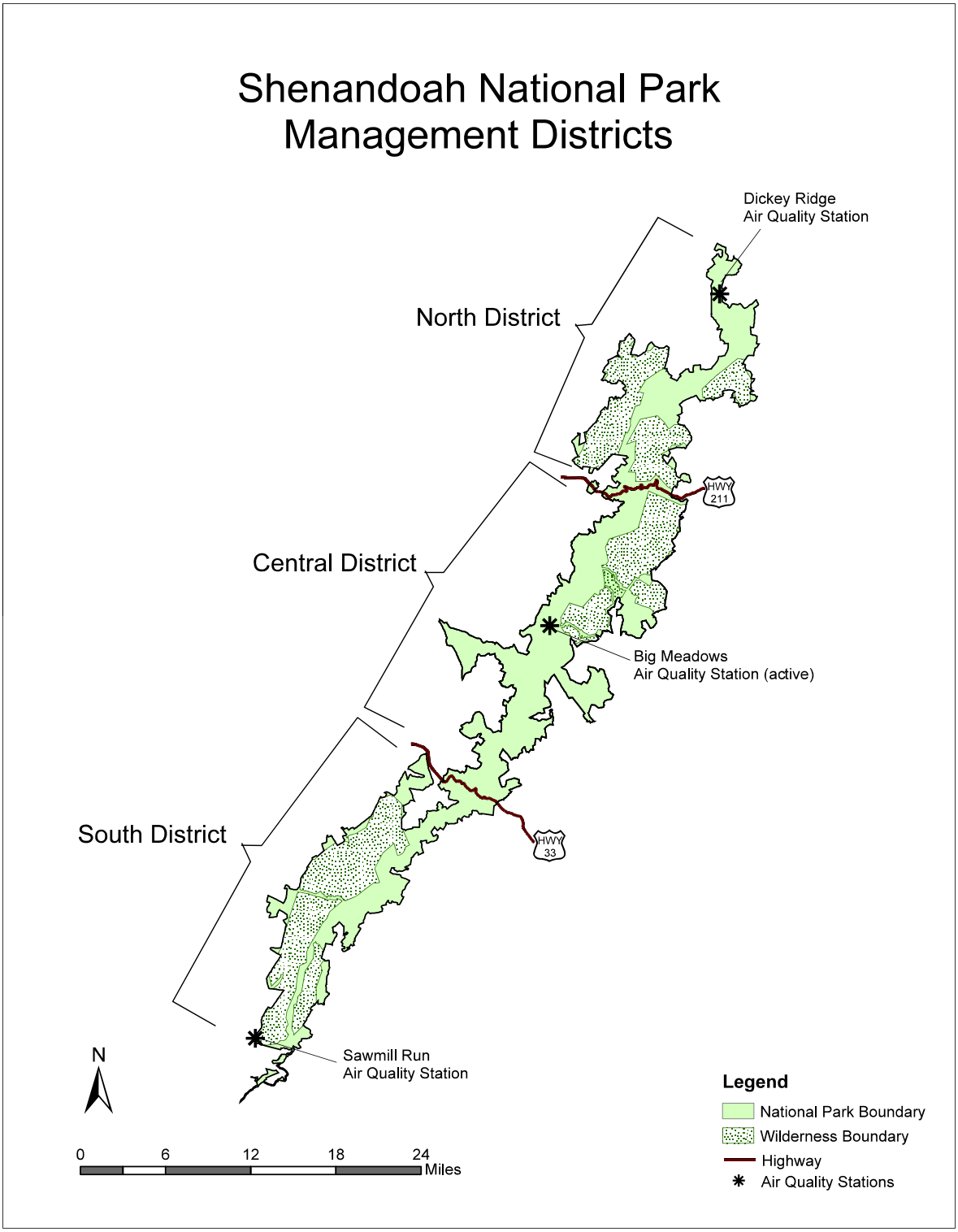

Figure II-1. Shenandoah National Park and division into three management districts. Also shown are the locations of federally-designated wilderness areas and air quality monitoring stations. The air quality stations at Dickey Ridge and Sawmill Run are no longer active.

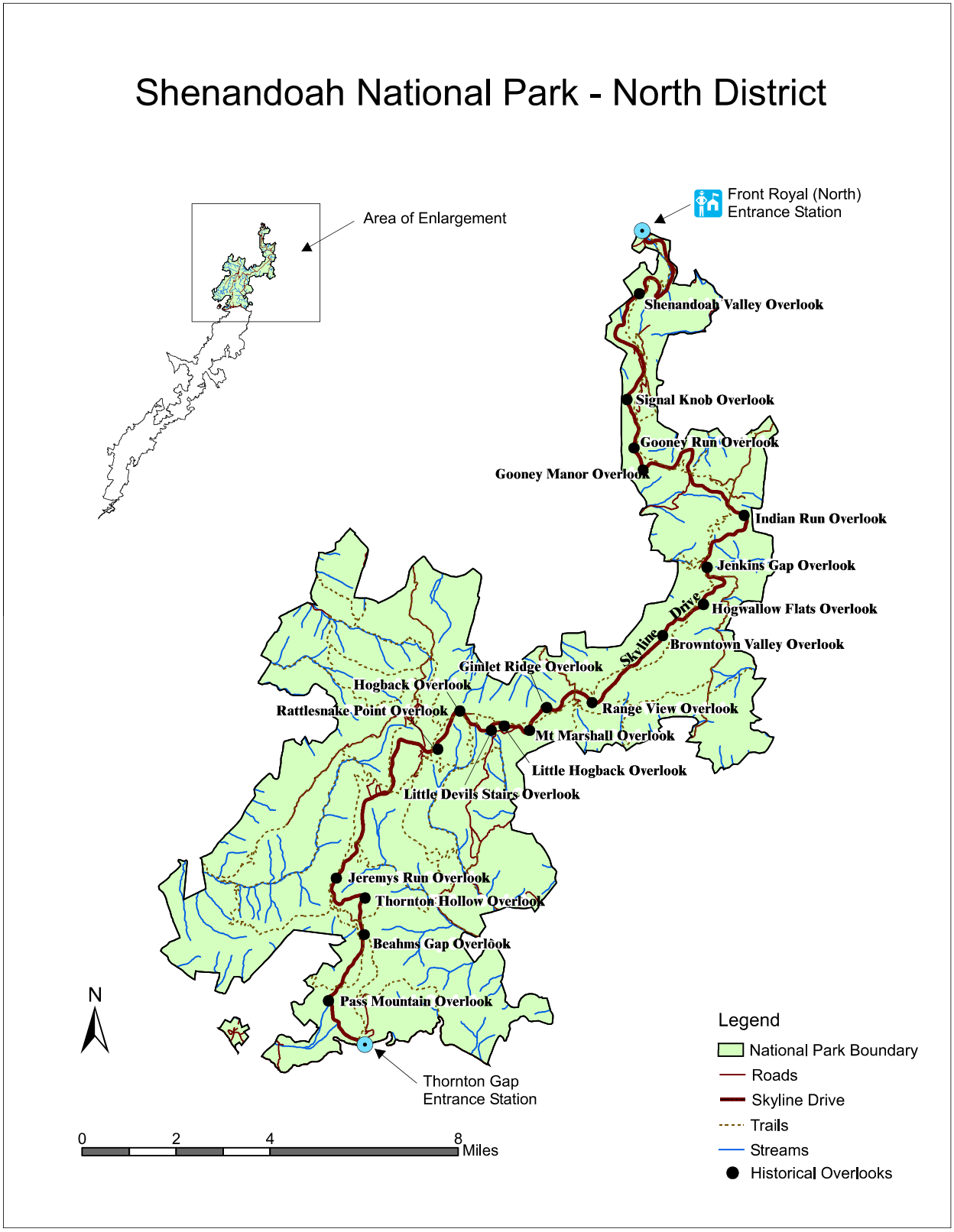

Figure II-2. Location of roads, trails, streams, and scenic historical overlooks within park boundaries: A) North District, B) Central District, C) South District. Skyline Drive is indicated by a thick red line, extending the length of the park.

Figure II-2. Continued.

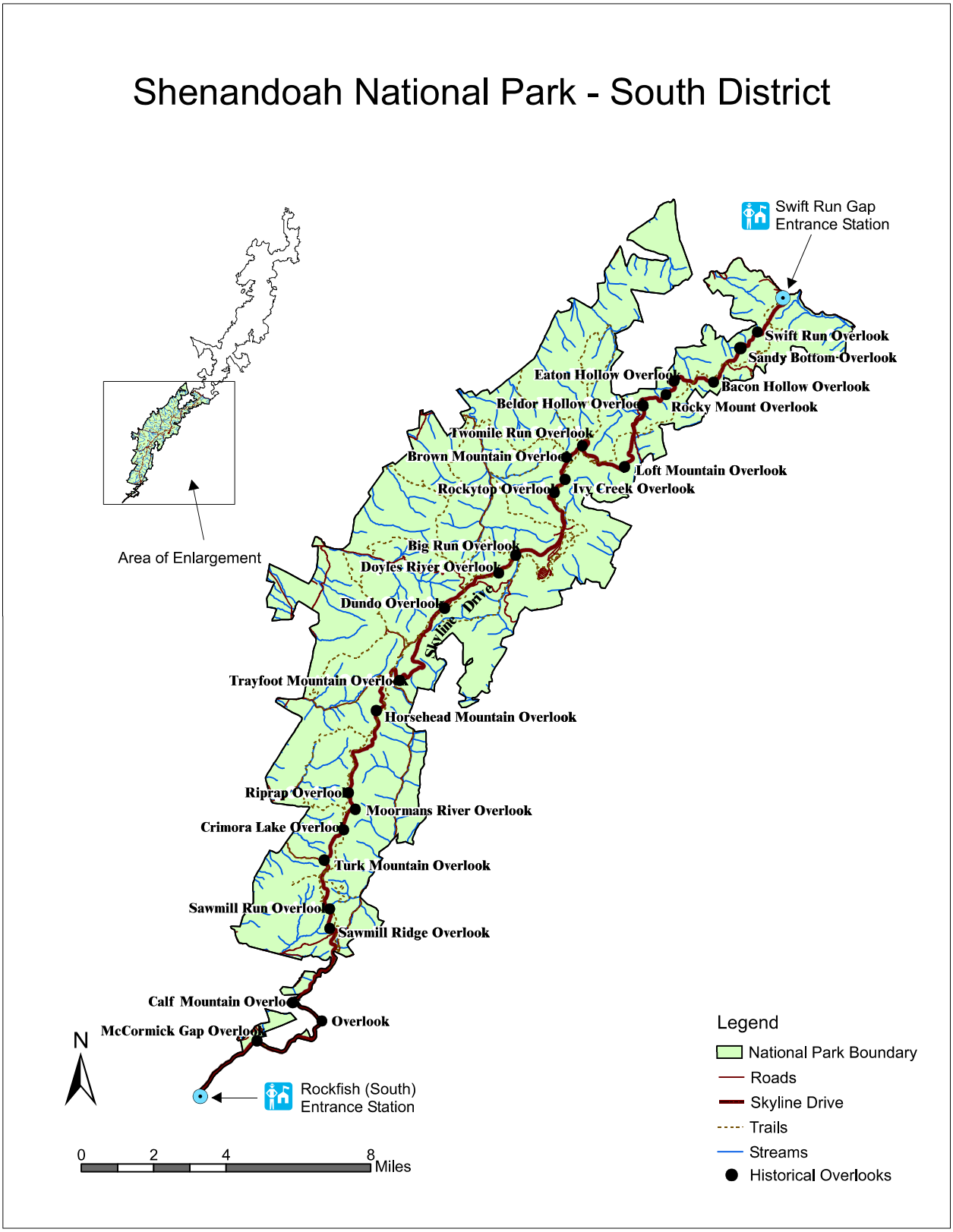

Figure II-2. Continued.

Ridge Province name to all contiguous high mountains underlain by crystalline rocks from south central Pennsylvania to northeastern Georgia, including SHEN and Great Smoky Mountains National Park. The Northern Blue Ridge (Roanoke River to Pennsylvania) is narrow (3-20-km wide overall), whereas the Southern Blue Ridge (Roanoke River to Georgia) widens to nearly 100 km, and increases in height southward. The Blue Ridge rocks are largely resistant to weathering, and streams are mostly of the softwater (low in calcium and magnesium) type.

The Blue Ridge Mountains in which SHEN is located are part of the Appalachian Range. The mountains are comprised of a series of long parallel folds with a single crest of rounded peaks and lower ridges that lies in a northeast to southwest direction. Elevation within the park ranges from 146 m at Front Royal to 1,234 m at Hawksbill Peak. Within the park, there are more than two dozen peaks that are over 900 m high. The land adjacent to the park is changing rapidly from recreational forest, agricultural, and seasonal residential uses to year- round residential use.

As mentioned earlier, interest in preserving areas in the southern Appalachian Mountains began near the turn of the 20th century. In 1924, the Southern Appalachian National Park Committee was appointed by the Secretary of the Interior to investigate the possible existence of sites suitable for the establishment of a national park. The result of the committee's work was an act that was passed in February, 1925 that directed the Secretary of the Interior to determine the boundaries and areas within the Blue Ridge Mountains of Virginia that could be recommended as a new national park. A subsequent act was passed in May, 1926 authorizing SHEN. Its provisions included that the lands could be secured by the United States only by public or private donation, and that the tract include approximately 210,800 ha. The task proved to be quite complicated and costly, and Congress reduced the minimum requirement to 64,735 ha. By 1935, the deeds were ready and the Commonwealth of Virginia donated about 71,400 ha to the Department of the Interior. On July 3, 1936, President Franklin D. Roosevelt dedicated SHEN "to the present and future generations of America for the recreation and re-creation which we shall find here."

SHEN was intended to be a sample of the southern Appalachian portion of primitive America, but approximately half of the forest was cleared at the time of park formation (Reed Engle, National Park Service, pers. comm.). The establishment of the park did, however, offer protection to what remained of Southern Appalachian plants and animals in portions of the park that were still forested, and nature continued its restorative process. The park is now about 95%

forested. Some of the animals that had been greatly reduced or eliminated have returned or have been reintroduced. So complete was the regeneration in the first four decades, that in 1976 nearly 132,370 ha were deemed of suitable primitive character to be included in the National Wilderness Preservation System.

Most homesites were located in the portions of the park that were suitable for farming (Gathright 1976). Farming was rare in the southwest because soils are thin and rocky and slopes are steep (Lynch and Dise 1985).

Logging began in the early 19th century and was most intense during the first two decades of the 20th century. Coupled with the outbreak of chestnut blight and subsequent large-scale tree mortality, logging removed much of the older timber prior to park formation. Mining activities were also conducted throughout the latter half of the 19th century, for iron, manganese, and copper, mainly in the southwestern portions of the park. Logging and farming ceased after the establishment of the park in 1935 (Lynch and Dise 1985).

Several areas of the park have received special recognition due to the significance of natural and cultural resources. For example, in 1985, the Shaver Hollow watershed was designated as the first Research Natural Area in a National Park Service (NPS) unit in eastern deciduous forest. It serves as a focal area for intensive watershed research within the park. In addition, in 1996 Skyline Drive and associated developed areas at Simmons Gap, Big Meadows, Piney River, Pinnacles, Dickey Ridge, and Park Headquarters were listed on the National Register of Historical Places.

SHEN has become significant for the following reasons:

- The park provides a traditional national park experience in the east.
- It is close to large metropolitan populations, providing relatively good accessibility to millions of citizens.
- Establishment of this park represented a conscious change in human use of the land. With ongoing vegetation recovery, the park has become a sizeable forested area, with large areas of designated wilderness.
- It includes developed areas that are listed on, or determined to be eligible for, the National Register or as national historical landmarks.
- The park includes the longest segment of the Appalachian National Scenic Trail that occurs in a national park.

Central to the significance of the park are the rural agricultural landscapes that surround it. These lands are the primary components of the vistas from Skyline Drive. They are additional components of the ecosystem that supports park wildlife and other values that are significant to the purposes for which the park was initially established. There are large blocks of undeveloped natural uplands, which contrast with the valley mosaic of privately owned farmland, forests, and settled areas. The wilderness contained in the park is the largest in Virginia and provides comparatively accessible opportunity for solitude, study, and experience in a natural area that has been allowed to revert to wilderness from past human land use.

B. CLIMATE

The Atlantic Ocean, and in particular the Gulf Stream, plays an important role in Virginia's precipitation regime. Winter storms generally track from the west to the east, and in the vicinity of the east coast move to the northeast paralleling the coast and the Gulf Stream. This shift to the northeast results partly from the tendency of storms to follow the boundary between the cold land and the warm Gulf Stream. When sufficiently cold air comes into Virginia from the west and the northwest, frontal storms can bring heavy snowfall. Thunderstorms occur in all months of the year, but are most common during summer. Precipitation is well distributed throughout the year, with a maximum in September and minimum in February. Storms and high runoff conditions can occur year-round at SHEN. Most locations receive 100 to 150 cm of precipitation per year. South to southwest winds predominate, with secondary maximum frequency from the north. Lower elevation areas of the park experience modified continental climate, with mild winters and warm, humid summers. The mean annual temperature in the lowland area at Luray averages 12 ^{o}C, and average annual precipitation is 91 cm, with about 43 cm of snow.

Higher elevation areas of the park experience winters that are moderately cold and summers that are relatively cool. The mean annual temperature at Big Meadows averages about 9 ^{o}C. Mean maximum daily temperatures in July average about 6 ^{o}C cooler at Big Meadows than in the lowland areas of the park. Temperatures in January range from about -7° to 4° C and in July from about 14° to 24° C. The average annual precipitation at Big Meadows is 132 cm, which includes about 94 cm of snow. Snow and ice are common in winter, but they usually melt quickly, leaving the ground bare. Occasional major snow or ice storms can cause considerable damage to the trees within the park.

Baseflow stream discharge is lowest in summer and early fall, reflecting evapotranspiration by terrestrial vegetation; highest baseflow occurs in winter and early spring. High discharges associated with storms can occur at anytime of year. For streams within forested mountain catchments, annual water yield is often 40-70% (annual discharge/annual precipitation; SAMAB 1996).

C. SCENERY

In its report to Congress, the Southern Appalachian National Park Committee highlighted the importance of scenery to the purpose and national significance of SHEN. The committee identified a possible sky-line drive as the greatest single feature of the area that was to become SHEN, and noted that the Blue Ridge mountains of northern Virginia met aesthetic requirements including but not limited to… "mountain scenery with inspiring perspectives and delightful details"…that contains…"forests, shrubs and flowers, and mountain streams, with picturesque cascades and waterfalls overhung with foliage…". The 163-km (105-mi) Skyline Drive was constructed by the Civilian Conservation Corps from 1931 to 1939. Most of the 157-km (101-mi) segment of the Appalachian National Scenic Trail found within the park was constructed by the Potomac Appalachian Trail Club in the 1930s. Today, the Appalachian National Scenic Trail forms the backbone for the park's extensive trails network totaling about 800 km (500 mi). Since the park's creation in 1935, millions of visitors have enjoyed the views from numerous vistas within the park.

SHEN has a unique blend of exceptional scenic beauty, outstanding natural features, diverse deciduous forests, wildlife, and historic sites in a mountain setting. Scenic views can be experienced by driving or cycling the Skyline Drive, walking the Appalachian National Scenic Trail and related trails, and experiencing the backcountry wilderness areas. The Drive's historic overlooks and the Appalachian National Scenic Trail afford scenic views of the pastoral Shenandoah Valley to the west or the Piedmont Plateau to the east (occasionally both) on clear days. The park is a popular destination to view fall colors in October. Old Rag Mountain in the Central District is one of the most popular hikes in the park. Rising from the edge of the Piedmont, its pinnacle of giant granite boulders, with challenging rock scrambles, makes this destination a unique regional attraction that provides 360-degree views. Visitors also enjoy numerous short hikes to picturesque waterfalls (Figure II-3).

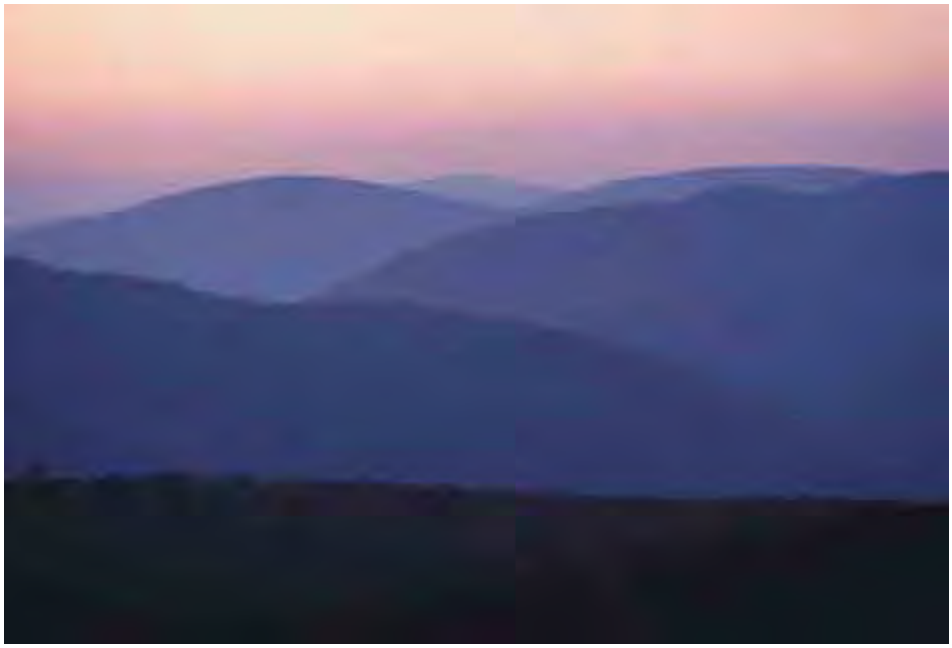

Figure II-3. Examples of outstanding scenery within SHEN.

D. SURFACE WATERS

High gradient is a chief feature of high-elevation streams in Virginia. Pools are interspersed with riffles, rapids, cascades and falls. Stream bottoms are chiefly comprised of large gravel, rubble, boulder and bedrock. Streams are cool or even cold in summer, typically clear, and rain-caused turbidity clears rapidly (Jenkins and Burkhead 1993). Patrick (1996) described typical Mid-Atlantic high-gradient mountain streams as heavily shaded in summer, having very few macrophytes and filamentous algae, with main primary productivity by diatoms. This description is also reflective of the mainly first-, second- and third-order streams of SHEN. Wallace et al. (1992) defined high-gradient streams as those with longitudinal gradients exceeding 0.15% slope (1.5 m per km), consistent with other definitions. Such streams typically occur between 330 and 2000 m above sea level. There are many such streams within the Valley and Ridge and Blue Ridge physiographic provinces, as well as in the Piedmont. The Blue Ridge (in which SHEN is located) is covered in dense deciduous and coniferous forests, with steep slopes up to 30%. High-gradient streams of the Blue Ridge are typically dendritic; stream density may be as high as 6.2 km/km^2. Streams in adjacent valleys may have different slopes and stream chemistry due to differences in bedrock composition.

Although acidic deposition is ubiquitous regionally, its interaction with local geological formations determines where effects on stream chemistry will occur. Stream concentrations of important ions (Ca^{2+}, Mg^{2+}, K^+, Na^+, Cl^-, NO_3^-, SO_4^{2-}) are usually low in regional mountain streams. Concentrations of NO_3^-, NH_4^+, and PO_4 may be very low (0.001-0.004 mg/L as nitrogen or phosphorus for each) in forested streams draining crystalline watersheds. Stream pH typically decreases with increasing elevation, as is the case within SHEN (Bulger et al. 1999).

There are 42 watershed basins on the west side of SHEN and 28 watershed basins on the east. In many places, the streams drop over ledges, creating waterfalls up to 28 m high. There are about 72 perennial streams in the park (Figure II-2), and over 50 of those contain native brook trout (*Salvelinus fontinalis*; Shenandoah National Park 1998b). Almost all of the streams in the park are at least largely headwater streams that drain into three major river basins, the Potomac River to the west and the Rappahannock and James Rivers to the east. This headwater status increases their potential sensitivity to adverse impacts from acidic deposition for a variety of reasons. In general, headwater streams are more likely than lower-elevation streams to be underlain by relatively homogeneous bedrock and soils, in many cases having low base cation supply. In addition, higher-elevation watershed areas are more likely to have shallow soils,

exhibit greater base cation leaching losses due to higher precipitation, and receive smaller base cation contributions from weathering due to colder temperatures.

Variation in bedrock geology plays a major role in determining variation in forest cover and streamwater chemistry within the park. The observed relationships between geology and water chemistry form the basis for relating intensively-studied watersheds in a hierarchical fashion to a geographically-extensive landscape coverage within the park and surrounding areas.

Loss of streamwater acid neutralizing capacity (ANC) in forested streams draining watersheds with crystalline or siliciclastic bedrock in response to acidic deposition occurs when concentrations of strong-acid anions (SO_4^{2-} and NO_3^-) increase relative to concentrations of base cations (Ca^{2+}, Mg^{2+}, K^+, Na^+). If surface water ANC is reduced to sufficiently low values, acidity may increase, as indicated by a depression in pH, to a range associated with adverse effects on fish and other aquatic life (Baker and Christensen 1991).

Acidic deposition can contribute to both chronic (long-term) and episodic (short-term) decline in streamwater ANC. The degree to which acidic deposition results in chronic loss of ANC in streams within SHEN depends mainly upon two watershed processes associated with acid-base status: 1) acid anion retention in watershed soils; and 2) base-cation release from watershed soils and rocks (Elwood 1991, Church et al. 1992). The degree to which acidic deposition results in episodic loss of ANC in surface water depends largely upon the hydrologic flow paths associated with high-runoff conditions (Turner et al. 1990, Wigington et al. 1990).

E. AQUATIC BIOTA

1. Fish

Table II-1 lists the species of fish most commonly found in SHEN. Rows 1-5 list the stream names, the SHEN district (North, Central, or South) where streams are located, the drainage (Potomac, James or Rappahannock Rivers) into which each stream flows, the side (East or West facing slope) where streams are located, and the total number of fish species recorded to date in each stream. There are a small number of additional fishless streams in the park. The next 34 rows record the presence of each of the fish species in each stream.

Table II-1. Fish species recorded in Shenandoah National Park streams (as of 2002)

Stream	Abundance	Bolton Branch	Happy Creek	Hickerson Hollow	Jeremy's Run	Land's Run	Overall Run	Piney River	Shenks Hollow	Thornton River, N. Fork	Berry Hollow	Broad Hollow Run	Brokenback Run	Cedar Run	Dry Run, N. Fork	Dry Run, S. Fork	East Hawksbill Creek	Fultz Run	Hannah Run	Hazel River	Hogcamp Branch	Hughes River	Little Hawksbill Creek	Naked Creek, E. Branch	Naked Creek, W. Branch	Pass Run	Pocosin Hollow Run	Ragged Run	Rapidan River	Rose River	South River	Staunton River	Swift Run	Thornton River, S. Fork	Whiteoak Canyon Run	Big Branch	Big Run	Doyles River	Eppert Hollow Run	Hawksbill Creek (Beldor)	Ivy Creek	Lower Lewis Run	Madison Run	Meadow Run	Moormans River, N. Fork	Onemile Run	Paine Run	Rocky Mt. Run	Sawmill Run	Twomile Run	# of Streams
Park District		N	N	N	N	N	N	N	N	N	C	C	C	C	C	C	C	C	C	C	C	C	C	C	C	C	C	C	C	C	C	C	C	C	C	C	S	S	S	S	S	S	S	S	S	S	S	S	S	S	S	
Drainage		R	P	P	P	P	P	R	P	R	R	R	R	R	P	P	P	P	R	R	R	R	P	P	P	P	R	R	R	R	R	R	J	R	R	J	P	J	P	P	J	P	P	P	J	P	P	P	P	P	
Side of Park		E	E	E	W	W	W	E	W	E	E	E	E	E	W	W	W	W	E	E	E	E	W	W	W	W	E	E	E	E	E	E	E	E	E	E	W	E	W	W	E	W	W	W	E	W	W	W	W	W	
# of Species		4	13	2	7	10	6	12	4	20	5	2	6	4	2	1	1	2	4	11	2	20	2	3	11	14	4	4	22	16	2	5	9	17	10	3	19	12	8	17	1	3	9	3	20	3	3	13	7	2	
Eel, American	C	◆				◆		◆		◆			◆						◆	◆		◆							◆	◆	◆	◆	◆	◆	◆			◆													16
Carp, Common	R																																				◆														1
Dace, Mountain Redbelly	U		◆							◆												◆							◆											◆					◆							6
Dace, Rosyside	A		◆		◆	◆	◆	◆		◆	◆		◆	◆						◆		◆			◆		◆	◆	◆	◆			◆	◆	◆	◆	◆	◆		◆			◆		◆			◆	◆		27
Dace, Longnose	A		◆		◆	◆	◆	◆		◆	◆			◆					◆	◆		◆			◆	◆	◆		◆	◆		◆	◆	◆	◆		◆	◆	◆	◆			◆		◆			◆	◆		28
Dace, Blacknose	A	◆	◆	◆	◆	◆	◆	◆	◆	◆	◆	◆	◆	◆	◆			◆	◆	◆	◆	◆	◆	◆	◆	◆	◆	◆	◆	◆		◆	◆	◆	◆	◆	◆	◆	◆	◆		◆	◆	◆	◆	◆	◆	◆	◆	◆	45
Stoneroller, Central	U		◆			◆				◆																◆											◆	◆		◆					◆			◆			9
Fallfish	U									◆										◆									◆					◆																	4
Chub, Creek	A		◆		◆	◆	◆	◆		◆										◆		◆			◆	◆			◆	◆				◆	◆		◆	◆	◆	◆			◆		◆			◆			21
Minnow, Cutlips	U									◆												◆							◆																						3
Chub, River	C					◆	◆	◆		◆										◆		◆				◆			◆	◆				◆	◆		◆	◆					◆					◆			15
Chub, Bluehead	C		◆			◆		◆	◆	◆										◆					◆				◆					◆			◆		◆	◆					◆			◆			14
Shiner, Satinfin	R																												◆																						1
Shiner, Common	C		◆							◆										◆		◆				◆			◆	◆			◆	◆			◆	◆	◆	◆			◆		◆						15
Minnow, Bluntnose	U		◆																																		◆			◆								◆			4
Hogsucker, Northern	U																			◆						◆								◆			◆			◆					◆						6
Sucker, Torrent	C							◆		◆			◆									◆						◆	◆	◆		◆	◆	◆	◆		◆	◆							◆				◆		15
Sucker, White	C		◆			◆		◆		◆												◆			◆	◆			◆	◆			◆	◆			◆	◆		◆			◆		◆			◆			17
Madtom, Margined	U																					◆							◆																◆						3
Trout, Brook	A	◆			◆	◆	◆	◆		◆	◆	◆	◆	◆	◆	◆	◆	◆	◆	◆	◆	◆	◆	◆	◆	◆	◆	◆	◆	◆	◆	◆	◆	◆	◆	◆	◆	◆	◆	◆	◆	◆	◆	◆	◆	◆	◆	◆	◆	46
Trout, Tiger	U																					◆								◆															◆						3
Trout, Brown	U									◆			◆									◆								◆															◆						5
Trout, Rainbow	U																					◆				◆				◆															◆						4
Sculpin, Mottled	A	◆	◆	◆	◆			◆	◆	◆	◆											◆		◆	◆	◆			◆	◆			◆	◆	◆		◆		◆	◆		◆						◆	◆		23
Sculpin, Potomac	U																								◆															◆											2

Table II-1. Continued.

Stream	Abundance	Bolton Branch	Happy Creek	Hickerson Hollow	Jeremy's Run	Land's Run	Overall Run	Piney River	Shenks Hollow	Thornton River, N. Fork	Berry Hollow	Broad Hollow Run	Brokenback Run	Cedar Run	Dry Run, N. Fork	Dry Run, S. Fork	East Hawksbill Creek	Fultz Run	Hannah Run	Hazel River	Hogcamp Branch	Hughes River	Little Hawksbill Creek	Naked Creek, E. Branch	Naked Creek, W. Branch	Pass Run	Pocosin Hollow Run	Ragged Run	Rapidan River	Rose River	South River	Staunton River	Swift Run	Thornton River, S. Fork	Whiteoak Canyon Run	Big Branch	Big Run	Doyles River	Eppert Hollow Run	Hawksbill Creek (Beldor)	Ivy Creek	Lower Lewis Run	Madison Run	Meadow Run	Moormans River, N. Fork	Onemile Run	Paine Run	Rocky Mt. Run	Sawmill Run	Twomile Run	# of Streams
Park District		N	N	N	N	N	N	N	N	N	C	C	C	C	C	C	C	C	C	C	C	C	C	C	C	C	C	C	C	C	C	C	C	C	C	S	S	S	S	S	S	S	S	S	S	S	S	S	S	S	S	
Drainage		R	P	P	P	P	P	R	P	R	R	R	R	R	P	P	P	P	R	R	R	R	P	P	P	P	R	R	R	R	R	R	J	R	R	J	P	J	P	P	J	P	P	P	J	P	P	P	P	P	
Side of Park		E	E	E	W	W	W	E	W	E	E	E	E	E	W	W	W	W	E	E	E	E	W	W	W	W	E	E	E	E	E	E	E	E	E	W	E	W	W	E	W	W	W	E	W	W	W	W	W	
# of Species		0	2	0	1	0	0	1	1	3	0	0	0	0	0	0	0	0	0	0	0	3	0	0	2	3	0	0	5	2	0	0	0	3	1	0	4	1	1	3	0	0	1	1	4	1	1	2	1	0	
Bass, Rock	U		◆							◆												◆							◆					◆			◆			◆											7
Bass, Smallmouth	U									◆												◆			◆				◆					◆			◆			◆								◆			8
Bass, Largemouth	U																									◆																									1
Sunfish, Redbreast	U																																												◆						1
Pumpkinseed	U							◆																					◆								◆							◆	◆						5
Darter, Greenside	R																									◆																									1
Darter, Johnny	R																																												◆						1
Darter, Tesselated	U									◆												◆							◆	◆				◆	◆																	6
Darter, Fantail	C		◆		◆				◆																◆	◆			◆	◆							◆	◆	◆	◆			◆		◆	◆	◆	◆	◆		17

Abundance	Description
R=Rarely encountered	Species found at intervals of five years or greater within the park.
U=Uncommon	Species with less than ten (<10) known populations in the park.
C=Common	Species with between ten and twenty (10 to 20) known populations in the park.
A=Abundant	Species with greater than twenty (>20) known populations in the park.

District	Drainage	Side of Park
N=North	J=James	E=East
C=Central	P=Potomac	W=West
S=South	R=Rappahanock	

Acidification is a conspicuous threat to three trout species in the region: brook trout, brown trout, and rainbow trout. Although brown and rainbow trout are found within SHEN, brook trout predominate. Of the three, native brook trout is the most acid tolerant, brown trout introduced from Europe is intermediate in acid tolerance, and rainbow trout introduced from the western United States is most sensitive. A recent survey (SAMAB 1996) concluded that trout populations are regarded by residents as among the region's most valuable aquatic natural resources, and trout populations and trout habitat are major concerns to the public in the southern Appalachians. Sources of concern generally fall into three categories: 1) fisheries for native brook trout and introduced rainbow and brown trout; 2) "existence value" for brook trout, regarded as a beautiful and intrinsically valuable native species; and 3) the presence of trout as indicators of high water quality.

2. Invertebrates

Benthic macroinvertebrates have been monitored in SHEN streams since 1986 as part of the Long-Term Ecological Monitoring System (LTEMS). They have several characteristics that make them particularly useful for biomonitoring (Moeykens and Voshell, 2002):

- Benthic macroinvertebrates occur in almost all types of freshwater habitats.
- There are many different taxa which include a wide range of sensitivity to environmental stress.
- They have mostly sedentary habits and are therefore likely to be exposed to ambient pollution or environmental stress.
- The duration of their life histories are sufficiently long such that they will likely be exposed to the environmental stress that is present, and the community will not recover so quickly that the impact will go undetected.
- Sampling the benthic macroinvertebrate assemblage is relatively simple and does not require complicated equipment or great effort.
- Taxonomic identification is almost always easy to the family level and usually easy to the genus level.

Since 1986, the benthic macroinvertebrate community at 17 core LTEMS sites in SHEN has been sampled at least once per year, and in 1995 SHEN personnel began to sample other sites with the goal of eventually sampling every permanent stream within park boundaries (Moeykens and Voshell, 2002). The sampling techniques and LTEMS protocols were described by Voshell

and Hiner (1990). The data summarized here cover samples taken between June 1988 and June 2000 (12 years) and include 43 streams.

There are five phyla of benthic macroinvertebrates represented in the samples from SHEN streams: Annelida (principally Oligochaeta), Arthropoda (including Insecta, Arachnida, and Crustacea), Mollusca (including Bivalvia and Gastropoda), Nematoda, and Platyhelminthes (principally Turbellaria).

Of particular importance to the ecology of the streams in the park are the aquatic insects (Class Insecta). There are nine orders of aquatic insects present in the SHEN LTEMS samples: Coleoptera, Collembola, Diptera, Ephemeroptera (mayflies), Hemiptera, Megaloptera, Odonata, Plecoptera (stoneflies), and Trichoptera (caddisflies). From these nine orders of aquatic insects, 79 families have been collected in SHEN streams. Not all families are present in each stream. The total number of insect families found in a given stream during the sampling period varies from 21 to 56 (Table II-2).

Some aquatic insect families are represented in only a few streams and some families are found in all streams (Table II-3). Nine families (Helicopsychidae, Ptychopteridae, Stratiomyiidae, Potamanthidae, Siplonuridae, Belostomatidae, Notonectidae, Haliplidae, and Helophoridae) have each been found in only one stream within SHEN (not all in the same stream). On the other hand, nine other families (Hydropsychidae, Chironomidae, Tipulidae, Baetidae, Ephemerellidae, Heptageniidae, Leuctridae, Perlodidae, and Psephenidae) have been found in all 43 streams that have been sampled.

F. GEOLOGY AND SOILS

The geology of the area in and around SHEN was formed in part as a result of plate tectonics. There were four collisional events involving eastern North America which contributed to the formation of the mountains and metamorphism of the existing rocks. There have also been two rifting events, which caused volcanic eruptions and the opening of ocean basins. The first resulted in extrusion of the Catoctin volcanic rocks about 570 million years ago. The second, which occurred about 200 million years ago, resulted in the opening of the Atlantic Ocean basin (Badger 1999).

The geology of the park represents one of its most outstanding natural resources. Exposed formations of the Blue Ridge Mountains are among the oldest in North America. The geologic history of the park has been the subject of frequent investigations by geologists and university

Table II-2. Total number of invertebrate families of each order present in SHEN streams (Phylum Arthropoda, Class Insecta).

Stream Name	Order Coleoptera	Order Collembola	Order Diptera	Order Ephemeroptera	Order Hemiptera	Order Megaloptera	Order Odonata	Order Plecoptera	Order Trichoptera	Total Families in Stream
Big Meadows Effluent	1	0	5	5	0	0	1	6	7	25
Big Run	3	1	10	5	2	1	1	8	11	42
Bolton Branch	4	0	7	4	0	2	1	7	7	32
Broad Hollow Run	2	1	8	6	2	0	1	7	10	37
Brokenback Run	3	1	7	6	1	1	2	7	9	37
Cedar Run	2	0	5	5	1	0	0	7	8	28
Deep Run	2	0	5	5	1	1	0	6	7	27
Doyles River	2	0	6	4	0	0	1	6	7	26
Dry Run, N. Fork	2	1	8	6	3	2	1	8	14	45
Eppert Hollow Run	1	0	3	4	1	1	1	8	6	25
Fultz Run	2	0	6	4	1	1	1	6	6	27
Hannah Run	2	0	6	4	1	1	1	6	5	26
Happy Creek	3	0	5	4	0	1	0	5	5	23
Hawksbill Creek (Beldor)	2	0	5	6	1	1	1	7	5	28
Hazel River	4	1	11	9	2	2	2	9	16	56
Hughes River	2	0	8	6	2	1	0	8	8	35
Ivy Creek	3	1	8	7	2	1	0	7	9	38
Jeremy's Run	3	1	8	8	2	2	1	9	13	47
Keyser Run	2	0	3	4	2	0	0	6	4	21
Land's Run	3	1	8	7	2	2	1	8	14	46
Little Hawhksbill Creek	2	0	7	4	1	1	1	6	8	30
Lower Lewis Run	2	1	6	6	2	1	1	7	12	38
Madison Run	4	1	7	5	2	1	1	9	11	41
Meadow Run	2	1	6	7	3	1	1	8	11	40
Moormans River, N. Fork	3	1	9	7	2	1	1	9	12	45
Naked Creek, E. Branch	2	0	6	6	1	1	1	7	7	31
Naked Creek, W. Branch	3	0	6	5	0	0	0	7	7	28
Onemile Run	2	1	6	6	3	2	1	8	11	40
Overall Run	1	0	5	5	0	0	0	5	6	22
Paine Run	4	1	9	5	4	2	2	9	14	50
Pass Run	3	0	6	7	0	2	1	9	10	38
Piney River	6	1	10	8	3	2	2	9	15	56
Rapidan River	4	0	9	7	2	1	1	8	12	44
Rose River	4	1	10	7	2	2	2	9	16	53
Sawmill Run	3	0	7	6	2	1	1	9	10	39
South River	2	0	6	5	0	0	0	7	8	28
Staunton River	4	1	12	7	2	2	1	9	16	54
Swift Run	2	0	8	6	0	0	2	6	7	31
Thornton River, N. Fork	2	1	5	5	1	1	0	6	8	29
Thornton River, S. Fork	3	0	9	8	1	1	1	8	12	43
Twomile Run	5	1	8	6	3	2	2	9	14	50
Whiteoak Canyon Run	6	1	11	7	2	2	1	9	14	53
Whiteoak Run	5	1	6	5	2	1	1	8	8	37

Table II-3. Invertebrate presence in SHEN streams (Phylum Arthropoda, Class Insecta).

Stream Name	Families of Order Trichoptera																
	Brachycentridae	Glossosomatidae	Goeridae	Helicopsychidae	Hydropsychidae	Hydroptilidae	Lepidostomatidae	Leptoceridae	Limnephilidae	Molannidae	Odontoceridae	Philopotamidae	Polycentropodidae	Psychomyiidae	Rhyacophilidae	Sericostomatidae	Uenoidae
Big Meadows Effluent					X		X		X		X			X	X		X
Big Run	X	X		X	X	X	X	X	X			X	X				X
Bolton Branch		X			X	X						X	X		X		X
Broad Hollow Run		X			X		X		X	X		X	X	X	X		X
Brokenback Run		X			X		X		X	X	X	X			X		X
Cedar Run	X	X			X		X		X			X	X				X
Deep Run		X			X		X					X	X		X		X
Doyles River		X			X				X			X	X		X		X
Dry Run, N. Fork	X	X	X		X	X	X		X	X	X	X	X	X	X		X
Eppert Hollow Run	X				X				X			X			X		X
Fultz Run		X			X				X			X	X				X
Hannah Run	X	X			X							X	X				
Happy Creek		X			X							X	X	X			
Hawksbill Creek (Beldor)					X	X						X	X				X
Hazel River	X	X	X		X	X	X	X	X	X	X	X	X	X	X	X	X
Hughes River	X	X			X				X			X	X		X		X
Ivy Creek					X	X	X	X	X			X	X		X		X
Jeremy's Run	X	X			X	X	X		X	X		X	X	X	X	X	X
Keyser Run					X				X			X			X		
Land's Run	X	X	X		X		X	X	X	X	X	X	X	X	X		X
Little Hawhksbill Creek	X	X			X		X		X			X	X		X		
Lower Lewis Run	X	X			X	X	X	X	X		X	X	X		X		X
Madison Run	X	X			X	X	X		X		X	X	X		X		X
Meadow Run	X	X			X	X	X	X	X			X	X		X		X
Moormans River, N. Fork	X	X			X	X	X		X	X	X	X	X		X		X
Naked Creek, E. Branch		X			X				X			X	X		X		X
Naked Creek, W. Branch	X	X			X				X			X	X		X		
Onemile Run	X	X			X	X	X		X	X		X	X		X		X
Overall Run					X	X	X		X			X			X		
Paine Run	X	X			X	X	X	X	X	X	X	X	X	X	X		X
Pass Run		X			X	X	X		X			X	X	X	X		X
Piney River	X	X	X		X	X	X	X	X	X	X	X	X	X	X		X
Rapidan River	X	X			X	X	X		X	X	X	X	X		X		X
Rose River	X	X	X		X	X	X	X	X	X	X	X	X	X	X	X	X
Sawmill Run	X	X			X	X	X			X		X	X		X		X
South River		X			X	X	X		X			X			X		X
Staunton River	X	X	X		X	X	X	X	X	X	X	X	X	X	X	X	X
Swift Run	X	X			X							X	X		X		X
Thornton River, N. Fork		X			X		X		X			X	X		X		X
Thornton River, S. Fork	X	X			X	X	X	X	X		X	X	X		X		X
Twomile Run	X	X			X	X	X	X	X	X	X	X	X	X	X		X
Whiteoak Canyon Run	X	X			X	X	X	X	X	X	X	X	X	X	X		X
Whiteoak Run		X			X	X	X		X			X	X		X		
Summary	26	37	6	1	43	25	31	13	36	16	16	42	37	14	37	4	36

Table II-3 Continued.

Stream Name	Families of Order Diptera														
	Athericidae	Blephariceridae	Ceratopogonidae	Chironomidae	Culicidae	Dixidae	Empididae	Ephydridae	Muscidae	Psychodidae	Ptychopteridae	Simuliidae	Stratiomyiidae	Tabanidae	Tipulidae
Big Meadows Effluent				X			X		X			X			X
Big Run		X	X	X	X	X	X		X			X		X	X
Bolton Branch		X	X	X		X	X					X			X
Broad Hollow Run		X	X	X		X	X		X			X			X
Brokenback Run	X	X	X	X		X						X			X
Cedar Run		X	X	X								X			X
Deep Run			X	X			X					X			X
Doyles River		X	X	X		X						X			X
Dry Run, N. Fork		X	X	X		X	X					X		X	X
Eppert Hollow Run			X	X											X
Fultz Run			X	X		X	X					X			X
Hannah Run		X		X		X	X					X			X
Happy Creek		X		X			X					X			X
Hawksbill Creek (Beldor)		X	X	X								X			X
Hazel River	X	X	X	X		X	X		X	X		X		X	X
Hughes River	X	X	X	X		X	X					X			X
Ivy Creek		X	X	X		X	X		X			X			X
Jeremy's Run		X	X	X		X	X	X				X			X
Keyser Run			X	X											X
Land's Run		X	X	X		X	X					X		X	X
Little Hawhksbill Creek	X	X	X	X			X					X			X
Lower Lewis Run			X	X		X	X					X			X
Madison Run		X	X	X		X	X					X			X
Meadow Run			X	X			X		X			X			X
Moormans River, N. Fork	X	X	X	X		X	X					X		X	X
Naked Creek, E. Branch		X	X	X			X					X			X
Naked Creek, W. Branch		X		X		X	X					X			X
Onemile Run		X	X	X			X					X			X
Overall Run		X	X	X								X			X
Paine Run		X	X	X		X	X		X			X		X	X
Pass Run		X	X	X			X					X			X
Piney River		X	X	X		X	X			X		X	X	X	X
Rapidan River	X	X	X	X			X	X				X		X	X
Rose River	X	X	X	X		X	X			X		X		X	X
Sawmill Run			X	X	X	X	X					X			X
South River		X	X	X			X					X			X
Staunton River	X	X	X	X	X	X	X		X	X	X	X			X
Swift Run	X	X	X	X		X	X					X			X
Thornton River, N. Fork		X	X	X								X			X
Thornton River, S. Fork	X	X	X	X		X	X					X		X	X
Twomile Run		X	X	X		X	X		X			X			X
Whiteoak Canyon Run	X	X	X	X	X	X	X		X	X		X			X
Whiteoak Run		X	X	X		X						X			X
Summary	11	35	39	43	4	27	34	2	10	5	1	41	1	10	43

Table II–3. Continued.

	Families of Order Ephemeroptera											Families of Order Hemiptera				
Stream Name	Ameletidae	Baetidae	Baetiscidae	Caenidae	Ephemerellidae	Ephemeridae	Heptageniidae	Isonychiidae	Leptophlebiidae	Potamanthidae	Siphlonuridae	Belostomatidae	Gerridae	Mesoveliidae	Notonectidae	Veliidae
Big Meadows Effluent	X	X			X		X		X							
Big Run	X	X			X		X		X				X			X
Bolton Branch		X			X	X	X									
Broad Hollow Run	X	X			X	X	X		X				X			X
Brokenback Run	X	X			X	X	X		X				X			
Cedar Run	X	X			X		X		X				X			
Deep Run	X	X			X		X		X				X			
Doyles River		X			X		X		X							
Dry Run, N. Fork	X	X			X		X	X	X				X	X		X
Eppert Hollow Run		X			X		X		X							X
Fultz Run		X			X		X		X				X			
Hannah Run		X			X		X		X				X			
Happy Creek		X			X		X	X								
Hawksbill Creek (Beldor)		X			X	X	X	X	X				X			
Hazel River	X	X	X	X	X	X	X	X	X				X			X
Hughes River	X	X			X		X	X	X				X			X
Ivy Creek	X	X			X	X	X	X	X				X			X
Jeremy's Run	X	X		X	X	X	X	X	X				X			X
Keyser Run		X			X		X		X				X			X
Land's Run	X	X			X	X	X		X	X			X			X
Little Hawhksbill Creek		X			X		X		X				X			
Lower Lewis Run	X	X			X		X	X	X				X			X
Madison Run	X	X			X		X		X				X			X
Meadow Run	X	X			X		X	X	X		X		X	X		X
Moormans River, N. Fork	X	X			X	X	X	X	X				X			X
Naked Creek, E. Branch		X			X	X	X	X	X				X			
Naked Creek, W. Branch		X			X		X	X	X							
Onemile Run	X	X			X		X	X	X				X	X		X
Overall Run	X	X			X		X		X							
Paine Run	X	X			X		X		X			X	X		X	X
Pass Run		X	X		X	X	X	X	X							
Piney River	X	X	X		X	X	X	X	X				X	X		X
Rapidan River	X	X			X	X	X	X	X				X			X
Rose River	X	X			X	X	X	X	X				X			X
Sawmill Run	X	X			X		X	X	X				X			X
South River	X	X			X		X		X							
Staunton River	X	X			X	X	X	X	X				X			X
Swift Run	X	X			X		X	X	X							
Thornton River, N. Fork		X			X		X	X	X				X			
Thornton River, S. Fork	X	X	X		X	X	X	X	X				X			
Twomile Run	X	X			X		X	X	X				X	X		X
Whiteoak Canyon Run	X	X			X	X	X	X	X				X			X
Whiteoak Run	X	X			X		X		X				X			X
Summary	30	43	4	2	43	17	43	24	41	1	1	1	33	5	1	24

Table II–3. Continued.

Stream Name	Families of Order												
	Plecoptera									Megaloptera		Odonata	
	Capniidae	Chloroperlidae	Leuctridae	Nemouridae	Peltoperlidae	Perlidae	Perlodidae	Pteronarcyidae	Taeniopterygidae	Corydalidae	Sialidae	Anisoptera	Zygoptera
Big Meadows Effluent		X	X	X	X		X		X			X	
Big Run		X	X	X	X	X	X	X	X	X		X	
Bolton Branch		X	X	X	X	X	X	X		X	X	X	
Broad Hollow Run		X	X	X	X	X	X	X				X	
Brokenback Run	X	X	X		X	X	X	X		X		X	X
Cedar Run	X	X	X		X	X	X	X					
Deep Run		X	X	X	X	X	X			X			
Doyles River		X	X		X	X	X	X				X	
Dry Run, N. Fork	X	X	X	X	X	X	X	X		X	X	X	
Eppert Hollow Run	X	X	X	X	X	X	X	X			X	X	
Fultz Run		X	X		X	X	X	X		X		X	
Hannah Run		X	X	X	X	X	X			X		X	
Happy Creek			X	X	X		X		X	X			
Hawksbill Creek (Beldor)		X	X	X	X	X	X	X		X		X	
Hazel River	X	X	X	X	X	X	X	X	X	X	X	X	X
Hughes River	X	X	X	X	X	X	X	X		X			
Ivy Creek		X	X	X	X	X	X	X		X			
Jeremy's Run	X	X	X	X	X	X	X	X	X	X	X	X	
Keyser Run	X	X	X			X	X	X					
Land's Run	X	X	X	X	X	X	X	X		X	X	X	
Little Hawhksbill Creek		X	X		X	X	X	X		X		X	
Lower Lewis Run		X	X	X	X	X	X	X		X		X	
Madison Run	X	X	X	X	X	X	X	X	X	X		X	
Meadow Run	X	X	X	X	X	X	X		X	X		X	
Moormans River, N. Fork	X	X	X	X	X	X	X	X	X	X		X	
Naked Creek, E. Branch		X	X	X	X	X	X	X		X		X	
Naked Creek, W. Branch		X	X	X	X	X	X	X					
Onemile Run	X	X	X	X	X	X	X	X		X	X	X	
Overall Run		X	X	X			X	X					
Paine Run	X	X	X	X	X	X	X	X	X	X	X	X	X
Pass Run	X	X	X	X	X	X	X	X	X	X	X	X	
Piney River	X	X	X	X	X	X	X	X	X	X	X	X	X
Rapidan River	X	X	X	X	X	X	X	X		X		X	
Rose River	X	X	X	X	X	X	X	X	X	X	X	X	X
Sawmill Run	X	X	X	X	X	X	X	X	X	X		X	
South River		X	X	X	X	X	X	X					
Staunton River	X	X	X	X	X	X	X	X	X	X	X	X	
Swift Run		X	X		X	X	X	X				X	X
Thornton River, N. Fork		X	X		X	X	X	X		X			
Thornton River, S. Fork		X	X	X	X	X	X	X	X	X		X	
Twomile Run	X	X	X	X	X	X	X	X	X	X	X	X	X
Whiteoak Canyon Run	X	X	X	X	X	X	X	X	X	X	X	X	
Whiteoak Run	X	X	X	X	X	X	X	X		X		X	
Summary	23	42	43	35	41	40	43	38	17	33	14	33	7

Table II-3. Continnued.

Stream Name	Families of Order									
	Coleoptera									Collembola
	Dryopidae	Dytiscidae	Elmidae	Gyrinidae	Haliplidae	Helophoridae	Hydrophilidae	Psephenidae	Ptilodactylidae	(Family not available)
Big Meadows Effluent								X		
Big Run	X		X					X		X
Bolton Branch	X		X					X	X	
Broad Hollow Run			X					X		X
Brokenback Run	X		X					X		X
Cedar Run			X					X		
Deep Run			X					X		
Doyles River			X					X		
Dry Run, N. Fork			X					X		X
Eppert Hollow Run								X		
Fultz Run			X					X		
Hannah Run			X					X		
Happy Creek	X		X					X		
Hawksbill Creek (Beldor)			X					X		
Hazel River	X		X					X	X	X
Hughes River			X					X		
Ivy Creek	X		X					X		X
Jeremy's Run	X		X					X		X
Keyser Run			X					X		
Land's Run	X		X					X		X
Little Hawhksbill Creek			X					X		
Lower Lewis Run			X					X		X
Madison Run	X		X				X	X		X
Meadow Run			X					X		X
Moormans River, N. Fork	X		X					X		X
Naked Creek, E. Branch			X					X		
Naked Creek, W. Branch			X			X		X		
Onemile Run			X					X		X
Overall Run								X		
Paine Run	X	X	X					X		X
Pass Run	X		X					X		
Piney River	X	X	X				X	X	X	X
Rapidan River	X		X				X	X		
Rose River	X		X			X		X		X
Sawmill Run	X		X					X		
South River			X					X		
Staunton River	X		X		X			X		X
Swift Run			X					X		
Thornton River, N. Fork			X					X		X
Thornton River, S. Fork			X					X	X	
Twomile Run	X	X	X				X	X		X
Whiteoak Canyon Run	X		X	X		X	X	X		X
Whiteoak Run	X	X	X				X	X		X
Summary	20	4	40	1	1	3	6	43	4	21

students. There are seven principal rock types that form the bedrock of the area, as described by Shenandoah National Park (1998b) and shown in Figure II-4. There are granitic rocks, known as Old Rag Granite and the Pedlar Formation, which exceed one billion years in age. They cover about 8% and 25% of the park area, respectively. The plutonic rocks of these two formations are among the oldest exposed rocks in the Appalachian Mountains. Old Rag Granite is a coarsely crystalline resistant granite. The Pedlar Formation is a medium-grained granodiorite that has gneissic foliation and is found mainly in the northern portion of the park (Gathright 1976). The Swift Run Formation is a conglomerate of debris from granitic rocks and the volcanism which laid down the Catoctin Formation. It is about 600 million years old and covers about 1% of the park. The Catoctin Formation is comprised of many layers of metamorphosed volcanic rocks, which were derived from a series of volcanic eruptions that began about 600 million years ago, with decades or centuries between flows. There are at least 12 of these layers remaining in the park. Many of the cliff faces that are found in the park occur along the boundaries of this formation, including nearly all of the numerous waterfalls. The Catoctin rocks dominate the central and northern park sections and cover about 38% of the park. Dense greenstone, which formed from lava, makes up much of the Catoctin Formation and underlies most of the high ridges, interlayered with thin bands of slate or phyllite. The latter formed from ash and tuff deposited by volcanic eruptions (Gathright 1976).

The other three rock types found in SHEN are metamorphosed sedimentary rocks, about 500 million years old. These rock formations were formed when the area was covered by a large sea. The Weverton, Hampton, and Erwin members of the Chilhowee Formation are exposed along western slopes in the southern portions of the park. The Hampton Member is the most extensive, covering about 17% of the park. It is a thick deposit (~ 600 m) of phyllite and shale in the lower sections and interbedded metasandstone and phyllite with intermittent quartzite in the upper sections. The Weverton Member, a sequence of interbedded quartzite, phyllite, and metasandstone, is of limited distribution in the park.

The Antietam Formation is extremely resistant and composed of light gray quartzite and quartz-rich clastics, which may be sparsely interbedded with less resistant metasandstone and phyllite. This 200 to 300 m thick formation is visible as quartzite ledges and sharp peaks in the southwestern part of the park (Lynch and Dise 1985).

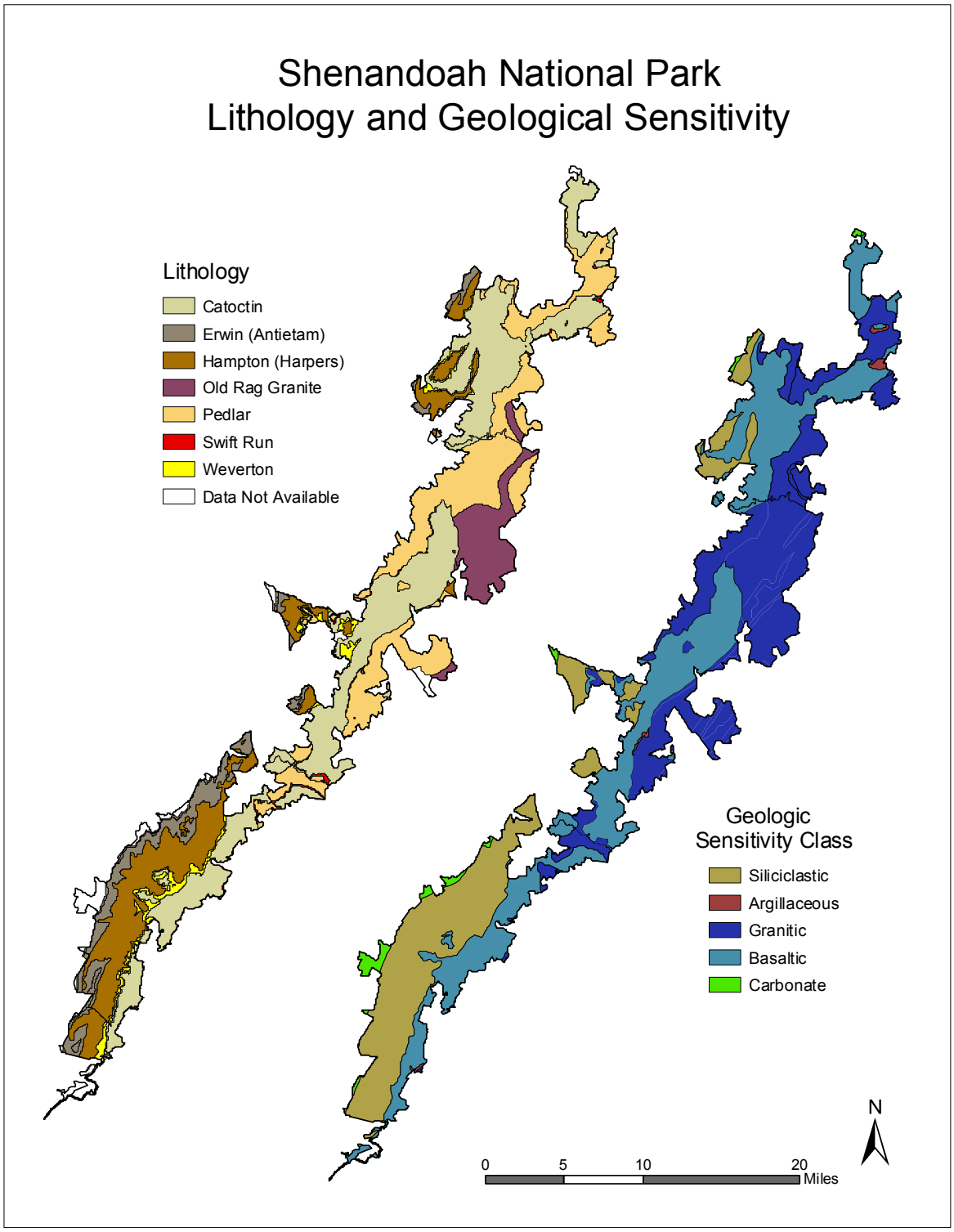

Figure II-4. Lithologic and geological sensitivity maps of SHEN. Lithology was taken from Gathright (1976). Geologic sensitivity classes are arranged in the legend from most (siliciclastic) to least (carbonate) sensitive to acidification. They can be derived from the lithological coverage as follows: siliciclastic (Erwin, Hampton, Weverton), granitic (Old Rag Granite, Pedlar, Swift Run), basaltic (Catoctin).

The geologic formations that are exposed within the park can be classified into three basic types of rock: granitic, basaltic, and siliciclastic (sedimentary rocks that contain abundant silica or sand). Siliciclastic rock types are most sensitive to acidification, followed by granitic rock types. Basaltic rock types are relatively insensitive. Each type covers approximately one-third of the park (Figure II-4). There are also minor amounts of argillaceous and carbonate rock types.

Sedimentary rocks in the park include sandstone, conglomerate phyllite, and quartzite. They are found mostly in the southern portion of the park and in a small area north of Thornton Gap. These siliciclastic rocks were deposited by streams, rivers, lakes, and the ocean. The granites are coarse-grained, crystalline rocks that contain quartz, feldspar, and small amounts of dark iron-bearing minerals, including pyroxine, hornblende, and biotite. Granitic rocks in the park include granite, granodiorite, and gneiss. These rocks are found in the Pedlar Formation and on Old Rag Mountain in the Old Rag Granite Formation. The granites and gneisses are between 1 and 1.2 billion years old and underlie other rock types. These rocks were part of a mountain range, that eroded long ago, called the Grenville Mountains, which once extended from Texas to Newfoundland (Badger 1999). Green volcanic rocks of the Catoctin Formation formed many outcrops. These green rocks were once basalts that metamorphosed into metabasalt called greenstones, which contain chlorite, epidote, and albite.

Furman et al. (1998) examined bedrock weathering properties for North Fork Dry Run, White Oak Run, and Deep Run watersheds in SHEN, using mass balance calculations. The North Fork Dry Run watershed is underlain by Precambrian granodiorite of the Pedlar Formation, with basalt dikes. White Oak Run has the Hampton and Weverton Members of the Chilhowee Formation as bedrock, and Deep Run has the Erwin and Hampton Members as bedrock. The calculations suggested that plagioclase feldspar is the dominant reactant in the granodiorite watershed, but the basalt dikes make significant contributions to the base cation budget even though they comprise a small fraction of the bedrock coverage. Calculations for the metamorphosed sedimentary watersheds suggested contributions from plagioclase feldspar, muscovite, and biotite.

The distribution of soil types in Virginia is closely related to bedrock distribution (USDA 1979). The region has not been glaciated and the typically rocky and patchy soils of the mountainous areas have formed in residual or colluvial material. Soils tend to be thin (< 2 m) and primarily classified as Ultisols and Inceptisols. Ultisols have formed from crystalline

bedrock materials along the crest and eastern flank of the Blue Ridge Province, whereas Inceptisols have formed from the sedimentary bedrock on the western flank of the Blue Ridge Province and on the ridges of the Ridge and Valley Province. All of these soils tend to be < 2 m in depth and skeletal, with a high percentage of rock fragments (Cosby et al. 1991). Depth to bedrock and extent of rock fragments are controlled mainly by slope position and orientation. The Inceptisols tend to have lower quantities of adsorbed base cations (Cosby et al. 1991).

Soils in SHEN are derived from *in-situ* weathering of bedrock or transport of weathered material from upslope positions (Elder and Pettry 1975, Carter 1961, Hockman et al. 1979, Lynch and Dise 1985). Soils characteristics therefore often reflect the underlying bedrock characteristics. The predominant soil associations include the Myersville-Catoctin, Porters-Halewood, Lew-Cataska-Harleton, and Hazleton-Drall. Colluvial fans, talus deposits, and exposed rock are also common. Soils of the park are generally classified as well-drained and medium to very strongly acidic (Lynch and Dise 1985). Soil chemistry was studied in the southwestern part of the park by Shaffer (1982). These soils tend to be thin, highly acidic, sandy loams to clay loams, derived from the Hampton and Antietam bedrock. They exhibit low cation exchange capacity (CEC; ~ 10 μeq/100 g) in the A and B horizons, low organic matter, and very low base saturation (~ 4 to 5%). The latter reflects the low weathering of the bedrock (Shaffer 1982, Lynch and Dise 1985) and to some extent might also reflect past base cation leaching in response to sulfur deposition.

In 2000, University of Virginia scientists collected and analyzed soil samples at 79 sites within SHEN in support of the acidic deposition component of this assessment. These soil samples have been archived at the University of Virginia. The samples were collected from 14 different watersheds, 5 each on primarily siliclastic and basaltic bedrock and 4 primarily on granitic bedrock. Between four and eight soil pits were excavated within each watershed, distributed across each watershed to account for differences in slope, aspect, land use history, fire history, and forest cover type. Laboratory analyses were conducted by Penn State University and Virginia Tech (Welsch et al. 2001).

The soils within watersheds situated primarily on siliciclastic bedrock generally showed the lowest soil pH (median 4.4 to 4.5), CEC (median 3.5 to 7.5 cmol/kg), and base saturation (median 8 to 12%). Values for watersheds having soils primarily on granitic bedrock were generally intermediate, and basaltic watersheds were higher in all three parameters (Table II-4).

Table II-4. Interquartile distribution of pH, cation exchange capacity (CEC), and percent base saturation for soil samples[a] collected in SHEN study watersheds during the 2000 soil survey.

Site ID	Watershed	n	pH			CEC (cmol/kg)			Percent Base Saturation		
			25th	Med	75th	25th	Med	75th	25th	Med	75th
Siliciclastic Bedrock Class[b]											
VT35	Paine Run	6	4.4	4.5	4.7	3.7	5.7	5.7	7.1	10.0	24.9
WOR1	White Oak Run	6	4.3	4.4	4.4	4.8	7.5	7.8	5.3	7.5	8.5
DR01	Deep Run	5	4.3	4.4	4.5	3.9	5.0	5.8	7.2	8.9	10.8
VT36	Meadow Run	6	4.4	4.4	4.5	3.1	3.5	7.6	7.8	8.7	11.3
VT53	Twomile Run	5	4.3	4.5	4.5	4.6	6.0	6.9	11.7	12.3	13.6
Granitic Bedrock Class											
VT59	Staunton River	6	4.7	4.8	4.9	6.5	7.5	9.2	9.1	13.9	29.5
NFDR	NF of Dry Run	5	4.4	4.5	4.7	7.3	8.0	9.2	7.5	10.8	12.4
VT58	Brokenback Run	5	4.6	4.7	4.7	7.3	8.4	9.6	6.0	6.7	9.7
VT62	Hazel River	4	4.5	4.7	4.8	5.3	5.3	6.5	12.3	12.8	21.6
Basaltic Bedrock Class											
VT60	Piney River	6	4.7	5.0	5.3	7.3	7.7	10.0	17.0	24.0	57.0
VT66	Rose River	8	4.8	5.0	5.3	7.3	10.1	10.7	19.1	38.0	63.5
VT75	White Oak Canyon	6	4.9	5.1	5.5	7.1	7.5	9.3	15.6	32.8	43.4
VT61	NF of Thornton River	7	5.1	5.2	5.3	7.7	9.6	10.8	35.6	54.4	71.2
VT51	Jeremys Run	4	4.7	5.0	5.3	6.3	7.6	7.7	15.0	22.8	46.1

[a] Samples collected from mineral soil >20cm depth
[b] Watersheds are stratified according to the predominant bedrock class present in each watershed.

Streamwater ANC, base cation, and silica concentrations vary in predictable ways in the streams of SHEN, depending on the characteristics of the underlying soils and bedrock (Lynch and Dise 1985). Each of the predominant rock formations, and its associated soils, is characterized by a particular set of minerals that control the chemical composition of drainage water.

Sullivan et al. (2002a) found that there were three soils types in the Southern Appalachian region that were associated with high percentages of acidic streams and streams having low ANC. All three of these soils types (Wallen-DeKalb-Drypond, Moomaw-Jefferson-Alonzville, and Shottower- Laidig-Weikert) are present within SHEN. For the Southern Appalachian Mountains Initiative (SAMI) assessment, each of these soil types was characterized by over 25% of sampled streams having ANC ≤ 20 μeq/L. Within SHEN, these soil types are most common in the South District, but are found within all districts along the western slope of the mountains, throughout the length of the park (Figure II-5). The Waller-DeKalb-Drypond type is the most common of the three within SHEN, and is the most prevalent soil type along the western slope within the park.

G. VEGETATION

The distribution of forest vegetation in the park (shown in Figure II-6) and surrounding region is largely determined by moisture availability, which in turn is strongly influenced by soil and bedrock characteristics and topographic features (Hack and Goodlett 1960, Edmunds et al. 1986). The Ultisols tend to have greater moisture holding capacity and are frequently dominated by red oak (*Quercus rubra*), maple (*Acer* spp.), yellow poplar (*Liriodendron tulipifera*), hemlock (*Tsuga canadensis*), rhododendron (*Rhododendron maximum*), and other moisture demanding species. Forests associated with the Inceptisols are more commonly dominated by chestnut oak (*Quercus prinus*), Virginia pine (*Pinus virginiana*), azalea (*Rhododendron calendulaceum*) and other dry habitat species (Cosby et al. 1991).

The park is located in a transitional area between northern and southern vegetation types. Higher elevations of the park and north-facing slopes tend to be dominated by northern species whereas lower elevations and south and west facing slopes are covered by central hardwood forests. There are seven primary vegetation types within the park. The chestnut oak forest type is common on the low to mid elevation drier slopes, which often have southern or southwestern exposure. This forest type is dominated by chestnut oak, with red oak as its primary associate. The second most common forest type in the park is yellow poplar. It is most frequently found on lower slopes of the more moist drainages in the north and central districts of the park, especially on north and east facing slopes. Yellow birch (*Betula alleghaniensis*), hemlock, white pine (*Pinus strobus*), and white oak (*Quercus alba*) are common associates. Cove hardwood is the third most common forest type, and is comprised of ash (*Fraxinus* sp.), red oak, and basswood

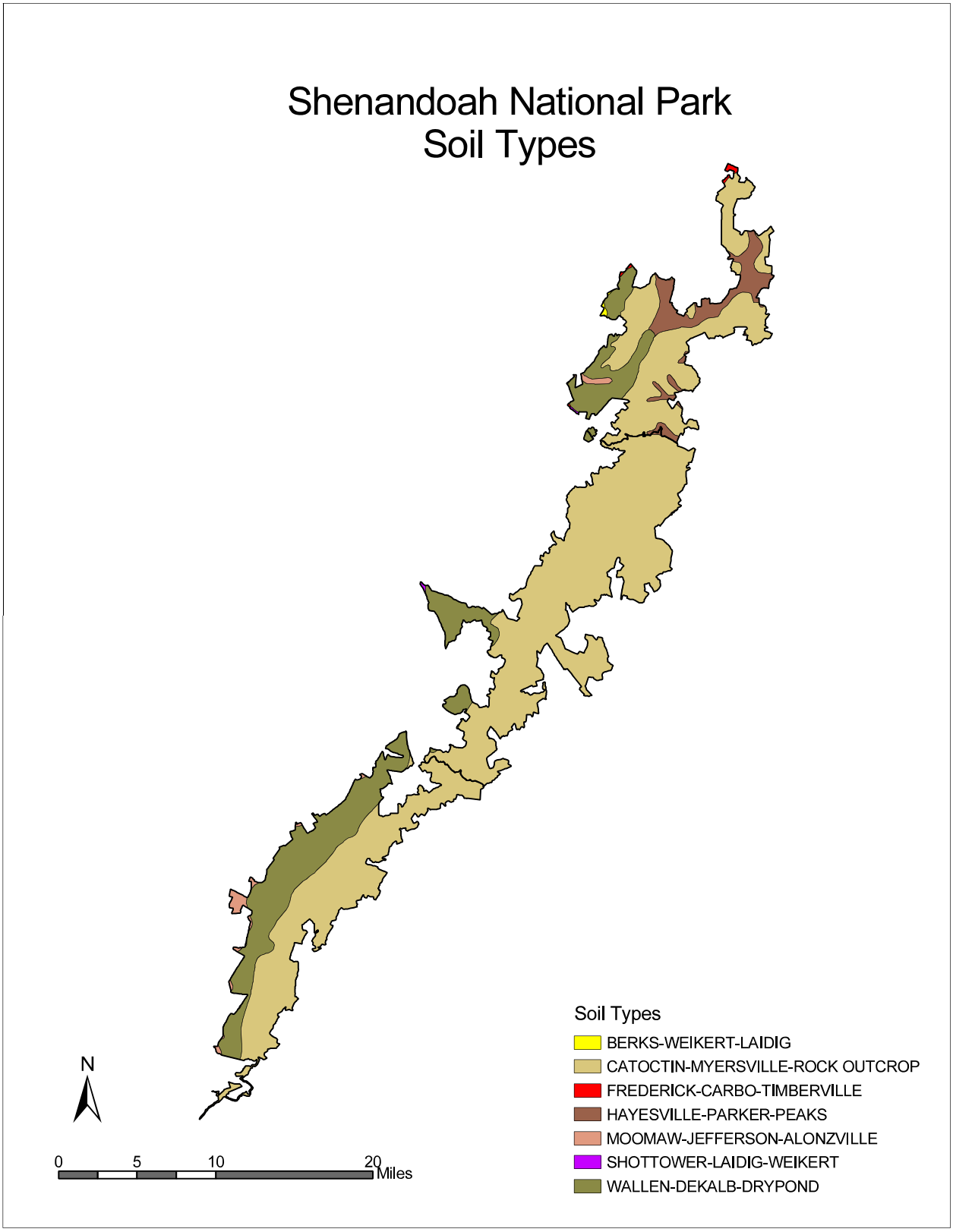

Figure II-5. Soils types in SHEN. All soil types in the legend are present within the park, but several are present only in very small areas.

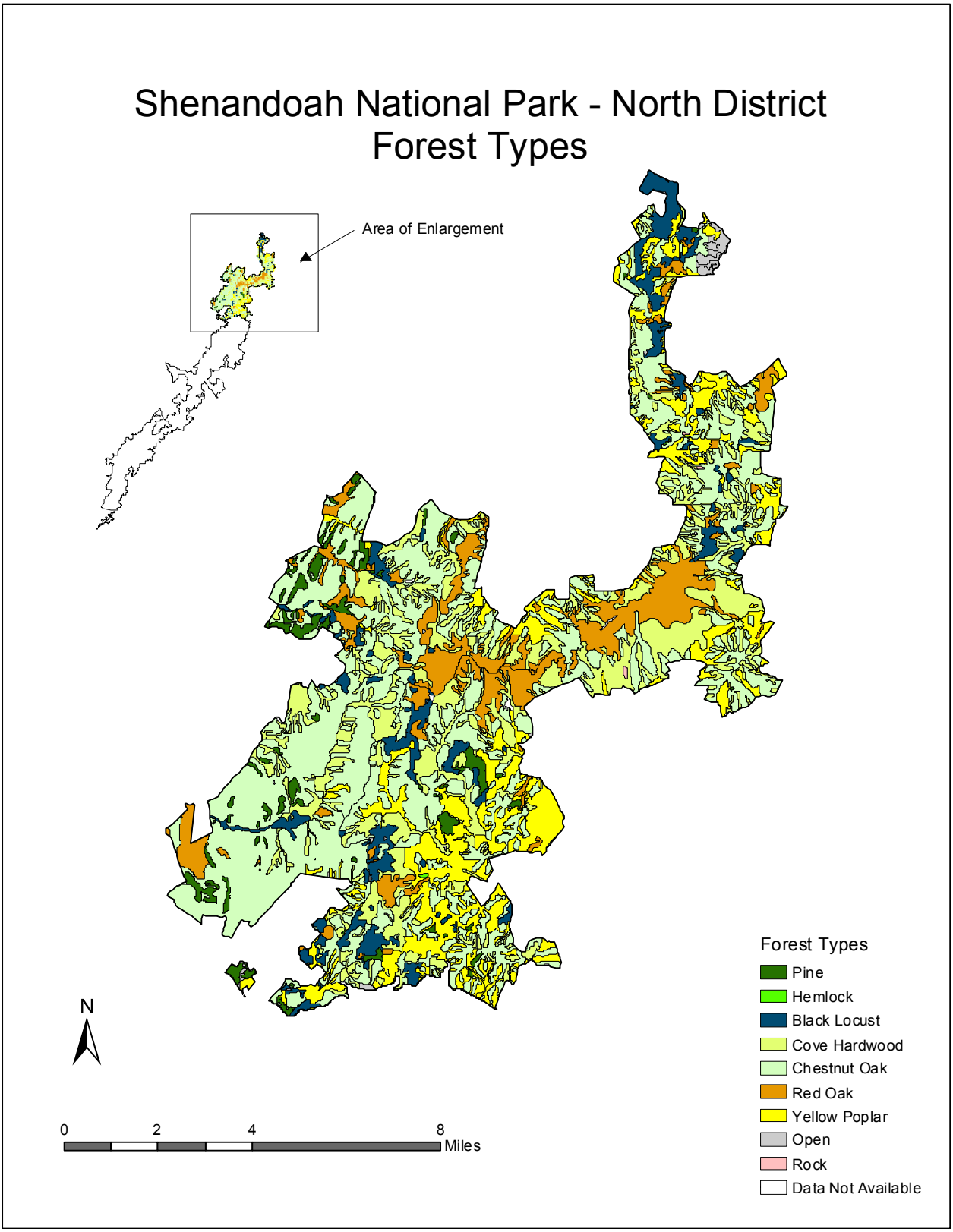

Figure II-6. Major forest types within SHEN, by district: A) North, B) Central, C) South.

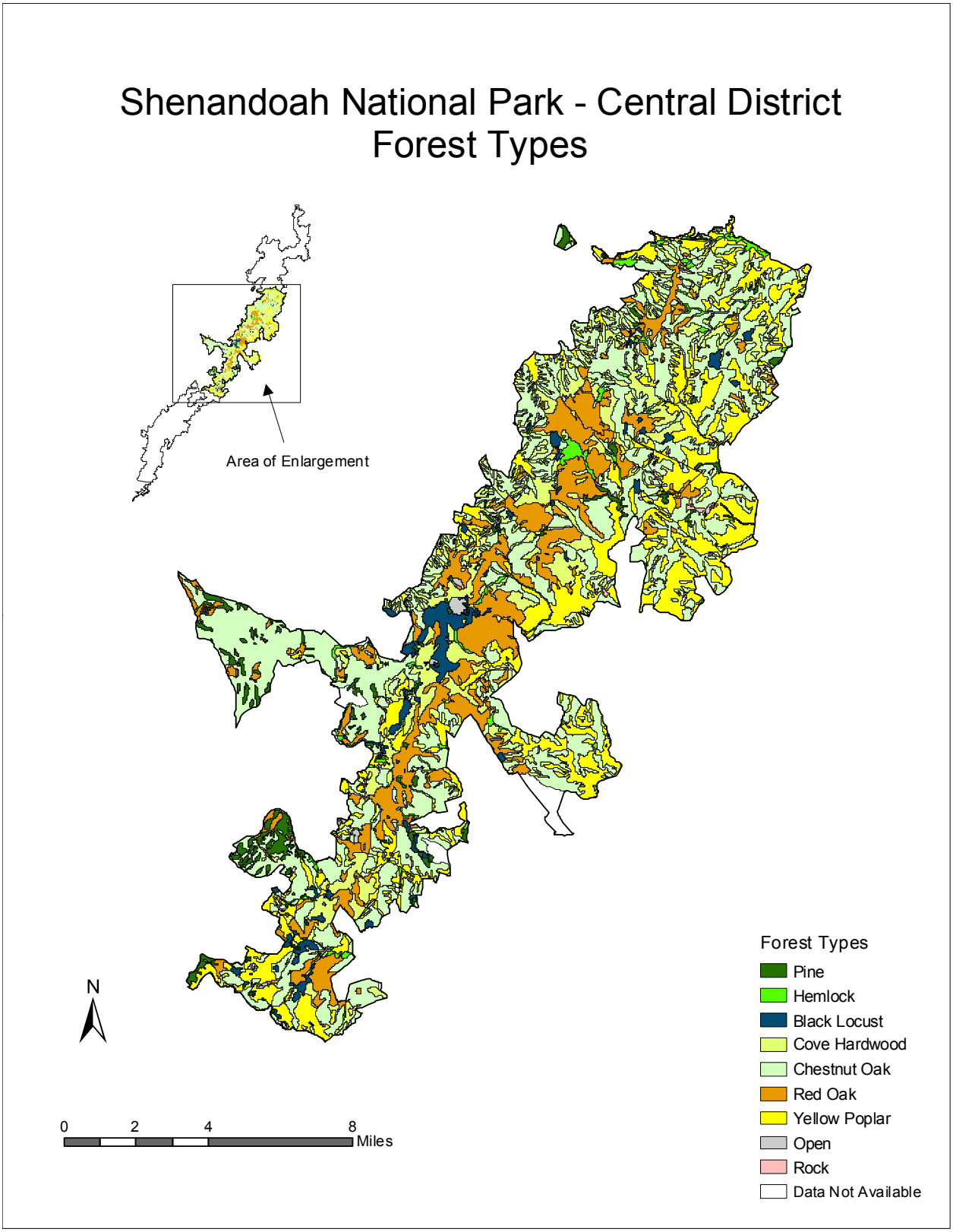

Figure II-6. Continued.

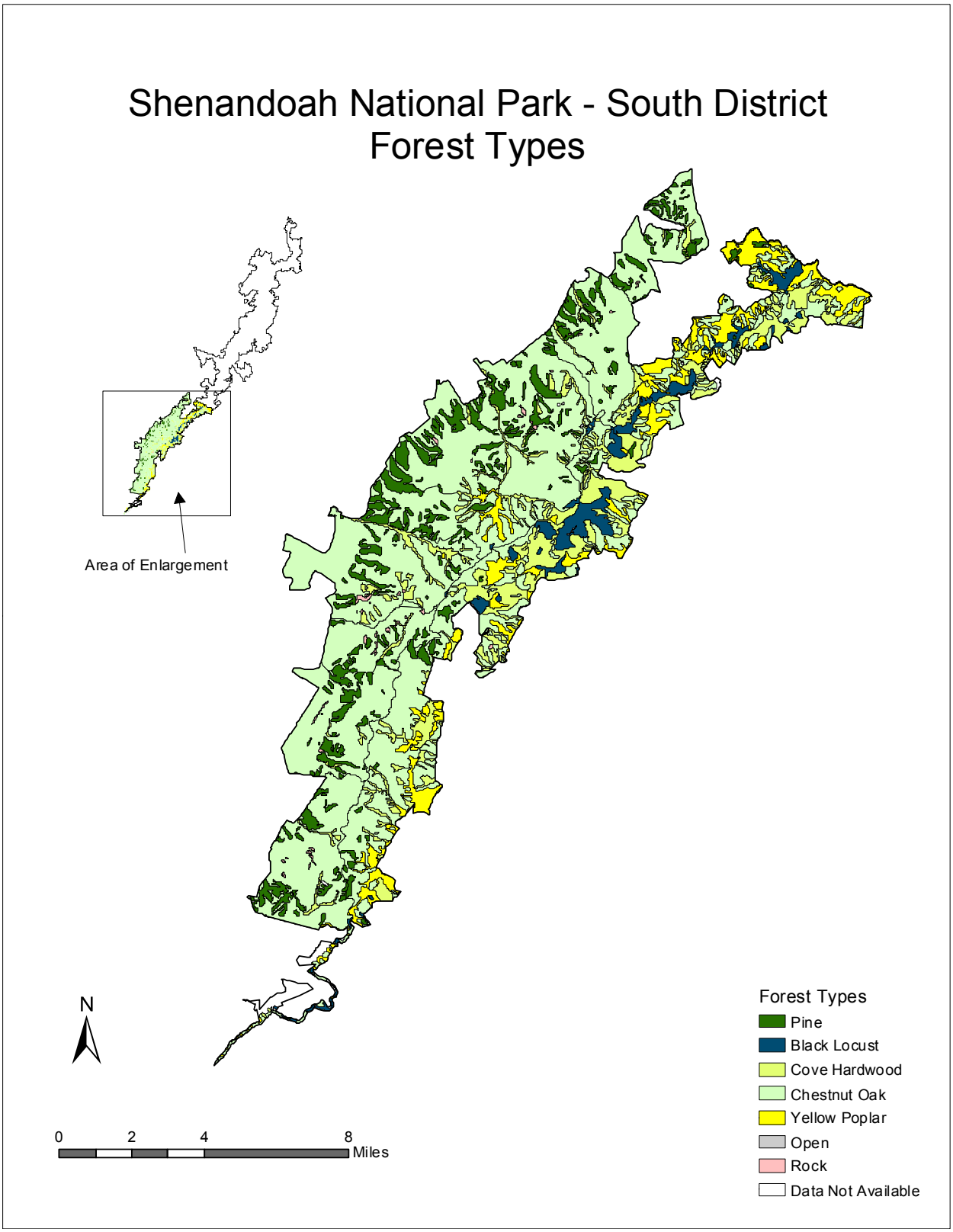

Figure II-6. Continued.

(*Tilia americana*). It is located mostly on moist sites in the hollows and along stream drainages. The red oak forest type is found over a fairly broad range of environmental conditions. It occupies the most mesic ridgetops and side slopes. Red oak is dominant in this forest type, which also includes mockernut hickory (*Carya tomentosa*), pignut hickory (*C. glabra*), chestnut oak, and white oak. The pine forest type includes eastern white pine (*Pinus strobus*), Virginia pine, and pitch pine (*P. rigida*). These species are primarily successional and are found on previously disturbed sites. Black locust (*Robinia pseudoacacia*) is an early successional forest type that is found in recently disturbed areas. It also includes black cherry (*Prunus serotina*), tree of heaven (*Ailanthus altissima*), and Virginia pine. Moist sites in association with spring seeps, streams, north facing slopes, and shaded drainage bottoms are often covered with hemlock forests, which occur in pure stands.

Big Meadows is a large (48 ha) high-elevation grass/shrub plant community that was maintained as a meadow in historic times by grazing and burning, and later by burning and mowing. A small bog occurs in its northeast corner, where many plant species are found that do not occur elsewhere in the park.

Limberlost is a high-elevation area of seeps and springs that contains an extensive old growth stand of eastern hemlock and red spruce (*Picea rubens*). The area also contains speckled alder (*Alnus rugosa*), Canada yew (*Taxus canadensis*), and the only occurrence in Virginia of alder-leaved buckthorn (*Rhamnus alnifolia*).

Cliffs and rocky north- and west-facing slopes support fragile populations of plants, including some boreal species such as balsam fir (*Abies balsamea*), mountain sandwort (*Minuartia groenlandica*), and bearberry (*Arctostaphylos uva-ursi*) at the tops of the highest peaks (e.g., Hawksbill, Stony Man and Old Rag). Crescent Rock, Black Rock, Hawksbill Summit, Stony Man Summit, and Old Rag Summit face prevailing winds and include heaths such as minnie bush (*Menziesia pilosa*) and northern bush honeysuckle (*Diervilla lonicera*), and crevice plants such as Allegheny stonecrop (*Sedum telephioides*), Michaux's saxifrage (*Saxifrage michauxii*), and three-toothed cinquefoil (*Potentilla tridentata*).

H. WILDLIFE

Explorers to the Shenandoah Valley and Blue Ridge Mountains in the early 1700s reported an abundance and variety of animals, some of which have since been extirpated. Woodland bison (*Bison bison*), the largest of Shenandoah's original fauna, inhabited the valleys and low-

elevation foothills with one documented trail crossing the Blue Ridge at Rockfish Gap. Eastern elk (*Cervus canadensis*) originally occurred throughout the entire northern Shenandoah Valley, including surrounding ridges. Timber wolves (*Canis lupus*) and mountain lions (*Felis concolor*) were also among the region's original inhabitants and together with the black bear (*Ursus americanus*), constituted the primary predators of large mammal species. As European settlers cleared the land, introduced exotic species, and hunted native animals, both the abundance and variety of wildlife decreased, with total elimination of some species. However, since the establishment of the park, some species have been reintroduced and some have naturally reestablished. Currently, the park sustains populations of white tailed deer (*Odocoileus virginianus*), black bear, bobcat (*Lynx rufus*), opossum (*Didelphis virginiana*), racoon (*Procyon lotor*), skunk (*Mephitis mephitis*), gray fox (*Urocyon cinereoargenteus*), and eastern cottontail (*Sylvilagus floridanus*; Shenandoah National Park 1993). There are over 200 species of resident and transient birds known to use the park's habitats, including turkey (*Meleagris gallopavo*). Sixty-one species of reptiles and amphibians have been recorded within the park. The Shenandoah salamander (*Plethodon shenandoah*) was listed as an endangered species in 1989. Its range is very limited and includes four areas located in the park at high elevation on rocky talus slopes (Shenandoah National Park 1998b).

I. DISTURBANCE

The forests of SHEN exist in an environment that includes insects and pathogens, competition and plant community dynamics, and abiotic factors, including air pollutants and disturbance. To understand how terrestrial ecosystems respond to air pollution requires an understanding of how plants normally grow in a stressful environment, in addition to the details of their response to pollutants and potential alterations in normal growth.

Forests make difficult experimental subjects. Plants grow in a variety of soils, in populations of mixed sizes and species, and under variable climatic conditions. Forests in national parks are even less amenable to experimentation—they are to be protected, studied, and enjoyed, not instrumented, poked, and prodded. On the other hand, it is important to understand how anthropogenic stresses affect the health and vigor of the forest.

SHEN comprises one of the nation's most diverse botanical reserves. The documented flora of the park includes over 1,400 species of plants. From the 1720s to the establishment of the park, much of the area was cleared. The invasion of non-native insects and pathogens during the

20th century seriously impacted the vegetation communities of the park. The chestnut blight (*Endothia parasitica*), a canker disease which kills American chestnuts (*Castanea dentata*), entered the United States in the early part of the 20th century. The disease spread quickly throughout the eastern United States. All chestnut trees in the park were affected by this disease. By about 1940, only remnant chestnut sprout growth existed. The loss of this tree species had a large impact on the structure and composition of park forests because some stands had contained 50% or greater numbers of chestnuts.

The gypsy moth (*Lymantria dispar*), which was introduced into the United States in the 1860s, began to impact the forests of the park in 1986. Because the preferred food of gypsy moths is oak, the forests of the park which were predominantly oak were vulnerable to widespread impact. Initial effects included defoliation of oaks, with as much as 16,000 ha defoliated in 1989 alone. Repeated defoliations, coupled with several years of drought, caused widespread oak mortality in the late 1980s and early 1990s. An introduced fungus (*Entomophaga maimaiga*), which attacks gypsy moths, reduced gypsy moth populations in the early 1990s. By 1996, effects on the forest canopies of the park were dramatically curtailed. The non-native hemlock woolly adelgid (*Adelges tsuga*) and the native southern pine beetle (*Dendroctonus frontalis*) have also had dramatic impacts on park forests.

Based on records kept since 1935, the park has approximately eight naturally-occurring fires per year. These fires tend to remain small, and are easily suppressed except during times of drought. Large fires within the park are overwhelmingly human-caused fires. The most notable of these was the Shenandoah Complex Fire, which burned 9,350 ha of park land in the fall of 2000. A fire management plan was prepared for the park (Shenandoah National Park 1993), with a primary objective of fire suppression. The plan details suppression strategies, prevention criteria, interagency cooperation, and programs to prevent adverse impacts of wildfire to life, property, and adjacent lands. In addition, increased emphasis is being directed towards prescribed fire components to determine appropriate actions regarding natural and management-ignited prescribed fires. The park is in the final review draft phase of updating its fire management plan.

I. INTRODUCTION

A. PURPOSE

The primary purpose of this report is to develop a state-of-the-science assessment of air quality and air pollution effects to support National Park Service (NPS) mandates under the Organic Act, the Clean Air Act (CAA), and other pertinent laws and policies to conserve, restore, and protect Shenandoah National Park's (SHEN) resources for current and future generations. This technical assessment is necessary to:

- enhance NPS and SHEN ability to meet "affirmative responsibility" obligations at national, regional, state, and park levels through effective synthesis of relevant data and information;
- enhance scientific understanding and quantification of key air pollutant emissions, transport, deposition, and current and projected future effects on SHEN resources;
- update a related 1990 technical document and quantify the range of critical loads of air pollutants;
- develop visual and ecological models and other educational tools aimed at non-technical audiences;
- provide state-of-science information for park staff, and in preparation for revision of the SHEN General Management Plan; and
- determine SHEN-specific acidic deposition analysis thresholds for New Source Review.

This assessment can also serve as a sub-regional case study regarding Class I area restoration and protection issues for those engaged in collaborative regional and state planning, policy-making, permit review, and scientific activities in the eastern United States. This information will be used for strategic outreach to key decision-makers and stakeholders in the development of regional and state air pollution control strategies and plans. Park managers and resource professionals will also use this assessment to communicate information regarding SHEN air quality and resource conditions to park employees and key local partners and other stakeholders, and to promote pollution prevention practices in the park. To support the NPS mandate to protect air quality related values (AQRVs) in Class I areas, the following specific objectives have been identified for the report:

- provide updated summaries of monitoring data on visibility, pollutant concentrations, and deposition, both temporally and spatially;

- conduct comprehensive analyses of documented and potential ecological effects of various atmospheric pollutants and exposures (chronic, episodic) on terrestrial and aquatic systems;
- summarize national ambient air quality standards (NAAQS) exceedances and potential non-attainment designation;
- utilize existing emissions inventories, meteorological data, and atmospheric models to assess current and future air quality conditions;
- utilize existing atmospheric deposition and terrestrial and aquatic effects models to evaluate potential future changes in air quality, deposition, and associated impacts;
- compile inventories of pollution-sensitive components or receptors of ecosystems, and assess the critical loading of pollutants that would be likely to cause changes in the sensitive receptors.

The report addresses these objectives by providing a summary of current and historical monitoring data for pollutants, a description of the resource base in the park, a synthesis of knowledge on the visual and ecological effects of atmospheric pollutants, model estimates of future atmospheric deposition associated with various emissions control scenarios, model estimates of future changes in the extent of streamwater acidification and associated effects on native brook trout (*Salvelinus fontinalis*) and species richness of aquatic biota, model estimates of potential future ground-level (tropospheric) ozone (O_3) effects on individual tree species and forest stands, and a park-specific assessment of pollution vulnerability and current and potential future impacts. The approach relies on published data summaries, new analyses, model output, journal articles, and technical reports. Some original data collection activities occurred in conjunction with this project; specifically, soils samples were collected and analyzed from 79 sites within the park during the summer of 2000.

This report is intended to serve diverse audiences, including various NPS, U.S. Fish and Wildlife (USFWS), and U.S. Forest Service (USFS) staff, state and Federal air regulators and scientists, regional planning organizations, conservation groups, industries, and others actively engaged in air quality issues in Virginia and throughout the eastern United States.

B. BACKGROUND

The NPS maintains the world's most admired system of national parks. The mission of the NPS is to preserve unimpaired the natural and cultural resources and values of the national park

system for the enjoyment, education, and inspiration of this and future generations. Air quality is fundamentally important to the preservation of these resources and values. In the 1977 Amendments to the Federal CAA, Congress formally recognized this when defining one of the purposes of the CAA, "…to preserve, protect and enhance the air quality in national parks, national wilderness areas, national monuments, national seashores and other areas of special national or regional natural, recreational, scenic, or historic value." Congress also designated 48 national parks managed by the NPS (including Shenandoah) and 108 wildernesses managed by the USFWS or the USFS as "mandatory Class I areas". The 1977 CAA outlined several special protections for Class I areas related to visibility and the prevention of significant deterioration of air quality and adverse impacts on Class I AQRVs. AQRVs include visibility, flora, fauna, bodies of water, soils, and other natural and cultural resources that may potentially be damaged by air pollution. Congress also delegated to Federal Land Managers (FLMs) "…an affirmative responsibility to protect the air quality related values…within a Class I area." The CAA legislative history further instructs FLMs "…to err on the side of protecting air quality related values for future generations". The 1990 CAA Amendments (CAAA) upheld and strengthened this affirmative responsibility and special protections afforded Class I areas.

In the late 1970s, the NPS responded to its new "affirmative responsibility" charge by forming a national Air Resources Division (ARD), staffed with air policy and technical experts, to assist Class I national parks with obtaining, analyzing and interpreting high-quality data to be used in the air policy-making, scientific, and educational arenas. Knowledge of pertinent laws, regulations, and policies, coupled with knowledge of emission inventories and scientific understanding of the effects of pollutants on park resources, provides the NPS with a framework to protect sensitive park resources from degradation due to air pollution.

Shenandoah National Park in Virginia (Figure I-1) is located downwind from and near major industrial and urban areas. The ARD targeted SHEN as one of the earliest atmospheric deposition, visibility, and air quality monitoring sites in the Class I national park network. In the early 1980s, SHEN

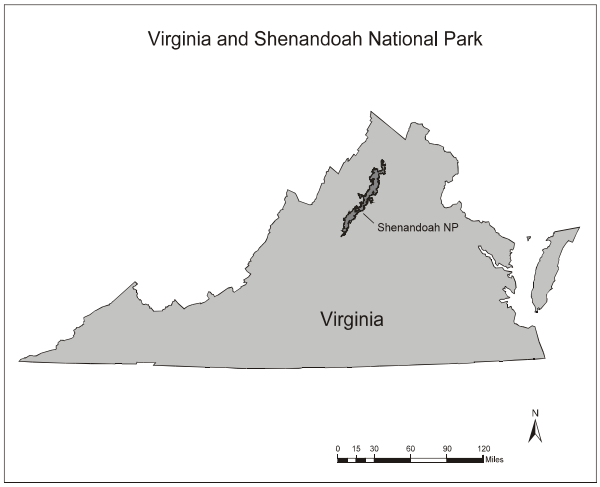

Figure I-1. Locational map for SHEN.

began long-term monitoring of ground-level O_3, sulfur (S) and nitrogen (N) wet deposition, and the size (coarse and fine), concentration, and chemical composition of airborne particulate matter that degrades visibility. The park's long-term monitoring program has since been expanded to include meteorology, sulfur dioxide (SO_2), dry deposition, visibility optical (e.g., light extinction and light scattering) monitoring, and (effective October, 2002) wet deposition of mercury. SHEN has also benefitted from a five-year photographic visibility monitoring project, a five-year research-grade O_3 precursor (nitrogen oxides [NO_x] and volatile organic compounds) study, and research projects related to visibility, cloud chemistry, streamwater chemistry, acidic deposition effects on fish, and O_3 effects on sensitive vegetation. In 1979, SHEN began a long-term cooperative agreement with acidic deposition scientists at the University of Virginia to monitor the acid-base status of two park streams and wet deposition in their respective watersheds. The Shenandoah Watershed Study's (SWAS) streamwater chemistry monitoring program was expanded to 14 streams by the mid-1990s. Today, SHEN maintains one of the most comprehensive long-term atmospheric deposition, air quality and related values (e.g., visibility and streamwater acid-base status) monitoring programs of the 48 Class I national parks. SHEN's strong scientific foundation, coupled with a solid legal and policy foundation (Section I.C), enhances NPS capability to uphold its "affirmative responsibility" to restore and protect key AQRVs in SHEN from the harmful effects of human-caused air pollution.

As described in this report, long-term monitoring and short-term research projects at SHEN testify that human-caused air pollution has adversely impacted the park's air quality, visibility, streamwater chemistry, and native fish at the individual, population, and community levels. Visibility has been significantly degraded, potentially detracting from visitor enjoyment of numerous vistas accessible from Skyline Drive (a Virginia State Scenic Highway), the Appalachian National Scenic Trail, and other trails and points within the park. Despite improvements in air quality under the CAA, the park's visibility and sensitive aquatic systems are still adversely impacted relative to estimated natural or pre-industrial background conditions (Church et al. 1992, Herlihy et al. 1993, Pitchford and Malm 1994, U.S. EPA 1995, Bulger et al. 2000, Malm et al. 2000, Stoddard et al. 2003) and, along with other Class I areas in the northeast and southeast, will remain at risk after full implementation of the 1990 CAAA. SHEN still suffers among the highest O_3 levels recorded at Class I national parks. Since the late 1980s, summertime ground-level O_3 at SHEN has consistently exceeded levels that are harmful to vegetation. Ozone foliar injury has been documented on several of the 40 known O_3-sensitive

plant species found at SHEN, and there is concern about potential effects of O_3 on forest growth and health. Visitor experience and visitor and employee health and safety are, or can be, impaired when summertime O_3 exposures exceed the human health protection standards established by the U.S. Environmental Protection Agency (U.S. EPA).

Based on a 1990 NPS technical assessment of air pollution impacts at SHEN, miscellaneous peer-reviewed literature and technical reports, and NPS air quality trends reports initiated in the late 1990s, it was evident that the NPS may not effectively uphold its "affirmative responsibility" to restore and protect SHEN AQRVs from adverse impacts of human-caused air pollution without an integrated state-of-the-science assessment. In early 1998, University of Virginia scientists notified SHEN of a pending report (Bulger et al. 1998) and paper (Bulger et al. 2000) that employed watershed acidification modeling to project substantial 1990 CAAA shortcomings in protecting and restoring the highly-prized, relatively acid-tolerant Appalachian brook trout (*Salvelinus fontinalis*) in some of the 65 streams (including 14 park streams) monitored in western Virginia. At the time, there was also uncertainty about the outcome of the Southern Appalachian Mountains Initiative's (SAMI) voluntary, consensus-based, multi-stakeholder effort to prepare an integrated regional assessment of air pollution effects on the vistas, streams, and forests of the southern Appalachians in eight states including Virginia. The goal of SAMI was to "recommend reasonable measures to remedy existing and prevent future adverse effects from human-induced air pollution". The park, recognized as a national example of significant air pollution impacts, obtained ARD support to acquire NPS Natural Resource Protection Program funds for this integrated, state-of-the-science SHEN Assessment. Park management and ARD support was based in large part on an understanding that this project would add value to the regional SAMI effort by providing:

- in-depth, park-specific data analyses and synthesis that capitalize on SHEN's comprehensive, high quality data sets, including new soils data collected within this project;
- airshed approach to determine SHEN-specific visibility, S and N deposition impacts, and state and source subregion contributions toward those impacts;
- landscape approach to assess SHEN-specific ground-level O_3 forest effects;
- defensible, SHEN-specific critical loads of air pollutants, enhanced in the case of S deposition by new soils data;

- objective disclosure of the environmental consequences at SHEN of two "On the Books" emissions scenarios based on the 1990 CAAA and two substantially more stringent emissions scenarios responsive to key known SHEN issues (e.g., visibility, acidic deposition, ground-level O_3); and

- objective disclosure of the current condition of SHEN AQRVs and prognosis for recovery under already promulgated regulations and SHEN Assessment emissions scenarios.

Long-range transport is involved with each of the pollutants of concern affecting SHEN, especially the secondary pollutants responsible for acidic deposition and visibility degradation, but also for O_3. Nonetheless, this SHEN Assessment (Section IV-C) and the final SAMI (2002) report both confirm that states are important contributors to air quality and air pollution impact problems within their own boundaries. Emissions from local sources within about 200 km produce greater haze- and acid-forming pollutants at receptors in SHEN (*on a per ton emissions basis*) than those farther away. The SAMI (2002) report also concluded that Class I areas in the central part of the eight-state SAMI region (e.g., Tennessee and North Carolina) would benefit the most from voluntary implementation of the SAMI emissions control scenarios. SHEN is greatly impacted by emissions from Great Lake states, mid-Atlantic states, and southeastern States (see Section IV-C), and is located between the borders of the respective regional planning areas for those states. The park's geographic location and impacted status demonstrates the need for significant trans-boundary communication and multi-stakeholder collaboration in development of clean air strategies. Since there are relatively few Class I national parks or wilderness areas in the eastern United States, the SHEN Assessment can serve as a "subregional case study" in the air policy, planning, scientific, and educational arenas at national, regional, and state levels. This assessment will also be a valuable tool in the park's resource stewardship, science, interpretation, education, and outreach programs.

C. LEGAL RESPONSIBILITIES AND MANAGEMENT POLICIES

The following is an explanation of how the NPS Organic Act, the CAA (as amended in 1977 and 1990), other pertinent environmental laws, and policies relate to air resource management on NPS lands, including SHEN. Key elements of these laws and policies are summarized below.

1. National Park Service Organic Act

In 1916, Congress created a new Federal agency in the U.S. Department of the Interior (DOI), the NPS, to manage and protect the National Park System. The general mandate of the 1916 Organic Act states that the NPS will:

> "promote and regulate the use of…national parks…by such means and measures as conform to the fundamental purpose of the said parks…which purpose is to conserve the scenery and the natural and historic objects and wildlife therein and to provide for the enjoyment of the same in such manner and by such means as will leave them unimpaired for the enjoyment of future generations" (16 USC 1).

The Organic Act and its 1970 and 1978 amendments do not directly address air pollution effects; however, they do specify what resources should be protected in the National Park System. The 1978 amendments further clarify the importance Congress placed on protecting park resources:

> "The authorization of activities shall be construed and the protection, management, and administration of these areas shall be conducted in light of the high public value and integrity of the National Park System and shall not be exercised in derogation of the values and purposes for which these various areas have been established, except as may have been or shall be directly and specifically provided by the Congress" (16 USC 1a-1).

2. Enabling Legislation for Shenandoah National Park

Interest in preserving lands in the southern Appalachians actually began even before the Organic Act was established. Shortly after the creation of the NPS in 1916, Director Stephen T. Mather began studying and advocating the creation of national parks in the East. In 1923, he proposed that a typical section of the Appalachian Mountains be established as a national park. In 1924, the Secretary of the Interior appointed the Southern Appalachian National Park Committee to investigate the possible existence of sites suitable for the establishment of such a park. The Committee commented as follows in their 1924 report:

> "The Blue Ridge of Virginia, one of the sections which had your committee's careful study, while secondary to the Great Smokies in altitude and some other features, constitute [sic], in our judgement, the outstanding and logical place for the creation of the first national park in the southern Appalachians.
>
> It will surprise the American people to learn that a national park site with fine scenic and recreational qualities can be found within a three-hour ride of our National Capitol and within a day's ride of 40,000,000 of our inhabitants. It has many canyons and gorges, with beautiful cascading streams. It has some

> splendid primeval forests, and the opportunity is there to develop an animal refuge of national importance… this area is full of historic interest, the mountains looking down on valleys with their…battlefields of Revolutionary and Civil War periods…and the birthplaces of many…Presidents…
>
> The greatest single feature, however, is a possible sky-line drive along the mountain top following a continuous ridge and looking down westerly on the Shenandoah Valley…and also commanding a view of the Piedmont Plain stretching easterly to the Washington Monument, which landmark of our National Capitol may be seen on a clear day. Few scenic drives in the world could surpass it."

Shortly following the Committee's report, an effort to formally establish SHEN began.

The enabling legislation for SHEN was passed in 1926 and provided for management and protection of the park by the NPS under the direction of the Secretary of the Interior, subject to the provisions of the 1916 NPS Organic Act, and subject to exemption from the 1920 Federal Water Power Act. SHEN was not actually created until 1935, after sufficient lands were acquired and donated by the Commonwealth of Virginia. The remainder of this section provides more specific legal (NPS 1994) and policy (NPS 2000a,b; SHEN 2001) information guiding an integrated approach to air resource management at SHEN.

3. Government Performance and Results Act

The 1993 Government Performance and Results Act was enacted to bring the Federal government into a contemporary performance management system that is mission- and results-oriented. This law requires Federal agencies to develop: 1) a Strategic Plan, 2) Annual Performance Plans, and 3) Annual Performance Reports in order to more effectively and efficiently manage their activities to achieve their missions, and to more effectively communicate with the Congress and the American people. The NPS developed its first Strategic Plan in 1997. Key NPS mission goals related to air resource management include:

- Natural and cultural resources and associated values are protected, restored, and maintained in good condition and managed within their broader ecosystem and cultural context, and

- NPS contributes to knowledge about natural and cultural resources and their associated values; management decisions about resources and visitors are based on adequate scholarly and scientific information.

The current NPS Strategic Plan is available on the internet at http://planning.den.nps.gov. The current Annual Performance Report for the NPS Air Quality Program is also available on the internet at http://www2.nature.nps.gov/ard.

Air pollution and associated resource impacts are integral parts of SHEN's Resource Management Plan and Strategic Management Plan. The Mission Statement of the park's Strategic Management Plan that was first developed in 1997 is:

> "Shenandoah National Park restores, where appropriate, and maintains the park as a functioning ecosystem that is the outstanding representative of the Blue Ridge/Central Appalachian biome. The park provides present and future generations outstanding opportunities to experience "recreation and re-creation" by driving the Skyline Drive, walking the Appalachian Trail and related trails, or experiencing the backcountry wilderness areas. The park preserves the fabric and tells the stories of the people and the land both before the park was established and as a result of the establishment of the park."

The SHEN Mission Goals most pertinent to air resource management include:

- Ecological integrity of this portion of the Blue Ridge/Central Appalachian biome is protected, maintained and restored as appropriate.

- Views of the Shenandoah Valley and Piedmont Plain, as seen from the park, are scenic and rural in character, and maintained in partnership with and integrating the needs of the surrounding communities.

- Visitors safely enjoy and are satisfied with the availability, accessibility, diversity and quality of park facilities; services; and appropriate recreational and "re-creational" opportunities.

Air resources and related values are also integral parts of the park's interpretation, education, and outreach programs. The SHEN Comprehensive Interpretive Plan (SHEN 2001) identifies primary parkwide interpretive themes that define the most important ideas or concepts to be communicated to the public about the park:

Primary Theme A. "Shenandoah National Park is a managed land area, representative of the central Appalachian biome, where science and law are the basis for making informed decisions to protect natural and human values inherent in the ecosystem."

Primary Theme B. "Shenandoah National Park was created and developed to bring the traditional national park experience to the densely populated east, and thereby generate support for the NPS mission of preserving America's heritage for all to enjoy."

4. Clean Air Act

The CAA of 1970 was enacted to protect public health and welfare from the harmful effects of human-made air pollution. Criteria pollutants are those pollutants for which the U.S. EPA has established NAAQS as directed by the CAA (Table I-1). Standards were established for the pollutants that are emitted in significant quantities throughout the country and that may endanger public health and welfare. The primary NAAQS are designed to protect human health while the secondary NAAQS are designed to protect public welfare from the adverse effects of the pollutant. The CAA defines public welfare effects to include, but not be limited to, "effects on soils, water, crops, vegetation, manmade materials, animals, wildlife, weather, visibility and climate, damage to and deterioration of property, and hazards to transportation, as well as effects on economic values and on personal comfort and well-being." The standards are defined in terms of deposition averaging times, such as annual or hourly, depending on the type of exposure associated with health and welfare effects. For some pollutants, there are both short-term and long-term standards. Criteria pollutants include O_3, carbon monoxide (CO), nitrogen dioxide (NO_2), SO_2, particulate matter less than 10 µm (PM_{10}), particulate matter less than 2.5 µm ($PM_{2.5}$), and lead. Data on criteria pollutants collected by a national monitoring system are used to determine if the NAAQS are met and to track pollutant trends. On July 17, 1997, the U.S. EPA announced changes to the NAAQS for O_3 and particulate matter. The U.S. EPA is phasing out the 1-hour O_3 standard, and replacing it with an 8-hour standard. For particulate matter, a standard for $PM_{2.5}$ has been added while retaining the PM_{10} standard. The U.S. EPA determined that these changes were necessary to protect public health and the environment.

In order to protect human health and welfare, the U. S. EPA has established primary and secondary O_3 NAAQS for maximum allowable O_3 concentration levels. Prior to 1997, these standards were based upon 1-hour average O_3 measurements. They were revised in 1997, when the U.S. EPA promulgated new standards, both primary and secondary, based upon an 8-hour average value. Under this rule, the annual fourth-highest daily maximum 8-hour O_3 concentration, averaged over three years, must not exceed 0.08 ppm (parts per million; 80 ppbv, which can be rounded up to 85 ppbv). This average is computed by first determining the highest 8-hour average O_3 value for each day of the year, and then identifying the 4th-highest of all daily maximum 8-hour O_3 values that occurred during the year. These 4th-highest values are then averaged over three successive years to determine the final concentration value that is compared to the standard. Because of rounding procedures, the U.S. EPA has indicated that 85 ppbv is the

Table I-1. National Ambient Air Quality Standards, published by the U.S. Environmental Protection Agency, in connection with the Clean Air Act and 40 CFR, Part 50.

Pollutant	Primary Standard		Secondary Standard	
	ug/m^3	ppm	ug/m^3	ppm
Carbon Monoxide				
8-hour concentration	10,000[a]	9[a]		
1-hour concentration	40,000[a]	35[a]		
Sulfur Dioxide				
Annual arithmetic mean	80	0.03		
24-hour concentration	365[a]	0.14[a]		
3-hour concentration			1300[a]	0.50[a]
Nitrogen Dioxide				
Annual arithmetic mean	100	0.053	Same as primary	
Ozone				
8-hour concentration	157[b]	0.08[b]	Same as primary	
1-hour concentration	235[c]	0.12[c]		
Lead				
Quarterly arithmetic mean	1.5		Same as primary	
Particulate Matter				
$PM_{2.5}$				
Annual arithmetic mean	15[d]			
24-hour concentration	65[e]			
PM_{10}			Same as primary	
Annual arithmetic mean	50[d]			
24-hour concentration	150[f]			

[a] Not to be exceeded more than once a year
[b] 3-year average of the 4th highest 8-hour concentration may not exceed 0.08 ppm
[c] Areas in nonattainment with the 1-hour standard must meet that standard before demonstrating attainment with the 8-hour standard.
[d] Based on a 3-year average of annual averages
[e] Based on a 3-year average of annual 98th percentile values
[f] Based on a 3-year average of annual 99th percentile values

lowest concentration that would exceed the 80 ppbv standard. The new secondary standard is identical to the primary standard.

The CAA (1977 Amendments) designated all national parks over 6,000 acres that were in existence as of August 7, 1977, as mandatory "Class I" areas. All other parks in existence at that time and all parks established since this date are designated as “Class II”, regardless of size. Class I areas, including SHEN, are afforded the greatest degree of air quality protection. The CAA assigns FLMs of Class I areas:

> "…an affirmative responsibility to protect air quality related values from adverse impacts due to manmade air pollution" (42 USC #7475(d)(2)(B)

The CAA legislative history further instructs FLMs to:

> "…assume an aggressive role in protecting the air quality related values of Class I areas from adverse impact…In cases of doubt the land manager should err on the side of protecting the air quality related values for future generations." (Senate Report No. 95-127, 95th Congress, 1st Session, 1977)

Congress placed special emphasis on visibility protection by setting a National Visibility Goal in the CAA:

> "…the prevention of any future, and the remedying of any existing, impairment of visibility in mandatory Class I Federal areas which impairment results from man-made air pollution…" (Section 169A(a)(1))

The 1977 amendments also require states to specifically address this goal in their State Implementation Plans (SIP), and to include Best Available Retrofit Technology (BART) for the appropriate emission sources.

The CAA as amended in 1977 also established the Prevention of Significant Deterioration (PSD) program. The primary objective of the PSD provisions is to prevent substantial degradation of air quality in areas that comply with NAAQS, and yet maintain a margin for industrial growth. A PSD permit from the appropriate air regulatory agency is required to construct a new pollution source or modify an existing source (Bunyak 1993). A permit application must demonstrate that the proposed polluting facility will 1) not violate national or state ambient air quality standards, 2) use the best available control technology to limit emissions, 3) not violate either Class I or Class II PSD increments for SO_2, NO_2, or particulate matter (Table I-2), and 4) not cause or contribute to adverse impacts to AQRVs in any Class I area (Peterson et al. 1992). The PSD increments are allowable pollutant concentrations that can be added to baseline concentrations.

The values chosen as PSD increments by Congress were not selected on the basis of concentration limits causing impacts to specific resources. Therefore, it is possible that pollution increases exceeding the legal Class I increments may not cause damage to Class I areas. It is also possible that resources in a Class I area could be adversely affected by pollutant concentrations that do not exceed the increments. The role of the FLM is to determine if there is potential for additional air pollution to cause damage to sensitive receptors whether or not the

Table I-2. Prevention of significant deterioration increments (in $\mu g/m^3$).[a]

Constituent	Averaging Time	Class I	Class II	Class III
Sulfur Dioxide	Annual Arith. Mean	2	20	40
	24-hour	5	91	182
	3-hour	25	512	700
PM_{10}	Annual Arith. Mean	4	17	34
	24-hour	8	30	60
Nitrogen Dioxide	Annual Arith. Mean	2.5	25	50

[a] PSD increments are not defined for ozone, $PM_{2.5}$, lead, or carbon monoxide.

PSD increments have been exceeded. Even if a proposed facility is not expected to violate Class I increments, the FLM can still recommend denial for a permit by demonstrating that there will be adverse impacts in the Class I area. Provisions for mitigation can be recommended by the FLM to the agency that issues permits.

The following questions may be addressed when reviewing PSD permit applications:

- What are the identified sensitive AQRVs in each Class I area that could be affected by the new source?
- What are the air pollutant levels that may affect the identified sensitive AQRVs?
- Will the proposed facility result in pollutant concentrations or atmospheric deposition that will cause the identified critical level to be exceeded or add to levels that already exceed the critical level?
- If the critical level is exceeded, what amount of additional pollution is considered "insignificant"?

The first two questions are largely land management issues that should be answered on the basis of management goals and objectives for the Class I area. The last two are technical and policy questions that must be answered on the basis of analyses of projected emissions from the proposed facility and predictions of environmental response to given pollutant concentrations (Peterson et al. 1992).

The U.S. EPA promulgated regulations in 1980 to address visibility impairment that is “reasonably attributable” to one or a small group of sources. Congress subsequently added section 169B as part of the CAA 1990 Amendments to focus attention on regional haze issues. On July 1, 1999, the U.S. EPA promulgated the Regional Haze Rule (RHR), which requires states (and tribes who choose to participate) to review how pollution emissions within the state

affect visibility at "Class I" areas across a broad region (not just Class I areas within the state). These rules also require states to make "reasonable progress" in reducing any effect this pollution has on visibility conditions in Class I areas and to prevent future impairment of visibility. The states are required by the rule to analyze a pathway that takes the Class I areas from current conditions to "natural conditions" in 60 years. "Natural conditions" is a term used in the CAA, which means that no human-caused pollution can impair visibility. This program, while aimed at Class I areas, will improve regional visibility throughout the country. In 2002, industry successfully challenged the BART portion of the RHR, which addresses older industrial sources. The U.S. EPA is currently in the process of updating that portion of the rule.

In Title IV of the 1990 CAAA, Congress called for the decrease of annual emissions of SO_2 and NO_x from utilities burning fossil fuels. The legislation specifically required a 10 million ton reduction (from 1980 levels) in annual SO_2 emissions and a 2 million ton reduction in NO_x emissions from utilities by the year 2010.

5. Clean Air Act Implementation Developments

On September 18, 1990, a preliminary notice of adverse impact on SHEN was published in the *Federal Register* by the Office of the Secretary, U.S. DOI (U.S. Dept. Interior 1990). This notice announced the preliminary determination by the Assistant Secretary for Fish and Wildlife and Parks, as the FLM of SHEN, that in accordance with the PSD air quality requirements of the CAA, the air pollution emissions from a proposed major emitting facility (1 of 19 new power plants proposed near the park) could contribute to or exacerbate adverse impacts on the AQRVs of this PSD Class I area. The FLM also recommended that the Virginia Department of Air Pollution Control not issue a permit to the facility unless measures were taken to ensure that this proposed source would not contribute to adverse impacts on park resources.

A technical support document was prepared by the ARD of the NPS and by SHEN in September 1990 in support of the adverse impact determination (National Park Service 1990). That review document supported the FLM's preliminary determination that:

> "although the Class I increments may not be exceeded at Shenandoah National Park, the increase in emissions resulting from the proposed PSD facilities will, together with the already permitted emissions, have an unacceptable adverse impact on visibility and other air quality related values in Shenandoah National Park. Visibility, aquatic, and terrestrial resources at Shenandoah National Park are currently being adversely affected by air pollution. The FLM reasonably believes that the effects of the additional sulfur dioxide, nitrogen oxide, and

> volatile organic compounds emissions associated with the electric generating stations proposed for the area would contribute to and exacerbate the existing adverse effects and are therefore unacceptable. In particular, increases in SO_2 and NO_x emissions associated with the pending permit applications are highly likely to (1) exacerbate existing adverse visibility conditions at Shenandoah National Park and cause a perceptible further degradation in park visibility; (2) hasten the acidification of sensitive streams within the park, with resulting effects on aquatic life; and (3) threaten sensitive park vegetation. The proposed increases in VOC and NO_x emissions will contribute to already high ozone levels, at times already higher than the national standard, and impacts on ozone sensitive vegetation."

The Virginia Department of Air Pollution Control issued a permit to the major emitting facility and it was appealed by environmental groups. The source was never built. Adverse impact determinations at SHEN (1990) and the Great Smoky Mountains National Park (1992) triggered the creation of two collaborative air quality planning bodies, SAMI (SAMI 2002) and the Interagency Work Group on Air Quality Models (U.S. EPA 1998a). In 1993, the NPS entered into a Memorandum of Understanding (MOU) with the Virginia Department of Air Pollution Control (since renamed the Virginia Department of Environmental Quality) regarding air permitting procedures. Although this MOU expired in 1998, the Virginia Department of Environmental Quality continues to honor its provisions at this writing.

In May 1998, the U.S. EPA issued the Interim Air Quality Policy on Wildland and Prescribed Burning, for FLMs and air regulators. Objectives of the new policy include avoidance of public health effects from increased prescribed burning and improvement of visibility in Class I areas. States are required by the policy to develop Smoke Management Programs. Virginia issued revised Smoke Management Guidelines in June 1998. The objectives of Virginia's guidelines were to: 1) identify and avoid smoke-sensitive areas, 2) reduce emissions, and 3) disperse and dilute smoke before it reaches smoke-sensitive areas. Air resource and fire management specialists are cooperating on a revision to the 1993 SHEN Fire Management Plan to ensure consistency with current air regulatory policies, regulations, and prescribed burning permitting requirements. In May 2001, Federal and state air regulators and FLMs agreed that natural fire emissions baselines required under the Regional Haze Rule would include certain amounts and types of management ignitions.

In June 2000, Virginia recommended to the U.S. EPA that about one-third of SHEN (parkland only in Page and Madison counties) be designated as a preliminary O_3 nonattainment area per the 1997 O_3 8-hour NAAQS and 1997-1999 O_3 levels recorded at the park's monitor at

Big Meadows. The U.S. EPA presumptive nonattainment boundaries included an additional 10% of parkland in Warren County for a total (Virginia and U.S. EPA) of 43% of the park. In May 2001, the U.S. Supreme Court generally upheld the U.S. EPA's 1997 O_3 8-hour and $PM_{2.5}$ NAAQS but delayed implementation until EPA addressed certain remanded issues. The U.S. EPA resolved these issues and established a final deadline of July, 2003 for recommendations from the states regarding O_3 nonattainment, and a deadline of July, 2004 for official designations by the U.S. EPA. In November, 2002, Virginia reaffirmed the Commonwealth's intent to recommend to the U.S. EPA in 2003 that the Page and Madison County portions of SHEN be designated as an O_3 nonattainment area. If Virginia or the U.S. EPA officially designates any of the park as an O_3 nonattainment area, SHEN managers must ensure that transportation and general management projects emitting O_3 precursors in the affected area are in compliance with Virginia's plan to attain and maintain the 8-hour O_3 standard.

On July 19, 2000, the U.S. DOI requested that the U.S. EPA initiate a rulemaking proceeding to restore and protect AQRVs in national parks and wilderness areas. Subsequently, the U.S. EPA posted a notice in the *Federal Register* soliciting public comments on the rulemaking requests from the U.S. DOI and several northeastern states (65 Fed. Reg. 48699-48701). Technical support documents were prepared by the NPS (NPS 2000c) and the USFWS and submitted to the U.S. EPA on December 6, 2000. These documents synthesized available scientific information regarding air pollution effects on natural resources in several units of the National Park System (including SHEN) and National Wildlife Refuge System. The NPS has observed chronic and episodic acidification of streams in both SHEN and Great Smoky Mountains National Park, as well as foliar injury from O_3 and visibility impairment in many park units. For further information, see the supporting technical documents at www2.nature.nps.gov/ard/epa. The NPS continues to work with the U.S. EPA to address Class I AQRV issues.

As indicated in Table I-1, secondary NAAQS for all criteria pollutants have not been proposed. Instead, the U.S. EPA has offered other policy tools to supplement NAAQS secondary implementation. For example, the 1997 O_3 8-hour and $PM_{2.5}$ NAAQS were supplemented with the 1998 NO_X SIP Call, the 1999 Regional Haze Rule, and the 2001 BART Rule. In addition, for O_3 secondary NAAQS, the U.S. EPA has also committed to sponsoring additional research regarding effects of O_3 on sensitive vegetation. It is not known at this time if the EPA will promulgate secondary standards for any of the other criteria pollutants.

6. Federal Water Pollution Control (Clean Water) Act

The Clean Water Act is summarized here because, like the Clean Air Act, it provides an additional tool to help the park meet NPS Organic Act mandates as well as NPS and SHEN management policies (I.C.8-9). The impaired streams and antidegradation sections of this law are pertinent to this assessment. Several acidified park streams may qualify for impaired streams listing and several others may be designated by Virginia as exceptional waters.

The Federal Water Pollution Control Act, commonly known as the Clean Water Act, was promulgated in 1972, and significantly amended in 1977, 1987, and 1990. The primary purpose of the act is to protect and to restore the physical, chemical, and biological quality of the nation's waters. Goals established by the act are to make all navigable waters "fishable and swimmable", and to eliminate the discharge of pollutants into the nation's waterways.

Congress recognized the primary role of the individual states in managing and regulating the quality of the nation's waters under the general framework provided by the Clean Water Act, and further defined by U.S. EPA regulations. All Federal agencies must comply with the requirements of state law for water quality management, regardless of other jurisdictional status or land ownership.

States manage and protect water quality through the development and enforcement of ambient water quality standards. Water quality standards are composed of the following three interrelated parts: 1) designated beneficial uses of a waterbody, such as contact recreation or cold water fishery; 2) numerical or narrative criteria that establish the limits of physical, chemical, and biological characteristics of water sufficient to protect beneficial uses; and 3) an antidegradation provision to protect water quality that exceeds criteria and to protect and maintain water quality in "Outstanding National Resource Waters", including certain waters in national parks and wildlife refuges. States comply with water quality standards by controlling the type and quantity of point source pollutants entering waters through the National Pollutant Discharge Elimination System, and implementing Best Management Practices for nonpoint sources of pollution. Section 303(d) of the act requires states to also formally identify waters that do not currently meet water quality standards, and bring them into compliance through the development and implementation of Total Maximum Daily Loads (TMDLs). The TMDL establishes the maximum loadings of pollutants that a waterbody can receive from point and nonpoint (including atmospheric deposition) sources of pollution without exceeding the standards.

Water quality standards for Virginia are developed and promulgated by the Virginia Department of Environmental Quality through the Virginia Administrative Code. Virginia has designated all of its waters for the following uses: recreational uses, e.g., swimming and boating; the propagation and growth of a balanced, indigenous population of aquatic life, including game fish, which might reasonably be expected to inhabit them; wildlife; and the production of edible and marketable natural resources, e.g., fish and shellfish.

Virginia's numeric criteria for three important parameters, dissolved oxygen, pH, and maximum temperature, are variable and categorized into the following "classes":

I. Open Ocean
II. Estuarine Waters (Tidal Water- Coastal Zone to Fall Line)
III. Nontidal Waters (Coastal and Piedmont Zones)
IV. Mountainous Zone Waters
V. Stockable Trout Waters
VI. Natural Trout Waters
VII. Wetlands

The waters of SHEN are placed into three of these classes. Tributaries to the Rappahannock and James Rivers and the South Fork of the Shenandoah River are classified as mountainous zone waters (Class IV), except those specifically classed as stockable trout waters (Class V) or natural trout waters (Class VI). No waters within SHEN have been formally identified as impaired, although long-term acid-base streamwater chemistry data collected under SWAS suggest that several park streams likely qualify for impaired stream (303[d]) listing per the water pH data parameter.

Virginia's antidegradation policy classifies water quality at three levels or "tiers":

- Tier 1 specifies that existing in-stream water uses and the level of water quality to protect the existing uses shall be maintained and protected. This means that, at a minimum, all waters should meet adopted water quality standards.

- Tier 2 protects water that is of higher quality than specified water quality standards. Only in limited circumstances may water quality be lowered in these waters.

- Tier 3 includes exceptional waters for which new, additional, or increased discharge of sewage , industrial wastes, or other pollution are not allowed. These waters must be specifically listed in the regulation.

Currently, none of SHEN's streams have been designated by Virginia as Tier 3, or Outstanding National Resources Waters, to be afforded special protection under anti-degradation provisions of the Clean Water Act. In 2002, however, SHEN evaluated and submitted comments on several park streams proposed by Virginia for Tier 3 designation.

7. Wilderness Act

The Wilderness Act of 1964 established the National Wilderness Preservation System, composed of Federal lands designated as Wilderness Areas where visitors have the opportunity for solitude, study, and experience in a natural area. Wilderness is an area where:

> "the earth and its community of life are untrammeled by man, where man himself is a visitor who does not remain…an area of undeveloped Federal Land retaining its primeval character and influence…which is protected and managed so as to preserve its natural conditions" (16 USC 1131(c)).

In October 1976, Congress designated over 40% of SHEN (79,019 ha or 195,256 ac) as Wilderness. An additional 227 ha (560 ac) was designated as Wilderness in September 1978. The Wilderness Act and its implementing regulations charge Federal land management agencies to preserve the wilderness character of such areas under their jurisdiction, and to protect them from human-caused effects not specifically allowed by law. The Wilderness Act and implementing regulations do not directly address air pollution effects; however, they do specify what should be protected in Wilderness (the earth and its community of life) and to what degree (preserve natural conditions). Within this context, each component of the Wilderness resource is important in itself, as well as in terms of how it interacts with other ecosystem components. Acid-sensitive watersheds and streams having low acid neutralizing capacity (ANC) within the park are primarily located within designated Wilderness. Air pollutants have significantly altered the park's natural visibility conditions, biogeochemical processes, and biodiversity of acid-sensitive streams, and also threaten terrestrial ecosystems.

8. Other Pertinent Laws

Several other laws are summarized here because they provide pertinent resource stewardship mandates to the park. Scenery is fundamentally important to the purpose and national significance of SHEN, home to more miles of the Appalachian National Scenic Trail than any other national park. The Federally-endangered Shenandoah salamander (*Plethodon*

shenandoah) may be at risk from acidic deposition effects. It is important to restore visual air quality and protect the park's cultural landscapes and cultural resources either placed on (e.g., Skyline Drive) or determined eligible for (e.g., Appalachian National Scenic Trail), the National Register of Historic Places.

The 1968 National Trails System Act established a national system of recreational and scenic trails to provide for the ever-increasing outdoor recreation needs of an expanding population and to promote enjoyment and appreciation of the open-air, outdoor areas of the nation. Congress designated the roughly 2,100-mile (3,380 km) Appalachian Trail and the approximately 2,350-mile (3,807 km) Pacific Crest Trail as the initial National Scenic Trail. The 101-mile (155 km) portion of the Appalachian National Scenic Trail within SHEN was constructed along the crest of the Blue Ridge between 1926 and 1936. Today, the Appalachian National Scenic Trail forms the backbone of SHEN's trail system. It includes fine examples of early trail construction techniques and is the longest segment of the Appalachian National Scenic Trail within a national park.

The 1973 Endangered Species Act (Amended in 1978, 1982, and 1988) was enacted to provide effective, long-term protection for threatened and endangered species. The Shenandoah salamander, a small terrestrial salamander found only within SHEN, was listed as endangered by the Commonwealth of Virginia in October 1987 (Wynn 1991), and was designated as Federally endangered in August 1989 (54 FR 34464). Initially, the Shenandoah salamander was believed to be endangered exclusively by natural biological causes (e.g., competition with the red-backed salamander, *Plethodon cinereus*), indicating that this species would not benefit from preparation of a recovery plan. However, key human-related factors affecting SHEN, such as acidic deposition and forest defoliation associated with exotic insects, prompted the USFWS to prepare a recovery plan in cooperation with the NPS. The 1994 recovery plan also addressed routine park management and permitted activities (e.g., trail maintenance, fire management, camping), in order to minimize potential human impacts to the species.

The 1966 National Historic Preservation Act authorized the Secretary of the Interior to "expand and maintain a national register of districts, sites, buildings, structures, and objects significant in American history, architecture, archeology, and culture". In 1996, Skyline Drive and 69 historic overlooks along its 105-mile length, as well as associated developed areas at Simmons Gap, Lewis Mountain, Big Meadows, Skyland, Piney River, Pinnacles, Dickey Ridge, Park Headquarters, Elkwallow and South River Picnic Campground, Camp Rapidan, Corbin

Cabin, Mount Vernon, Iron Furnace, and the Shenandoah cultural landscape, including the 101-mile segment of the Appalachian National Scenic Trail, were placed on, or determined eligible for, the National Register of Historic Places. National significance of the Skyline Drive and Park Headquarters cultural landscapes reflects their association with the Civilian Conservation Corps, the Works Progress Administration, and the presence of several hundred architectural and landscape structures and features. The park's Strategic Plan includes a long-term goal to clear and maintain vegetation obscuring views from historic overlooks along Skyline Drive. Improving visual air quality by reducing haze-forming air pollution is an important complementary goal to restoring and protecting scenic, natural, and cultural resources and landscapes at SHEN.

9. National Park Service Management Policies

In carrying out their responsibilities under the 1916 National Park Service Organic Act and other pertinent statutes, all NPS officials and employees must be knowledgeable about the laws, regulations, and policies that pertain to their work. The NPS, like other Federal agencies, develops policy to interpret the ambiguities of the law and to fill in the details left unaddressed by Congress in statutes. Agency policy must be consistent with the Constitution, public laws, Executive Orders, and all other higher authorities.

The NPS Management Policies 2001 clarifies that the fundamental purpose of the National Park System established by the Organic Act begins with a mandate to conserve park resources and values (National Park Service 2000a). When there is a conflict between conserving resources and values and providing for enjoyment of them, conservation is given priority. The Management Policies prohibit impairment of park resources and values unless directly and specifically provided for by legislation or by the proclamation establishing the park. The Management Policies also recognize that parks are integral parts of larger regional environments, thereby increasing the importance of constructively managing external threats from non-agency as well as agency activities. Air resource management policies are summarized below:

- Seek to perpetuate the best possible air quality in parks to preserve natural and cultural resources, and sustain visitor enjoyment, human health, and scenic vistas
- Embrace affirmative responsibilities to protect AQRVs in Class I areas
- Proactively help states (and interested Tribes) achieve the National Visibility Goal

- Strive to protect integral vistas (specific views from Class I areas to outside the boundary of the Class I areas) through cooperative means
- Take advantage of opportunities to protect air quality in Class II areas
- Integrate air resource management requirements into NPS operations and planning to ensure environmental compliance of in-park air pollution sources
- Acquire and evaluate information needed to effectively participate in decision-making that affects park AQRVs
- Participate in the development of Federal, state, and local air pollution control plans and regulations
- Participate in permit application reviews for major new or modified air pollution sources and develop recommendations to permitting authority to mitigate adverse impacts
- Promote public understanding of park air quality issues through educational and interpretive programs

D. SCOPE

This report is based on a concern for the scenic resources, cultural landscape, and ecological integrity of SHEN. The legal and policy foundation, described above, addresses the pertinent Federal mandates and guidance that must be considered in upholding the NPS affirmative responsibility to restore and protect AQRVs in SHEN, which include water, aquatic biota, soil, vegetation, and visibility. The scientific foundation and scope are generally limited to addressing these known AQRVs and the key air pollutants that threaten: 1) aquatic resources (primarily from S and N deposition), 2) terrestrial resources (primarily from O_3 exposure and N and S deposition [including gaseous form]), and 3) visibility (primarily from fine particles suspended in the air). Estimates of the isolated effects of ground-level O_3 on trees and forests and acidification effects on aquatic biota may be conservative because they did not consider effects from other, potentially exacerbating, stresses. Exposure to trace metals, pesticides, radionuclides, and organic toxins are not addressed.

The fine particulate matter standard set by the U.S. EPA to protect public health and welfare is not addressed because, barring substantial increases in SO_2 or NO_x emissions in key states or source subregions affecting the park, SHEN air quality will likely meet this standard. Nitrate air concentrations are not addressed for visibility effects due to time and funding constraints and the

current dominant role of sulfate air concentrations. However, nitrate air concentrations would increase in relative importance under any air pollution control strategy that calls for substantial reductions in SO_2 emissions beyond the 1990 CAA. This assessment focuses on regional or uniform haze attributable to haze-forming emissions from numerous distant and local sources over a wide geographic area. Visibility degradation can also be caused by local sources and specific meteorological conditions that result in coherent plumes or layered hazes observed from park vistas. However, plumes and layered hazes are usually evaluated on a case-by-case basis, and robust data sets needed to support such analyses are generally not available.

The Enhanced Regional Acid Deposition Model (RADM) was selected for atmospheric modeling, in part because it was published and fully operational for strategic atmospheric modeling applications at the onset of this project. Time and funding constraints prohibited the supplementary use of the CALPUFF model for higher resolution in the park's local modeling domain. Critical loads are threshold amounts of pollutants at which specific potentially harmful effects on sensitive resources begin to occur. Target loads are pollutant levels at which it is believed that the environment will be protected to a specified level and/or over a specified period of time. Critical load ranges for N deposition are not addressed in this report, in part due to modeling limitations. Target loads entail policy decisions by the NPS and are therefore beyond the scope of this assessment.

Although the report attempts to assess many of the critical issues facing the park, partial coverage or absence of coverage of some topics should not be interpreted as a judgment that these topics are not important or relevant to the issue of air pollution effects. These omissions often reflect the lack of information on these topics rather than any reflection on their scenic or ecological significance.

IX. REFERENCES

Aber, J.D. and C.T. Driscoll. 1997. Effects of land use, climate variation and N deposition on N cycling and C storage in northern hardwood forests. Global Biogeochem. Cycles 11:639-648.

Aber, J. D. and C. A. Federer. 1992. A generalized, lumped-parameter model of photosynthesis, evapotranspiration and net primary production in temperate and boreal forest ecosystems. Oecologia 92:463-474.

Aber, J., W. McDowell, K. Nadelhoffer, A. Magill, G. Berntson, M. Kamakea, S. McNulty, W. Currie, L. Rustad, and I. Fernandez. 1998. Nitrogen saturation in temperate forest ecosystems. Bioscience 48:921-934.

Aber, J.D., S.V. Ollinger, and C.T. Driscoll. 1997. Modeling nitrogen saturation in forest ecosystems in response to land use and atmospheric deposition. Ecol. Model. 101:61-78.

Aber, J.D., A. Magill, S.G. McNulty, R.D. Boone, K.J. Nadelhoffer, M. Downs, and R. Hallett. 1995a. Forest biogeochemistry and primary production altered by nitrogen saturation. Water Air Soil Pollut. 85:1665-1670.

Aber, J.D., S.V. Ollinger, C.A. Federer et al. 1995b. Predicting the effects of climate change on water yield and forest production in the northeastern U.S. Climate Res. 5:207-222.

Aber, J.D., J.M. Melillo, K.J. Nadelhoffer, J. Pastor, and R.D. Boone. 1991. Factors controlling nitrogen cycling and nitrogen saturation in northern temperate forest ecosystems. Ecol. Appl. 1(3):303-315.

Aber, J.D., K.J. Nadelhoffer, P. Steudler, and J.M. Melillo. 1989. Nitrogen saturation in northern forest ecosystems: excess nitrogen from fossil fuel combustion may stress the biosphere. BioScience 39:378-386.

Adams, S. A. and C. T. Hackney. 1992. Ecological processes of the southeastern United States aquatic ecosystems. In Hackney, C. T., S. M. Adams and W. H. Martin (eds.). Biodiversity of the Southeastern United States Aquatic Communities. John Wiley and Sons, New York. 779 pp.

Agren, G.I. and E. Bosatta. 1988. Nitrogen saturation of terrestrial ecosystems. Environ. Pollut. 54:185-197.

Air Resource Specialists, Inc. 1996a. Standard Operating Procedures and Technical Instructions for Optec LPV-2 Transmissometer Systems.

Air Resource Specialists, Inc.. 1996b. Standard Operating Procedures and Technical Instructions for Optec NGN-2 Nephelometer.

Althshuller, A.P. and A.S. LeFohn. 1996. Background ozone in the planetary boundary layer over the United States. J. Air Waste Manage. Assoc. 46:134-141.

Altman, D., T. Bryant, M. Gardner, and D. Machin. 2000. Statistics with Confidence. BMJ Books, London.

Andersen, C.P. and P. T. Rygiewicz. 1995. Allocation of carbon in mycorrhizal *Pinus ponderosa* seedlings exposed to ozone. New Phytol. 131:471-480.

Andersen, C.P. and P. T. Rygiewicz. 1991. Stress interactions and mycorrhizal plant response: understanding carbon allocation priorities. Environ. Pollut. 73:217-244.

Andersen, C.P. and C. F. Scagel. 1997. Nutrient availability alters below-ground respiration of ozone-exposed ponderosa pine. Tree Phys. 17:377-387.

Andersen, C.P., W. E. Hogsett, R. Wessling, and M. Plocher. 1991. Ozone decreases spring root growth and root carbohydrate content in ponderosa pine the year following exposure. Can. J. For. Res. 21:1288-1291.

Aneja, V.P., S. Businger, Z. Li, C.S. Claiborn, and A. Murthy. 1991. Ozone climatology at high elevations in southern Appalachians. J. Geophys. Res. 96:1007-1021.

Badger, R.L. 1999. Geology Along Skyline Drive, Shenandoah National Park, Virginia. A Self-Guided Tour for Motorists. Falcon Publishing, Inc., Helena, MT. 100 pp.

Baker, L.A. 1991. Ion enrichment analysis for the Regional Case Studies Project. In: Charles, D.F. (ed.). Acidic Deposition and Aquatic Ecosystems: Regional Case Studies. Springer-Verlag, New York. pp. 641-644.

Baker, J.P. and S.W. Christensen. 1991. Effects of acidification on biological communities. In: Charles, D.F. (ed.). Acidic Deposition and Aquatic Ecosystems. Springer-Verlag, New York, pp. 83-106.

Baker, J.P., J. Van Sickle, C.J. Gagen, D.R. DeWalle, W.E. Sharpe, R.F. Carline, B.P. Baldigo, P.S. Murdoch, D.W. Bath, W.A. Kretser, H.A. Simonin, and P.J. Wigington, Jr. 1996. Episodic acidification of small streams in the northeastern United States: Effects on fish populations. Ecol. Appl. 6:422-437.

Baker, L.A., A.T. Herlihy, P.R. Kaufmann, and J.M. Eilers. 1991. Acidic lakes and streams in the United States: the role of acidic deposition. Science 252:1151-1154.

Baker, L.A., P.R. Kaufmann, A.T. Herlihy, and J.M. Eilers. 1990a. Current Status of Surface Water Acid-Base Chemistry. State of the Science SOS/T 9, National Acid Precipitation Program.

Baker, J. P., D. P. Bernard, S.W. Christensen, M.J. Sale, J. Freda, K. Heltcher, D. Marmorek, L. Rowe, P. Scanlon, G. Suter, W. Warren-Hicks, P. Welbourn. 1990b. Biological Effects of Changes in Surface Water Acid-base Chemistry. SOS/T Report 13. Acid Precipitation Assessment Program, Washington, DC.

Barmuta, L.A., S.D. Cooper, S.K. Hamilton, J.W. Kratz, and J.M. Melack. 1990. Responses of zooplankton and zoobenthos to experimental acidification in a high-elevation lake (Sierra Nevada, California, U.S.A.). Freshw. Biol. 23:571-586.

Beck, J. P. and P. Grennfelt. 1994. Estimate of ozone production and destruction over northwestern Europe. Atmos. Environ. 28:129-140.

Binkley, D. and D. Richter. 1987. Nutrient cycles and H^+ budgets of forest ecosystems. Adv. Ecol. Res. 16:1-51.

Binkley, D., C. Driscoll, H.L. Allen, P. Schoeneberger, and D. McAvoy. 1989. Acidic Deposition and Forest Soils: Context and Case Studies in the Southeastern U.S. Springer -Verlag Ecological Studies No. 72, New York. 149 p.

Binkley, D., D. Valentine, C. Wells, and U. Valentine. 1989. An empirical model of the factors contributing to 20-year decrease in soil pH in an old-field plantation of loblolly pine. Biogeochemistry 8:39-54.

Binkowski, F.S. and U. Shankar. 1995. The Regional Particulate Matter Model, 1. Model description and preliminary results. J. Geophys. Res., 100(26):191-209.

Binkowski, F.S., J.S. Chang, R.L. Dennis, S. Reynolds, P.J. Samson and J.D. Shannon. 1990. Regional Acid Deposition Modeling. NAPAP State of Science and Technology Report No. 3 in Acidic Deposition: State of Science and Technology, Volume 1, National Acid Precipitation Assessment Program, Washington D.C.

Böhm, M. 1992. Air quality and deposition. In Olson, R., D. Binkley, and M. Böhm (eds.) The Response of Western Forests to Air Pollution. Springer-Verlag, New York. pp. 63-152.

Brace, S. and D.L. Peterson. 1998. Tropospheric ozone distribution in the Mount Rainier region of the Cascade Mountains, U.S.A. Atmos. Environ. 32:3629-3637.

Brace, S. and D.L. Peterson. 1996. Spatial patterns of ozone exposure in Mt. Rainier National Park. In: Proceedings of the Meeting of the Air Waste Manage. Assoc. AWMA, Pacific Northwest Chapter, Spokane, WA.

Brace, S., D.L. Peterson, and D. Bowers. 1999. Ozone injury in vascular plants of the Pacific Northwest. USDA For. Serv. Gen. Tech. Rep. GTR-PNW-446.

Brakke, D.F., A. Henriksen, and S.A. Norton. 1989. Estimated background concentrations of sulfate in dilute lakes. Water Resour. Bull. 25:247-253.

Bricker, O.P. and K.C. Rice. 1989. Acidic deposition to streams – a geology-based method predicts their sensitivity. Environ. Sci. Technol. 23:379-385.

Brook, J.R., P.J. Samson, and S. Sillman. 1995a. Aggregation of selected three-day periods to estimate annual and seasonal wet deposition totals for sulfate, nitrate, and acidity. Part I: A synoptic and chemical climatology for eastern North America. J. Appl. Meteorol. 34:297-325.

Brook, J.R., P.J. Samson, and S. Sillman. 1995b. Aggregation of selected three-day periods to estimate annual and seasonal wet deposition totals for sulfate, nitrate, and acidity. Part II: Selection of events, deposition totals, and source-receptor relationships. J. Appl. Meteorol. 34:326-339.

Bugas, Jr., P.E., L.O. Mohn, and J.W. Kauffman. 1999. Impacts of acid deposition on fish populations in the St. Marys River, Augusta County, Virginia. Banisteria 13:191-200.

Bulger, A.J. 1986. Coincident peaks in serum osmolality and heat-tolerance rhythms in seawater-acclimated killifish (*Fundulus heteroclitus*). Physiol. Zool. 59(2):169-174.

Bulger, A.J., B.J. Cosby and J.R. Webb. 2000. Current, reconstructed past and projected future status of brook trout *(Salvelinus fontinalis)* streams in Virginia. Can. J. Fish. Aq. Sci. 57:1515-1523.

Bulger, A.J., B.J. Cosby, C.A. Dolloff, K.N. Eshleman, J.R. Webb, and J.N. Galloway. 1999. The "Shenandoah National Park: Fish in Sensitive Habitats (SNP: FISH)" Project Final Report. An Integrated Assessment of Fish Community Responses to Stream Acidification. National Park Service. 570 pages plus interactive computer model.

Bulger, A.J., B.J. Cosby and J.R. Webb. 1998. Acid Rain: Current and projected status of coldwater fish communities in the Southeastern U.S. in the context of continued acid deposition. Trout Unlimited, Arlington Virginia. 28 p.

Bulger, A.J., L. Lien, B.J. Cosby and A. Henriksen. 1993. Trout status and chemistry from the Norwegian thousand lake survey: statistical analysis. Can. J. Fish. Aq. Sci. 50(3):575-585.

Bull, K.R. 1992. An introduction to critical loads. Environ. Pollut. 77:173-176.

Bull, K.R. 1991. The critical loads/levels approach to gaseous pollutant emission control. Environ. Pollut. 69:105-123.

Bunyak, J. 1993. Permit application guidance for new air pollution sources. Natural Resources Report 93-09. U.S. Department of the Interior, National Park Service Report. B-79-2.

Bureau of Economic Analysis (BEA). 1995. Regional State Projections of Economic Activity and Population to 2045, Bureau of Economic Analysis, U.S. Department of Commerce, Washington, DC, July 1995.

Bytnerowicz, A. and N.E. Grulke. 1992. Physiological effects of air pollutants on western trees. In Olson, R.K., D. Binkley, and M. Böhm (eds.). Response of Western Forests to Air Pollution, Springer-Verlag, New York. pp. 183-233.

Bytnerowicz, A. M.E. Fenn, P.R. Miller, and M.J. Arbaugh. 1999. Wet and dry pollutant deposition to the mixed conifer forest. In Miller, P.R. and J.R. McBride (eds.). Oxidant Air Pollution Impacts in the Montane Forests of Southern California. Springer-Verlag, New York. pp. 235-269.

Bytnerowicz, A., K.E. Percy, G. Riechers, P. Padgett, and M. Krywult. 1998. Nitric acid vapor effects on forest trees: deposition and cuticular changes. Chemosphere 36:697-702.

California Air Resources Board. 2001. Buyers' Guide to Cleaner Cars, published on the web at http://arbis.arb.ca.gov/msprot/CCBG/ccbg.htm, March 13, 2001.

Cambell, R.W. 1981. Population Dynamics. In: Doane, C.C. and M.L. McManus (eds). The Gypsy Moth: Research Toward Integrated Pest Management. U.S. Department of Agriculture, Washington, D.C. pp. 65-214.

Carter, J.B. 1961. Soil survey of Rappahannock County, Virginia. USDA Soil Conservation Service. 85 pp.

Chang, J.S., F.S. Binkowski, N.L. Seaman, J.N. McHenry, D. Byun, P.J. Samson, W.R. Stockwell, C.J. Walcek, S. Madronich, P. Middleton, J.E. Pleim., and H.H. Lansford. 1990. The Regional Acid Deposition Model and engineering model, NAPAP SOS/T Report No. 4. In National Acid Precipitation Assessment Program: State of Science and Technology, Vol 1. National Acid Precipitation Assessment Program, Washington, D.C.

Chang, J.S., R.A. Brost, I.S.A. Isaksen, S. Madronich, P. Middleton,, W.R. Stockwell, and C.J. Walcek. 1987. A three-dimensional Eulerian acid deposition model: Physical concepts and formation. J. Geophys. Res. 92(14):681-700.

Chappelka, A.H. and B.I. Chevone. 1992. Tree response to ozone. In Lefohn, A.S. (ed.), Surface Level Ozone Exposures and their Effects on Vegetation. Lewis Publishers, Chelsea, MI. pp. 271-324.

Chappelka, A.H. and L.J. Samuelson. 1998. Ambient ozone effects on forest trees in the eastern United States: a review. New Phytol. 139:91-108.

Chestnut, L.G. and R.D. Rowe. 1990. Preservation Values for Visibility Protection at the National Parks. Final Report prepared for Office of Air Quality Planning and Standards, U.S. Environmental Protection Agency; and Air Quality Management Division, National Park Service. RCG/Hagler, Bailly, Inc., Boulder, CO.

Christophersen, N., H.M. Seip, and R.F. Wright. 1982. A model for streamwater chemistry at Birkenes, Norway. Water Resour. Res. 18:977-997.

Church, M.R. and J. Van Sickle. 1999. Potential relative future effects of sulfur and nitrogen deposition on lake chemistry in the Adirondack Mountains, United States. Water Resour. Res. 35:2199-2211.

Church, M.R., P.W. Shaffer, K.W. Thornton, D.L. Cassell, C.I. Liff, M.G. Johnson, D.A. Lammers, J.J. Lee, G.R. Holdren, J.S. Kern, L.H. Liegel, S.M. Pierson, D.L. Stevens, B.P. Rochelle, and R.S. Turner. 1992. Direct/Delayed Response Project: Future Effects of Long-Term Sulfur Deposition on Stream Chemistry in the Mid-Appalachian Region of the Eastern United States. U.S. Environmental Agency, EPA/600/R-92/186, Washington, DC. 384 pp.

Church, M.R., K.W. Thornton, P.W. Shaffer, D.L. Stevens, B.P. Rochelle, R.G. Holdren, M.G. Johnson, J.J. Lee, R.S. Turner, D.L. Cassell, D.A. Lammers, W.G. Campbell, C.I. Liff, C.C. Brandt, L.H. Liegel, G.D. Bishop, D.C. Mortenson, and S.M. Pierson. 1989. Future Effects of Long-Term Sulfur Deposition on Surface Water Chemistry in the Northeast and Southern Blue Ridge Province (Results of the Direct/Delayed Response Project). U.S. Environmental Protection Agency Environmental Research Laboratory, Corvallis, OR.

Cole, D.W., H. Van Miegroet, and N.W. Foster. 1992. Retention or loss of N in IFS sites and evaluation of relative importance of processes, pp. 196-199. In Johnson, D.W. and S.E. Lindberg (eds.). Atmospheric Deposition and Forest Nutrient Cycling. Ecological Studies 91, Springer-Verlag, New York.

Cooper, O.R. and J.L. Moody. 2000. Meteorological controls on ozone at an elevated eastern United States regional background monitoring site. J. Geophys. Res. 105:6855-6869.

Cooper, S.M. and D.L. Peterson. 2000. Tropospheric ozone distribution in western Washington. Environ. Pollut. 107:339-347.

Cooperative Institute for Research in the Atmosphere (CIRA), 2001, Graphics revised by Jeff Lemke (currently not in publication), Original graphics published in Malm W. C. 2000. Introduction to Visibility. Cooperative Institute for Research in the Atmosphere (CIRA). Colorado State University, Fort Collins, CO. ISSN: 0737-5352-40.

Cosby, B.J. and T.J. Sullivan. 2001. Quantification of dose response relationships and critical loads of sulfur and nitrogen for six headwater catchments in Rocky Mountain, Grand Teton, Sequoia, and Mount Rainier National Parks. Report 97-15-01. E&S Environmental Chemistry, Inc., Corvallis, OR.

Cosby, B.J., R.C. Ferrier, A. Jenkins and R.F. Wright. 2001. Modelling the effects of acid deposition: refinements, adjustments and inclusion of nitrogen dynamics in the MAGIC model. Hydrol. Earth Syst. Sci. 5:499-517.

Cosby, B.J., R.C. Ferrier, A. Jenkins, B.A. Emmett, R.F. Wright, and A. Tietema. 1997. Modelling the ecosystem effects of nitrogen deposition: Model of Ecosystem Retention and Loss of Inorganic Nitrogen (MERLIN). Hydrol. Earth Sys. Sci. 1:137-158.

Cosby, B.J., S.A. Norton, and J.S. Kahl. 1996. Using a paired-catchment manipulation experiment to evaluate a catchment-scale biogeochemical model. Sci. Tot. Environ. 183:49-66.

Cosby, B.J., R.F. Wright, and E. Gjessing. 1995. An acidification model (MAGIC) with organic acids evaluated using whole-catchment manipulations in Norway. J. Hydrol. 170:101-122.

Cosby, B.J., P.F. Ryan, J.R. Webb, G.M. Hornberger, and J.N. Galloway. 1991. Mountains of West Virginia. In: Charles, D.F. (Ed.). Acidic Deposition and Aquatic Ecosystems. Regional Case Studies. Springer-Verlag, New York. pp. 297-318.

Cosby, B.J., R.F. Wright, G.M. Hornberger, and J.N. Galloway. 1985a. Modelling the effects of acid deposition: assessment of a lumped parameter model of soil water and streamwater chemistry. Water Resour. Res. 21:51-63.

Cosby, B.J., R.F. Wright, G.M. Hornberger, and J.N. Galloway. 1985b. Modelling the effects of acid deposition: estimation of long-term water quality responses in a small forested catchment. Water Resour. Res. 21:1591-1601.

Cosby, B.J., G.M. Hornberger, J.N. Galloway, and R.F. Wright. 1985c. Time scales of catchment acidification: a quantitative model for estimating freshwater acidification. Environ. Sci. Technol. 19:1144-1149.

Cowling, E.B. and L.S. Dochinger. 1980. Effects of acidic precipitation on health and productivity of forests: USDA Forest Service Technical Report. PSW-43. pp. 165-173.

Cronan, C.S. and D.F. Grigal. 1995. Use of calcium/aluminum ratios as indicators of stress in forest ecosystems. J. Environ. Qual. 24:209-226.

Cronan, C.S. and C.L. Schofield. 1990. Relationships between aqueous aluminum and acidic deposition in forested watersheds of North America and northern Europe. Environ. Sci. Technol. 24:1100-1105.

Davis, D.D. and R.G. Wilhour. 1976. Susceptibility of woody plants to sulfur dioxide and photochemical oxidants. EPA Ecological Research Series, EPA-600/3-76-102.

Dennis, R.L., 1997. Using the Regional Acid Deposition Model to determine the nitrogen deposition airshed of the Chesapeake Bay watershed, in Baker, J.E. (ed.). Atmospheric Deposition of Contaminants to the Great Lakes and Coastal Waters, SETAC Press, Pensacola, Florida. pp 393-413.

Dennis, T. E., and A. J. Bulger. 1995. Condition factor and whole-body sodium concentration in a freshwater fish: evidence of acidification stress and possible ionoregulatory over-compensation. Water Air Soil Pollut. 85:377-382.

Dennis R.L. and R. Mathur. 2001. Airshed domains for modeling atmospheric deposition of oxidized and reduced nitrogen to the Neuse/Pamlico system of North Carolina. Hydrolog. Sci. Technol., Special Issue, 17(1-4):107-117.

Dennis, T.E., S.E. MacAvoy, M.B. Steg, and A.J. Bulger. 1995. The association of water chemistry variables and fish condition in streams of Shenandoah National Park (USA). Water Air Soil Pollut. 85:365-370.

Dennis, R.L., F.S. Binkowski, T.L. Clark, J.N. McHenry, S. Reynolds, and S.K. Seilkop. 1990. Evaluation of Regional Acid Deposition Models: Appendix 5F: Selected Applications of RADM (Part II). NAPAP State of Science and Technology Report No 5. In Acidic Deposition: State of Science and Technology, Volume 1. National Acid Precipitation Assessment Program, Washington D.C.

Dillon, P.J., R.A. Reid, and E. DeGrosbois. 1987. The rate of acidification of aquatic ecosystems in Ontario, Canada. Nature 329:45-48.

Dise, N.B. and R.F. Wright. 1995. Nitrogen leaching from European forests in relation to nitrogen deposition. For. Ecol. Manage. 71:153-161.

Dise, N.B., E. Matzner, and P. Gundersen. 1998. Synthesis of nitrogen pools and fluxes from European forest ecosystems. Water Air Soil Pollut. 105:143-154.

Doddridge, B. G., R. R. Dickerson, J. Z. Holland, J. N. Cooper, R. G. Wardell, and O. Poulida. 1991. Observations of tropospheric trace gases and meteorology in rural Virginia using an unattended monitoring system: Hurricane Hugo (1989), a case study. J. Geophys. Res. 96:9341-9360.

Driscoll, C.T. and R. Van Dreason. 1993. Seasonal and long-term temporal patterns in the chemistry of Adirondack lakes. Water Air Soil Pollut. 67:319-344.

Driscoll, C.T., G.B. Lawrence, A.J. Bulger, T.J. Butler, C.C. Cronan, C. Eager, K.L. Lambert, G.E. Likens, J.L. Stoddard, and K.C. Weathers. 2001a. Acidic Deposition in the Northeastern United States: Sources and inputs, ecosystem effects, and management strategies. Bioscience 51:180-198.

Driscoll, C.T., G.B. Lawrence, A.J. Bulger, T.J. Butler, C.C. Cronan, C. Eager, K.L. Lambert, G.E. Likens, J.L. Stoddard, and K.C. Weathers. 2001b. Acid Rain Revisited: Advances in scientific understanding since the passage of the 1970 and 1990 Clean Air Act Amendments. Hubbard Brook Research Foundation. Science Links Publication. Vol. 1, no. 1.

Driscoll, C.T., K.M. Postek, W. Kretser, and D.J. Raynal. 1995. Long-term trends in the chemistry of precipitation and lake water in the Adirondack region of New York, USA. Water Air Soil Pollut. 85:583-588.

Driscoll, C.T., G.E. Likens, L.O. Hedin, J.S. Eaton, and F.H. Bormann. 1989. Changes in the chemistry of surface waters. Environ. Sci. Technol. 23:137-143.

Duchelle, S.F., J.M. Skelly, T.L. Sharick, B.I. Chevone, Y-S. Yang, and J.E. Nellessen. 1983. Effects of ozone on the productivity of natural vegetation in a high meadow of the Shenandoah National Park of Virginia. J. Environ. Manage. 17:299-308.

Duchelle, S. F., J. M. Skelly, and B. I. Chevone. 1982. Oxidant effects on forest tree seedling growth in the Appalachian Mountains. Water Air Soil Pollut. 18: 363-373.

Eager, C., H. Van Miegroet, S.B. McLaughlin, and N.S. Nicholas. 1996. Evaluation of existing effects of acidic deposition on vegetation in the Southern Appalachians. Unpublished Report. Southern Appalachian Mountains Initiative, Asheville, NC.

EarthInfo, Inc., 1992. EARTHINFO's NCDC Summary of the Day, User's Manual. EarthInfo, Inc., Boulder, Colorado. 111 pp.

Edmunds, W.J., D.D. Rector, N.O. Wilson, and T.L. Arnold. 1986. Properties, Classification, and Upland Oak Site Quality for Residual Soils Derived from Shales, Phyllites, Siltstones, and Sandstones in Southwestern Virginia. Bulletin 86-5. July. Virginia Agricultural Experiment Station.

Elder, J.H. and D.E. Pettry. 1975. Soil Survey of Madison County, Virginia. USDA Soil Conservation Survey. 143 pp.

Elwood, J. W. 1991. Southeast Overview. In Charles, D.F. (ed.). Acidic Deposition and Aquatic Ecosystems. Springer-Verlag, New York. pp. 291-295.

Elwood, J.W., M.J. Sale, P.R. Kaufmann, and G.F. Cada. 1991. The Southern Blue Ridge Province. In Charles, D.F. (ed.). Acidic Deposition and Aquatic Ecosystems. Springer-Verlag, New York pp. 319-364.

Emmett, B.A., D. Boxman, M. Bredemeier, P. Gundersen, O.J. Kjønaas, F. Moldan, P. Schleppi, A. Tietema, and R.F. Wright. 1998. Predicting the effects of atmospheric nitrogen deposition in conifer stands: evidence from the NITREX ecosystem-scale experiments. Ecosystems 1:352-360.

Emmett, B.A., B.J. Cosby, R.C. Ferrier, A. Jenkins, A. Tietema, and R.F. Wright. 1997. Modelling the ecosystem effects of nitrogen deposition: simulation of nitrogen saturation in a Sitka spruce forest, Aber, Wales, UK. Biogeochemistry 38:129-148.

Emmett, B.A., B. Reynolds, P.A. Stevens, D.A. Norris, S. Hughes, J. Görres, and I. Lubrecht. 1993. Nitrate leaching from afforested Welsh catchments – Interactions between stand age and nitrogen deposition. Ambio 22:386-394.

Eshleman, K.N. 1988. Predicting regional episodic acidification of surface waters using empirical models. Water Resour. Res. 34:1118-1126.

Eshleman, K.N. and K.E. Hyer. 2000. Discharge and water chemistry at the three intensive sites. In: Bulger, A.J., B.J. Cosby, C.A. Dolloff, K.N. Eshleman, J.R. Webb, and J.N. Galloway. Shenandoah National Park: Fish in Sensitive Habitats. Project Final Report - Vol. II. Stream Water Chemistry and Discharge, and Synoptic Water Quality Surveys. pp. 51-92.

Eshleman, K.N., D.A. Fiscus, N.M. Castro, J.R. Webb, and F.A. Deviney, Jr. 2001. Computation and visualization of regional-scale forest disturbance and associated dissolved nitrogen export from Shenandoah National Park, Virginia. The Scientific World 1(S2):539-547.

Eshleman, K.N., J.L. Moody, K.E. Hyer, and F.A. Deviney. 1999. Episodic Acidification of Streams in Shenandoah National Park, Virginia. Final report to U.S. Dept. of Interior, NPS - Mid-Atlantic Region and NPS - Air Resources Division.

Eshleman, K.N., R.P. Morgan II, J.R. Webb, F.A. Deviney, and J.N. Galloway. 1998. Temporal patterns of nitrogen leakage from mid-Appalachian forested watersheds: Role of insect defoliation. Water Resour. Res. 34:2005-2016.

Eshleman, K.N., T.D. Davies, M. Tranter, and P.J. Wigington, Jr. 1995. A two-component mixing model for predicting regional episodic acidification of surface waters during spring snowmelt periods. Water Resour. Res. 31:1011-1021.

Estes, M.J. 1990. The chemical composition of cloud water in the Shenandoah National Park and its variation with long-range atmospheric transport and season. Masters Thesis, Department of Environmental Sciences, University of Virginia, Charlottesville.

Farmer, G.J. and F.W.H. Beamish. 1969. Oxygen consumption of *Tilapia nilotica* in relation to swimming speed and salinity. J. Fish Res. Bd. Can. 26:2807-2821.

Federal Land Managers' Air Quality Related Values Workgroup (FLAG). 2002. Guidance on Nitrogen and Sulfur Deposition Analysis Thresholds. Federal Land Managers Air Quality Related Values Work Group. Submitted by letter to S.W. Becker, Executive Director, STAPPA/ ALAPCO, from C.L. Shaver, Air Resources Division, National Park Service, and S.V. Silva, Air Quality Branch, U.S. Fish and Wildlife Service. Posted at www.aqd.nps.gov/ard/flagfree.

Federal Land Managers' Air Quality Related Values Workgroup (FLAG). 2000. Phase I Report. U.S. Forest Service-Air Quality Program, National Park Service - Air Resources Division, and U.S. Fish and Wildlife Service - Air Quality Branch.

Federer, C.A., J.W. Hornbeck, L.M. Tritton, C.W. Martin, R.S. Pierce, and C.T. Smith. 1989. Long-term depletion of calcium and other nutrients in eastern U.S. forests. Environ. Manage. 13:593-601.

Feger, K.H. 1992. Nitrogen cycling in two Norway spruce (*Picea abies*) ecosystems and effects of a $(NH_4)_2SO_4$ addition. Water Air Soil Pollut. 61:295-307.

Feldman, R., and E. Connor. 1992. The relationship between pH and community structure of invertebrates in streams of the Shenandoah National Park, Virginia, U.S.A. Freshw. Biol. 27:261-276.

Fenn, M.E. and P.H. Dunn. 1989. Litter decomposition across an air-pollution gradient in the San Bernardino Mountains. Soil Sci. Soc. Am. J. 53:1560-1567.

Fenn, M.E., M.A. Poth, J.D. Aber, J.S. Baron, B.T. Bormann, D.W. Johnson, A.D. Lemly, S.G. McNulty, D.F. Ryan, and R. Stottlemyer. 1998. Nitrogen excess in North American ecosystems: predisposing factors, ecosystem responses, and management strategies. Ecol. Appl. 8:706-733.

Fenn, M.E., M.A. Poth, and D.W. Johnson. 1996. Evidence for nitrogen saturation in the San Bernardino Mountains in southern California. For. Ecol. Manage. 82:211-230.

Ferrier, R.C., A. Jenkins, B.J. Cosby, R.C. Hall, R.F. Wright, and A.J. Bulger. 1995. Effects of future N deposition scenarios on the Galloway region of Scotland using a coupled sulphur and nitrogen model (MAGIC-WAND). Water Air Soil Pollut. 85:707-712.

Fievet, C.J. 2001. Application of the PnET-CN Terrestrial Ecosystem Model to Shenandoah National Park, Virginia. Distinguished Majors Thesis. Department of Environmental Sciences, University of Virginia, Charlottesville, VA.

Fiore, A.M., D.J. Jacob, I. Bey, R.M. Yantosca, B.D. Field, and A.C. Fusco. 2002. Background ozone over the United States in summer: Origin, trend, and contribution to pollution episodes. J. Geophys. Res. 107:D15.

Foster, N.W., J.D. Aber, J.M. Melillo, R.D. Bowden, and F.A. Bazazz. 1997. Forest response to disturbance and anthropogenic stress. BioScience 47:437-445.

Furman, T., P. Thompson, and B. Hatchl. 1998. Primary mineral weathering in the central Appalachians: A mass balance approach. Geochim. Cosmochim. Acta 62(17):2889-2904.

Galloway, J.N., F.A, Deviney, Jr., and J.R. Webb, 1999. Shenandoah Watershed Study Data Assessment: 1980-1993. Project Final Report, submitted to National Park Service, Luray, VA.

Galloway, J.N., G.E. Likens, and M.E. Hawley. 1984. Acid precipitation: natural versus anthropogenic components. Science 226:829-831.

Galloway, J.N., S.A. Norton, and M.R. Church. 1983. Freshwater acidification from atmospheric deposition of sulfuric acid: a conceptual model. Environ. Sci. Tech. 17:541-545.

Garner, J.H.B., T. Pagano, and E.B. Cowling. 1989. An evaluation of the role of ozone, acid deposition, and other airborne pollutants in the forests of eastern North America. Tech. Rept. SE-59. USDA Forest Service, Southeastern Forest Experiment Station, Asheville, NC. 172 pp.

Gathright, T.M. II. 1976. Geology of The Shenandoah National Park, Virginia. Virginia Division of Mineral Resources Bulletin 86, Charlottesville, VA. 93 pp.

Gilliam, F.S., M.B. Adams, and B.M. Yurish. 1996. Ecosystem nutrient responses to chronic nitrogen inputs at Fernow Experimental Forest, West Virginia. Can. J. For. Res. 26:196-205.

Goldan P.D., D.D. Parrish, W.C. Kuster, M. Trainer, S.A. McKeen, J. Holloway, B.T. Jobson, D.T. Sueper, and F.C. Fehsenfeld. 2000. Airborne measurements of isoprene, CO, and anthropogenic hydrocarbons and their implications. J. Geophys. Res. 105:9091-9105.

Grulke, N.E. 1999. Physiological responses of ponderosa pine to gradients of environmental stressors. In Miller, P.R. and J.R. McBride (eds.). Oxidant Air Pollution Impacts in the Montane Forests of Southern California. Springer-Verlag, New York. pp. 126-163.

Grulke, N.E., P.R. Miller, and D. Scioli. 1996. Response of giant sequoia canopy foliage to experimentally manipulated levels of atmospheric ozone. Tree Phys. 16:575-581.

Gundersen, P. 1992. Mass balance approaches for establishing critical loads for nitrogen in terrestrial ecosystems. Background document for UN-ECE workshop Critical Loads for Nitrogen, Lökeberg, Sweden, 6-10 April, 1992.

Hack, J.T. and J.C. Goodlett. 1960. Geomorphology and Forest Ecology of a Mountain Region in the Central Appalachians. Prof. Paper 347. U.S. Geol. Surv., Reston, VA.

Hallock-Waters, K. A. 2000. Trace gas observations over rural Virginia: Photochemistry and transport, Ph.D. dissertation, Dept. of Chemistry, University of Maryland, College Park, MD.

Hallock-Waters, K.A., B.G. Doddridge, R.R. Dickerson, S. Spitzer, and J.D. Ray. 1999. Carbon monoxide in the US Mid-Atlantic troposphere: Evidence for a decreasing trend. Geophys. Res. Letters 26:2861-2864.

Hansen, M.H., T. Frieswyk, J.F. Glover, and J.F. Kelly. 1992. The Eastwide forest inventory data base: Users manual. Gen. Tech. Rep. NC-151. U.S. Department of Agriculture, Forest Service, North Central Forest Experiment Station, St. Paul, MN. 48 p.

Harr, R.D. 1982. Fog drip in the Bull Run Municipal Watershed, Oregon. Water Resour. Bull. 18:785-789.

Heath, R.L. and G.E. Taylor. 1997. Physiological processes and plant responses to ozone exposure. In Sandermann, H., A.R. Wellburn, and R.L. Heath (eds.). Forest Decline and Ozone: A Comparison of Controlled Chamber and Field Experiments. Springer-Verlag, New York. pp. 310-368.

Heck, W.W. and E.B. Cowling. 1997. The need for a long-term cumulative secondary ozone standard. Air & Waste Management Association, Pittsburgh, PA, January, 1997. pp 22-33.

Hedin, L. O.; L. Granat; G.E. Likens; T.A. Bulshand; J.N. Galloway; T.J. Butler, and H. Rodhe. 1994. Steep declines in atmospheric base cations in regions of Europe and North America. Nature 367:351-354.

Henriksen, A. and D.F. Brakke. 1988. Increasing contributions of nitrogen to the acidity of surface waters in Norway. Water Air Soil Pollut. 42:183-201.

Herlihy, A.T., D.P. Larsen, S.G. Paulsen, N.S. Urquhart, and B.J. Rosenbaum. 2000. Designing a spatially balanced, randomized site selection process for regional stream surveys: the EMAP Mid-Atlantic Pilot Study. Environ. Monit. Assess. 63:95-113.

Herlihy, A.T., P.R. Kaufmann, J.L. Stoddard, K.N. Eshleman, and A.J. Bulger. 1996. Effects of acidic deposition on aquatic resources in the Southern Appalachians with a special focus on Class I wilderness areas. Report prepared for the Southern Appalachian Mountains Initiative (SAMI), Asheville, NC.

Herlihy, A.T., P.R. Kaufmann, M.R. Church, P.J. Wigington, Jr., J.R. Webb, and M.J. Sale. 1993. The effects of acid deposition on streams in the Appalachian Mountain and Piedmont region of the mid-Atlantic United States. Water Resour. Res. 29:2687-2703.

Hildebrand, E., J.M. Skelly, and T.S. Fredericksen. 1996. Foliar response of ozone-sensitive hardwood trees species from 1991 to1993 in Shenandoah National Park, Virginia. Can. J. For. Res. 26:658-669.

Hirsch, R.M. and J.R. Slack, 1984. A nonparametric trend test for seasonal data with serial dependence. Water Res. Res. 20:727.

Hirsch, A. I., J. W. Munger, D. J. Jacob, L,. W. Horowitz, and A. H. Goldstein. 1996. Seasonal variation of the ozone production efficiency per unit NOx at Harvard Forest, Massachusetts. J. Geophys. Res. 101:12,659-12,666.

Hirsch, R.M., J.R. Slack, and R.A. Smith. 1982. Techniques of trend analysis for monthly water quality analysis. Water Resour. Res. 18:107.

Hockman, J.R., J.C. McKinney, T.R. Burruss, D. Jones, R.E. Modesitt, L.G. Manhart, and W.R. Waite. 1979. Soil survey of Augusta County, Virginia. USDA Soil Conservation Service. 249 pp.

Hogsett, W. E., D. T. Tingey, C. Hendricks, and D. Rossi. 1989. Sensitivity of western conifers to SO_2 and seasonal interaction of acid fog and ozone. In: Olson, R. K. and A. S. Lefohn (eds.). Effects of Air Pollution on Western Forests. Transactions of the Air and Waste Management Society. Pittsburgh, PA. pp. 469-491.

Hogsett, W.E., M. Plocher, V. Wildman, D.T. Tingey, and J.P. Bennett. 1985. Growth response of two varieties of slash pine seedlings to chronic ozone exposures. Can. J. Bot. 63:2369-2376.

Hov, Ø. and B.A. Hjøllo, 1994. Transport distance of ammonia and ammonium in Northern Europe 2. Its relation to emissions of SO_2 and NO_x, J. Geophys. Res. 99:749-755.

Hyer, K.E. 1997. Episodic acidification of streams in Shenandoah National Park. Masters Thesis. Department of Environmental Sciences, University of Virginia.

Hyer, K.E., J. R. Webb, and K. N. Eshleman. 1995. Episodic acidification of three streams in Shenandoah National Park, Virginia, USA. Water Air Soil Pollut. 85:523-528.

Ingersoll, S.K. 1995. Differences in soil sulfate adsorption within a headwater catchment in Shenandoah National Park, Virginia. Masters Thesis. Department of Environmental Sciences, University of Virginia.

Innes, J.L. 1993. Forest Health: Its Assessment and Status. CAB International, Wallingford, UK.

Isphording, W. C. and J. F. Fitzpatrick, Jr. 1992. Geological and evolutionary history of drainage systems in the southeastern United States. In: Hackney, C. T., S. M. Adams and W. H. Martin (eds). Biodiversity of the Southeastern United States Aquatic Communities. John Wiley and Sons, New York. 779 pp.

Jacob D. J., L. Horowitz, J.W. Munger, B.G. Heikes, R.R. Dickerson, R.S. Artz, and W.C. Keene. 1995. Seasonal transition from NO_x- to hydrocarbon-limited conditions for ozone production over the eastern United States in September. J. Geophys. Res. 100:9315-9324.

Jacob, D. J., J. A. Logan, R. M. Yevich, G. M. Gardner, C. M Spivakovsky, S. C. Wofsy, J. W. Munger, S. Sillman, M. J. Prather, M. O. Rodgers, H. Westberg, and P. R. Zimmerman. 1993. Simulation of summertime ozone over North America. J. Geophys. Res. 98:14,797-14,816.

Jenkins, R. E. and N. M. Burkhead. 1993. Freshwater Fishes of Virginia. .American Fisheries Society, Bethesda, MD. 1079 pp.

Jenkins, A., R.C. Helliwell, P.J. Swingewood, C. Seftron, M. Renshaw, and R.C. Ferrier. 1998. Will reduced sulphur emissions under the Second Sulphur Protocol lead to recovery of acid sensitive sites in UK? Environ. Pollut. 99:309-318.

Jenkins, A., R.C. Ferrier, and B.J. Cosby. 1997. A dynamic model for assessing the impact of coupled sulphur and nitrogen deposition scenarios on surface water acidification. J. Hydrol. 197:111-127.

Johnson, D.W. and D.W. Cole. 1980. Mobility in soils: relevance to nutrient transport from forest ecosystems. Environ. Internat. 3:79-90.

Johnson, D.W. and S.E. Lindberg, eds. 1992. Atmospheric Deposition and Forest Nutrient Cycling: A Synthesis of the Integrated Forest Study. Springer-Verlag, New York. 707 pp.

Johnson, D.W. and D.E. Todd. 1990. Nutrient cycling in forests of Walker Branch Watershed Tennessee: roles of uptake and leaching in causing soil changes. J. Environ. Qual. 19:97-104.

Johnson, A.H., S.B. McLaughlin, M.B. Adams, and others. 1992. Synthesis and conclusions from epidemiological and mechanistic studies of red spruce decline. In: Eager, C. and M.B. Adams (eds.). Ecology and Decline of Red Spruce in the Eastern United States. Ecology Studies: Analysis and Synthesis. Vol. 96, Chapter 10. Springer-Verlag, New York. pp. 385-411.

Johnson, D.W., H. Van Miegroet, S.E. Lindberg, R.B. Harrison and D.E. Todd. 1991. Nutrient cycling in red spruce forests of the Great Smoky Mountains. Can. J. For. Res. 21:769-787.

Johnson, D.W., J.M. Kelly, W.T. Swank, D.W. Cole, H. Miegroet, J.W. Hornbeck, R.S. Pierce, and D. Van Lear. 1988. The effects of leaching and whole-tree harvesting on cation budgets of several forests. J. Environ. Qual. 17:418-424.

Joseph, D. B., and M. I. Flores. 1993. Statistical Summary of Ozone Measurements in the National Park System, 1981-1991. Volume II: Quick Look Yearly and Growing Season Frequency Distribution Reports, National Park Service, Technical Report NPS/NRAQD/NRTR-93/111.

Kaeser, A.J. and W.E. Sharpe. 2001. The influence of acidic run-off episodes on slimy sculpin reproduction in Stone Run. Trans. Amer. Fish Soc. 130:1106-1115.

Kahl, J.S., T.A. Haines, S.A. Norton, and R.B. Davis. 1993. Recent temporal trends in the acid-base chemistry of surface waters in Maine, USA. Water Air Soil Pollut. 67:281-300.

Kämäri, J., M. Amann, Y.-W Brodin, M.J. Chadwick, A. Henriksen, J.P. Hettelingh, J.C.I. Kuylenstierna, M. Posch, and H. Sverdrup. 1992. The use of critical loads for the assessment of future alternatives to acidification. Ambio 21:377-386.

Kang, D., V.P. Aneja, R. Mathur, and J. Ray. In review. Non-methane hydrocarbons and ozone In the rural southeast United States national parks: A model sensitivity analysis and its comparison with measurement. J. Geophys. Res. – Atmospheres.

Kang, D., V.P. Aneja, R.G. Zika, C. Farmer, and J.D. Ray. 2001. Non-methane hydrocarbons in the rural southwest US National Parks. J. Geophys. Res. 106:3133-3155.

Kasibhatla, P., H. Levy II, A. Klonecki, and W. L. Chameides. 1996. Three-dimensional view of the large-scale tropospheric ozone distribution over the North Atlantic Ocean during summer. J. Geophys. Res. 101:29,305-29,316.

Kauffman, J.W., L.O. Mohn, and P.E. Bugas, Jr.. 1999. Effects of Acidification on Benthic Fauna in St. Marys River, Augusta County, VA. Banisteria 13:183-190.

Kaufmann, P.R., A.T. Herlihy, J.W. Elwood, M.E. Mitch, W.S. Overton, M.J. Sale, J.J. Messer, K.A. Cougar, D.V. Peck, K.H. Reckhow, A.J. Kinney, S.J. Christie, D.D. Brown, C.A. Hagley, and H.I. Jager. 1988. Chemical Characteristics of Streams in the Mid-Atlantic and Southeastern United States. Volume I: Population Descriptions and Physico-Chemical Relationships. EPA/600/3-88/021a. U.S. Environmental Protection Agency, Washington, D.C.

Kauppi, P.E., K. Mielikäinen, and K. Kuusela. 1992. Biomass and carbon budget of European forests, 1971 to 1990. Science 256:70-74.

Kelso, J.R.M., M.A. Shaw, C.K. Minns, and K.H. Mills. 1990. An evaluation of the effects of atmospheric acidic deposition on fish and the fishery resource of Canada. Can. J. Fish. Aq. Sci. 47:644-655.

Kimmel, W.G., and D.J. Murphy. 1985. Macroinvertebrate community structure and detritus processing rates in two southern Pennsylvania streams acidified by atmospheric deposition. Hydrobiologia, 124:97-102.

Kirchner, J.W. and E. Lydersen. 1995. Base cation depletion and potential long-term acidification of Norwegian catchments. Environ. Sci. Technol. 29:1953-1960.

Kleinman, L.I. 1991. Seasonal dependence of boundary layer peroxide concentration: The low and high NOx regimes. J. Geophys. Res. 96(20)721-20,733.

Kobuszewski, D.M. and S.A. Perry. 1993. Aquatic insect community structure in an acidic and circumneutral stream in the Appalachian mountains of West Virginia. J. Freshw. Ecol. 8:37-45.

Kozlowski, T.T. and H.A. Constantinidou. 1986. Responses of woody plants to environmental pollution. For. Abstr. 47:1-51.

Kratz, K., S.D. Cooper, and J.M. Melack. 1994. Effects of single and repeated experimental acid pulses on invertebrates in a high altitude Sierra Nevada stream. Freshw. Biol. 32:161-183.

Kretser, W.A., J. Gallagher, and J. Nicolette. 1989. Adirondack Lakes Study 1984-1987: an evaluation of fish communities and water chemistry. Adirondack Lake Survey Corporation, Ray Brook, NY, USA.

Krupa, S. and W.J. Manning. 1988. Atmospheric ozone: formation and effects on vegetation. Environ. Pollut. 50:101-137.

Krupa, S.V., A.E.G. Tonneijck, and W.J. Manning. 1998. Ozone. In Flagler, R.B. (ed.). Recognition of Air Pollution Injury to Vegetation: A Pictorial Atlas, 2nd edition. Air Waste Manage. Assoc., Pittsburgh. pp. 2.1-2.28.

Langner J, and H. Rodhe, 1991. A global three-dimensional model of the tropospheric sulfur cycle. J. Atmos. Chem. 13:225-263.

Laurence, J.A., 1981. Effects of air pollutants on plant-pathogen interactions. Z. Pflanzenkr. Pflanzenschutz 88:156-172.

Laurence, J.A., W.A. Retzlaff, J.S. Kern, E.H. Lee, W.E. Hogsett, and D.A. Weinstein. 2001. Predicting the regional impact of ozone and precipitation on the growth of loblolly pine and yellow-poplar using linked TREGRO and ZELIG models. For. Ecol. Mgmt. 146:247-263.

Laurence, J.A., S.V. Ollinger, and P.B. Woodbury. 2000. Regional impacts of ozone on forest productivity. In: Mickler, R.A., R. Birdsey, and J. Hom (eds.). Responses of Northern Forests to Environmental Change. Springer-Verlag Ecological Studies Series. pp 425-453

Laurence, J.A., R.J. Kohut, R.G. Amundson, D.A. Weinstein, and D.C. MacLean. 1996. Response of sugar maple to multiple year exposures to ozone and simulated acidic precipitation. Environ. Pollut. 92:119-126.

Laurence, J.A., R.G. Amundson, A.L. Friend, E.J. Pell, and P.J. Temple. 1994. Allocation of carbon in plants under stress: an analysis of the ROPIS experiments. J. Environ. Qual. 23:412-417.

Lawrence, G.B. and T.G. Huntington. 1999. Soil-calcium depletion linked to acid rain and forest growth in the eastern United States. USGS WRIR 98-4267.

Lawrence, G.B., M.B. David, and W.C. Shortle. 1995. A new mechanism for calcium loss in forest-floor soils. Nature 378:162-165.

Legge, A.H., H-J. Jäger, and S.V. Krupa. 1998. Sulfur dioxide. In Flagler, R.B. (ed.). 1998. Recognition of Air Pollution Injury to Vegetation: A Pictorial Atlas, 2nd edition. Air Waste Manage. Assoc., Pittsburgh. pp. 3.1-3.42.

Likens, G.E., C.T. Driscoll, and D.C. Buso. 1996. Long-term effects of acid rain: response and recovery of a forest ecosystem. Science 272:244-246.

Likens, G.E., F.H. Bormann, N.M Johnson, D.W. Fisher, and R.S. Pierce. 1970. Effects of forest cutting and herbicide treatment on nutrient budgets in the Hubbard Brook watershed ecosystem. Ecolog. Monogr. 40:23-47.

Lin, C.Y., D.J. Jacob, J.W. Munger, and A.M. Fiore. 2000. Increasing background ozone in surface air over the United States. Geophys. Res. Letters 27:3465-3468.

Lindberg, S.E., D. Silsbee, D.A. Schaefer, J.G. Owens, and W. Petty. 1988. A comparison of atmospheric exposure conditions at high- and low-elevation forests in the southern Appalachian Mountain range. In: Unsworth, M.M. and D. Fowler (eds.). Acid Deposition at High Elevation Sites. Kluwer Academic Publishers, Dordrecht, The Netherlands. pp. 321-344.

Liu, S., R. Munson, D.W. Johnson, S. Gherini, K. Summers, R. Hudson, K. Wilkinson, and L.F. Pitelka. 1992. The Nutrient Cycling Model (NuCM): Overview and Application. In Johnson, D.W. and S.E. Lindberg (eds.). Atmospheric Deposition and Forest Nutrient Cycling. Springer Verlag, New York.

Liu, S., R. Munson, D. Johnson, S. Gherini, K. Summers, R. Hudson, K. Wilkinson, and L. Pitelka. 1991. Application of a nutrient cycling model (NuCM) to northern mixed hardwood and southern coniferous forest. Tree Phys. 9:173-182.

Loibl, W., W. Winiwarter, A. Kopsca, J. Zueger and R. Bauman. 1994. Estimating the spatial distribution of ozone concentrations in complex terrain. Atmos. Environ. 28:2557-2566.

Lovett, G.M. and J.D. Kinsman. 1990. Atmospheric pollutant deposition to high-elevation ecosystems. Atmos. Environ. 24A:2767-2786.

Lynch, J.A. and E.S. Corbett 1989. Hydrologic control of sulfate mobility in a forested watershed. Water Resour. Res. 25(7):1695-1703.

Lynch, D.D. and N.B. Dise. 1985. Sensitivity of Stream Basins in Shenandoah National Park to Acid Deposition. U.S. Geol. Surv. Water-Resources Investigations Report 85-4115. Prepared in cooperation with University of Virginia Department of Environmental Sciences. U.S. Geological Survey, Richmond, VA.

Lynch, J.A., V.C. Bowersox, and J.W. Grimm. 1996. Trends in precipitation chemistry in the United States, 1983-94: an analysis of the effects in 1995 of Phase I of the Clean Air Act Amendments of 1990, Title IV. U.S. Geological Survey open-file report. 96-0346. U.S. Geological Survey, Denver, CO.

MacAvoy, S. E. and A. J. Bulger. 1995. Survival of brook trout *(Salvelinus fontinalis)* embryos and fry in streams of different acid sensitivity in Shenandoah National Park, USA. Water Air Soil Pollut. 85:439-444.

Malm, W.C. 2000. Introduction to Visibility. Cooperative Institute for Research in the Atmosphere (CIRA). Colorado State University, Fort Collins, CO. ISSN: 0737-5352-40.

Malm, W.C., R. Ames, S. Copeland, D. Day, K. Gebhart, M. Pitchford, M. Scruggs, and J. Sisler. 2000. IMPROVE Report, Spatial and Seasonal Patterns and Temporal Variability of Haze and its Constituents in the United States: Report III, Cooperative Institute for Research in the Atmosphere (CIRA), Colorado State University, Ft. Collins, CO 80523. ISSN: 0737-5352-47.

Mathur, R., A. Hanna, M.T. Odman, J. McHenry, U. Shankar, C. Coats, K. Alapaty, A. Xiu, C. Jang, D. Olerud, S. Fine, K. Galluppi, D. Byun, K. Schere, F. Binkowski, J. Ching, R. Dennis, J. Novak, T. Pierce, J. Pleim, S. Roselle, and J. Young. In review. The Multiscale Air Quality Simulation Platform (MAQSIP): An overview of model formulation and initial applications. J. Geophys. Res.

Matyssek, R. and J.L. Innes. 1999. Ozone - a risk factor for trees and forests in Europe. Water Air Soil Pollut. 116:199-226.

McCool, P.M., 1988. Effect of air pollutants on mycorrhizae. In: Schulte-Hostede, S., N.M. Darrall, L.W. Blank, and A.R. Wellburn (eds.). Air Pollution and Plant Metabolism. Elsevier Applied Science, London, UK, pp. 356-365.

McLaughlin, S.B. and D.J. Downing. 1995. Interactive effects of ambient ozone and climate measured on growth of mature forest trees. Nature 374:252-254.

McNulty, S.G., J.D. Aber, and S.D. Newman. 1996. Nitrogen saturation in a high elevation spruce-fir stand. For. Ecol. Manage. 84:109-121.

Miller P.R., G.J. Longbotham, and C.R. Longbotham. 1983. Sensitivity of selected western conifers to ozone. Plant Dis. 67:1113-1115.

Miller, P.R., O.C. Taylor, and R.G. Wilhour. 1982. Oxidant air pollution effects on a western coniferous forest ecosystem. EPA report No. EPA-600/D-82-276. U.S. Environmental Protection Agency, Environmental Research Laboratory, Corvallis, OR.

Miller-Marshall, L.M. 1993. Mechanisms controlling variation in stream chemical composition during hydrologic episodes in the Shenandoah National Park, Virginia. Masters Thesis, Department of Environmental Science, University of Virginia.

Moeykens, M.D. and J.R. Voshell. 2002. Studies of Benthic Macroinvertebrates for the Shenandoah National Park Long-Term Ecological Monitoring System: Statistical Analysis of LTEMS Aquatic Dataset from 1986 to 2000 on Water Chemistry, Habitat and Macroinvertebrates. Report to Shenandoah National Park from the Dept. of Entomology, Virginia Polytechnic and State University, Blacksburg, VA. 49 pp.

Mohnen, V.A. 1988a. Mountain cloud chemistry project – wet, dry and cloud water deposition. EPA-600/3-89-009. U.S. Environmental Protection Agency, Research Triangle Park, NC.

Mohnen, V.A. 1988b. Exposure of forests to air pollutants, clouds, precipitation and climate variables. EPA-600/3-89-003. U.S. Environmental Protection Agency, Research Triangle Park, NC.

Molot, L.A., P.J. Dillon, and B.D. LaZerte. 1989. Changes in ionic composition of streamwater during snowmelt in central Ontario. Can. J. Fish. Aquat. Sci. 46:1658-1666.

Moyle. P.B. and J.J. Cech,. Jr. 2000. Fishes: An Introduction to Ichthyology. 4th Edition. Prentice Hall, New Jersey. 612 pp.

Mudd, J.B. 1975. Peroxyacyl nitrates. In: Mudd, J.B. and T.T. Kozlowski (eds.). Responses of Plants to Air Pollution. Academic Press. New York, NY. pp. 97-119.

Munson, R.K. and S.A. Gherini. 1991. Processes influencing the acid-base chemistry of surface waters. In: Charles, D.F. (ed.). Acidic Deposition and Aquatic Ecosystems: Regional Case Studies. Springer-Verlag, Inc., New York. pp. 9-34.

National Academy of Sciences. 1978. Sulfur Oxides. National Academy of Sciences, Washington, DC. 209 pp.

National Academy of Sciences. 1977. Nitrogen Oxides. National Academy of Sciences, Washington, DC. 333 pp.

National Acid Precipitation Assessment Program. 1998. Biennial Report to Congress: An Integrated Assessment. National Acid Precipitation Assessment Program, Silver Spring, MD.

National Acid Precipitation Assessment Program. 1991. Integrated Assessment Report. National Acid Precipitation Assessment Program, Washington, DC.

National Park Service. 2000a. Management Policies 2001, U.S. Dept. of Interior, National Park Service, NPS D1416/December 2000.

National Park Service. 2000b. Five Year Strategic Plan, Shenandoah National Park. Fiscal Years 2001-2005.

National Park Service. 2000c. Agency technical support document regarding the Department of the Interior request for a U.S. Environmental Protection Agency rule to restore and protect air quality values in Class I national parks and wilderness areas.

National Park Service. 1994. An introduction to selected laws important for resources management in the National Park Service. NPS/NRPO/NRR-94/15, Washington, DC. 48 pp.

National Park Service. 1990. Agency technical support document regarding adverse impact determination for Shenandoah National Park. Air Quality Division and Shenandoah National Park.

National Park Service. 1981. Biogeography of red spruce in Shenandoah National Park.

Neufeld, H.S., E.H. Lee, J.R. Renfro, W.D. Hacker, and B. Yu. 1995. Sensitivity of seedlings of black cherry (*Prunus serotina* Ehrh.) to ozone in Great Smoky Mountains National Park. 1. Exposure-response curves for biomass. New Phytol. 130:447-459.

Nilsson, J. (Ed.). 1986. Critical Loads for Sulphur and Nitrogen. Miljørapport 1986:11, Nordic Council of Ministers, Copenhagen.

Nilsson, J. and P. Grennfelt (eds.). 1988. Critical loads for sulphur and N, report from a workshop held at Skokloster, Sweden, 19-24 March 1988, NORD Miljørapport 1988:15, Nordic Council of Ministers, Copenhagen. pp. 225-268.

North American Research Strategy for Tropospheric Ozone (NARSTO). 2000. An Assessment of Tropospheric Ozone Pollution - A North American Perspective. Printed by Electric Power Research Institute for NARSTO, Palo Alto, California.

Ollinger, S.V., J.D. Aber, G.M. Lovett, S.E. Millham, R.G. Lathrop, and J.M. Ellis. 1993. A spatial model of atmospheric deposition for the northeastern U.S. Ecol. Appl. 3:459-472.

Olszyna, K.J., E.M. Bailey, R. Simonaitis, and J.F. Meagher. 1994. O_3 and NO_y relationships at a rural site. J. Geophys. Res. 99:14,557-14,563.

Oltmans, S.J., A.S. Lefohn, H.E. Scheel, J.M. Harris, H. Levy II, I.E. Galbally, E.-G. Brunke, C.P. Meyer, J.A. Lathrop, B.J. Johnson, D.S. Shadwick, E. Cuevas, F.J. Schmidlin, D.W. Tarasick, H. Claude, J.B. Kerr, O. Uchino, and V. Mohnen 1998. Trends of ozone in the troposphere. Geophys. Res. Letters 25:139-142.

Parker, D.R., L.W. Zelazny, and T.B. Kinraide. 1989. Chemical speciation and plant toxicity of aqueous aluminum. In: Lewis, T.E. (ed.). Environmental Chemistry and Toxicology of Aluminum. American Chemical Society. pp. 117-145.

Patrick, R. 1996. Rivers of the United States. Volume III. The Eastern and Southeastern States. John Wiley and Sons, New York. 829 pp.

Patterson, M.T. and P.W. Rundel. 1989. Seasonal physiological responses of ozone stressed Jeffrey pine in Sequoia National Park, California. In Olson, R.K. and A.S. Lefohn (eds.). Effects of Air Pollution on Western Forests. Transactions Series 16. Air Waste Manage. Assoc. Pittsburgh. pp. 419-428.

Pechan, E.H. 2001. NO_x and SO_2 Emissions Reduction Assessment. Draft report prepared for Clean Air Markets Division, U.S. Environmental Protection Agency, Washington, DC. E.H. Pechan & Associates, Inc. 5528-B Hempstead Way Springfield, VA.

Peet, R.K. 1992. Community structure and ecosystem function. In Glenn-Lewis, D.L., R.K. Peet, and T.T. Veblen (eds.). Plant Succession: Theory and Prediction. Chapman and Hall, London, UK. pp. 103-151.

Pell, E.J., N.A. Eckardt, and R.E. Glick. 1994a. Biochemical and molecular basis for impairment of photosynthetic potential. Photosynthesis Res. 39:453-462.

Pell, E.J., P.J. Temple, A.L. Friend, H.A. Mooney, and W.E. Winner. 1994b. Compensation as a plant response to ozone and associated stresses: an analysis of ROPIS experiments. J. Environ. Qual. 23:429-436.

Peterjohn, W.T., M.B. Adams, and F.S. Gilliam. 1996. Symptoms of nitrogen saturation in two central Appalachian hardwood forest ecosystems. Biogeochemistry 35:507-522.

Peterson, D.L. and T.J. Sullivan. 1998. Assessment of Air Quality and Air Pollutant Impacts in National Parks of the Rocky Mountains and Northern Great Plains. NPS D-657. U.S. Dept. of the Interior, National Park Service, Air Resources Division.

Peterson, R.H., and L. Van Eeckhaute. 1992. Distribution of Ephemeroptera, Plecoptera, and Trichoptera of maritime catchments differing in pH. Freshw. Biol. 27:65-78.

Peterson, D.L., D.L. Schmoldt, J.M. Eilers, R.W. Fisher, and R.D. Doty. 1992. Guidelines for evaluating air pollution impacts on Class I areas in California. USDA Forest Service Gen. Tech. Rep. PSW-GTR-136.

Pitchford, M.L., and W.C. Malm. 1994. Development and Applications of a Standard Visual Index. Atmos. Environ. 28(5):1049-1054.

Posch, M., J.-P. Hettelingh, P.A.M. de Smet, and R.J. Downing. 1997. Calculation and mapping of critical thresholds in Europe: CCE status report 1997. RIVM Report 259101007. National Institute for Public Health and the Environment. Gilthoven, Netherlands.

Poulida O., R.R. Dickerson, B.G. Doddridge, J.Z. Holland, R.G. Wardell, and J.G. Watkins. 1991. Trace gas concentrations and meteorology in rural Virginia, 1. Ozone and carbon monoxide. J. Geophys. Res. 96:22461-22475.

Pronos, J., L. Merrill, and D. Dahlsten. 1999. Insects and pathogens in a pollution-stressed forest. In Miller, P.R. and J.R. McBride (eds.). Oxidant Air Pollution Impacts in the Montane Forests of Southern California. Springer-Verlag, New York. pp. 317-337.

Ray, J.D., C.C. Van Valin, M. Luria, and J.F. Boatman. 1990. Oxidants in the marine troposphere over the western Atlantic Ocean. Global Biogeochem. Cycles 34(2):201.

Raynal, D.J., N.W. Foster, M.J. Mitchell, and D.W. Johnson. 1992. In: Johnson, D.W. and S.E. Lindberg (eds.). Atmospheric Deposition and Forest Nutrient Cycling: A Synthesis of the Integrated Forest Study. Springer-Verlag, New York. pp. 526-543.

Reich, P.B. and R. G. Amundson. 1985. Ambient levels of ozone reduce net photosynthesis in tree and crop species. Science 230:566-570.

Retzlaff. W.A., D.A. Weinstein, J.A. Laurence, and B. Gollands. 1996. Simulating the growth of a 160-year-old sugar maple (*Acer saccharum* Marsh.) tree with and without ozone exposure using the TREGRO model. Can. J. For. Res. 27:783-789

Reuss, J.O., and D.W. Johnson. 1986. Acid deposition and the acidification of soil and water. Springer-Verlag, New York.

Rice, K.C., S.W. Maben, and J.R. Webb. 2001. Water-Quality Data of Soil Water from Three Watersheds, Shenandoah National Park, Virginia, 1999-2000. USGS, Open-File Report 01-236.

Rochelle, B.P. and M.R. Church. 1987. Regional patterns of sulfur retention in watersheds of the eastern U.S. Water Air Soil Pollut. 36:61-73.

Runeckles, V.C. and B.I. Chevone. 1992. Crop responses to ozone. In: Lefohn, A.S. (ed.). Surface Level Ozone Exposures and their Effects on Vegetation. Lewis Publishers, Chelsea, MI. pp. 189-270.

Rygiewicz, P.T. and C.P. Andersen. 1994. Mycorrhizae alter quality and quantity of carbon allocated below ground. Nature 369:58-60.

Samuelson, L.J. and J.M. Kelly. 1996. Carbon partitioning and allocation in northern red oak seedlings and mature trees in response to ozone. Tree Phys. 16:853-858.

Sandroni S., P. Bacci, G. Boffa , U. Pellegrini, and A. Ventura. 1994. Tropospheric ozone in the pre-alpine and alpine regions. Sci. Total Environ. 156:169-182.

SAS Institute Inc. 1988. SAS/STAT User's Guide, Release 6.03 Edition. SAS Institute, Inc., Cary, NC.

Saxe, H. 1994. Relative sensitivity of greenhouse pot plants to long-term exposures of NO- and NO_2-containing air. Environ. Pollut. 85:283-290.

Schichtel, B., R.B. Husar; S.R. Falke; W.E. Wilson. 2001. Haze trends over the United States, 1980-1995. Atmos. Environ. 35:5205-5210 .

Schofield, C.L., and C.T. Driscoll. 1987. Fish species distribution in relation to water quality gradients in the North Branch of the Moose River Basin. Biogeochemistry 3:63-85.

Schreck, C.B. 1982. Stress and compensation in teleostean fishes: response to social and physical factors. In: Pickering, A.D. (ed.). Stress and Fish. Academic Press, London. pp. 295-321.

Schreck, C.B. 1981. Stress and rearing of salmonids. Aquaculture 28:241-249.

Schulze, E.-D. 1989. Air pollution and forest decline in a spruce (*Picea abies*) forest. Science 244:776-783.

Shaffer, P.W. 1982. Soil and bedrock mineralogy: Soil chemistry in the SWAS watersheds. Appendix VII In: Galloway, J.N., G.M. Hornberger, and K.J. Beven. Shenandoah watershed acidification study: three year summary report, September 1979-September 1982. Department of Environmental Sciences, University of Virginia, Charlottesville, VA. 31 pp., 8 appendices.

Shannon, J.D. 1998. Calculation of Trends from 1900 through 1990 for Sulfur and NO_x-N Deposition Concentrations of Sulfate and Nitrate in Precipitation, and Atmospheric Concentrations of SO_x and NO_x Species over the Southern Appalachians. Report to SAMI, April 1998.

Shannon, J.D. 1985. User's Guide for the Advanced Statistical Trajectory Regional Air Pollution (ASTRAP) Model. U. S. Environmental Protection Agency Report EPA/600/8-85/016 (NTIS PB85-236784/XAB).

Shannon, J.D. 1981. A model of regional long-term average sulfur atmospheric pollution, surface removal, and net horizontal flux. Atmos. Environ. 15:689-701.

Shenandoah National Park. 2001. Comprehensive Interpretive Plan. U.S. Dept. of the Interior, National Park Service.

Shenandoah National Park. 1998a. Backcountry & Wilderness Management Plan. U.S. Dept. of Interior, National Park Service.

Shenandoah National Park. 1998b. Resource Management Plan. U.S. Dept. of Interior, National Park Service.

Shenandoah National Park. 1993. Wildland Fire Management Plan. U.S. Dept. of the Interior, National Park Service.

Sigmon, J.T., F.S. Gilliam, and M.E. Partin. 1989. Precipitation and throughfall chemistry for a montane hardwood forest ecosystem: potential contributions from cloud water. Can. J. For. Res. 19:1240-1247.

Sillman, S. , J.A. Logan, and S.C. Wofsy. 1990. The sensitivity of ozone to nitrogen oxides and hydrocarbons in regional ozone episodes. J. Geophys. Res. 95:1,837-1,852.

Sisler J. F. and W.C. Malm. 2000. Interpretation of trends of $PM_{2.5}$ and reconstructed visibility from the IMPROVE network. J. Air Waste Manage. Assoc. 50:775-789.

Sisterson, D.L., V.C. Bowersox, T.P. Meyers, A.R. Olsen, and R.J. Vong. 1990. Deposition monitoring: Methods and results. State of Science and Technology Report 6. National Acid Precipitation Assessment Program, Washington, DC.

Skeffington, R.A. 1999. The use of critical loads in environmental policy making: A critical appraisal. Environ. Sci. Technol. 33(11):245A-252A.

Skelly, J.M., D.D. Davis, K.C. Steiner, J. Zhang, M. Schaub, J. Ferdinand, J.E. Savage, and R.E. Stevenson. 2001. Final Report. Impact of ambient ozone on physiological, visual, and growth responses of sensitive eastern hardwood tree species under natural and varying conditions. Assistance ID No. 825244-01-0. National Center for Environmental Research and Quality Assurance, United States Environmental Protection Agency, Washington, DC.

Smith, W.H. 1990. Air Pollution and Forests: Interactions Between Air Contaminants and Forest Ecosystems. Springer-Verlag, New York. 618 pp.

Southern Appalachian Man and the Biosphere (SAMAB). 1996. Southern Appalachian Man and the Biosphere. The Southern Appalachian Assessment Aquatics Technical Report. Report 2 of 5. Atlanta, USDA, Forest Service, Southern Region.

Southern Appalachian Mountains Initiative (SAMI). 2002. Southern Appalachian Mountains Initiative Final Report, August, 2002. Asheville, NC. Available at http://www.saminet.org/reports

Stehr J. W., R.R. Dickerson, K.A. Hallock-Waters, B.G. Doddridge, and D. Kirk. 2000. Observations of NO_y, CO, and SO_2 and the origin of reactive nitrogen in the eastern United States. J. Geophys. Res. 105:3553-3564.

Stoddard, J.L. 1994. Long-term changes in watershed retention of nitrogen: its causes and aquatic consequences, pp. 223-284. In: Baker, L.A. (ed.). Environmental Chemistry of Lakes and Reservoirs. Advances in Chemistry Series, No. 237, American Chemical Society, Washington, DC.

Stoddard, J.L., J.S. Kahl, F.A. Deviney, D.R. DeWalle, C.T. Driscoll, A.T. Herlihy, J.H. Kellogg, P.S. Murdoch, J.R. Webb, and K.E. Webster. 2003. Response of surface water chemistry to the Clean Air Act Amendments of 1990. EPA/620/R-03/001, U.S. Environmental Protection Agency, Washington, DC.

Stoddard, J.L., D.S. Jeffries, A. Lukewille, T.A. Clair, P.J. Dillon, C.T. Driscoll, M. Forsius, M. Johannessen, J.S. Kahl, J.H. Kellogg, A. Kemp, J. Mannio, D. Monteith, P.S. Murdoch, S. Patrick, A. Rebsdorf, B.L. Skjelkvååle, M. Stainton, T. Traaen, H. van Dam, K.E. Webster, J.

Wieting, and A. Wilander. 1999. Regional trends in aquatic recovery from acidification in North America and Europe. Nature 401:575.

Stoddard, J.L., C.T. Driscoll, J.S. Kahl, and J.H. Kellogg. 1998. Can site-specific trends be extrapolated to a region? An acidification example for the Northeast. Ecol. Appl. 8:288-299.

Stolte, K.W. 1996. Symptomology of ozone injury to pine foliage. In P.R. Miller, K.W. Stolte, D.M. Duriscoe, and J. Pronos (tech. coords.), Evaluating ozone air pollution effects on pines in the western United States. USDA For. Serv. Gen. Tech. Rep. PSW-GTR-155. pp. 11-18.

Stroo, H.F., P.B. Reich, A.W. Schoettle, and R.G. Amundson. 1988. Effects of ozone and acid rain on white pine (*Pinus strobus*) seedlings grown in five soils. II. Mycorrhizal infection. Can. J. Bot. 66:1510B1516.

Sullivan, T.J. 2000. Aquatic Effects of Acidic Deposition. Lewis Publ., Boca Raton, FL. 373 pp.

Sullivan, T.J. 1993. Whole ecosystem nitrogen effects research in Europe. Environ. Sci. Technol. 27(8):1482-1486.

Sullivan, T.J. 1990. Historical Changes in Surface Water Acid-Base Chemistry in Response to Acidic Deposition. State of the Science, SOS/T 11, National Acid Precipitation Assessment Program. 212 pp.

Sullivan, T.J. and B.J. Cosby. 1995. Testing, improvement, and confirmation of a watershed model of acid-base chemistry. Water Air Soil Pollut. 85:2607-2612.

Sullivan, T.J. and J.M. Eilers. 1994. Assessment of Deposition Levels of Sulfur and Nitrogen Required to Protect Aquatic Resources in Selected Sensitive Regions of North America. Final Report prepared for Technical Resources, Inc., Rockville, MD, Under Contract to U.S. Environmental Protection Agency, Environmental Research Laboratory-Corvallis, Corvallis, OR.

Sullivan, T.J., B.J. Cosby, J.R. Webb, K.U. Snyder, A.T. Herlihy, A.J. Bulger, E.H. Gilbert, and D. Moore. 2002a. Assessment of the effects of acidic deposition on aquatic resources in the Southern Appalachian Mountains. Report prepared for the Southern Appalachian Mountains Initiative (SAMI). E&S Environmental Chemistry, Inc., Corvallis, OR. (Available at www.esenvironmental.com/sami_download.htm)

Sullivan, T.J., D.W. Johnson, and R. Munson. 2002b. Assessment of effects of acid deposition on forest resources in the Southern Appalachian Mountains. Report prepared for the Southern Appalachian Mountains Initiative (SAMI). E&S Environmental Chemistry, Inc., Corvallis, OR. (Available at www.esenvironmental.com/sami_download.htm)

Sullivan, T.J., D.L. Peterson, C.L. Blanchard, K. Savig, and D. Morse. 2001. Assessment of air quality and air pollutant impacts in Class I national parks of California. NPS D-1454. U.S. Dept. of the Interior, National Park Service, Air Resources Division.

Sullivan, T.J., J.M. Eilers, B.J. Cosby, and K.B. Vaché. 1997. Increasing role of nitrogen in the acidification of surface waters in the Adirondack Mountains, New York. Water Air Soil Pollut. 95:313-336.

Sullivan, T.J., B.J. Cosby, C.T. Driscoll, D.F. Charles, and H.F. Hemond. 1996. Influence of organic acids on model projections of lake acidification. Water Air Soil Pollut. 91:271-282.

Sullivan, T.J., R.S. Turner, D.F. Charles, B.F. Cumming, J.P. Smol, C.L. Schofield, C.T. Driscoll, B.J. Cosby, H.J.B. Birks, A.J. Uutala, J.C. Kingston, S.S. Dixit, J.A. Bernert, P.F. Ryan, and D.R. Marmorek. 1992. Use of historical assessment for evaluation of process-based model projections of future environmental change: Lake acidification in the Adirondack Mountains, New York, U.S.A. Environ. Pollut. 77:253-262.

Surber, E.W., 1951. Bottom fauna and temperature conditions in relation to trout management in St. Marys River, Augusta County, Virginia. Virginia J. Sci. 2:190-202.

Sverdrup, J., P. Warfvinge, and K. Rosen. 1992. A model for the impact of soil solution Ca:Al ratio on tree base cation uptake. Water Air Soil Pollut. 61:365-383.

Sverdrup, H., W. de Vries, and A. Henriksen. 1990. Mapping critical loads. Nordic Council of Ministers, Copenhagen.

Swank, W.T. 1988. Stream chemistry responses to disturbance. In: Swank, W.T. and D.S. Crossley (eds). Forest Hydrology at Coweeta. Springer-Verlag, New York. pp. 339-358.

Takemoto, B.K. 2000. Effects of ozone and atmospheric nitrogen on mixed conifer forests: considerations for a critical/target N load to protect forests from N-saturation. Draft report. California Air Resources Board, Sacramento.

Takemoto, B.K., A. Bytnerowicz, and M.E. Fenn. 2001. Current and future effects of ozone and atmospheric nitrogen deposition on California's mixed conifer forests. For. Ecol. Manage. 144:159-173.

Taylor, O.C. 1968. Effects of oxidant air pollutants. Occup. Med. 10:53-60.

Taylor, A. and J. Blum. 1995. Relation between soil age and silicate weathering rates determined from the chemical evolution of a glacial chronosequence Geology 23:979-982.

Taylor, O.C., C.R. Thompson, D.T. Tingey, and R.A. Reinert. 1975. Oxides of nitrogen. In: Mudd, J.B. and T.T. Kozlowski (eds.). Responses of Plants to Air Pollution. Academic Press. New York, NY. pp. 121-139.

Temple, P.J. 1988. Injury and growth of Jeffrey pine and giant sequoia in response to ozone and acidic mist. Environ. Exp. Bot. 28:323-333.

Theil, H. 1950. A rank-invariant method of linear and polynomial regression analysis. I. Proc. Kon. Ned. Akad, V. Wetensch. A. 53:386-392.

Thompson, C.R., D.M. Olszyk, G. Kats, A. Bytnerowicz, P.J. Dawson, and J. Wolf, and C.A. Fox. 1984a. Air pollutant impacts on plants of the Mojave Desert. Southern California Edison, Rosemead.

Thompson, C.R., D.M. Olszyk, G. Kats, A. Bytnerowicz, P.J. Dawson, and J.W. Wolf. 1984b. Effects of ozone and sulfur dioxide on annual plants of the Mojave Desert. J. Air Pollut. Control Assoc. 34:1017-1022.

Thompson, C.R., G. Kats, and R.W. Lennox. 1980. Effects of SO_2 and/or NO_2 on native plants of the Mojave Desert and Eastern Mojave-Colorado Desert. J. Air Pollut. Control Assoc. 30:1304-1309.

Thornton, K., D. Marmorek, and P. Ryan. 1990. Methods for Projecting Future Changes in Surface Water Acid-Base Chemistry. State of the Science, SOS/T 14, National Acid Precipitation Assessment Program, Washington, DC. .

Tietema, A. and C. Beier. 1995. A correlative evaluation of nitrogen cycling in the forest ecosystems of the EC projects NITREX and EXMAN. For. Ecol. Mgmt. 71:143-151.

Tingey, D.T., J. A. Laurence, J.A. Weber, J. Greene, W.E. Hogsett, S. Brown, and E.H. Lee. 2001. Effects of elevated CO_2 and temperature on the response of *Pinus ponderosa* to ozone: A simulation analysis. Ecol. Appl. 11(5):1412-1424.

Treshow, M. and F.K. Anderson. 1989. Plant Stress from Air Pollution. John Wiley and Sons, New York. 283 pp.

Trijonis, J.C. 1990. Acidic Deposition: State of Science and Technology. Report No. 24. Visibility: Existing Conditions – Causes and Effects. National Acid Precipitation Assessment Program, Washington, DC.

Turner, R.S., P.F. Ryan, D.R. Marmorek, K.W. Thornton, T.J. Sullivan, J.P. Baker, S.W. Christensen, and M.J. Sale. 1992. Sensitivity to change for low-ANC eastern US lakes and streams and brook trout populations under alternative sulfate deposition scenarios. Environ. Pollut. 77:269-277.

Turner, R.S., R.B. Cook, H. van Miegroet, D.W. Johnson, J.W. Elwood, O.P. Bricker, S.E. Lindberg, and G.M. Hornberger. 1990. Watershed and Lake Processes Affecting Chronic Surface Water Acid-Base Chemistry. State of the Science, SOS/T 10. National Acid Precipitation Assessment Program, Washington, DC.

Turner, D.P., D.T. Tingey, and W.E. Hogsett. 1989. Acid fog effects on conifer seedlings. In J.B. Bucher and I. Bucher-Wallin (eds.). Air Pollution and Forest Decline. Swiss Institute for Forest, Snow and Landscape Research, Birmensdorf, Switzerland. pp. 125-129.

Ulrich, B. 1983. Soil acidity and its relations to acid deposition. In Ulrich, B. and J. Pankrath (eds.). Effects of Accumulation of Air Pollutants on Forest Ecosystems. D. Reidel Publ. Co., Boston. pp. 127-146.

Urban, D. L. 1990. A versatile model to simulate forest pattern: a user's guide to ZELIG version 1.0. University of Virginia, Charlottesville, Virginia, USA.

Urban, D.L., G.B. Bonan, T.M. Smith, and H.H. Shugart. 1991. Spatial applications of gap models. For. Ecol. Manage. 42:95-110.

U.S. Department of Agriculture. 1979. General soil map of Virginia. U.S.D.A., Soil Conservation Service, Lanham, MD.

U.S. Department of Agriculture Forest Service. 2000. Preliminary Air Quality Related Screening Values for the James River Face Wilderness, a Class I Area in Virginia. Posted at www.fs.fed.us/r6/aq/natarm/document.htm.

U.S. Department of Agriculture Forest Service. 1998. Preliminary Air Quality Related Screening Values for Three Class I Areas in North Carolina and Tennessee. USDA Forest Service Air Resource Management Program. Posted at www.fs.fed.us/r6/aq/natarm/ document.htm.

U.S. Department of Agriculture Forest Service, Southern Region; and U.S. Department of the Interior National Park Service, Shenandoah National Park and Great Smoky Mountains National Park. 1996. Southern Appalachian Clean Air Partnership. Tech. Publ. R8-TP-30.

U.S. Department of the Interior (USDOI), Office of the Secretary. 1990. Preliminary Notice of Adverse Impact on Shenandoah National Park. Federal Register. September 18, 1990. 55(181):38403-38409.

U.S. Environmental Protection Agency. 2002a. Documentation of EPA Modeling Applications (V.2.1) Using the Integrated Planning Model, EPA Report No. EPA 430/R-02-004, Office of Air and Radiation (6204N), Clean Air Markets Division, Washington, D.C., March 2002.

U.S. Environmental Protection Agency. 2002b. IPM Documentation, U.S. Environmental Protection Agency Web Page: http://www.epa.gov/airmarkets/epa-ipm/index.html.

U.S. Environmental Protection Agency. 2001a. Draft Guidance for Tracking Progress Under the Regional Haze Rule, U.S. EPA, Office of Air Quality Planning and Standards, Research Triangle Park, NC . September 27, 2001.

U.S. Environmental Protection Agency. 2001b. Draft Guidance for Estimating Natural Visibility Conditions Under the Regional Haze Rule, U.S. EPA, Office of Air Quality Planning and Standards, Research Triangle Park, NC. September 27, 2001.

U.S. Environmental Protection Agency. 2001c. National Air Quality and Emissions Trends Report, Office of Air Quality Planning and Standards Research Triangle Park, NC. (EPA 454/R-01-004).

U.S. Environmental Protection Agency. 2000a. Procedures for Developing Base Year and Future Year Mass and Modeling Inventories for the Heavy-Duty Engine and Vehicle Standards and Highway Diesel Fuel (HDD) Rulemaking, EPA Report No. EPA420-R-00-020, US Environmental Protection Agency, Office of Air Quality Planning and Standards, Research Triangle Park, NC. October 2000.

U.S. Environmental Protection Agency. 2000b. National Air Pollutant Emission Trends, 1900-1998, EPA Report No. EPA-454/R-00-002, US Environmental Protection Agency, Office of Air Quality Planning and Standards, Research Triangle Park, NC. March 2000.

U.S. Environmental Protection Agency. 1999. Procedures for Developing Base Year and Future Year Mass and Modeling Inventories for the Tier 2 Final Rulemaking, EPA Report No. EPA420-R-99-034, US Environmental Protection Agency, Office of Air Quality Planning and Standards, Research Triangle Park, NC. September 1999.

U.S. Environmental Protection Agency. 1998a. Interagency Workgroup on Air Quality Modeling (IWAQM). Phase 2 Summary Report and Recommendations for Modeling Long-Range Transport and Impacts on Regional Visibility. EPA-454/R-98-019.

U.S. Environmental Protection Agency. 1998b. National Air Quality and Emission Trends Report, 1997. Rep. EPA-454/R-98-016. Research Triangle Park, N.C. 112pp

U.S. Environmental Protection Agency. 1997. National Ambient Air Quality Standards for Ozone; Final Rule. Federal Register Vol. 62, No. 138.

U.S. Environmental Protection Agency. 1996a. Air quality criteria for ozone and related photochemical oxidants, Vol. II. EPA/600/P-93/ 004bF, Washington, DC.

U.S. Environmental Protection Agency. 1996b. Review of National Ambient Air Quality Standards for Ozone. Assessment of Scientific and Technical Information. OAQPS Staff Paper. Office of Air Quality Planning and Standards, Research Triangle Park, NC. EPA-452/R-96-007.

U.S. Environmental Protection Agency. 1995. Acid Deposition Standard Feasibility Study: Report to Congress, EPA Report No. 430-R-95-001a, Office of Air and Radiation, Acid Rain Division, Washington D.C.

U.S. Environmental Protection Agency, Office of Research and Development. 1993. Air Quality Criteria for Oxides of Nitrogen. Vol. II. U.S. Environmental Protection Agency, Research Triangle Park, NC. EPA/600/8-91/049bf.

U.S. General Accounting Office (USGAO). 2000. Acid Rain: Emissions Trends and Effects in the Eastern United States. GAO/RCED-00-47, U.S. General Accounting Office, Washington, D.C.

van Miegroet, H., D.W. Cole, and N.W. Foster. 1992. Nitrogen distribution and cycling. In Johnson, D.W. and S.E. Lindberg (eds.). Atmospheric Deposition and Forest Nutrient Cycling: A Synthesis of the Integrated Forest Study. Springer-Verlag, New York. pp. 178-196.

van Sickle, J. and M.R. Church. 1995. Methods for Estimating the Relative Effects of Sulfur and Nitrogen Deposition on Surface Water Chemistry. U.S. Environmental Protection Agency, EPA/600/R-95/172, Washington, DC. 121 pp.

Vitousek, P.M. 1977. The regulation of element concentrations in mountain streams in the northeastern United States. Ecol. Monogr. 47:65-87.

Vong, R.J., J.T. Sigmon, and S.F. Mueller. 1991. Cloud water deposition to Appalachian forests. Environ. Sci. Technol. 25:1014-1021.

Voshell, J.R. Jr, and S.W. Hiner. 1990. Shenandoah National Park Long-Term Ecological Monitoring System: Section III, Aquatic component user manual. In: United States Department of Interior, Shenandoah National Park long-term ecological monitoring system users manual. USDI, NPS, Shenandoah National Park, Luray, VA 14-16-0009-1558.

Wallace, B., J.R. Webster and R.L. Lowe. 1992. High-Gradient Streams of the Appalachians. In: Hackney, C.T., S.M. Adams and W.H. Martin (eds.). Biodiversity of the Southeastern United States Aquatic Communities. John Wiley and Sons, New York. 779 pp.

Wang, D., F.H. Bormann, and D.F. Karnosky. 1986. Regional tree growth reductions due to ambient ozone: evidence from field experiments. Environ. Sci. Tech. 20:1122-1125.

Weathers, K.C., G.E. Likens, F.H. Bormann, S.H. Bicknell, B.T. Bormann, B.C. Daube, Jr., J.S. Eaton, J.N. Galloway, W.C. Keene, K.D. Kimball, W.H. McDowell, T.G. Siccama, D. Smiley, and R. Tarrant. 1988. Cloud water chemistry from ten sites in North America. Environ. Sci. Technol. 22:1018-1026.

Webb, J.R. 1999. Synoptic Stream Water Chemistry. In Bulger, A.J., B.J. Cosby, C.A. Dolloff, K.N. Eshleman, J.R. Webb, and J.N. Galloway. Shenandoah National Park: Fish in Sensitive Habitats. Project Final Report Volume II for U.S. National Park Service. pp. 1-50.

Webb, J.R. 1988. Retention of atmospheric sulfate by catchments in Shenandoah National Park, Virginia. Masters Thesis. Department of Environmental Sciences, University of Virginia.

Webb, J.R. and F.A. Deviney. 1999. The Acid-Base Status of the St. Marys River: Trout Stream Sensitivity Study Results. Banisteria 13:171-182.

Webb, J.R., F.A. Deviney, Jr., B.J. Cosby, A.J. Bulger, and J.N. Galloway. 2000. Change in the acid-base status of streams in Shenandoah National Park and the mountains of Virginia. Amer. Geophys. Union, Biogeochemical Studies of Shenandoah National Park.

Webb, J.R., B.J. Cosby, F.A. Deviney, K.N. Eshleman, and J.N. Galloway. 1995. Change in the acid-base status of Appalachian Mountain catchments following forest defoliation by the gypsy moth. Water Air Soil Pollut. 85:535-540.

Webb, J.R., F.A. Deviney, J.N. Galloway, C.A. Rinehart, P.A Thompson, and S. Wilson. 1994. The acid-base status of native brook trout streams in the mountains of Virginia. A regional assessment based on the Virginia Trout Stream Sensitivity Study. Univ. of Virginia, Charlottesville, VA.

Webb, J.R., F.A. Deviney, and J.N. Galloway. 1993. Shenandoah Watershed Study: Program Evaluation. Report to U.S. National Park Service.

Webb, J.R., B.J. Cosby, J.N. Galloway, and G.M. Hornberger. 1989. Acidification of native brook trout streams in Virginia. Water Resour. Res. 25:1367-1377.

Wedemeyer, G.A., B.A. Barton, and D.J. MeLeay. 1990. Stress and acclimation. In Schreck, C.B. and P.B. Moyle (eds). Methods for Fish Biology. American Fisheries Society, Bethesda, Maryland. pp. 178-196.

Weinstein, D.A. and R.D. Yanai. 1994. Integrating the effects of simultaneous multiple stresses on plants using the simulation model TREGRO. J. Environ. Qual. 23:418-428.

Weinstein, D.A., B. Gollands, and W.A. Retzlaff. 2001. The effects of ozone on a lower slope forest of the Great Smoky Mountain National Park: Simulations linking an individual tree model to a stand model. For. Sci. 47:29-42.

Weinstein, D.A., L.J. Samuelson, and M.A. Arthur. 1998. Comparison of the response of red oak (*Quercus rubra* L.) seedlings and mature trees to ozone exposure using simulation modeling. Environ. Pollut. 102:307-320.

Weinstein, D.A., Beloin, R.M., Yanai, R.D., 1991. Modeling changes in red spruce carbon balance and allocation in response to interacting ozone and nutrient stresses. Tree Physiol. 9:127-146.

Wellburn, A.R. 1988. Air Pollution and Acid Rain: The Biological Impact. Longman Scientific and Technical, Burnt Mill, UK.

Welsch, D.L., J.R. Webb, B.J. Cosby. 2001. Description of Summer 2000 Field Work. Collection of Soil Samples and Tree Corps in the Shenandoah National Park with Summary Soils Data. Dept. of Environ. Sci., Univ. of Virginia.

Wigington, P.J., Jr., D.R. DeWalle, P.S. Murdoch, W.A. Kretser, H.A. Simonin, J. Van Sickle, and J.P. Baker. 1996. Episodic acidification of small streams in the northeastern United States: Ionic controls of episodes. Ecological Applications 6:389-407.

Wigington, P.J., J.P. Baker, D.R. DeWalle, W.A. Kretser, P.S. Murdoch, H.A. Simonin, J. Van Sickle, M.K. McDowell, D.V. Peck, and W.R. Barchet. 1993. Episodic acidification of streams in the northeastern United States: Chemical and biological results of the Episodic Response Project. EPA/600/R-93/190, U.S. Environmental Protection Agency, Washington, DC.

Wigington, P.J., Jr., T.D. Davies, M. Tranter, and K.N. Eshleman. 1990. Episodic acidification of surface waters due to acidic deposition. State of Science and Technology Report No. 12, National Acid Precipitation Assessment Program, Washington, DC.

Williams, M.W., J. S. Baron, N. Caine, R. Sommerfeld, and R. Senford, Jr. 1996. Nitrogen saturation in the Rocky Mountains. Environ. Sci. Technol. 30:640-646.

Winner, W.E., A.S. Lefohn, I.S. Cotter, C.S. Greitner, J. Nellessen, L.R. McEvoy, Jr., R.L. Olson, C.J. Atkinson, and L.D. Moore. 1989. Plant responses to elevational gradients of ozone exposures in Virginia. Proceedings National Academy of Sciences 86:8828-8832.

Wojcik, G.S. and J.S. Chang. 1997. A re-evaluation of sulfur budgets, lifetimes, and scavenging ratios for Eastern North America, J. Atmos. Chem. 26:109-145.

Wood, C.M. 1989. The physiological problems of fish in acid waters. In: Morris, R., E.W. Taylor, D.J.A. Brown, and J.A. Brown (eds.). Acid Toxicity and Aquatic Animals. Cambridge University Press, Cambridge. pp. 125-152

Woodbury, P.B., J.E. Smith, D.A. Weinstein, and J.A. Laurence. 1998. Assessing potential climate change effects on loblolly pine growth: a probabilistic regional modeling approach. For. Ecol. and Mgmt. 107:99-116.

Woodbury, P.B., J.E. Smith, D.A. Weinstein and J.A. Laurence. 1995. Incorporating uncertainty in regional ecological risk assessments: Ozone effects on Alabama forests. Bull. Ecolog. Soc. Amer. 76(3):404

Woodbury, P.B., J.A. Laurence, and G.W. Hudler. 1994. Chronic ozone exposure alters the growth of leaves, stems, and roots of hybrid *Populus*. Environ. Pollut. 85:103-108.

Wright, R.F. and N. van Breemen. 1995. The NITREX project: An introduction. For. Ecol. Manage. 71:1-5.

Wright, R.F., E.T. Gjessing, N. Christophersen, E. Lotse, H.M. Seip, A. Semb, B. Sletaune, R. Storhaug, and K. Wedum. 1986. Project RAIN: changing acid deposition to whole catchments. The first year of treatment. Water Air Soil Pollut. 30:47-64.

Wynn, A.H. 1991. Shenandoah salamander. Species account. In: Terwilliger, K. (Coord.). Virginia's Endangered Species. McDonald and Woodward Publishing Co., Blacksburg, Virginia. pp. 439-42.

Zika, R.G. 2001. Study of source and composition of VOCs that impact Shenandoah National Park. Final Tech. Rept. of EPA Grant R825-2570R.

Appendix I

Equations Describing the Simulated Effect of Ground-level Ozone on Vegetative Mass

Appendix I Spline Regression Parameters

Spline regression equation parameters for TREGRO model simulations for 8 tree species.
Y = percent change in mass and X = 3-yr ozone exposure index in ppm-h. The model is of the form:

Model: $Y = A + B*X$ if $X<X0$
$Y = C + D*X$ if $X>X0$

NOTE: A=. means A was set to 0 and not estimated by PROC NLIN. In the table below, species are black cherry (BC), basswood (BW), chestnut oak (CO), red maple (RM), red oak (RO), sugar maple (SM), white ash (WA), and yellow poplar (YP). X refers to the ozone metric used in the regression, with 3 and 5 referring to either a 3 or 5 month averaging period. SSE (sum square error), RMSE (root mean standard error), and R2 (r-squared) are measures of fit. X0 is the threshold value for ozone exposure.

Obs	SPECIES	Y	X	B	C	D	SSE	R2	RMSE	X0	A
1	BC	root	aot403	-0.000935	6.0553	-0.025000	0.00149	0.99955	0.01931	251.157	.
2	BC	root	aot405	-0.000603	9.7764	-0.025000	0.00144	0.99956	0.01898	400.281	.
3	BC	root	sum003	-0.000218	0.4992	-0.002508	0.00360	0.99891	0.03002	218.001	.
4	BC	root	sum005	-0.000025	0.4264	-0.001437	0.00255	0.99923	0.02527	301.998	.
5	BC	root	sum063	-0.000533	9.1547	-0.025000	0.00058	0.99983	0.01203	373.664	.
6	BC	root	sum065	-0.000336	0.3362	-0.001353	0.00039	0.99988	0.00982	330.852	.
7	BC	root	w1263	-0.000661	8.8858	-0.025000	0.00070	0.99979	0.01319	364.641	.
8	BC	root	w1265	-0.000426	0.2181	-0.001200	0.00066	0.99980	0.01284	281.891	.
9	BC	shoot	aot403	-0.000606	5.4753	-0.030000	0.00063	0.99981	0.01256	186.275	.
10	BC	shoot	aot405	-0.000391	7.8874	-0.025000	0.00061	0.99982	0.01233	316.627	.
11	BC	shoot	sum003	-0.000174	4.1324	-0.016534	0.00200	0.99939	0.02238	252.596	.
12	BC	shoot	sum005	-0.000108	4.2018	-0.010453	0.00202	0.99939	0.02246	406.164	.
13	BC	shoot	sum063	-0.000346	7.2656	-0.025000	0.00025	0.99993	0.00785	290.797	.
14	BC	shoot	sum065	-0.000217	2.8524	-0.008564	0.00014	0.99996	0.00582	341.745	.
15	BC	shoot	w1263	-0.000430	6.9967	-0.025000	0.00024	0.99993	0.00781	280.861	.
16	BC	shoot	w1265	-0.000275	2.1047	-0.007595	0.00022	0.99993	0.00746	287.543	.
17	BC	stem	aot403	-0.000652	5.3613	-0.030000	0.00085	0.99974	0.01460	182.681	.
18	BC	stem	aot405	-0.000421	7.7734	-0.025000	0.00082	0.99975	0.01435	312.180	.
19	BC	stem	sum003	-0.000183	4.3188	-0.017297	0.00242	0.99927	0.02458	252.363	.
20	BC	stem	sum005	-0.000113	4.3914	-0.010935	0.00243	0.99927	0.02466	405.794	.
21	BC	stem	sum063	-0.000372	7.1516	-0.025000	0.00041	0.99988	0.01008	286.286	.
22	BC	stem	sum065	-0.000230	2.9797	-0.008959	0.00022	0.99993	0.00737	341.374	.
23	BC	stem	w1263	-0.000463	6.8827	-0.025000	0.00035	0.99990	0.00930	276.404	.
24	BC	stem	w1265	-0.000292	2.1976	-0.007945	0.00030	0.99991	0.00863	287.140	.
25	BC	total	aot403	-0.000669	5.8465	-0.030000	0.00076	0.99977	0.01374	199.329	.
26	BC	total	aot405	-0.000432	8.2585	-0.025000	0.00073	0.99978	0.01349	332.926	.
27	BC	total	sum003	-0.000193	3.4268	-0.013800	0.00243	0.99927	0.02465	251.839	.

Obs	SPECIES	Y	X	B	C	D	SSE	R2	RMSE	X0	A
28	BC	total	sum005	-0.000119	3.4847	-0.008724	0.00245	0.99926	0.02474	404.960	.
29	BC	total	sum063	-0.000382	7.6368	-0.025000	0.00029	0.99991	0.00847	306.959	.
30	BC	total	sum065	-0.000240	2.3585	-0.007148	0.00016	0.99995	0.00636	341.430	.
31	BC	total	w1263	-0.000474	7.3679	-0.025000	0.00030	0.99991	0.00868	297.173	.
32	BC	total	w1265	-0.000304	1.7344	-0.006339	0.00028	0.99992	0.00832	287.399	.
33	BW	root	aot403	-0.010810	0.6179	-0.033550	0.44594	0.96348	0.33389	27.173	.
34	BW	root	aot405	-0.007157	0.4345	-0.020806	0.48324	0.96043	0.34758	31.836	.
35	BW	root	sum003	-0.002272	5.2161	-0.034152	0.27289	0.97765	0.26119	163.617	.
36	BW	root	sum005	0.000000	5.3509	-0.021575	0.26644	0.97818	0.25809	248.015	.
37	BW	root	sum063	-0.015553	3.5103	-0.030000	0.31049	0.97457	0.27861	242.988	.
38	BW	root	sum065	-0.009479	1.7035	-0.015981	0.10593	0.99133	0.16273	261.988	.
39	BW	root	w1263	-0.018579	0.6150	-0.023147	0.28595	0.97658	0.26737	134.646	.
40	BW	root	w1265	-0.012255	0.4138	-0.014367	0.27817	0.97722	0.26371	195.972	.
41	BW	shoot	aot403	-0.000752	4.7546	-0.025000	0.00127	0.99990	0.01785	193.161	.
42	BW	shoot	aot405	-0.000485	8.4758	-0.025000	0.00122	0.99990	0.01749	342.920	.
43	BW	shoot	sum003	-0.000208	2.9740	-0.012099	0.00245	0.99980	0.02475	250.113	.
44	BW	shoot	sum005	-0.000129	3.0248	-0.007649	0.00247	0.99980	0.02485	402.224	.
45	BW	shoot	sum063	-0.000429	7.8540	-0.025000	0.00071	0.99994	0.01334	316.785	.
46	BW	shoot	sum065	-0.000254	2.0374	-0.006266	0.00023	0.99998	0.00757	338.858	.
47	BW	shoot	w1263	-0.000535	7.5851	-0.025000	0.00045	0.99996	0.01060	307.208	.
48	BW	shoot	w1265	-0.000323	1.4903	-0.005557	0.00025	0.99998	0.00795	284.723	.
49	BW	stem	aot403	-0.000628	4.7459	-0.025000	0.00089	0.99993	0.01494	191.775	.
50	BW	stem	aot405	-0.000405	8.4670	-0.025000	0.00086	0.99993	0.01464	341.393	.
51	BW	stem	sum003	-0.000173	3.0417	-0.012293	0.00170	0.99986	0.02062	250.978	.
52	BW	stem	sum005	-0.000107	3.0932	-0.007771	0.00171	0.99986	0.02069	403.598	.
53	BW	stem	sum063	-0.000358	7.8452	-0.025000	0.00050	0.99996	0.01120	315.473	.
54	BW	stem	sum065	-0.000212	2.0900	-0.006367	0.00016	0.99999	0.00630	339.552	.
55	BW	stem	w1263	-0.000447	7.5764	-0.025000	0.00032	0.99997	0.00889	305.693	.
56	BW	stem	w1265	-0.000270	1.5341	-0.005647	0.00017	0.99999	0.00661	285.312	.
57	BW	total	aot403	-0.010818	3.6180	-0.030000	0.20496	0.98322	0.22636	188.617	.
58	BW	total	aot405	-0.006978	6.0300	-0.025000	0.19653	0.98391	0.22166	328.253	.
59	BW	total	sum003	-0.000000	3.0970	-0.018506	0.02016	0.99835	0.07099	167.351	.
60	BW	total	sum005	-0.000000	3.1712	-0.011693	0.02079	0.99830	0.07210	271.208	.
61	BW	total	sum063	-0.006174	5.4083	-0.025000	0.08455	0.99308	0.14539	279.804	.
62	BW	total	sum065	-0.003521	1.6464	-0.009593	0.04490	0.99632	0.10595	271.162	.
63	BW	total	w1263	-0.007674	5.1394	-0.025000	0.06765	0.99446	0.13004	289.500	.
64	BW	total	w1265	-0.004834	1.0674	-0.008984	0.05455	0.99553	0.11678	257.203	.
65	CO	root	aot403	-0.006125	1.6289	-0.045527	0.14327	0.98886	0.18926	41.341	.
66	CO	root	aot405	-0.004055	1.5592	-0.028860	0.13825	0.98925	0.18591	62.860	.
67	CO	root	sum003	0.000000	7.5170	-0.045204	0.05037	0.99609	0.11221	166.289	.
68	CO	root	sum005	-0.000000	7.6985	-0.028562	0.05058	0.99607	0.11245	269.532	.
69	CO	root	sum063	-0.006619	3.0257	-0.033919	0.75854	0.94104	0.43547	110.833	.
70	CO	root	sum065	-0.008815	3.7000	-0.022873	0.38517	0.97006	0.31031	263.183	.
71	CO	root	w1263	-0.017228	2.1487	-0.033158	0.52368	0.95930	0.36183	134.886	.
72	CO	root	w1265	-0.012362	2.4053	-0.021578	0.47937	0.96274	0.34618	260.984	.
73	CO	shoot	aot403	-0.000291	5.4920	-0.025000	0.00048	0.99996	0.01096	220.580	.

Obs	SPECIES	Y	X	B	C	D	SSE	R2	RMSE	X0	A
74	CO	shoot	aot405	-0.000188	9.2131	-0.025000	0.00047	0.99996	0.01086	369.651	.
75	CO	shoot	sum003	-0.000067	1.7969	-0.007237	0.00054	0.99996	0.01161	250.605	.
76	CO	shoot	sum005	-0.000041	1.8273	-0.004576	0.00054	0.99996	0.01164	403.016	.
77	CO	shoot	sum063	-0.000166	8.5914	-0.025000	0.00039	0.99997	0.00993	344.271	.
78	CO	shoot	sum065	-0.000088	1.2366	-0.003749	0.00015	0.99999	0.00605	337.790	.
79	CO	shoot	w1263	-0.000209	8.3225	-0.025000	0.00030	0.99998	0.00859	334.040	.
80	CO	shoot	w1265	-0.000112	0.9093	-0.003325	0.00014	0.99999	0.00594	283.060	.
81	CO	stem	aot403	-0.000354	5.5293	-0.025000	0.00057	0.99996	0.01195	222.735	.
82	CO	stem	aot405	-0.000228	9.2504	-0.025000	0.00056	0.99996	0.01182	371.843	.
83	CO	stem	sum003	-0.000086	1.7054	-0.006910	0.00078	0.99994	0.01400	249.880	.
84	CO	stem	sum005	-0.000053	1.7344	-0.004369	0.00079	0.99994	0.01404	401.863	.
85	CO	stem	sum063	-0.000202	8.6287	-0.025000	0.00044	0.99997	0.01052	346.351	.
86	CO	stem	sum065	-0.000111	1.1704	-0.003579	0.00018	0.99999	0.00667	337.461	.
87	CO	stem	w1263	-0.000253	8.3598	-0.025000	0.00033	0.99997	0.00904	336.228	.
88	CO	stem	w1265	-0.000141	0.8579	-0.003174	0.00018	0.99999	0.00664	282.877	.
89	CO	total	aot403	-0.009865	3.5522	-0.030000	0.20074	0.98440	0.22402	176.421	.
90	CO	total	aot405	-0.006364	5.9642	-0.025000	0.19341	0.98497	0.21989	313.004	.
91	CO	total	sum003	-0.000505	3.4497	-0.019581	0.04056	0.99685	0.10069	180.843	.
92	CO	total	sum005	-0.000312	3.5318	-0.012379	0.04058	0.99685	0.10072	292.679	.
93	CO	total	sum063	-0.005631	5.3425	-0.025000	0.10024	0.99221	0.15830	267.968	.
94	CO	total	sum065	-0.003066	1.9056	-0.010117	0.05680	0.99559	0.11916	270.237	.
95	CO	total	w1263	-0.007009	5.0736	-0.025000	0.07452	0.99421	0.13649	274.212	.
96	CO	total	w1265	-0.004343	1.3371	-0.009552	0.05552	0.99568	0.11781	256.664	.
97	RM	root	aot403	-0.000133	4.6201	-0.047107	0.05092	0.99579	0.11282	98.354	.
98	RM	root	aot405	-0.000086	4.5407	-0.029840	0.05177	0.99572	0.11376	152.609	.
99	RM	root	sum003	-0.000036	10.7424	-0.046861	0.04959	0.99590	0.11135	229.412	.
100	RM	root	sum005	-0.000022	10.9389	-0.029626	0.04956	0.99590	0.11131	369.511	.
101	RM	root	sum063	-0.000096	7.0708	-0.038261	0.00003	1.00000	0.00269	185.268	.
102	RM	root	sum065	-0.000064	6.7029	-0.023560	0.00002	1.00000	0.00248	285.283	.
103	RM	root	w1263	-0.000106	5.0236	-0.033909	0.00074	0.99994	0.01358	148.615	.
104	RM	root	w1265	-0.000070	4.7288	-0.021046	0.00266	0.99978	0.02580	225.438	.
105	RM	shoot	aot403	-0.000415	5.1397	-0.030000	0.00818	0.99932	0.04521	173.729	.
106	RM	shoot	aot405	-0.000269	7.5518	-0.025000	0.00814	0.99933	0.04510	300.863	.
107	RM	shoot	sum003	-0.000013	4.6404	-0.018676	0.00005	1.00000	0.00352	248.648	.
108	RM	shoot	sum005	-0.000008	4.7188	-0.011807	0.00005	1.00000	0.00352	399.938	.
109	RM	shoot	sum063	-0.000236	6.9300	-0.025000	0.00809	0.99933	0.04496	275.335	.
110	RM	shoot	sum065	-0.000018	3.1945	-0.009673	0.00003	1.00000	0.00271	330.876	.
111	RM	shoot	w1263	-0.000308	6.6611	-0.025000	0.00736	0.99939	0.04289	265.263	.
112	RM	shoot	w1265	-0.000024	2.3500	-0.008579	0.00003	1.00000	0.00263	274.688	.
113	RM	stem	aot403	-0.000412	5.3386	-0.030000	0.00792	0.99934	0.04450	180.427	.
114	RM	stem	aot405	-0.000266	7.7506	-0.025000	0.00788	0.99935	0.04439	309.214	.
115	RM	stem	sum003	-0.000014	4.2798	-0.017255	0.00005	1.00000	0.00360	248.226	.
116	RM	stem	sum005	-0.000009	4.3522	-0.010909	0.00005	1.00000	0.00361	399.272	.
117	RM	stem	sum063	-0.000233	7.1288	-0.025000	0.00783	0.99935	0.04425	283.680	.
118	RM	stem	sum065	-0.000019	2.9439	-0.008937	0.00003	1.00000	0.00275	330.097	.
119	RM	stem	w1263	-0.000305	6.8600	-0.025000	0.00712	0.99941	0.04219	273.627	.

Obs	SPECIES	Y	X	B	C	D	SSE	R2	RMSE	X0	A
120	RM	stem	w1265	-0.000025	2.1636	-0.007926	0.00003	1.00000	0.00266	273.815	.
121	RM	total	aot403	-0.000068	2.7327	-0.024960	0.00003	1.00000	0.00291	109.783	.
122	RM	total	aot405	-0.000754	6.4644	-0.025000	0.07182	0.99406	0.13399	260.218	.
123	RM	total	sum003	-0.000020	5.9802	-0.024839	0.00006	0.99999	0.00398	240.956	.
124	RM	total	sum005	-0.000012	6.0844	-0.015703	0.00006	0.99999	0.00399	387.772	.
125	RM	total	sum063	-0.000039	4.2581	-0.020893	0.00003	1.00000	0.00266	204.193	.
126	RM	total	sum065	-0.000026	4.0572	-0.012865	0.00003	1.00000	0.00257	316.019	.
127	RM	total	w1263	-0.000864	5.5738	-0.025000	0.06555	0.99458	0.12801	224.473	.
128	RM	total	w1265	-0.000034	2.9340	-0.011410	0.00002	1.00000	0.00248	257.919	.
129	RO	root	aot403	-0.003422	4.6018	-0.042316	0.02398	0.99382	0.07742	118.319	.
130	RO	root	aot405	-0.002213	4.5280	-0.026798	0.02325	0.99401	0.07623	184.174	.
131	RO	root	sum003	-0.001060	10.1075	-0.042111	0.07975	0.97945	0.14120	246.218	.
132	RO	root	sum005	-0.000656	10.2842	-0.026623	0.08029	0.97931	0.14168	396.050	.
133	RO	root	sum063	-0.001980	7.1879	-0.035421	0.01088	0.99720	0.05215	214.947	.
134	RO	root	sum065	-0.001324	6.8474	-0.021811	0.00909	0.99766	0.04768	334.235	.
135	RO	root	w1263	-0.002561	5.2514	-0.031273	0.01026	0.99736	0.05065	182.897	.
136	RO	root	w1265	-0.001686	4.9431	-0.019344	0.00995	0.99744	0.04987	279.943	.
137	RO	shoot	aot403	0.000010	5.7693	-0.025000	0.00000	1.00000	0.00042	229.380	.
138	RO	shoot	aot405	0.000007	9.4905	-0.025000	0.00000	1.00000	0.00042	378.219	.
139	RO	shoot	sum003	0.000004	1.4276	-0.005595	0.00000	1.00000	0.00042	254.939	.
140	RO	shoot	sum005	0.000003	1.4511	-0.003537	0.00000	1.00000	0.00042	409.893	.
141	RO	shoot	sum063	0.000006	8.8687	-0.025000	0.00000	1.00000	0.00038	353.367	.
142	RO	shoot	sum065	0.000005	0.9944	-0.002898	0.00000	1.00000	0.00023	342.533	.
143	RO	shoot	w1263	0.000007	8.5998	-0.025000	0.00000	1.00000	0.00044	342.596	.
144	RO	shoot	w1265	0.000006	0.7414	-0.002570	0.00000	1.00000	0.00027	287.739	.
145	RO	stem	aot403	0.000001	5.7988	-0.025000	0.00000	1.00000	0.00048	230.697	.
146	RO	stem	aot405	0.000001	9.5200	-0.025000	0.00000	1.00000	0.00048	379.542	.
147	RO	stem	sum003	0.000002	1.3697	-0.005374	0.00000	1.00000	0.00024	254.818	.
148	RO	stem	sum005	0.000001	1.3923	-0.003397	0.00000	1.00000	0.00024	409.700	.
149	RO	stem	sum063	0.000001	8.8982	-0.025000	0.00000	1.00000	0.00048	354.673	.
150	RO	stem	sum065	0.000002	0.9537	-0.002783	0.00000	1.00000	0.00027	342.454	.
151	RO	stem	w1263	0.000001	8.6293	-0.025000	0.00000	1.00000	0.00049	343.919	.
152	RO	stem	w1265	0.000002	0.7107	-0.002468	0.00000	1.00000	0.00028	287.679	.
153	RO	total	aot403	-0.001214	5.6578	-0.030000	0.00714	0.99816	0.04224	196.551	.
154	RO	total	aot405	-0.000784	8.0699	-0.025000	0.00698	0.99820	0.04176	329.795	.
155	RO	total	sum003	-0.000290	3.4666	-0.014380	0.00793	0.99796	0.04453	246.030	.
156	RO	total	sum005	-0.000179	3.5269	-0.009091	0.00798	0.99794	0.04466	395.761	.
157	RO	total	sum063	-0.000693	7.4481	-0.025000	0.00567	0.99854	0.03765	302.909	.
158	RO	total	sum065	-0.000370	2.3533	-0.007448	0.00176	0.99955	0.02095	332.463	.
159	RO	total	w1263	-0.000871	7.1792	-0.025000	0.00405	0.99896	0.03182	294.062	.
160	RO	total	w1265	-0.000472	1.7030	-0.006605	0.00166	0.99957	0.02037	277.676	.
161	SM	root	aot403	-0.000052	-2.8810	0.020000	0.00000	0.99998	0.00105	143.679	.
162	SM	root	aot405	-0.000034	-2.0897	0.010824	0.00000	0.99998	0.00104	192.463	.
163	SM	root	sum003	-0.000018	-4.3433	0.017009	0.00002	0.99991	0.00230	255.082	.
164	SM	root	sum005	-0.000011	-4.4147	0.010753	0.00002	0.99991	0.00231	410.120	.
165	SM	root	sum063	-0.000030	-3.1641	0.014307	0.00000	0.99999	0.00059	220.696	.

Obs	SPECIES	Y	X	B	C	D	SSE	R2	RMSE	X0	A
166	SM	root	sum065	-0.000020	-3.0265	0.008809	0.00000	0.99999	0.00055	342.768	.
167	SM	root	w1263	-0.000039	-2.3819	0.012631	0.00000	0.99999	0.00073	187.994	.
168	SM	root	w1265	-0.000026	-2.2574	0.007813	0.00000	0.99999	0.00072	287.986	.
169	SM	shoot	aot403	-0.000005	5.5292	-0.025000	0.00000	1.00000	0.00014	219.523	.
170	SM	shoot	aot405	-0.000004	9.2503	-0.025000	0.00000	1.00000	0.00014	368.373	.
171	SM	shoot	sum003	-0.000001	1.8638	-0.007313	0.00000	1.00000	0.00018	254.916	.
172	SM	shoot	sum005	-0.000001	1.8945	-0.004623	0.00000	1.00000	0.00018	409.854	.
173	SM	shoot	sum063	-0.000003	8.6285	-0.025000	0.00000	1.00000	0.00012	343.493	.
174	SM	shoot	sum065	-0.000002	1.2976	-0.003788	0.00000	1.00000	0.00004	342.762	.
175	SM	shoot	w1263	-0.000004	8.3597	-0.025000	0.00000	1.00000	0.00010	332.747	.
176	SM	shoot	w1265	-0.000002	0.9670	-0.003359	0.00000	1.00000	0.00005	288.048	.
177	SM	stem	aot403	-0.000007	5.6700	-0.025000	0.00000	1.00000	0.00017	225.402	.
178	SM	stem	aot405	-0.000004	9.3911	-0.025000	0.00000	1.00000	0.00017	374.252	.
179	SM	stem	sum003	-0.000002	1.6047	-0.006297	0.00000	1.00000	0.00021	254.890	.
180	SM	stem	sum005	-0.000001	1.6312	-0.003981	0.00000	1.00000	0.00021	409.813	.
181	SM	stem	sum063	-0.000004	8.7694	-0.025000	0.00000	1.00000	0.00014	349.370	.
182	SM	stem	sum065	-0.000002	1.1172	-0.003262	0.00000	1.00000	0.00005	342.736	.
183	SM	stem	w1263	-0.000005	8.5005	-0.025000	0.00000	1.00000	0.00012	338.626	.
184	SM	stem	w1265	-0.000003	0.8324	-0.002893	0.00000	1.00000	0.00006	288.024	.
185	SM	total	aot403	-0.000010	6.0244	-0.025000	0.00000	1.00000	0.00021	240.212	.
186	SM	total	aot405	-0.000007	9.7456	-0.025000	0.00000	1.00000	0.00021	389.063	.
187	SM	total	sum003	-0.000003	0.9527	-0.003742	0.00000	1.00000	0.00038	254.803	.
188	SM	total	sum005	-0.000002	0.9684	-0.002366	0.00000	1.00000	0.00038	409.674	.
189	SM	total	sum063	-0.000006	9.1238	-0.025000	0.00000	1.00000	0.00013	364.173	.
190	SM	total	sum065	-0.000004	0.6630	-0.001938	0.00000	1.00000	0.00009	342.743	.
191	SM	total	w1263	-0.000007	8.8549	-0.025000	0.00000	1.00000	0.00013	353.437	.
192	SM	total	w1265	-0.000005	0.4938	-0.001719	0.00000	1.00000	0.00012	288.064	.
193	WA	root	aot403	-0.070814	-10.4119	-0.030000	9.54811	0.70941	1.54500	255.107	.
194	WA	root	aot405	-0.045678	-7.9998	-0.025000	9.17936	0.72063	1.51487	385.404	.
195	WA	root	sum003	-0.003934	11.6592	-0.078529	7.16223	0.78202	1.33812	156.300	.
196	WA	root	sum005	-0.002428	11.9708	-0.049613	7.08727	0.78430	1.33110	253.701	.
197	WA	root	sum063	-0.044220	-8.6216	-0.025000	7.61706	0.76818	1.37995	453.145	.
198	WA	root	sum065	-0.014025	1.7817	-0.033129	0.62599	0.98095	0.39560	93.265	.
199	WA	root	w1263	-0.050267	-8.8905	-0.025000	3.36739	0.89751	0.91752	350.921	.
200	WA	root	w1265	-0.032975	-2.2855	-0.027069	3.16793	0.90359	0.88993	386.939	.
201	WA	shoot	aot403	-0.000375	4.5941	-0.030000	0.00395	0.99988	0.03143	155.073	.
202	WA	shoot	aot405	-0.000242	7.0062	-0.025000	0.00392	0.99988	0.03131	277.559	.
203	WA	shoot	sum003	-0.000040	5.7223	-0.022808	0.00036	0.99999	0.00945	251.324	.
204	WA	shoot	sum005	-0.000025	5.8180	-0.014419	0.00036	0.99999	0.00947	404.170	.
205	WA	shoot	sum063	-0.000213	6.3844	-0.025000	0.00386	0.99988	0.03105	252.130	.
206	WA	shoot	sum065	-0.000050	3.9565	-0.011813	0.00026	0.99999	0.00806	336.330	.
207	WA	shoot	w1263	-0.000276	6.1155	-0.025000	0.00336	0.99990	0.02896	241.904	.
208	WA	shoot	w1265	-0.000065	2.9251	-0.010477	0.00024	0.99999	0.00773	280.931	.
209	WA	stem	aot403	-0.000847	4.6151	-0.030000	0.00756	0.99977	0.04347	158.309	.
210	WA	stem	aot405	-0.000547	7.0272	-0.025000	0.00746	0.99977	0.04317	281.996	.
211	WA	stem	sum003	-0.000157	5.4725	-0.022121	0.00239	0.99993	0.02444	249.164	.

Obs	SPECIES	Y	X	B	C	D	SSE	R2	RMSE	X0	A
212	WA	stem	sum005	-0.000097	5.5653	-0.013985	0.00240	0.99993	0.02451	400.743	.
213	WA	stem	sum063	-0.000483	6.4054	-0.025000	0.00694	0.99979	0.04164	255.856	.
214	WA	stem	sum065	-0.000200	3.7599	-0.011457	0.00060	0.99998	0.01226	334.005	.
215	WA	stem	w1263	-0.000613	6.1365	-0.025000	0.00556	0.99983	0.03728	246.216	.
216	WA	stem	w1265	-0.000256	2.7596	-0.010161	0.00056	0.99998	0.01182	278.603	.
217	WA	total	aot403	-0.005273	0.9688	-0.030265	0.07204	0.99781	0.13420	38.763	.
218	WA	total	aot405	-0.003491	0.9224	-0.019185	0.06986	0.99787	0.13215	58.772	.
219	WA	total	sum003	0.000000	4.9206	-0.030171	0.00108	0.99997	0.01643	163.093	.
220	WA	total	sum005	0.000000	5.0392	-0.019058	0.00070	0.99998	0.01327	264.410	.
221	WA	total	sum063	-0.005698	1.9081	-0.022599	0.22356	0.99320	0.23641	112.897	.
222	WA	total	sum065	-0.006281	2.2434	-0.015018	0.09766	0.99703	0.15625	256.763	.
223	WA	total	w1263	-0.011021	0.9894	-0.021015	0.20128	0.99387	0.22432	98.999	.
224	WA	total	w1265	-0.008683	1.2009	-0.013814	0.19158	0.99417	0.21885	234.055	.
225	YP	root	aot403	-0.003464	7.9055	-0.070866	0.05856	0.98996	0.12099	117.289	.
226	YP	root	aot405	-0.002240	7.7819	-0.044879	0.05773	0.99010	0.12014	182.506	.
227	YP	root	sum003	-0.001027	17.1259	-0.070523	0.13435	0.97697	0.18327	246.432	.
228	YP	root	sum005	-0.000635	17.4218	-0.044585	0.13501	0.97686	0.18372	396.405	.
229	YP	root	sum063	-0.002008	12.2365	-0.059319	0.04413	0.99244	0.10503	213.508	.
230	YP	root	sum065	-0.001347	11.6661	-0.036526	0.04018	0.99311	0.10023	331.619	.
231	YP	root	w1263	-0.002616	8.9933	-0.052372	0.03884	0.99334	0.09854	180.748	.
232	YP	root	w1265	-0.001723	8.4771	-0.032395	0.03825	0.99344	0.09779	276.385	.
233	YP	shoot	aot403	-0.000371	5.6696	-0.025000	0.00068	0.99988	0.01302	228.840	.
234	YP	shoot	aot405	-0.000239	9.3907	-0.025000	0.00066	0.99989	0.01287	377.926	.
235	YP	shoot	sum003	-0.000087	1.4320	-0.005860	0.00067	0.99989	0.01293	248.057	.
236	YP	shoot	sum005	-0.000054	1.4566	-0.003705	0.00067	0.99988	0.01297	398.976	.
237	YP	shoot	sum063	-0.000212	8.7689	-0.025000	0.00054	0.99991	0.01166	352.393	.
238	YP	shoot	sum065	-0.000111	0.9783	-0.003035	0.00013	0.99998	0.00563	334.529	.
239	YP	shoot	w1263	-0.000266	8.5001	-0.025000	0.00039	0.99993	0.00992	342.324	.
240	YP	shoot	w1265	-0.000141	0.7133	-0.002692	0.00012	0.99998	0.00559	279.668	.
241	YP	stem	aot403	-0.000448	5.8646	-0.025000	0.00080	0.99986	0.01417	237.869	.
242	YP	stem	aot405	-0.000289	9.5858	-0.025000	0.00078	0.99987	0.01400	386.942	.
243	YP	stem	sum003	-0.000110	1.0446	-0.004381	0.00098	0.99983	0.01562	244.565	.
244	YP	stem	sum005	-0.000068	1.0630	-0.002770	0.00098	0.99983	0.01567	393.436	.
245	YP	stem	sum063	-0.000255	8.9640	-0.025000	0.00061	0.99990	0.01231	361.259	.
246	YP	stem	sum065	-0.000139	0.7055	-0.002269	0.00015	0.99997	0.00613	331.112	.
247	YP	stem	w1263	-0.000320	8.6951	-0.025000	0.00043	0.99993	0.01035	351.347	.
248	YP	stem	w1265	-0.000177	0.5073	-0.002012	0.00015	0.99997	0.00622	276.349	.
249	YP	total	aot403	-0.000871	1.9987	-0.017851	0.00324	0.99944	0.02846	117.706	.
250	YP	total	aot405	-0.000769	7.5915	-0.025000	0.00923	0.99842	0.04803	308.968	.
251	YP	total	sum003	-0.000260	4.3213	-0.017765	0.00782	0.99866	0.04422	246.869	.
252	YP	total	sum005	-0.000161	4.3959	-0.011231	0.00786	0.99865	0.04434	397.098	.
253	YP	total	sum063	-0.000680	6.9698	-0.025000	0.00801	0.99863	0.04474	282.202	.
254	YP	total	sum065	-0.000338	2.9460	-0.009201	0.00211	0.99964	0.02298	332.404	.
255	YP	total	w1263	-0.000858	6.7009	-0.025000	0.00605	0.99896	0.03890	273.187	.
256	YP	total	w1265	-0.000433	2.1427	-0.008160	0.00202	0.99965	0.02246	277.272	.

Appendix H

Details of Regional Ground-level Ozone Interpolation

Methods

The study area of Shenandoah National Park in Virginia was expanded to six eastern states (VA, MD, PA, WV, NC, and OH) in order to interpolate ozone exposures in the area of interest. By interpolating over a larger region we believe our estimate of ozone exposure in the Park is more robust. The expanded study area was represented by a 15-arc-second digital elevation model (DEM) and projected to an Albers equal-area conic map projection. Elevation data are from the United States Geological Survey (USGS) Conterminous U.S. Advanced Very High Resolution Radiometer Companion Disc (Loveland et al. 1991) and re-sampled by the USGS to 1 km resolution. Elevation data from the DEM on a 4 km grid were used to spatially interpolate monthly air temperature at high spatial resolution and, subsequently with air temperature, to interpolate ozone exposure at the same resolution.

The loess regression/kriging statistical interpolation approach presented in Lee and Hogsett (2001) was used to generate high-resolution maps of monthly SUM06 values using monitoring data for ozone in conjunction with elevation and temperature data sampled at higher spatial density. The inclusion of elevation and temperature significantly improved the ability to predict ozone exposures over complex terrain and overcomes the data limitations imposed by poor spatial coverage of the ozone-monitoring network. The elevation-based interpolation method produced accurate and precise temperature and ozone exposure surfaces that had desirable statistical properties and were logically consistent with topographical features and atmospheric conditions known to influence ozone formation and transport.

Ambient ozone exposure was characterized using the 5-month 12-h SUM06 index for assessing the ecological risk of ozone to tree species in Shenandoah National Park. Monthly SUM06 values were calculated as the sum of all hourly ozone concentrations $\geq$0.06 ppm between 0800 and 2000 for May to September 1997-1999. Prediction surfaces for the monthly SUM06 values were generated using the loess/kriging interpolation method and summed to calculate the prediction surface for the 5-month SUM06 index.

Hourly ozone monitoring data were obtained from the EPA's Aerometric Information Retrieval System (AIRS). About 150 AIRS monitoring stations denoted as either rural or suburban and reporting a land use of forest, agricultural, residential, desert or mobile received highest priority in the analysis. Urban, city-center monitoring sites in close proximity to a "non-urban" site were excluded from the analysis to minimize the effect of nitric oxide scavenging in urban areas (Logan 1989). The majority of monitoring sites in the AIRS database were located nearby major urban centers and at lower elevation. Consequently, background ozone concentrations at the suburban and rural sites are likely influenced by pollutant plume transport from downwind urban sources to varying degrees.

Monthly 12-h SUM06 values were calculated as the sum of hourly ozone concentrations $\geq$0.06 ppm between 0800 and 2000 and were adjusted for missing values by a multiplicative factor equal to the number of days in the month times 12 divided by the number of available hourly ozone concentrations. Daily SUM06 values were considered valid if at least nine hourly ozone concentrations between 8:00 AM and 8:00 PM were available for calculation. The adjusted monthly SUM06 values were retained for analysis if there were at least 75 percent valid days in the month. Initially, the number of ozone monitoring stations that met our data completeness criterion ranged from 140 for May 1997 to 158 for July 1999. There were large gaps in spatial coverage in non-urban areas and at higher elevations (Figure H-1).

Maximum daily temperature data were obtained from monitoring stations from the National Weather Service (NWS) cooperative network archived at the National Climatic Data Center

(NCDC). Daily temperature data for 1997 and 1998 were available for about 550 meteorological stations from the NCDC Summary of the Day TD-3200 database purchased from EarthInfo (EarthInfo 1992). Daily temperature data for 158 meteorological stations for 1999 were obtained directly from NCDC. The locations of these stations are shown in Figure H-2. The more densely sampled temperature data were used in the first stage of the analysis to predict mean monthly temperature values at the geographic locations of the ozone monitoring stations.

Results

The monthly mean daily maximum temperature was interpolated at the geographic locations for the ozone monitoring stations based on separate loess/kriging models for each month. Loess regression was used to model the large-scale variability in monthly temperature as a function of geographic location, elevation, and coastal proximity. Kriging of the loess residuals was used to model the small-scale spatial dependencies as a function of relative spatial location. All calculations were performed in MathSoft Splus V5.1 and its accompanying module S+Spatialstats V1 (MathSoft, 1996, 1998). The loess fits had R^2 values ranging from 0.78 to 0.89 and residual standard errors (RSEs) ranging from 0.78 C to 0.92 C (Table H-1).

For each region, the weighted nonlinear least squares approach was used to fit a spherical variogram model to the empirical one as a function of relative spatial location (Cressie 1985). A dominant nugget effect was observed for most months and indicated a weak covariance structure among neighboring sampled points (Table H-2). Consequently, kriging gave marginal improvements in accuracy and precision in temperature predictions for the eastern United States.

Loess regression was used to model the large-scale variability in monthly SUM06 values as a function of geographic location, elevation, and predicted monthly mean daily maximum temperature. The loess fits had R^2 values ranging from 0.17 to 0.78 and residual standard errors (RSEs) ranging from 1.37 to 3.23 ppm-h (Table H-3). The low R^2 value for May 1998 was attributed to low spatial variability in monthly SUM06 values and did not indicate poor predictive ability. The loess predictions for monthly SUM06 values were as precise for May 1998 as other months in 1998 based on the RSE.

Except for September 1997 and 1999, the range parameter in the spherical variogram model was less than 70 km indicating that sampled points within a 70 km radius largely influence the kriged prediction of the SUM06 residual at an unsampled point. Consequently, kriging gave marginal improvements in accuracy and precision in SUM06 predictions for the Shenandoah National Park area because of the sparse spatial coverage of the ozone-monitoring network (Table H-4).

Figures H-3 to H-5 show the spatial extrapolation of ozone over the region for 1997-1999.

Table H-1. Locally quadratic loess fits for monthly mean daily maximum air temperature as a function of elevation, geographic location and coastal proximity.

	1997[1]				1998				1999[2]			
Month	# Obs.	Residual SE (C)	R^2	Span	# Obs.	Residual SE (C)	R^2	Span	# Obs.	Residual SE (C)	R^2	Span
May	685	0.83	0.92	0.65	521	0.85	0.80	0.50	556	0.81	0.79	0.60
June	686	0.81	0.80	0.50	524	0.89	0.89	0.60	559	0.83	0.78	0.50
July	685	0.88	0.84	1.00	523	0.87	0.86	0.60	558	0.84	0.81	0.60
August	685	0.84	0.89	1.00	527	0.82	0.83	0.50	561	0.83	0.88	0.60
Sept	685	0.82	0.89	0.80	538	0.86	0.86	0.40	563	0.78	0.81	0.70

[1] Meteorological stations for TN and KY were included in 1997 but were excluded in 1998 and 1999.
[2] Maximum daily temperature data for 1999 were obtained from NCDC by Chris Daly.

Table H-2. Kriging models for loess residuals for monthly mean daily maximum air temperature as a function of spatial distance.

.	1997			1998			1999		
Month	Range (km)	Sill ($^oC^2$)	Nugget ($^oC^2$)	Range (km)	Sill ($^oC^2$)	Nugget ($^oC^2$)	Range (km)	Sill ($^oC^2$)	Nugget ($^oC^2$)
May	NA	NA	NA	72	0.32	0.34	112	0.14	0.47
June	161	0.14	0.48	72	0.29	0.41	82	0.24	0.42
July	112	0.17	0.52	109	0.24	0.47	93	0.17	0.52
August	169	0.20	0.46	89	0.20	0.47	68	0.26	0.37
Sept	114	0.19	0.44	107	0.19	0.52	118	0.17	0.42

Table H-3. Locally quadratic loess fits for monthly 12-h SUM06 ozone exposure index as a function of elevation, geographic location and monthly mean daily maximum temperature.

	1997[1]				1998				1999[2]			
Month	# Obs.	Residual SE (ppm-h)	R^2	Span	# Obs.	Residual SE (ppm-h)	R^2	Span	# Obs.	Residual SE (ppm-h)	R^2	Span
May	140	1.45	0.77	2.50	150	2.01	0.17[1]	1.80	156	2.58	0.32	2.00
June	142	2.08	0.51	1.80	151	1.91	0.63	1.80	157	2.14	0.50	1.80
July	142	2.71	0.55	2.50	151	2.48	0.59	1.00	158	3.23	0.44	2.00
August	143	1.93	0.67	1.40	151	2.30	0.53	1.00	158	2.49	0.78	2.00
Sept	143	1.37	0.70	1.00	150	1.97	0.66	0.60	155	1.44	0.69	2.00

[1] Low r^2 in May 1998 was due to low spatial variability in monthly SUM06 values which had an interquartile range equal to 2.4 ppm- h. Note that the RSE was 2.01 ppm-h for May 1998 so that the loess regression had as much precision in spatial predictions as other months.

Table H-4. Kriging models for loess residuals for monthly 12-h SUM06 ozone exposure index as a function of spatial distance.

.	1997			1998			1999		
Month	Range (km)	Sill $(ppm\text{-}h)^2$	Nugget $(ppm\text{-}h)^2$	Range (km)	Sill $(ppm\text{-}h)^2$	Nugget $(ppm\text{-}h)^2$	Range (km)	Sill $(ppm\text{-}h)^2$	Nugget $(ppm\text{-}h)^2$
May	NA	NA	NA	NA	NA	NA	46	3.59	1.26
June	NA	NA	NA	30	2.80	0.41	48	3.05	0.87
July	48	4.38	1.55	38	5.21	0.29	69	5.32	3.08
August	41	2.71	0.12	48	2.62	2.06	48	2.62	2.06
Sept	113	0.61	0.71	NA	NA	NA	203	0.47	1.20

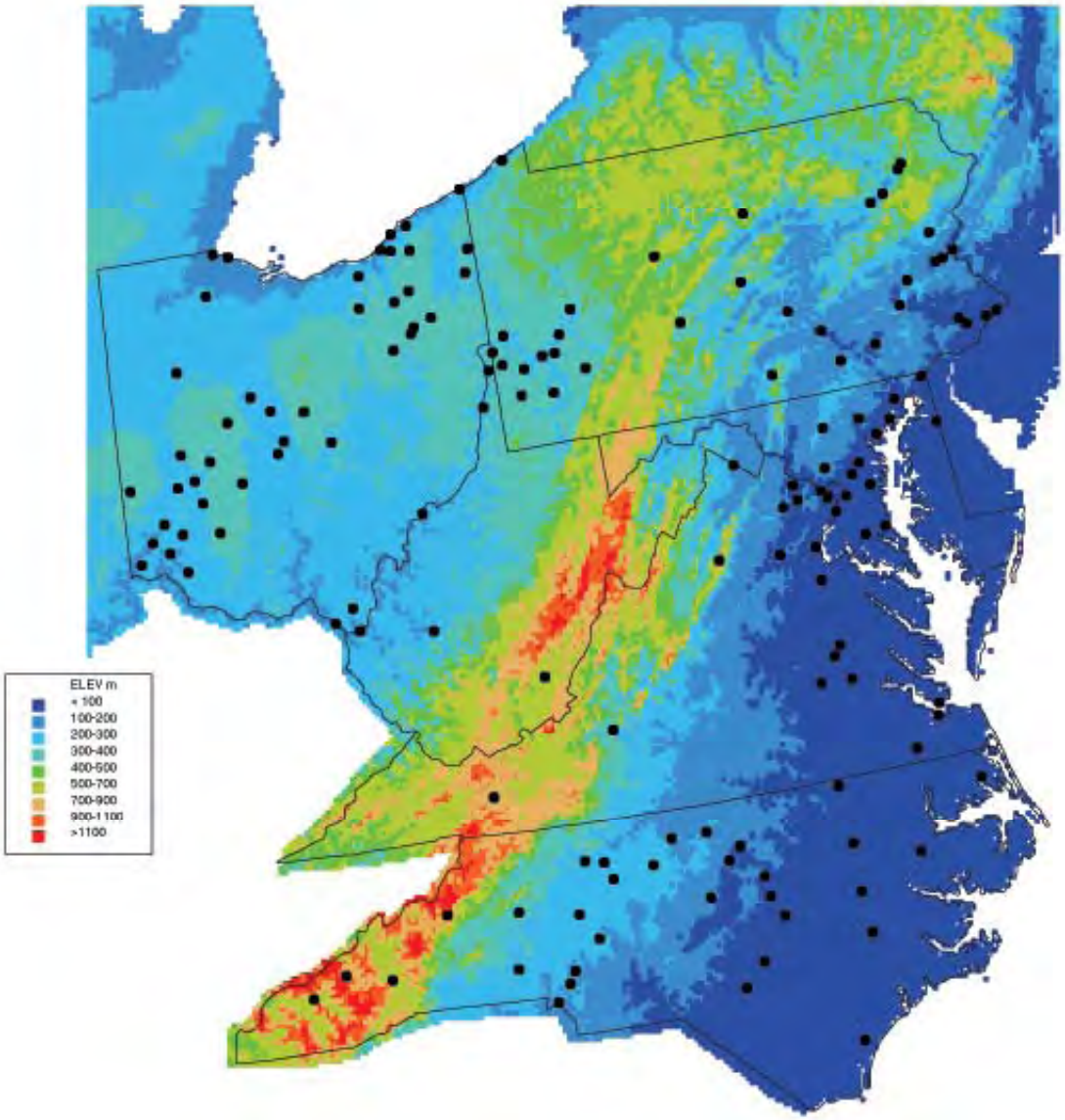

U.S. EPA's AIRS monitoring stations for 1998.

Figure H-1. EPA AIRS ozone monitoring stations for 1998.

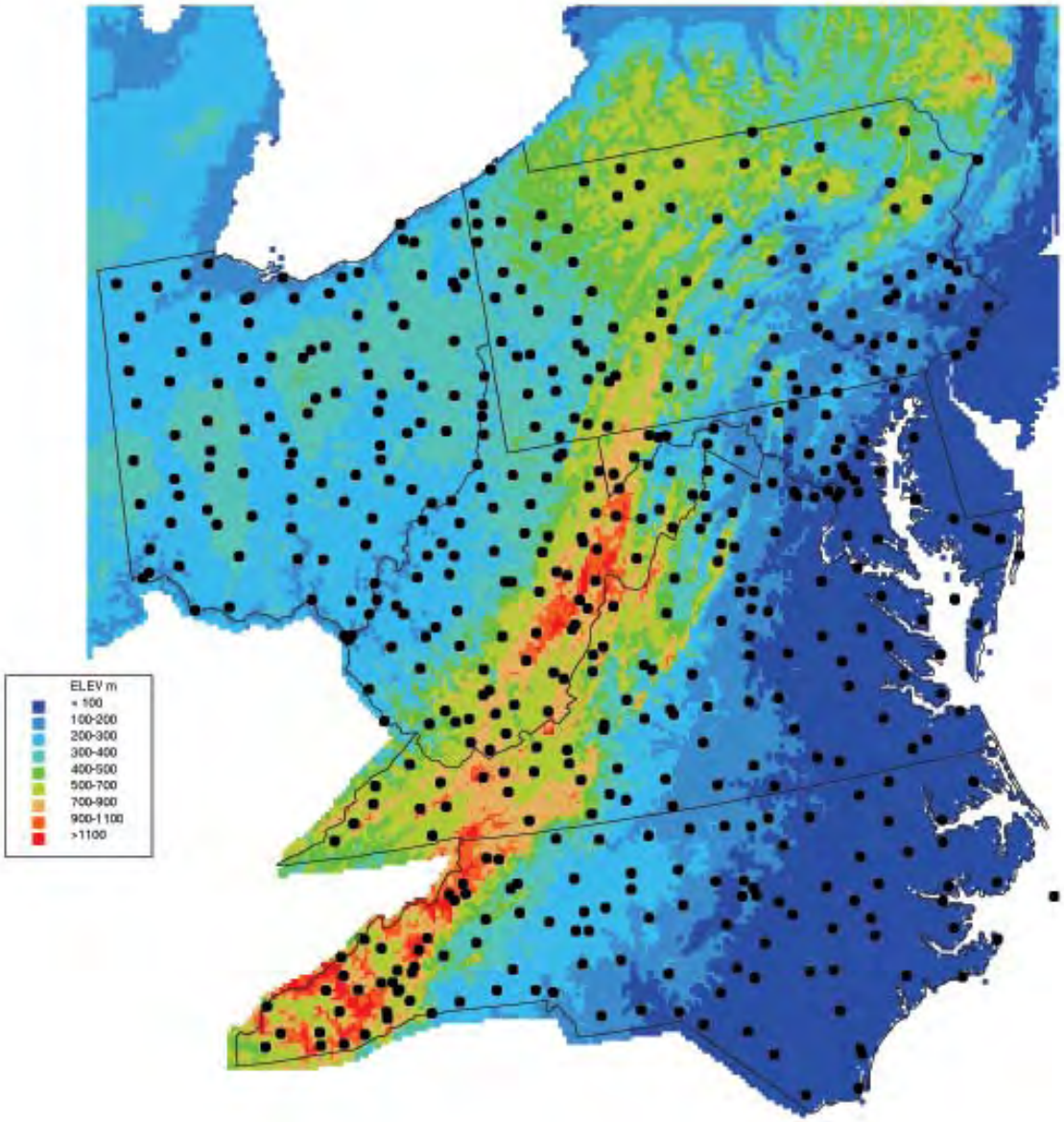

Earthinfo meteorological monitoring stations for 1998.

Figure H-2. NCDC meteorological stations in 1998.

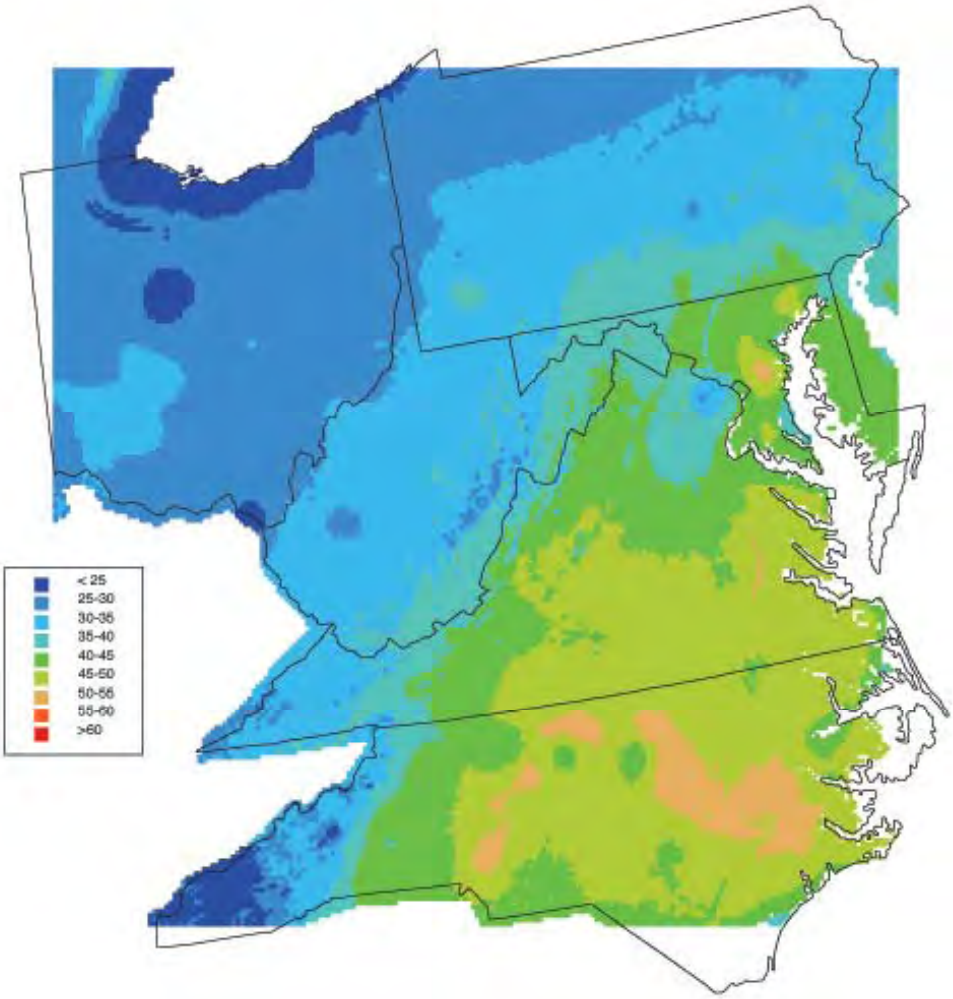

Spatial interpolation of 5-month 12-h SUM06 for 1997 on 4-km grid.

Figure H-3. Spatial extrapolation of the 5 month 12 hour SUM06 for 1997 on a 4 km grid.

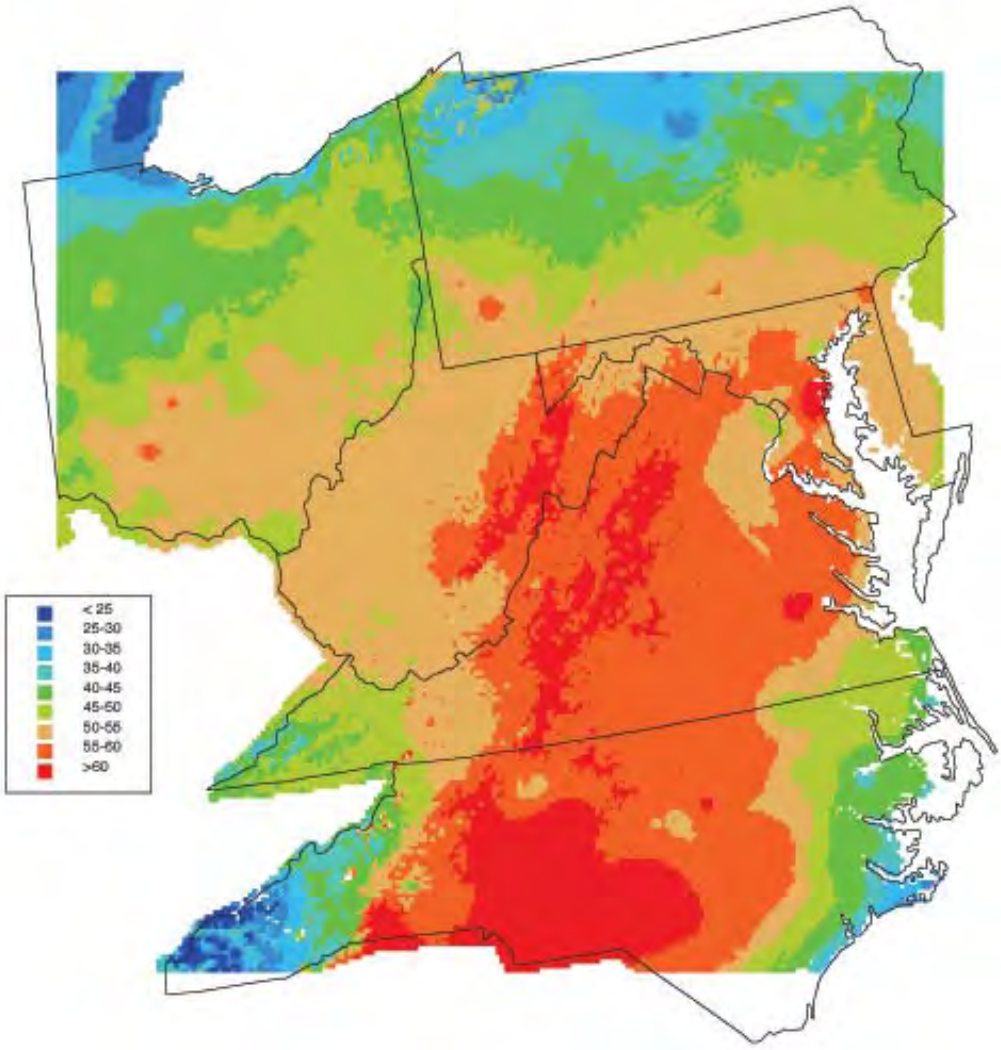

Spatial interpolation of 5-month 12-h SUM06 for 1998 on 4-km grid.

Figure H-4. Spatial extrapolation of the 5 month 12 hour SUM06 for 1998 on a 4 km grid.

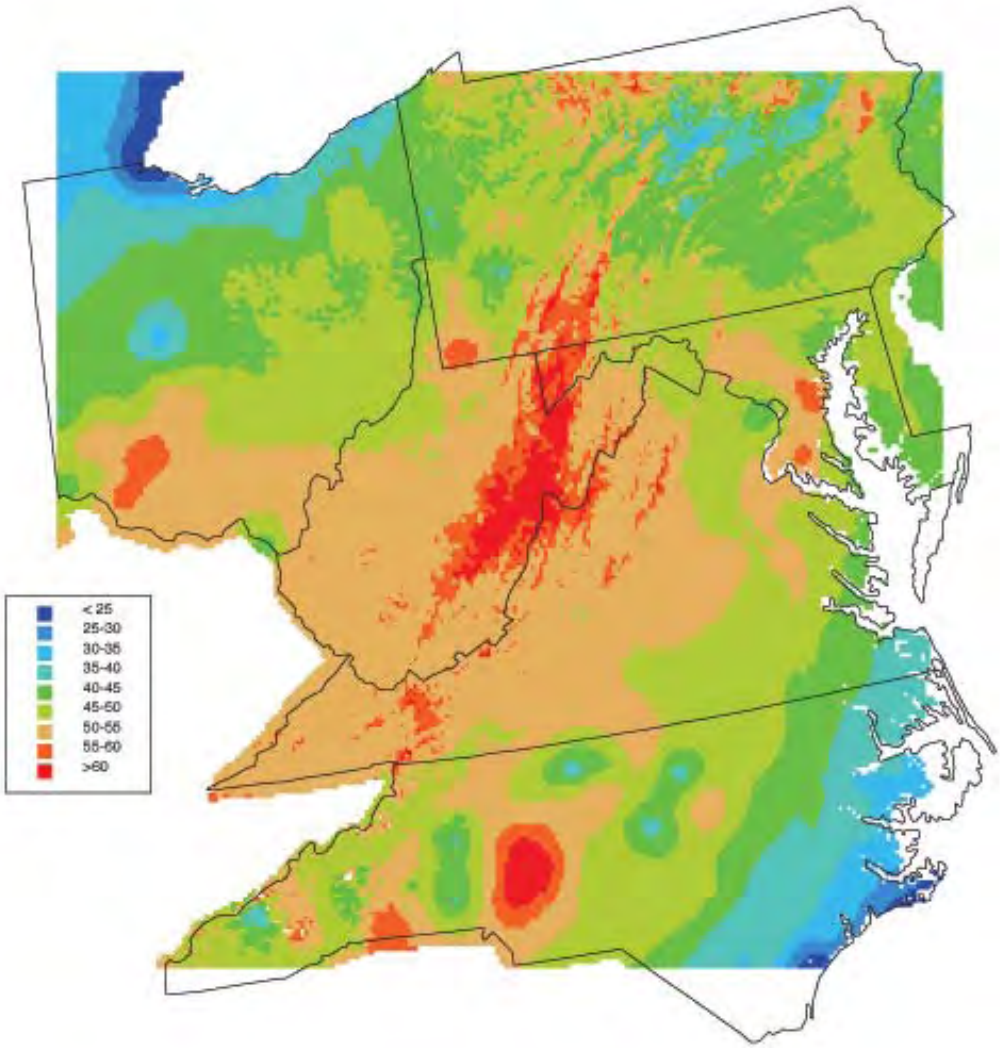

Figure H-5. Spatial extrapolation of the 5 month 12 hour SUM06 for 1999 on a 4 km grid.

References

Cressie, N. 1985. Fitting variogram models by weighted least squares. Math. Geol. 17:563-586.

EarthInfo, Inc., 1992. EARTHINFO's NCDC Summary of the Day, User's Manual. EarthInfo, Inc., Boulder, Colorado. 111 pp.

Lee, E.H. and W. E. Hogsett. 2001. Interpolation of temperature and non-urban ozone exposure at high spatial resolution over the western United States. Accepted for publication. Climate Res.

Logan, J.A. 1989. Ozone in rural areas of the United States. J. Geophys. Res. [Atmos] 94: 8511-8532.

Loveland, T. R., J. W. Merchant, D. O. Ohlen, and J. F. Brown. 1991. Development of a land-cover characteristics database for the conterminous United States. Photogramm. Eng. Remote. Sens. 57: 1453-1463.

Appendix G

Details of TREGRO Parameterization

Basswood - Parameterization Procedure

A TREGRO parameter set for basswood was developed to simulate the growth of the species at Shenandoah National Park. At present, no ozone response has been documented for the species, but based on personal communication with Howard Neufeld at Appalachian State University, it is most likely intermediate in sensitivity, along the lines of red maple. The parameter set is called Basswood and the allometry is contained in an Excel spreadsheet titled basswood allometry.

Initial tree biomass

Estimates of initial tree biomass were generated from the allometry of Ter-Mikaelian and Korzukhin (1997). Trees of 30 and 31.2 cm dbh were estimated based on measurements of Abrams et al. (1998). No allometry was available for roots, so a root to shoot ratio of 0.35 was assumed. Of the root mass, 60 percent was assigned to coarse roots (divided equally between a and b1) and 40 percent assigned to fine roots (divided equally between a, b1, and b2). Similarly, no detail was available to partition wood, structure, and TNC so 70 percent of branch, stem, and coarse root mass was assigned to wood. The remaining 30 percent was divided between structure (70 percent) and TNC (30 percent), thus 21 percent was structure and 9 percent was TNC.

Seasonal phenology

Seasonal phenology was based on estimates supplied by Christi Gordon, US NPS, Shenandoah National Park, based on her conversations with Park Naturalists.

Carbon assimilation

Net carbon assimilation on a high light (1000 $\mu E\ m^{-2}\ s^{-1}$; 25 - 30 ˚C), midsummer (DoY 200-210) period was set to approximately 0.0086 g carbon g^{-1} leaf carbon hr^{-1} based on values reported by Abrams et al. (1994). No measurements of respiration were available.

Final tree biomass

The target was to grow a basswood tree based on three years of meteorological data from Big Meadows, Virginia. The final TREGRO simulated tree was calibrated by adjusting tissue growth rates and senescence rates in fine roots until two conditions were met: (1) the simulated C gain of each of the tree components, foliage, branch, stem, and coarse and fine roots, and the total tree C gain were within 10 percent of the value for projected C gain from the literature-based allometric relationships and (2) when the proportion of TNC, structure, and wood in each of the tree components at the end of a simulation matched that parameterized for the tree at the beginning of the simulation (see Basswood allometry spreadsheet).

Basswood Literature Citations:

Abrams, M. D., M. E. Kubiske, and S. A. Mostoller. 1994. Relating wet and dry year ecophysiology to leaf structure in contrasting temperate tree species. Ecology 75: 123-133.

Abrams, M. D., C, M. Ruffner, and T. E. DeMeo. 1998. Dendroecology and species co-existence in an old-growth *Quercus-Acer-Tilia* talus slope forest in the central Appalachians, USA. For. Ecol. Mgmt. 106: 9-18.

Ter-Mikaelian, M. T. and M. D. Korzukhin. 1997. Biomass equations for sixty-five North American tree species. For. Ecol. Mgmt. 97: 1-24

Chestnut Oak - Parameterization Procedure

A TREGRO parameter set for chestnut oak was developed to simulate the growth of the species at Shenandoah National Park. At present, no ozone response has been documented for the species. It might be assumed to be similar in response to red oak. The parameter set is called ChestnutOak and the allometry is contained in an Excel spreadsheet titled chestnut oak allometry.

Initial tree biomass

Estimates of initial tree biomass were generated from the allometry of Martin et al. (1998). Trees of 30 and 31.008 cm dbh were estimated based on measurements of Rauscher and Smith (1979). No allometry was available for roots, so a root to shoot ratio of 0.35 was assumed. Of the root mass, 60 percent was assigned to coarse roots (divided equally between a and b1) and 40 percent assigned to fine roots (divided equally between a, b1, and b2). Similarly, no detail was available to partition wood, structure, and TNC so 70 percent of branch, stem, and coarse root mass was assigned to wood. The remaining 30 percent was divided between structure (70 percent) and TNC (30 percent), thus 21 percent was structure and 9 percent was TNC.

Seasonal phenology

Seasonal phenology was based on estimates supplied by Christi Gordon, US NPS, Shenandoah National Park, based on her conversations with Park Naturalists.

Carbon assimilation

Net carbon assimilation on a high light (1000 μE m^{-2} s^{-1}; 25 - 30 ˚C), midsummer (DoY 200-210) period was set to approximately 0.026 g carbon g^{-1} leaf carbon hr^{-1} based on values reported by Sullivan et al. (1996). No measurements of respiration were available.

Final tree biomass

The target was to grow a chestnut oak tree based on three years of meteorological data from Big Meadows, Virginia. The final TREGRO simulated tree was calibrated by adjusting tissue growth rates and senescence rates in fine roots until two conditions were met: (1) the simulated C gain of each of the tree components, foliage, branch, stem, and coarse and fine roots, and the total tree C gain were within 10 percent of the value for projected C gain from the literature-based allometric relationships and (2) when the proportion of TNC, structure, and wood in each of the tree components at the end of a simulation matched that parameterized for the tree at the beginning of the simulation (see Chestnut Oak allometry spreadsheet).

Chestnut Oak Literature Citations:

Martin, J. G., B. D. Kloeppel, T. L. Schaefer, D. L. Kimbler, and S. G. McNulty. 1998. Aboveground biomass and nitrogen allocation of ten deciduous southern Appalachian tree species. Can. J. For. Res. 28:1648-1659.

Rauscher, H. M. and D. W. Smith. 1979. Predicting daily radial growth of chestnut oak and pitch pine on a dry mountain site. For. Sci. 25: 233-236.

Sullivan, N. H., P. V. Bolstad, and J. M. Vose. 1996. Estimates of net photosynthetic parameters for twelve tree species in mature forests of the southern Appalachians. Tree Phys. 16: 397-406.

White Ash - Parameterization Procedure

A TREGRO parameter set for white ash was developed to simulate the growth of the species at Shenandoah National Park. The ozone dose-response is not set at this time. The parameter set is called Whiteash and the allometry is contained in an Excel spreadsheet titled white ash allometry.

Initial tree biomass

Estimates of initial tree biomass were generated from the allometry of Ter-Mikaelian and Korzukhin (1997). Trees of 30 and 32.5 cm dbh were estimated based on measurements of Abrams et al. (1994, 1997). No allometry was available for roots, so a root to shoot ratio of 0.35 was assumed. Of the root mass, 60 percent was assigned to coarse roots (divided equally between a and b1) and 40 percent assigned to fine roots (divided equally between a, b1, and b2). Similarly, no detail was available to partition wood, structure, and TNC so 70 percent of branch, stem, and coarse root mass was assigned to wood. The remaining 30 percent was divided between structure (70 percent) and TNC (30 percent), thus 21 percent was structure and 9 percent was TNC.

Seasonal phenology

Seasonal phenology was based on estimates supplied by Christi Gordon, US NPS, Shenandoah National Park, based on her conversations with Park Naturalists.

Carbon assimilation

Net carbon assimilation on a high light (1000 $\mu E\ m^{-2}\ s^{-1}$; 25 - 30 ˚C), midsummer (DoY 200-210) period was set to approximately 0.013 g carbon g^{-1} leaf carbon hr^{-1} based on values reported by Kubiske et al. (1996). No measurements of respiration were available.

Final tree biomass

The target was to grow a white ash tree based on three years of meteorological data from Big Meadows, Virginia. The final TREGRO simulated tree was calibrated by adjusting tissue growth rates and senescence rates in fine roots until two conditions were met: (1) the simulated C gain of each of the tree components, foliage, branch, stem, and coarse and fine roots, and the total tree C gain were within 10 percent of the value for projected C gain from the literature-based allometric relationships and (2) when the proportion of TNC, structure, and wood in each of the tree components at the end of a simulation matched that parameterized for the tree at the beginning of the simulation (see white ash allometry spreadsheet).

White Ash Literature Citations:

Abrams, M. D., M. E. Kubiske, and S. A. Mostoller. 1994. Relating wet and dry year ecophysiology to leaf structure in contrasting temperate tree species. Ecology 75: 123-133.

Abrams, M. D., D. A. Orwig, and M. J. Dockry. 1997. Dendroecology and successional status of two contrasting old-growth oak forests in the Blue Ridge Mountains, U. S. A. Can. J. For. Res. 27: 994-1002.

Kubiske, M. E., M. D. Abrams, and S. A. Mostoller. 1996. Stomatal and nonstomatal limitations of photosynthesis in relation to the drought and shade tolerance of tree species in open and understory environments. Trees (Berlin) 11: 76-82.

Ter-Mikaelian, M. T. and M. D. Korzukhin. 1997. Biomass equations for sixty-five North American tree species. For. Ecol. Mgmt. 97: 1-24

Appendix F

Description of the MAGIC Model and Application Methods Employed

Background

The principal tools that can be used to evaluate the potential response of aquatic resources to changes in acidic deposition are mathematical models. One of the prominent models developed to estimate acidification of lakes and streams is MAGIC (Model of Acidification of Groundwater In Catchments, Cosby et al., 1985a-c). MAGIC was the principal model used by the National Acid Precipitation Assessment Program (NAPAP) in assessment of potential future damage to lakes and streams in the eastern United States (NAPAP 1991, Thornton et al. 1990). Most recently MAGIC has been the principal model used for aquatic assessment in the Southern Appalachian Mountain Initiative Assessment activities (Sullivan et al., 2002). The validity of the model has been confirmed by comparison with estimates of lake acidification inferred from paleolimnological reconstructions of historical lake changes in pH (Sullivan et al. 1991, 1996) and with the results of several catchment-scale experimental acidification and de-acidification experiments (e.g., Cosby et al. 1995, 1996). MAGIC has been used to reconstruct the history of acidification and to simulate future trends on a regional basis and in a large number of individual watersheds in both North America and Europe (e.g., Lepisto et al. 1988; Whitehead et al. 1988; Cosby et al. 1990, 1994, 1996; Jenkins et al. 1990; Wright et al. 1990, 1994). Information contained in this Appendix was taken from the model summary provided by Sullivan et al. (2002).

Conceptual Basis of the Model

MAGIC is a lumped-parameter model of intermediate complexity, developed to predict the long-term effects of acidic deposition on surface water chemistry. The model simulates soil solution chemistry and surface water chemistry to predict the monthly and annual average concentrations of the major ions in these waters. MAGIC consists of: 1) a section in which the concentrations of major ions are assumed to be governed by simultaneous reactions involving sulfate adsorption, cation exchange, dissolution-precipitation- speciation of aluminum and dissolution-speciation of inorganic carbon; and 2) a mass balance section in which the flux of major ions to and from the soil is assumed to be controlled by atmospheric inputs, chemical weathering, net uptake and loss to biomass and runoff. At the heart of MAGIC is the size of the pool of exchangeable base cations in the soil. As the fluxes to and from this pool change over time in response to changes in atmospheric deposition, the chemical equilibria between soil and soil solution shift to give changes in surface water chemistry. The degree and rate of change of surface water acidity thus depend both on flux factors and the inherent characteristics of the affected soils.

Cation exchange is modeled using equilibrium (Gaines-Thomas) equations with selectivity coefficients for each base cation and aluminum. Sulfate adsorption is represented by a Langmuir isotherm. Aluminum dissolution and precipitation are assumed to be controlled by equilibrium with a solid phase of aluminum trihydroxide. Aluminum speciation is calculated by considering hydrolysis reactions as well as complexation with sulfate and fluoride. Effects of carbon dioxide on pH and on the speciation of inorganic carbon are computed from equilibrium equations. Organic acids are represented in the model as tri-protic analogues. First-order rates are used for retention (uptake) of nitrate and ammonium in the catchment. Weathering rates are assumed to be constant. A set of mass balance equations for base cations and strong acid anions are included. Given a description of the historical deposition at a site, the model equations are solved numerically to give long-term reconstructions of surface water chemistry (for complete details of the model see Cosby et al. 1985 a-c).

Equilibrium Equations

Cation and Anion Exchange in Soil Water

Cation exchange reactions between the soil matrix and soil solution are assumed to result in an equilibrium partitioning of calcium, magnesium, sodium, potassium and trivalent aluminum between solid and aqueous phases. The equilibrium expressions for cation exchange (Table F-1) are constructed using a Gaines-Thomas expression (Gaines and Thomas, 1953). E represents exchangeable fractions of each base cation on the soil (equivalents of each base cation per total cation exchange capacity of the soil). The sum of all exchangeable fractions must equal 1.0. Base saturation of the soil is defined as the sum of the exchangeable fractions of the base cations (Table F-2). The selectivity coefficients (Table F-3) must be calibrated for each aggregated soil layer in the model. The calibration procedure relies on observations of the exchangeable fractions of base cations in soils and measured base cation concentrations in streamwater (see Cosby et al. 1985a,b for details).

Anion exchange reactions are assumed to occur only for sulfate ion. The relationship between dissolved and adsorbed sulfate (Table F-1) is assumed to follow a Langmuir isotherm (Couto et al. 1979, Hasan et al. 1970). MAGIC is a catchment-scale model and it is often the case that the effective values of aggregated parameters intended to represent large-scale function cannot be derived by a direct scaling-up of similar parameters measured in a laboratory setting (see Rastetter et al. 1992). The sulfate adsorption parameters (Table F-3) used in MAGIC must, therefore, be calibrated for each site. Cosby et al. (1986) described the method for calibrating sulfate adsorption parameters in whole catchment simulations based on input/output budgets and deposition histories for the site.

Inorganic Aluminum in Soil Water and Surface Water

Inorganic aluminum speciation consists of one reaction involving the equilibrium dissolution of a solid phase of aluminum trihydroxide and twelve reactions involving formation of aqueous complexes of Al^{3+}. These reactions are assumed to occur both in soil solution and in surface waters in the model and can be represented by a series of equilibrium equations (Table F-1). The aluminum solubility constants for the soils in the model are represented by aggregated values. These values are not, therefore, necessarily associated with a particular crystalline form of $Al(OH)_3$ and must be selected as part of the calibration process.

Inorganic and Organic Carbon in Soil Water and Surface Water; and Dissociation of Water

Inorganic carbon reactions in MAGIC consist of dissolution of CO_2 to form carbonic acid, followed by dissociation to bicarbonate and carbonate. These reactions are assumed to occur both in soil solution and in surface waters in the model and can be represented by equilibrium equations (Table F-1) that are temperature-dependent.

Organic acids are the dominant form of dissolved organic material in natural waters (e.g., McKnight et al. 1985, David and Vance 1991). Organic acids are effective hydrogen ion buffers and can form complexes with inorganic aluminum. Considerable evidence has accumulated suggesting that organic acids influence the response of surface waters to changes in strong acid inputs, most likely by changes in the protonation of the organic acid anions (see Wright 1989). Organic acids were not included in the original formulation of MAGIC because specification (and calibration) of organic acid analog models was hampered by lack of data on organic acid behavior (e.g., Jenkins and Cosby 1989). In 1994, Driscoll et al. (1994) compared several organic acid analog models (mono-, di-, and triprotic organic acid analogs and the model of Oliver et al. 1983) with respect to their abilities to resolve mass balance discrepancies in measured water samples from Adirondack lakes. They concluded that organic acids were

Table F-1. Equations in the MAGIC model.

Equilibrium Equations

Cation and Anion Exchange in Soil Water

$$E_{Ca} + E_{Mg} + E_{Na} + E_K + E_{Al} = 1.0$$

$$\frac{\{Ca^{2+}\}^3 E_{Al}^2}{\{Al^{3+}\}^2 E_{Ca}^3} = S_{AlCa} \qquad \frac{\{Mg^{2+}\}^3 E_{Al}^2}{\{Al^{3+}\}^2 E_{Mg}^3} = S_{AlMg} \qquad \frac{\{Na^{+}\}^3 E_{Al}}{\{Al^{3+}\}\ E_{Na}^3} = S_{AlNa} \qquad \frac{\{K^{+}\}^3 E_{Al}}{\{Al^{3+}\}\ E_K^3} = S_{AlK} \qquad \frac{\{SO_4^{2-}\}}{C_{1/2} + \{SO_4^{2-}\}} * E_{mx} = E_{SO4}$$

Inorganic Aluminum in Soil Water and Surface Water

$$\{Al^{3+}\} = [K_{Al}] * \{H^+\}^{S_{Al}}$$

$$\frac{\{Al(OH)^{2+}\}\ \{H^+\}}{\{Al^{3+}\}} = K_{Al_1} \qquad \frac{\{Al(OH)_2^+\}\ \{H^+\}^2}{\{Al^{3+}\}} = K_{Al_2} \qquad \frac{\{Al(OH)_3^0\}\ \{H^+\}^3}{\{Al^{3+}\}} = K_{Al_3} \qquad \frac{\{Al(OH)_4^-\}\ \{H^+\}^4}{\{Al^{3+}\}} = K_{Al_4}$$

$$\frac{\{AlF^{2+}\}}{\{Al^{3+}\}\ \{F^-\}} = K_{Al_5} \qquad \frac{\{AlF_2^+\}}{\{Al^{3+}\}\ \{F^-\}^2} = K_{Al_6} \qquad \frac{\{AlF_3^0\}}{\{Al^{3+}\}\ \{F^-\}^3} = K_{Al_7} \qquad \frac{\{AlF_4^-\}}{\{Al^{3+}\}\ \{F^-\}^4} = K_{Al_8}$$

$$\frac{\{AlF_5^{2-}\}}{\{Al^{3+}\}\ \{F^-\}^5} = K_{Al_9} \qquad \frac{\{AlF_6^{3-}\}}{\{Al^{3+}\}\ \{F^-\}^6} = K_{Al_{10}} \qquad \frac{\{Al(SO_4)^+\}}{\{Al^{3+}\}\ \{SO_4^{2-}\}} = K_{Al_{11}} \qquad \frac{\{Al(SO_4)_2^-\}}{\{Al^{3+}\}\ \{SO_4^{2-}\}^2} = K_{Al_{12}}$$

Inorganic and Organic Carbon in Soil Water and Surface Water; Dissociation of Water

$$\{H^+\}\{OH^-\} = K_w \qquad \frac{\{H_2CO_3^*\}}{P_{CO2}} = K_{CO2_1} \qquad \frac{\{HCO_3^-\}\ \{H^+\}}{\{H_2CO_3^*\}} = K_{CO2_2} \qquad \frac{\{CO_3^{2-}\}\ \{H^+\}}{\{HCO_3^-\}} = K_{CO2_3} \qquad \frac{\{H_2A^-\}\ \{H^+\}}{\{H_3A\}} = K_{OA_1}$$

$$\frac{\{HA^{2-}\}\ \{H^+\}}{\{H_2A^-\}} = K_{OA_2} \qquad \frac{\{A^{3-}\}\ \{H^+\}}{\{HA^{2-}\}} = K_{OA_3} \qquad \frac{\{AlA\ \}}{\{Al^{3+}\}\ \{A^{3-}\}} = K_{OA_4} \qquad \frac{\{Al(H)A^+\}}{\{Al^{3+}\}\ \{H^+\}\{A^{3-}\}} = K_{OA_5}$$

Braces denote activities (calculated from concentrations using the extended Debye-Huckel equation)

Mass and Ionic Balance Equations

Ionic Balance in Soil Water and Surface Water (parentheses denote molar concentrations)

$$\begin{aligned} & 2(Ca^{2+}) + 2(Mg^{2+}) + (Na^+) + (K^+) + (NH_4^+) + (H^+) + 3(Al^{3+}) + 2(AlOH^{2+}) + (Al(OH)_2^+) + 2(AlF^{2+}) + (AlF_2^+) + (AlSO_4^+) + (Al(H)A^+) \\ = \ & 2(SO_4^{2-}) + (Cl^-) + (NO_3^-) + (F^-) + (OH^-) + (HCO_3^-) + 2(CO_3^{2-}) + (H_2A^-) + 2(HA^{2-}) + 3(A^{3-}) + (Al(OH)_4^-) + (AlF_4^-) + 2(AlF_5^{2-}) \\ & + 3(AlF_6^{3-}) + (Al(SO_4)_2^-) \end{aligned}$$

Mass Balance for Ions in Soil Water and Surface Water (rates of change in eq m^{-2} yr^{-1})

$$\frac{dCa_T}{dt} = AD_{Ca} + W_{Ca} + SS_{Ca} - Q*2(Ca^{2+}) \qquad \frac{dNO3_T}{dt} = AD_{NO3} + W_{NO3} + SS_{NO3} + NIT - IM_{NO3} - UP_{NO3} - DEN - Q*(NO_3^-)$$

$$\frac{dMg_T}{dt} = AD_{Mg} + W_{Mg} + SS_{Mg} - Q*2(Mg^{2+}) \qquad \frac{dNH4_T}{dt} = AD_{NH4} + W_{NH4} + SS_{NH4} + MIN - IM_{NH4} - UP_{NH4} - NIT - Q*(NH_4^+)$$

$$\frac{dNa_T}{dt} = AD_{Na} + W_{Na} + SS_{Na} - Q*(Na^+) \qquad \frac{dSO4_T}{dt} = AD_{SO4} + W_{SO4} + SS_{SO4} - Q*2\left[(SO_4^{2-}) + (AlSO_4^+) + 2(Al(SO_4)_2^-)\right]$$

$$\frac{dK_T}{dt} = AD_K + W_K + SS_K - Q*(K^+) \qquad \frac{dCl_T}{dt} = AD_{Cl} + W_{Cl} + SS_{Cl} - Q*(Cl^-)$$

$$\frac{dF_T}{dt} = AD_F + W_F + SS_F - Q*\left[(F^-) + (AlF^{2+}) + 2(AlF_2^+) + 3(AlF_3^0) + 4(AlF_4^-) + 5(AlF_5^{2-}) + 6(AlF_6^{3-})\right]$$

Table F-2. Variables in the MAGIC model.

State Variables (functions of time, calculated by model)

Aqueous Phase - Ionic Concentrations in Soil Water and Surface Water (mol m^{-3})

Base Cations: $(Ca^{2+})(Mg^{2+})(Na^{+})(K^{+})(NH_4^{+})$

Strong Acid Anions: $(SO_4^{2-})(Cl^{-})(NO_3^{-})(F^{-})$

Hydrogen and Hydroxyl Ions: $(H^{+})(OH^{-})$

Inorganic Carbon: $(H_2CO_3^{*})(HCO_3^{-})(CO_3^{2-})$

Aluminum: $(Al^{3+})(AlOH^{2+})(Al(OH)_2^{+})(Al(OH)_3^{0})(Al(OH)_4^{-})(AlF^{2+})(AlF_2^{+})(AlF_3^{0})(AlF_4^{-})(AlF_5^{2-})(AlF_6^{3-})(AlSO_4^{+})(Al(SO_4)_2^{-})$

Organic Carbon: $(H_3A)(H_2A^{-})(HA^{2-})(A^{3-})(AlA)(Al(H)A^{+})$

Solid Phase - Exchangeable Ions on Soil Matrix; Soil Organic Matter Constituents

Exchangeable Cations (fraction): $E_{Ca}, E_{Mg}, E_{Na}, E_K, E_{Al}$

Exchangeable Sulphate (eq kg^{-1}): E_{SO4}

Organic Carbon and Nitrogen (mol m^{-2}): C_{Org}, N_{Org}

Defined Variables (derived from state variables)

Total Ions for Mass Balance (eq m^{-2})

$SO_{4T} = SM*E_{SO4} + SV*TOT_{SO4}$

$Ca_T = SM*CEC*E_{Ca} + SV*2(Ca^{2+})$

$Na_T = SM*CEC*E_{Na} + SV*(Na^{+})$

$NO_{3T} = SV*(NO_3^{-})$

$Cl_T = SV*(Cl^{-})$

$Mg_T = SM*CEC*E_{Mg} + SV*2(Mg^{2+})$

$K_T = SM*CEC*E_K + SV*(K^{+})$

$NH_{4T} = SV*(NH_4^{+})$

$F_T = SV*TOT_F$

Total Aqueous Concentrations (eq m^{-3})

$SBC = 2(Ca^{2+}) + 2(Mg^{2+}) + (Na^{+}) + (K^{+})$

$TOT_{Al} = 3(Al)_{TOT}$

$TOT_F = (AlF^{2+}) + 2(AlF_2^{+}) + 3(AlF_3^{0}) + 4(AlF_4^{-}) + 5(AlF_5^{2-}) + 6(AlF_6^{3-})$

$SAA = 2(SO_4^{2-}) + (Cl^{-}) + (NO_3^{-}) + (F^{-})$

$DOC_{Al} = 3(Al)_{DOC}$

$TOT_{SO4} = 2(SO_4^{2-}) + 2(AlSO_4^{+}) + 4(Al(SO_4)_2^{-})$

Summed Species (mol m^{-3})

$(Al)_{SO4} = (AlSO_4^{+}) + (Al(SO_4)_2^{-})$

$(Al)_{DOC} = (AlA) + (Al(H)A^{+})$

$(Al)_{OH} = (AlOH^{2+}) + (Al(OH)_2^{+}) + (Al(OH)_3^{0}) + (Al(OH)_4^{-})$

$(Al)_F = (AlF^{2+}) + (AlF_2^{+}) + (AlF_3^{0}) + (AlF_4^{-}) + (AlF_5^{2-}) + (AlF_6^{3-})$

$(Al)_{TOT} = (Al^{3+}) + (Al)_{SO4} + (Al)_{OH} + (Al)_F + (Al)_{DOC}$

$(OA)_{TOT} = (H_3A) + (H_2A^{-}) + (HA^{2-}) + (A^{3-}) + (AlA) + (Al(H)A^{+})$

Charge Balance Alkalinity (eq m^{-3}) $CALK = SBC + (NH_4^{+}) - SAA$

Soil C/N ratio $C/N = \frac{C_{Org}}{N_{Org}}$

Solution pH, pAl $pH = -\log_{10}(H^{+})$ $pAl = -\log_{10}(Al^{3+})$

Soil Base Saturation $BS = E_{Ca} + E_{Mg} + E_{Na} + E_K$

Table F-3. Parameters in the MAGIC model.

Parameters (constant values that must be specified)

Soil Physical/Chemical Properties

D = depth (m)
P = porosity (fraction)
BD = bulk density (kg m^{-3})
SM = soil mass (D*BD)
SV = soil pore volume (D*P)

CEC = cation exchange capacity (eq kg^{-1})
$C_{1/2}$ = sulphate adsorption half saturation (eq m^{-3})
E_{mx} = sulphate adosrption maximum (eq kg^{-1})
K_{Al} = aluminum solubility constant (log_{10})
S_{Al} = slope of pH-pAl relationship

Surface Water Properties

RT = retention time (yr)
RA = relative area of lake/stream (fraction)
K_{Al} = aluminum solubility constant (log_{10})
S_{Al} = slope of pH-pAl relationship

Aqueous Phase - Equilibrium Constants (log_{10})

Organic Acid: pK_1, pK_2, pK_3 $[-\log_{10}(K_{OA_1}, K_{OA_2}, K_{OA_3})]$
Organic Aluminum: K_{OA_4}, K_{OA_5}
Inorganic Aluminum Speciation: $K_{Al_1}, K_{Al_2}, K_{Al_3}, K_{Al_4}, K_{Al_5}, K_{Al_6}, K_{Al_7}, K_{Al_8}, K_{Al_9}, K_{Al_{10}}, K_{Al_{11}}, K_{Al_{12}}$
Inorganic Carbon Speciation and Dissociation of Water: $K_{CO2_1}, K_{CO2_2}, K_{CO2_3}, K_w$

Solid Phase - Weathering and Exchange Constants

Cation Exchange Selectivity Coefficients (log_{10}): $S_{AlCa}, S_{AlMg}, S_{AlNa}, S_{AlK}$
Weathering Rates (eq m^{-2} yr^{-1}): $W_{Ca}, W_{Mg}, W_{Na}, W_K, W_{NH4}, W_{SO4}, W_{Cl}, W_{NO3}, W_F$ (can be pH dependent)

important buffers in surface waters even when dissolved organic carbon was low. They obtained the best agreement between predicted and observed pH values using a triprotic organic acid analog model. The triprotic organic acid analog model can also be used to describe the complexation of Al by organic solutes (Schecher and Driscoll 1993, Driscoll et al. 1994). A triprotic organic acid analog model is currently incorporated into the structure of MAGIC.

Mass and Ionic Balance Equations

Mass balance is required for the total amounts of base cations and strong acid anions in each compartment of the simulated watershed (Table F-1). That is, input minus output of each mass balance ion must equal the rate of change of the total amount of that ion in each compartment of the model. Total amounts in surface water compartments are calculated from aqueous concentrations and water volume. In soil compartments, total amounts include both dissolved amounts in the pore water and adsorbed amounts (if applicable) on the soil matrix. Process-related inputs (Table F-4) are by atmospheric deposition, primary mineral weathering (in soil compartments) and biological production (decomposition and mineralization). Process-related outputs are by drainage water discharge or biological removal (uptake or immobilization). Unspecified sources and sinks of each ion are also available in the model. These may be used to simulate processes or perturbations not explicitly represented in the model (such as experimental additions of ions, losses of ions resulting from land use changes, etc.). At each time step during model simulation, inputs and outputs are added or subtracted from each compartment, new total amounts are calculated, and the equilibrium equations are solved subject to the constraint of ionic balance (Table F-1) to derive an estimate of the concentrations of the state variables (Table F-2) for that time step.

Nitrogen Immobilization Equations

Concern was expressed more than a decade ago about the possible adverse effects of atmospheric deposition of nitrogen compounds on soils, forests and waters. There is now

Table F-4. Inputs to the MAGIC model.

Input Fluxes and Conditions (functions of time that must be specified)
Conditions are annual averages (monthly averages are specified for seasonal simulations)
Temperature (^oC), Carbon Dioxide (atm), Organic Acid (mol m^{-3}): TEMP, P_{CO2}, $(OA)_{TOT}$
[CO_2 partial pressure and Organic Acid concentration control the weak inorganic and organic carbon buffers]
Fluxes are annual values (monthly fractions of annual fluxes are specified for seasonal simulations)
Catchment Discharge (m yr^{-1}) and Flow Fractions: Q, F_1, F_2, F_3
[Flow fractions specify the pathway of water flux through the modelled system and can vary seasonally]
Atmospheric Deposition (eq m^{-2} yr^{-1}): AD_{Ca}, AD_{Mg}, AD_{Na}, AD_K, AD_{NH4}, AD_{SO4}, AD_{Cl}, AD_{NO3}, AD_F
[Deposition is specified as the product of precipitation concentrations and amount, scaled by a dry deposition factor]
Sources and Sinks of Ions (eq m^{-2} yr^{-1}): SS_{Ca}, SS_{Mg}, SS_{Na}, SS_K, SS_{NH4}, SS_{SO4}, SS_{Cl}, SS_{NO3}, SS_F
[Sources and sinks are distinct and represent processes, inputs or outputs not explicitly included in the model]
The flow fractions determine atmospheric deposition fluxes into each soil and surface water compartment. Other fluxes and conditions must be specified separately for each model compartment (if appropriate).
Initial Values
Initial values of these state variables must be specified for each model compartment (if appropriate)
Cation and Anion Concentrations (mol m^{-3}): (Ca^{2+}), (Mg^{2+}), (Na^+), (K^+), (NH_4^+), (SO_4^{2-}), (Cl^-), (NO_3^-), (F^-)
Exchangeable Ions (fraction): E_{Ca}, E_{Mg}, E_{Na}, E_K

evidence that some forests in Europe and North America are becoming nitrogen saturated, leading to enhanced nitrate leaching in drainage waters (e.g., Emmett et al.1993, Stoddard 1994, Dise and Wright 1995). Recent Experimental results from the NITREX Project (Wright and van Breemen 1995, Gundersen et al. 1998, Emmett et al. 1998) have provided insights into the controls on nitrogen cycling and have enabled the development of empirical models that relate nitrogen retention to the carbon and nitrogen characteristics of soil organic matter. It is important to incorporate this new process level understanding into dynamic models of acidification responses.

There were no process-based mechanisms for nitrogen retention in soils in the original version of MAGIC. Ferrier et al. (1995) and Jenkins et al. (1997) modified MAGIC to produce a new coupled sulfur and nitrogen model (MAGIC-WAND) to address concerns over the interaction of sulfur and nitrogen deposition on soil and surface water acidification. MAGIC-WAND used many of the same processes included in the latest version of MAGIC but did not introduce an internal pool of stored nitrogen in the soil compartments. All of the nitrogen processes in MAGIC-WAND were rate-based and there was no internal state variable that could change the rates as nitrogen accumulated in the simulated systems (no feedback). Cosby et al. (1997) and Emmett et al. (1997) constructed a model (MERLIN) to deal explicitly with nitrogen dynamics in soils. The MERLIN model was based on both rates and internal pools and proved more capable of simulating nitrogen dynamics. However, MERLIN did not simulate the acid-base processes. The nitrogen dynamics included in the current version of MAGIC are based conceptually on the empirical model described by Gundersen et al. (1998) (see also Tietema and Beier 1995, Emmett et al. 1995). The mathematical formulation and process representations of

the nitrogen dynamics in the current version of MAGIC (Cosby et al. 2001) derive from a simplification of the structure of the MERLIN model.

Even though the current version of MAGIC has the capability to simulate dynamic nitrogen changes, these dynamics can be turned off. In this case, simple sink and source terms for nitrogen species are used in MAGIC to simulate N retention and release. In the absence of direct evidence that the N dynamics of a catchment are changing, it is appropriate to use the simple sink/source representation. For nitrate, this procedure specifies that retention (uptake) is a constant percentage loss of all inputs of nitrate (deposition, nitrification, etc). For ammonium, this procedure specifies that retention (uptake) is a constant percentage of all inputs of ammonium left over after nitrification has occurred. For the AQRV simulations presented in this report, nitrification of ammonium inputs was assumed to be 100%, and the % retention of the nitrate was calibrated based on observed input/output fluxes. This procedure assures that simulated and observed nitrate and ammonium agree very closely for the calibration period. The percentages of nitrification and nitrate retention were assumed to remain constant throughout the historical and future simulations.

Model Implementation

Atmospheric deposition and net uptake-release fluxes for the base cations and strong acid anions are required as inputs to the model. These inputs are generally assumed to be uniform over the catchment. Atmospheric fluxes are calculated from concentrations of the ions in precipitation and the rainfall volume into the watershed. The atmospheric fluxes of the ions must be corrected for dry deposition of gas, particulates and aerosols and for inputs in cloud/fog water. An estimate of the streamflow volume must also be provided to the model. In general, the model is implemented using average hydrologic conditions and meteorological conditions in annual or seasonal simulations. Mean annual or mean monthly deposition, precipitation and streamflow are used to drive the model. The model is not designed to provide temporal resolution greater than monthly. Most simulations are based on annual average conditions. Values for soil and streamwater temperature, partial pressure of carbon dioxide in the soil and streamwater, and organic acid concentrations in soilwater and streamwater must also be provided.

As implemented for this project, MAGIC is a two-compartment representation of each watershed. Atmospheric deposition enters the soil compartment and the equilibrium equations are used to calculate soil water chemistry. The water is then routed to the stream compartment, and the appropriate equilibrium equations are reapplied to calculate streamwater chemistry.

Once initial conditions (initial values of variables in the equilibrium equations) have been established, the equilibrium equations are solved for soil water and streamwater concentrations of the remaining variables. These concentrations are used to calculate the streamwater output fluxes of the model for the first time step. The mass balance equations are (numerically) integrated over the time step, providing new values for the total amounts of base cations and strong acid anions in the system. These in turn are used to calculate new values of the remaining variables and new streamwater fluxes. The output from MAGIC is thus a time trace for all major chemical constituents for the period of time chosen for the integration.

Model Calibration Procedure

The aggregated nature of the model requires that it be calibrated to observed data from a watershed before it can be used to examine potential system response. Calibration is achieved by setting the values of certain parameters within the model which can be directly measured or observed in the system of interest (called “fixed” parameters). The model is then run (using

observed atmospheric and hydrologic inputs) and the output (streamwater and soil chemical variables, called "criterion" variables) are compared to observed values of these variables. If the observed and simulated values differ, the values of another set of parameters in the model (called "optimized" parameters) are adjusted to improve the fit. After a number of iterations, the simulated-minus-observed values of the criterion variables usually converge to zero (within some specified tolerance). The model is then considered calibrated. If new assumptions (or values) for any of the fixed variables or inputs to the model are subsequently adopted, the model must be re-calibrated by re-adjusting the optimized parameters until the simulated-minus-observed values of the criterion variables again fall within the specified tolerance.

Because the estimates of the fixed parameters and deposition inputs are subject to uncertainties, a "fuzzy" optimization procedure can be implemented for calibrating the model. The fuzzy optimization procedure consists of multiple calibrations of each watershed using random values of the fixed parameters drawn from the observed possible range of values, and random values of deposition from the range of model estimates. Each of the multiple calibrations begins with (1) a random selection of values of fixed parameters and deposition, and (2) a random selection of the starting values of the adjustable parameters. The adjustable parameters are then optimized using the Rosenbrock (1960) algorithm to achieve a minimum error fit to the target variables. This procedure is undertaken ten times for each stream. The final calibrated model is represented by the ensemble of parameter values and variable values of the successful calibrations.

Calibrations are based on volume-weighted mean annual fluxes for a given period of observation. The length of the period of observation used for calibration is variable, but model output will be more reliable if the annual flux estimates used in calibration are based on a number of years rather than just one year. There is considerable year-to-year variability in atmospheric deposition and catchment runoff. Averaging over a number of years reduces the likelihood that an "outlier" year (very dry, etc.) constitutes the primary data on which model forecasts are based. On the other hand, averaging over too long a period may remove important trends in the data that need to be simulated by the model. For this study, the model was calibrated using five-year average values of deposition and five years of streamwater data.

The model results presented in this report are based on the median values of the simulated water quality variables from the multiple calibrations of each site. The use of median values for each stream helps to assure that the simulated responses are neither over- nor underestimates, but approximate the most likely behavior of each stream (given the assumptions inherent in the model and the data used to constrain and calibrate the model). The uncertainty analyses make use of the maximum and minimum simulated values from the multiple calibrations for each site to calculate uncertainty "widths" (or confidence intervals) around the median simulated values.

Comments on Model Applicability

The MAGIC model of acidification is a model that has been extensively subjected to the process of testing and confirmation over a 15-year period and thousands of applications. MAGIC has been used in scientific studies, as a tool in establishing management practices, and as an aid in making policy decisions regarding controls on emissions and deposition. Overall, the model has proven to be robust, reliable, and useful in all of these activities. The longevity and utility of MAGIC results as much from the philosophical approach to its formulation (empirically-based, compatible with readily available data, technically easy to implement, and capable of being tested), as from the soundness of the hydrobiogeochemical concepts and understanding on which the model is based. The success of this conceptual approach in the

qualitative and quantitative description of acidification responses of ecosystems suggests that it is also an appropriate tool for examining recovery responses as well.

References

Cosby, B.J., R.C. Ferrier, A. Jenkins and R.F. Wright. 2001. Modelling the effects of acid deposition: refinements, adjustments and inclusion of nitrogen dynamics in the MAGIC model. Hydrol. Earth Syst. Sci. 5: 499-517.

Cosby, B.J., R.C. Ferrier, A. Jenkins, B.A. Emmett, R.F. Wright and A. Tietema. 1997. Modelling the ecosystem effects of nitrogen deposition at the catchment scale: model of ecosystem retention and loss of inorganic nitrogen (MERLIN). Hydrology and Earth System Sciences 1:137-158.

Cosby, B.J., S.A. Norton, and J.S. Kahl. 1996. Using a paired-catchment manipulation experiment to evaluate a catchment-scale biogeochemical model. Sci. Tot. Environ. 183:49-66.

Cosby, B.J., R.F. Wright, and E. Gjessing. 1995. An acidification model (MAGIC) with organic acids evaluated using whole-catchment manipulations in Norway. J. Hydrol. 170:101-122.

Cosby, B. J., Bulger, A.J., and Wright, R.F. 1994. Predicting recovery of freshwater ecosystems: Trout in Norwegian lakes. *In* Acidification of Freshwater Ecosystems: Implication for the Future. *Edited by* C.E.W. Steinberg and R.F. Wright. John Wiley and Sons, Ltd., New York. pp 355-373.

Cosby, B.J., A. Jenkins, R.C. Ferrier, J.D. Miller and T.A.B. Walker. 1990. Modelling stream acidification in afforested catchments: long-term reconstruction at two sites in central Scotland. J. Hydrol. 120:143-162.

Cosby, B. J., G. M. Hornberger, R. F. Wright, and J. N. Galloway. 1986. Modeling the effects of acid deposition: Control of long-term sulfate dynamics by soil sulfate adsorption, Water Resour. Res. 22(8):1283-1302.

Cosby, B.J., R.F. Wright, G.M. Hornberger, and J.N. Galloway. 1985a. Modelling the effects of acid deposition: assessment of a lumped parameter model of soil water and streamwater chemistry. Water Resour. Res. 21:51-63.

Cosby, B.J., R.F. Wright, G.M. Hornberger, and J.N. Galloway. 1985b. Modelling the effects of acid deposition: estimation of long-term water quality responses in a small forested catchment. Water Resour. Res. 21:1591-1601.

Cosby, B.J., G.M. Hornberger, J.N. Galloway, and R.F. Wright. 1985c. Time scales of catchment acidification: a quantitative model for estimating freshwater acidification. Environ. Sci. Technol. 19:1144-1149.

Cosby, B. J., R. F. Wright, G. M. Hornberger and J. N. Galloway. 1984. Model of acidification of groundwater in catchments. Project completion report, Proj. E2-14, EPA/NCSU Acid Precipitation Program, Environ. Prot. Agency, N. C. State Univ., October 1984.

Couto, W., D. J. Lathwell, and D. R. Bouldin. 1979. Sulfate sorption by two oxisols and an alfisol of the tropics, Soil Sci. 127:108-116.

David, M.B. and G.F. Vance. 1991. Chemical character and origin of organic acids in streams and seepage lakes of central Maine. Biogeochemistry 12:17-41.

Dise, N.B. and R.F. Wright. 1995. Nitrogen leaching from Europoean forests in relation to nitrogen deposition. Forest Ecol. Management 71:153-163.

Driscoll, C.T., M.D. Lehtinen, and T.J. Sullivan. 1994. Modeling the acid-base chemistry of organic solutes in Adirondack, New York, lakes. Water Resour. Res. 30:297-306.

Emmett, B.A., B. Reynolds, P.A. Stevens, D.A. Norris, S. Hughes, J. Gorres and I. Lubrecht. 1993. Nitrate leaching from afforested Welsh catchments - interactions between stand age and nitrogen deposition. Ambio 22:386-394.

Emmett, B.A., B.J. Cosby, R.C. Ferrier, A. Jenkins, A. Tietema and R.F. Wright. 1997. Modelling the ecosystem effects of nitrogen deposition at the catchment scale: simulation of nitrogen saturation in a Sitka spruce forest, Aber, Wales, UK. Biogeochemistry 38:129-148.

Emmett, B.A., P.A. Stevens and b. Reynolds. 1995. Factors influencing nitrogen saturation in Sitka spruce stands in Wales. Water Air Soil Pollut. 85:1629-1634.

Emmett, B.A., D. Boxman, M. Bredemeier, F. Moldan, P. Gundersen, O.J. Kjonaas, P. Schleppi, A. Tietema and R.F. Wright. 1998. Predicting the effects of atmospheric nitrogen deposition in conifer stands: evidence from the NITREX ecosystem-scale experiments. Ecosystems.

Ferrier, R.C., A. Jenkins, B.J. Cosby, R.C. Helliwell, R.F. Wright, and A.J. Bulger. 1995. Effects of future N deposition scenarios on the Galloway region of Scotland using a coupled sulphur & nitrogen model (MAGIC-WAND). Water Air Soil Pollut. 85:707-712.

Gaines, G. L., and H. C. Thomas. 1953. Adsorption studies on clay minerals, II. A formulation of the thermodynamics of exchange adsorption. J. Chem. Phys. 21:714-718.

Gundersen, P., B.A. Emmett, O.J. Kjonaas, C.J. Koopmans and A. Tietema. 1998. Impact of nitrogen deposition on nitrogen cycling in forests: a synthesis of NITREX data. Forest Ecol. Management 101:37-55.

Hasan, S. M., R. L. Fox, and C. C. Boyd. 1970. Solubility and availability of sorbed sulfate in Hawaiian soils. Soil Sci. Soc. Am. Proc. 34:897-901.

Jenkins, A. and B.J. Cosby. 1989. Modelling surface water acidification using one and two soil layers and simple flow routing. In: J. Kamari, D.F. Brakke, A. Je?nkins, S.A. Norton and R.F.

Wright (eds), Regional Acidification Models: Geographic Extent and Time Development, Springer, New York, 1989, pp. 253-266.

Jenkins, A., R.C. Ferrier and B.J. Cosby. 1997. A dynamic model for assessing the impact of coupled sulphur and nitrogen deposition scenarios on surface water acidification. J. Hydrol. 197:111-127.

Jenkins, A., B.J. Cosby, R.C. Ferrier, T.A.B. Walker, and J.D. Miller. 1990. Modelling stream acidification in afforested catchments: An assessment of the relative effects of acid deposition and afforestation. J. Hydrol. 120:163-181.

Lepistö, A., Whitehead, P. G., Neal, C., and Cosby, B. J. 1988. Modelling the effects of acid deposition: estimation of longterm water quality responses in forested catchments in Finland. 19: 99120. Nordic Hydrology 19: 99-120.

McKnight, D.M., E.M. Thurman, R.L. Wershaw and H.F.Hemond. 1985. Biogeochemistry of aquatic humic substances in Thoreau's Bog, Concord, Massachusetts. Ecology 66:1339-1352.

NAPAP. 1991. Integrated Assessment Report. National Acid Precipitation Assessment Program, Washington, DC.

Oliver, B.G., E.M. Thurman, and R.L. Malcolm. 1983. The contribution of humic substances to the acidity of colored natural waters. Geochim. Cosmochim. Acta 47:2031-2035.

Rastetter, E. B., A. W. King, B. J. Cosby, G. M. Hornberger, R. O. O'Neill, and J. E. Hobbie. 1992. Aggregating fine-scale ecological knowledge to model coarser-scale attributes of ecosystems, Ecolog. Applic. 2:55-70.

Rosenbrock, H.H. 1960. An automatic method for finding the greatest or least value of a function. Computer J. 3:175-184.

Schecher, W.D. and C.T. Driscoll. 1993. ALCHEMI: A chemical equilibrium model to assess the acid-base chemistry and speciation of aluminum in dilute solutions. In R. Loeppert, A.P. Schwab, and S. Goldberg. Chemical Equilibrium and Reaction Models. Soil Sci. Soc. Amer., Madison, WI.

Stoddard, J.L. 1994. Long-term changes in watershed retention of nitrogen: Its causes and aquatic consequences. In: L. Baker (ed) Environmental Chemistry of Lakes and Reservoirs. Advances in Chemistry Series, No. 237, American Chemical Society, Washington, D.C., pp 223-284.

Sullivan, T.J., B.J. Cosby, J.R. Webb, K.U. Snyder, A.T. Herlihy, A.J. Bulger, E.H. Gilbert, and D. Moore. 2002. Assessment of the effects of acidic deposition on aquatic resources in the Southern Appalachian Mountains. Report prepared for the Southern Appalachian Mountains Initiative (SAMI). E&S Environmental Chemistry, Inc., Corvallis, OR.

Sullivan, T.J., B.J. Cosby, C.T. Driscoll, D.F. Charles, and H.F. Hemond. 1996. Influence of organic acids on model projections of lake acidification. Water Air Soil Pollut. 91:271-282.

Sullivan, T.J., J. A. Bernert, E. A. Jenne, J. M. Eilers, B. J. Cosby, D. F. Charles, and A. R. Selle. 1991. Comparison of MAGIC and diatom paleolimnological model hindcasts of lakewater acidification in the Adirondack region of New York. Prepared for the U.S. Department of Energy under Contract DE-AC06-76RLO 1830. Pacific Northwest Laboratory, Richland, WA.

Thornton, K., D. Marmorek, and P. Ryan. 1990. Methods for Projecting Future Changes in Surface Water Acid-Base Chemistry. State of the Science, SOS/T 14, National Acid Precipitation Assessment Program.

Tietema, A. and C. Beier. 1995. A correlative evaluation of nitrogen cycling in the forest ecosystems of the EC projects NITREX and EXMAN. Forest Ecol. Management 71: 143-151.

Whitehead, P. G., Bird, S., Hornung, M., Cosby, B. J., Neal, C., and Paricos, P. 1988. Stream acidification trends in the Welsh Uplands: a modelling study of the Llyn Brianne catchments. J.Hydrol. 101: 191-212.

Wright, R.F. 1989. RAIN project: role of organic acids in moderating pH change following reduction in acid deposition. Water Air Soil Pollut. 46:251-259.

Wright, R.F. and N. van Breemen. 1995. The NITREX project: an introduction. Forest Ecol. Management 71:1-5.

Wright, R. F., Cosby, B. J., Ferrier, R. C., Jenkins, A., Bulger, A. J., and Harriman, R. 1994. Changes in the acidification of lochs in Galloway, southwestern Scotland, 1979-1988: the MAGIC model used to evaluate the role of afforestation, calculate critical loads, and predict fish status. J.Hydrol. 161: 257-285.

Wright, R.F., B.J. Cosby, M.B. Flaten, and J.O. Reuss. 1990. Evaluation of an acidification model with data from manipulated catchments in Norway. Nature 343:53-55.

Appendix E

Water Chemistry Trends Data

This Appendix presents an analysis of time trends in water quality for 14 intensively-studied streams in Shenandoah National Park. The analysis covers the water years from 1988 through 2001 and provides 14 years of quarterly sampled data for all streams (occasional missing values may occur at some sites).

Streams on Siliciclastic Bedrock include DR01 (Deep Run), VT35 (Paine Run), VT36 (Meadow Run), VT53 (Twomile Creek), and WOR1 (White Oak Run). Streams on Granitic Bedrock include NFDR (North Fork Dry Run), VT58 (Brokenback Run), VT59 (Staunton River), and VT62 (Hazel River). Streams on Basaltic Bedrock include VT51 (Jeremys Run), VT60 (Piney River), VT61 (North Fork Thornton River), VT66 (Rose River), and VT75 (White Oak Canyon).

Analyses of the following water quality constituents are presented:

ANC (Acid Neutralizing Capacity; ueq/L),

Hydrogen ion concentration (ueq/L),

Sulfate concentration (ueq/L),

Nitrate concentration (ueq/L),

SBC (Sum of Base Cation concentrations – calcium + magnesium + sodium + potassium; ueq/L),

SAA (Sum of Acid Anion concentrations – sulfate + nitrate + chloride; ueq/L), and

Calculated ANC (SBC – SAA; ueq/L).

The concentrations of each analyte for each stream are plotted vs time in this appendix. The coefficients of a linear regression equation fitted to each time series are given in each plot.

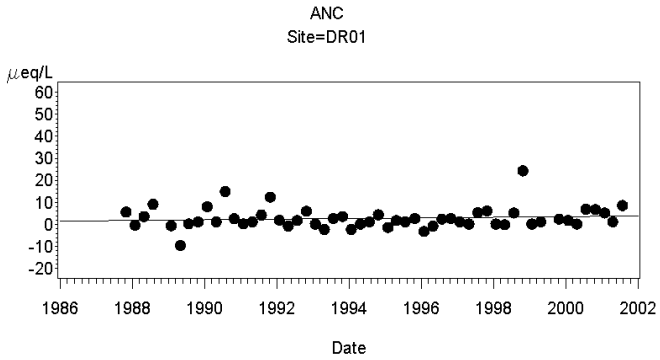

Regression Equation:
ALK = -279.8736 + 0.141773*Date

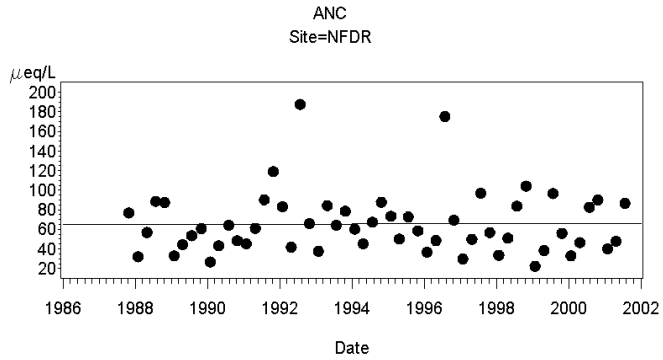

Regression Equation:
ALK = -61.84063 + 0.063902*Date

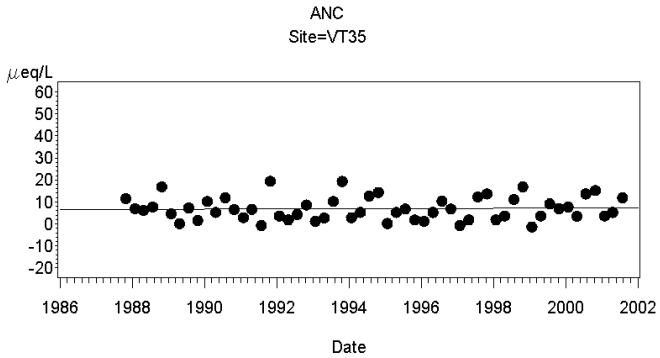

Regression Equation:
ALK = -87.14083 + 0.047204*Date

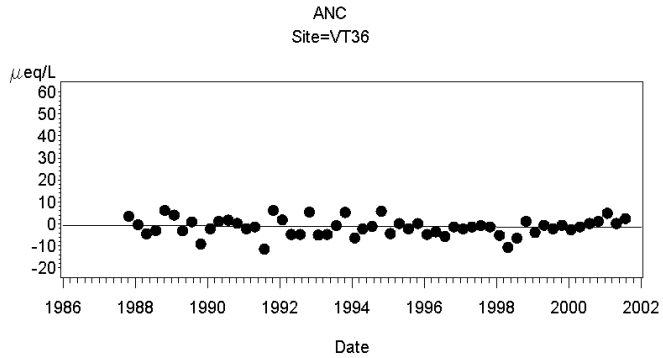

Regression Equation:
ALK = 95.96497 - 0.048751*Date

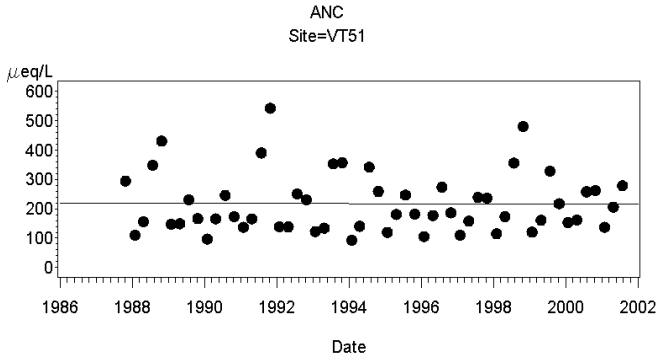

Regression Equation:
ALK = 684.2502 - 0.234162*Date

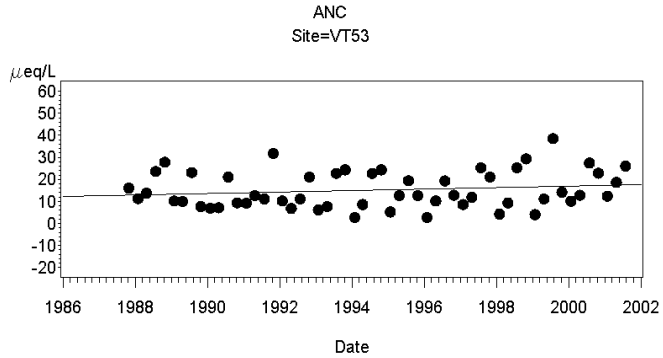

Regression Equation:
ALK = -652.815 + 0.33492*Date

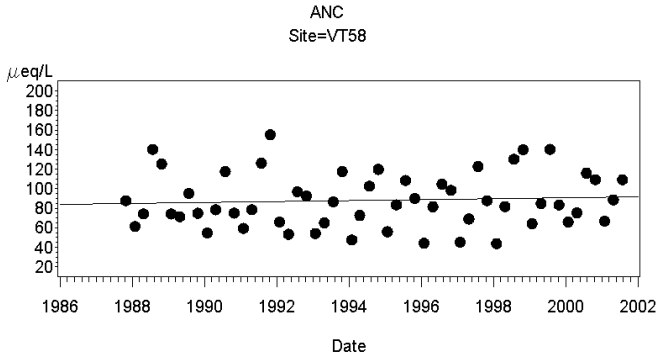

Regression Equation:
ALK = -887.2494 + 0.488895*Date

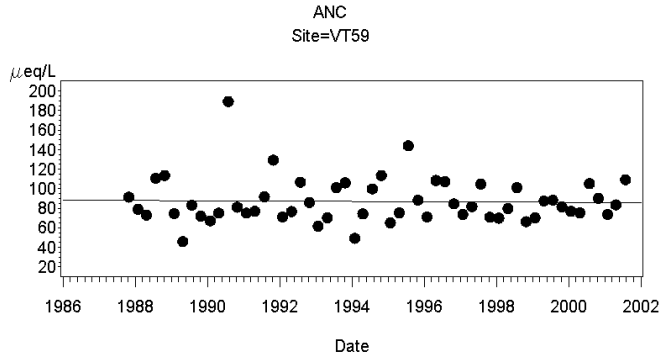

Regression Equation:
ALK = 413.075 - 0.163335*Date

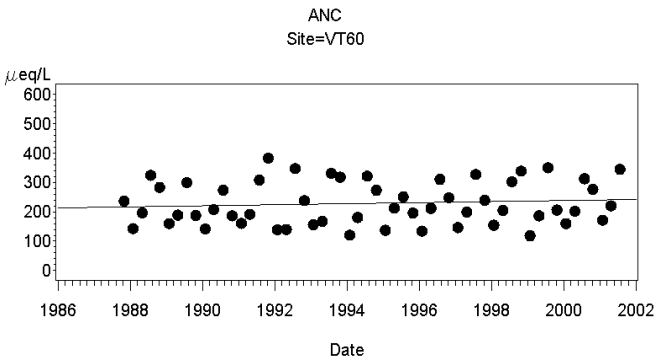

Regression Equation:
ALK = -3126.787 + 1.682061*Date

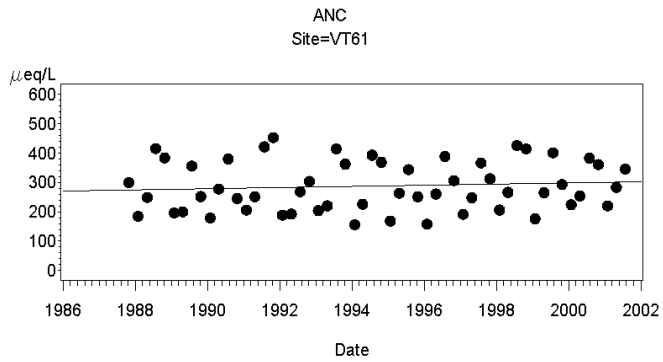

Regression Equation:
ALK = -3669.388 + 1.983243*Date

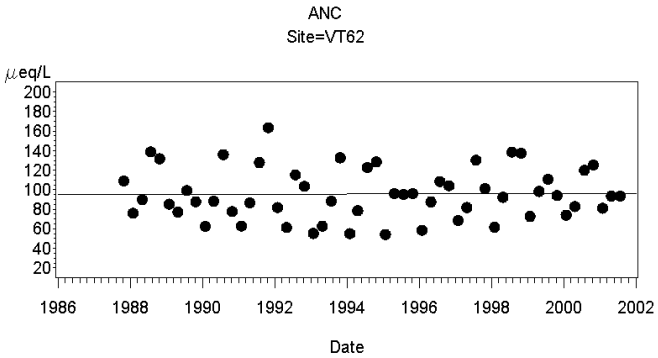

Regression Equation:
ALK = -78.44445 + 0.087236*Date

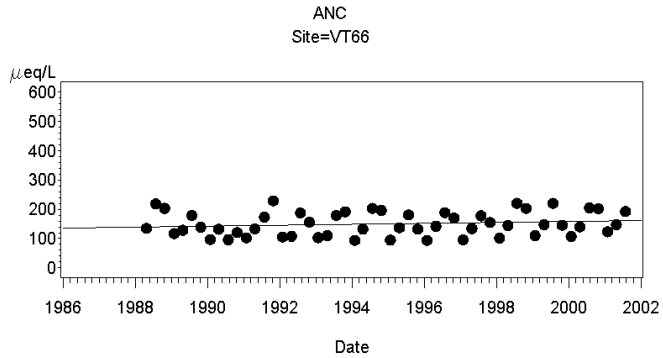

Regression Equation:
ALK = -2847.6 + 1.502688*Date

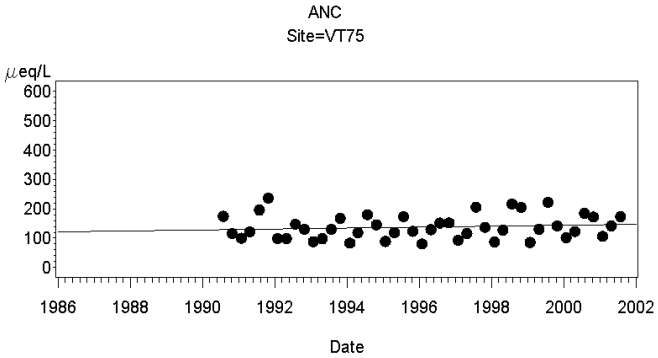

Regression Equation:
ALK = -3079.654 + 1.612302*Date

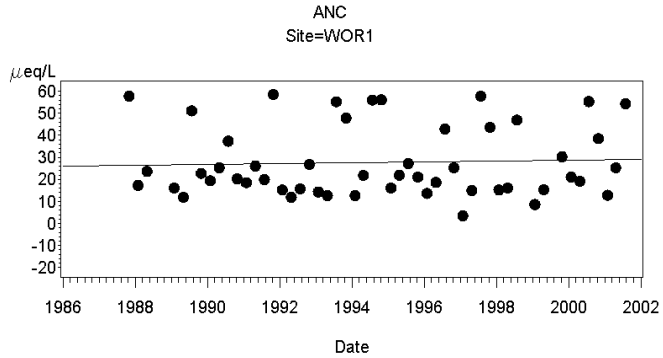

Regression Equation:
ALK = -360.3259 + 0.194536*Date

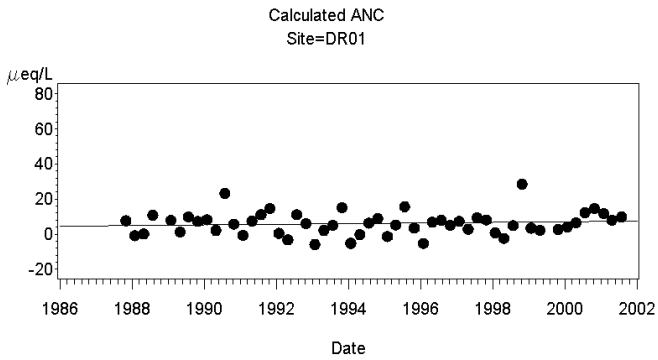

Regression Equation:
calk = -347.2313 + 0.177164*Date

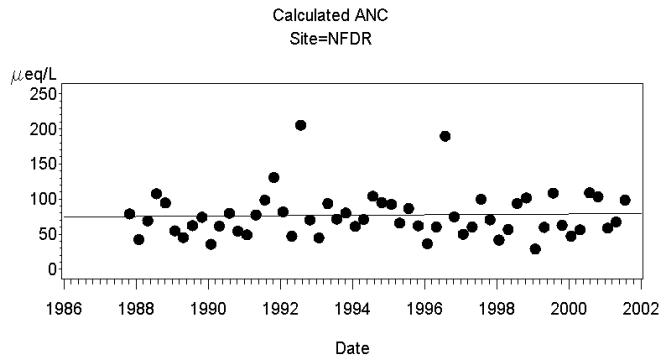

Regression Equation:
calk = -522.785 + 0.300522*Date

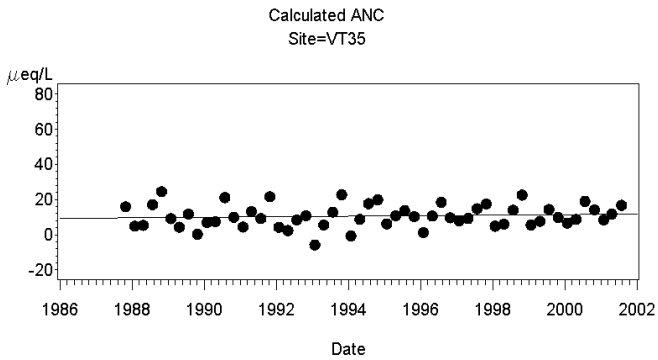

Regression Equation:
calk = -315.078 + 0.163325*Date

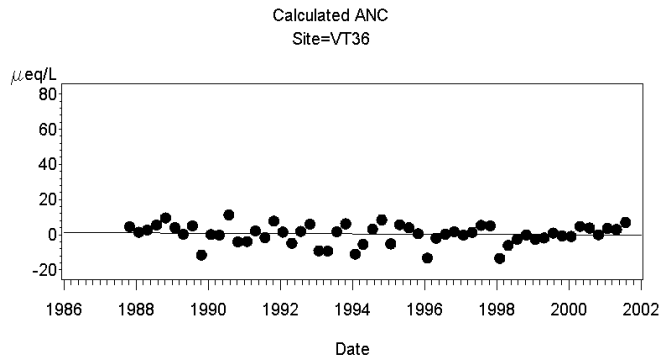

Regression Equation:
calk = 214.8213 - 0.10747*Date

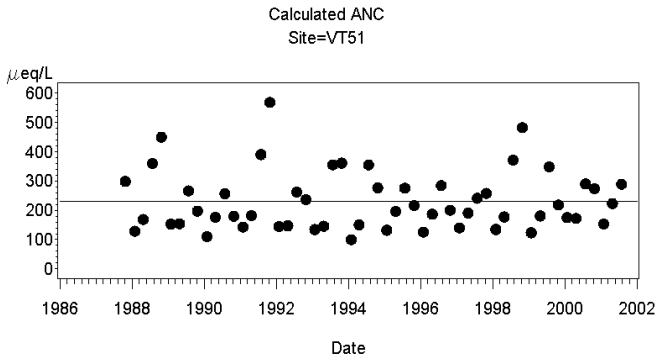

Regression Equation:
calk = 201.9913 + 0.014514*Date

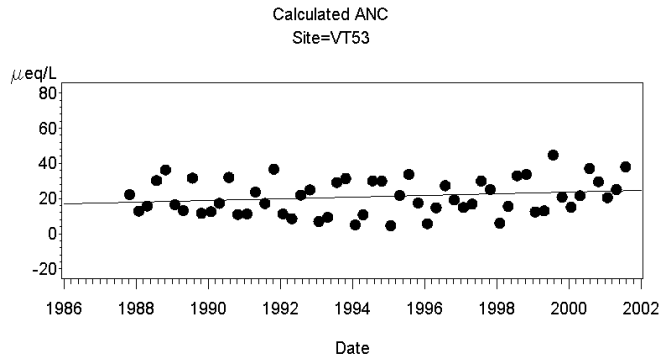

Regression Equation:
calk = -921.4713 + 0.472465*Date

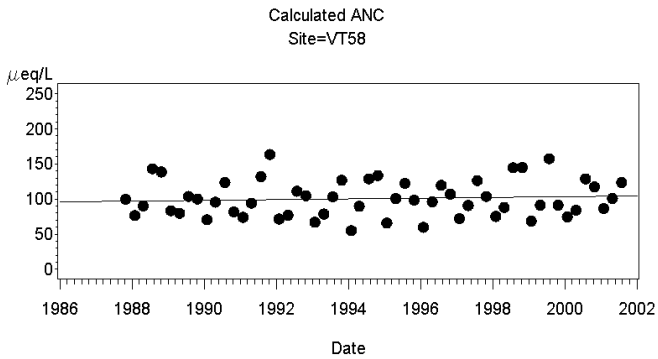

Regression Equation:
calk = -918.2002 + 0.5109*Date

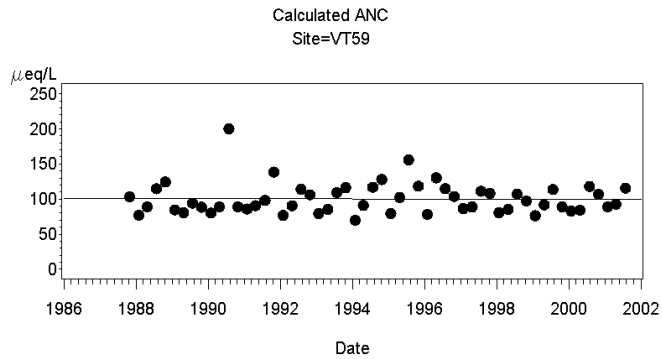

Regression Equation:
calk = 279.8399 - 0.089909*Date

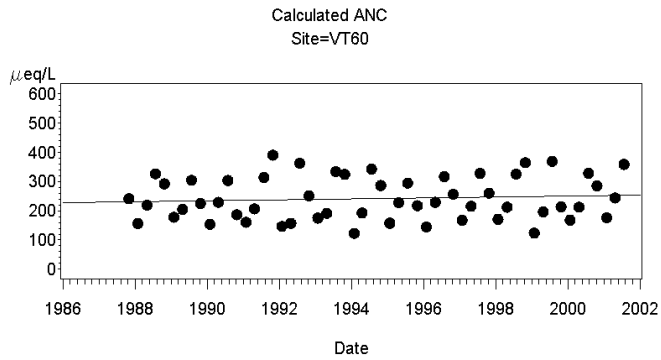

Regression Equation:
calk = -3152.46 + 1.701905*Date

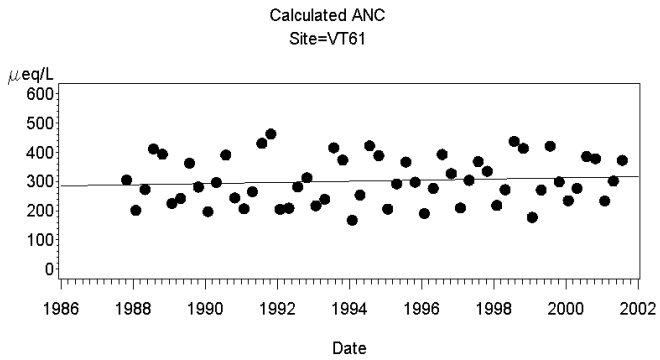

Regression Equation:
calk = -3732.547 + 2.023038*Date

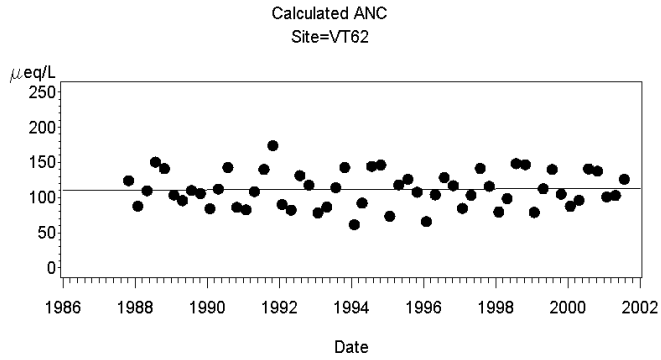

Regression Equation:
calk = -129.4677 + 0.120792*Date

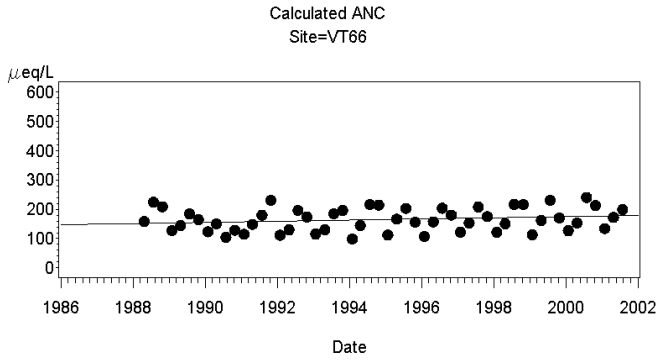

Regression Equation:
calk = -3436.066 + 1.804952*Date

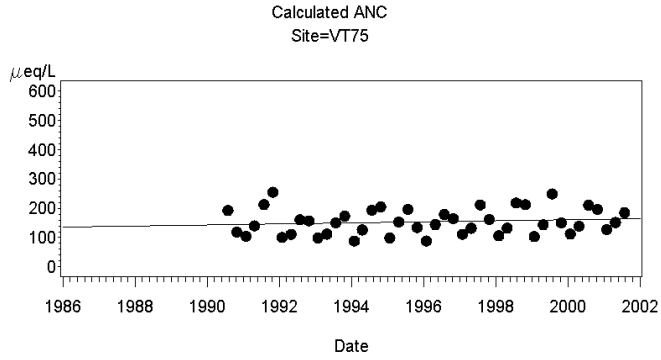

Regression Equation:
calk = -3567.981 + 1.864714*Date

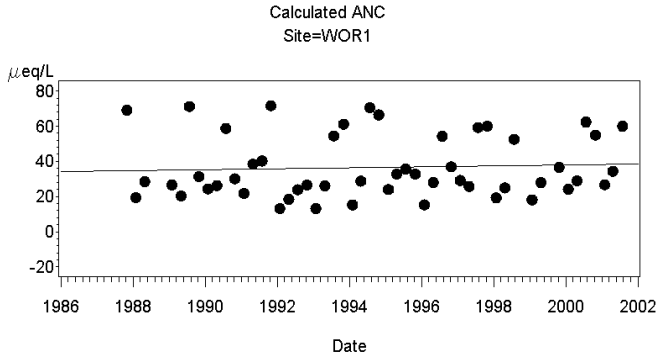

Regression Equation:
calk = -535.3522 + 0.286743*Date

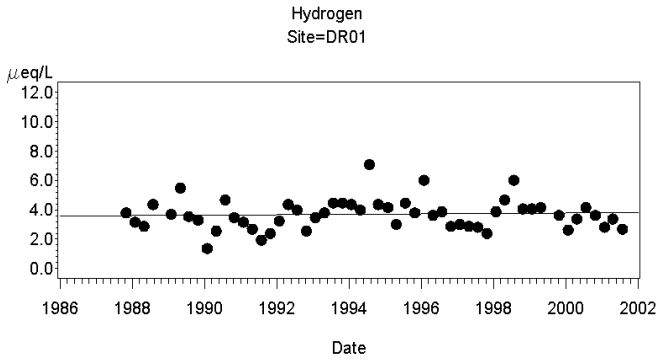

Regression Equation:
H = -27.33784 + 0.015553*Date

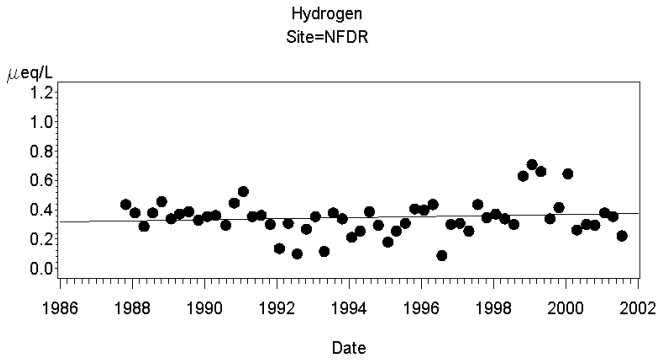

Regression Equation:
H = -6.484087 + 0.003425*Date

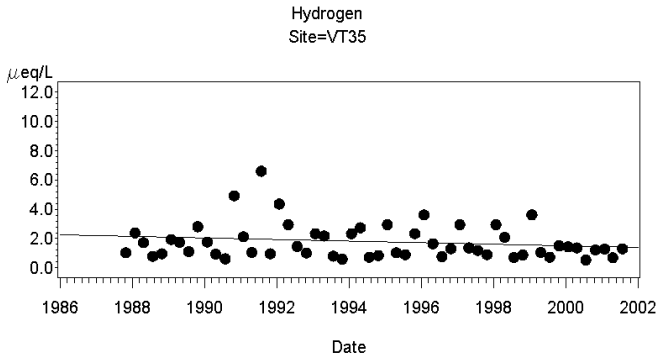

Regression Equation:
H = 109.1118 - 0.053817*Date

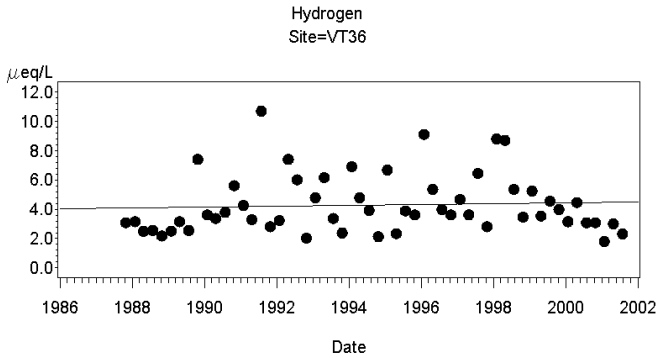

Regression Equation:
H = -51.43175 + 0.027941*Date

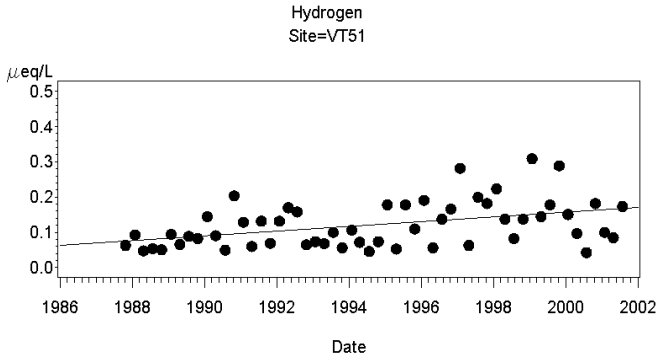

Regression Equation:
H = -13.42908 + 0.006793*Date

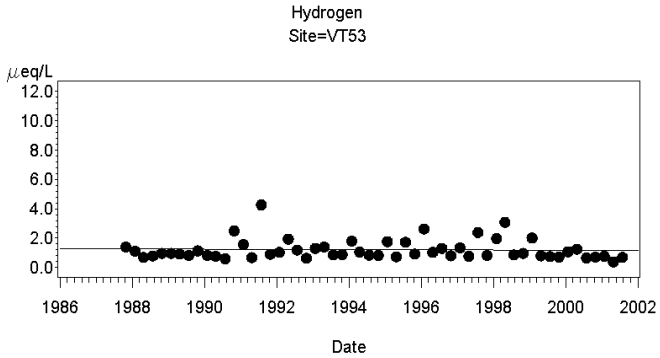

Regression Equation:
H = 17.79643 - 0.008311*Date

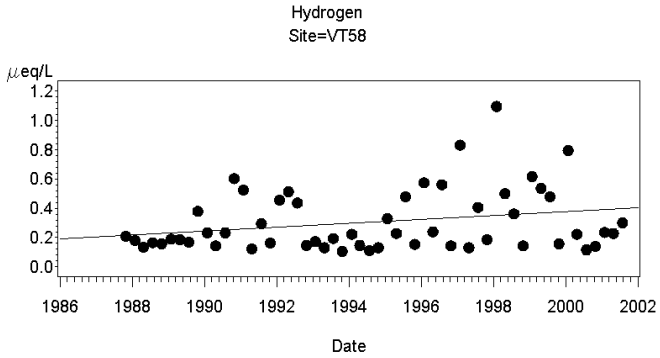

Regression Equation:
H = -25.77014 + 0.013072*Date

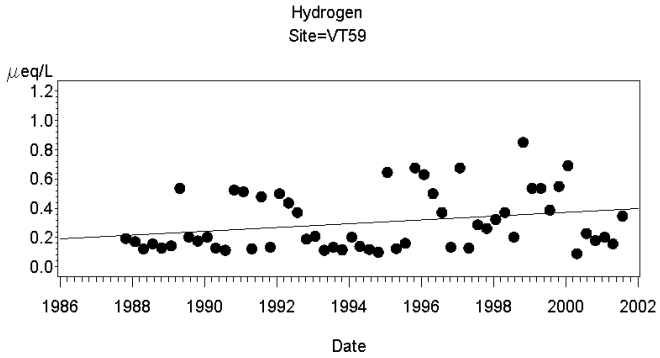

Regression Equation:
H = -25.82814 + 0.0131*Date

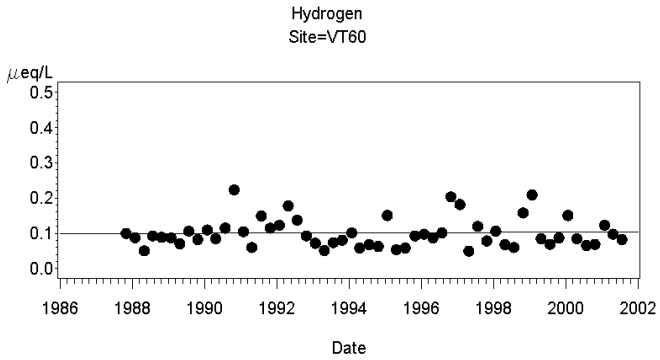

Regression Equation:
H = -0.409651 + 0.000256*Date

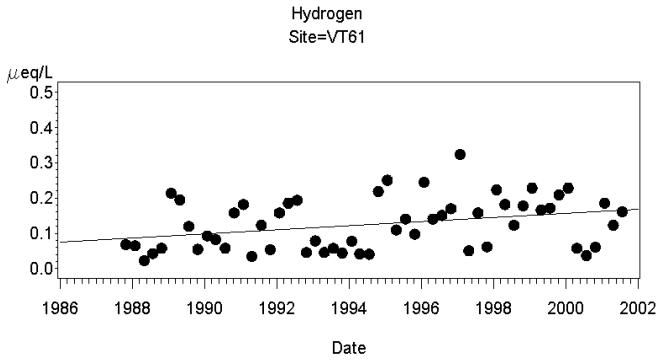

Regression Equation:
H = -11.42078 + 0.005789*Date

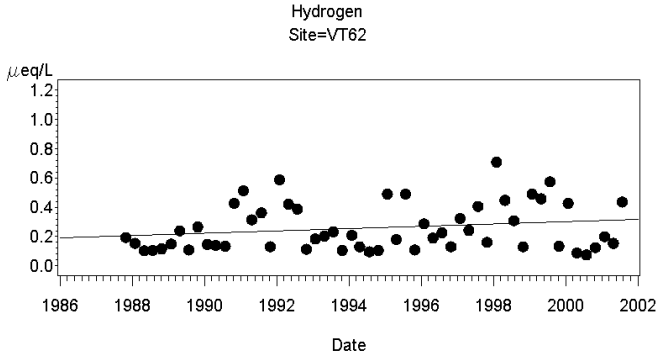

Regression Equation:
H = -15.32971 + 0.007814*Date

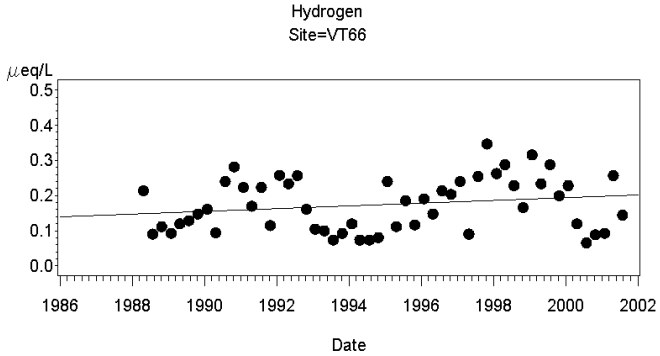

Regression Equation:
H = -7.507262 + 0.00385*Date

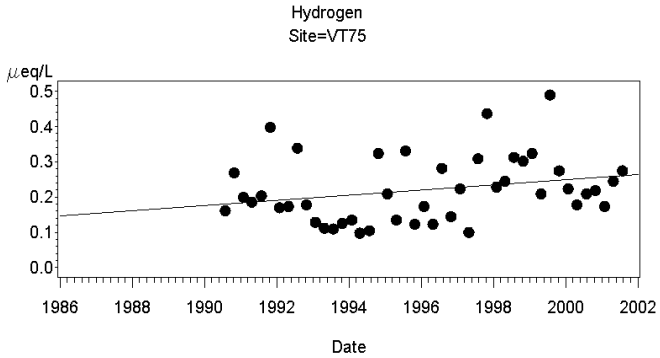

Regression Equation:
H = -14.60083 + 0.007425*Date

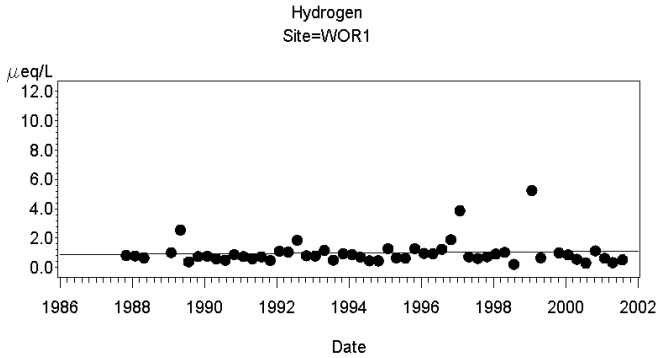

Regression Equation:
H = -32.2156 + 0.01665*Date

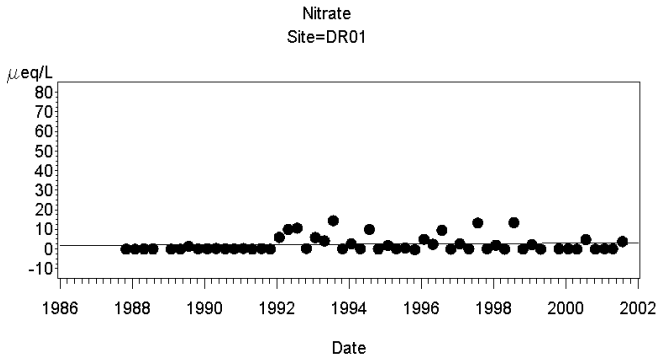

Regression Equation:
NO3 = -198.4712 + 0.100716*Date

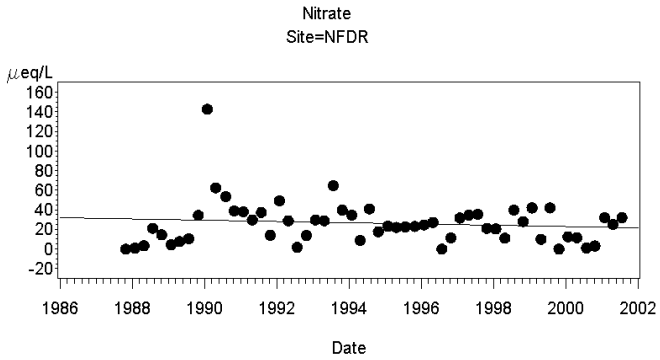

Regression Equation:
NO3 = 1362.745 - 0.670062*Date

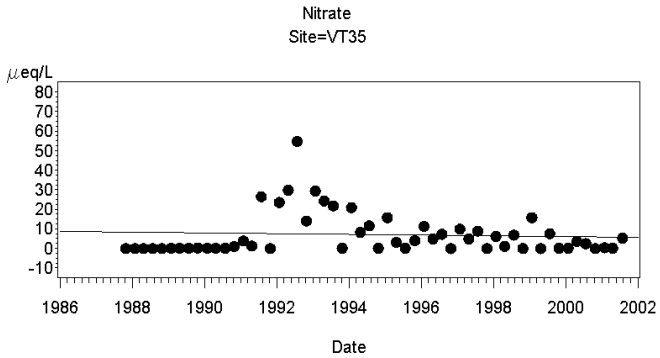

Regression Equation:
NO3 = 369.6376 - 0.181794*Date

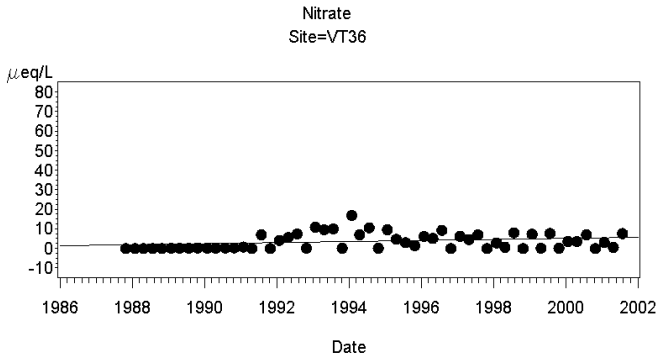

Regression Equation:
NO3 = -504.736 + 0.254847*Date

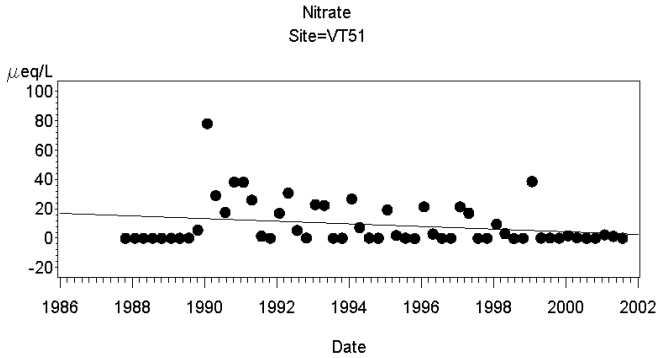

Regression Equation:
NO3 = 1740.047 - 0.86777*Date

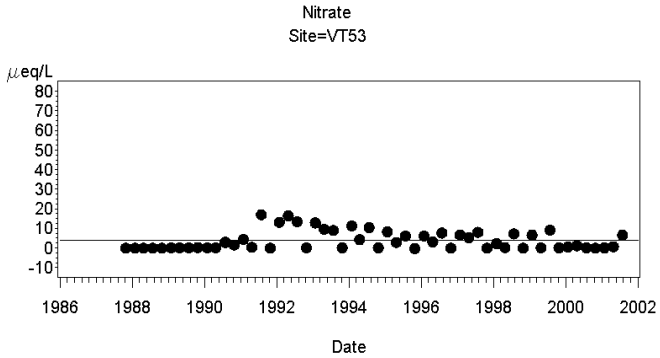

Regression Equation:
NO3 = -29.85814 + 0.016926*Date

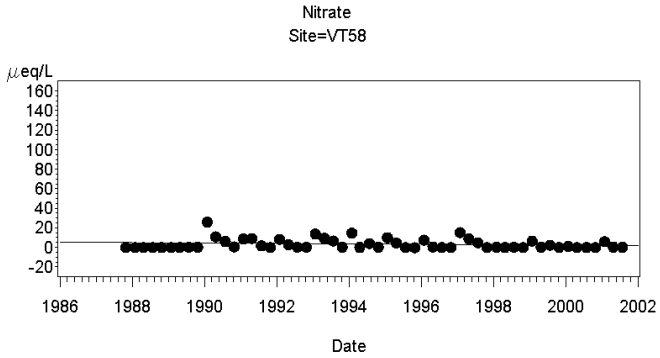

Regression Equation:
NO3 = 362.2943 - 0.179892*Date

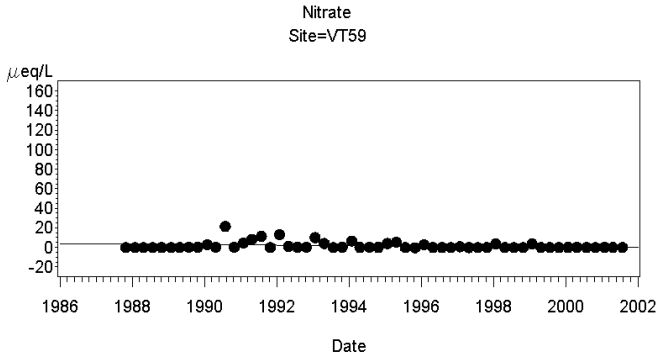

Regression Equation:
NO3 = 461.6683 - 0.230485*Date

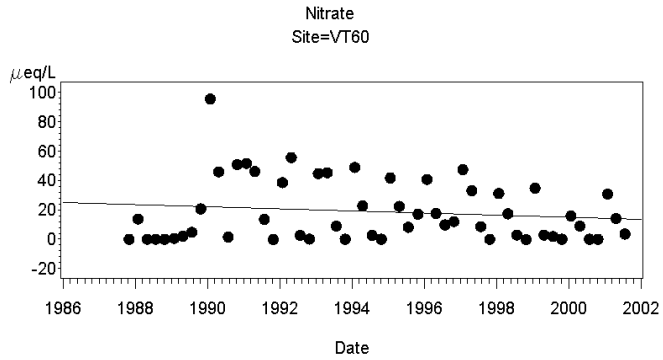

Regression Equation:
NO3 = 1482.256 - 0.733764*Date

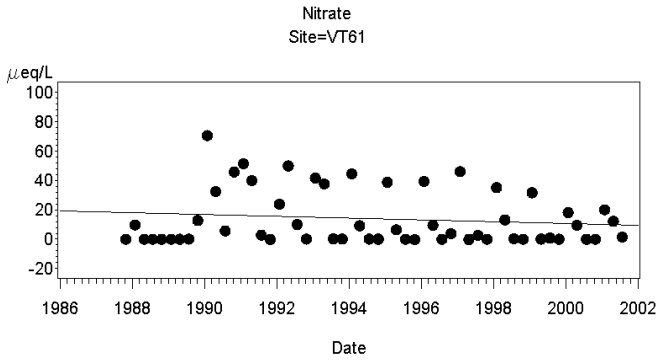

Regression Equation:
NO3 = 1286.58 - 0.638013*Date

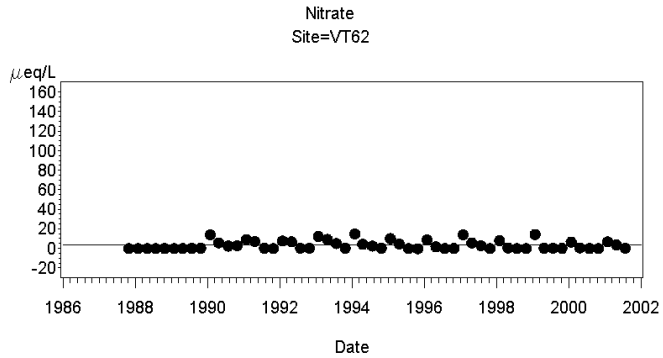

Regression Equation:
NO3 = -47.34606 + 0.025482*Date

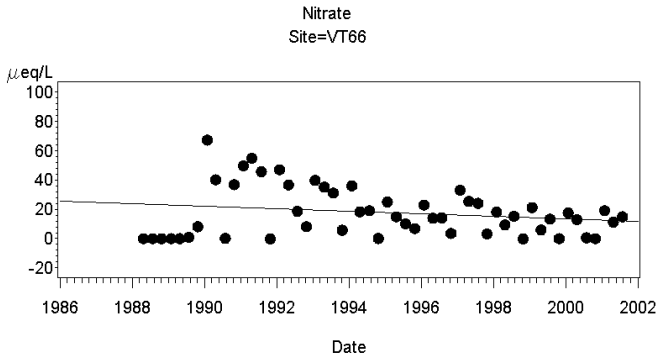

Regression Equation:
NO3 = 1747.833 - 0.867226*Date

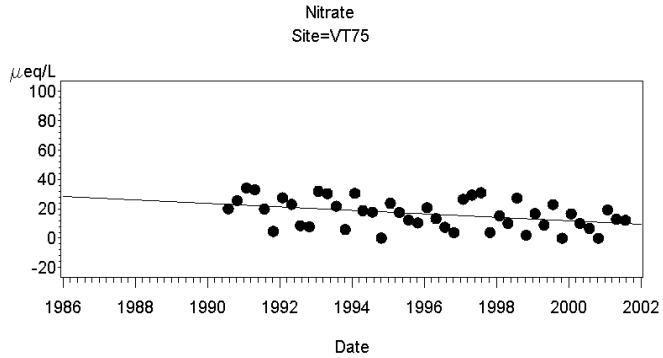

Regression Equation:
NO3 = 2385.95 - 1.187013*Date

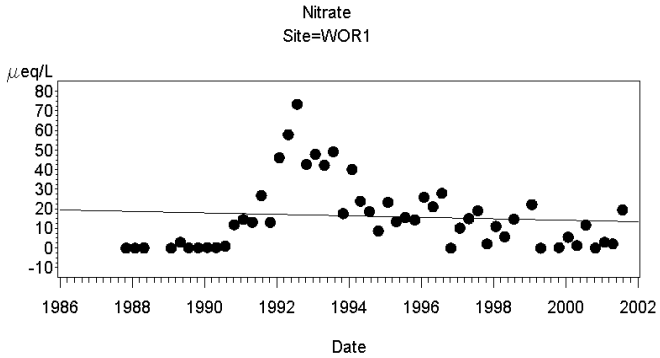

Regression Equation:
NO3 = 743.4187 - 0.364593*Date

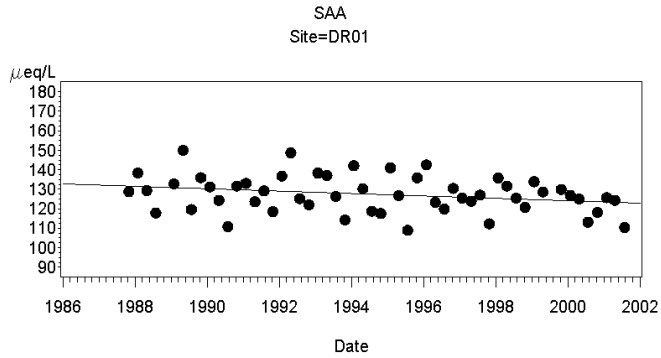

Regression Equation:
saa = 1350.433 - 0.613106*Date

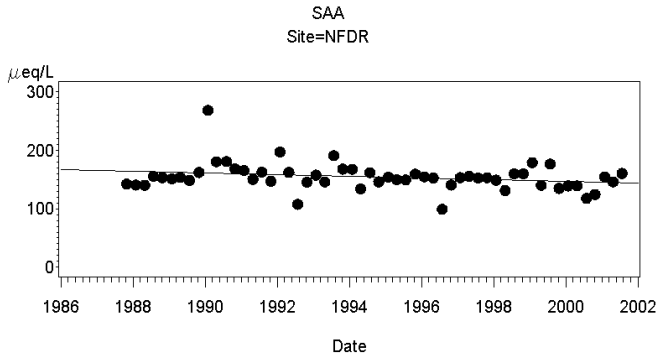

Regression Equation:
saa = 3119.964 - 1.486661*Date

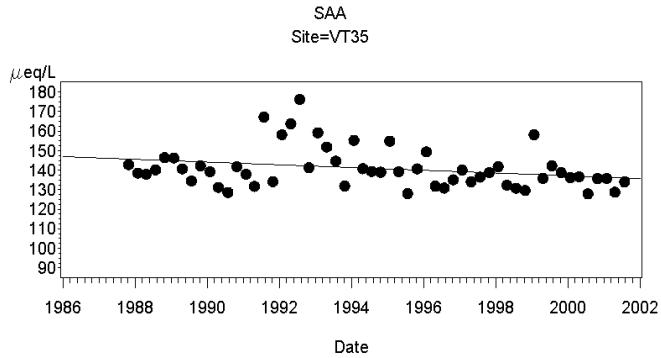

Regression Equation:
saa = 1494.26 - 0.678476*Date

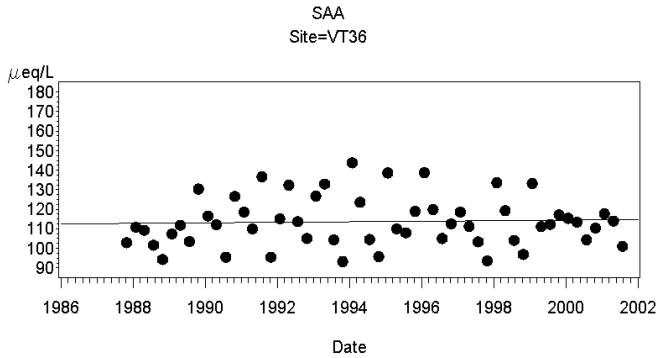

Regression Equation:
saa = -171.8407 + 0.143097*Date

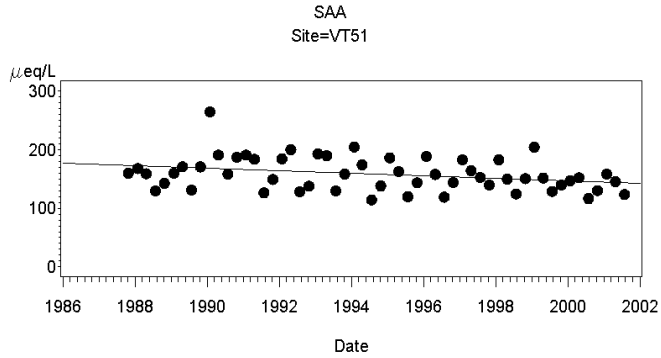

Regression Equation:
saa = 4333.26 - 2.09296*Date

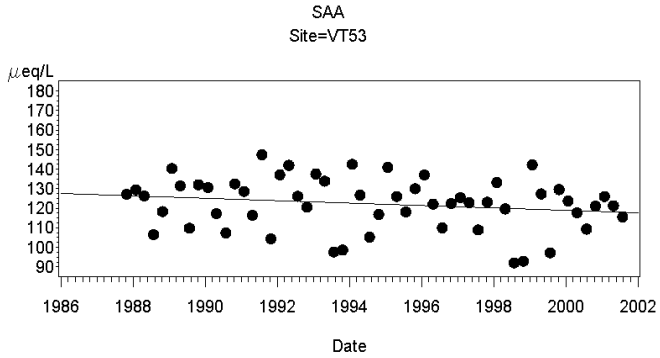

Regression Equation:
saa = 1368.182 - 0.624574*Date

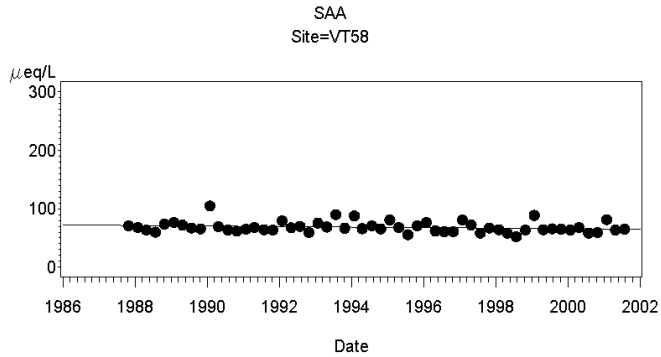

Regression Equation:
saa = 931.3231 - 0.432369*Date

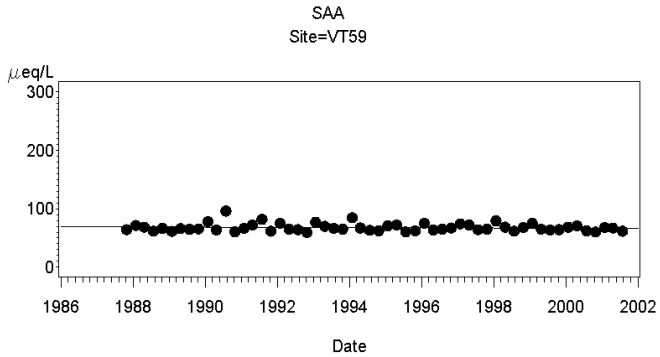

Regression Equation:
saa = 412.1573 - 0.172398*Date

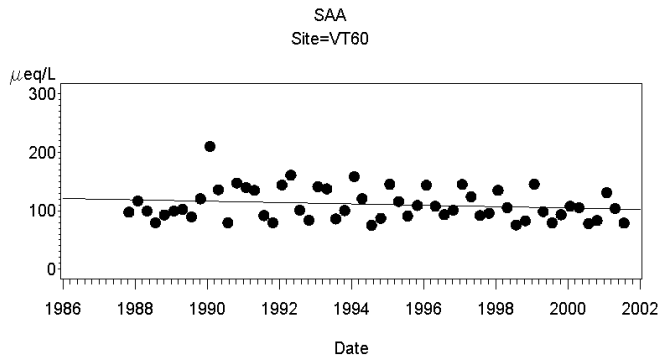

Regression Equation:
saa = 2561.052 - 1.228497*Date

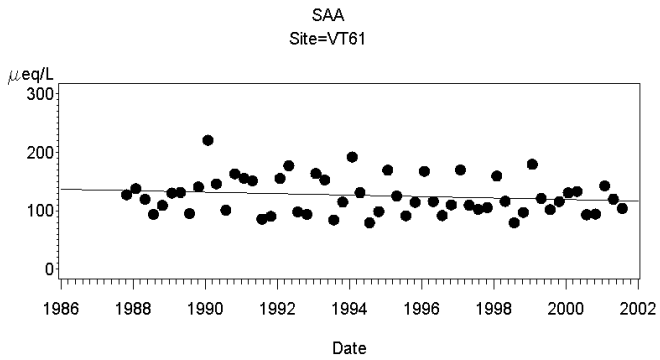

Regression Equation:
saa = 2634.723 - 1.258068*Date

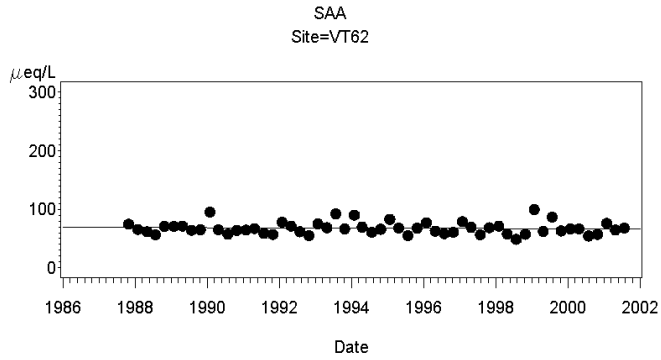

Regression Equation:
saa = 294.7419 - 0.113692*Date

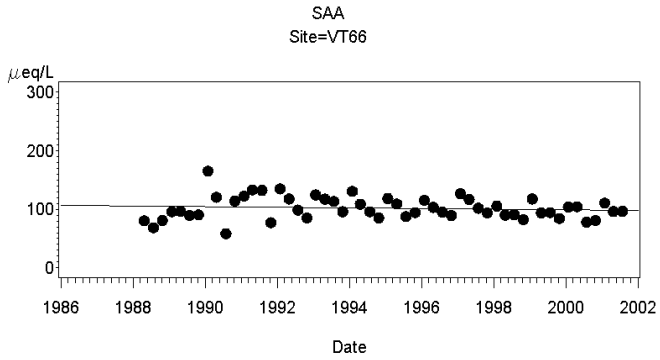

Regression Equation:
saa = 1185.596 - 0.542991*Date

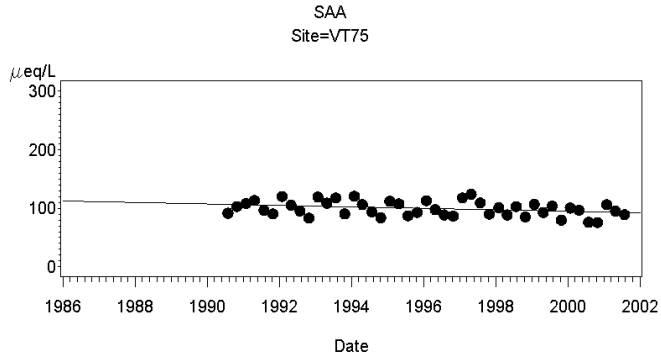

Regression Equation:
saa = 2475.23 - 1.190102*Date

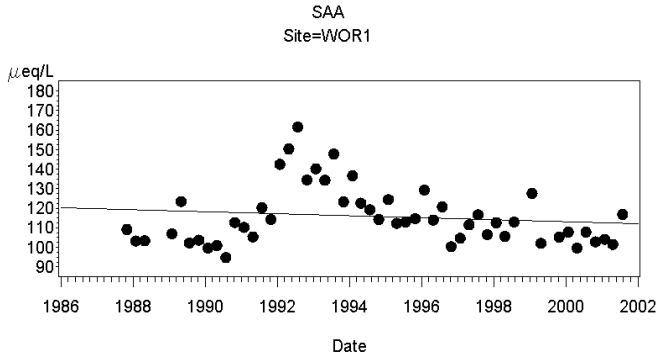

Regression Equation:
saa = 1110.296 - 0.4986*Date

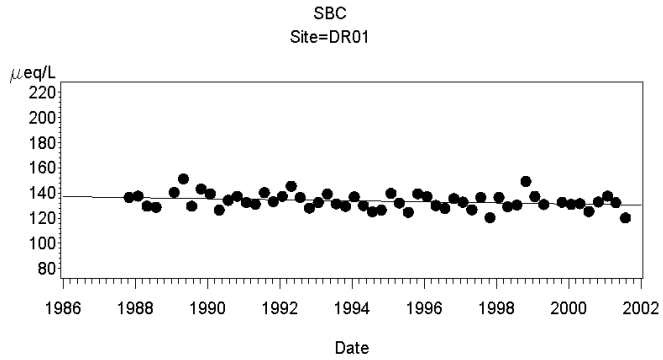

Regression Equation:
sbc = 1003.202 - 0.435942*Date

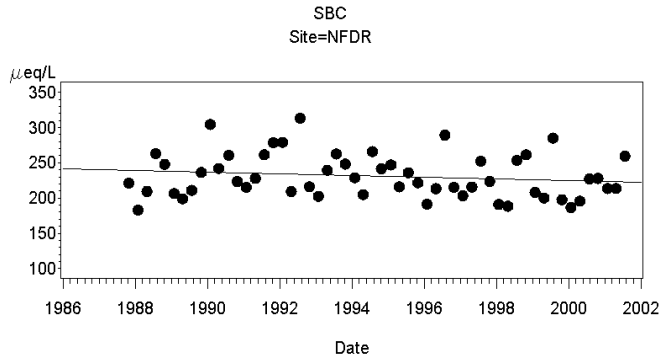

Regression Equation:
sbc = 2597.179 - 1.186139*Date

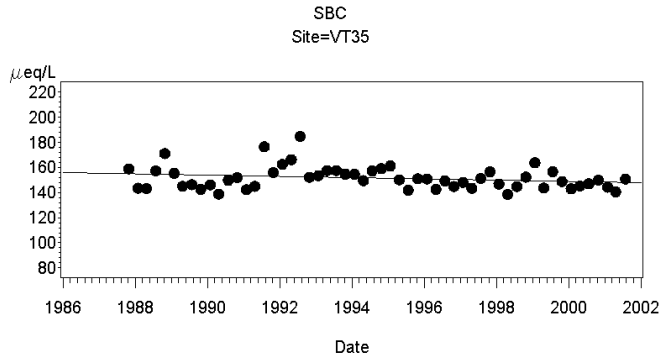

Regression Equation:
sbc = 1179.182 - 0.515152*Date

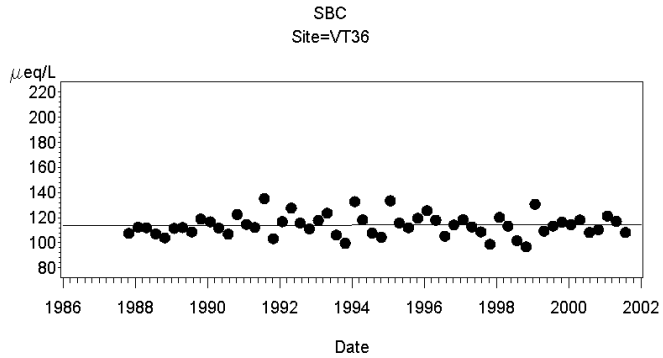

Regression Equation:
sbc = 42.98058 + 0.035626*Date

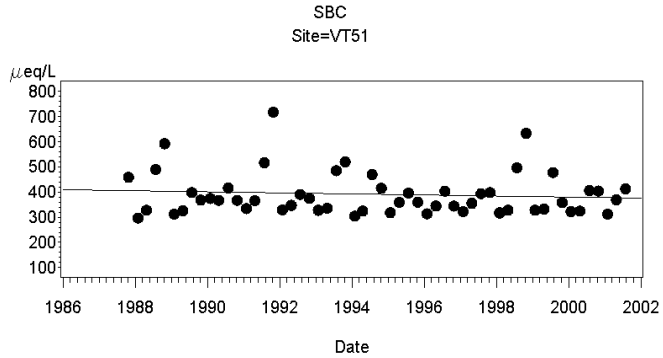

Regression Equation:
sbc = 4535.251 - 2.078446*Date

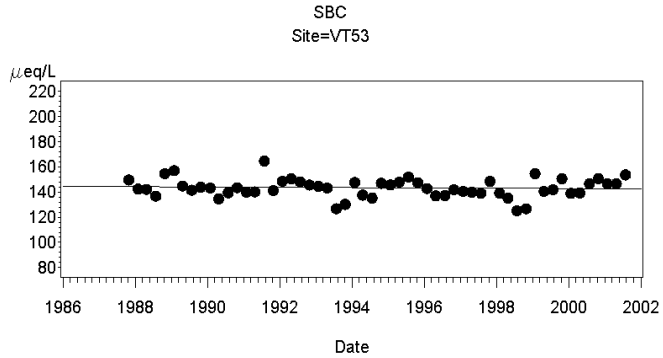

Regression Equation:
sbc = 446.7112 - 0.152108*Date

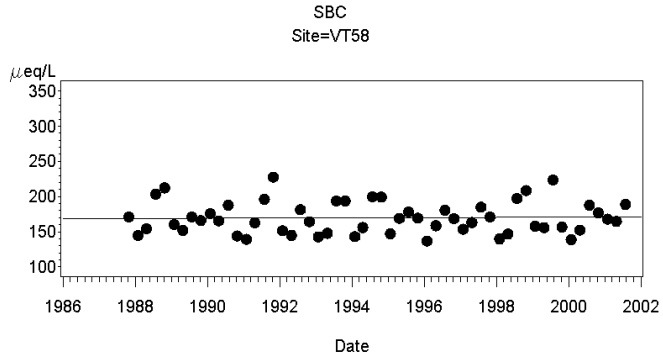

Regression Equation:
sbc = 13.12284 + 0.078531*Date

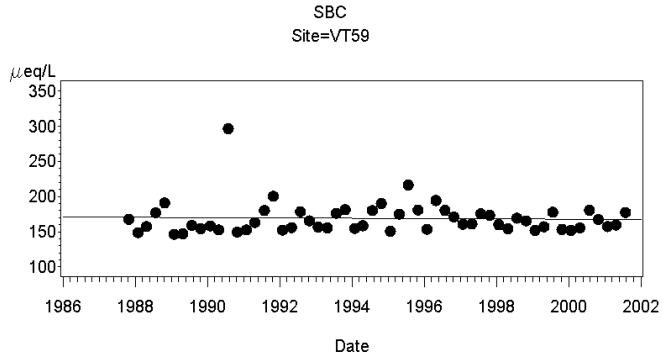

Regression Equation:
sbc = 691.9972 - 0.262306*Date

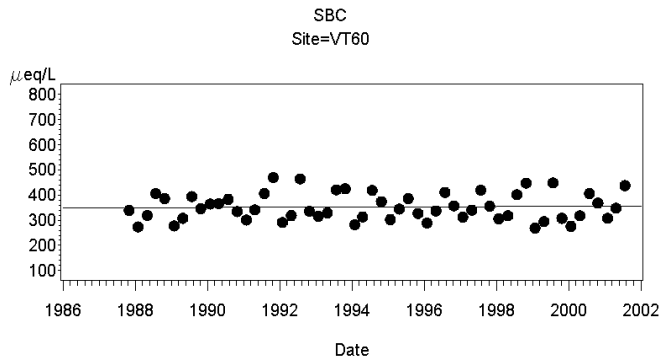

Regression Equation:
sbc = -591.4077 + 0.473409*Date

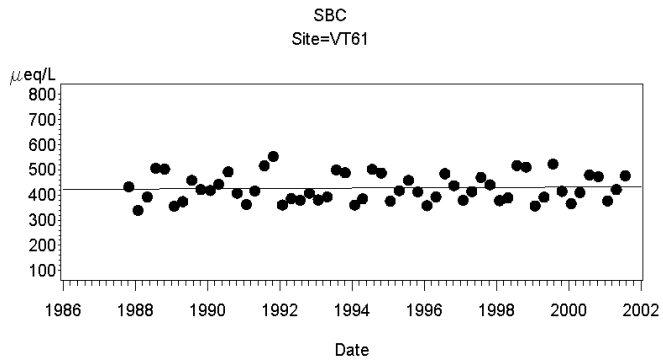

Regression Equation:
sbc = -1097.824 + 0.764971*Date

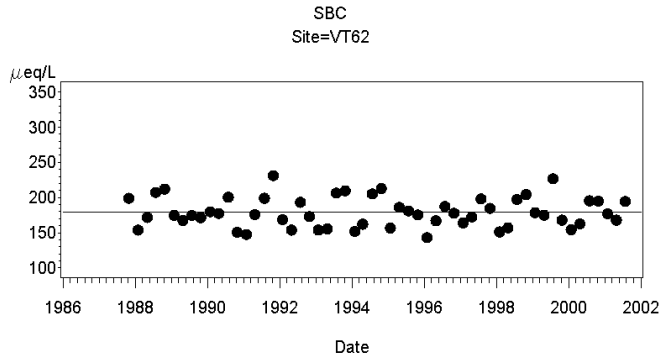

Regression Equation:
sbc = 165.2742 + 0.0071*Date

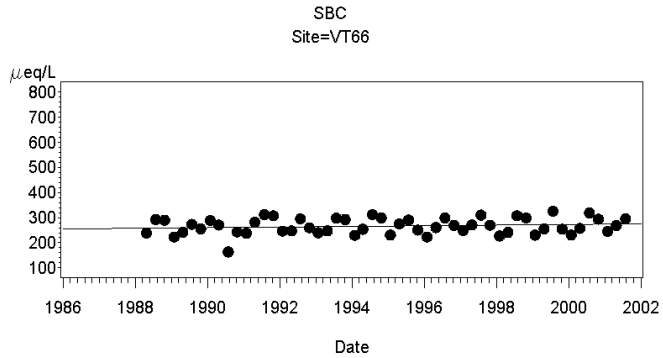

Regression Equation:
sbc = -2250.47 + 1.261961*Date

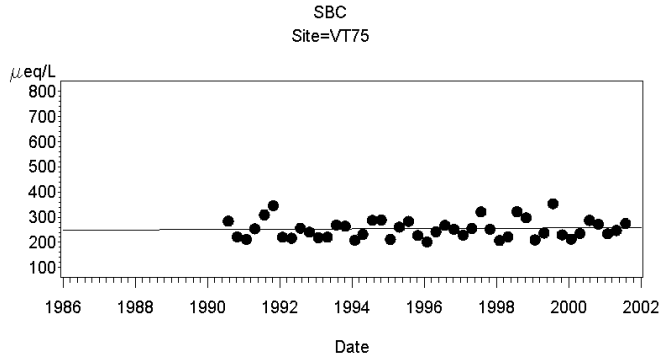

Regression Equation:
sbc = -1092.751 + 0.674612*Date

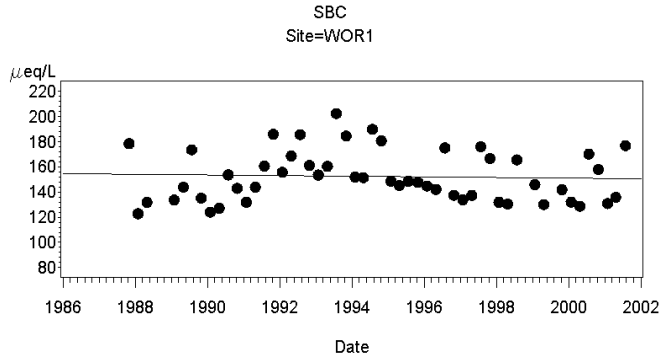

Regression Equation:
sbc = 574.9436 - 0.211857*Date

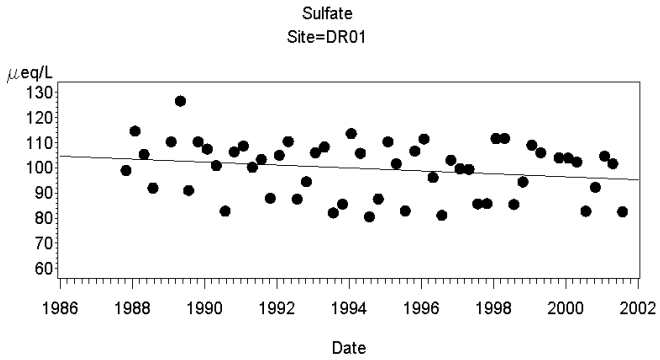

Regression Equation:
SO4 = 1244.275 - 0.573908*Date

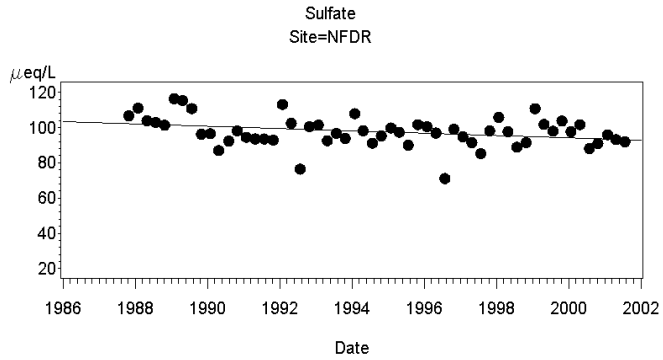

Regression Equation:
SO4 = 1358.48 - 0.632081*Date

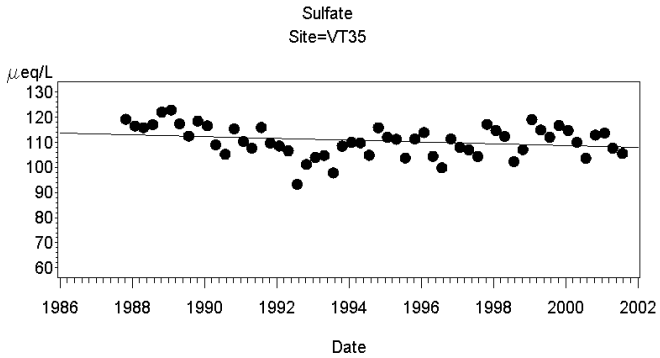

Regression Equation:
SO4 = 806.08 - 0.34869*Date

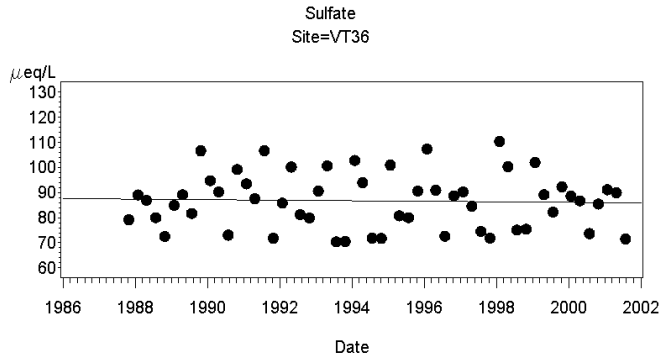

Regression Equation:
SO4 = 281.5882 - 0.097693*Date

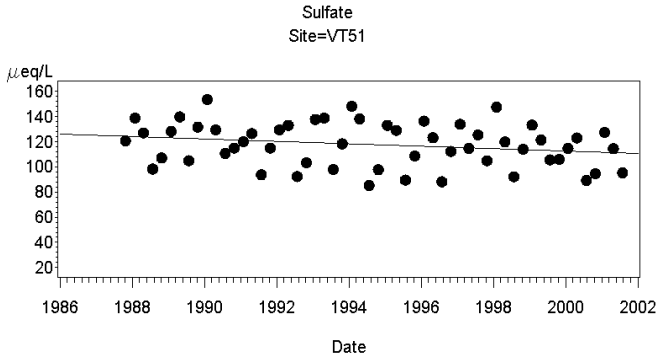

Regression Equation:
SO4 = 2055.77 - 0.971697*Date

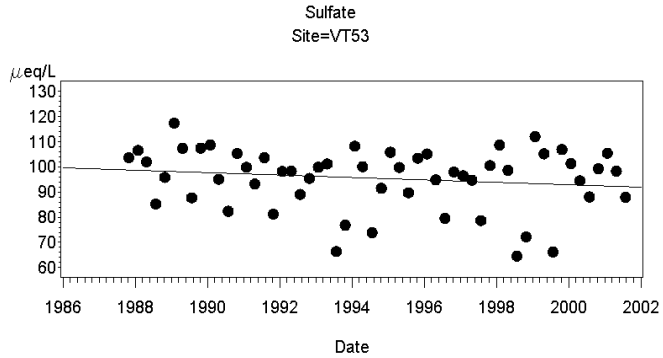

Regression Equation:
SO4 = 1075.546 - 0.491399*Date

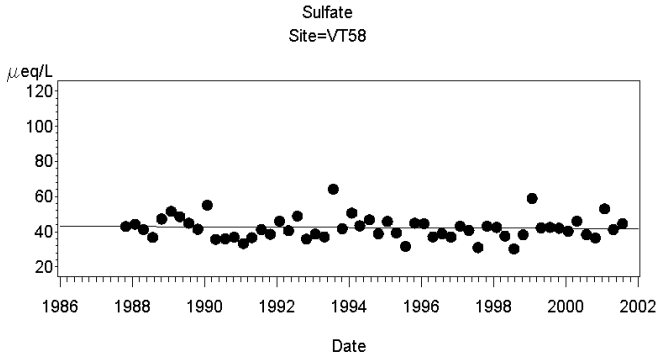

Regression Equation:
SO4 = 229.2576 - 0.093803*Date

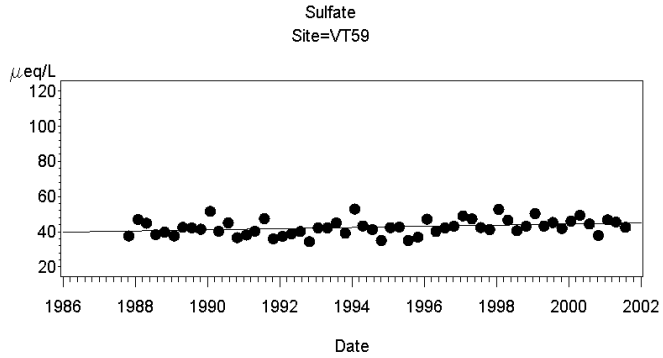

Regression Equation:
SO4 = -614.4821 + 0.329446*Date

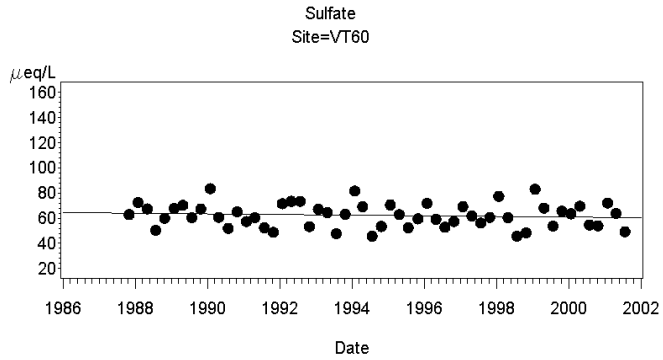

Regression Equation:
SO4 = 553.6827 - 0.246309*Date

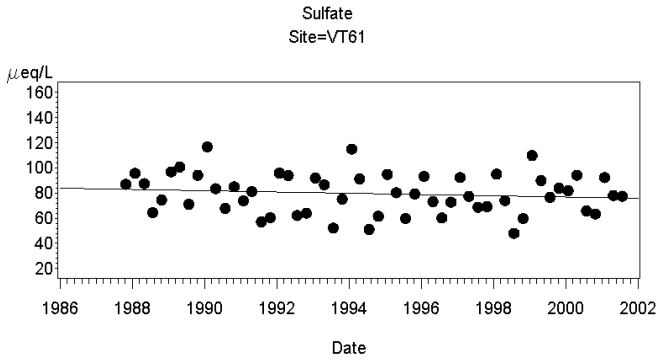

Regression Equation:
SO4 = 1126.814 - 0.525022*Date

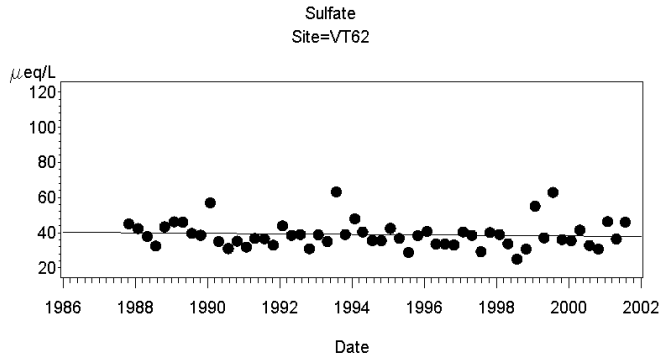

Regression Equation:
SO4 = 309.4081 - 0.135551*Date

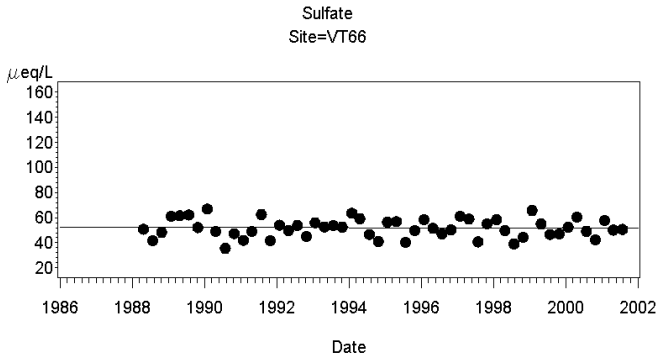

Regression Equation:
SO4 = 171.9832 - 0.060212*Date

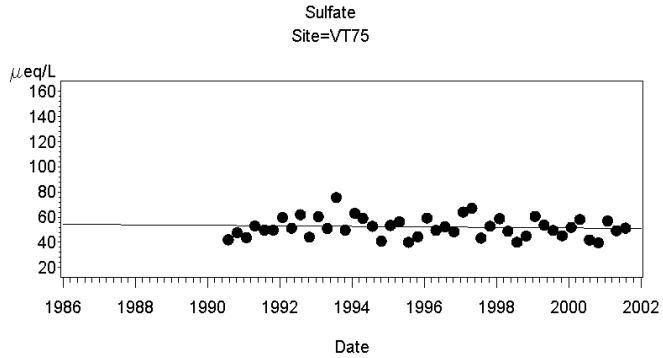

Regression Equation:
SO4 = 473.8638 - 0.211298*Date

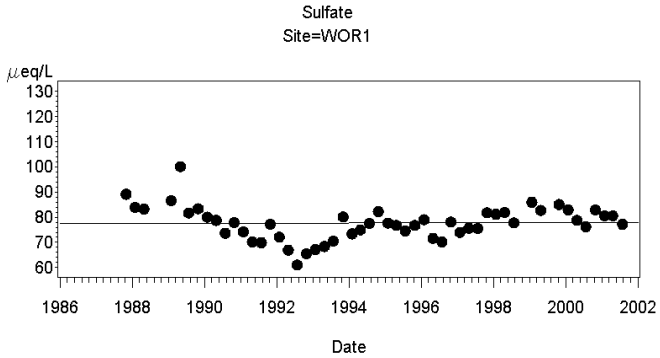

Regression Equation:
SO4 = 52.37576 + 0.012667*Date

Appendix D

Characteristics of Streams Surveyed within SHEN

Available data on streamwater ANC within SHEN are summarized in this appendix, along with locational information, site elevation, watershed area, and percent of watershed in the various geologic sensitivity classes. Locational and physical data are listed in Table D-1. Geological and chemical data are provided in Table D-2. Modeled sites are indicated with bold characters in the site identification column.

For some purposes in this report the site pairs, VT59/STAN, VT60/PINE, and VT35/PAIN, are treated as single sites. In these cases, routine monitoring, established at the first site, was continued at the second site when discharge gauges were installed. The paired sites, VT59/STAN and VT60/PINE, are in close proximity. The paired sites, VT35/PAIN are identical and only PAIN is listed in this Appendix.

Table D-1. Location and physical information for streams surveyed in SHEN.

Frequency[1]	Site ID[2]	Stream	Watershed	District	Elev[3]	Area[4]	UTM EW	UTM NS
Quarterly	**VT51**	Jeremys Run	Jeremys Run	North	930	21.97	727652	4288251
Survey	JR04	Jeremys Run	Jeremys Run	North	940	20.87	728093	4287965
Survey	JR02	Jeremys Run	Jeremys Run	North	980	0.83	728092	4288021
Survey	JR05	Jeremys Run	Jeremys Run	North	1080	20.11	728804	4287838
Survey	JR15	Jeremys Run	Jeremys Run	North	1090	0.71	730312	4288131
Survey	JR18	Jeremys Run	Jeremys Run	North	1090	1.25	729940	4287735
Survey	JR17	Jeremys Run	Jeremys Run	North	1090	15.79	730006	4287855
Survey	JR16	Jeremys Run	Jeremys Run	North	1100	14.62	730416	4288048
Survey	JR06	Jeremys Run	Jeremys Run	North	1140	18.15	729689	4287892
Survey	JR11	Jeremys Run	Jeremys Run	North	1180	12.95	730933	4288242
Survey	JR12	Jeremys Run	Jeremys Run	North	1190	1.21	730923	4288103
Survey	JR03	Jeremys Run	Jeremys Run	North	1200	0.28	728445	4288803
Survey	JR87	Jeremys Run	Jeremys Run	North	1320	11.85	731340	4288599
Survey	JR13	Jeremys Run	Jeremys Run	North	1330	0.62	731111	4287677
Survey	JR14	Jeremys Run	Jeremys Run	North	1330	0.35	730998	4287618
Survey	JR86	Jeremys Run	Jeremys Run	North	1390	0.56	731601	4289106
Survey	JR85	Jeremys Run	Jeremys Run	North	1390	10.30	731499	4289169
Survey	JR84	Jeremys Run	Jeremys Run	North	1450	9.41	731584	4289739
Survey	JR83	Jeremys Run	Jeremys Run	North	1570	8.11	731747	4290336
Survey	JR19	Jeremys Run	Jeremys Run	North	1580	0.44	729958	4287180
Survey	JR20	Jeremys Run	Jeremys Run	North	1590	0.41	730013	4287240
Survey	JR82	Jeremys Run	Jeremys Run	North	1670	7.12	731959	4290909
Survey	JR81	Jeremys Run	Jeremys Run	North	1730	6.01	732211	4291562
Survey	JR80	Jeremys Run	Jeremys Run	North	1820	5.56	732537	4292084
Survey	JR77	Jeremys Run	Jeremys Run	North	1880	3.26	733044	4292058
Survey	JR79	Jeremys Run	Jeremys Run	North	1900	1.43	733083	4291965
Survey	JR78	Jeremys Run	Jeremys Run	North	2040	2.69	733638	4292288
Survey	JR76	Jeremys Run	Jeremys Run	North	2310	1.96	733910	4292996
Survey	JR75	Jeremys Run	Jeremys Run	North	2540	1.03	734505	4293257

Table D-1. Continued.

Frequency[1]	Site ID[2]	Stream	Watershed	District	Elev[3]	Area[4]	UTM EW	UTM NS
Survey	WN02	Lands Run	Lands Run	North	1120	3.55	742616	4300590
Quarterly	**VT61**	North Fork Thornton River	North Fork Thornton River	North	1100	19.08	736982	4286022
Survey	TH02	North Fork Thornton River	North Fork Thornton River	North	1140	18.72	736798	4286102
Survey	TH03	North Fork Thornton River	North Fork Thornton River	North	1150	18.57	736617	4286191
Survey	TH04	North Fork Thornton River	North Fork Thornton River	North	1180	17.89	736246	4286419
Survey	TH11	North Fork Thornton River	North Fork Thornton River	North	1190	12.50	736061	4286517
Survey	TH05	North Fork Thornton River	North Fork Thornton River	North	1190	5.26	736127	4286431
Survey	TH12	North Fork Thornton River	North Fork Thornton River	North	1260	11.93	735680	4286949
Survey	TH07	North Fork Thornton River	North Fork Thornton River	North	1350	2.34	735060	4286197
Survey	TH30	North Fork Thornton River	North Fork Thornton River	North	1360	0.85	735150	4287712
Survey	TH06	North Fork Thornton River	North Fork Thornton River	North	1370	4.50	735270	4286242
Survey	TH27	North Fork Thornton River	North Fork Thornton River	North	1400	7.68	734636	4287811
Survey	TH09	North Fork Thornton River	North Fork Thornton River	North	1410	1.84	735146	4286107
Survey	TH29	North Fork Thornton River	North Fork Thornton River	North	1420	9.13	734694	4287682
Survey	TH28	North Fork Thornton River	North Fork Thornton River	North	1440	1.41	734584	4287714
Survey	TH10	North Fork Thornton River	North Fork Thornton River	North	1450	1.16	735020	4285648
Survey	TH08	North Fork Thornton River	North Fork Thornton River	North	1480	1.18	734312	4286383
Survey	TH24	North Fork Thornton River	North Fork Thornton River	North	1620	6.39	733955	4288486
Survey	TH25	North Fork Thornton River	North Fork Thornton River	North	1640	2.81	733790	4288491
Survey	TH23	North Fork Thornton River	North Fork Thornton River	North	1650	3.50	733869	4288594
Survey	TH26	North Fork Thornton River	North Fork Thornton River	North	1840	1.35	733074	4288212
Survey	TH22	North Fork Thornton River	North Fork Thornton River	North	1880	2.76	733642	4289402
Survey	TH21	North Fork Thornton River	North Fork Thornton River	North	1960	1.39	733649	4289752
Survey	TH20	North Fork Thornton River	North Fork Thornton River	North	1970	0.89	733581	4289740
Survey	WN01	Overall Run	Overall Run	North	690	10.41	731320	4297461
Quarterly	VT60	Piney River	Piney River	North	1140	12.59	737939	4286960
Weekly	**PINE**	Piney River	Piney River	North	1180	12.44	737523	4287155
Survey	PI03	Piney River	Piney River	North	1240	12.15	737501	4287198
Survey	PI02	Piney River	Piney River	North	1250	0.94	737350	4287363
Survey	PI04	Piney River	Piney River	North	1260	10.85	737109	4287446

Table D-1. Continued.

Frequency[1]	Site ID[2]	Stream	Watershed	District	Elev[3]	Area[4]	UTM EW	UTM NS
Survey	PI04	Piney River	Piney River	North	1260	10.85	737109	4287446
Survey	PI05	Piney River	Piney River	North	1320	9.86	736905	4287866
Survey	PI06	Piney River	Piney River	North	1420	8.68	736475	4288516
Survey	PI07	Piney River	Piney River	North	1540	7.44	736356	4289152
Survey	PI08	Piney River	Piney River	North	1620	6.46	735827	4289718
Survey	PI09	Piney River	Piney River	North	2180	3.62	735621	4291028
Survey	PI29	Piney River	Piney River	North	2280	0.40	735654	4291207
Survey	PI28	Piney River	Piney River	North	2520	2.99	735745	4291210
Survey	PI27	Piney River	Piney River	North	2520	2.16	736179	4291759
Survey	PI26	Piney River	Piney River	North	2550	1.41	736283	4291947
Survey	PI25	Piney River	Piney River	North	2780	0.68	736315	4291825
Survey	PI24	Piney River	Piney River	North	2800	0.42	736859	4292186
Survey	PI22	Piney River	Piney River	North	2800	0.67	736420	4292770
Survey	PI23	Piney River	Piney River	North	3000	0.23	736981	4292818
Survey	PI21	Piney River	Piney River	North	3140	0.08	736265	4293219
Survey	PI20	Piney River	Piney River	North	3230	0.08	736972	4293318
Survey	RA09	Rush River	Rush River	North	1280	2.14	740701	4292313
Survey	MA10	Berry Hollow	Berry Hollow	Central	1440	1.40	731636	4269703
Survey	PG09	Big Creek	Big Creek	Central	1740	3.51	719494	4259953
Survey	RA02	Bolton Branch	Bolton Branch	Central	1090	4.36	747377	4298770
Survey	RA07	Broad Hollow	Broad Hollow	Central	1180	2.35	737300	4275098
Quarterly	**VT58**	Brokenback Run	Brokenback Run	Central	1080	9.86	735102	4272372
Survey	MA04	Brokenback Run	Brokenback Run	Central	1080	9.84	735181	4272388
Survey	BB01	Brokenback Run	Brokenback Run	Central	1100	9.86	734833	4272338
Survey	BB02	Brokenback Run	Brokenback Run	Central	1160	0.78	734628	4272252
Survey	BB03	Brokenback Run	Brokenback Run	Central	1160	8.92	734645	4272393
Survey	BB04	Brokenback Run	Brokenback Run	Central	1320	8.14	734055	4272323
Survey	BB05	Brokenback Run	Brokenback Run	Central	1370	7.87	733852	4272058

Table D-1. Continued.

Frequency[1]	Site ID[2]	Stream	Watershed	District	Elev[3]	Area[4]	UTM EW	UTM NS
Survey	BB07	Brokenback Run	Brokenback Run	Central	1440	4.88	733706	4271972
Survey	BB06	Brokenback Run	Brokenback Run	Central	1490	2.42	733724	4271893
Survey	BB08	Brokenback Run	Brokenback Run	Central	1780	4.07	732999	4272433
Survey	BB09	Brokenback Run	Brokenback Run	Central	2050	2.98	732356	4272805
Survey	BB10	Brokenback Run	Brokenback Run	Central	2440	2.06	731575	4272989
Survey	BB11	Brokenback Run	Brokenback Run	Central	2680	1.09	730965	4272920
Survey	MA07	Cedar Run	Cedar Run	Central	1400	5.43	730203	4268452
Survey	GR03	Devils Ditch	Conway River	Central	1460	5.88	723745	4256431
Survey	GR05	Pocosin Hollow	Conway River	Central	1520	7.38	723527	4253556
Survey	GR02	Bootens Run	Conway River	Central	1720	2.07	723729	4258194
Survey	GR04	Bush Mountain Stream	Conway River	Central	1720	2.49	723630	4258088
Survey	GR01	Conway River (Upper Reach)	Conway River	Central	1940	5.09	723748	4258986
Survey	PG08	East Branch of Naked Creek	East Branch of Naked Creek	Central	1780	9.10	719673	4261628
Survey	PG05	Fultz Run	Fultz Run	Central	1170	5.89	712824	4264047
Survey	MA05	Hannah Run	Hannah Run	Central	1260	7.49	733964	4274404
Quarterly	**VT62**	Hazel River	Hazel River	Central	1080	13.24	738348	4277397
Survey	RA05	Hazel River	Hazel River	Central	1120	11.27	738171	4277525
Survey	HR20	Hazel River	Hazel River	Central	1140	11.05	738064	4277672
Survey	HR02	Hazel River	Hazel River	Central	1160	1.73	738074	4277421
Survey	HR21	Hazel River	Hazel River	Central	1280	10.48	737916	4278205
Survey	HR22	Hazel River	Hazel River	Central	1380	9.99	737671	4278559
Survey	HR23	Hazel River	Hazel River	Central	1450	9.25	737399	4279011
Survey	HR24	Hazel River	Hazel River	Central	1490	0.59	737314	4279098
Survey	HR25	Hazel River	Hazel River	Central	1500	8.55	737411	4279217
Survey	HR26	Hazel River	Hazel River	Central	1575	8.27	737013	4279571
Survey	HR03	Hazel River	Hazel River	Central	1700	1.34	737265	4277194
Survey	HR27	Hazel River	Hazel River	Central	1800	7.90	736410	4279484
Survey	HR28	Hazel River	Hazel River	Central	1830	3.15	736302	4279480

Table D-1. Continued.

Frequency[1]	Site ID[2]	Stream	Watershed	District	Elev[3]	Area[4]	UTM EW	UTM NS
Survey	HR29	Hazel River	Hazel River	Central	1880	4.67	736348	4279381
Survey	HR30	Hazel River	Hazel River	Central	2000	4.37	736035	4278852
Survey	HR04	Hazel River	Hazel River	Central	2000	0.78	736982	4277392
Survey	HR33	Hazel River	Hazel River	Central	2090	3.03	735780	4279449
Survey	HR07	Hazel River	Hazel River	Central	2180	1.37	735401	4278333
Survey	HR10	Hazel River	Hazel River	Central	2180	2.28	735337	4278475
Survey	HR08	Hazel River	Hazel River	Central	2200	2.20	735245	4278432
Survey	HR32	Hazel River	Hazel River	Central	2200	2.66	735460	4278992
Survey	HR09	Hazel River	Hazel River	Central	2210	1.96	734988	4278270
Survey	HR05	Hazel River	Hazel River	Central	2220	0.65	736819	4277649
Survey	HR31	Hazel River	Hazel River	Central	2300	1.92	734722	4279046
Survey	HR06	Hazel River	Hazel River	Central	2330	0.84	735581	4277775
Survey	HR11	Hazel River	Hazel River	Central	2440	1.25	734136	4279199
Survey	MA06	Hughes Run	Hughes Run	Central	1240	13.76	733901	4274400
Survey	GR08	Ivy Creek	Ivy Creek	Central	1300	7.02	707154	4239119
Survey	MA14	Kinsey Run	Kinsey Run	Central	1560	2.56	727326	4256535
Survey	MA02	Negro Run	Negro Run	Central	1500	3.43	730718	4270608
Weekly	**NFDR**	North Fork Dry Run	North Fork Dry Run	Central	1600	2.31	729933	4279183
Survey	NF01	North Fork Dry Run	North Fork Dry Run	Central	1620	2.17	729897	4279070
Survey	NF02	North Fork Dry Run	North Fork Dry Run	Central	1700	1.70	729933	4278796
Survey	NF03	North Fork Dry Run	North Fork Dry Run	Central	1820	1.41	730081	4278473
Survey	NF04	North Fork Dry Run	North Fork Dry Run	Central	1920	1.24	730195	4278299
Survey	NF05	North Fork Dry Run	North Fork Dry Run	Central	2180	1.01	730387	4278006
Survey	NF06	North Fork Dry Run	North Fork Dry Run	Central	2220	0.99	730433	4277961
Survey	NF07	North Fork Dry Run	North Fork Dry Run	Central	2260	0.44	730435	4277873
Survey	NF09	North Fork Dry Run	North Fork Dry Run	Central	2290	0.18	730521	4277866
Survey	NF10	North Fork Dry Run	North Fork Dry Run	Central	2340	0.16	730595	4277830
Survey	NF08	North Fork Dry Run	North Fork Dry Run	Central	2500	0.37	730310	4277639

Table D-1. Continued.

Frequency[1]	Site ID[2]	Stream	Watershed	District	Elev[3]	Area[4]	UTM EW	UTM NS
Survey	MA03	Ragged Run	Ragged Run	Central	1120	3.04	735507	4268139
Survey	MA16	Rapidan River	Rapidan River	Central	970	25.26	729559	4258134
Survey	MA13	Laurel Prong	Rapidan River	Central	2500	5.37	724901	4263174
Survey	MA12	Mill Prong	Rapidan River	Central	2540	4.34	724908	4263397
Quarterly	**VT66**	Rose River	Rose River	Central	1120	23.73	729550	4266066
Survey	RR01	Rose River	Rose River	Central	1120	23.74	729549	4266069
Survey	RR30	Rose River	Rose River	Central	1280	20.57	728812	4265696
Survey	RR21	Rose River	Rose River	Central	1360	18.80	728204	4265611
Survey	RR19	Rose River	Rose River	Central	1400	4.06	727835	4265518
Survey	RR07	Rose River	Rose River	Central	1560	13.34	727455	4266147
Survey	RR16	Rose River	Rose River	Central	1660	3.32	727219	4265193
Survey	RR06	Rose River	Rose River	Central	1830	10.87	726693	4266716
Survey	RR17	Rose River	Rose River	Central	1900	1.15	726529	4264792
Survey	RR05	Rose River	Rose River	Central	2120	9.90	726085	4267073
Survey	RR04	Rose River	Rose River	Central	2180	4.38	725928	4267399
Survey	RR03	Rose River	Rose River	Central	2180	3.34	725793	4267829
Survey	RR18	Rose River	Rose River	Central	2210	0.40	727007	4264842
Survey	RR15	Rose River	Rose River	Central	2520	4.09	725654	4267202
Survey	RR14	Rose River	Rose River	Central	2540	3.19	725070	4266824
Survey	RR02	Rose River	Rose River	Central	2580	2.70	725841	4268376
Survey	RR11	Rose River	Rose River	Central	2870	2.24	724642	4266442
Survey	RR13	Rose River	Rose River	Central	3160	0.73	724407	4266157
Survey	RR12	Rose River	Rose River	Central	3220	0.91	724424	4266299
Survey	RA06	Sams Run	Sams Run	Central	1160	1.89	738136	4277455
Survey	GR07	South River	South River	Central	1760	4.81	718798	4250506
Quarterly	VT59	Staunton River	Staunton River	Central	1010	10.50	729380	4258243
Weekly	**STAN**	Staunton River	Staunton River	Central	1010	10.50	729396	4258233
Survey	SR01	Staunton River	Staunton River	Central	1030	10.50	729380	4258243

Table D-1. Continued.

Frequency[1]	Site ID[2]	Stream	Watershed	District	Elev[3]	Area[4]	UTM EW	UTM NS
Survey	SR02	Staunton River	Staunton River	Central	1320	10.15	729072	4258302
Survey	SR03	Staunton River	Staunton River	Central	1340	8.34	728978	4258370
Survey	SR06	Staunton River	Staunton River	Central	1340	0.35	728486	4258305
Survey	SR04	Staunton River	Staunton River	Central	1350	1.75	728961	4258294
Survey	SR18	Staunton River	Staunton River	Central	1360	0.06	728617	4258725
Survey	SR07	Staunton River	Staunton River	Central	1420	7.50	728723	4259103
Survey	SR08	Staunton River	Staunton River	Central	1550	6.75	728390	4259560
Survey	SR05	Staunton River	Staunton River	Central	1620	0.73	728177	4258043
Survey	SR09	Staunton River	Staunton River	Central	1900	0.19	727672	4259808
Survey	SR11	Staunton River	Staunton River	Central	2140	1.00	726808	4259595
Survey	SR13	Staunton River	Staunton River	Central	2200	0.40	726718	4259562
Survey	SR14	Staunton River	Staunton River	Central	2220	3.37	726711	4259652
Survey	SR15	Staunton River	Staunton River	Central	2380	2.50	726028	4260028
Survey	SR16	Staunton River	Staunton River	Central	2510	0.25	725878	4260102
Survey	SR17	Staunton River	Staunton River	Central	2870	1.21	725257	4260562
Survey	MA17	Whiteoak Canyon (Robinson River)	Whiteoak Canyon (Robinson River)	Central	1120	14.10	730986	4268888
Quarterly	**VT75**	Whiteoak Canyon (Robinson River)	Whiteoak Canyon (Robinson River)	Central	1160	14.08	730905	4268968
Survey	WO02	Whiteoak Canyon (Robinson River)	Whiteoak Canyon (Robinson River)	Central	1280	12.00	730614	4269771
Survey	WO04	Whiteoak Canyon (Robinson River)	Whiteoak Canyon (Robinson River)	Central	1450	11.23	730730	4270476
Survey	WO05	Whiteoak Canyon (Robinson River)	Whiteoak Canyon (Robinson River)	Central	1485	3.33	730715	4270617
Survey	WO03	Whiteoak Canyon (Robinson River)	Whiteoak Canyon (Robinson River)	Central	1490	7.87	730654	4270569
Survey	MA01	Whiteoak Canyon (Robinson River)	Whiteoak Canyon (Robinson River)	Central	1540	7.85	730643	4270577
Survey	WO06	Whiteoak Canyon (Robinson River)	Whiteoak Canyon (Robinson River)	Central	2060	2.87	730837	4271345
Survey	WO20	Whiteoak Canyon (Robinson River)	Whiteoak Canyon (Robinson River)	Central	2260	6.89	730045	4271107
Survey	WO07	Whiteoak Canyon (Robinson River)	Whiteoak Canyon (Robinson River)	Central	2420	1.39	730646	4272174
Survey	WO21	Whiteoak Canyon (Robinson River)	Whiteoak Canyon (Robinson River)	Central	2700	4.45	729523	4271694
Survey	WO22	Whiteoak Canyon (Robinson River)	Whiteoak Canyon (Robinson River)	Central	2920	3.83	729219	4272304
Survey	WO23	Whiteoak Canyon (Robinson River)	Whiteoak Canyon (Robinson River)	Central	3080	3.49	729031	4272765

Table D-1. Continued.

Frequency[1]	Site ID[2]	Stream	Watershed	District	Elev[3]	Area[4]	UTM EW	UTM NS
Survey	WO25	Whiteoak Canyon (Robinson River)	Whiteoak Canyon (Robinson River)	Central	3110	2.35	728973	4272917
Survey	WO24	Whiteoak Canyon (Robinson River)	Whiteoak Canyon (Robinson River)	Central	3130	0.89	728917	4272823
Survey	WO26	Whiteoak Canyon (Robinson River)	Whiteoak Canyon (Robinson River)	Central	3160	2.13	728941	4273082
Survey	WO28	Whiteoak Canyon (Robinson River)	Whiteoak Canyon (Robinson River)	Central	3200	2.02	728788	4273217
Survey	WO27	Whiteoak Canyon (Robinson River)	Whiteoak Canyon (Robinson River)	Central	3240	1.11	728816	4273323
Survey	WO30	Whiteoak Canyon (Robinson River)	Whiteoak Canyon (Robinson River)	Central	3260	0.55	728582	4273306
Survey	WO29	Whiteoak Canyon (Robinson River)	Whiteoak Canyon (Robinson River)	Central	3295	0.29	728581	4273226
Survey	RH51	Bearwallow Run	Bearwallow Run	South	1300	2.55	702490	4243656
Survey	RH48	Big Run (Lower Reach)	Big Run	South	1220	28.05	700744	4242055
Survey	RH50	Rocky Mountain Run	Big Run	South	1340	8.34	701415	4239995
Survey	RH49	Big Run (Upper Reach)	Big Run	South	1340	14.92	701398	4239982
Weekly	**DR01**	Deep Run	Deep Run	South	1360	3.12	695591	4238919
Survey	AB06	Doyle River	Doyle River	South	1460	5.45	701825	4233751
Survey	AB07	Jones Run	Jones Run	South	1460	4.55	701746	4233666
Survey	RH47	Lower Lewis Run	Lower Lewis Run	South	1340	2.90	698203	4241434
Quarterly	**MAD2**	Madison Run	Madison Run	South	1460	5.15	697162	4235896
Survey	AU02	Meadow Run	Meadow Run	South	1480	8.95	691714	4225474
Quarterly	**VT36**	Meadow Run	Meadow Run	South	1480	8.86	691758	4225462
Survey	MR01	Meadow Run	Meadow Run	South	1510	8.86	691759	4225463
Survey	MR17	Meadow Run	Meadow Run	South	1600	8.11	692900	4225947
Survey	MR11	Meadow Run	Meadow Run	South	1640	6.67	692958	4226043
Survey	MR12	Meadow Run	Meadow Run	South	1640	1.41	692985	4225926
Survey	MR10	Meadow Run	Meadow Run	South	1700	1.29	693172	4226210
Survey	MR09	Meadow Run	Meadow Run	South	1700	5.23	693129	4226294
Survey	MR16	Meadow Run	Meadow Run	South	1800	1.00	693516	4225613
Survey	MR18	Meadow Run	Meadow Run	South	1880	8.51	692496	4225694
Survey	MR08	Meadow Run	Meadow Run	South	1920	4.49	693404	4227008
Survey	MR13	Meadow Run	Meadow Run	South	1950	1.03	693694	4225991

Table D-1. Continued.

Frequency[1]	Site ID[2]	Stream	Watershed	District	Elev[3]	Area[4]	UTM EW	UTM NS
Survey	MR06	Meadow Run	Meadow Run	South	1960	3.12	693512	4227017
Survey	MR07	Meadow Run	Meadow Run	South	1960	1.24	693499	4227164
Survey	MR15	Meadow Run	Meadow Run	South	2050	0.51	694098	4225637
Survey	MR05	Meadow Run	Meadow Run	South	2060	2.66	694267	4227050
Survey	MR14	Meadow Run	Meadow Run	South	2150	0.64	694272	4225993
Survey	MR04	Meadow Run	Meadow Run	South	2160	1.90	694718	4227333
Survey	MR02	Meadow Run	Meadow Run	South	2175	1.27	694814	4227429
Survey	MR03	Meadow Run	Meadow Run	South	2175	0.50	694810	4227321
Survey	AB09	Pond Ridge Branch of Mormans River	Mormans River	South	1040	2.96	697017	4223567
Survey	AB01	NF of Mormans River(lower Reach)	Mormans River	South	1040	26.09	697129	4223849
Survey	AB08	South Fork of Mormans River	Mormans River	South	1100	12.59	696615	4222643
Survey	AB05	Big Branch of Mormans River	Mormans River	South	1460	3.64	697493	4226388
Survey	AB04	NF Mormans River (Upper Reach)	Mormans River	South	1820	6.59	698839	4230351
Survey	AB02	NF Mormans River (Blackrock Gap)	Mormans River	South	1880	2.10	697976	4229654
Survey	RH52	Onemile Run	Onemile Run	South	1380	4.26	702654	4243570
Weekly	**PAIN**	Paine Run	Paine Run	South	1390	12.39	693243	4229927
Survey	PR02	Paine Run	Paine Run	South	1400	12.28	693534	4229863
Survey	PR03	Paine Run	Paine Run	South	1440	10.34	693589	4229817
Survey	PR06	Paine Run	Paine Run	South	1440	9.28	693708	4229596
Survey	PR04	Paine Run	Paine Run	South	1440	10.27	693632	4229707
Survey	PR07	Paine Run	Paine Run	South	1480	9.09	694059	4229494
Survey	PR08	Paine Run	Paine Run	South	1480	8.24	694162	4229461
Survey	PR05	Paine Run	Paine Run	South	1480	0.95	693606	4229610
Survey	PR12	Paine Run	Paine Run	South	1510	7.43	694640	4229680
Survey	PR11	Paine Run	Paine Run	South	1510	7.75	694538	4229631
Survey	PR09	Paine Run	Paine Run	South	1520	0.68	694079	4229369
Survey	PR15	Paine Run	Paine Run	South	1540	7.18	694958	4229830
Survey	PR16	Paine Run	Paine Run	South	1550	6.21	695057	4229840

Table D-1. Continued.

Frequency[1]	Site ID[2]	Stream	Watershed	District	Elev[3]	Area[4]	UTM EW	UTM NS
Survey	PR10	Paine Run	Paine Run	South	1560	0.18	694428	4229467
Survey	PR38	Paine Run	Paine Run	South	1560	0.88	694434	4230709
Survey	PR19	Paine Run	Paine Run	South	1580	5.80	695385	4229812
Survey	PR24	Paine Run	Paine Run	South	1580	4.08	695499	4229980
Survey	PR18	Paine Run	Paine Run	South	1600	0.91	695041	4230005
Survey	PR13	Paine Run	Paine Run	South	1600	0.25	694670	4229513
Survey	PR21	Paine Run	Paine Run	South	1600	1.15	695509	4229769
Survey	PR25	Paine Run	Paine Run	South	1640	0.44	695683	4229919
Survey	PR14	Paine Run	Paine Run	South	1640	0.24	695201	4229650
Survey	PR27	Paine Run	Paine Run	South	1670	1.88	695935	4230481
Survey	PR28	Paine Run	Paine Run	South	1720	0.28	696003	4230359
Survey	PR17	Paine Run	Paine Run	South	1720	0.55	695055	4230622
Survey	PR29	Paine Run	Paine Run	South	1720	2.52	696385	4230964
Survey	PR30	Paine Run	Paine Run	South	1750	1.96	696494	4231005
Survey	PR20	Paine Run	Paine Run	South	1780	0.50	695799	4229190
Survey	PR32	Paine Run	Paine Run	South	1840	1.67	696790	4231262
Survey	PR31	Paine Run	Paine Run	South	1840	0.52	696388	4231118
Survey	PR26	Paine Run	Paine Run	South	1860	3.78	695846	4230375
Survey	PR33	Paine Run	Paine Run	South	1925	1.31	696900	4231761
Survey	PR36	Paine Run	Paine Run	South	1970	0.06	696763	4231066
Survey	PR34	Paine Run	Paine Run	South	2000	0.36	696839	4231855
Survey	PR35	Paine Run	Paine Run	South	2000	0.87	696956	4231867
Survey	AU12	Sawmill Run	Sawmill Run	South	1520	6.18	604510	4217237
Quarterly	**VT53**	Twomile Run	Twomile Run	South	1220	5.56	703527	4245225
Survey	TM12	Twomile Run	Twomile Run	South	1270	5.03	703899	4244635
Survey	TM10	Twomile Run	Twomile Run	South	1340	3.58	704438	4244174
Survey	TM09	Twomile Run	Twomile Run	South	1425	0.79	704444	4244360
Survey	TM07	Twomile Run	Twomile Run	South	1440	3.09	704677	4243829

Table D-1. Continued.

Frequency[1]	Site ID[2]	Stream	Watershed	District	Elev[3]	Area[4]	UTM EW	UTM NS
Survey	TM05	Twomile Run	Twomile Run	South	1520	2.23	705206	4243527
Survey	TM04	Twomile Run	Twomile Run	South	1660	1.45	705478	4242795
Survey	TM03	Twomile Run	Twomile Run	South	1680	0.80	705485	4242630
Survey	TM02	Twomile Run	Twomile Run	South	1680	0.59	705577	4242654
Weekly	**WOR1**	White Oak Run	White Oak Run	South	1480	5.13	696960	4235772
Survey	WR02	White Oak Run	White Oak Run	South	1520	4.71	697296	4235290
Survey	WR03	White Oak Run	White Oak Run	South	1540	4.56	697390	4235185
Weekly	LUCK	White Oak Run	White Oak Run	South	1560	1.96	697418	4234929
Weekly	WOR3	White Oak Run	White Oak Run	South	1560	2.43	697496	4234955
Survey	WR04	White Oak Run	White Oak Run	South	1580	4.48	697458	4235023
Survey	WR06	White Oak Run	White Oak Run	South	1580	2.43	697470	4234973
Survey	WR07	White Oak Run	White Oak Run	South	1620	2.30	697688	4234790
Survey	WR08	White Oak Run	White Oak Run	South	1690	1.99	697746	4234407
Survey	WR09	White Oak Run	White Oak Run	South	1840	1.16	698100	4233971
Survey	WR10	White Oak Run	White Oak Run	South	1840	1.66	698052	4234108

[1] FREQUENCY = Sampling frequency: Weekly (may include higher frequency episode sampling), Quarterly (January, April, July, October), or Survey (occasional).
[2] Bold indicates primary site
[3] Elev = Feet above MSL for sampling site. Based on 1:24,000-scale USGS topographic maps.
[4] Area = Watershed area (km^2). Based on 1:24,000-scale USGS topographic maps.

Table D-2. Geological and chemical information for streams surveyed in SHEN.

Site ID [a]	GEO[b]	Silic.[c]	Gran.[d]	Basa.[e]	Min Date[f]	Max Date[g]	Cold ANC[h]	Cold n[i]	Warm ANC[j]	Warm n[k]
VT51	A	31.00	0.00	68.97	4/25/87	7/31/01	143.3	30	295.2	29
JR04	A	28.80	0.00	71.20	3/20/92	3/20/92	114.5	1		
JR02	A	90.60	0.00	9.40	3/20/92	3/20/92	16.2	1		
JR05	A	28.20	0.00	71.80	3/20/92	3/20/92	111.2	1		
JR15	A	50.00	0.00	50.00	3/20/92	3/20/92	101.9	1		
JR18	A	57.10	0.00	42.90	3/20/92	3/20/92	22.8	1		
JR17	A	18.40	0.00	81.60	3/20/92	3/20/92	121.2	1		
JR16	A	17.50	0.00	82.50	3/20/92	3/20/92	120.0	1		
JR06	A	24.40	0.00	75.60	3/20/92	3/20/92	112.0	1		
JR11	A	16.00	0.00	84.00	3/20/92	3/20/92	126.7	1		
JR12	A	39.10	0.00	60.90	3/20/92	3/20/92	41.1	1		
JR03	A	100.00	0.00	0.00	3/20/92	3/20/92	12.8	1		
JR87	A	15.70	0.00	84.30	3/20/92	3/20/92	129.4	1		
JR13	A	54.20	0.00	45.80	3/20/92	3/20/92	29.5	1		
JR14	A	38.50	0.00	61.50	3/20/92	3/20/92	31.2	1		
JR86	A	52.40	0.00	47.60	3/20/92	3/20/92	38.7	1		
JR85	A	13.40	0.00	86.60	3/20/92	3/20/92	134.5	1		
JR84	A	12.70	0.00	87.30	3/20/92	3/20/92	134.5	1		
JR83	A	9.30	0.00	90.70	3/20/92	3/20/92	138.7	1		
JR19	A	94.10	0.00	5.90	3/20/92	3/20/92	8.7	1		
JR20	A	60.00	0.00	40.00	3/20/92	3/20/92	12.8	1		
JR82	A	6.20	0.00	93.80	3/20/92	3/20/92	136.1	1		
JR81	A	1.30	0.00	98.70	3/20/92	3/20/92	146.1	1		
JR80	A	0.50	0.00	99.50	3/20/92	3/20/92	146.7	1		
JR77	A	0.00	0.00	100.00	3/20/92	3/20/92	165.4	1		
JR79	A	0.00	0.00	100.00	3/20/92	3/20/92	131.2	1		
JR78	A	0.00	0.00	100.00	3/20/92	3/20/92	176.9	1		
JR76	A	0.00	0.00	100.00	3/20/92	3/20/92	226.7	1		
JR75	A	0.00	0.00	100.00	3/20/92	3/20/92	220.4	1		
WN02	B	0.00	87.35	9.75	4/26/87	4/24/00	154.1	2		
VT61	A	5.18	27.02	67.79	4/26/87	7/30/01	219.8	30	354.3	28
TH02	A	5.30	26.30	68.50	3/16/92	3/16/92	174.4	1		
TH03	A	5.30	25.70	69.00	3/16/92	3/16/92	174.4	1		
TH04	A	5.50	23.20	71.30	3/16/92	3/16/92	169.4	1		
TH11	A	7.90	10.80	81.40	3/16/92	3/16/92	188.6	1		
TH05	A	0.00	50.70	49.30	3/16/92	3/16/92	141.9	1		
TH12	A	8.20	6.50	85.20	3/16/92	3/16/92	185.4	1		
TH07	A	0.00	22.00	78.00	3/16/92	3/16/92	153.6	1		
TH30	A	0.00	0.00	100.00	3/16/92	3/16/92	186.1	1		
TH06	A	0.00	42.20	57.80	3/16/92	3/16/92	136.1	1		
TH27	A	12.80	0.00	87.20	3/16/92	3/16/92	158.5	1		
TH09	A	0.00	59.20	40.80	3/16/92	3/16/92	106.9	1		
TH29	A	10.80	0.00	89.20	3/16/92	3/16/92	165.5	1		
TH28	A	0.00	0.00	100.00	3/16/92	3/16/92	155.4	1		

Table D-2. Continued.

Site ID [a]	GEO[b]	Silic.[c]	Gran.[d]	Basa.[e]	Min Date[f]	Max Date[g]	Cold ANC[h]	Cold n[i]	Warm ANC[j]	Warm n[k]
TH10	A	0.00	68.90	31.10	3/16/92	3/16/92	105.3	1		
TH08	A	0.00	0.00	100.00	3/16/92	3/16/92	181.1	1		
TH24	A	15.40	0.00	84.60	3/16/92	3/16/92	166.9	1		
TH25	A	23.10	0.00	76.90	3/16/92	3/16/92	154.2	1		
TH23	A	8.90	0.00	91.10	3/16/92	3/16/92	166.1	1		
TH26	A	33.30	0.00	66.70	3/16/92	3/16/92	80.4	1		
TH22	A	8.50	0.00	91.50	3/16/92	3/16/92	93.7	1		
TH21	A	0.00	0.00	100.00	3/16/92	3/16/92	142.9	1		
TH20	A	26.50	0.00	73.50	3/16/92	3/16/92	61.9	1		
WN01	B	15.07	16.80	68.13	4/26/87	4/24/00	263.5	2		
VT60	B	0.00	41.29	58.71	4/26/87	4/27/00	163.6	19	292.3	16
PINE	A	0.00	31.27	68.73	9/1/92	9/26/01	166.4	504	245.9	530
PI03	A	0.00	29.90	70.10	3/17/92	6/7/95	158.1	3	285.8	4
PI02	A	0.00	100.00	0.00	3/17/92	6/7/95	132.2	3	202.2	3
PI04	A	0.00	21.50	78.50	3/17/92	6/7/95	157.9	3	293.4	4
PI05	A	0.00	17.60	82.40	3/17/92	6/7/95	156.6	3	272.7	3
PI06	A	0.00	12.50	87.50	3/17/92	6/7/95	134.8	3	259.2	4
PI07	A	0.00	14.60	85.40	3/17/92	6/7/95	125.8	3	245.6	4
PI08	A	0.00	16.90	83.10	3/17/92	6/7/95	122.4	3	228.3	4
PI09	A	0.00	30.00	70.00	3/17/92	6/7/95	102.9	3	184.2	4
PI29	A	0.00	0.00	100.00	3/17/92	6/7/95	151.4	3	281.6	3
PI28	A	0.00	36.50	63.50	3/17/92	6/7/95	88.6	3	151.0	4
PI27	A	0.00	50.60	49.40	3/17/92	6/7/95	64.7	3	118.3	4
PI26	A	0.00	50.90	49.10	3/17/92	6/7/95	61.2	3	106.1	4
PI25	A	0.00	53.80	46.20	3/17/92	6/7/95	92.8	3	127.3	3
PI24	A	0.00	82.40	17.60	3/17/92	10/28/94	31.4	3	81.9	2
PI22	A	0.00	96.20	3.80	3/17/92	6/7/95	27.9	3	63.1	4
PI23	A	0.00	100.00	0.00	3/17/92	10/28/94	33.1	3	57.8	2
PI21	A	0.00	100.00	0.00	3/17/92	6/7/95	45.5	3	57.5	1
PI20	A	0.00	100.00	0.00	3/17/92	6/7/95	46.1	3	46.0	4
RA09	B	0.00	0.00	100.00	4/25/87	4/27/00	185.0	2		
MA10	B	0.00	100.00	0.00	4/25/87	4/24/00	40.0	2		
PG09	B	24.32	0.01	75.67	4/25/87	4/26/00	121.4	2		
RA02	B	0.00	86.09	7.83	4/25/87	4/26/00	107.9	2		
RA07	B	0.00	100.00	0.00	4/26/87	4/29/00	49.3	2		
VT58	A	0.00	93.41	6.59	8/12/87	7/31/01	67.3	29	110.0	29
MA04	B	0.00	94.24	5.76	4/26/87	4/29/00	51.6	2		
BB01	A	0.00	93.40	6.60	3/18/92	10/10/94	55.3	3	113.4	3
BB02	A	0.00	100.00	0.00	3/18/92	10/10/94	40.3	2	75.0	3
BB03	A	0.00	92.70	7.30	3/18/92	10/10/94	56.3	2	115.6	3
BB04	A	0.00	92.00	8.00	3/18/92	10/10/94	51.2	2	105.5	3
BB05	A	0.00	91.80	8.20	3/18/92	10/10/94	52.8	2	104.9	3

Table D-2. Continued.

Site ID [a]	GEO[b]	Silic.[c]	Gran.[d]	Basa.[e]	Min Date[f]	Max Date[g]	Cold ANC[h]	Cold n[i]	Warm ANC[j]	Warm n[k]
BB07	A	0.00	86.70	13.30	3/18/92	10/10/94	51.1	2	99.3	3
BB06	A	0.00	100.00	0.00	3/18/92	10/10/94	50.6	2	95.1	3
BB08	A	0.00	84.10	15.90	3/18/92	10/10/94	50.8	2	100.9	3
BB09	A	0.00	78.30	21.70	3/18/92	10/10/94	50.8	2	102.3	3
BB10	A	0.00	68.80	31.30	3/18/92	10/10/94	52.4	2	99.4	3
BB11	A	0.00	45.20	54.80	3/18/92	10/10/94	73.6	2	136.8	3
MA07	B	0.00	0.00	100.00	4/25/87	4/29/00	114.1	2		
GR03	B	0.00	89.96	4.35	4/25/87	4/24/00	53.6	2		
GR05	B	0.00	80.68	19.03	5/2/87	4/24/00	123.9	2		
GR02	B	0.00	100.00	0.00	4/26/87	4/24/00	61.0	2		
GR04	B	0.00	91.75	3.14	4/26/87	4/24/00	48.5	2		
GR01	B	0.00	90.91	9.10	4/26/87	4/24/00	83.2	2		
PG08	B	16.11	0.00	83.89	4/25/87	4/26/00	130.5	2		
PG05	B	79.87	9.00	11.13	4/25/87	4/26/00	30.8	2		
MA05	B	0.00	100.00	0.00	4/26/87	4/29/00	71.0	2		
VT62	A	0.00	100.00	0.00	8/12/87	7/30/01	76.1	28	116.2	29
RA05	B	0.00	100.00	0.00	4/26/87	4/29/00	74.1	2		
HR20	A	0.00	100.00	0.00	3/21/92	3/21/92	72.5	1		
HR02	A	0.00	100.00	0.00	3/21/92	3/21/92	53.3	1		
HR21	A	0.00	100.00	0.00	3/21/92	3/21/92	71.2	1		
HR22	A	0.00	100.00	0.00	3/21/92	3/21/92	68.7	1		
HR23	A	0.00	100.00	0.00	3/21/92	3/21/92	66.9	1		
HR24	A	0.00	100.00	0.00	3/21/92	3/21/92	63.7	1		
HR25	A	0.00	100.00	0.00	3/21/92	3/21/92	67.0	1		
HR26	A	0.00	100.00	0.00	3/21/92	3/21/92	64.4	1		
HR03	A	0.00	100.00	0.00	3/21/92	3/21/92	46.9	1		
HR27	A	0.00	100.00	0.00	3/21/92	3/21/92	61.9	1		
HR28	A	0.00	100.00	0.00	3/21/92	3/21/92	54.4	1		
HR29	A	0.00	100.00	0.00	3/21/92	3/21/92	66.2	1		
HR30	A	0.00	100.00	0.00	3/21/92	3/21/92	67.0	1		
HR04	A	0.00	100.00	0.00	3/21/92	3/21/92	53.7	1		
HR33	A	0.00	100.00	0.00	3/21/92	3/21/92	58.7	1		
HR07	A	0.00	100.00	0.00	3/21/92	3/21/92	69.5	1		
HR10	A	0.00	100.00	0.00	3/21/92	3/21/92	71.9	1		
HR08	A	0.00	100.00	0.00	3/21/92	3/21/92	66.1	1		
HR32	A	0.00	100.00	0.00	3/21/92	3/21/92	50.4	1		
HR09	A	0.00	100.00	0.00	3/21/92	3/21/92	58.7	1		
HR05	A	0.00	100.00	0.00	3/21/92	3/21/92	56.2	1		
HR31	A	0.00	100.00	0.00	3/21/92	3/21/92	45.4	1		
HR06	A	0.00	100.00	0.00	3/21/92	3/21/92	73.7	1		
HR11	A	0.00	100.00	0.00	3/21/92	3/21/92	43.8	1		
MA06	B	0.00	90.19	9.81	4/26/87	4/29/00	82.7	2		

Table D-2. Continued.

Site ID [a]	GEO[b]	Silic.[c]	Gran.[d]	Basa.[e]	Min Date[f]	Max Date[g]	Cold ANC[h]	Cold n[i]	Warm ANC[j]	Warm n[k]
GR08	B	26.16	0.74	73.11	4/26/87	4/29/00	112.4	2		
MA14	B	0.00	100.00	0.00	4/26/87	4/29/00	82.0	2		
MA02	B	0.00	22.06	77.95	4/25/89	4/24/00	95.3	2		
NFDR	A	0.00	100.00	0.00	3/12/87	9/26/01	50.6	357	82.1	372
NF01	A	0.00	100.00	0.00	7/6/92	10/31/94	40.4	1	85.6	3
NF02	A	0.00	100.00	0.00	7/6/92	10/31/94	32.8	1	77.7	3
NF03	A	0.00	100.00	0.00	7/6/92	10/31/94	28.7	1	62.3	3
NF04	A	0.00	100.00	0.00	7/6/92	10/31/94	26.1	1	56.1	3
NF05	A	0.00	100.00	0.00	7/6/92	10/31/94	26.2	1	49.8	3
NF06	A	0.00	100.00	0.00	7/6/92	10/31/94	23.7	1	40.1	3
NF07	A	0.00	100.00	0.00	7/6/92	10/31/94	16.9	1	26.7	3
NF09	A	0.00	100.00	0.00	7/6/92	4/23/94	33.7	1	69.5	2
NF10	A	0.00	100.00	0.00	7/6/92	4/23/94	30.3	1	53.7	1
NF08	A	0.00	100.00	0.00	7/6/92	10/31/94			25.8	2
MA03	B	0.00	100.00	0.00	4/26/87	4/24/00	61.7	2		
MA16	B	0.00	69.51	30.50	4/26/87	4/26/00	96.6	2		
MA13	B	0.00	56.29	43.71	4/25/87	4/24/00	56.6	2		
MA12	B	0.00	0.00	100.00	4/25/87	4/24/00	108.0	2		
VT66	A	0.00	9.05	90.95	4/25/87	7/31/01	121.1	30	180.7	27
RR01	A	0.00	9.20	90.80	3/14/92	3/14/92	104.5	1		
RR30	A	0.00	7.80	92.20	3/14/92	3/14/92	85.7	1		
RR21	A	0.00	0.00	0.00	3/14/92	3/14/92	93.7	1		
RR19	A	0.00	2.40	97.60	3/14/92	3/14/92	85.4	1		
RR07	A	0.00	8.20	91.80	3/14/92	3/14/92	92.8	1		
RR16	A	0.00	3.10	96.90	3/14/92	3/14/92	86.9	1		
RR06	A	0.00	10.00	90.00	3/14/92	3/14/92	92.0	1		
RR17	A	0.00	0.00	100.00	3/14/92	3/14/92	33.7	1		
RR05	A	0.00	11.00	89.00	3/14/92	3/14/92	96.2	1		
RR04	A	0.00	5.30	94.70	3/14/92	3/14/92	83.7	1		
RR03	A	0.00	7.00	93.00	3/14/92	3/14/92	83.7	1		
RR18	A	0.00	66.70	33.30	3/14/92	3/14/92	98.6	1		
RR15	A	0.00	12.70	87.30	3/14/92	3/14/92	87.8	1		
RR14	A	0.00	4.00	96.00	3/14/92	3/14/92	101.2	1		
RR02	A	0.00	8.70	91.30	3/14/92	3/14/92	77.8	1		
RR11	A	0.00	0.00	100.00	3/14/92	3/14/92	103.7	1		
RR13	A	0.00	0.00	100.00	3/14/92	3/14/92	65.3	1		
RR12	A	0.00	0.00	100.00	3/14/92	3/14/92	164.4	1		
RA06	B	0.00	100.00	0.00	4/26/87	4/29/00	68.8	2		
GR07	B	0.00	0.00	100.00	4/26/87	4/29/00	148.1	2		
VT59	B	0.00	100.00	0.00	4/26/87	4/27/95	69.4	18	104.4	16
STAN	A	0.00	100.00	0.00	9/1/92	9/25/01	68.9	426	87.2	595
SR01	A	0.00	100.00	0.00	3/15/92	11/18/99	72.2	6	86.8	8

Table D-2. Continued.

Site ID [a]	GEO[b]	Silic.[c]	Gran.[d]	Basa.[e]	Min Date[f]	Max Date[g]	Cold ANC[h]	Cold n[i]	Warm ANC[j]	Warm n[k]
SR02	A	0.00	100.00	0.00	3/15/92	12/8/00	73.0	8	90.3	7
SR03	A	0.00	100.00	0.00	3/15/92	12/8/00	74.2	8	89.8	7
SR06	A	0.00	100.00	0.00	3/15/92	10/5/94	49.8	2	98.7	1
SR04	A	0.00	100.00	0.00	3/15/92	4/19/00	55.6	6	87.6	6
SR18	A	0.00	100.00	0.00	3/15/92	12/8/00	84.9	7	83.0	3
SR07	A	0.00	100.00	0.00	3/15/92	12/8/00	75.7	7	90.1	7
SR08	A	0.00	100.00	0.00	3/15/92	12/8/00	74.9	7	85.7	6
SR05	A	0.00	100.00	0.00	3/15/92	5/17/99	61.5	5	76.6	7
SR09	A	0.00	0.00	0.00	3/15/92	12/8/00	71.5	8	87.2	7
SR11	A	0.00	100.00	0.00	3/15/92	12/8/00	56.0	8	71.5	7
SR13	A	0.00	100.00	0.00	3/15/92	12/8/00	67.5	8	81.3	7
SR14	A	0.00	100.00	0.00	3/15/92	12/8/00	69.8	8	85.4	7
SR15	A	0.00	100.00	0.00	3/15/92	12/8/00	63.0	8	74.2	7
SR16	A	0.00	100.00	0.00	3/15/92	12/8/00	66.8	8	77.5	5
SR17	A	0.00	100.00	0.00	3/15/92	12/8/00	57.2	8	67.4	7
MA17	B	0.00	14.41	85.59	4/25/87	4/29/00	107.5	2		
VT75	A	0.00	14.10	85.90	7/31/90	7/31/01	106.6	22	169.2	23
WO02	A	0.00	14.50	83.20	3/19/92	7/15/92	86.2	1	170.4	1
WO04	A	0.00	13.90	83.60	3/19/92	7/15/92	86.2	1	172.0	1
WO05	A	0.00	21.10	78.90	3/19/92	7/15/92	72.8	1	137.9	1
WO03	A	0.00	10.80	85.70	3/19/92	7/15/92	91.2	1	182.9	1
MA01	B	0.00	6.96	93.04	4/25/87	4/29/00	107.4	2		
WO06	A	0.00	18.90	81.10	3/19/92	7/15/92	76.2	1	145.4	1
WO20	A	0.00	11.50	84.50	3/19/92	7/15/92	94.4	1	184.4	1
WO07	A	0.00	0.00	100.00	3/19/92	7/15/92	90.3	1	166.1	1
WO21	A	0.00	17.50	76.50	3/19/92	7/15/92	100.3	1	181.1	1
WO22	A	0.00	20.10	73.00	3/19/92	7/15/92	101.2	1	191.9	1
WO23	A	0.00	21.90	70.50	3/19/92	7/15/92	102.8	1	196.1	1
WO25	A	0.00	14.40	79.40	3/19/92	7/15/92	101.2	1	219.2	1
WO24	A	0.00	45.00	42.50	3/19/92	7/15/92	93.7	1	151.1	1
WO26	A	0.00	15.90	77.30	3/19/92	7/15/92	100.3	1	198.6	1
WO28	A	0.00	16.70	76.20	3/19/92	7/15/92	75.4	1	147.2	1
WO27	A	0.00	2.30	95.50	3/19/92	7/15/92	76.9	1	158.6	1
WO30	A	0.00	20.80	66.70	3/19/92	3/19/92	91.1	1		
WO29	A	0.00	61.50	23.10	3/19/92	7/15/92	75.4	1	105.4	1
RH51	B	100.00	0.00	0.00	4/25/87	4/29/00	-7.5	2		
RH48	B	84.08	0.00	15.92	4/25/87	4/24/00	42.5	2		
RH50	B	100.00	0.00	0.00	4/25/87	4/24/00	12.1	2		
RH49	B	70.06	0.00	29.94	4/26/87	4/24/00	62.5	2		
DR01	A	100.00	0.00	0.00	11/2/79	9/25/01	2.2	545	7.6	497
AB06	B	0.03	0.00	99.97	4/26/87	4/28/00	163.3	2		
AB07	B	19.19	0.00	80.81	4/26/87	4/28/00	133.8	2		

Table D-2. Continued.

Site ID [a]	GEO[b]	Silic.[c]	Gran.[d]	Basa.[e]	Min Date[f]	Max Date[g]	Cold ANC[h]	Cold n[i]	Warm ANC[j]	Warm n[k]
RH47	B	99.99	0.00	0.00	4/25/87	4/29/00	1.9	2		
MAD2	A	73.40	0.00	26.60	3/31/81	7/31/01	77.2	299	131.5	304
AU02	B	100.00	0.00	0.00	4/26/87	4/29/00	0.6	2		
VT36	A	100.00	0.00	0.00	8/16/87	7/31/01	-2.3	28	-0.2	29
MR01	A	100.00	0.00	0.00	3/12/92	8/28/93	-3.0	2	-0.6	2
MR17	A	100.00	0.00	0.00	3/12/92	11/1/94	-2.7	2	1.7	3
MR11	A	100.00	0.00	0.00	3/12/92	11/1/94	-5.2	2	-1.3	3
MR12	A	100.00	0.00	0.00	3/12/92	11/1/94	4.1	2	18.1	3
MR10	A	100.00	0.00	0.00	3/12/92	11/1/94	-4.4	2	-3.6	3
MR09	A	100.00	0.00	0.00	3/12/92	11/1/94	-4.4	2	0.0	3
MR16	A	100.00	0.00	0.00	3/12/92	11/1/94	4.9	2	28.6	3
MR18	A	100.00	0.00	0.00	3/12/92	11/1/94	-4.3	2	1.4	3
MR08	A	100.00	0.00	0.00	3/12/92	11/1/94	-6.6	2	-4.9	3
MR13	A	100.00	0.00	0.00	3/12/92	11/1/94	-2.2	2	7.0	3
MR06	A	100.00	0.00	0.00	3/12/92	11/1/94	-1.9	2	-1.4	3
MR07	A	100.00	0.00	0.00	3/12/92	11/1/94	-16.9	2	-10.8	3
MR15	A	100.00	0.00	0.00	3/12/92	11/1/94	6.6	2	25.0	3
MR05	A	100.00	0.00	0.00	3/12/92	8/28/93	1.6	2	5.8	2
MR14	A	100.00	0.00	0.00	3/12/92	11/1/94	3.3	2	21.1	3
MR04	A	100.00	0.00	0.00	3/12/92	11/1/94	-1.4	2	8.3	3
MR02	A	100.00	0.00	0.00	3/12/92	11/1/94	-0.6	2	3.1	3
MR03	A	100.00	0.00	0.00	3/12/92	11/1/94	3.2	2	13.1	3
AB09	B	59.99	0.00	39.08	4/28/87	4/26/00	58.3	2		
AB01	B	30.66	0.00	68.78	4/28/87	4/26/00	133.5	2		
AB08	B	23.99	0.00	76.01	4/24/87	4/26/00	171.2	2		
AB05	B	79.78	0.00	20.22	4/24/87	4/28/00	42.4	2		
AB04	B	17.22	0.00	82.78	4/29/87	4/28/00	85.5	2		
AB02	B	88.42	0.00	11.58	4/29/87	4/28/00	20.1	2		
RH52	B	100.00	0.00	0.00	4/25/87	4/29/00	9.2	2		
PAIN	A	100.00	0.00	0.00	8/14/87	9/25/01	1.9	446	7.8	355
PR02	A	100.00	0.00	0.00	3/8/92	10/6/94	2.3	3	10.5	4
PR03	A	100.00	0.00	0.00	3/8/92	10/6/94	0.6	3	6.2	4
PR06	A	100.00	0.00	0.00	3/8/92	10/6/94	2.1	3	6.6	4
PR04	A	100.00	0.00	0.00	3/8/92	10/6/94	2.0	3	4.1	4
PR07	A	100.00	0.00	0.00	3/8/92	10/6/94	1.1	3	4.1	4
PR08	A	100.00	0.00	0.00	3/8/92	10/6/94	1.7	3	9.4	4
PR05	A	100.00	0.00	0.00	3/8/92	10/6/94	-6.4	3	-5.1	4
PR12	A	100.00	0.00	0.00	3/8/92	10/6/94	1.4	3	11.7	4
PR11	A	100.00	0.00	0.00	3/8/92	10/6/94	2.3	3	11.3	4
PR09	A	100.00	0.00	0.00	3/8/92	10/6/94	-4.5	3	-1.8	4
PR15	A	100.00	0.00	0.00	3/8/92	4/9/94	1.4	3	2.8	2
PR16	A	100.00	0.00	0.00	3/8/92	4/9/94	0.6	3	2.0	2

Table D-2. Continued.

Site ID [a]	GEO[b]	Silic.[c]	Gran.[d]	Basa.[e]	Min Date[f]	Max Date[g]	Cold ANC[h]	Cold n[i]	Warm ANC[j]	Warm n[k]
PR10	A	100.00	0.00	0.00	3/8/92	4/9/94	0.6	3	1.9	1
PR38	A	100.00	0.00	0.00	3/8/92	4/9/94	5.1	3	15.8	2
PR19	A	100.00	0.00	0.00	3/8/92	4/9/94	0.6	3	5.3	3
PR24	A	100.00	0.00	0.00	3/8/92	10/6/94	1.1	3	5.9	4
PR18	A	100.00	0.00	0.00	3/8/92	10/6/94	4.8	3	10.7	4
PR13	A	100.00	0.00	0.00	3/8/92	4/9/94	3.6	3	6.9	1
PR21	A	100.00	0.00	0.00	3/8/92	10/6/94	-3.3	3	2.0	4
PR25	A	100.00	0.00	0.00	3/8/92	4/9/94	5.5	3	12.4	2
PR14	A	100.00	0.00	0.00	3/8/92	4/9/94	3.6	3	10.3	2
PR27	A	100.00	0.00	0.00	3/8/92	10/6/94	2.0	3	6.3	4
PR28	A	100.00	0.00	0.00	3/8/92	10/6/94	-3.6	3	2.2	4
PR17	A	100.00	0.00	0.00	3/8/92	10/6/94	3.7	3	14.3	4
PR29	A	100.00	0.00	0.00	3/8/92	10/6/94	1.1	3	8.2	4
PR30	A	100.00	0.00	0.00	3/8/92	10/6/94	-0.5	3	4.1	4
PR20	A	100.00	0.00	0.00	3/8/92	4/9/94	-1.1	3	4.8	3
PR32	A	100.00	0.00	0.00	3/8/92	10/6/94	0.3	3	5.5	4
PR31	A	100.00	0.00	0.00	3/8/92	10/6/94	5.0	3	19.0	4
PR26	A	100.00	0.00	0.00	3/8/92	4/9/94	1.4	3	5.8	3
PR33	A	100.00	0.00	0.00	3/8/92	10/6/94	3.0	3	10.1	4
PR36	A	100.00	0.00	0.00	3/8/92	10/6/94	-74.8	3	-40.4	4
PR34	A	100.00	0.00	0.00	3/8/92	10/6/94	3.3	3	7.0	4
PR35	A	100.00	0.00	0.00	3/8/92	10/6/94	3.5	3	9.9	4
AU12	B	81.00	0.00	19.00	4/26/87	4/26/87	8.0	1		
VT53	A	100.00	0.00	0.00	8/14/87	7/31/01	9.3	28	21.8	29
TM12	A	100.00	0.00	0.00	3/13/92	11/19/94	8.6	3	19.1	2
TM10	A	100.00	0.00	0.00	3/13/92	8/19/93	3.7	2	20.8	2
TM09	A	100.00	0.00	0.00	3/13/92	4/1/93	4.3	2		
TM07	A	100.00	0.00	0.00	3/13/92	8/19/93	-0.1	2	10.8	2
TM05	A	100.00	0.00	0.00	3/13/92	4/1/93	-0.2	2	8.7	1
TM04	A	100.00	0.00	0.00	3/13/92	4/1/93	-3.1	2	-3.1	1
TM03	A	100.00	0.00	0.00	3/13/92	4/1/93	5.8	2	11.9	1
TM02	A	100.00	0.00	0.00	3/13/92	4/1/93	-5.8	2	-16.4	1
WOR1	A	100.00	0.00	0.00	11/2/79	9/25/01	19.2	531	40.3	451
WR02	B	100.00	0.00	0.00	11/2/94	11/2/94			49.3	1
WR03	B	100.00	0.00	0.00	11/2/94	11/2/94			47.8	1
LUCK	B	100.00	0.00	0.00	3/29/86	6/20/95	11.3	223	29.8	193
WOR3	B	100.00	0.00	0.00	3/29/86	6/20/95	22.9	224	41.1	226
WR04	A	100.00	0.00	0.00	11/2/94	11/2/94			46.8	1
WR06	A	100.00	0.00	0.00	11/2/94	11/2/94			49.3	1
WR07	A	100.00	0.00	0.00	11/2/94	11/2/94			51.8	1
WR08	A	100.00	0.00	0.00	11/2/94	11/2/94			42.8	1
WR09	A	100.00	0.00	0.00	11/2/94	11/2/94			24.4	1

Table D-2. Continued.

Site ID [a]	GEO[b]	Silic.[c]	Gran.[d]	Basa.[e]	Min Date[f]	Max Date[g]	Cold ANC[h]	Cold n[i]	Warm ANC[j]	Warm n[k]
WR10	A	100.00	0.00	0.00	11/2/94	11/2/94			32.8	1

[a] Bold indicates primary sampling site.
[b] GEO = Source information for determination of watershed bedrock percentages.
A = Gathright (1976); manually digitized catchments based on 1:24,000-scale USGS topographic maps.
B = Sullivan et al. (2002); catchment areas determined based on 30-m DEM data.
[c] Silic. = Percentage of watershed area underlain by siliciclastic bedrock.
[d] Gran. = Percentage of watershed area underlain by granitic bedrock.
[e] Basa. = Percentage of watershed area underlain by basaltic bedrock..
[f] Min Date = First collection date in 1980-2001 water year period.
[g] Max Date = Last collection date in 1980-2001 water year period.
[h] Cold ANC = mean ANC for all samples collected between May 16 and November 15.
[i] Cold N = number of sample values included in COLD_ANC mean.
[j] Warm ANC = mean ANC for all samples collected between May 16 and November 15.
[k] Warm N = number of sample values included in WARM_ANC mean.

Appendix C

Description of the Extended RADM Model

1. Model Description

The Regional Acid Deposition Model (RADM) (Chang et al., 1987) was used as the basis for the Extended RADM. The RADM is an Eulerian model that was developed under the National Acidic Precipitation Assessment Program (NAPAP) to address regional photochemistry, aqueous chemistry, cloud processes, transport and wet and dry deposition. A primary deficiency in the use of RADM to study nitrogen deposition and inorganic particles, however, was the lack of representation of the important role of NH_3 to affect deposition and particle composition through conversion of HNO_3 to NO_3^- and of NH_3 to aerosol NH_4^+. In order to synthesize the current knowledge of the processes governing the fate of inorganic nitrogen in a consistent modeling framework, RADM was enhanced, by adding several additional modules to represent the various atmospheric physical and chemical pathways governing the fate of emitted NH_3. These processes, their model representation, and assumptions in their formulation are described here.

The partitioning of reduced and oxidized nitrogen forms between the gas and the aerosol phases is governed by thermodynamic equilibrium (Seinfeld and Pandis, 1998). To model this partitioning, an additional process module representing aerosol equilibrium was added to the RADM framework. This module calculates equilibrium chemical composition of the sulfate-nitrate-ammonium-water aerosol, and is based on the work of Saxena et al. (1986) with further modifications described in Binkowski and Shankar (1995) and Binkowski (1999). Zhang et al. (2000) compared the performance of this thermodynamic module with other more comprehensive approaches and found results to be comparable for the sulfate-nitrate-ammonium-water system.

Two additional species, representing particulate NH_4^+ and particulate NO_3^-, were also added to RADM. Existing transport modules were modified to account for advective and turbulent transport and dry deposition of these additional particulate species. The dry deposition velocities for particulate NH_4^+ and NO_3^- were set to be the same as that of SO_4^{2-} already computed in RADM, and are based on the assumption of an internally mixed aerosol. Further, no distinction of aerosol size was retained since inorganic particles over the continental region are primarily in the fine aerosol size fraction. The representation of aqueous chemistry was modified to include the participation of particulate nitrate and ammonium. Further, the cloud transport and cloud scavenging portions of the model were modified to include the impact of these important processes in the representation of particulate ammonium and nitrate and to include their contribution to the eventual ammonium and nitrate wet deposition amounts. This enhanced version of the model is termed the *Extended-RADM*.

RADM was developed with grids that are 80-km on a side. More recently, a 20-km grid covering the northeastern U.S. nested within the 80-km grid was created for Chesapeake Bay studies as a one-way nest. For this study, the 20-km grid was extended south to include all of North and South Carolina. Both grids are shown in Figure C-1. The extended 20-km grid is the principal grid used for this assessment.

The RADM parameterization of dry deposition velocities for various gaseous species, including NH_3, is based on the resistance analog method of Wesley (1989) and is detailed in Chang et al. (1990) and Walmsley and Wesley (1996). The value of the deposition velocity, V_d, is dependent on three terms representing the bulk properties of the lower atmosphere and the underlying surface: the aerodynamic resistance (r_a), the laminar sub-layer resistance (r_b), and the canopy resistance (r_c). For the various cases considered in this study, over most of the continental eastern U.S. we found the mean daytime values of V_d computed using this approach to be about 0.5-0.7 cm s^{-1}. These estimates are considerably lower than those reported in the

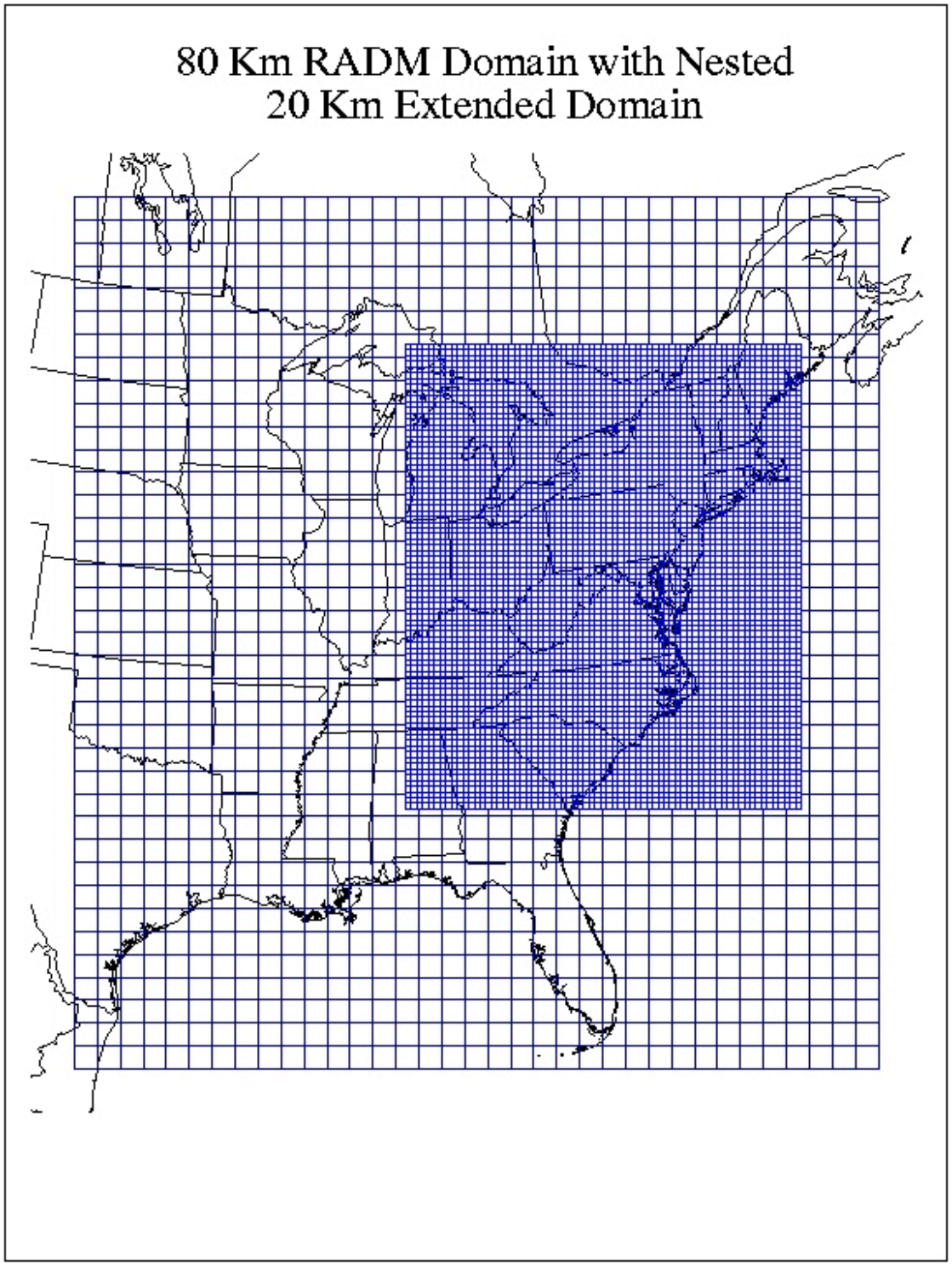

Figure C-1. Map of the 80-km grid Eastern U.S. domain with the embedded 20-km nest covering the mid-Atlantic and midwest regions.

measurements discussed earlier, but cannot be verified given the lack of comprehensive observational data on NH_3 deposition velocity over the eastern U.S. These lower estimates of V_d could be related to the computed canopy resistance (r_c) in the model. The r_a and r_b are dependent on prevalent meteorological conditions and standard methods for their estimation are widely used (Wesley and Hicks, 2000). The canopy or surface resistance describes the uptake process at the surface and in turn is dependent on the vegetative characteristics of the underlying surface, with smaller r_c for surfaces with stronger uptake. The r_c paramterization in RADM was inferred from limited deposition measurements for other species (e.g., SO_2) since reliable measurements of atmospheric NH_3 were lacking. It appears that this approach results in modeled r_c values which are overestimated. To account for this overestimation and to be more consistent with European measurements, we modified the calculation of the NH_3 deposition velocity through reducing the computed canopy resistance for NH_3, by one-third. (For a description of the European measurements see Mathur and Dennis, in press.) Though somewhat approximate, this simplistic approach yields V_d values in the upper range of 1-1.25 cm s^{-1}, while retaining the regional spatial heterogeneity in its distribution due to variations in micrometeorology, land-use, and surface wetness (Walmsley and Wesley, 1996).

The thickness of the lowest model layer used in this study was 75 m. In Eulerian model calculations, inadequate resolution of the lowest model layer thickness can potentially create a bias in the estimated dry deposition. RADM uses a constant flux regime computation to deal with estimation of r_a and takes the surface layer thickness into account (Byun, 1990 and 1991). The turbulent flux is integrated over the lower height of the cell to compute r_a. During day time conditions, when the PBL height is high relative to the height of the lowest layer, the constant flux concept is valid (the eddy diffusivity, K_z, near the surface monotonically increases with height) and the bias in V_d is small and typically on the order of ±20% (Byun and Dennis 1995). Under these conditions, ambient concentrations are relatively well mixed in the vertical; thus, the bias in deposition due to layer thickness is small. At night, under stable conditions, the constant flux concept may not be entirely valid, leading to r_a being a factor of 2-4 too high. However, RADM has been shown to systematically over-predict nighttime surface-level concentrations by factors of 2 and larger (Dennis, et al, 1990a). For nighttime calculations of deposition, these two biases are in opposite directions and to a large degree cancel each other out. Because the nighttime V_d is typically much smaller than the daytime V_d, the overall deposition bias is estimated to be the order of +20% to -50%. Given the large uncertainty in deposition velocity estimates, this degree of bias is considered acceptable.

Unlike most gas phase pollutants, which are consistently deposited, NH_3 is both emitted from and deposited to land and water surfaces (Quinn et al., 1988; Asman et al., 1994). In characterizing the air-surface exchange of NH_3, several measurement studies point towards the existence of a "compensation point" (e.g., Farquhar et al., 1979; Lemon and Van Houtte, 1980). These studies report that, depending on whether the difference between NH_3 concentrations in the air and those in the depositing surface is positive or negative, either dry deposition to the surface or emission from the surface could occur. This could imply that there may be no NH_3 dry deposition to surfaces that contain substantial amounts of NH_3, such as fields within a few weeks of spreading of manure or cattle-grazing meadows (Asman and van Jaarsveld, 1992). Asman and Janssen (1987) estimated average annual reductions in NH_3 deposition on the order of 20% for such fields. Measurements from Langford and Fehsenfeld (1992) demonstrated that under circumstances of high atmospheric NH_3 concentrations, a pine forest acted as a sink, but it acted as a source at low NH_3 concentrations. These studies imply that natural vegetation may be a net sink in the vicinity of source regions but a net source of NH_3 in regions where un-neutralized

acidic aerosols could depress gaseous NH_3 concentrations below the compensation point. The representation of this bi-directional air-surface exchange in regional models employing relatively coarse grid resolution is challenging, however, because detailed information on land management practices employed for the mosaic of land-use categories represented within each coarse model grid cell is currently lacking. Further, the characterization of this net NH_3 emission from surfaces such as intensively grazed pastures and fertilized croplands requires detailed information on local surface environmental conditions, including form of nitrogen input, NH_x status in plant leaves, nitrogen status in the soil, plant growth stage, and micrometeorology. These conditions vary considerably spatially and temporally, are not typically well known, are subject to significant uncertainty, and are not likely to be resolved by model grid resolution typical of regional scale models. In addition, our intent in this study is to characterize mean seasonal and annual features of the distribution of NH_x compounds. We therefore ignore the explicit treatment of such NH_3 emission sources, except where they are already accounted for in the base inventory (e.g., fertilized croplands).

2. Development of Annual Averages

The Extended RADM is very computationally intensive because it predicts hourly photochemistry. Although recent advances in computational technology and computer code optimization have enabled the application of regional models over monthly to seasonal scales, their applications to study long-term pollutant behavior and deposition patterns over several seasonal and annual cycles challenge the practical limits of current computer resources. Aggregation techniques are available that combine into seasonal and annual totals a limited number of episodic estimates representing a variety of meteorological cases. Such approaches have emerged as useful practical methods for modeling the long-term relationships among changing emission patterns and regional air quality and atmospheric deposition. These techniques are based on the assumption that the atmospheric chemistry, transport, and deposition at a given location are governed by a number of different recurring weather patterns that can be combined to produce a realistic estimate of annual and seasonal synoptic and chemical climatology (Brook et al., 1995a).

The aggregation technique used here has been previously used during the NAPAP study to develop climatological seasonal and annual estimates of acid deposition totals (Dennis et al., 1990b). The approach involves the selection of a set of events for model simulations that are representative of the cross section of synoptic conditions occurring on a climatological annual cycle. Meteorological cases of 5-day durations during the 1979-1983 period were grouped by wind flow patterns through cluster analysis and sampled proportionate to their frequency of occurrence as detailed in Brook et al. (1995a, b). A total of 30 cases constitute the aggregation sample. The precipitation predicted for each case within a cluster was adjusted to the long-term mean precipitation for that cluster to estimate average deposition. This procedure was selected because the spatial pattern of precipitation during an individual event will not necessarily resemble the cluster average. The aggregation method produces a climatological average of transport and deposition representative of the transport of the 1980s and the seven-year average precipitation of that period. This precipitation average approximates well the 30-year normal precipitation.

3. Defining an Applications Version of the Extended RADM

To account for the low bias in the NH_3 emission estimates for the U.S. from the 1985 NAPAP inventory, we developed seasonal correction factors for NH_3 emissions through successive applications of the Extended-RADM and systematic comparisons with observed data. This simple "brute-force" inversion analysis allowed us to develop a seasonal modeling inventory for NH_3 that, as will be discussed subsequently, provides model results that are consistent with observed values for both ambient atmospheric concentrations and wet deposition amounts. We adjusted the NH_3 emission fields input to the Extended-RADM through successive model application and comparison with a suite of ambient and wet measurements. In these analyses, we included comparisons of model results against measurements of ambient levels of HNO_3, SO_4^{2-}, NO_3^-, and NH_4^+ and wet deposition amounts of SO_4^{2-}, NO_3^-, and NH_4^+, but gave more weight towards satisfying three specific criteria: 1) the adjustment in NH_3 emissions should not disturb the modeled ambient and wet deposition for sulfate through perturbations in cloud pH-related oxidation pathways, such as through ozone oxidation, 2) since NH_3 provides a pathway for formation of particulate NO_3^-, the predicted ambient $NO_3^-/(HNO_3 + NO_3^-)$ ratio should retain the spatial regional signature indicated by measurements, and 3) any bias structure in modeled NH_4^+ wet deposition should be similar to that for $SO_4^{2-}$and NO_3^- wet deposition. This approach provided a physically-based, self-consistent constraint for potential growth in NH_3 emissions as opposed to a purely empirically based one in which NH_3 increases are dictated solely by discrepancies between model and observed ambient NH_x levels without accounting for other modeled species.

Table C-1. Seasonal correction factors to the 1985 NAPAP ammonia emissions inventory developed for the Extended RADM

Season	Factor
Summer	4.9
Fall	1.32
Winter	1.31

Table C-1 presents the resulting estimated domain mean seasonal adjustment factors for NH_3 emissions in the NAPAP inventory. The estimates are representative of the late 1980's to early 1990's period of ammonia emissions. These results suggest that on an annual basis, the 1985 NAPAP NH_3 emissions inventory was a factor of 2.75 too low, confirming suspicions of previous studies (e.g., Chang et al., 1990) and giving annual emissions rates consistent with EPA's 1990 National Emissions Inventory. Additionally, the adjustment factors showed a pronounced seasonal variation and yielded maximum NH_3 emissions during summer, followed by spring, fall and winter. These trends are in agreement with recent NH_3 flux measurements reported by Aneja et al. (2000), who observed similar seasonal variation in NH_3 emissions from waste storage and treatment lagoons. It should be noted, however, that since the ambient and wet deposition measurements used in our simple inversion analysis were for the late 1980s to early 1990s period, the magnitude of regional estimated NH_3 emissions should be taken as representative emissions only for that period. Also, since the method only scaled the emissions based on a fixed inventory, growth in local NH_3 emissions was only captured to the extent that they were detailed in the base inventory. The seasonally-adjusted NH_3 emissions were used in the model simulations. For this study, the NH_3 emissions were kept constant at the effective 1990 levels.

4. Comparison of Model Predictions with Measurements

The development, application and evaluation of RADM, which formed the basis for the Extended RADM, has been documented extensively by NAPAP (Chang, et al. 1987, Chang, et al., 1990 and Dennis, et al., 1990a). RADM continued to undergo periodic peer review, evaluations and improvements since completion of the NAPAP assessment in 1991 (Dennis, et al., 1993; McHenry and Dennis, 1994; Cohen and Dennis, 1994; External Review Panel, 1994; Eder and LeDuc, 1996; Eder, et al., 1996). RADM has been used in more recent U.S. EPA studies of acidic deposition (e.g. U.S. EPA 1995), assessments of fine particle mass and light extinction, and assessments of deposition of nitrogen to coastal estuaries (Dennis 1997, U.S. EPA 1997). Here are presented comparisons specifically for the Extended RADM.

a. Annual deposition and ambient concentrations

To assess the performance of the Extended-RADM, annual predictions of both ambient concentrations and wet deposition amounts were compared with measurements from the Clean Air Status and Trends Network (CASTNet; CASTNet 2002) and precipitation chemistry data from the NADP (2002), respectively. To develop climatologically-representative measurements to compare with aggregated model results, we used several years of measurements from the CASTNet (1988-1992) and NADP (1984-1993) networks. Recognizing the intrinsic bias in using a small sample of precipitation events to approximate average rainfall (since no single storm event can replicate long-term average rainfall patterns), the modeled wet deposition amounts were scaled by climatologically observed precipitation within each model grid cell following the approach of Dennis et al. (1990b); these were then compared with measured wet deposition amounts. For the comparisons reported here, measurements from 44 CASTNet sites and 124 NADP sites located within the model domain were used. A 75% completeness criterion was used for averaging the ambient measurements from CASTNet. To minimize possible bias arising from missing data, a more stringent 90% completeness criterion was used in accumulating the NADP deposition measurements. Both networks have excellent spatial coverage across the eastern U.S. as shown in Figure C-2 and thus the comparisons provide an opportunity to assess the performance of the model in capturing the spatial variability in both ambient levels and wet deposition amounts.

The degree of correspondence between the modeled and measured ambient concentrations and wet deposition amounts was examined for various species both on a climatological annual and seasonal basis. In the subsequent discussion, we use the term correlation to denote this degree of correspondence between the model and measurements. Figure C-3 presents scatter-plots of the relationship between model predicted climatological annual averages and corresponding measurements of ambient concentrations and wet deposition amounts for selected ions that are important in determining aerosol composition and wet deposition amounts in the eastern United States. A summary of the comparisons in Figure C-3, plus additional comparisons between model- predicted, climatological annual averages and NADP and CASTNet measurements, is given in Table C- 2.

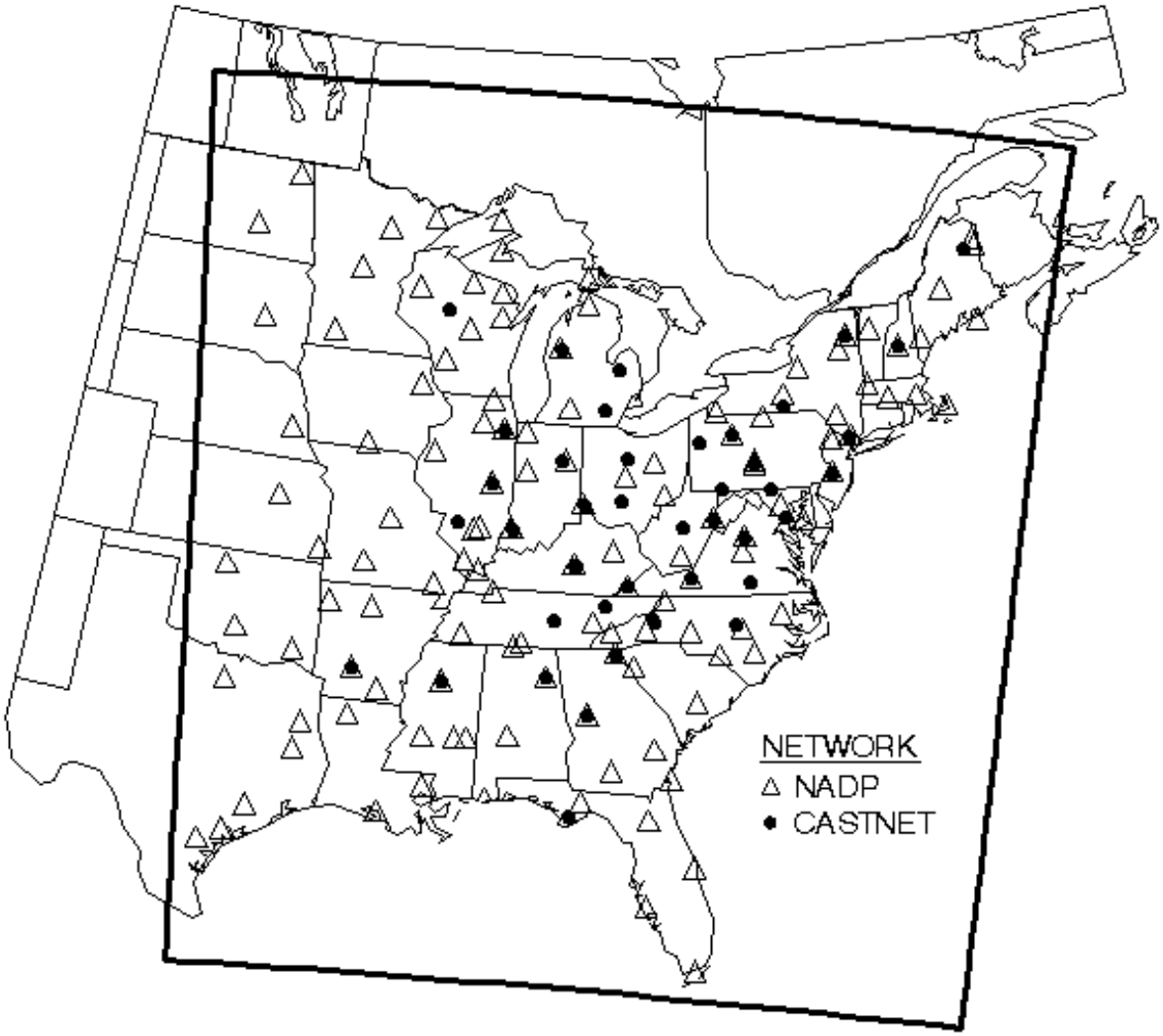

Figure C-2. Map of the Extended RADM Domain showing locations of the two monitoring networks, NADP and CASTNet, and their spatial coverage.

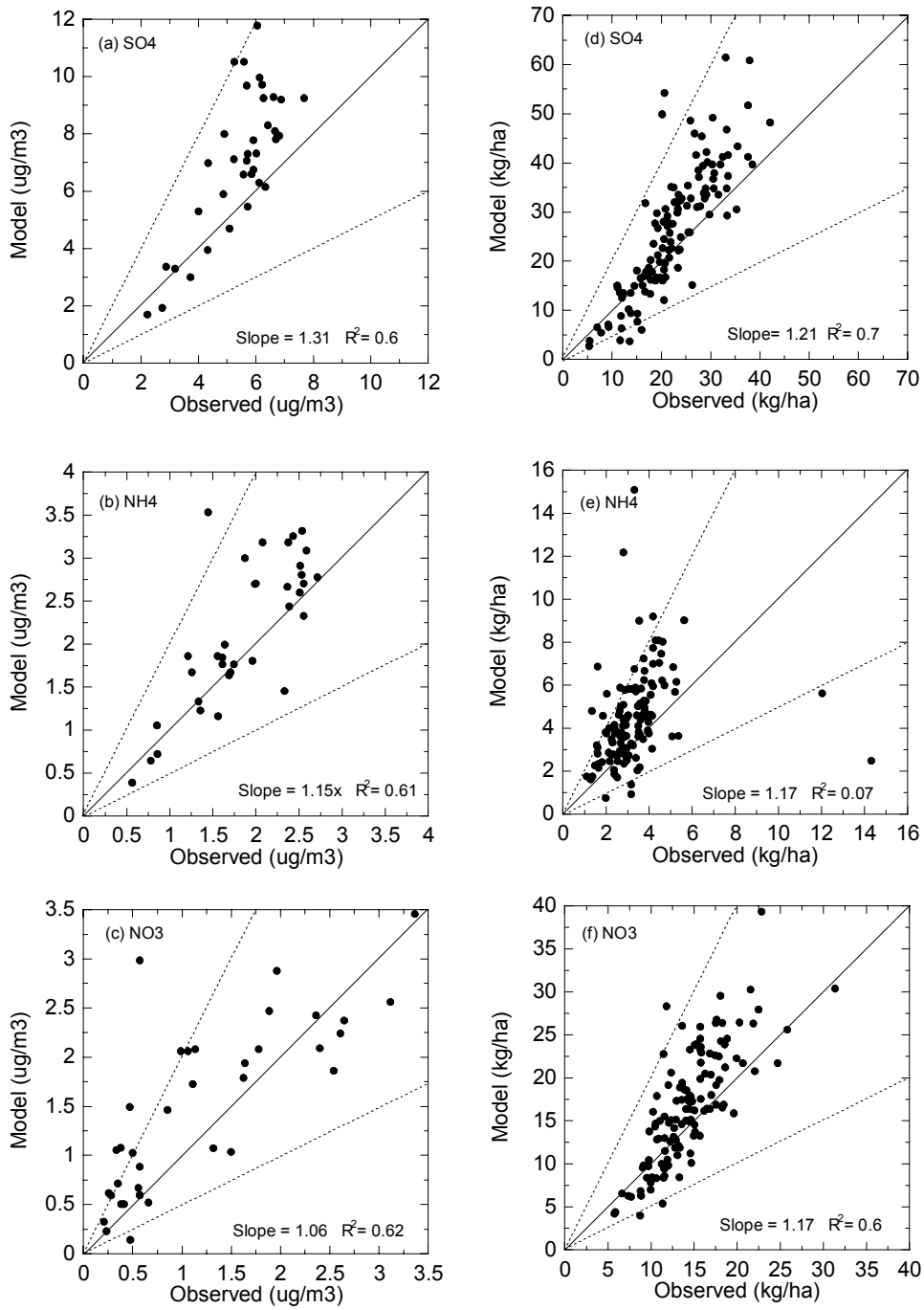

Figure C-3. Comparison of model simulated annual climatological averages with measurements: panels a to c are comparisons of ambient levels with CASTNet data; panels d to f are comparisons of wet deposition amounts with NADP data. The solid line indicates the 1:1 relationship, dotted lines indicate 1:2 and 2:1 comparison bounds as aids for judgment. Slope and coefficient of determination (r^2) of the correlation between model and observed are indicated in each panel.

Table C-2. Summary of comparisons between predicted and measured values of wet and dry deposition.		
NADP Wet Deposition		
$SO_4^{=}$	Ext.RADM = 1.21 x NADP	r^2 = 0.73, (n=124)
NH_4^+	Ext.RADM = 1.17 x NADP	r^2 = 0.36, (n=121)*
NO_3^-	Ext.RADM = 1.17 x NADP	r^2 = 0.64, (n=124)
CASTNet Ambient Concentrations		
HNO_3	Ext.RADM = 1.37 x CASTNet	r^2 = 0.36, (n=44)
$HNO_3 + NO_3^-$	Ext RADM = 1.41 x CASTNet	r^2 = 0.61, (n=44)
NO_3^-	Ext.RADM = 1.28 x CASTNet	r^2 = 0.63, (n=44)
$NO_3^-/(HNO_3 + NO_3^-)$	Ext.RADM = 1.04 x CASTNet	r^2 = 0.47, (n=43)
NH_4^+	Ext.RADM = 1.25 x CASTNet	r^2 = 0.60, (n=41)

* with the four outliers removed

In general, with the exception of NH_4^+ wet deposition, good agreement for model predicted annual estimates are noted, with r^2 in the range of 0.6-0.7 for both ambient concentrations (Figure C-3a-c) and wet deposition amounts (Figure C-3d-f). These correlations are reasonable, given that they are based on comparing grid-averaged values with point measurements (Schere, 1988; McKeen et al., 1991). It is difficult for a grid model operating from first principle descriptions of the processes, combined with comparing its grid predictions with point measurements, to achieve correlations greater than 0.7 (r^2 = 0.49). The poor r^2 for wet NH_4^+ deposition (Figure C-3e) results from discrepancies between model and measurements at a few sites characterized by relatively large model over- and under-predictions, though the overall correlation was good (without the four outliers, the r^2 = 0.36). Since similar outliers were not noted for SO_4^{2-} and NO_3^- wet deposition, these discrepancies in NH_4^+ wet deposition can be attributed primarily to large uncertainties associated with spatial variability of NH_3 emissions in the inventory. As discussed earlier, the NH_3 emissions correction factors are intended to be regionally representative and do not account for local spatial variability in the emissions. Thus, if a particular source category is missing in the base inventory, the corrected emissions would still be under-estimated. Consequently, poor estimation of local NH_3 emissions can contribute to local poor prediction of wet NH_4^+ deposition. More recent modeling studies of NH_3 indicate that large uncertainty in NH_3 emissions can significantly affect model performance, supporting this conclusion (Gilliland 2001). For HNO_3 during the warm half of the year when the spatial signal is more pronounced due to more active photochemistry, the r^2 is 0.52, more comparable to wet nitrate deposition. For ambient NO_3^- during the cold half of the year when its spatial signal is more pronounced, the r^2 is 0.71. The r^2 of 0.61 for total nitrate ($HNO_3 + NO_3^-$), for which there is less concern about measurement bias, is reasonable and the partitioning of total nitrate is basically unbiased, with an acceptable r^2 of 0.47. Thus, we believe the Extended RADM to a

sufficient degree is capturing the spatial patterns in annual wet deposition, ambient concentrations and partitioning of key species.

b. Growing season ozone

The ozone predictions of relevance for ozone exposure analysis relate to the distribution of ozone during the growing season, rather than a seasonal average, because it is largely an hourly exposure above a defined threshold (e.g., 60 ppb) that is of concern. The ozone analysis for this assessment focused on daylight hours, for which the model does best and when ozone levels dominate the overall exposure. The model has a large nighttime bias (Byun and Dennis, 1995; Dennis et al., 1990a), but this is less relevant to estimation of the effects of ozone exposure because the plant stomata are more frequently closed at night. Daytime ozone predictions provide the most reliable indicators of change in ozone exposure . A concentration distribution of hourly ozone can be constructed for the Extended RADM to represent exposure during the growing season, using a warm-season subset of the aggregation cases. The daytime (8 a.m. to 8 p.m.) hourly ozone distribution from the Extended RADM, defined by the decile cutpoints, is compared to the daytime hourly and daytime maximum ozone distribution observed at SHEN across several years (1989-1995) in Figure C-4. The model distribution is in excellent agreement with the shape of the observed distribution, and is biased high by only about 10%. The model distribution is more similar to the high ozone years observed at SHEN and is between the maximum year distribution and the daily maximum distribution. These distributions are all quite similar because the diurnal ozone pattern is broad with little amplitude. Most of the range in the distribution comes from synoptic differences among days. The extent of agreement is unusually good.

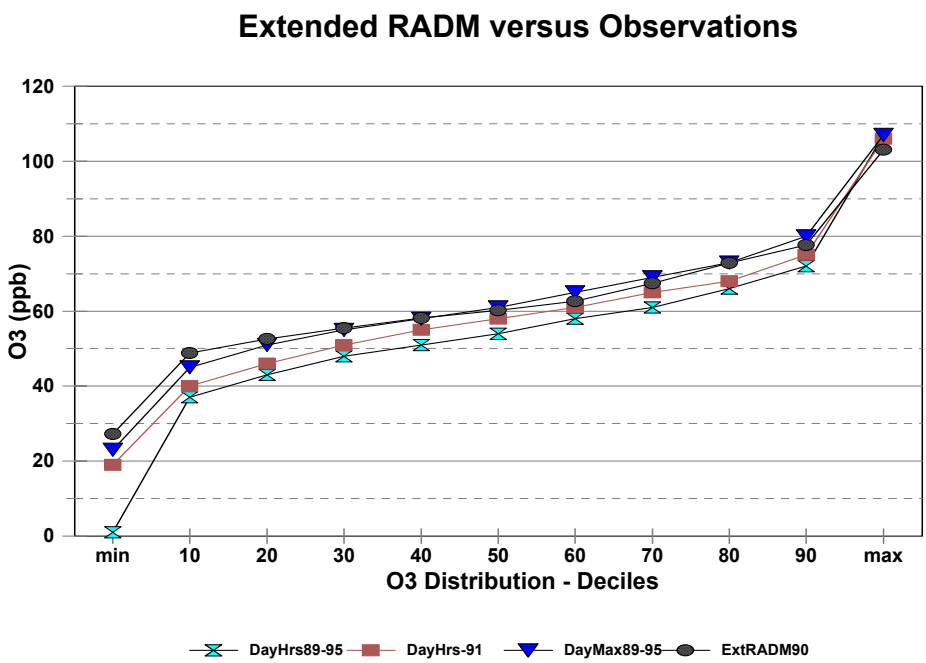

Figure C-4. Comparison of the growing season daytime (8 a.m. - 8 p.m.) ozone distribution predicted by the Extended RADM with the average distribution observed in SHEN from 1989 to 1995, the distribution for 1991, and the 1989 to 1995 daily maximum ozone distribution.

Given this degree of agreement, the Extended RADM should provide a reasonable vehicle for estimating changes in ozone exposure above a defined threshold for the growing season. It is key that the model does an adequate job of estimating the change in the upper end of the distribution. We should take into consideration, however, the observed 10% bias in the modeled ozone distribution. Also, we should consider that the system is potentially nonlinear in its response at different points along the distribution, in part because the number of hours per day above the defined threshold is not constant, but is itself a distribution. A representative threshold for the exposure change calculations from the model would not necessarily simply be the same threshold as defined for the ecological models. As demonstrated in the assessment calculations, the change in overall exposure-hours is dominated by the change in number of hours, rather than the change in the daily maximum ozone. Therefore, a threshold should be defined that best represents the overall pattern of hours above threshold. This was done for the Extended RADM. Several modeled hours-above-threshold distributions, using several model thresholds, were compared with the observed distribution above 60 ppb. The model hours-above-threshold distribution that was found to have a good match with the observed distribution of hours above 60 ppb, be consistent with the 10% bias, and show stable response across the emissions changes was a model threshold of 65ppb. The modeled (threshold = 65ppb) and observed (threshold = 60ppb) distributions are shown in Figure C-5. Thus, 65 ppb ozone was the threshold used with the Extended RADM in this assessment to best represent change in exposure associated with a "real world" threshold of 60ppb used by the ecological models. If the ecological model exposure threshold were to be changed, this procedure with the Extended RADM should be repeated to develop a new representative threshold. We believe the comparisons are sufficiently in agreement that this approach with the Extended RADM is reasonable and appropriate for the growing season exposure-hour calculations.

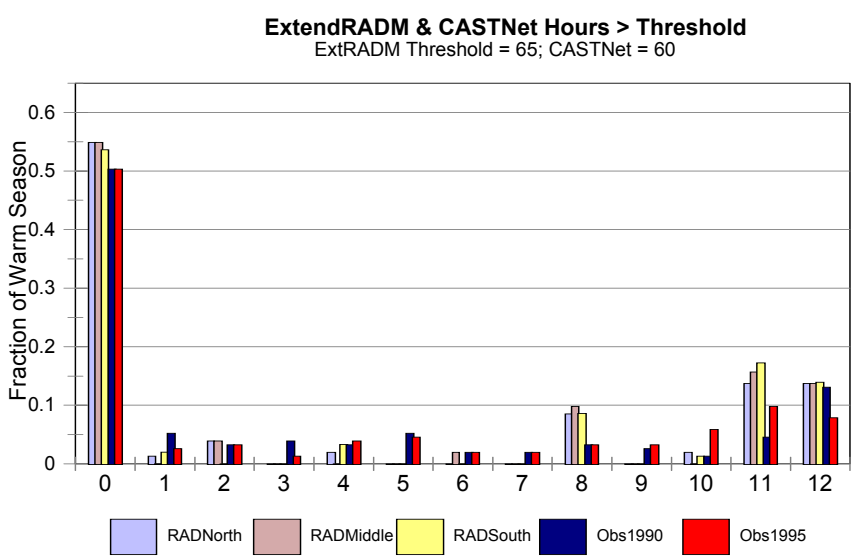

Figure C-5. Histogram of the number of growing-season daylight hours (8 a.m.-8 p.m.) within a day for which the defined threshold is exceeded for SHEN. Extended RADM O_3 threshold = 65 ppb, measurements O_3 threshold = 60 ppb. Extended RADM calculations are shown for the three cells covering the northern, middle and southern portions of SHEN.

5. References

Aneja, V. P., J. P. Chauhan, and J. T. Walker, Characterization of atmospheric ammonia emissions from swine waste storage and treatment lagoons, *J. Geophys. Res.*, *105*, 11,535-11,545, 2000.

Asman, W. A. H. and A. J. Janssen, A long-range transport model for ammonia and ammonium for Europe, *Atmos. Environ.*, *21*, 2099-2119, 1987.

Asman, W. A. H. and H. A. van Jaarsveld, A variable resolution model applied for NHx in Europe, *Atmos. Environ., 26*, 445-464, 1992.

Asman, W. A. H., R. M. Harrison, and C. J. Ottley, Estimation of the net air-sea flux of ammonia over the southern bight of the north sea, *Atmos. Environ.*, *28*, 3647-3654, 1994.

Binkowski, F. S., and U. Shankar, The Regional Particulate Matter Model 1. Model description and preliminary results, *J. Geophys. Res.*, *100*, 26,191-26,209, 1995.

Binkowski, F. S., *Aerosols in Models-3 CMAQ, Chapter 10, Science Algorithms of the EPA Models-3 Community Multiscale Air Quality (CMAQ) Modeling System*, D. Byun and J. Ching (Eds.), EPA/600/R-99/030, Office of Research and Development, U.S. Environmental Protection Agency, 1999.

Brook, J. R. P. J. Samson, and S. Sillman, Aggregation of selected three-day periods to estimate annual and seasonal wet deposition totals for sulfate, nitrate, and acidity. Part I: A synoptic and chemical climatology for eastern North America, *J. Applied Meteor.*, *34*, 297-325, 1995a.

Brook, J. R. P. J. Samson, and S. Sillman, Aggregation of selected three-day periods to estimate annual and seasonal wet deposition totals for sulfate, nitrate, and acidity. Part II: Selection of events, deposition totals, and source-receptor relationships, *J. Applied Meteor.*, *34*, 326-339, 1995b.

Byun, D.W., On the analytical solutions of flux-profile relationships for the atmospheric surface layer, *J. Applied Meteor.*, 29, 652-657, 1990.

Byun, D.W., Determination of similarity functions of resistance laws for the planetary boundary layer using surface-layer-similarity functions, *Boundary Layer Meteorology*, 57, 17-48, 1991.

Byun, D.W. and R.L. Dennis, Design artifacts in Eulerian air quality models: Evaluation of the effects of layer thickness and vertical profile correction on surface ozone concentrations, *Atmos. Environ.*, 29, 105-126, 1995.

Clean Air Status Trends Network (CASTNet), World wide web site, http://www.epa.gov/castnet, 2002.

Chang, J. S., R. A. Brost, I. S. A. Isaksen, S. Madronich, P. Middleton, W. R. Stockwell, and C. J. Walcek, A three-dimensional Eulerian acid deposition model: Physical concepts and formulation, *J. Geophys. Res.*, *92*, 14,681-14,700, 1987.

Chang, J. S., F. S. Binkowski, N. L. Seaman, D. W. Byun, J. N. McHenry, P. J. Samson, W. R. Stockwell, C. J. Walcek, S. Madronich, P. B. Middleton, J. E. Pleim, and H. L. Landsford, The regional acid deposition model and engineering model, *NAPAP SOS/T Report 4, in National Acid Precipitation Assessment Program, Acidic Deposition: State of Science and Technology*, *Volume I.*, National Acid Precipitation Assessment Program, Washington, DC, 1990.

Cohn, R. D. and Dennis R. L., 1994. The Evaluation of Acid Deposition Models Using Principal Component Spaces, *Atmospheric Environment*, **28**, 2531-2543.

Dennis, R.L., F.S. Binkowski, T.L. Clark, S.J. Reynolds and S.K. Seilkop, Evaluation of regional acidic deposition models (Part I), *NAPAP SOS/T Report 5, in National Acid Precipitation Assessment Program: State of Science/Technology, Volume 1*, National Acid Precipitation Program, 722 Jackson Place, Washington D.C., 1990a.

Dennis, R.L., F.S. Binkowski, T.L. Clark, J.N. McHenry, S.J. Reynolds, and S.K. Seilkop, Selected applications of the regional acid deposition model and engineering Model, *Appendix 5F (Part 2) of NAPAP SOS/T Report 5, in National Acid Precipitation Assessment Program: State of Science and Technology, Volume I*, National Acid Precipitation Assessment Program, Washington, D.C., 1990b.

Dennis, R.L., J.N. McHenry, W.R. Barchet, F.S. Binkowski, and D.W. Byun, 1993. Correcting RADM's sulfate underprediction: Discovery and correction of model errors and testing the correction s through comparisons against field data. *Atmospheric Environment,* **27A**(6), 975-997.

Dennis R.L., 1997. Using the Regional Acid Deposition Model to Determine the Nitrogen Deposition Airshed of the Chesapeake Bay Watershed. in Joel E. Baker, editor, *Atmospheric Deposition to the Great Lakes and Coastal Waters*, Society of Environmental Toxicology and Chemistry, Pennsacola, FL, pp 393-413.

External Review Panel. 1994: Report on RADM evaluation for the Eulerian Model Evaluation Field Study Program, Anton Eliassen, editor. Norwegian Meteorological Institute, Norway.

Eder B.K. and S.K. LeDuc, 1996. Can selected RADM simulations be aggregated to estimate annual concentrations of fine particulate matter? In *Measurement of toxic and related air pollutants*. VIP-64. Proceedings of an International Specialty Conference, Research Triangle Park, NC, May 7-9, 1996. Air & Waste Management Association, Pittsburgh, PA, pp 732-739.

Eder B.K., S.K. LeDuc, and F.D. Vestal, 1996. Aggregation of selected RADM simulations to estimate annual ambient air concentrations of fine particulate matter. in Preprints, Ninth Joint conference of Applications of Air Pollution Meteorology with A&WMA, January 28-February 2, 1996, Atlanta, Georgia. American Meteorological Society, Boston, MA, pp 390-392.

Farquhar, G.D., R. Wetselaar, and P.M. Firth, Ammonia volatalization from scenescing leaves of maize, *Science*, *203*, 1257-1258, 1979.

Gilliland, A.B., R.L. Dennis, S.J. Roselle, T.E. Pierce, and L.E. Bender, Developing seasonal ammonia emission estimates with an inverse modeling technique*, Proc. of the 2nd International Nitrogen Conference on Science and Policy*, *TheScientificWorld*, 1(S2), 356-362, 2001.

Langford, A.O. and F.C. Fehsenfeld, Natural vegetation as a source or sink for atmospheric ammonia: A case study, *Science*, *255*, 581-583, 1992.

Lemon, E. and R. Van Houte, Ammonia exchange at the land surface, *Agron. J.*, *72*, 876-883, 1980.

Mathur R. and R. L. Dennis, 2003. Seasonal and Annual Modeling of Reduced Nitrogen Compounds Over the Eastern United States: Emissions, Ambient Levels, and Deposition Amounts, *Journal of Geophysical Research*, (in press).

McHenry, J. N.and R. L. Dennis, The relative importance of oxidation pathways and clouds to atmospheric ambient sulfate production as predicted by the regional acid deposition model, *J. Appl. Meteor.*, *33*, 890-905, 1994.

McKeen, S.A, E.-Y. Hsie, M. Trainer, R. Tallamraju, and S. C. Liu, A regional model study of the ozone budget in the eastern United States, *J. Geophys. Res.*, *96*, 10,809-10,845, 1991.

National Atmospheric Deposition Program (NADP), World wide web site, http://nadp.sws.uiuc.edu, 2002.

Quinn, P. K., R. J. Charlson, and T.S. Bates, Simultaneous observations of ammonia in the atmosphere and ocean, *Nature*, *335*, 336-338, 1988.

Saxena, P., A. B. Hudischewskyj, C. Seigneur, and J. H. Seinfeld, A comparative study of equilibrium approaches to the chemical characterization of secondary aerosols, *Atmos. Environ.*, *20*, 1471-1484, 1986.

Schere, K.L., Modeling ozone concentrations, *Environ. Sci. Technol.*, *22*, 488-495, 1988.

Seinfeld, J. H. and S. N. Pandis, *Atmospheric Chemistry and Physics*, John Wiley, New York, 1998.

U.S. Environmental Protection Agency, 1995. *Acid Deposition Standard Feasibility Study Report to Congress*, EPA Report 430-R-95-001a, Office of Air and Radiation, Acid Rain Division, Washington, D.C.

U.S. Environmental Protection Agency, 1997. *Deposition of Air Pollutants to the Great Waters*, EPA Report 453/R-97-011, Office of Air Quality Planning and Standards, Research Triangle Park, NC.

Wamsley, J.L. and M.L. Wesley, Modification of coded parameterizations of surface resistances to gaseous dry deposition, *Atmos. Environ.*, 30, 1181-1188, 1996.

Wesley, M. L., Parameterizations of surface resistances to gaseous dry deposition in regional scale numerical models, *Atmos. Environ.*, 23, 1293-1304, 1989.

Wesley, M. L., and B. B. Hicks, A review of the current status of knowledge on dry deposition, *Atmos. Environ.*, *34*, 2261-2282, 2000.

Zhang Y., C. Seigneur, J. H. Seinfeld, M. Jacobson, S. L. Clegg, and F. S. Binkowski, A comparative review of inorganic aerosol thermodynamic equilibrium models: similarities, differences, and their likely causes, *Atmos. Environ.*, *34*, 117-137, 2000.

Appendix B

Description of Metrics Used to Quantify Visibility Effects

Light Extinction Coefficient

Aerosol data are used to calculate the atmospheric light extinction coefficient from experimentally determined extinction efficiencies of important aerosol species. The equation used by the IMPROVE Program to estimate reconstructed particle light extinction in Mm^{-1} is:

$$b_{ext} = b_{ray} + 3f(RH)[\text{sulfates}] + 3f(RH)[\text{nitrates}] + (4)[\text{organics}] + (1)[\text{soil}] + (0.6)[\text{coarse mass}] + (10)[\text{light absorbing carbon}]$$

where [ ] indicates mass concentration of the individual species (Malm et al. 2000). Some sulfates and nitrates are hygroscopic, so their scattering properties must be adjusted for the effects of relative humidity (f(RH)).

Visual Range

Visual Range (VR) can be expressed in terms of the light extinction coefficient as:

$$VR = 3912/(b_{ext} + b_{ray})$$

where b_{ext} is the extinction coefficient expressed in Mm^{-1}; b_{ray} is the site specific Rayleigh values (elevation dependent) and 3912 is the constant derived from assuming 2% contrast detection threshold. The theoretical maximum VR is 391 km. Note that b_{ext} and VR are inversely related: for example, as the air becomes cleaner, b_{ext} values decrease and VR values increase. A related metric is the Standard Visual Range (SVR). This metric is indexed to Rayleigh conditions at 1800 meters elevation rather than actual Rayleigh conditions at a specific location, (i.e., set to 10 Mm^{-1}).

Haziness

Haziness as expressed in deciview is defined as:

$$(\text{Haziness})\ dv = 10 \ln(b_{ext}/10\ Mm^{-1})$$

where b_{ext} is the extinction coefficient expressed in Mm^{-1} (Pitchford and Malm 1994). A one dv change is approximately a 10% change in b_{ext}, which is a small but perceptible scenic change under many circumstances. The deciview scale is near zero (0) for a pristine atmosphere and increases as visibility is degraded.

References

Malm, W.C., R. Ames, S. Copeland, D. Day, K. Gebhart, M. Pitchford, M. Scruggs, and J. Sisler. 2000. IMPROVE Report, Spatial and Seasonal Patterns and Temporal Variability of Haze and its Constituents in the United States: Report III, Cooperative Institute for Research in the Atmosphere (CIRA), Colorado State University, Ft. Collins, CO 80523. ISSN: 0737-5352-47.

Pitchford, M.L., and W.C. Malm. 1994. Development and Applications of a Standard Visual Index. Atmos. Environ. 28(5):1049-1054.

Appendix A

Weighting Function for W126 Ground-level Ozone Exposure Index

The W126 ozone exposure index is represented as the sum of all hourly ozone concentrations, where each measured concentration is weighted by a function, w_i, to assign greater emphasis to the higher measured concentrations. This weighting function provides a weighting value that is unique for each hourly ozone concentration. The weighting function, as described by Lefohn et al. [1988] is:

$$w_i = \frac{1}{1 + 4403\exp(-0.126c_i)}$$

where

w_i = weighting value for hourly concentration *i*, and
c_i = hourly concentration i in ppb.

The graph of weighting value versus ozone concentration illustrates the greater weights given to higher hourly ozone concentrations (Figure A-1). Each hour's weighting value is multiplied by its corresponding hourly concentration. This product is summed over all valid hours to calculate the W126 exposure. Thus, the W126 exposure is:
where
W126 = W126 exposure index, and
n = number of hours with valid ozone concentrations.

The exposure unit for both indices are parts per million-hours (ppm-hr). As in the case of the SUM06 index, W126 exposures are calculated using values measured during the 12 hours from 8 AM to 8 PM in the months of May through September of each year.

$$W126 = \sum_{i=1}^{n} w_i c_i$$

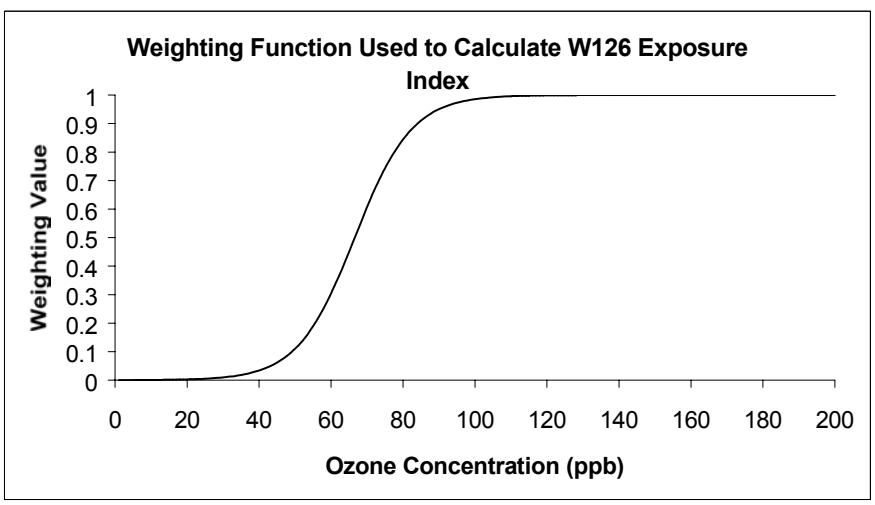

Figure A-1. Weighting function used to calculate the W126 ozone exposure index (Lefohn et al. 1988).

References

Lefohn A. S., J.A. Laurence, and R.J. Kohut. 1988. A comparison of indices that describe the relationship between exposure to ozone and reduction in the yield of agricultural crops. Atmospheric Environment 22:1229-1240.

Appendix J

Projected Changes in Tree Mass in Response to Ambient Ground-level Ozone Exposure During the Period 1997 to 1999, for Species That Showed Only Minor Response

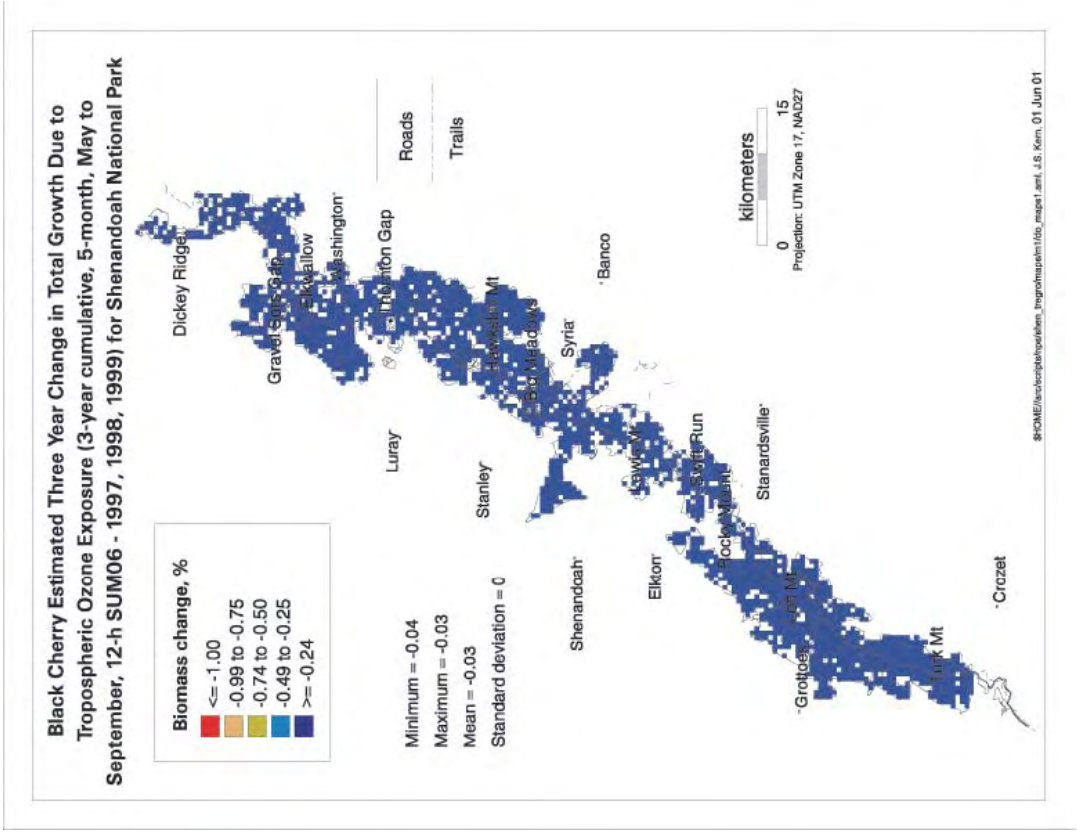

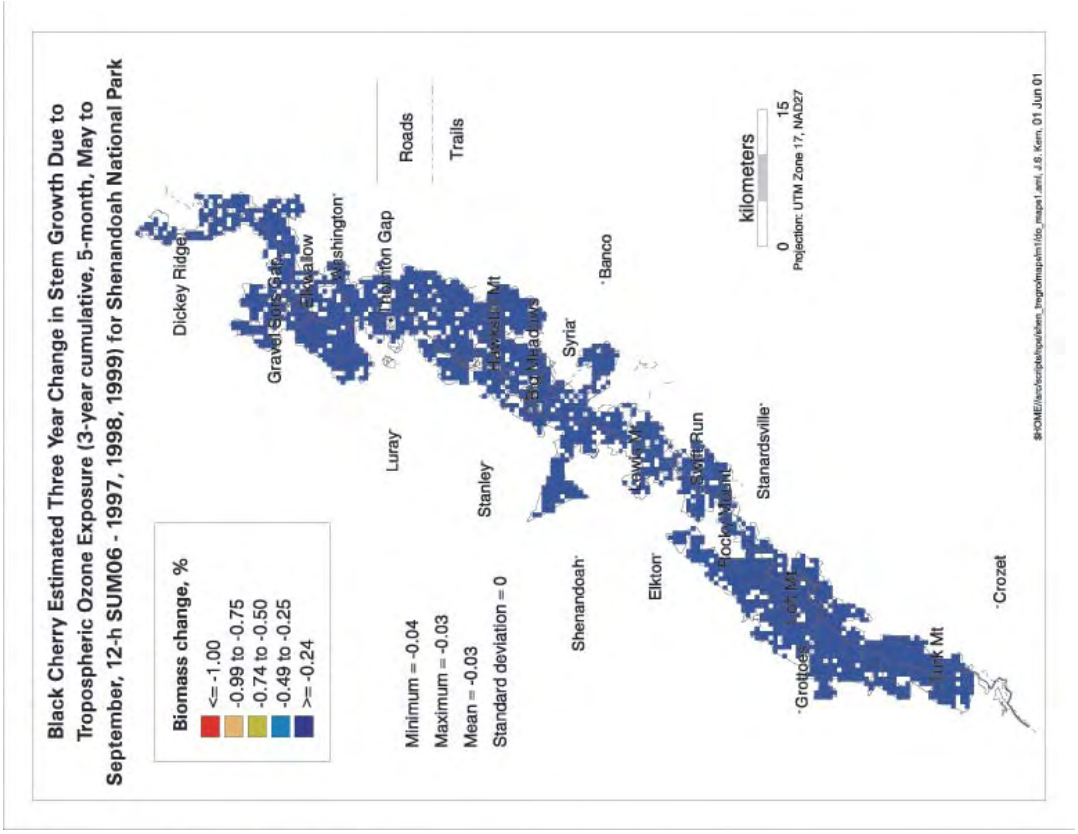

Figure J-1. Predicted change in stem (left) and total (right) mass of black cherry in response to ozone exposures in 1997-1999.

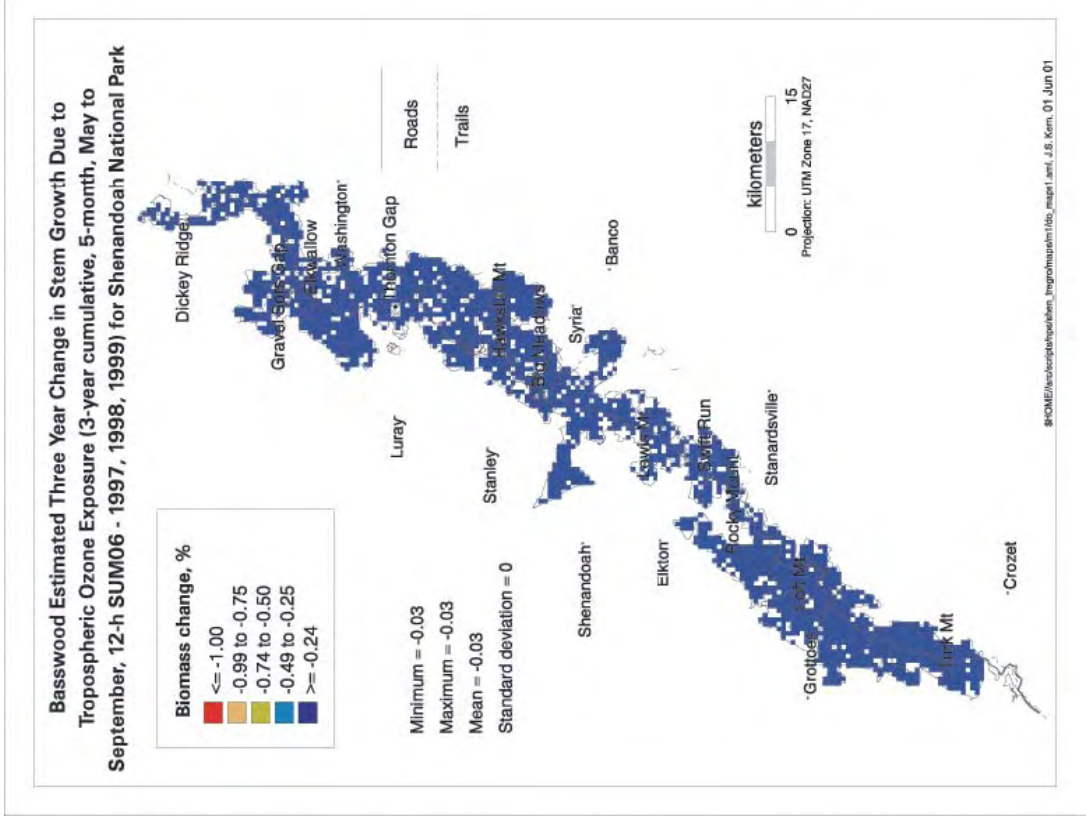

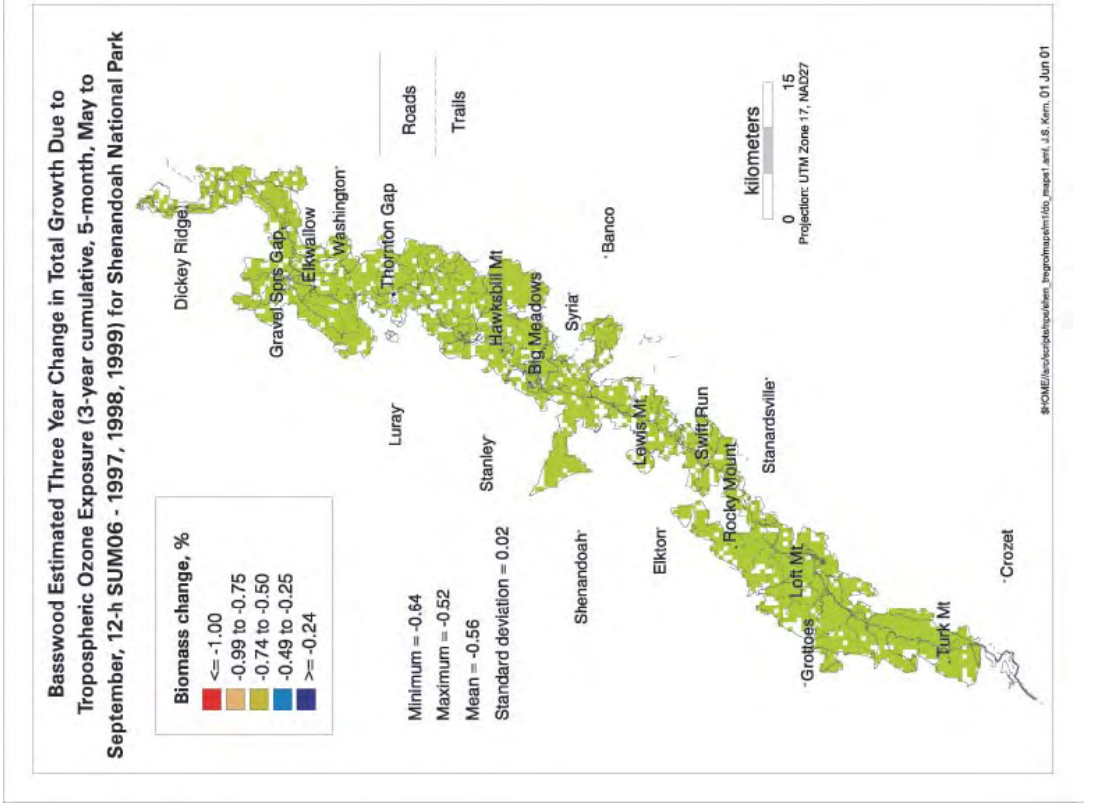

Figure J-2. Predicted change in stem (top) and total (right) mass of basswood in response to ozone exposures in 1997-1999.

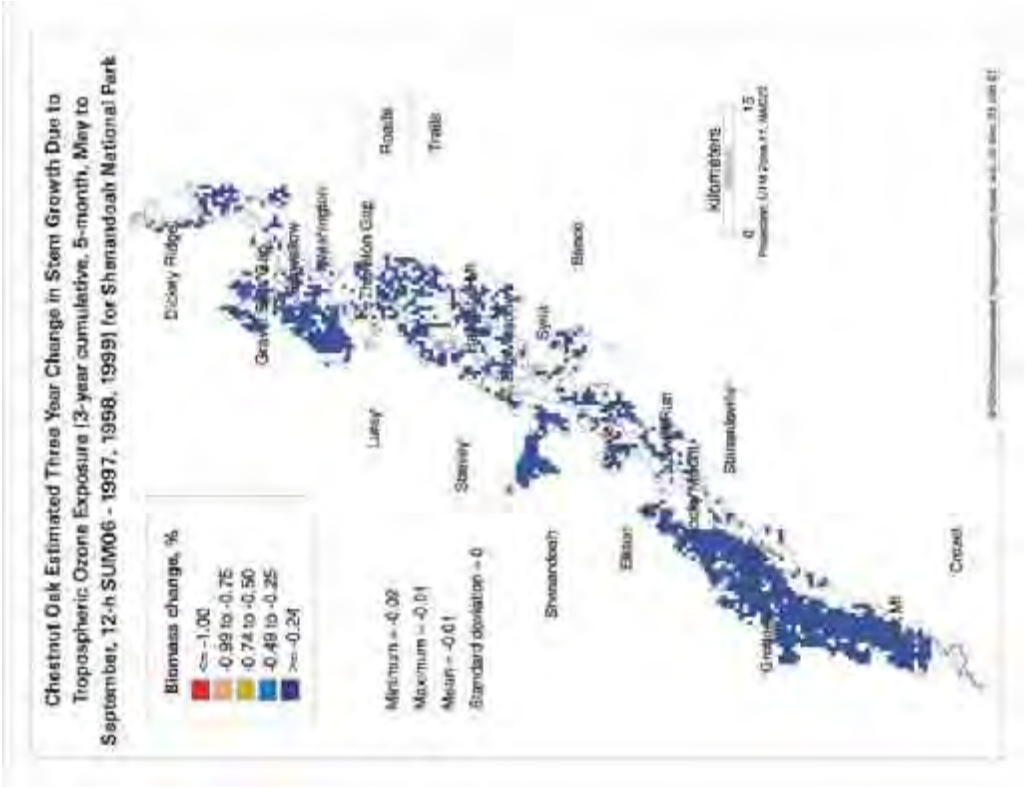

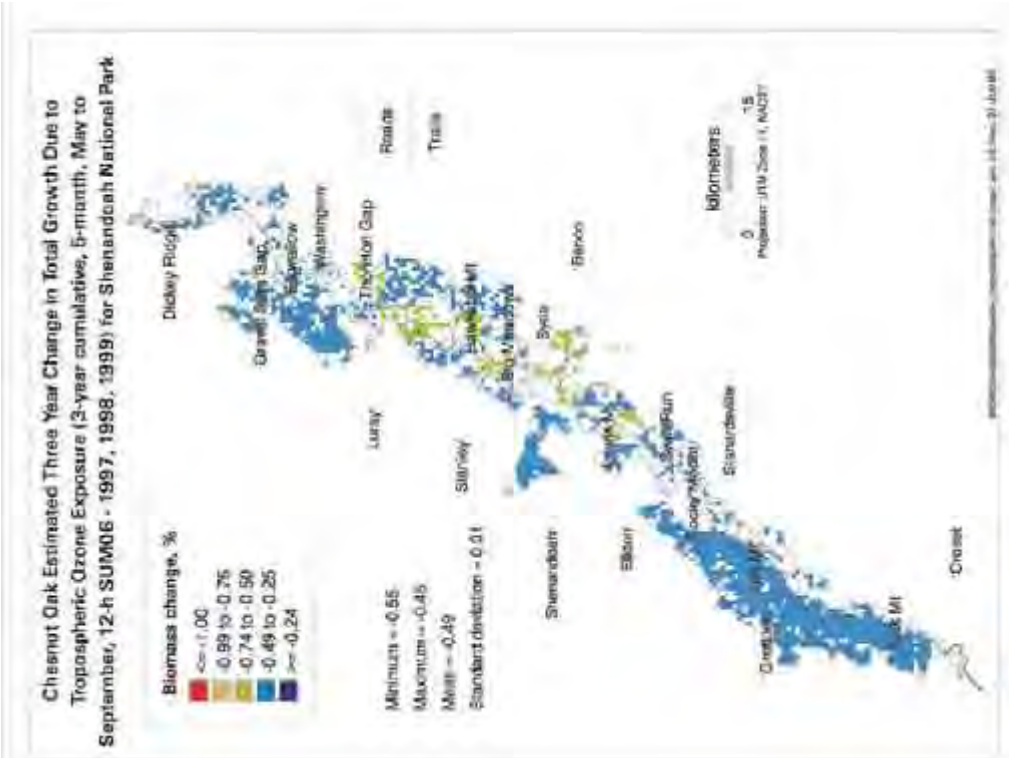

Figure J-3. Predicted change in stem (left) and total (right) mass of chestnut oak in response to ozone exposures in 1997-1999.

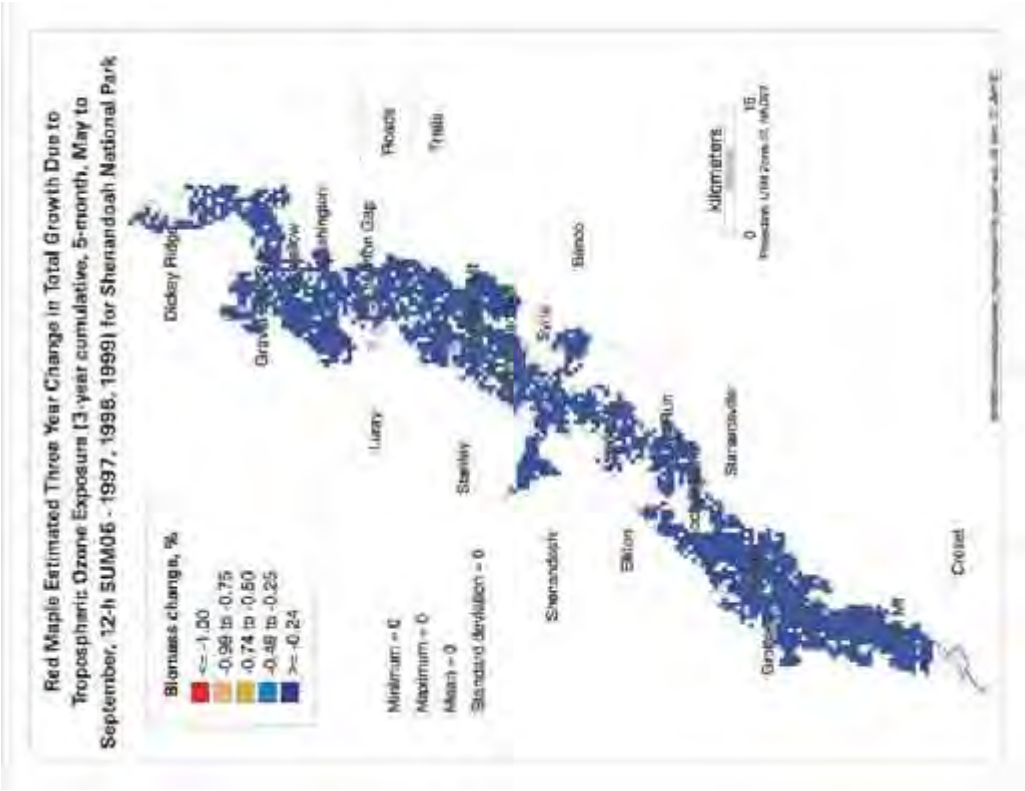

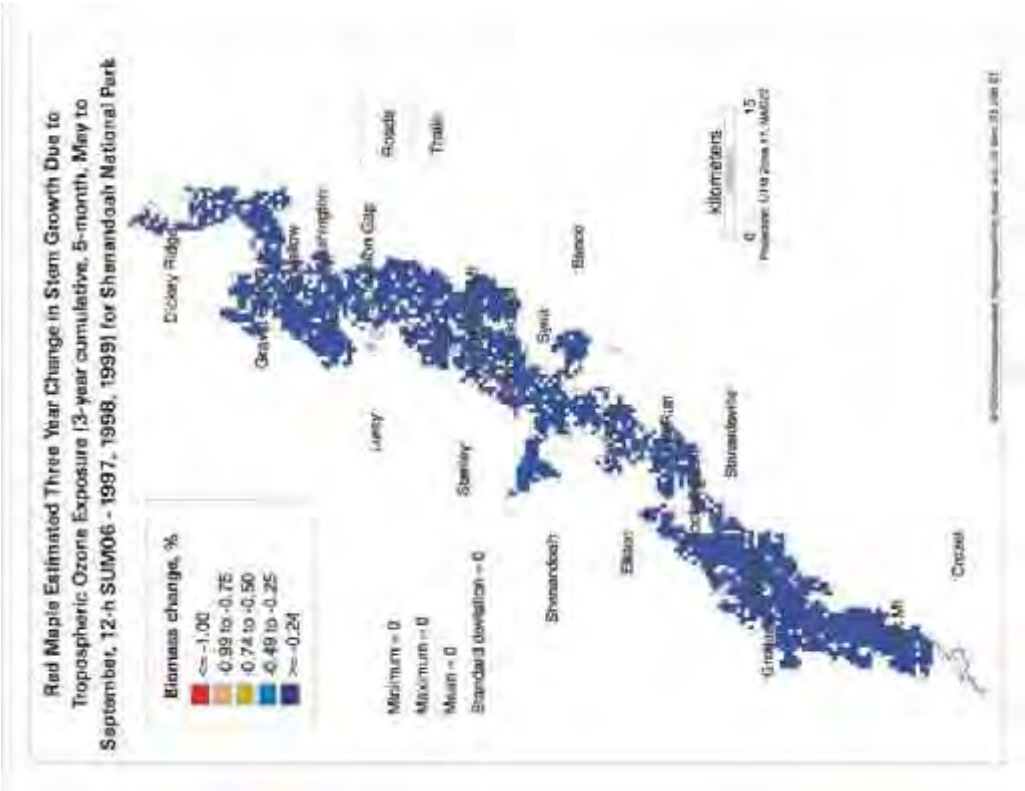

Figure J-4. Predicted change in stem (left) and total (right) mass of red maple in response to ozone exposures in 1997-1999.

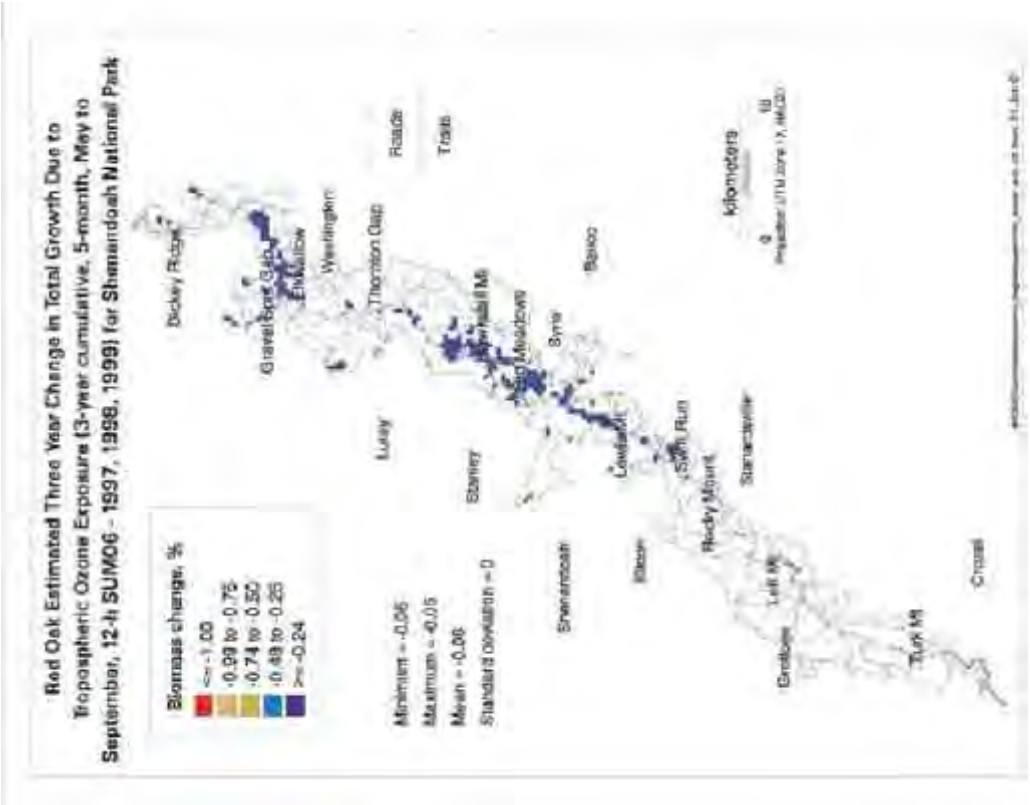

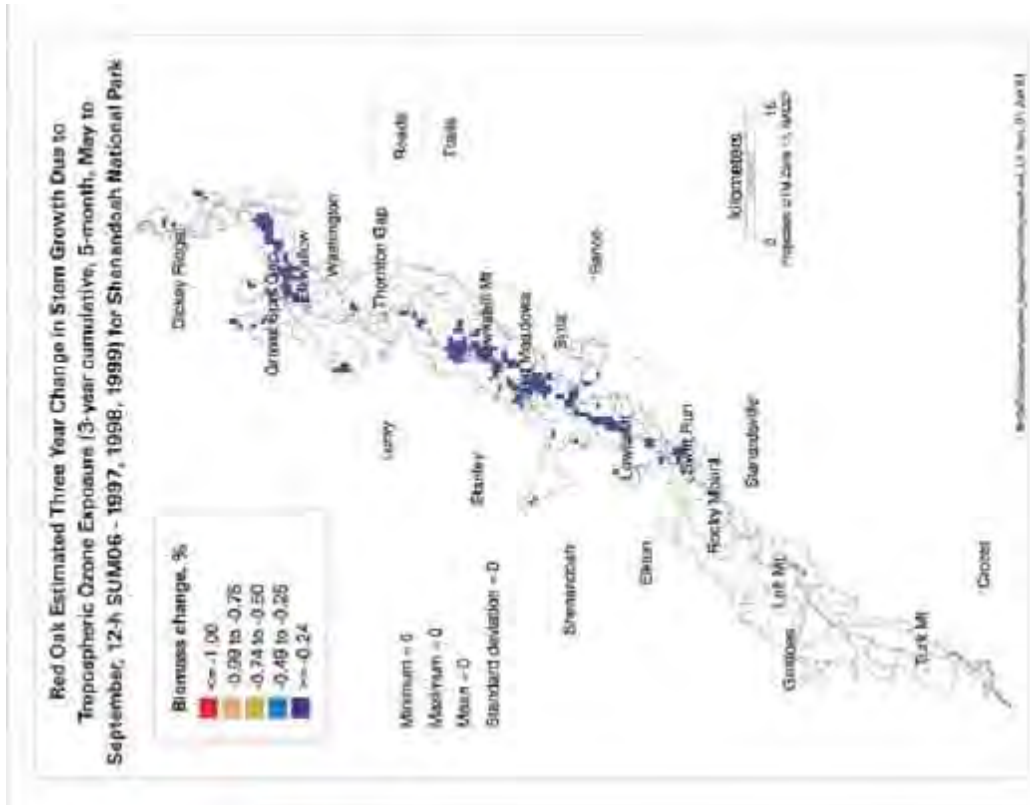

Figure J-5. Predicted change in stem (left) and total (right) mass of red oak in response to ozone exposures in 1997-1999.

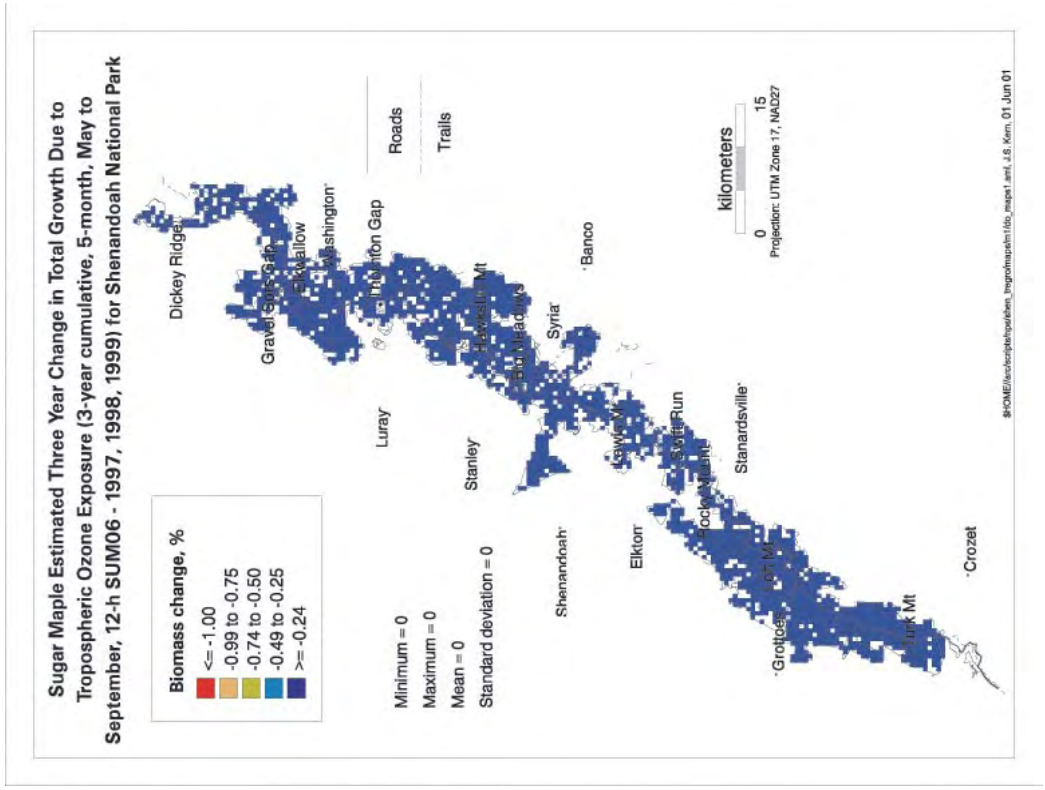

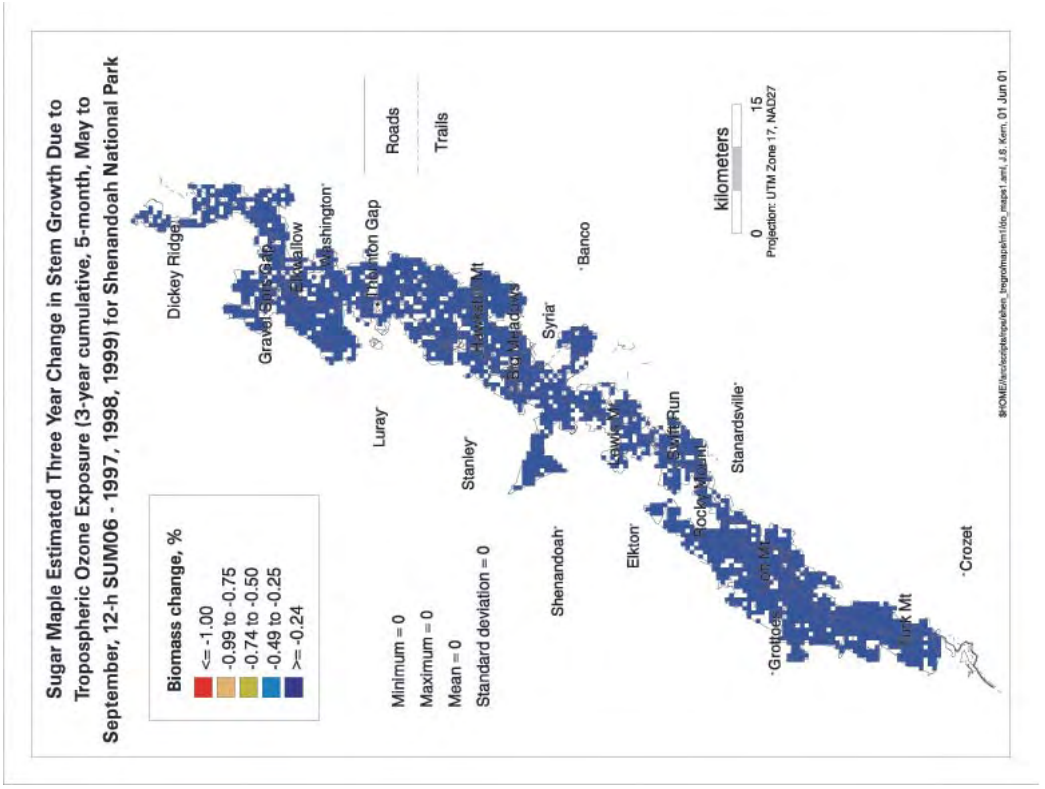

Figure J-6. Predicted change in stem (left) and total (right) mass of sugar maple in response to ozone exposures in 1997-1999.

United States Department of the Interior

NATIONAL PARK SERVICE
Northeast Region
United States Custom House
200 Chestnut Street
Philadelphia, PA 19106

IN REPLY REFER TO:

N3615(NER/RS&S-NRP)

AUG 7 2003

Dear Interested Party:

We are pleased to provide you with a copy of the technical report entitled, "Assessment of Air Quality and Related Values in Shenandoah National Park." The report documents current air quality conditions at Shenandoah National Park in Virginia. It is the culmination of several years of data compilation, analysis, modeling and evaluation. The report can better inform regulatory decision-making by providing an objective technical assessment by scientific experts on the quality of air and related resource conditions in this Federal Class I area.

This report is a technical assessment that evaluates the past, current and potential future status of air quality and air pollution effects on the sensitive resources in Shenandoah National Park. It focuses on the park's key known air quality related values, including visibility, streamwater chemistry, fish, soils and vegetation, and the human-made air pollutants that most affect them. The assessment summarizes the park's current and historical air quality and resource conditions, synthesizes knowledge on the visibility and ecological effects of atmospheric pollutants and documents park-specific critical load ranges for sulfur deposition effects on surface waters and ground-level ozone effects on forests. The report attempts to predict future air quality and resource conditions assuming implementation of the 1990 Clean Air Act as well as two substantially more stringent alternative emission control scenarios developed by the authors. The report also provides an overview of pertinent national and park-specific laws and policies.

Findings highlighted in the report include:

- Shenandoah has one of the highest monitored concentrations of airborne sulfate particles, acidic deposition and ground-level ozone of all U.S. national parks.
- Current annual average visual range is about 20% of the park's estimated natural range.
- Current annual average haziness is about three times greater than the park's estimated natural haziness.
- The park's most acid-sensitive streams have generally lost one or two species, and some streams may have lost up to four species of fish in response to acidic deposition.

- White ash is more sensitive to growth and species composition impacts from ground-level ozone than seven other modeled tree species.
- In-park emissions comprise less than 1% of total emissions of five human-caused air pollutants in the eight counties encompassing the park.

This assessment takes into account over 20 years of monitoring and research at the park. Results show that despite some recently improving trends, the park's sensitive scenic and aquatic resources remain significantly degraded by air pollution. The genesis of this report was the realization by park managers that there was a need for a comprehensive, state-of-the-science assessment of Shenandoah National Park's air quality and related values for use as a tool in the air-related regional, State, and park planning, policy, permit review, science and outreach arenas. As such, it is intended that this technical assessment should be used as guidance when developing new or implementing existing regulatory programs, which affect Federal Class I areas such as Shenandoah National Park.

We look forward to our continued cooperation with your agency in the mitigation and protection of air quality and related values in Shenandoah National Park, as well as other park areas in the Mid-Atlantic and Chesapeake Bay regions.

Sincerely,

Marie Rust
Regional Director
Northeast Region